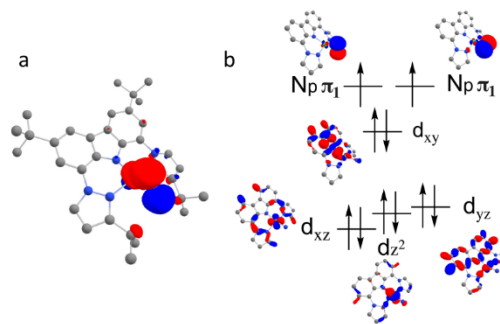
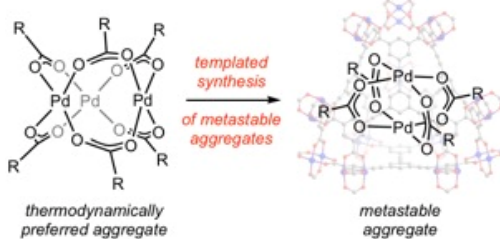
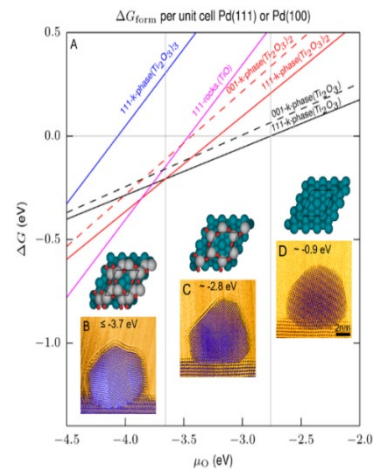
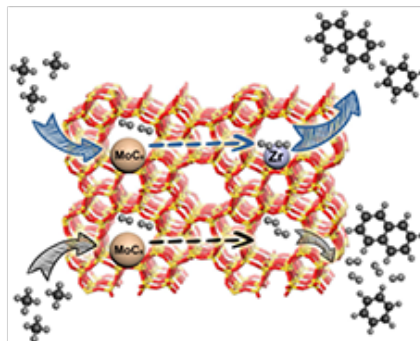
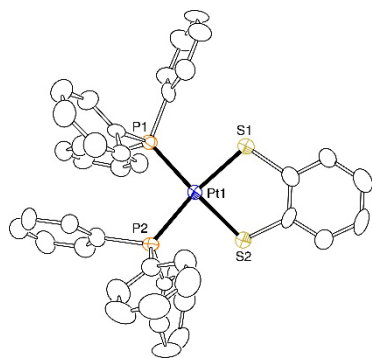


U.S. DEPARTMENT OF
ENERGY

Office of
Science

2019 Catalysis Science PI Meeting
Resources and Opportunities
 Gaithersburg Marriott Washingtonian Center
 Gaithersburg, MD
 July, 24 – 26, 2019



Program and Abstracts for the
2019 BES Catalysis Science Research PI Meeting:
“Resources and Opportunities”



Gaithersburg Marriot Washingtonian Center
Gaithersburg, MD
July 24 - 26, 2019

The research grants and contracts described in this document are supported by the U.S. Department of Energy, Office of Science/Basic Energy Sciences, as part of the Catalysis Science Program within the Chemical Sciences, Geosciences and Biosciences Division

FOREWORD

The 2019 Catalysis Science Research PI Meeting is sponsored by the Division of Chemical Sciences, Geosciences and Biosciences, Office of Basic Energy Sciences (BES), U.S. Department of Energy. It is held on July 24-26, 2019, at the Marriott Washingtonian Hotel in Gaithersburg, Maryland. The purposes of this meeting are to discuss the recent advances in the chemical, physical, and biological bases of catalysis science, to foster exchange of ideas and cooperation among BES/Catalysis Science Program PIs, and to discuss the new science challenges and opportunities recently emerging in catalytic technologies for energy production and use.

Catalysis research activities within BES emphasize fundamental research aimed at understanding reaction mechanisms and, ultimately, controlling the chemical conversion of natural and artificial feedstocks to useful energy carriers. The long-term goals of this research are to discover fundamental scientific principles, and to produce insightful approaches for the prediction of catalyst structure-reactivity behavior. Such knowledge, integrated with advances in chemical and materials synthesis, *in-situ* and *operando* analytical instrumentation, chemical kinetics and dynamics measurements, and computational chemistry methods, will allow the control of chemical reactions along desired pathways. This new knowledge will impact the efficiency of conversion of natural resources into fuels, chemicals, materials, or other forms of energy, while minimizing the impact to the environment.

The purpose of this meeting is to highlight the fundamental advances in catalysis science of relevance to the energy, economic and environmental future of the U.S. This year's meeting "*Resources and Opportunities*" is aimed at focusing the attention of the scientific community to existing tools and facilities that can enable novel discoveries and more in depth understanding of catalytic systems. Examples of resources and opportunities discussed in this meeting include sessions presenting the Synchrotron Catalysis Consortium and Co-Access, ultrafast spectroscopy, and the Advanced Scientific Computing Resources (ASCR), all of which provide unique and state of the art tools for interrogating and understanding catalytic systems. This year's program includes two plenary sessions featuring 7 talks, as well as 17 oral and 56 poster presentations by BES/Catalysis Science PIs.

Special thanks to the program investigators and their students, postdocs, and collaborators for their dedication to the continuous success and visibility of the BES/Catalysis Science Program. We also thank the Oak Ridge Institute for Science and Education staff (Linda Sievers, Connie Lansdon and Teresa Crockett) for the logistical and web support of the meeting. Finally, very special thanks go to Raul Miranda³ for his longstanding and continuing contributions to the BES/Catalysis Science Program, now from his role as Team Lead for Chemical Transformations in the BES/Chemical Sciences, Geosciences and Biosciences Division.

Maria Flytzani-Stephanopoulos¹, Manos Mavrikakis², Viviane Schwartz³ and Chris Bradley³

¹Tufts University

²University of Wisconsin, Madison

³Catalysis Science Program, Office of Basic Energy Sciences, US Department of Energy

2019 Catalysis Science PI Meeting
Catalysis Science – Resources and Opportunities

July 24th – 26th, 2019
Marriott Washingtonian, Gaithersburg, MD

Program Chairs: Maria Flytzani-Stephanopoulos and Manos Mavrikakis

Wednesday Morning, July 24

7:30-8:30 am **Registration and Breakfast**

OPENING SESSION

Session Chairs: Maria Flytzani-Stephanopoulos and Manos Mavrikakis

8:30-9:20 am *Welcoming Remarks and Program Updates*

Viviane Schwartz and Chris Bradley, DOE/BES/Catalysis Science Program

9:20-9:30 am PI Meeting Theme – “*Resources and Opportunities*”

Maria Flytzani-Stephanopoulos, Tufts University and **Manos Mavrikakis**,
University of Wisconsin-Madison

PI SESSION I

Session Chair: Alex Bell (LBNL)

9:30 – 10:00 am *Functionalization Reactions Controlled by Non-Covalent Interactions*

John Hartwig (LBNL)

10:00 – 10:10 am Discussion

10:10 – 10:30 am Coffee Break

10:30 – 11:00 am *Boron-Containing Materials as Selective Catalysts for the Oxidative
Dehydrogenation of Alkanes*

Ive Hermans (U. Wisconsin-Madison)

11:00 – 11:10 am Discussion

11:10 – 11:40 am *Mechanistic Understanding of Methane Activation Catalysts from First Principles*

Ping Liu (BNL)

11:40 – 11:50 am Discussion

11:50 - 1:30 pm **Working Lunch**

Wednesday Afternoon, July 24

PI SESSION II

Session Chair: Donna Chen (U. South Carolina)

1:30-2:00 pm *The Chemical Potential of Metal Atoms in Supported Nanoparticles: a Key Descriptor for Catalyst Performance*

Charles Campbell (U. Washington)

2:00-2:10 pm Discussion

2:10-2:40 pm *Emerging Electron Microscopy for Heterogeneous Catalysis Research*

Miaofang Chi (ORNL)

2:40-2:50 pm Discussion

2:50-3:20 pm *Bridging Molecular and Heterogeneous Catalysis Through Graphite-Conjugated Solids*

Yogesh Surendranath (MIT)

3:20-3:30 pm Discussion

3:30-3:50 pm **Coffee Break**

PLENARY SESSION I – Resources

Session Chairs: **Maria Flytzani-Stephanopoulos**, Tufts University and **Manos Mavrikakis**, University of Wisconsin-Madison

3:50-4:15 pm *Make It Work! Accessing Office of Science Cyberinfrastructure*

Ben Brown, DOE Advanced Science Computing Research (ASCR), Acting Facilities Division Director

4:15- 4:25 pm Discussion

4:25 - 4:45 pm Synchrotron *Catalysis Consortium (SCC)*
Jingguang Chen (Columbia University/BNL)

4:45 – 5:05 pm *Consortium for Operando and Advanced Catalysts Characterization via
Electronic Spectroscopy and Structure (Co-ACCESS)*
Simon Bare, SLAC

5:05 - 5:15 pm Discussion

5:15-7:15 pm **Dinner (on your own)**

Wednesday Evening, July 24

Poster SESSION I

7:15-9:15 pm (Odd numbers)

Thursday Morning, July 25

7:30-8:30 am **Breakfast**

8:30-8:50 am CSGB/BES *Update*

Raul Miranda, Chemical Transformations Team Lead, DOE/BES/Chemical
Sciences, Geosciences and Biosciences Division

PI SESSION III

Session Chair: Shannon Stahl (U. Wisconsin)

8:50-9:20 am *Electrocatalytic Applications of Heteroatom-doped Carbon Nanostructures:
Thinking Beyond PEM Fuel Cells*
Umit Ozkan (Ohio State University)

9:20-9:30 am Discussion

9:30-10:00 am *Exploring Protonated Metallocenes as PCET Relays in N₂RR*
Jonas Peters (Caltech)

10:00-10:10 am Discussion

10:10-10:30 am **Coffee Break**

10:30-11:00 am *Selective Catalytic Oxidations: Mechanistically-Informed Catalyst Design and Optimization*

Robert Waymouth (Stanford University)

11:00-11:10 am Discussion

Plenary Session II – Opportunities

Maria Flytzani-Stephanopoulos, Tufts University and **Manos Mavrikakis**, University of Wisconsin-Madison

11:10-11:40 am *Following Ultrafast Reaction Dynamics in Heterogeneous Catalysis*

Tony Heinz (SLAC)

11:40-11:50 am Discussion

11:50-12:20 am *Tabletop Femtosecond M-edge XANES as a New Tool for Inorganic Spectroscopy*

Josh Vura-Weis (UIUC)

12:20-12:30 am Discussion

12:30-1:30 pm **Working Lunch**

Thursday Afternoon, July 25

Panel Session – Opportunities

Session Chairs: **Viviane Schwartz** and **Chris Bradley**, DOE/BES/Catalysis Science Program

Recent CSGB/BES Workshop Activities

1:30-1:45 pm *Update on the CSGB Council Workshop on Earth Abundant Catalysis*

Morris Bullock (PNNL)

1:45-2:15 pm Q & A Panel Discussion of the Workshop (with Catalysis Science PI participants)

2:15-2:30 pm *Update on the BES Roundtable Workshop on Polymer Upcycling*

Geoff Coates (Cornell)

2:30-3:00 pm Q & A Panel Discussion of the Workshop (with Catalysis Science PI participants)

3:00-3:10 pm *Updates on Upcoming Workshops/Activities*
Viviane Schwartz, DOE BES

3:10-3:30 pm **Coffee Break**

PI SESSION IV

Session Chair: Ged Parkin (Columbia)

3:30-4:00 pm *Control and Understanding of Molecular Catalysts on Surfaces*
Alex Katz (U. California-Berkeley)

4:00-4:10 pm Discussion

4:10-4:40 pm *Metal-ligand Cooperativity- an Ir(III)-H and its Corresponding Ligand Protonated Tautomer*
Karen Goldberg (U. Pennsylvania)

4:40-4:50 pm Discussion

4:50-5:20 pm *Advances in Catalysts for Heterocycle Carbonylation*
Geoff Coates (Cornell)

5:20-5:30 pm Discussion

5:30-7:30 pm **Dinner (on your own)**

Thursday Evening, July 25

Poster SESSION II

7:30-9:30 pm (Even numbers)

Friday Morning, July 26

7:30-8:30 am **Breakfast**

PI SESSION V

Session Chair: Susannah Scott (UCSB)

8:30-9:00 am *Understanding Oxide Catalysis Through Collaborative Science in the Institute for Catalysis in Energy Processes (ICEP)*

Justin Notestein (Northwestern University)

9:00-9:10 am Discussion

9:10-9:40 am *Organofunctionalized Surfaces for Controlling the Behavior of Interfacial Catalysts*

Igor Slowing (Ames National Laboratory)

9:40-9:50 am Discussion

9:50-10:20 am *Olefination and the Catalytic Monoborylation of Methane by Combining Synthesis, Theory, and High-Throughput Optimization*

Daniel Mindiola (U. Pennsylvania)

10:20-10:30 am Discussion

10:30-10:50 am **Coffee Break**

PI SESSION VI

Session Chair: Thomas Bligaard (SLAC)

10:50-11:20 am *Bimetallic Catalysts for Bio-oil Upgrading: A Multi-scale Modeling Approach*

Jean-Sabin McEwen (Washington State University)

11:20-11:30 am Discussion

11:30-12:00 pm *Catalytic Hydrogenation of Arenes: Evolution of the Conversion of a Molecular Rh-CAAAC Complex to Rh Nanoparticles*, **Morris Bullock** (PNNL)

12:00-12:10 pm Discussion

CLOSING SESSION

12:10-12:25 pm Final Remarks

12:25 pm Adjourn

POSTER SESSION I

Wednesday, July 24

1. Kinetics of ethylene and 1-hexene co-oligomerization/co-polymerization

Chan Y. Park,^a Joshua Speer,^a Jeffrey Switzer,^b Grigori Medvedev,^b James M. Caruthers,^b and Mahdi M. Abu-Omar^a

^a Department of Chemistry and Biochemistry, University of California, Santa Barbara, California 93106.

^b School of Chemical Engineering, Purdue University, West Lafayette, Indiana 47907

2. Electronic Cooperativity in Supported Organometallic Catalysts for Low Temperature Upgrading of Light Alkenes

Alon Chapovetsky,¹ Gokhan Celik,¹ Ryan R. Langeslay,² Frédéric A. Perras,² Marek Pruski,² Magali S. Ferrandon,¹ Evan C. Wegener,¹ Hacksung Kim,¹ Jacob White,³ Laura Gagliardi,³ Alfred P. Sattelberger,¹ David M. Kaphan,¹ Massimiliano Delferro¹

¹Chemical Sciences and Engineering Division, Argonne National Laboratory

²Ames Laboratory

³Department of Chemistry, University of Minnesota

3. Development of Silica Supported Single-Site Metal Ion Catalysts for Alkenes Hydrogenation and Alkanes Dehydrogenation

Cong Liu, Magali Ferrandon, A. Jeremy Kropf, David M. Kaphan, Massimiliano Delferro
Chemical Sciences and Engineering Division, Argonne National Laboratory

4. Mechanistic Aspects of a Surface Organovanadium(III) Catalyst for Hydrocarbon Hydrogenation and Dehydrogenation

David M. Kaphan, Magali S. Ferrandon, Ryan R. Langeslay, Gokhan Celik, Evan C. Wegener, Cong Liu, Jens Niklas, Oleg G. Poluektov, Massimiliano Delferro
Chemical Sciences and Engineering Division, Argonne National Laboratory

5. Heterogeneous Catalysts for Strategic Formation of C-C, C-O, and C-N Bonds

Alexis T. Bell

Chemical Sciences Division, Lawrence Berkeley National Laboratory, Berkeley, CA

6. Lewis Acid and Solvent Effects on Carbon Dioxide Insertion and Valorization Processes

Nilay Hazari¹ and Wesley H. Bernskoetter²

¹Yale University

²University of Missouri

7. Clusters as catalysts for small molecule activation

Amymarie M. Bartholomew, Justin J. Teesdale, Brian J. Malbrecht
Harvard University, 12 Oxford Street, Cambridge, MA

- 8. Polyfunctional Catalysis for C₁ Conversion: Appraisal and Circumvention of Thermodynamic Limits in Non-Oxidative Methane Dehydroaromatization**
Neil K. Razdan, Anurag Kumar, Aditya Bhan
Chemical Engineering and Materials Science, University of Minnesota
- 9. Interplay of Electrochemical Hydrogenation and Hydrogenolysis of Furfural on Copper with Undesired Side Reactions**
Elizabeth J. Biddinger, Andrew May, Sungyup Jung
Department of Chemical Engineering, The City College of New York, CUNY, New York
- 10. Machine Learning Accelerated Catalysis Simulations**
Thomas Bligaard
SLAC National Accelerator Laboratory, Energy Sciences Division
- 11. In-situ Studies for the Conversion of C-O Bonds on Complex Metal-Oxide and Metal-Carbide Interfaces**
José A. Rodriguez, Ping Liu, Sanjaya D. Senanayake and Michael G. White
Brookhaven National Laboratory, Chemistry Department
- 12. Catalytic Hydrogenation of Arenes: Evolution of the Conversion of a Molecular Rh-CAAC Complex to Rh Nanoparticles**
R. Morris Bullock, Ba L. Tran, John L. Fulton, John C. Linehan, and Johannes A. Lercher
Institute for Integrated Catalysis, Pacific Northwest National Laboratory, Richland, WA
- 13. Transition Metal Catalysts Encapsulated in a Metal-Organic Framework for the Autocatalytic Conversion of CO₂ to Methanol**
Jeffery A. Byers, Chia-Kuang “Frank” Tsung, Zhehui Li, Thomas M. Rayder, Adam T. Benselah, Enric Adillon, Noella D’Souza
Department of Chemistry, Boston College
- 14. Metal Nodes in Bimetallic Metal-Organic Frameworks as Isolated Sites for Hydrogenation Reactions**
Donna A. Chen¹, Natalia B. Shustova¹, and Konstantinos Vogiatzis²
¹Department of Chemistry and Biochemistry, University of South Carolina
²Department of Chemistry, University of Tennessee
- 15. Dedicated Beamline Facilities for Catalytic Research –Synchrotron Catalysis Consortium (SCC)**
Jingguang G. Chen, Anatoly I. Frenkel, Jose A. Rodriguez
Columbia University and Brookhaven National Laboratory
- 16. Emerging Electron Microscopy for Heterogeneous Catalysis Research**
Miaofang Chi,¹ Michael Zachman¹, Wenpei Gao³, Ahmed O. Elnabawy⁴, Victor Fung¹, Felipe Polo Garzon², Luke T. Roling⁴, De-en Jiang⁵, Younan Xia⁶, Manos Mavrikakis⁴, Zili Wu^{1,2}

¹Center for Nanophase Materials Sciences, ²Chemical Sciences Division, Oak Ridge National Laboratory; ³Department of Materials Science and Engineering, University of California–Irvine; ⁴Department of Chemical and Biological Engineering, University of Wisconsin–Madison; ⁵Department of Chemistry, University of California–Riverside; ⁶Department of Biomedical Engineering, Georgia Institute of Technology

17. The Consortium for Operando and Advanced Catalyst Characterization via Electronic Spectroscopy and Structure (Co-ACCESS) at SSRL

Simon R. Bare

Chemical Science Division, Energy Sciences Directorate, and SSRL, SLAC National Accelerator Laboratory

18. Modeling of Catalytic Processes for More Efficient Utilization of Hydrocarbon Resources

Thomas R. Cundari (t@unt.edu)

Department of Chemistry, Center for Advanced Scientific Computing and Modeling (CASCAM), University of North Texas, Denton, TX

19. Tailoring Boron Nitride for Catalysis Applications

Hao Chen,¹ Zhenzhen Yang,¹ Miaofang Chi,¹ De-en Jiang,² Zili Wu,¹ and Sheng Dai¹

¹Oak Ridge National Laboratory and ²University of California Riverside

20. Sub Nanometer Sized Clusters for Heterogeneous Catalysis

Abhaya Datye¹ and Yong Wang²

¹University of New Mexico and ²Washington State University

21. Conversion of Ethanol to Butanol and Butadiene over Bifunctional Acid-Base Catalysts

Robert J. Davis, Sabra Hanspal, Naomi Miyake, J. Tyler Prillaman, Zachary Young
Department of Chemical Engineering, University of Virginia Charlottesville, VA

22. Theory, Simulation, and Design of High-Oxidation State Main-Group Metal Catalysts for Hydrocarbon C-H Functionalization

Daniel H. Ess

Department of Chemistry and Biochemistry, Brigham Young University, Provo, UT

23. Controlling Catalytic Activity by Redesigning Enzymatic Scaffolds

Bojana Ginovska, Greg Schenter, Joseph Laureanti and Wendy Shaw

Institute for Integrated Catalysis, Pacific Northwest National Laboratory, Richland, WA

24. Spectroscopic Characterization of Polynuclear Copper Species in Chabazite Zeolites for Partial Methane Oxidation to Methanol

Laura N. Wilcox¹, Ishant Khurana¹, Hui Li², Christopher Paolucci², William F. Schneider², Rajamani Gounder^{1*}

¹Davidson School of Chemical Engineering, Purdue University, West Lafayette, IN

²Chemical and Biomolecular Engineering, University of Notre Dame, Notre Dame, IN

25. Electrocatalysis at Liquid-Solid Interfaces: Principles and Reactivity-Stability Trends

Siddharth Deshpande, Zhenhua Zeng, Ankita Morankar, Joseph Kubal, Jeffrey Greeley

Davidson School of Chemical Engineering, Purdue University, West Lafayette, IN

26. From Single Atoms to Clusters: Controlling CO₂ Reduction through Molecular Affinity on Rh Catalysts

Oliver Y. Gutierrez, Janos Szanyi, Libor Kovarik, John Fulton, Johannes A. Lercher
Pacific Northwest National Laboratory

27. N₂O Elimination from *cis*-Pt(PPh₃)₂(κ^2 -N₂O₂) and *trans*-Ph₃Sn-ONNO-SnPh₃

Jack V. Davis¹, Mohan M. Gamage¹, Musa Ahmadi¹, Leonardo Farias Serafim¹, Jake Sirlin¹, Manuel Temprado², Burjor Captain¹, Carl D. Hoff¹.

University of Miami, Coral Gables, Florida¹, University of Alcalá, Madrid, Spain²

28. Catalysis by Au: Au-TiO₂ Interfacial Sites in Oxidation Catalysis and Selective Ethylbenzene Oxidation by Coupling with Au-catalyzed Cyclooctene Epoxidation

Harold H. Kung

Chemical and Biological Engineering, Northwestern University, Evanston, IL

Thursday, July 24

29. Surface Science Meets Homogeneous Catalysis. Surfaces as Unique Activators and Ligands

Tobin J. Marks

Department of Chemistry, Northwestern University, Evanston IL

30. Fundamental Understanding and Catalyst Development for Electrochemical Processes Involving H₂O, H₂, O₂, and H₂O₂

McKenzie Hubert, Zhihua Chen, Shuchung Chen, Alaina Strickler, Yi Cui, Frank Abild-Pedersen, Christopher Hahn, Drew Higgins, Laurie A. King, Samira Siahrostami, Zhenan Bao, Jens K. Nørskov, Thomas F. Jaramillo

SLAC National Accelerator Laboratory & Stanford University

31. Well-Defined Active-Site Environments on Silicate Supports

Alexander Katz,# Nicolás Grosso-Giordano,# Christian Schöttle,# Andrew Palermo,# Christian Schroeder,* Alexander Okrut,# Andrew Solovyov,# Shengjie Zhang,^ David Dixon,^ Heinz Frei,† Bruce C. Gates,% Hubert Koller,* Stacey I. Zones‡

#Department of Chemical and Biomolecular Engineering, University of California, Berkeley, California

*Institut für Physikalische Chemie, Westfälische Wilhelms-Universität Münster, Münster, Germany

[^]Department of Chemistry, The University of Alabama, Tuscaloosa, Alabama
[†]Molecular Biophysics and Integrated Bioimaging Division, Lawrence Berkeley National Laboratory, Berkeley, California
[%]Department of Chemical Engineering, University of California at Davis, Davis, California
[‡]Chevron Energy Technology Company, Richmond, California

32. Strategies for Enhancement of Catalytic Performance of Mo-based Catalysts in Methane Dehydroaromatization

Mustafizur Rahman¹, Apoorva Sridhar¹, Antonia Infantes-Molina², Alexey Boubnov³, Simon R. Bare³, Eli Stavitski⁴, Sheima J. Khatib¹

¹ Department of Chemical Engineering, Texas Tech University, Lubbock, Texas

² Department of Inorganic Chemistry, Crystallography and Mineralogy. Faculty of Science. Campus de Teatinos, 29071 Malaga, Spain.

³ Stanford Synchrotron Radiation Lightsource, SLAC National Accelerator Laboratory, Menlo Park, CA

⁴ National Synchrotron Light Source II, Brookhaven National Laboratory, Upton, NY

33. Applications and advances in machine learned potentials

John Kitchin, Jenny Zhan, Mingjie Liu and Yilin Yang
Carnegie Mellon University, Department of Chemical Engineering

34. Surface Chemistry and Reactions for Bimetallic Au Catalysis

Bruce E. Koel¹, Simon G. Podkolzin²

¹Department of Chemical and Biological Engineering, Princeton University, Princeton, NJ

²Department of Chemical Engineering and Materials Science, Stevens Institute of Technology, Hoboken, NJ

35. Inter- and Intramolecular “Inverse” Frustrated Lewis Pairs – Catalysis and Small Molecule Activation

Clemens Krempner
Department of Chemistry & Biochemistry, Texas Tech University, Lubbock, Texas.

36. Electrocatalytic H₂ Evolution by Metal Dithiolene Frameworks

Smaranda C. Marinescu,^a Keying Chen,^a Courtney A. Downes,^a Eugene Schneider,^b Jason D. Goodpaster^b

^aUniversity of Southern California, Los Angeles, CA

^bUniversity of Minnesota – Twin Cities, MN

37. Atomic-scale Design of Metal and Alloy Catalysts: A Combined Theoretical and Experimental Approach

Manos Mavrikakis,[†] James A. Dumesic,[†] Younan Xia[‡]

[†] Department of Chemical & Biological Engineering, University of Wisconsin – Madison

[‡] School of Chemistry & Biochemistry, Georgia Institute of Technology

38. Selective Conversion of Carbon Dioxide to Formaldehyde via a Bis(silyl)acetal: Carbon Dioxide as a C₁ Source for the Synthesis of Organic Molecules

Michael Rauch and Gerard Parkin

Columbia University, Department of Chemistry

39. Understanding Kinetics of Reconstructed Catalyst Surfaces to Build Reactivity Descriptors

Felipe Polo-Garzon,¹ Victor Fung,² Yongqiang Cheng,³ Luke L. Daemen,³ Anibal J. Ramirez-Cuesta,³ Miaofang Chi,² Franklin Tao,⁴ De-en Jiang,⁵ Zili Wu^{1,2}

¹Chemical Sciences Division, ²Center for Nanophase Materials Sciences, ³Neutron Scattering Division, Oak Ridge National Laboratory, Oak Ridge, TN; ⁴Department of Chemical Engineering and Chemistry, The University of Kansas, Lawrence, KS;

⁵Department of Chemistry, University of California, Riverside, CA

40. Characterization of, and Hydrocarbon Functionalization with, Lattice-Confined Reactive Intermediates

David C. Powers

Texas A&M University, Department of Chemistry

41. Solvent Effects on Elementary Steps in Solid Acid Catalyzed Reactions: Acid-Base Interactions

Robert M. Rioux^{1,2}, Yanyu Mu¹, Susanna Ogozaly², William A Elliott¹, Christopher Titman¹

¹Department of Chemical Engineering, The Pennsylvania State University, University Park, PA

²Department of Chemistry, The Pennsylvania State University, University Park, PA

42. Activation of Atomically-dispersed Oxometal Catalysts for Olefin Transformations

Susannah L. Scott,¹ Albert E. Stiegman,² Baron Peters^{1,3}

¹ Department of Chemical Engineering, University of California, Santa Barbara

² Department of Chemistry, Florida State University

³ Department of Chemical Engineering, University of Illinois, Urbana-Champaign

43. Pathways for Methanol Synthesis from the Conversion of C-H bonds over Well-defined Metal-Oxide Surfaces

Sanjaya D. Senanayake, Feng Zhang, Zongyuan Liu, Ivan Orozco, Luis E. Betancourt Ping Liu, Jose A. Rodriguez

Chemistry Department, Brookhaven National Laboratory, Upton, NY

44. Design of Highly Durable Multimetallic Electrocatalysts

Jocelyn T. L. Gamler,¹ Hannah M. Ashberry,¹ Alberto Leonardi,² Xiahan Sang,³ Raymond R. Unocic,³ Michael Engel,² and Sara E. Skrabalak^{1,*}

¹Department of Chemistry, Indiana University, Bloomington, IN

²Institute for Multiscale Simulation, Friedrich-Alexander Universität Erlangen-Nürnberg, Erlangen, Germany

³Center for Nanophase Materials Sciences, Oak Ridge National Laboratory, Oak Ridge, TN

- 45. Catalytic Environments at the Interface: Characterization of Sites and Distributions, Catalytic Activity and Reaction Mechanisms**
Aaron D. Sadow, Takeshi Kobayashi, Marek Pruski, Frédéric A. Perras, Long Qi, Igor I. Slowing
U.S. DOE Ames Laboratory and Iowa State University, Ames, IA
- 46. Two-State Reactivity in Iron(I)-Catalyzed Alkene Isomerization**
Yafei Gao, Sean A. Lutz, Anne K. Hickey and Jeremy M. Smith
Indiana University
- 47. Copper-Catalyzed Oxidation of O–H and N–H Bonds**
Shannon S. Stahl
Department of Chemistry, University of Wisconsin-Madison
- 48. Influence of Temperature and Ti substitution on Oxygen Electroadsorption and Electrocatalysis: A Progress on Theory-Experiment Convergence**
Jin Suntivich
Cornell University, Department of Materials Science and Engineering
- 49. Bridging Molecular and Heterogeneous Catalysis Through Graphite-Conjugated**
Yogesh Surendranath
Massachusetts Institute of Technology, Department of Chemistry
- 50. Activation of shale gas on singly dispersed catalytic sites anchored on oxide**
Yu Tang, ^a Luan Nguyen, ^a De-en Jiang, ^b Philippe Sautet, ^c Franklin (Feng) Tao^a
Department of Chemical and Petroleum Engineering, University of Kansas ^a
Department of Chemistry, University of California, Riverside ^b
Department of Chemical and Bimolecular Engineering, University of California, Los Angeles ^c
- 51. Catalytic Transformations and Bond Activation Processes Promoted by Zr/Co Heterobimetallic Complexes**
Christine M. Thomas, Hongtu Zhang, Kathryn M. Gramigna, and Nathanael H. Hunter
The Ohio State University, Department of Chemistry and Biochemistry
- 52. Synthesis and Properties of Ruthenium–Cobalt Oxo Cubane Clusters Bearing a High-Valent, Terminal Ru^V–Oxo with Significant Oxo Radical Character**
Jaruwat Amtawong and T. Don Tilley
Chemical Sciences Division, Lawrence Berkeley National Laboratory
- 53. Chemical and Electrocatalytic Oxidation of Ammonia**
Mahdi Raghbi Borougeni, Christine Greene, and Timothy H. Warren
Georgetown University, Department of Chemistry

54. Alkane Activation and Oxidation on IrO₂(110)

Jason F. Weaver,¹ Aravind Asthagiri,² Minkyu Kim,² Rachel Martin,¹ Austin Franklin,¹
Yingxue Bian,¹ Tao Li¹

¹ Department of Chemical Engineering, University of Florida, Gainesville, FL

² Department of Chemical and Biomolecular Engineering, The Ohio State University,
Columbus, OH

55. Size-Selected Metal Oxide Clusters as Model Inverse Catalysts

Michael G. White,^{1,2} Kenneth R. Goodman,¹ Yilin Ma,¹ and Jason Wang¹

¹Department of Chemistry, Stony Brook University, Stony Brook, NY

²Chemistry Division, Brookhaven National Laboratory, Upton, NY

56. Force/Activity Relationships in Transition Metal-Catalysis

Ross A. Widenhoefer, Stephen L. Craig, Liqi Wang, Yichen Yu

Department of Chemistry, Duke University

TABLE OF CONTENTS

TITLE PAGE	i
FOREWORD	ii
AGENDA	iii
POSTER SESSIONS	ix
TABLE OF CONTENTS	xvii
ABSTRACTS	1
ORAL PRESENTATION ABSTRACTS	2
Functionalization Reactions Controlled by Non-Covalent Interactions John F. Hartwig, <i>Lawrence Berkeley National Laboratory</i>	3
Boron-containing Materials as Selective Catalysts for the Oxidative Dehydrogenation of Alkanes Ive Hermans, <i>University of Wisconsin-Madison</i>	9
Mechanistic Understanding of Methane Activation Catalysts from First Principles Ping Liu, <i>Brookhaven National Laboratory</i>	14
The Chemical Potential of Metal Atoms in Supported Nanoparticles: a Key Descriptor for Catalyst Performance Charles T. Campbell, <i>University of Washington</i>	15
Emerging Electron Microscopy for Heterogeneous Catalysis Research Miaofang Chi, <i>Oak Ridge National Laboratory</i>	19
Bridging Molecular and Heterogeneous Catalysis Through Graphite-Conjugated Solids Yogesh Surendranath, <i>Massachusetts Institute of Technology</i>	21
Electrocatalytic Applications of Heteroatom-doped Carbon Nanostructures: Thinking Beyond PEM Fuel Cells Umit S. Ozkan, <i>The Ohio state University</i>	22
Exploring Protonated Metallocenes as PCET Relays in N₂RR Jonas C. Peters, <i>California Institute of Technology</i>	28

Selective Catalytic Oxidations: Mechanistically-Informed Catalyst Design and Optimization Robert M. Waymouth, <i>Stanford University</i>	30
Following ultrafast reaction dynamics in heterogeneous catalysis Tony F. Heinz, <i>SLAC National Accelerator Laboratory</i>	34
Tabletop Femtosecond M-edge XANES as a New Tool for Inorganic Spectroscopy Josh Vura-Weis, <i>University of Illinois at Urbana-Champaign</i>	35
Control and Understanding of Molecular Catalysts on Surfaces Alexander Katz, <i>University of California at Berkeley</i>	36
Metal-ligand cooperativity - an Ir(III)-H and its Corresponding Ligand Protonated Tautomer Karen I. Goldberg, <i>University of Pennsylvania</i>	40
New Advances in Catalysts for Heterocycle Functionalization Geoffrey W. Coates, <i>Cornell University</i>	41
Understanding oxide catalysis through collaborative science in the Institute for Catalysis in Energy Processes (ICEP) Justin M Notestein, <i>Northwestern University</i>	43
Organofunctionalized Surfaces for Controlling the Behavior of Interfacial Catalysts Igor I. Slowing, <i>Ames National Laboratory</i>	56
Olefination and the Catalytic Monoborylation of Methane by Combining Synthesis, Theory and High-Throughput Optimizations. Daniel J. Mindiola, <i>University of Pennsylvania</i>	57
Bimetallic Catalysts for Bio-oil Upgrading: A Multi-Scale Modeling Approach Jean-Sabin McEwen, <i>Washington State University</i>	61
Catalytic Hydrogenation of Arenes: Evolution of the Conversion of a Molecular Rh-CAAC Complex to Rh Nanoparticles R. Morris Bullock, <i>Pacific Northwest National Laboratory</i>	67
NATIONAL LABORATORIES ABSTRACTS	68
Catalytic Environments at the Interface: Characterization of Sites and Distributions, Catalytic Activity and Reaction Mechanisms Aaron D. Sadow, <i>Ames National Laboratory</i>	69
Electronic Cooperativity in Supported Organometallic Catalysts for Low Temperature Upgrading of Light Alkenes Massimiliano Delferro, <i>Argonne National Laboratory</i>	79

In-situ Studies for the Conversion of C-O Bonds on Complex Metal-Oxide and Metal-Carbide Interfaces José A. Rodriguez, <i>Brookhaven National Laboratory</i>	87
The Consortium for Operando and Advanced Catalyst Characterization via Electronic Spectroscopy and Structure (Co-ACCESS) at SSRL Simon Bare, <i>Co-ACCESS</i>	99
Harnessing Complexity for Catalytic Efficiency John F. Hartwig, <i>Lawrence Berkeley National Laboratory</i>	104
Fundamentals of Catalysis and Chemical Transformations Zili Wu, <i>Oak Ridge National Laboratory</i>	125
Self-Organization Around Active Centers Influencing Catalytic Rates for Brønsted Acid Catalyzed Reactions Johannes Lercher, <i>Pacific Northwestern National Laboratory</i>	141
Fundamental Understanding and Catalyst Development for Electrochemical Processes Involving H₂O, H₂, O₂, and H₂O₂ Thomas F. Jaramillo, <i>SLAC National Accelerator Laboratory</i>	168
POSTER PRESENTATION ABSTRACTS	185
Kinetics of ethylene and 1-hexene co-oligomerization/co-polymerization Mahdi M. Abu-Omar, <i>University of California, Santa Barbara</i>	186
Development of Silica Supported Single-Site Metal Ion Catalysts for Alkenes Hydrogenation and Alkanes Dehydrogenation Cong Liu, <i>Argonne National Laboratory</i>	191
Mechanistic Aspects of a Surface Organovanadium(III) Catalyst for Hydrocarbon Hydrogenation and Dehydrogenation David M. Kaphan, <i>Argonne National Laboratory</i>	192
Heterogeneous Catalysts for Strategic Formation of C-C, C-O, and C-N Bonds Alexis T. Bell, <i>Lawrence Berkeley National Laboratory</i>	193
Lewis Acid and Solvent Effects on Carbon Dioxide Insertion and Valorization Processes Wesley H. Bernskoetter, <i>University of Missouri</i>	197
Clusters as catalysts for small molecule activation Theodore A. Betley, <i>Harvard University</i>	202

Polyfunctional Catalysis for C₁ conversion: Appraisal and circumvention of thermodynamic limits in non-oxidative methane dehydroaromatization Aditya Bhan, <i>University of Minnesota</i>	204
Interplay of Electrochemical Hydrogenation and Hydrogenolysis of Furfural on Copper with Undesired Side Reactions Elizabeth J. Biddinger, <i>The City College of New York, CUNY</i>	209
Machine Learning Accelerated Catalysis Simulations Thomas Bligaard, <i>SLAC National Accelerator Laboratory</i>	211
Catalytic Hydrogenation of Arenes: Evolution of the Conversion of a Molecular Rh-CAAC Complex to Rh Nanoparticles R. Morris Bullock, <i>Pacific Northwest National Laboratory</i>	212
Transition Metal Catalysts Encapsulated in a Metal-Organic Framework for the Autocatalytic Conversion of CO₂ to Methanol Jeffery A. Byers, <i>Boston College</i>	213
Metal Nodes in Bimetallic Metal-Organic Frameworks as Isolated Sites for Hydrogenation Reactions Donna A. Chen, <i>University of South Carolina</i>	217
Dedicated Beamline Facilities for Catalytic Research – Synchrotron Catalysis Consortium (SCC) Jingguang G. Chen, <i>Columbia University and Brookhaven National Laboratory</i>	220
Emerging Electron Microscopy for Heterogeneous Catalysis Research Miaofang Chi, <i>Oak Ridge National Laboratory</i>	224
Modeling of Catalytic Processes for More Efficient Utilization of Hydrocarbon Resources Thomas R. Cundari, <i>University of North Texas</i>	226
Tailoring Boron Nitride for Catalysis Applications Sheng Dai, <i>Oak Ridge National Laboratory</i>	231
Sub Nanometer Sized Clusters for Heterogeneous Catalysis Abhaya Datye, <i>University of New Mexico</i>	232
Conversion of Ethanol to Butanol and Butadiene over Bifunctional Acid-Base Catalysts Robert J. Davis, <i>University of Virginia Charlottesville</i>	240
Theory, Simulation, and Design of High-Oxidation State Main-Group Metal Catalysts for Hydrocarbon C-H Functionalization Daniel H. Ess, <i>Brigham Young University</i>	243

Controlling Catalytic Activity by Redesigning Enzymatic Scaffolds Bojana Ginovska, <i>Pacific Northwest National Laboratory</i>	247
Spectroscopic Characterization of Polynuclear Copper Species in Chabazite Zeolites for Partial Methane Oxidation to Methanol Rajamani P. Gounder, <i>Purdue University</i>	248
Electrocatalysis at Liquid-Solid Interfaces: Principles and Reactivity-Stability Trends Jeffrey Greeley, <i>Purdue University</i>	252
From Single Atoms to Clusters: Controlling CO₂ Reduction through Molecular Affinity on Rh Catalysts Oliver Y. Gutierrez, <i>Pacific Northwest National Laboratory</i>	256
N₂O Elimination from <i>cis</i>-Pt(PPh₃)₂(κ²-N₂O₂) and <i>trans</i>-Ph₃Sn-ONNO-SnPh₃ Carl D. Hoff, <i>University of Miami</i>	257
Catalysis by Au: Au-TiO₂ Interfacial Sites in Oxidation Catalysis and Selective Ethylbenzene Oxidation by Coupling with Au-catalyzed Cyclooctene Epoxidation Harold H. Kung, <i>Northwestern University</i>	261
Surface Science Meets Homogeneous Catalysis. Surfaces as Unique Activators and Ligands Tobin J. Marks, <i>Northwestern University</i>	262
Well-Defined Active-Site Environments on Silicate Supports Alexander Katz, <i>University of California, Berkeley</i>	263
Strategies for Enhancement of Catalytic Performance of Mo-based Catalysts in Methane Dehydroaromatization Sheima J. Khatib, <i>Texas Tech University</i>	264
Applications and advances in machine learned potentials John Kitchin, <i>Carnegie Mellon University</i>	270
Surface Chemistry and Reactions for Bimetallic Au Catalysis Bruce E. Koel, <i>Princeton University</i>	274
Inter- and Intramolecular “Inverse” Frustrated Lewis Pairs – Catalysis and Small Molecule Activation Clemens Krempner, <i>Texas Tech University</i>	278
Electrocatalytic H₂ Evolution by Metal Dithiolene Frameworks Smaranda C. Marinescu, <i>University of Southern California</i>	283

Atomic-scale Design of Metal and Alloy Catalysts: A Combined Theoretical and Experimental Approach Manos Mavrikakis, <i>University of Wisconsin – Madison</i>	284
Selective Conversion of Carbon Dioxide to Formaldehyde via a Bis(silyl)acetal: Carbon Dioxide as a C₁ Source for the Synthesis of Organic Molecules Gerard Parkin, <i>Columbia University</i>	292
Understanding Kinetics of Reconstructed Catalyst Surfaces to Build Reactivity Descriptors Felipe Polo-Garzon, <i>Oak Ridge National Laboratory</i>	296
Characterization of, and Hydrocarbon Functionalization with, Lattice-Confined Reactive Intermediates David C. Powers, <i>Texas A&M University</i>	298
Solvent Effects on Elementary Steps in Solid Acid Catalyzed Reactions: Acid-Base Interactions Robert M. Rioux, <i>The Pennsylvania State University</i>	301
Activation of Atomically-dispersed Oxometal Catalysts for Olefin Transformations Susannah L. Scott, <i>University of California, Santa Barbara</i>	305
Pathways for Methanol Synthesis from the Conversion of C-H bonds over Well-defined Metal-Oxide Surfaces Sanjaya D. Senanayake, <i>Brookhaven National Laboratory</i>	309
Design of Highly Durable Multimetallic Electrocatalysts Sara E. Skrabalak, <i>Indiana University</i>	310
Two-State Reactivity in Iron(I)-Catalyzed Alkene Isomerization Jeremy M. Smith, <i>Indiana University</i>	313
Copper-Catalyzed Oxidation of O–H and N–H Bonds Shannon S. Stahl, <i>University of Wisconsin-Madison</i>	314
Influence of Temperature and Ti substitution on Oxygen Electroadsorption and Electrocatalysis: A Progress on Theory-Experiment Convergence Jin Suntivich, <i>Cornell University</i>	321
Bridging Molecular and Heterogeneous Catalysis Through Graphite-Conjugated Yogesh Surendranath, <i>Massachusetts Institute of Technology</i>	325
Activation of Shale Gas on Singly Dispersed Catalytic Sites Anchored on Oxide Franklin (Feng) Tao, <i>University of Kansas</i>	329

Catalytic Transformations and Bond Activation Processes Promoted by Zr/Co Heterobimetallic Complexes	
Christine M. Thomas, <i>The Ohio State University</i>	337
Synthesis and Properties of Ruthenium–Cobalt Oxo Cubane Clusters Bearing a High-Valent, Terminal Ru^V–Oxo with Significant Oxo Radical Character	
T. Don Tilley, <i>Lawrence Berkeley National Laboratory</i>	341
Chemical and Electrocatalytic Oxidation of Ammonia	
Timothy H. Warren, <i>Georgetown University</i>	342
Alkane Activation and Oxidation on IrO₂(110)	
Jason F. Weaver, <i>University of Florida</i>	346
Size-Selected Metal Oxide Clusters as Model Inverse Catalysts	
Michael G. White, <i>Stony Brook University and Brookhaven National Laboratory</i>	350
Force/Activity Relationships in Transition Metal-Catalysis	
Ross A. Widenhoefer, <i>Duke University</i>	351
LIST OF PARTICIPANTS	355

ABSTRACTS

ORAL PRESENTATION ABSTRACTS

Functionalization Reactions Controlled by Non-Covalent Interactions

John F. Hartwig

Division of Chemical Sciences, Lawrence Berkeley National Laboratory Department of Chemistry, University of California, Berkeley

Presentation Abstract

This presentation will focus on the influence of non-covalent interactions on the reactivity and selectivity of catalysts for C-H bond functionalization and olefin hydrofunctionalization. We have discovered, developed and studied the mechanism of the hydroarylation of unactivated alkenes with unactivated arenes to form the products from anti-Markovnikov addition with regioselectivities exceeding 50:1. The catalyst for this reaction is a Ni(0) species ligated by an *N*-heterocyclic carbene containing very sterically demanding substituents on the *N*-aryl groups. A combination of experimental and computational studies show that the rate-determining step of the process is reductive elimination to form the aryl-alkyl C-C bond and that the rate of this reaction is enhanced by non-covalent electrostatic and London dispersion interactions, rather than steric repulsion. In addition, we have sought to achieve regioselective functionalizations of C-H bonds catalyzed by artificial metalloenzymes, and have shown that one can achieve regioselectivity reactions of C-H bonds that differ only by the presence of remote substituents. These data show that metalloenzymes for abiological processes can lead to selectivities that would be difficult to achieve with small-molecule systems.

FWP Number: DE-AC02-05CH11231 Harnessing Complexity for Catalytic Efficiency

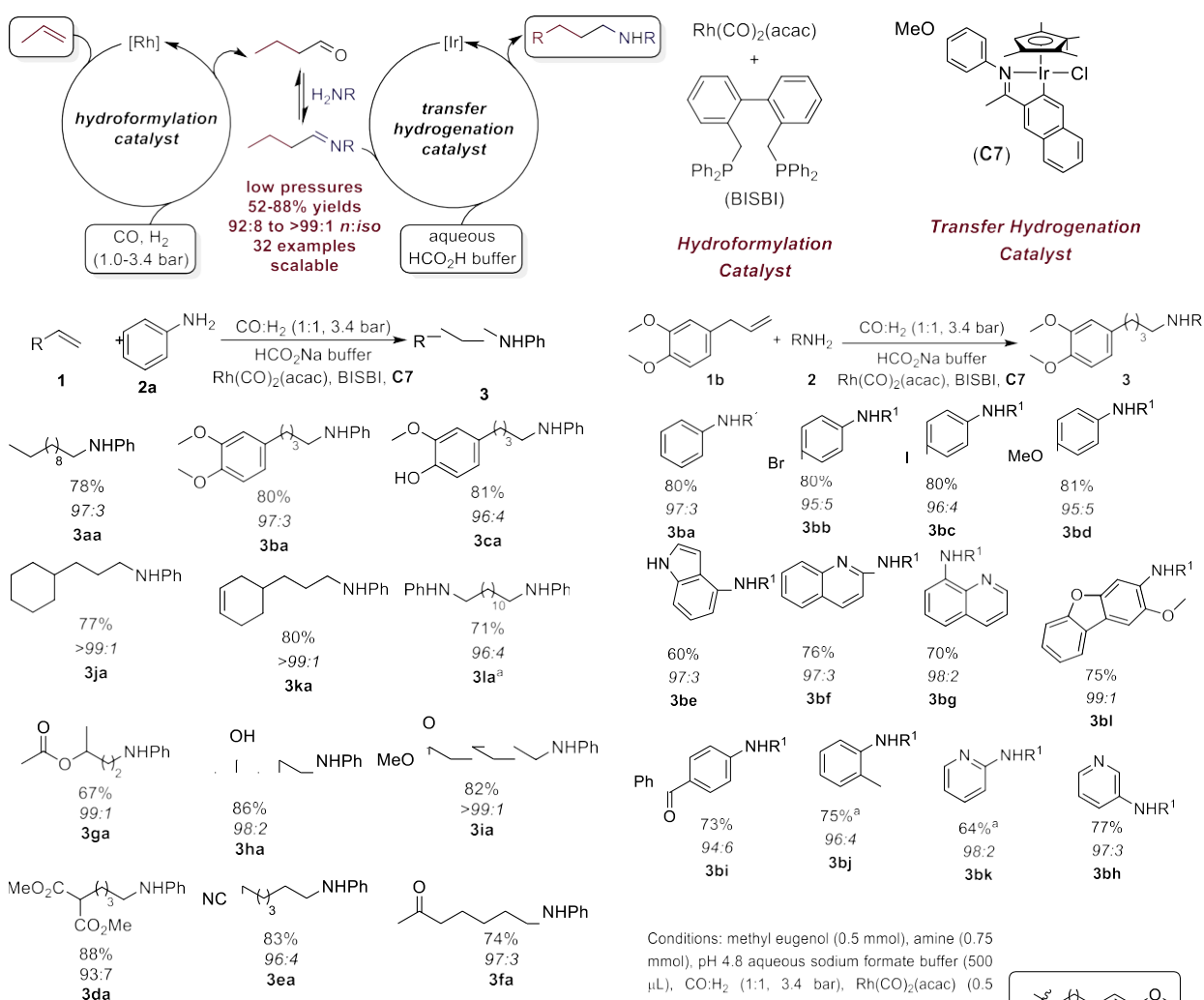
PI: John F. Hartwig

Postdocs: Yang Gu, Sean Natoli

Students: Zhennan Liu, Brandon Bloomer, Yumeng Xi, Noam Saper, Steven Hanna

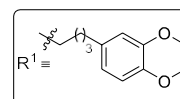
One research thrust in the LBNL Catalysis Program is the discovery of multicatalytic processes. We have focused on reactions that would involve mutually compatible catalysts whose orthogonal requirements of reaction conditions enable cooperative process to occur. In one case we focused on the hydroaminomethylation of alkenes in which aldehydes are formed by hydroformylation and reductive amination of the resulting aldehyde gives the amine. Typically, a different catalyst is the optimal one for these two steps; thus, we focused on developing conditions and catalysts that would enable highly active and regioselective catalysts for hydroformylation to operate with catalysts for mild reductive aminations. As a result of this strategy, we developed and reported on the hydroaminomethylation of diverse α -olefins with a wide range of alkyl, aryl, and

heteroarylamines at low temperatures (70-80 °C) and pressures (1.0-3.4 bar) of synthesis gas. The hydroformylation step was catalyzed by a rhodium diphosphine complex. The reductive amination step was conducted as a transfer hydrogenation with aqueous, buffered sodium formate as the reducing agent. This reaction was catalyzed by a cyclometallated iridium complex that is stable to the CO and hydrogen of hydroformylation. By adjusting the ratio of CO to H₂, we conducted the reaction at one atmosphere of gas in yields that were similar to those obtained with 3.4 bar of synthesis gas. A diverse array of olefins and amines, including heteroarylamines that do not react under more conventional conditions with a single catalyst, underwent hydroaminomethylation with this new system, and the pharmaceutical ibutilide was prepared in higher yield and under milder conditions than those reported with a single catalyst.

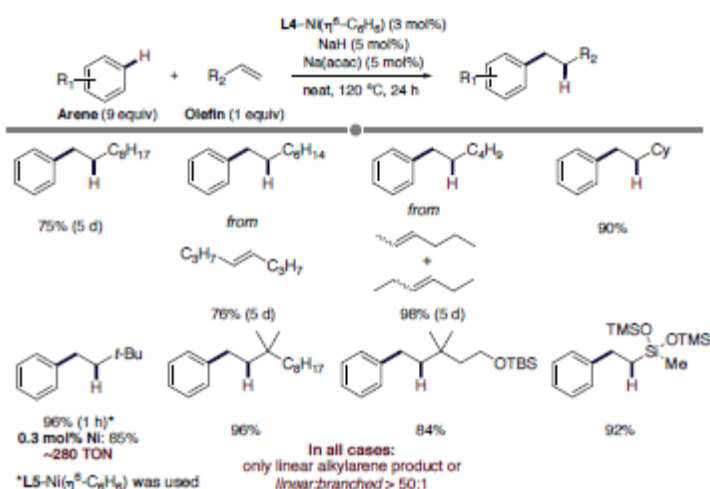


Conditions: olefin (0.5 mmol), aniline (0.75 mmol), pH 4.8 aqueous sodium formate buffer (500 μL), CO:H₂ (1:1, 3.4 bar), Rh(CO)₂(acac) (0.5 mol%), BISBI (2.5 mol%), Xiao's catalyst (1 mol%), 9:1 PhMe:MeOH (2.5 mL), 80 °C, 20 h. All yields reported are isolated yields. Regioselectivities were determined by GC analysis of the crude reaction mixture. ^a0.25 mmol olefin.

Conditions: methyl eugenol (0.5 mmol), amine (0.75 mmol), pH 4.8 aqueous sodium formate buffer (500 μL), CO:H₂ (1:1, 3.4 bar), Rh(CO)₂(acac) (0.5 mol%), BISBI (2.5 mol%), Xiao's catalyst (1 mol%), 9:1 PhMe:MeOH (2.5 mL), 80 °C, 20 h. All yields reported are isolated yields. Regioselectivities were determined by GC analysis of the crude reaction mixture. ^a1.25 mmol amine

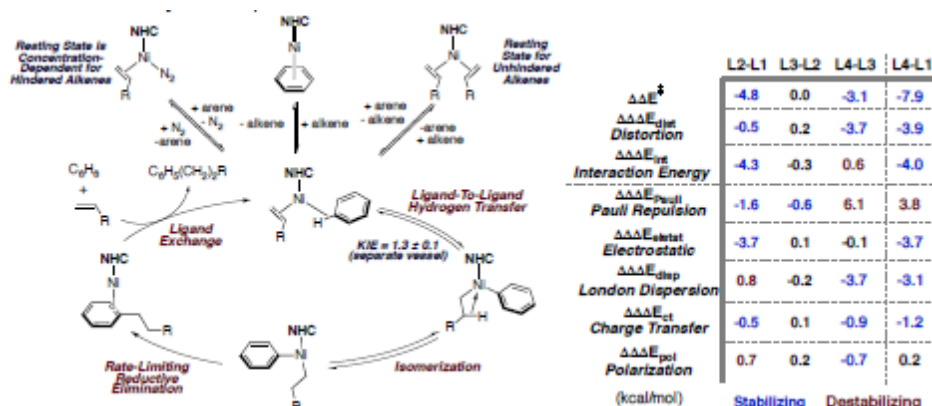


A second theme of the LBNL catalysis program is to exploit the second coordination sphere for controlling the activity and selectivity of catalytic systems. Anti-Markovnikov additions to alkenes have been a longstanding goal of catalysis, and anti-Markovnikov addition of arenes to alkenes would produce alkylarenes that are distinct from those formed by acid-catalyzed processes. Existing hydroarylations are either directed or occur with low reactivity and low regioselectivities for the linear alkylarene. We have developed a catalyst system for the first anti-Markovnikov hydroarylation of unactivated alkenes with unactivated arenes that occurs with high regioselectivity. This reaction also occurs in good yield in many cases with turnover numbers an order of magnitude higher than prior homogeneous catalysts. The reaction occurs with a Ni catalyst ligated by an outsized *N*-heterocyclic carbene ligand. Catalytically relevant arene- and alkene-bound Ni complexes have been characterized, and the rate-limiting step was shown to be reductive elimination to form the C-C bond.

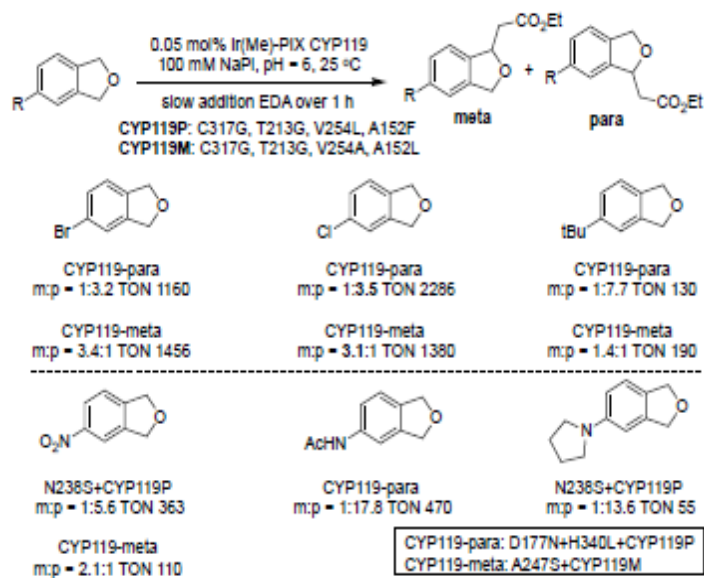


To begin to reveal the origin of the higher rates of hydroarylation with **L1** as ligand versus those of a smaller NHC ligands, such as IPr, we computed the barrier to reductive elimination with both ligands (Figure 4a). Consistent with our experimental results, the computed barrier for reductive elimination by the complex bound by **L1** was almost 4 kcal/mol lower in energy than the barrier for the complex bound by IPr. One might envision this difference in barriers

to result from a steric effect on the rate of reductive elimination. However, computation of the geometry and non-covalent interactions provided a much different origin of high activity of the complexes of **L1**. Most striking, the geometrical parameters around the Ni center in the transition state for reductive elimination from the complex of **L1** were identical to those of the analog containing IPr, suggesting that an effect beyond simple steric effects within the transition state controls the rate.



To reveal the alternative effects on the barrier for reductive elimination from the complexes containing IPr and **L1**, we used the ligand-substrate interaction model pioneered by Houk and the second-generation absolutely-localized molecular orbital energy decomposition analysis (ALMO-EDA) developed by Head-Gordon (Figure 4b). Both the distortion energies and interaction energies of the reductive elimination transition state (relative to the ground state) were more favorable with **L1** than they were with other NHC ligands. Instead of accelerating the reductive elimination by steric repulsion, the larger steric profile of **L1** versus other NHC ligands such as IPr actually increased the energy of the transition state for reductive elimination. Analysis of the pairwise contributions between different ligands indicated that the multiple aryl groups in ligand **L1** of the most active catalyst lead to favorable electrostatic interactions, and the large number of methyl groups in **L1** leads to favorable London dispersion interactions and lower distortion energy. Together these attractive electrostatic and dispersion interactions of the large ligand, rather than steric effects (Pauli repulsions), lead to the higher rates of reaction with the large ligands.



We have also sought to use non-covalent interactions in the form of a protein host to influence the regioselectivity of reactions. We developed a series of site-selective functionalizations of C–H bonds, differentiated solely by remote substituents, catalyzed by artificial metalloenzymes (ArM's). These artificial metalloenzymes were generated from the combination of P450 scaffold and an iridium-porphyrin cofactor. The scaffold was evolved to generate catalysts for the insertion of carbenes into the C–H bonds of a range of phthalan derivatives containing substituents that render the two methylene positions in each phthalan inequivalent. These reactions occur with site-selectivities up to 17.8:1. In most cases, we identified pairs of enzyme mutants that preferentially form each of the two constitutional isomers. This study demonstrates the potential of artificial metalloenzymes to catalyze C–H bond functionalization with site-selectivity that is difficult to achieve with small-molecule catalysts.

Publications Acknowledging this Grant in 2015-2018

1. Wang, J. Y.; Strom, A. E.; Hartwig, J. F., Mechanistic Studies of Palladium-Catalyzed Aminocarbonylation of Aryl Chlorides with Carbon Monoxide and Ammonia. *J. Am. Chem. Soc.* **2018**, *140* (25), 7979-7993.
2. Xi, Y. M.; Hartwig, J. F., Mechanistic Studies of Copper-Catalyzed Asymmetric Hydroboration of Alkenes. *J. Am. Chem. Soc.* **2017**, *139* (36), 12758-12772.
3. Troshin, K.; Hartwig, J. F., Snap deconvolution: An informatics approach to high-throughput discovery of catalytic reactions. *Science* **2017**, *357* (6347), 175-180.
4. Saper, N. I.; Hartwig, J. F., Mechanistic Investigations of the Hydrogenolysis of Diaryl Ethers Catalyzed by Nickel Complexes of N-Heterocyclic Carbene Ligands. *J. Am. Chem. Soc.* **2017**, *139* (48), 17667-17676.
5. Hartwig, J. F., Catalyst-Controlled Site-Selective Bond Activation. *Acc. Chem. Res.* **2017**, *50* (3), 549-555.
6. Dydio, P.; Key, H. M.; Hayashi, H.; Clark, D. S.; Hartwig, J. F., Chemoselective, Enzymatic C-H Bond Amination Catalyzed by a Cytochrome P450 Containing an Ir(Me)-PIX Cofactor. *J. Am. Chem. Soc.* **2017**, *139* (5), 1750-1753.
7. Zhang, J.; Shrestha, R.; Hartwig, J. F.; Zhao, P. J., A decarboxylative approach for regioselective hydroarylation of alkynes. *Nat. Chem.* **2016**, *8* (12), 1144-1151.
8. Xi, Y. M.; Hartwig, J. F., Diverse Asymmetric Hydrofunctionalization of Aliphatic Internal Alkenes through Catalytic Regioselective Hydroboration. *J. Am. Chem. Soc.* **2016**, *138* (21), 6703-6706.
9. Xi, Y. M.; Butcher, T. W.; Zhang, J.; Hartwig, J. F., Regioselective, Asymmetric Formal Hydroamination of Unactivated Internal Alkenes. *Angew. Chem. Int. Ed.* **2016**, *55* (2), 776-780.
10. Lee, S. Y.; Hartwig, J. F., Palladium-Catalyzed, Site-Selective Direct Allylation of Aryl C-H Bonds by Silver-Mediated C-H Activation: A Synthetic and Mechanistic Investigation. *J. Am. Chem. Soc.* **2016**, *138* (46), 15278-15284.
11. Key, H. M.; Dydio, P.; Clark, D. S.; Hartwig, J. F. Abiological catalysis by artificial haem proteins containing noble metals in place of iron. *Nature* **2016**, *534* (7608), 534-537.
12. Jiang, X. Y.; Chen, W. Y.; Hartwig, J. F., Iridium-Catalyzed Diastereoselective and Enantioselective Allylic Substitutions with Acyclic α -Alkoxy Ketones. *Angew. Chem. Int. Ed.* **2016**, *55* (19), 5819-5823.
13. Gao, F.; Webb, J. D.; Hartwig, J. F., Chemo- and Regioselective Hydrogenolysis of Diaryl Ether C- O Bonds by a Robust Heterogeneous Ni/C Catalyst: Applications to the Cleavage of Complex Lignin-Related Fragments. *Angew. Chem. Int. Ed.* **2016**, *55* (4), 1474-1478.
14. Dydio, P.; Key, H. M.; Nazarenko, A.; Rha, J. Y. E.; Seyedkazemi, V.; Clark, D. S.; Hartwig, J. F., An artificial metalloenzyme with the kinetics of native enzymes. *Science* **2016**, *354* (6308), 102-106.

15. Schramm, Y.; Takeuchi, M.; Semba, K.; Nakao, Y.; Hartwig, J. F., Anti-Markovnikov Hydroheteroarylation of Unactivated Alkenes with Indoles, Pyrroles, Benzofurans, and Furans Catalyzed by a Nickel-N-Heterocyclic Carbene System. *J. Am. Chem. Soc.* **2015**, *137* (38), 12215- 12218.
16. Key, H. M.; Clark, D. S.; Hartwig, J. F., Generation, Characterization, and Tunable Reactivity of Organometallic Fragments Bound to a Protein Ligand. *J. Am. Chem. Soc.* **2015**, *137* (25), 8261- 8268.

Boron-containing Materials as Selective Catalysts for the Oxidative Dehydrogenation of Alkanes

Ive Hermans

Department of Chemistry & Department of Chemical and Biological Engineering University of Wisconsin-Madison, 1101 University Ave, Madison, WI 53706

Presentation Abstract

The oxidative dehydrogenation of propane (ODHP) has been broadly studied as an and energy-efficient alternative to naphtha cracking and dehydrogenation for propylene production. However, decades of research establishing supported vanadium oxide as the state-of-the-art catalyst for ODHP still does not achieve commercially attractive selectivity to the olefin due to the facile over-oxidation of propylene to CO and CO₂ (CO_x). In this presentation, I will expound upon our discovery of boron and boron containing materials (like BN, B₄C, NiB, amongst others) as highly selective catalysts for the ODHP reaction. FTIR, Raman, XPS, XAS and MAS NMR spectroscopic studies indicate that all tested boron-containing materials commonly share a partially oxidized surface—formed *in situ*. We have since proposed that this surface layer likely contains the active site denoted BO_xH_y and utilize a suite of solid-state NMR experiments to further resolve the near surface chemical environment of these catalysts. We believe that the surface layer is likely influenced by the properties of the bulk material, opening new possibilities for future catalyst development. Our recent kinetic experiments align with our hypothesis that boron-catalyzed ODHP reaction mechanism likely proceeds via a surface-initiated reaction and continues via gas phase radical oxidation chemistry. Additionally, we employ TPD and H₂O cofeeding experiments to investigate the properties of the active site, as well as determine structural and reaction parameter descriptors that influence the reaction network and overall catalyst performance.

DE-SC0017918: Controlled Activation of Molecular Oxygen on Boron Nitride Materials for Selective Oxidation Catalysis

Postdoc(s): Somphonh Peter Phivilay

Student(s): Juan M. Venegas^a, Theodore Agbi^a, Will McDermott

Affiliations(s): ^a Department of Biological and Chemical Engineering, University of Wisconsin-Madison, 1415 Engineering Dr., Madison, Wisconsin 53706, United States

RECENT PROGRESS

We have shown that boron and boron containing materials are catalytically active and highly selective for the oxidative dehydrogenation of light alkanes to olefins. We have since studied the activation of oxygen and alkane on boron-containing catalysts (e.g. h-BN) to determine a fundamental reaction mechanism, the properties of the boron active site, and methods to enhance catalytic performance.

Evidencing a surface-gas reaction network in boron catalyzed ODHP

We have analytically shown that our reactor design is free of heat and mass transport limitations and pass a suite of criterion for these limitations. However complementary experimental checks illustrated unpredictable behavior upon changing the catalyst mass. Attempting to address this behavior with SiC diluent, which is ODHP inactive, showed that increasing the concentration of SiC in the catalyst bed (i.e. increasing the bed volume) at a given h-BN mass resulted in a non-linear increase in the rate of propane consumption, figure 1a, with no observable change in the conversion-selectivity trend. We conclude that SiC does not react with reaction intermediates via layered bed experiment, wherein the h-BN bad is segregated atop a SiC bed, that did not exhibit the same rate enhancement. We show, rather, that increased residence time in the homogeneously mixed (e.g. SiC and h-BN) catalyst bed was a more accurate descriptor for the observed increase in h-BN's reactivity, shown figure 1b. Given that the contact time remained constant (e.g. a constant h-BN mass) across these experiments, these studies suggest an ODH mechanism which proceeds via a surface-initiated reaction and continues into the gas phase.

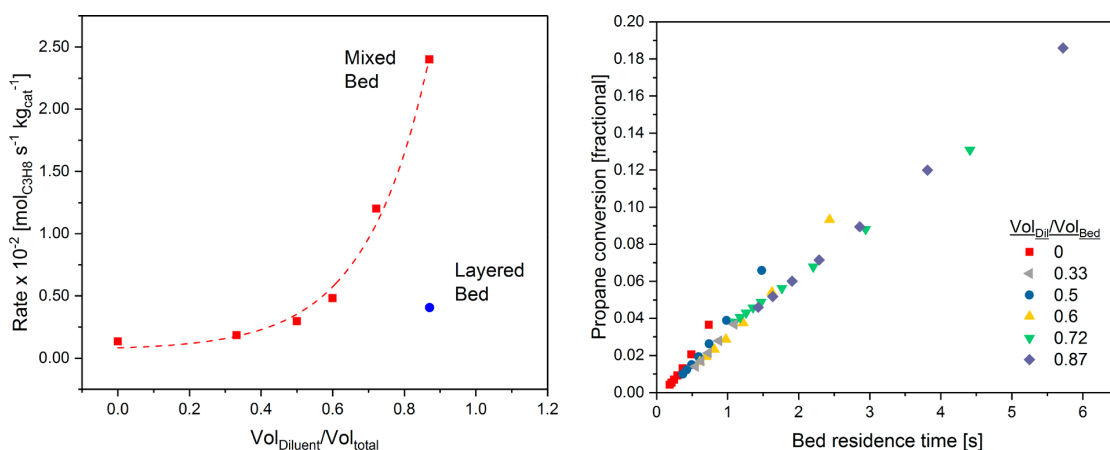


Figure 1. (a) Propane consumption rate calculated on a catalyst mass basis as a function of SiC dilution. Red symbols indicate a homogeneously mixed h-BN and SiC catalyst bed. Blue symbol indicates a layered bed configured with h-BN layered over a bed of SiC. (b) Propane conversion as a function of total residence time in the catalyst bed at various SiC dilutions. Both (a) and (b) are from the same data set where the mass of h-

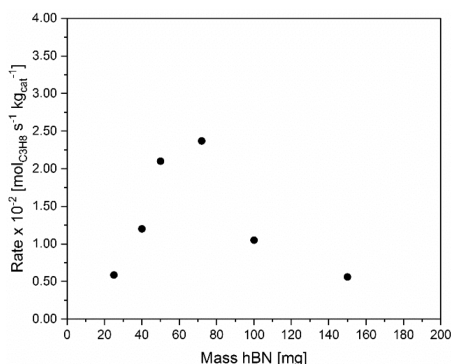


Figure 2. Reaction rate as a function of h-BN mass. A total catalyst bed height of 1.8 cm and bed volume of 0.9 cm³ were maintained via SiC diluent.

We further observe that increasing the concentration of h-BN in fixed catalyst bed volume (i.e. fixed residence time) results in a volcano like trend in the rate of propane consumption, figure 2. We hypothesize that the activated boron surface both initiates gas phase radicals that further react via gas phase radical oxidation chemistry or are terminated on the boron surface.

Probing the transformation of the boron surface during ODH

(DNP-)SSNMR and SEM experiments reveal significant oligomerization of surface boron species, and a particle size increase (i.e. surface area decrease) post ODH catalytic testing of both spent h-BN and boron nitride nanotubes (BNNT). Quantitative ^{11}B and ^1H solid-state SS-NMR resonance experiments of these materials support structural assignments and differentiation of boron coordination environments that suggest a large degree of oxidized/hydrolyzed boron species throughout the surface. Herein, along with complimentary X-ray absorption spectroscopy, we further resolve this amorphous network of three-coordinate boron surface sites comprised of hydroxyl and bridging oxygen groups denoted $\text{B}(\text{OH})_x\text{O}_{3-x}$ (where $x = 0-3$). We suspect that hydroxyl groups present under ODH conditions may be an indicator of the active site.

TPD chemisorption experiments on our synthesized BO_x/SiO_2 materials were used to examine the properties of the active site. A mixture of vaporized isopropanol, a probe molecule for our propane substrate, and inert gas was used as the adsorption gas feed. We observed a broad desorption peak for BO_x/SiO_2 suggesting a distribution of boron sites (as expected) that were less active than a reference VO_x/SiO_2 ODH catalysts studied under the same conditions. Propylene was the main product of both catalysts as confirmed by MS. However, addition of O_2 to the desorption gas feed resulted in a narrower desorption peak for BO_x/SiO_2 that appeared more active and produced acetone as the main product—a result not observed in VO_x/SiO_2 under the same oxidative conditions. This may indicate that under these oxidative conditions BO_x/SiO_2 exhibits a low variety of site strengths which preferentially abstract hydrogen from the alcohol. We propose a mechanism for the surface mediated chemistry present, wherein the active boron site likely abstracts a hydrogen from the alkane to produce gas phase alkyl radicals.

Investigating gas phase-radical chemistry

We investigated the influence of the reactants' partial pressures on the observed product distribution and product formation rates. The relative bond dissociation energy for secondary vs. primary C-H bond breakage suggests that the active site would initiate a more isopropyl than *n*-propyl gas phase radicals from adsorbed propane. Both propyl radicals would readily react with O_2 to produce propylene and a peroxy radical. However, while the isopropyl radical may readily undergo thermal C-H bond breaking to produce propylene and a hydrogen radical, the *n*-propyl radical would more readily undergo thermal C-C cracking to produce ethylene and a methyl radical given the β -scission rule. We therefore expect the relative rate of isopropyl to *n*-propyl formation and the fate of *n*-propyl radical to be reasonable descriptors for the propylene selectivity. To examine this, we observed the ratio for the rate of formation of C-H bond breaking products (e.g.

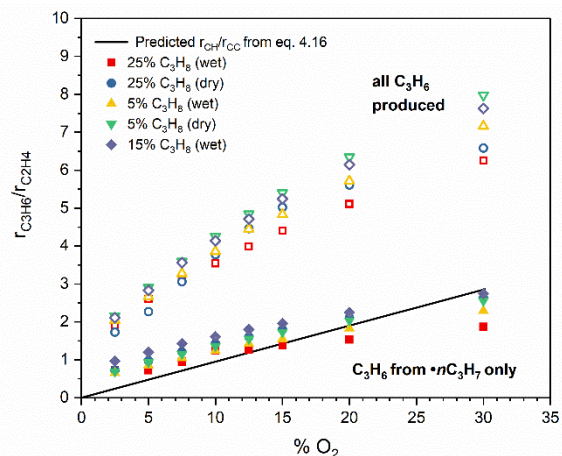


Figure 3. Comparison of experimental rates of propylene and ethylene formation as a function of O_2 concentration. Solid line is the calculated ratio between C-H and C-C bond breaking. Ratio of overall $r_{\text{C}_3\text{H}_6}/r_{\text{C}_2\text{H}_4}$ (open symbols) and $r_{\text{C}_3\text{H}_6}/r_{\text{C}_2\text{H}_4}$ accounting for only the C_3H_6 estimated to originate from *n*-propyl radicals (filled symbols) based on relative reaction rate constants.

propylene) and C-C cracking products (e.g. ethylene). Experimentally, we found a linear increase in this ratio with increasing O₂ partial pressure, figure 3. When we adjust this data to account solely for products formed via a *n*-propyl intermediate relatively good agreement with our theoretical ratio, devised from reported kinetic parameters solely for the two aforementioned *n*-propyl reaction pathways. Figure 3, illustrated this trend independent of alkane concentration and the presence of cofed H₂O, at varying O₂ partial pressures.

We also found that cofeeding 10% molar concentration of steam into the reaction mixture greatly enhances the reaction rate under both propane rich and lean conditions with no significant impact on the selectivity-conversion trend, figure 4. There was no observable impact on the rate dependence of O₂, suggesting that water did not impact the activation of O₂ on the oxidized boron surface. Water cannot maintain the ODH reaction in the absence of O₂, suggesting that water does not directly carry out the H abstraction from propane. There was no significant impact on the apparent activation energy of propane, oxygen conversion, or the formation of products which further suggests that water likely influences the concentration of the reactive intermediates. Therefore, we hypothesize that the presence of water likely increases the radical pool concentration resulting in an enhanced rate of propane activation via a gas phase mediated process.

Spectroscopic characterization (FTIR, and Raman) of the spent h-BN showed an increased degree of oxidation and hydrolysis on the surface of the catalyst, while the bulk remained as h-BN. We hypothesize that water may also restructure the surface to expose H abstracting sites that can further activate both propane and water. However, we expect this surface effect to occur on long time scales given that we observe consistent wet or dry steady state reactivities upon cycling the H₂O feed into the reaction over approximately 4 days' time on stream.

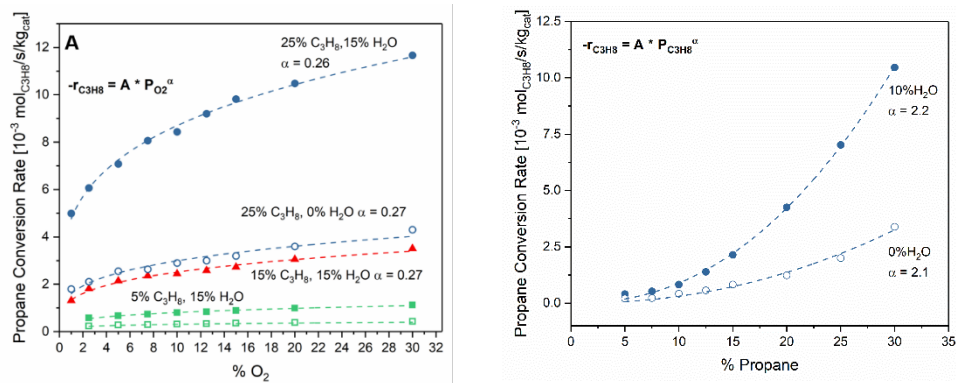


Figure 4. Propane consumption rate as a function of the partial pressure of (a) O₂ and (b) propane under various wet (closed symbols) and dry (open symbols)

To our knowledge this is the first experimental explanation of h-BN's performance. Concurrently, we have shown a similar higher selectivity to cracking products with decreasing O₂ partial pressure for *n*-butane ODH over h-BN. The catalytic tests show that the product distribution can be shifted between oxidative cracking products and oxidative dehydrogenation products by increasing the O₂ partial pressure. We propose that oxidative cracking of C₄ and C₃ alkanes over h-BN likely proceeds mechanistically similarly to other catalysts, like Li/MgO, which are attributed to homogeneous gas-phase chemistry, albeit with decreased CO_x (especially CO₂) production. These studies suggest that increasing the partial pressure of O₂ and catalytic surfaces that favor isopropyl radicals may enhance the catalytic performance of these boron-materials.

Publications Acknowledging this Grant in 2015-2018

(I) Exclusively funded by this grant;

1. Venegas, J. M., McDermott, W. P. & Hermans, I. Serendipity in Catalysis Research: Boron-Based Materials for Alkane Oxidative Dehydrogenation. *Acc. Chem. Res.* **51**, 2556–2564 (2018).
2. Venegas, J. M. & Hermans, I. The Influence of Reactor Parameters on the Boron Nitride-Catalyzed Oxidative Dehydrogenation of Propane. *Org. Process Res. Dev.* **22**, 1644–1652 (2018)
3. McDermott, W. P., Venegas, J and Hermans, I. Selective Oxidative Cracking of *n*-Butane to Light Olefins over Hexagonal Boron Nitride with Limited Formation of CO_x submitted

(II) Jointly funded by this grant and other grants with leading intellectual contribution from this grant;

4. Love, A. M. *et al.* Probing the Transformation of Boron Nitride Catalysts under Oxidative Dehydrogenation Conditions. *J. Am. Chem. Soc.* **141**, 182–190 (2019).

(III) Jointly funded by this grant and other grants with relatively minor intellectual contribution from this grant;

Mechanistic Understanding of Methane Activation Catalysts from First Principles

Zhijun Zuo,¹ Shizhong Liu,² Sanjaya D. Senanayake,³ Jose A. Rodriguez³ and Ping Liu³

1. *Key Laboratory of Coal Science and Technology of Ministry of Education and Shanxi Province, Taiyuan University of Technology, Taiyuan 030024, Shanxi, China*
2. *Chemistry Department, State University of New York (SUNY) at Stony Brook, Stony Brook, NY 11794, USA*
3. *Chemistry Department, Brookhaven National Laboratory, Upton, NY 11973, USA*

Presentation Abstract

Methane is the main component of natural gas and a greenhouse gas. It is one of the most important research areas to convert methane into value-added chemical. However, due to the high stability of the molecule the catalysts often suffer low conversion and/or selectivity. Here, we take dry reforming of methane (DRM, $\text{CO}_2 + \text{CH}_4 \rightarrow 2\text{CO} + 2\text{H}_2$) over single site catalysts, which have drawn considerable attentions due to their superior behaviors in catalysis, as a case study, specifically over $\text{Ni}_n/\text{Mg}(100)$. Conventional Ni catalysts for the DRM deactivate quickly due to sintering of the active metal phase and carbon deposition. Possible solutions include the formation of small Ni particles supported on MgO. However, due to the complexity of the reaction, the origin of promoting effects remains elusive. The combined theoretical modeling (Density Functional Theory and kinetic Monte Carlo simulation) and experimental studies show that the formation of single Ni atom helps in improving the binding property of MgO; yet it is not enough to dissociate CO_2 and CH_4 . This can be achieved by the formation of the single site $\text{Ni}_4/\text{MgO}(100)$ catalyst, enabling the formations of CO, H_2 and H_2O under the DRM conditions. During this process, coking, as observed for bulk-like Ni particles, is eliminated. By confining the reaction to occur at the isolated Ni ensemble the single site $\text{Ni}_4/\text{MgO}(100)$ catalyst is able to balance the CO_2 and CH_4 activations, which is identified as the key for tuning the DRM activity and selectivity of Ni/MgO catalysts. Our study highlights the independent roles of confined sites in tuning the performance of single site catalysts during complex catalytic processes.

FWP-BNL-CO040: Catalysis for Advanced Fuel Synthesis and Energy

Charles T. Campbell

**The Chemical Potential of Metal Atoms in Supported Nanoparticles:
a Key Descriptor for Catalyst Performance**

Charles T. Campbell
University of Washington, Seattle, WA 98195-1700

Presentation Abstract

Metal nanoparticles anchored to support surfaces form the basis for many industrial catalysts and promise to play an ever-increasing role in future energy and environmental technologies. The “chemical potential” of a species i in a mixture of species is a quantitative way to describe the thermodynamic stability of that species. It quantifies the potential for that species to do chemistry. The chemical potential of metal atoms in supported metal nanoparticle catalysts is a measure of the stability of the metal atoms, closely related to the strength of bonding between the metal atoms on the exposed surfaces of the nanoparticles and the rest of the catalyst material. It is shown here that this chemical potential of the metal atoms in these particles is an important descriptor which helps explain a great deal regarding the performance of such catalysts, especially with respect to their strength of binding to adsorbed reaction intermediates and their resistance to deactivation by sintering (or lack thereof). A predictive equation for metal chemical potential versus effective particle radius in supported metal nanoparticles will be presented. All of the parameters in the equation are well known for late transition metals *except* the adhesion energy of the metal to the support. Recent results that provide some predictive ability for this adhesion energy will also be presented. This opens new avenues for catalysts design, and provides new understanding of catalyst structure / performance relations. If time permits, some recent success in analyzing microkinetic models using the degree of rate control and for understanding the effects of solvents on adsorption energies (relative to gas phase) will also be summarized.

Grant #DE-FG02-96ER14630: Supported Metal Nanoparticles: Correlating Structure with Catalytic Function through Energetics

Student(s): Zhongtian Mao, John R. Rumptz and Wei Zhang

RECENT PROGRESS

Overview

Nanoparticles of late transition metals are used as catalysts and electrocatalysts for industrial chemical reactions that produce fuels and clean up pollution associated with the generation and use of fuels. This experimental research program aims to provide the basic understanding needed to develop new and improved catalysts for these important reactions involving nanoparticles of late transition metals supported on oxides and carbon. Specifically, we study well-defined model catalysts consisting of metal nanoparticles supported on single-crystalline oxide, mixed-oxide and carbon surfaces, structurally characterized using a variety of ultrahigh vacuum surface science techniques. We use calorimetry techniques invented here and available nowhere else in the world

to measure the energies of the metal atoms in these particles, the metal/support adhesion energies (E_{adh}) and the energies of adsorbed intermediates on these particles.

Measuring and predicting metal chemical potential versus particle size and support

We continued our calorimetric studies of the adsorption energies of metal atoms as they grow nanoparticles on oxide supports, which provides the metal atom chemical potential (\square_m) versus particle size.

We proved that for large hemispherical metal particles of the same diameter, D , \square_m differs between two supports by $-2(E_{adh,A} - E_{adh,B})V_m / D$, where $E_{adh,i}$ is the adhesion energy between the metal and support i , and V_m is the molar volume of the bulk metal. This is consistent with calorimetric measurements of metal vapor adsorption energies onto clean oxide surfaces where the metal grows as 3D particles, which proved that \square_m increases with decreasing particle size below 6 nm, and, for a given size, decreases with E_{adh} .

We also showed that catalytic activity and sintering rates correlate with metal chemical potential. Therefore, it is crucial to understand what properties of catalyst materials control metal/oxide adhesion energies. Trends in how E_{adh} varies with the metal and the support oxide were discovered.

By comparing to our calorimetric measurements of metal adsorption energies, from which we extracted the metal atom chemical potential on oxide-supported metal nanoparticles as a function of particle size for different metal / oxide combinations, we more recently found that this chemical potential for late transition metals is well approximated for a particle of effective diameter D (even down to tiny size) by:

$$\square_m(D) = [(3\square_m - E_{adh})(1 + D_o/D)](2V_m / D),$$

where \square_m is the surface energy of the bulk metal, E_{adh} is the adhesion energy at the bulk metal / oxide interface, and D_o is ~ 1.5 nm, and V_m is the molar volume of the bulk metal.

Our discovery that E_{adh} for different metals on a given oxide increases linearly with increasing heat of formation of the most stable oxide of the metal from metal gas atoms plus $O_2(\text{gas})$ per mole of metal atoms allowed us to predict that E_{adh} on any oxides should be much larger for Ni particles than for any other metal particles we had studied so far. We measured E_{adh} for Ni on MgO(100) and confirmed those predictions. For Ni on CeO₂(111), we found that E_{adh} is significantly smaller than predicted, which we attribute to interfacial Ni²⁺.

New Methods for Analyzing MicroKinetic Models of Catalytic Reactions

The “degree of rate control” (DRC) is a mathematical approach invented by the PI for analysing multi-step reaction mechanisms that has proven very useful in catalysis research. It identifies the “rate-controlling transition states and intermediates” (i.e., those whose DRCs are large in magnitude). Since the energies of these key adsorbed intermediates and transition states can be adjusted by modifying the catalyst or solvent, or even a reactant’s molecular structure, DRC values provide important ideas for understanding structure / activity relationships and catalyst improvement. We published an invited review on DRC analysis. We discovered ways to use DRC analysis to more easily interpret and predict kinetic isotope effects and apparent activation energies for multistep reactions. We are currently two writing papers about these discoveries.

Connecting Gas-Phase Catalytic Reactions Energetics to those in Aqueous Phase

In collaboration with Jonannes Lercher’s team at PNNL, we studied both electrocatalytic hydrogenation (ECH) and thermal catalytic hydrogenation (TCH) of phenol by carbon-supported

Pt, Rh and Pd particles. We characterized the mechanism and surface intermediates in the TCH and ECH reaction using kinetics and in situ spectroscopies. We showed that both reactions have the same rate-determining step whereby an H adatom adds to adsorbed phenol, and that phenol and H compete for sites. The dependence of the TCH rate on the concentration of the organics and H₂ were fitted to a Langmuir-Hinshelwood model. The equilibrium constants for the adsorption of the organics (e.g., phenol) that gave the best fits to the rate data agreed closely with the values that we independently measured by quantifying the fraction of sites for H adsorption (measured by cyclic voltammetry) blocked by the organic's surface coverage.

For phenol adsorption on Pt(111), we have been able to compare the low-coverage heat of adsorption measured in aqueous solution (21 kJ/mol) with the value we measured in ultrahigh vacuum by calorimetry (200 kJ/mol, under funding from my NSF grant), and found a huge difference (179 kJ/mol). We were able to show that this difference is largely due to the heat of solvation of phenol gas (~50 kJ/mol) and the energy costs to break up the bond between liquid water and Pt(111) (i.e., the water / Pt(111) adhesion energy, E_{adh}) and to de-solvate the face of phenol that binds to Pt.

In comparing gas-phase adsorption energies with those in liquid solvents, we found it useful to know the solvent/metal adhesion energies. By using an analysis method we had developed earlier under this DOE grant to extract E_{adh} at metal/solid interfaces from the calorimetric heat of adsorption of metal vapor versus coverage (up to bulk-like multilayer film thickness), we could also extract E_{adh} at the following solvent / metal interfaces from earlier calorimetric data we had published for Pt(111) and Ni(111) surfaces: water, methanol, HCOOH, benzene and phenol. We are writing a paper about these results, which are crucial for understanding solvent effects in catalysis.

Publications Acknowledging this Grant in 2016-2019

A. Publications Resulting from this DOE Grant Support alone.

0. Adsorption and Adhesion of Au on Reduced CeO₂(111) Surfaces at 300 K and 100 K, S. L. Hemmingson, T. E. James, G. M. Feeley, A. M. Tilson and C. T. Campbell, *J. Physical Chemistry C* **2016**, 120, 12113–12124.
1. Calorimetric Measurement of Adsorption and Adhesion Energies of Cu on Pt(111), T. E. James, S. L. Hemmingson, J. R.V. Sellers and C. T. Campbell, *Surface Science* **2017**, 657, 58–62 (Selected as *Editor's Choice*).
2. Trends in Adhesion Energies of Metal Nanoparticles on Oxide Surfaces: Understanding Support Effects in Catalysis and Nanotechnology, S. L. Hemmingson and C. T. Campbell, *ACS Nano* **2017**, 11, 1196-1203.
3. Correction to: "Trends in Adhesion Energies of Metal Nanoparticles on Oxide Surfaces: Understanding Support Effects in Catalysis and Nanotechnology", S. L. Hemmingson and C. T. Campbell, *ACS Nano* 11, 1196-1203 (2017), *ACS Nano* 11, **2017**, 4373.
4. Energetics of 2D and 3D Gold Nanoparticles on MgO(100): Influence of Particle Size and Defects on Gold Adsorption and Adhesion Energies, S. L. Hemmingson, G. M. Feeley, N. J. Miyake and C. T. Campbell, *ACS Catalysis* **2017**, 7, 2151-2163.
5. The Degree of Rate Control: A Powerful Tool for Catalysis Research, C. T. Campbell, *ACS Catalysis (Invited Viewpoint)* **2017**, 7, 2770-2779.
6. The Chemical Potential of Metal Atoms in Supported Nanoparticles: Dependence upon Particle Size and Support, Charles T. Campbell and Zhongtian Mao, *ACS Catalysis* **2017**, 7,

- 8460-8466.
7. Correction to “The Chemical Potential of Metal Atoms in Supported Nanoparticles: Dependence upon Particle Size and Support”, Charles T. Campbell and Zhongtian Mao, *ACS Catalysis* 2017, 7, 8460-8466. Charles T. Campbell and Zhongtian Mao, *ACS Catalysis* **2018**, 8, 8763–8764.
 8. Energetics of Au adsorption and film growth on Pt(111) by single-crystal adsorption calorimetry, Gabriel M. Feeley, Stephanie L. Hemmingson and Charles T. Campbell, *Journal of Physical Chemistry C* **2019**, 123, 5557-5561.

B. Publications jointly funded by this DOE grant and other grants of the PI and/or his co-authors, with a leading intellectual contribution from this grant.

9. The physical chemistry and materials science behind sinter-resistant catalysts, Yunqian Dai, Ping Lu, Charles T. Campbell and Younan Xia, *Chemical Society Reviews* **2018**, 47, 4314-4331.
10. Impact of pH on Aqueous-Phase Phenol Hydrogenation Catalyzed by Carbon-Supported Pt and Rh, Nirala Singh, Mal-Soon Lee, Sneha A. Akhade, Guanhua Cheng, Donald M. Camaioni, Oliver Y. Gutiérrez, Vassiliki-Alexandra Glezakou, Roger Rousseau, Johannes A. Lercher and Charles T. Campbell, *ACS Catalysis* **2019**, 9, 1120-1128.
11. Heats of Adsorption of N₂, CO, Ar and CH₄ versus Coverage on the Zr-Based MOF NU-1000: Measurements and DFT Calculations, Graeme Vissers, Wei Zhang, Oscar E. Vilches, Wei-Guang Liu, Haoyu S. Yu, Donald G. Truhlar and Charles T. Campbell, *Journal of Physical Chemistry C* **2019**, 123, 6586–6591.
12. Quantifying adsorption of organic molecules on platinum in aqueous phase by hydrogen site blocking and in situ X-ray absorption spectroscopy, Nirala Singh, Udishnu Sanyal, John L. Fulton, Oliver Y. Gutiérrez, Johannes A. Lercher and Charles T. Campbell, *ACS Catalysis* (**submitted**).
13. A Simple Bond-Additivity Model Explains Large Decreases in Heats of Adsorption in Solvents Versus Gas Phase: A Case Study with Phenol on Pt(111) in Water, Nirala Singh and Charles T. Campbell, *ACS Catalysis* (**submitted**).

C. Publication jointly funded by this DOE grant and other grants of the PI and/or his co-authors, where a leading intellectual contribution is not from this grant.

14. Towards Benchmarking in Catalysis Science: Best Practices, Opportunities, and Challenges, T. Bligaard, R. M. Bullock, C. T. Campbell, J. G. Chen, B. C. Gates, R. J. Gorte, C. W. Jones, W. D. Jones, J. R. Kitchin, S. L. Scott, *ACS Catalysis* (Perspective), **2016**, 6, 2590–2602. (featured as *ACS Editor’s Choice*).
15. Electrocatalytic Hydrogenation of Phenol over Platinum and Rhodium: Unexpected Temperature Effects Resolved, N. Singh, Y. Song, O. Y. Gutiérrez, D. M. Camaioni, C. T. Campbell, J. A. Lercher, *ACS Catalysis* **2016**, 6, 7466–7470.

Emerging Electron Microscopy for Heterogeneous Catalysis Research

Miaofang Chi,¹ Michael Zachman¹, Wenpei Gao⁵, Ahmed O. Elnabawy³, Victor Fung⁴, Felipe Polo Garzon,² Luke T. Roling³, De-en Jiang⁴, Younan Xia⁶, Manos Mavrikakis³, Zili Wu²

¹*Center for Nanophase Materials Sciences,* ²*Chemical Sciences Division, Oak Ridge National Laboratory;* ³*Department of Materials Science and Engineering, University of California–Irvine;* ³*Department of Chemical and Biological Engineering, University of Wisconsin–Madison;* ⁴*Department of Chemistry, University of California–Riverside;* ⁵ *Department of Biomedical Engineering, Georgia Institute of Technology*

An aim of our BES program titled “Fundamentals of Catalysis and Chemical Transformations (ERKCC96)” is to fundamentally understand how synergism can be tailored at the metal-oxide interface to control catalytic activity and selectivity in heterogenous catalysts. Various interactions can occur at a metal- oxide interface, e.g., interfacial anchoring via vacancies, impurities, and/or elemental inter-diffusion, formation of interfacial interphases, encapsulation of NPs by the support material, atomic structural rearrangement at the interfaces and surfaces, and/or charge transfer between the NP and support, each of which impacts reactivity and selectivity. These interfacial interactions are sensitive not only to the selection of metal and oxides, but also to their contacting surface atomic arrangements. Our work is to provide mechanistic insight into the role of interfaces in heterogenous catalysts at the single atom and electron levels for the design of more efficient catalysts.

Scanning transmission electron microscopy (STEM) has long been a primary imaging tool for interface research in catalysis because of its exceptional spatial resolution and simultaneous chemical analysis with single-atom sensitivity. In this talk, we will go beyond atomic-resolution imaging and chemical analysis, and introduce two emerging STEM techniques. We will discuss how these new techniques can benefit heterogenous catalysis research, especially understanding of the formation and function of interfaces through two examples. The first example features the use of four-dimensional (4-D STEM) –based differential phase contrast (DPC) imaging to probe charge transfer at an interface of Au- SrTiO₃, a prototype metal catalyst–oxide support system. Among the various tunable interaction parameters, charge transfer is the least understood, largely because there is no reliable technique to directly probe charge distribution at the inherent sub-nanometer length scale. Herein, we directly probe the charge distribution at Au-SrTiO₃ interfaces down to the atomic scale, revealing the nature of the charge transfer in this system. Further, by combining the experimental results with density functional theory calculations, we provide new insights into the origins and characteristics of charge transfer at the atomic scale. The second example focuses on understanding the formation mechanism of core-shell nanoparticles using *in situ* liquid cell STEM imaging. Syntheses of core-shell nanoparticles are generally realized through liquid phase deposition of shell atoms on core seed particles. However, synthesizing core-shell

particles with atomic precision has not yet been accessible, because of our limited knowledge of the deposition mechanism at sufficient spatial and time resolution. In this work, we observe the dynamic process of depositing individual platinum (Pt) atoms onto palladium (Pd) nanocube seeds at atomic scale. The dynamic interplay between the deposited Pt atoms and the surface of the Pd cube is revealed. The role of the synthesis parameters— e.g., precursor concentration and capping agent, that dictate the deposition kinetics and surface energy of evolving core-shell particles are elucidated. These examples demonstrate how new STEM imaging techniques allow us to access information regarding catalyst interfaces that before was not possible.

FWP ERKCC96: Fundamentals of Catalysis and Chemical Transformations. For a full description of recent progress see Extended Abstract for ERKCC96.

Bridging Molecular and Heterogeneous Catalysis Through Graphite-Conjugated Solids

Yogesh Surendranath

Massachusetts Institute of Technology, Department of Chemistry

Presentation Abstract

The efficient interconversion of electrical and chemical energy requires catalysts capable of accelerating complex multi-electron reactions at electrified interfaces. These reactions can be carried out at the metallic surface sites of heterogeneous electrocatalysts or via redox mediation at molecular electrocatalysts. Molecular catalysts yield readily to synthetic alteration of their redox properties and secondary coordination sphere, permitting systematic tuning of their activity and selectivity. Similar control is difficult to achieve with heterogeneous electrocatalysts because they typically exhibit a distribution of active site geometries and local electronic structures, which are recalcitrant to molecular-level synthetic modification. However, metallic heterogeneous electrocatalysts benefit from a continuum of electronic states which distribute the redox burden of a multi-electron transformation, enabling more efficient catalysis. We have developed a simple synthetic strategy for conjugating well-defined molecular catalyst active sites with the extended states of graphitic solids. Electrochemical and spectroscopic data indicate that these graphite-conjugated catalysts do not behave like their molecular analogues, but rather as metallic active sites with molecular definition, providing a unique bridge between the traditionally disparate fields of molecular and heterogeneous electrocatalysis.

Electrocatalytic Applications of Heteroatom-doped Carbon Nanostructures: Thinking Beyond PEM Fuel Cells

Umit S. Ozkan, Deeksha Jain, Qiang Zhang, Vance Gustin, Dishari Basu, Kuldeep Mamtani, Anne Co, Aravind Asthagiri

The Ohio state University, Department of Chemical & Biomolecular Engineering

Presentation Abstract

The tunable electrical, mechanical and catalytic properties of heteroatom-doped carbon nanostructures have resulted in their widespread use for the development of sustainable electrocatalytic technologies such as PEM fuel cells. Particularly, nitrogen-doped carbon nanostructures (CN_x) and transition metal catalysts such as iron-nitrogen coordinated carbon-supported materials (FeNC) have been widely studied as precious metal-free cathode catalysts for oxygen reduction reaction (ORR) in PEM fuel cells. This work focusses on determining the applicability of these materials for other important electrocatalytic applications including: (i) bifunctional oxygen reduction (ORR) and oxygen evolution reaction (OER) catalysts for regenerative PEM fuel cells, (ii) catalysts for oxygen depolarized cathode technology used in the electrochemical production of halogens such as Cl₂ and Br₂, (iii) catalysts/catalyst supports for low temperature bromine evolution reaction and (iv) cathode catalysts for intermediate temperature phosphoric acid fuel cells. We have combined results from electrocatalytic half-cell measurements with spectroscopic characterization techniques and density functional theory (DFT) predictions to gain useful insights into the nature of active sites of carbon-based catalysts for different applications.

Grant or FWP Number:

PI: Prof. Umit S. Ozkan, Prof. Aravind Asthagiri, Prof. Anne C. Co

Postdoc(s): Dr. Seval Gunduz

Student(s): Graduate students: Deeksha Jain, Qiang Zhang, Vance Gustin, Jonathan Hightower, Dishari Basu; Undergraduate students: Corey Sceranka, Benjamin Rudzinski, Callista Krebs, Benjamin Naragon

RECENT PROGRESS

ORR and OER bifunctional characteristics of nitrogen-doped carbon nanostructures for unitized regenerative PEM fuel cells

The ORR activity of CN_x is found to be higher than Ir/C but lower than Pt/C (Figure 1(a)). Similarly, OER activity of CN_x is significantly higher than Pt/C but comparable to Ir/C (Figure 1(b)). The total bifunctional overpotentials for Pt/C and Ir/C catalysts are significantly higher than CN_x. Operando mass spectrometry measurements shown in Figure 1(c), confirm that the effluent stream from the electrochemical reactor does not contain any CO₂ gas, but contains O₂ gas produced during OER on CN_x catalyst. Moreover, the ORR and OER activity, and hence the overall bifunctional activity of CN_x catalysts increase with increasing pyridinic-N content in the samples (Figure 1(d)). This study demonstrates the promise of using CN_x as efficient ORR and OER bifunctional catalysts for unitized regenerative PEM fuel cells.

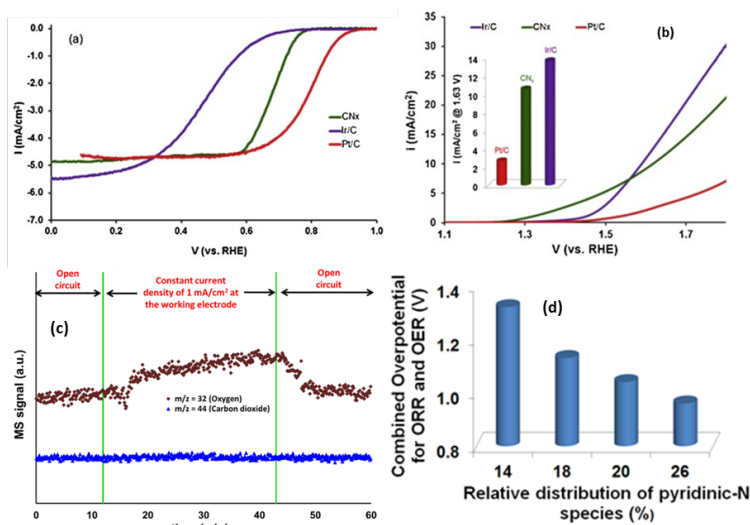


Figure 1: (a) Cathodic polarization curves of CN_x, Ir/C and Pt/C samples for ORR, (b) LSVs of CN_x, Ir/C and Pt/C samples for OER; inset: OER current at 1.63 V for all samples, (c) operando mass spectrometry analysis of the exit stream from an electrochemical cell with CN_x working electrode held at current density of 1 mA/cm², (d) correlation between pyridinic N content and bifunctional overpotential of CN_x catalysts

measurements reveal that the ORR onset and half-wave potentials of CN_x-Cl are higher than CN_x (Figure 2(a)). Ex-situ near edge X-ray absorption fine structure (NEXAFS) for both CN_x and CN_x-Cl samples in the C K-edge region are shown in Figure 2(b). The additional shoulder at ~288 eV in CN_x-Cl sample is attributed to the formation of C-Cl bonds. We hypothesize that the difference in electronegativity of C and Cl facilitates side-on adsorption of O₂ molecule leading to the enhancement in ORR activity.

For FeNC catalyst, in-situ electrochemical Cl⁻ poisoning measurements show a significant decrease in kinetic current density at 0.8 V with increasing Cl⁻ concentration as shown in Figure 2(c). DFT calculations of the crossover potential when OOH* or O₂* outcompetes (based on free energy or reaction) Cl⁻ ion adsorption on various models for FeNC indicate that Cl⁻ ions block the initial steps of ORR until a larger overpotential is applied. These DFT results match qualitatively the experimental observation of the increase in overpotential due to Cl⁻ poisoning. Post-reaction X-ray absorption near edge structure (XANES) spectra collected in the Fe

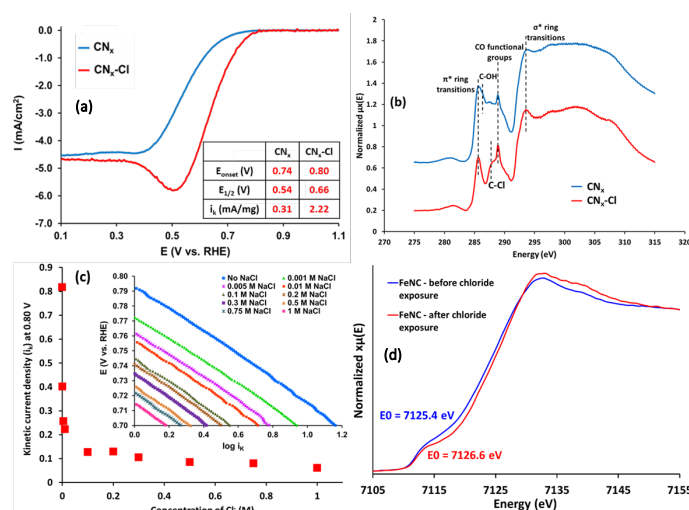


Figure 2: (a) ORR activity of CN_x and CN_x-Cl, (b) NEXAFS C K-edge spectra of CN_x and CN_x-Cl, (c) Change in *i_k* at 0.8 V (inset: mass transport corrected polarization curves of FeNC catalysts with increasing Cl⁻ concentration), (d) XANES spectra on FeNC in the Fe K-edge region before and after exposure to Cl⁻

CN_x and FeNC catalysts as oxygen depolarized cathodes (ODCs) for Cl₂ production

In-situ Cl⁻ poisoning electrocatalytic measurements were performed for four catalysts – Pt/C, Rh_xS_y/C, FeNC and CN_x. A significant drop in ORR activity of Pt/C and Rh_xS_y/C is observed with increasing concentration of Cl⁻ ions in the electrolyte. FeNC catalyst also shows a decrease in ORR activity, while CN_x catalyst shows no reduction in ORR activity after exposure to Cl⁻ ions.

CN_x-Cl catalysts were synthesized by soaking CN_x in 0.3 M HCl at room temperature. ORR activity

K-edge region of FeNC reveals an increase in the Fe K-edge energy by 1.2 eV after Cl^- exposure, indicating oxidation of the catalyst, consistent with the predicted increase in DFT-calculated Bader charges on Fe in the different FeN_x sites after adsorption of Cl^- (Figure 2(d)).

Electrocatalytic bromine evolution reaction (BER) using CN_x catalyst

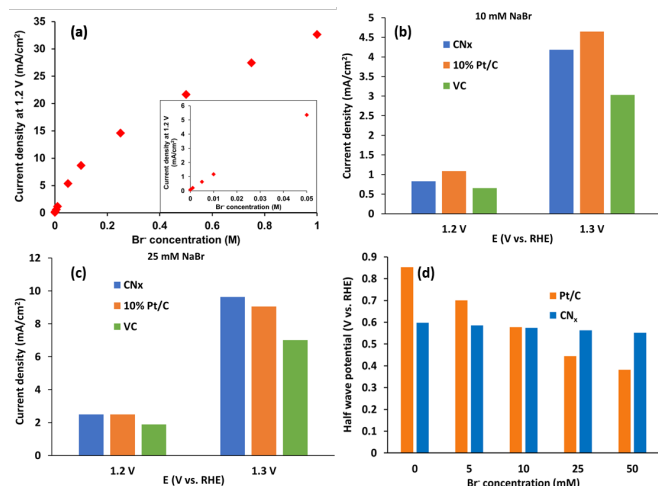


Figure 3: (a) Current density at 1.2 V obtained from LSVs collected under BER conditions, current densities obtained in electrolyte containing Br^- : (b) 10 mM NaBr, (c) 25 mM NaBr, (d) ORR activity of CN_x and 10% Pt/C catalysts in the presence of bromide ions in acidic electrolyte

As shown in Figure 3(a), the current density associated with BER increases with increasing Br^- concentration and BER using CN_x begins at Br^- concentration as low as 5 mM. Figures 3(b) and (c) compare the BER activity in terms of current density on the three model catalysts – CN_x , 10% Pt/C (commercial) and Vulcan Carbon (VC, commercial). At 10 mM Br^- concentration, the BER activity of CN_x is slightly lower compared to Pt/C. However, at 25 mM Br^- concentration, the BER activity of CN_x is better than 10% Pt/C. Another important aspect of this technology is the use of ODCs for BER. CN_x shows high resistance to Br^- poisoning, while Pt/C is significantly poisoned in the presence of Br^- under ORR conditions (Figure 3(d)). These results show

the promise of using CN_x as both anode and cathode catalysts for BER using ODCs.

FeNC catalysts for phosphoric acid fuel cells

Figures 4(a-c) indicate the phosphate poisoning resistance of FeNC under both ex-situ and in-situ conditions. In-situ phosphate poisoning experiments reported in Figure 4(b) were performed by evaluating the ORR characteristics of FeNC in 0.1 M H_2SO_4 , followed by adding H_3PO_4 in the electrolyte. The ORR selectivity of FeNC, determined using rotating ring disk electrode (RRDE) measurements, remains unchanged after exposure to H_3PO_4 . The reason behind the resistance of FeNC catalyst to phosphate poisoning could be the high surface area and pore volume of the Black Pearls® carbon support resulting in Fe sites being incorporated inside its pores, thus preventing large anions such as phosphate from adsorbing onto the Fe sites inside the catalyst pores.

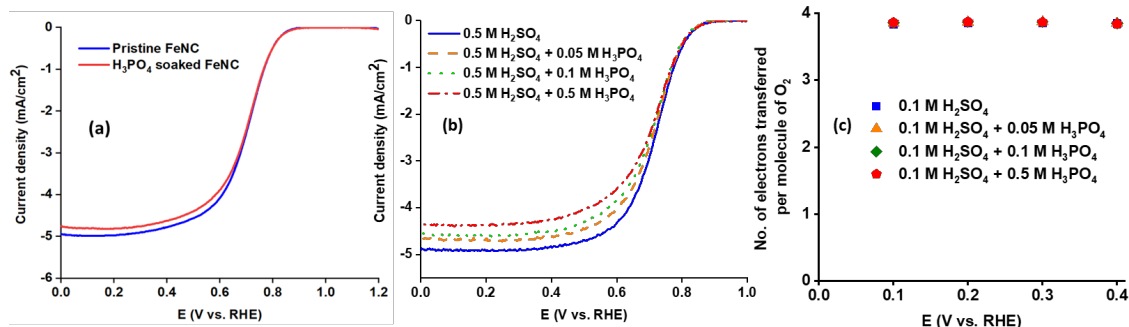


Figure 4: ORR voltammograms of FeNC catalyst obtained (a) before and after soaking in 0.1 M H₃PO₄, (b) by addition of increasing amounts of H₃PO₄ in 0.1 M H₂SO₄ electrolyte during half-cell measurements, (c) ORR selectivity of FeNC catalyst obtained using RRDE measurements during H₃PO₄ additions

Solvation Effects on DFT Predictions of ORR on CN_x

DFT calculations examining the free energy of the 4 proton-electron transfer steps (going through the intermediates OOH*, O*, OH* to form water) for ORR under acidic conditions allow for a quick prediction of the ORR onset potential. Such calculations have provided insight into volcano plots for ORR on metal surfaces, and can be valuable to examine the large range of possible ORR active sites on CN_x catalysts. Nevertheless, solvation effects can dramatically affect the DFT predictions of onset potential. We have used continuum solvation methods (based on VASPSol implementation) to show that continuum solvation methods do not reproduce the stabilization of OH* on metal surfaces leading to inaccurate onset potentials for metal surfaces. We have extended this comparison to solvation effects for ORR on basal CN_x. Table 1 shows the results for DFT predicted onset potentials for basal CN_x using several solvation methods. We find that the water bilayer results are sensitive to the details of the relationship of the ORR intermediate and water bilayer. This sensitivity is greater than what is found on metal surfaces due to the weaker interaction of the water bilayer to the CN_x surface. This allows the bilayer structure to be more flexible and more easily disrupted by the ORR intermediate. If we take the most favorable configurations from the water bilayer calculations, we find that a hybrid method (1 explicit H₂O + VASPSol) gives generally good agreement and might be the most practical approach to incorporate solvation to DFT studies of ORR on CN_x catalysts.

Table 1. DFT results for stabilization of the ORR intermediates on basal CN_x with different solvation approaches along with the resulting DFT predictions for the onset potential and rate-limiting step.

Method	E _{stabilization} /(eV)			Onset potential/V	Rate-limiting step
	OOH*	O*	OH*		
No solvation	0	0	0	0.64	O* to OH*
VASPSol	-0.25	-0.49	-0.17	0.32	O* to OH*
1 explicit H ₂ O	-0.26	-0.46	-0.22	0.41	O* to OH*
Two water bilayer	-0.01 to -0.19	-0.71 to -0.97	-0.10 to -0.33	-0.24 to 0.25	O* to OH*
Hybrid	-0.48	-0.77	-0.36	0.23	O* to OH*

Publications Acknowledging this Grant in 2015-2018

Exclusively funded by this grant

1. Mamtani, K.; Ozkan, U.S. Heteroatom-doped Carbon nanostructures as Oxygen Reduction Reaction Catalysts in Acidic Media: An Overview. *Catal Lett.* **2015**, *145*, 436-450.
2. Mamtani, K.; Jain, D.; Co, A.; Ozkan, U.S. Investigation of Chloride Poisoning Resistance for Nitrogen-Doped Carbon Nanostructures as Oxygen Depolarized Cathode Catalysts in Acidic Media. *Catal. Lett.* **2017**, *147*, 11, 2903-2909.
3. Jain, D.; Mamtani, K.; Gustin, V.; Gunduz, S.; Celik, G.; Waluyo, I.; Hunt, A.; Co, A.; Ozkan, U.S.; Enhancement in Oxygen Reduction Reaction Activity of Nitrogen-Doped Carbon Nanostructures in Acidic Media through Chloride-Ion Exposure. *ChemElectroChem.* **2018**, *5*, 1-11
4. Gunduz, S.; Deka, D.J.; Ozkan, U.S. Chapter Three - Advances in High-Temperature Electrocatalytic Reduction of CO₂ and H₂O. *Adv. Catal.* **2018**, *62*, 113-165.
5. Deka, D.J.; Gunduz, S.; Fitzgerald, T.; Miller, J. T.; Co, A.; Ozkan, U.S. Production of syngas with controllable H₂/CO ratio by high temperature co-electrolysis of CO₂ and H₂O over Ni and Co- doped lanthanum strontium ferrite perovskite cathodes. *Appl. Catal., B.* **2019**, *248*, 487-503.
6. Dogu, D.; Gunduz, G.; Meyer, K.E.; Deka, D.J.; Co, A.; Ozkan, U.S. CO₂ and H₂O Electrolysis Using Solid Oxide Electrolyzer Cell (SOEC) with La and Cl- doped Strontium Titanate Cathode. *Catal. Lett.* **2019**, *149*, 7, 1743–1752.
7. Zhang, A., and Asthagiri, A., Solvation effects on DFT predictions of ORR activity on metal surfaces *Catalysis Today* 323 (2019) 35-43

Jointly funded by this grant and other grants with leading intellectual contribution from this grant

8. Zhang, Q.; Mamtani, K.; Jain, D.; Ozkan, U.S.; Asthagiri, A. CO Poisoning Effects on FeNC and CN_x ORR Catalysts: A Combined Experimental– Computational Study. *J. Phys. Chem. C* **2016**, *120*, 28, 15173-15184.
9. Mamtani, K.; Singh, D.; Millet, J-M.; Miller, J.T.; Co, A. C.; Ozkan, U.S. Evolution of N-Coordinated Iron–Carbon (FeNC) Catalysts and Their Oxygen Reduction (ORR) Performance in Acidic Media at Various Stages of Catalyst Synthesis: An Attempt at Benchmarking. *Catal Lett.* **2016**, *146*, 1749-1770.
10. Mamtani, K.; Jain, D.; Zemyanov, G.; Celik, G.; Luthman, J.; Renkes, G.; Co, A.; Ozkan, U.S. Probing the ORR Active Sites Over Nitrogen-doped Carbon Nanostructures (CN_x) in Acidic Media Using Phosphate Anion *ACS Catal.* **2016**, *6*, 10, 7249-7259.
11. Mamtani, K.; Jain, D.; Shankaran, K.; Co, A.; Ozkan, U.S. Nitrogen-coordinated iron-carbon (FeNC) Materials as Efficient Bifunctional Electrocatalysts for Oxygen Reduction

Reaction and Oxygen Evolution Reaction in Acidic Media. *Energy Fuels* **2017**, *31*, 6, 6541-6547.

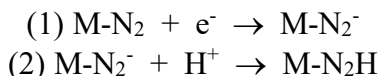
12. Mamtani, K.; Bruening, C.; Co, A.; Ozkan, U.S. A Comparison of Oxygen Reduction Reaction (ORR) Performance for Iron-nitrogen-carbon (FeNC) Catalysts in Acidic and Alkaline Media. *Res. Rev. Electrochem.* **2017**, *8*, 2, 1-9.
13. Mamtani, K.; Jain, D.; Dogu, D.; Gustin, V.; Gunduz, S.; Co, A.; Ozkan, U.S. Insights into Oxygen Reduction Reaction (ORR) and Oxygen Evolution Reaction (OER) Active Sites for Nitrogen-doped Carbon Nanostructures (CN_x) in Acidic Media. *Appl. Catal., B.* **2018**, *220*, 88-97.
14. Mamtani, K.; Singh, D.; Dogu, D.; Jain, D.; Millet, J.-M.; Ozkan, U.S. Effect of Acid-washing on the Nature of Bulk Characteristics of Nitrogen-doped Carbon Nanostructures (CN_x) as Oxygen Reduction Reaction (ORR) Electrocatalysts in Acidic Media. *Energy Fuels.* **2018**, *32*, 10, 11038-11045.

Exploring Protonated Metallocenes as PCET Relays in N₂RR

Jonas C. Peters, Matthew J. Chalkley, Paul H. Oyala,
Marcus W. Drover, and Dirk J. Schild
*Division of Chemistry and Chemical Engineering,
California Institute of Technology, Pasadena CA 91125*

Presentation Abstract

An important challenge in advancing the field of N₂RR reduction catalysis by molecular (and possibly heterogenous) systems is to identify means to accomplish the challenging reduction protonation of N₂ efficiently. While there are various metrics by which to consider efficiency, one of the themes we and other labs are targeting concerns the generation of N-H bonds during N₂RR via proton-coupled-electron-transfer (PCET) steps. Such an approach can in principle avoid, or at least attenuate, the strongly reducing potentials otherwise needed to access M-N₂ species that are sufficiently basic to undergo a subsequent, uncoupled protonation step, as for:



During the course of N₂RR studies by a tris(phosphine)borane iron catalyst our lab discovered some years ago, we began to wonder whether a common metallocene reducing agent, such as Cp*₂Co or Cp*₂Cr, might undergo in situ protonation by an organic acid to generate a highly reactive, protonated form of the metallocene. We have undertaken detailed studies to explore this hypothesis, and to characterize the site/s of protonation, in one such species (Cp*₂Co). These studies, in addition to combined physical and experimental data, establish that protonation at the ring of Cp*₂Co generates a species with a very weak and hence highly reactive C-H bond. We also found that including Cp*₂Co in electrocatalytic N₂RR experiments using the same iron catalyst improves the overall modest efficiency of the system.

Encouraged by these findings, we are pursuing related systems as plausible targets for PCET, with an eye towards incorporating such systems within an electrocatalytic scheme. At this stage, we have synthesized and characterized several systems where ring protonation occurs, and leads to a similarly weak C-H bond. This talk will focus on our recent progress, opportunities, and some of the challenges we are facing.

DE-SC0019136: Towards Electrocatalytic N₂-to-NH₃ Conversion with Molecular Catalysts

Publications Acknowledging this Grant in 2015-2018

(1)

1. Gu, N. X.; Ung, G.; Peters, J. C. Catalytic hydrazine disproportionation mediated by a thiolate-bridged VFe complex. *Chem. Commun.* **2019**, 55, 5363-5366.

2. Chalkley, M.; Oyala, P.; Peters, J. C. Cp* Non-Innocence Leads to a Remarkably Weak C–H Bond via Metallocene Protonation. *J. Am. Chem. Soc.* **2019**, 141, 4721-4729.
3. Nance, P.; Oyala, P.; Thompson, N.; Peters, J. C. Zerovalent Rh and Ir Silatranes Featuring 2-center, 3-electron Polar Sigma Bonds. *Angew. Chem. Int. Ed.* **2019**, 58, 6220-6224.

Selective Catalytic Oxidations: Mechanistically-Informed Catalyst Design and Optimization

Robert M. Waymouth
Department of Chemistry, Stanford University

Presentation Abstract

The cationic Pd dimer [(neocuproine)Pd(μ -OAc)]₂[OTf]₂ (neocuproine = 2,9-dimethyl-1,10-phenanthroline) is an active catalyst precursor for the oxidation of a variety of alcohols, vicinal diols, polyols and carbohydrates. Complex polyols, such as glycerol, threitol and unprotected alkyl pyranosides are also oxidized in high selectivity to the hydroxyketones; for alkyl pyranosides oxidation occurs selectively to afford the 3-ketoses.

For aerobic alcohol oxidations, competitive oxidative degradation of the ligand limited the catalyst lifetime and turnover numbers (TON). Mechanistic studies, including *in situ* mass spectrometry techniques, provided insights that guided the development of effective strategies for mitigating catalyst deactivation. Specifically, the addition of H-atom donors and appropriate ligand modifications improved the catalyst lifetime, enabling the efficient aerobic oxidations of a variety of polyols on a multigram scale with as little as 0.25 mol% Pd without any appreciable loss in chemoselectivity.

During the course of these studies, we identified more oxidatively resistant ligands based on 2,2'-biquinoline (**L**₂) and 6,7-dihydrodibenzo[b,j]-[1,10]phenanthroline (**L**₃). Cationic Pd complexes ligated by these ligands are effective for the aerobic oxidation of 1,2-propanediol and afford significantly longer lifetimes and higher turnover numbers (TON > 80) without the need of additives. However, the rates of these aerobic oxidations are considerably lower than those of the Pd neocuproine complexes, due to the competitive formation of insoluble trinuclear species [(**L**₂Pd)₃(μ^3 -O)₂]²⁺ (**L**₂ = 2,2'-biquinoline).

DOE DE-SC00181168, "Selective Catalytic Oxidations: Opportunities and Challenges for Selective Conversion of Renewable Resources"

PI: Lead PI; Robert M. Waymouth

Postdoc: Trevor Del Castillo

Students: Wilson Ho, Summer Ramsay-Burrough, Katherine Walker, Conor Galvin

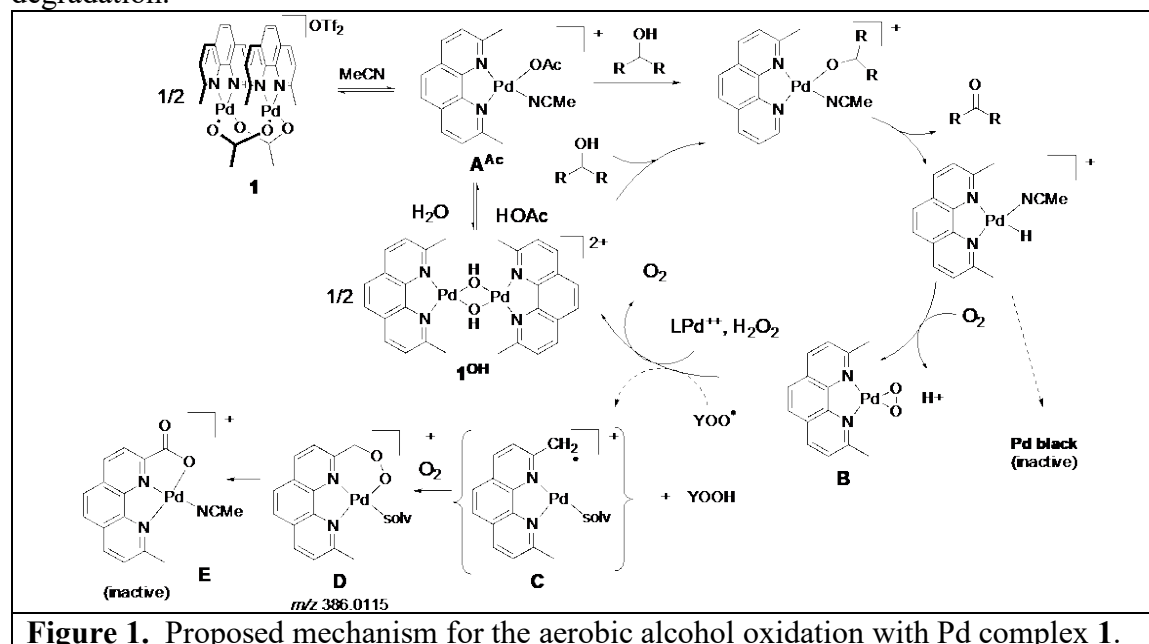
RECENT PROGRESS

Extension of Catalyst Lifetimes and Improvement of Turnover Numbers for Aerobic Oxidation of Alcohols with cationic Pd neocuproine catalysts.

The cationic Pd complex [LPd(OAc)]₂(OTf)₂ complex **1** (**L**₁ = neocuproine = 2,9-dimethyl-1,10-phenanthroline) is a selective catalyst for the oxidation of primary and secondary alcohols; vicinal diols, polyols,¹ and sugar glycosides.²

Limited aerobic lifetime is a key challenge in the application of the otherwise promising [LPd(OAc)]₂(OTf)₂ complex **1** (**L**₁ = neocuproine = 2,9-dimethyl-1,10-phenanthroline) which

exhibits highly selective and rapid aerobic oxidation of polyols and sugars. Prior studies had revealed a competitive oxidative degradation of the neocuproine ligand when O₂ or air is used as the terminal oxidant (Figure 1). *In-operando* mass spectrometry studies, carried out in collaboration with the Zare group at Stanford, revealed several ions (**D** and **E**, Figure 1) whose intensities increased in an inverse correlation with the decrease in rate during the course of the aerobic oxidation reactions.³⁻⁴ These studies collectively reveal that H atom abstraction from the methyl groups at the 2 and 9 positions of the neocuproine ligand is a key event in initiating catalyst degradation.

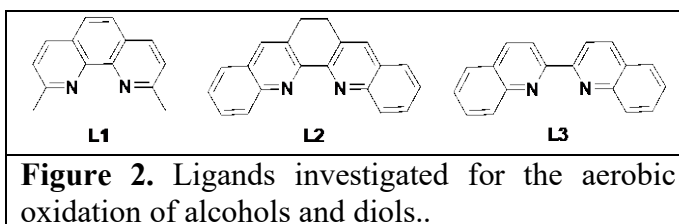


Several strategies were employed to illuminate the pathways for the competitive oxidative degradation of the neocuproine during aerobic oxidations with the goal of increasing turnover numbers and enabling lower catalyst loadings.⁴ Phenol anti-oxidants proved a particularly useful additive for mitigating oxidative degradation of the catalyst. In addition, styrene additives proved to improve catalyst lifetimes by intercepting Pd hydrides, facilitating aerobic re-oxidation of the Pd hydride species and mitigating the formation of Pd black.⁴

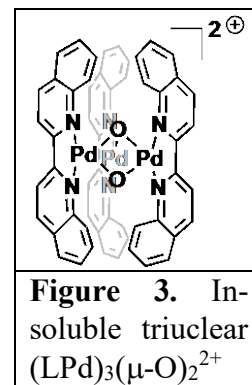
New Oxidatively Resistant Ligands for Aerobic Pd-catalyzed Oxidations.

As a strategy to increase the lifetimes of catalysts under aerobic conditions, we investigated a new class of ligands, 6,7-dihydrodibenzo[*b,j*]-[1,10]-phenanthroline (**L2**, Figure 2) and 2,2'-biquinoline (**L3**, Figure 2). Catalytic aerobic oxidation of 1,2 propane diol with cationic Pd catalysts ligated by ligands **L2** and **L3** led to a significant improvement in TON compared to the Pd neocuproine complex **1**; with ligand **L3**, TON of 84 were observed.

Pd catalysts with ligands **L2** and **L3** retain the high selectivity for the oxidation of 1,2-propanediol, polyols and glycosides affording the α -hydroxy ketones or 3-ketoses with



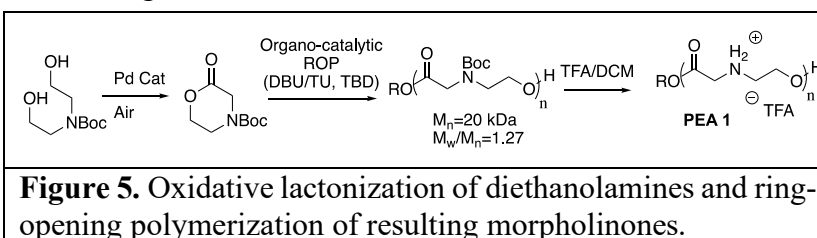
selectivities > 85%. However, the rate of oxidation of polyol substrates by these new oxidatively robust ligands is substantially reduced compared to the neocuproine system, limiting their synthetic utility. Preliminary mass spectrometry studies suggest that reaction rates with **L3** may be limited due to buildup of a poorly soluble trimeric species $(\text{LPd})_3(\mu\text{-O})_2^{2+}$ ($\text{L} = 2,2'$ -biquinoline). Further ligand modifications and mechanistic studies are underway to improve the rates of catalysis and to understand the origin of high chemoselectivities for the oxidation of vicinal diols, polyols and unprotected carbohydrates by this class of Pd compounds. Additional mass spectrometry studies will be combined with DFT to investigate the relative stabilities of $(\text{LPd})_3(\mu\text{-O})_2^{2+}$ with a number of bisquinoline ligand variants. Related trinuclear compounds were observed for the neocuproine (**L1**) complexes, but these complexes were more soluble and were competent to regenerate monomeric Pd complexes under catalytic conditions.⁵ Computationally guided synthesis of sterically encumbered bisquinoline ligands anticipated to destabilize $(\text{LPd})_3(\mu\text{-O})_2^{2+}$ may potentially improve rates of catalysis.



Scope and Utility of Chemoselective Catalytic Oxidations:

The fundamental investigations to improve the scope of the Pd-catalyzed alcohol oxidations have proven an enabling advance for collaborative studies with the Wender group at Stanford to generate functional polyesters as novel degradable polymers useful for the delivery of messenger RNA in cells and live animals.⁶⁻⁷ The oxidative lactonization of substituted diethanolamines with Pd catalyst **1** generates morpholinones (aza-lactones), which have proven a versatile class of monomers for generating functionalized, degradable

polyesters.⁸ Lactones accessed via the Pd-catalyzed oxidative lactonization of α - ω diols were polymerized (by organocatalytic ROP)⁹ to generate functionalized poly(\square -aminoester)s (PAEs)



of precise molecular weight and low polydispersity.⁸ Removal of the Boc protecting group affords novel cationic, water soluble PAEs (Figure 5) that we have shown efficient vectors for the transfection of cells with mRNA, DNA and other bioactive oligonucleotides.⁶⁻⁷

References.

1. Chung, K.; Banik, S. M.; De Crisci, A. G.; Pearson, D. M.; Blake, T. R.; Olsson, J. V.; Ingram, A. J.; Zare, R. N.; Waymouth, R. M., Chemoselective Pd-Catalyzed Oxidation of Polyols: Synthetic Scope and Mechanistic Studies. *J. Am. Chem. Soc.* **2013**, *135* (20), 7593-7602.
2. Chung, K.; Waymouth, R. M., Selective Catalytic Oxidation of Unprotected Carbohydrates. *ACS Catalysis* **2016**, *6* (7), 4653-4659.
3. Ingram, A. J.; Walker, K. L.; Zare, R. N.; Waymouth, R. M., Catalytic Role of Multinuclear Palladium–Oxygen Intermediates in Aerobic Oxidation Followed by Hydrogen Peroxide Disproportionation. *J. Am. Chem. Soc.* **2015**, *137* (42), 13632-13646.

4. Ho, W. C.; Chung, K.; Ingram, A. J.; Waymouth, R. M., Pd-Catalyzed Aerobic Oxidation Reactions: Strategies To Increase Catalyst Lifetimes. *J. Am. Chem. Soc.* **2018**, *140* (2), 748-757.
5. Ingram, A. J.; Solis-Ibarra, D.; Zare, R. N.; Waymouth, R. M., Trinuclear Pd₃O₂ Intermediate in Aerobic Oxidation Catalysis. *Angew. Chem., Int. Ed.* **2014**, *53* (22), 5648-5652.
6. McKinlay, C. J.; Benner, N. L.; Haabeth, O. A.; Waymouth, R. M.; Wender, P. A., Enhanced mRNA delivery into lymphocytes enabled by lipid-varied libraries of charge-altering releasable transporters. *Proc. Natl. Acad. Sci* **2018**, *115* (26), E5859-E5866.
7. Benner, N. L.; Near, K. E.; Bachmann, M. H.; Contag, C. H.; Waymouth, R. M.; Wender, P. A., Functional DNA Delivery Enabled by Lipid-Modified Charge-Altering Releasable Transporters (CARTs). *Biomacromolecules* **2018**, *19* (7), 2812-2824.
8. Blake, T. R.; Waymouth, R. M., Organocatalytic Ring-Opening Polymerization of Morpholinones: New Strategies to Functionalized Polyesters. *J. Am. Chem. Soc.* **2014**, *136* (26), 9252-9255.
9. Zhang, X.; Fevre, M.; Jones, G. O.; Waymouth, R. M., Catalysis as an Enabling Science for Sustainable Polymers. *Chem. Rev.* **2018**, *118* (2), 839-885.

Publications Acknowledging this Grant in 2017-2019

(I) Exclusively funded by this grant.

1. Ho, W. C., Chung, K.; Ingram, A. J., Waymouth, R. M. "Pd-Catalyzed Aerobic Oxidation Reactions: Strategies to Increase Catalyst Lifetimes", *J. Am. Chem. Soc.*, **2018**, *140*, 748-757.

(III) Jointly funded by this grant and other grants with relatively minor intellectual contribution from this grant;

2. Zhang, X.; Fevre, M.; Jones, G. O.; Waymouth, R. M. "Catalysis as an Enabling Science for Sustainable Polymers" *Chem. Rev.* **2018**, *118*, 839-885.
3. Benner, N. L.; Near, K. E.; Bachmann, M. H.; Contag, C. H.; Waymouth, R. M.; Paul A. Wender, P. A. "Functional DNA Delivery Enabled by Lipid-Modified Charge-Altering Releasable Transporters (CART)s", *Biomacromolecules*, **2018**, *19*, 2812-2824.
4. McKinlay, C.J.; Benner, N.L.; Haabeth, O.A.; Waymouth, R. M.; Wender, P.A. "Enhanced mRNA delivery into lymphocytes enable by lipid-varied libraries of Charge-Altering Releasable Transporters" *Proc. Nat. Acad. Sci.*, **2018**, *115*(26), E5859-E5866

Following ultrafast reaction dynamics in heterogeneous catalysis

Tony F. Heinz

*SLAC National Accelerator Laboratory, Menlo Park, CA 94025 and
Dept. of Applied Physics, Stanford University, Stanford, CA 94305*

Mechanistic understanding of chemical transformation through heterogeneous catalysis requires knowledge of short-lived intermediates and of the behavior of reactants in the region of transition states. Because of their low concentration in steady state, these states are difficult to observe and characterize directly. In this talk, we discuss approaches to harnessing ultrafast laser techniques, particularly the revolutionary capabilities of the x-ray free electron lasers, to obtain detailed information about these transient states and to explore fundamental aspects of the related electron dynamics on time scales down to a few femtoseconds.

Central to this research is use of x-ray free electron lasers (XFELs), such as the LCLS XFEL at SLAC National Accelerator Laboratory and the LCLS-II upgrade now under construction. These new light sources provide tunable coherent x-ray radiation in the form of a collimated x-ray beam consisting of pulses shorter than 100 fs (10^{-13} s). Such intense pulses are ideally suited for probing the ultrafast dynamics of catalytic processes through x-ray spectroscopy of atom-specific core-level transitions. The expected capability of the LCLS-II XFEL to produce x-ray pulses as short as a few femtoseconds further enhances the time resolution and permits access to strongly non-equilibrium processes underlying energy exchange and the dynamics of photocatalytic processes.

After a general discussion of the motivation and progress in this new field, we present recent results on the transient K-edge spectra of chemisorbed C atoms on the Ni(100) surface from studies carried out using the Fermi x-ray free electron laser in Trieste, Italy. Under excitation by femtosecond visible laser pulses, no lasting change in structure of the adsorbate-covered surface is expected, but the system provides an attractive model for understanding ultrafast electron and vibrational dynamics. Experimentally, transient response was recorded in C K-edge x-ray spectra in both absorption and emission measurements. Distinct time scales from 100-fs to several ps were identified and attributed to different phases of adsorbate-substrate coupling -- first electronic, then vibrational.

This research has been carried out as part of a new DOE-BES funded program (FWP SCW0063) in collaboration with SLAC co-investigators Tom Jaramillo, Alan Luntz, Hirohito Ogasawara, Frank Abild-Pederson, and Johannes Voss and with Stockholm University co-investigator Anders Nilsson.

Tabletop Femtosecond M-edge XANES as a New Tool for Inorganic Spectroscopy

Josh Vura-Weis

University of Illinois at Urbana-Champaign, Department of Chemistry

Presentation Abstract

X-ray absorption near edge spectroscopy (XANES or NEXAFS) is a powerful technique for measuring the electronic structure of transition metal complexes. With the advent of free-electron lasers, there is increased interest in using time-resolved XANES to observe catalytic reaction intermediates. However, widespread use of this technique is limited by scarce beamtime and the need to travel to shared facilities. We have developed $M_{2,3}$ -edge XANES, corresponding to $3p \rightarrow 3d$ transitions, as a reliable technique for measuring the electronic structure of first-row transition metal coordination complexes. The tabletop high-harmonic source provides femtosecond time resolution and 24/7 accessibility. In this talk, we will introduce the instrumentation and show how M-edge XANES spectra are sensitive to the oxidation state, spin state, and ligand field of the metal center in coordination complexes. We will describe the photophysics of several transition metal complexes relevant to photocatalysis, and present progress on solution-phase XANES of Co_4O_4 cubane water oxidation catalysts.

DE-SC0018904: Catalytic Reaction Intermediates Revealed with Femtosecond M-edge XANES

Students: Clare Leahy, Yusef Shari'ati, Kori Sye

Control and Understanding of Molecular Catalysts on Surfaces

Alexander Katz,[#] Nicolás Grosso-Giordano,[#] Christian Schöttle,[#] Andrew Palermo,^{#%}
Alexander Okrut,[#] Andrew Solovyov,[#] Christian Schroeder,^{*} Erjia Guan,[%] Hubert Koller,^{*}
Stacey I. Zones,[‡] Bruce Gates[%]

[#]*Department of Chemical and Biomolecular Engineering, University of California at Berkeley,
Berkeley, California 94720, United States*

^{*}*Institut für Physikalische Chemie, Westfälische Wilhelms-Universität Münster, Münster 48149,
Germany*

[‡]*Chevron Energy Technology Company, Richmond, California 94804, United States*

[%]*Department of Chemical Engineering, University of California at Davis, One Shields Avenue,
Davis, California 95616, United States*

Presentation Abstract

In the first part of this talk, we describe the effect of dynamic reorganization and confinement of isolated Ti^{IV} catalytic centers supported on silicates as catalysts for olefin epoxidation. Catalysts investigated consist of grafted single-site calix[4]arene- Ti^{IV} centers on a siliceous support, or their calcined counterparts. Their location is synthetically controlled to be either unconfined at terminal T-atom positions (denoted as type-(i)) or within confining 12-MR pockets (denoted as type-(ii); diameter $\sim 7 \text{ \AA}$) composed of hemispherical cavities on the external surface of zeotypes with *-SVY topology. When active sites are located at unconfined type-(i) environments, the rate constants for cyclohexene epoxidation are $9 \pm 2 \text{ M}^{-2} \text{ s}^{-1}$; whereas within confining type-(ii) 12-MR pockets, there is a ~ 5 -fold enhancement to $48 \pm 8 \text{ M}^{-2} \text{ s}^{-1}$. While activation enthalpies are $\Delta H_{\text{app}}^{\ddagger} = 43 \pm 1 \text{ kJ mol}^{-1}$ irrespective of active site location, confining environments exhibit diminished entropic barriers ($\Delta S_{\text{app}}^{\ddagger} = -68 \text{ J mol}^{-1} \text{ K}^{-1}$ for unconfined type-(i) vs $-56 \text{ J mol}^{-1} \text{ K}^{-1}$ for confining type-(ii)), indicating that confinement leads to more facile association of reactants at active sites to form transition state structures. In a second part of this talk, we describe an approach for stabilizing supported weakly interacting active sites (i.e. those that interact non-covalently with the support) against aggregation and coalescence. We use silica as a prototypical example of a support, and an iridium pair-site catalyst incorporating bridging calixarene ligands as an active site. Atomic-resolution imaging of the Ir centers before and after ethylene-hydrogenation catalysis show the metals resisted aggregation and deactivation, remaining atomically dispersed and accessible for catalysis. These two examples represent new opportunities for understanding reactivity on surfaces by synthetically controlling active site reaction environments.

DE-FG02-05ER15696: Control of Supported Molecular Catalysts Using Metallocalixarene Active Sites

Postdoc(s): Alexander Okrut, Christian Schöttle, Andrew Solovyov, Mizuho Yabushita

Student(s): Nicolás Grosso-Giordano, Andrew Palermo

RECENT PROGRESS

Introduction

In the first part of the talk, by grafting calix[4]arene-Ti^{IV} (**cTi**) complexes on crystalline zeolitic silicates as supports, we synthesize well-defined active centers for olefin epoxidation with confining and non-confining surrounding surface environments. In the second part of this talk, we demonstrate the synthesis and supporting an Ir dimer catalyst stabilized by bulky calix[4]arene ligands. These ligands prevent Ir aggregation and deactivation that are observed in other common molecular hydrogenation catalysts.

Materials and Methods

Molecular Ti^{IV} sites active for olefin epoxidation consist of calix[4]arene-Ti (**cTi**) molecular complexes, which are grafted onto silanols on silicate supports to result in **cTi/X** catalyst. In the second part of the talk, active sites consist of an Ir dimer stabilized by P-bridging calix[4]arene ligands, supported on a silica SiO₂ support.

Results and Discussion

In **cTi/X**, Ti^{IV} centers are found within identical inner-sphere oxo coordination environments, as confirmed by physicochemical characterization, UV-visible, and X-ray absorption spectroscopies; therefore, higher rates observed for **cTi/3-a** and **cTi/3-b** are a consequence of support structures occurring beyond the active center, and not due to any difference in coordination of Ti^{IV} active centers. Activation enthalpies are the same between **cTi/3-a** (confined) vs **cTi/2** (unconfined) at 41 ± 1 kJ mol⁻¹, suggesting that elementary steps involved in reactions are the same. However, entropies of activation are less negative by 20 J mol⁻¹ K⁻¹ for sites found within nanocavities in **cTi/3-a**.

The successful synthesis and immobilization of the Ir dimer catalyst on SiO₂ was confirmed by structural characterization data from single-crystal X-ray diffraction, ³¹P and ¹H NMR, and EXAFS (data not shown). Ethylene hydrogenation proceeds after on-stream catalyst activation, resulting in a stable catalyst for continuous ethylene hydrogenation (Figure 1, right side panel inset shows steady activity up to 84 h of reaction). HAADF STEM imaging confirms that Ir dimer active sites remain isolated after catalysis. In contrast, other Ir molecular hydrogenation catalyst such as the well-known Crabtree's catalyst, rapidly deactivate when supported on SiO₂. This demonstrates that calix[4]arene ligands are able to act as bulky ligands that stabilize Ir pair active sites.

Significance

Taken together, these examples demonstrate the importance of synthetically controlling active sites structures, in order to obtain well-defined active sites that are stable under catalytic conditions. This enables understanding how reaction events are influenced by the surrounding surface environment. In particular for Ti^{IV} catalyzed epoxidation, partially confining external-surface nanocavities on 2-D zeotypes are accessible to bulk fluid phases and therefore to reactants that cannot be typically activated within zeotype pores. In the second part of the talk, new approaches for stabilizing supported molecular sites are demonstrated through an "accessible but protected" mechanism.

Publications Acknowledging this Grant in 2016-2019

(I) Exclusively funded by this grant

1. N. A. Grosso-Giordano, S. I. Zones and A. Katz. Opportunities for controlling catalysis by designing molecular environments around active sites: cations supported on amorphous versus crystalline zeolitic silicate supports. *Catalysis (published by RSC; edited by J. Spivey, Y.-F. Han, D. Shekhawat)* **2019**, *31*, 72–126.

(II) Jointly funded by this grant and other grants with leading intellectual contribution from this grant

- 1 N. A. Grosso-Giordano, A. S. Hoffman, A. Boubnov, D. W. Small, S. R. Bare, S. I. Zones, A. Katz. Dynamic reorganization and confinement of Ti(IV) active sites controls olefin epoxidation catalysis on two-dimensional zeotypes. *J. Am. Chem. Soc.*, **2019**, *141*, 7090–7106.
- 2 A. Okrut, N. A. Grosso-Giordano, C. Schöttle, S. Zones, A. Katz. Understanding the role of Zn(II) in surfactant-free layered silicate delamination: exfoliation of magadiite. *Microporous Mesoporous Mater.*, **2019**, *283*, 55–63.
- 3 C. Schöttle, E. Guan, A. Okrut, N. A. Grosso-Giordano, A. Palermo, A. Solovyov, B. C. Gates, A. Katz. Bulky Calixarene Ligands Stabilize Supported Iridium Pair-Site Catalysts. *J. Am. Chem. Soc.*, **2019**, *149*, 4010–4015.
- 4 A. Okrut, M. Aigner, C. Schöttle, N. A. Grosso-Giordano, S.-J. Hwang, X. Ouyang, S. Zones, A. Katz. SSZ-70 borosilicate delamination without sonication: effect of framework topology on olefin epoxidation catalysis. *Dalt. Trans.*, **2018**, *47*, 15082–15090.
- 5 M. Yabushita, N. A. Grosso-Giordano, A. Fukuoka, A. Katz. Selective sequestration of aromatics from aqueous mixtures with sugars by hydrophobic molecular calixarene cavities grafted on silica. *ACS Appl. Mater. Interfaces*, **2018**, *10*, 39670–39678.
- 6 A. Palermo, S. Zhang, S.-J. Hwang, D.A. Dixon, B.C. Gates, A. Katz. Weakly interacting solvation spheres surrounding a calixarene-protected tetrairidium carbonyl cluster: contrasting effects on reactivity of alkane solvent and silica support. *Dalton Trans.*, **2018**, *47*, 13550–13558.
- 7 N. A. Grosso-Giordano, C. Schroeder, A. Okrut, A. Solovyov, C. Schöttle, W. Chassé, N. Marinković, H. Koller, S. I. Zones, A. Katz. Outer-sphere control of catalysis on surfaces: a comparative study of Ti(IV) single-sites grafted on amorphous versus crystalline silicates for alkene epoxidation. *J. Am. Chem. Soc.*, **2018**, *140*, 4956–4960.
- 8 M. Aigner, N. A. Grosso-Giordano, C. Schöttle, A. Okrut, S. Zones, A. Katz. Epoxidation of 1-octene under harsh tail-end conditions in a flow reactor II: impact of delaminated-zeolite catalyst surface area and structural integrity on catalytic performance. *React. Chem. Eng.*, **2017**, *2*, 852–861.
- 9 M. Aigner, N. A. Grosso-Giordano, A. Okrut, S. Zones, A. Katz. Epoxidation of 1-octene under harsh tail-end conditions in a flow reactor I: a comparative study of crystalline vs. amorphous catalysts. *React. Chem. Eng.*, **2017**, *2*, 842–851.
- 10 C. Schöttle, E. Clark, A. Harker, A. Solovyov, A. T. Bell, A. Katz. Nanoporous gold assemblies of calixarene-phosphine-capped colloids. *ChemComm* **2017**, *53*, 10870–10873.

- 11 B. C. Gates, M. Flytzani-Stephanopoulos, D. A. Dixon, A. Katz. Atomically Dispersed Supported Metal Catalysts: Perspectives and Suggestions for Future Research. *Catal. Sci. Technol.* **2017**, *7*, 4259–4275.
- 12 N. A. Grosso-Giordano, A. Yeh, A. Okrut, D. J. Xiao, F. Grandjean, G. J. Long, S. I. Zones, A. Katz. Effect of defect site pre-organization on Fe(III) grafting and stability: A Comparative Study of Delaminated Zeolite vs. Amorphous Silica Supports. *Chem. Mater.* **2017**, *29*, 6480–6392.
- 13 S. Zhang, S. D. Foyle, A. Okrut, A. Solovyov, A. Katz, B. C. Gates, D. A. Dixon. Role of N-heterocyclic carbenes as ligands in iridium carbonyl clusters. *J. Phys. Chem. A* **2017**, *121*, 5029–5044.
- 14 A. Palermo, A. Solovyov, D. Ertler, A. Okrut, B.C. Gates, A. Katz. Dialing in single-site reactivity of a supported calixarene-protected tetrairidium cluster catalyst. *Chem. Sci.*, **2017**, *8*, 4951–4960.
- 15 M. Yabushita, N. A. Grosso-Giordano, A. Fukuoka, A. Katz. Selective Metal-Organic Framework Catalysis of Glucose to 5-Hydroxymethylfurfural Using Phosphate-Modified NU-1000. *Ind. Eng. Chem. Res.* **2017**, *56*, 7141–7148.
- 16 M. Yabushita, P. Li, K. A. Durkin, H. Kobayashi, A. Fukuoka, O. K. Farha, and A. Katz. Insights into Supramolecular Sites Responsible for Complete Separation of Biomass-Derived Phenolics and Glucose in Metal-Organic Framework NU-1000. *Langmuir* **2017**, *33*, 4129–4137.
- 17 M. Yabushita, K. Techikawara, H. Kobayashi, A. Fukuoka, A. Katz. Zeolite-Templated Carbon Catalysts for Adsorption and Hydrolysis of Cellulose-Derived Long-Chain Glucans: Effect of Post-Synthetic Surface Functionalization. *ACS Sustainable Chemistry & Engineering* **2016**, *4*, 6844–6851.
- 18 Y. Guo, A. Solovyov, N. A. Grosso-Giordano, S.-J. Hwang and A. Katz. Stabilizing Single Sites on Solid Supports: Robust Grafted Ti(IV)-Calixarene Olefin Epoxidation Catalysts via Surface Polymerization and Cross-Linking. *ACS Catal.*, **2016**, *6*, 7760–7768.
- 19 E. M. May, A. Solovyov, Y. Guo, A. Drapailo, Y. Matveev, V. Kalchenko, H. Nitsche, A. Katz. Unprecedented increase in affinity for Eu(III) over Am(III) through silica grafting of a carbamoylmethylphosphine oxide-calix[4]arene site. *European Journal of Inorganic Chemistry* **2016**, *29*, 4542–4545.
- 20 A. Charmot, A. Solovyov, A. Katz. Silica-supported phosphonic acids as thermally and oxidatively stable organic acid sites. *Chem. Mater.* **2016**, *28*, 6166–6177.
- 21 N. A. Grosso-Giordano, A. Solovyov, S.-J. Hwang and A. Katz. Effect of coordination environment in grafted single-site Ti-SiO₂ olefin epoxidation catalysis. *Top. Catal.*, **2016**, *59*, 1110–1122.
- 22 M. Yabushita, P. Li, H. Kobayashi, A. Fukuoka, O. K. Farha, A. Katz. Complete furanics-sugar separations with metal-organic framework NU-1000. *ChemComm* **2016**, *52*, 11791–11794.
- 23 M. Yabushita, P. Li, V. Bernales, H. Kobayashi, A. Fukuoka, L. Gagliardi, O. K. Farha, A. Katz. Unprecedented Selectivity in Molecular Recognition of Carbohydrates by a Metal–Organic Framework. *ChemComm* **2016**, *52*, 7094–7097.

Metal-ligand cooperativity - an Ir(III)–H and its Corresponding Ligand Protonated Tautomer

Jonathan L. Kuo and Karen I. Goldberg
University of Pennsylvania, Department of Chemistry

Presentation Abstract

Our DOE sponsored project explores strategies for facilitating the rarely observed oxygen atom transfer from a late metal peroxo (M-O₂) or hydroperoxo (M-OOH) complex to an olefin. Ultimately our goal is to combine this oxygen atom transfer step with two reactions that have been previously studied in our laboratory: insertion of molecular oxygen into late metal-hydride bonds and hydrogenolysis of late metal-hydroxide complexes. Working together, the three reactions would comprise a catalytic cycle for aerobic olefin epoxidation, a transformation of considerable industrial interest.

One particularly promising approach to promote oxygen atom transfer from a late metal peroxo or hydroperoxo is through metal-ligand cooperativity. Acidic functional groups on the ligand may assist in oxygen atom transfer via acid-base chemistry and/or hydrogen bonding interactions with the metal dioxygen or hydroperoxide moiety.

Square-planar Ir(I) complexes supported by a protic bispyrazolato-pincer ligand have been prepared. The pyrazolato protons were found to play both expected and unexpected roles in the reactivity of these compounds. Predictably, hydrogen bonding and deprotonation with bases were observed. In addition, transfer of the proton from the ligand to the metal to generate octahedral Ir(III)–hydride compounds was also observed. While isolable under particular reaction conditions, the Ir(III)–hydrides decompose by formal H• loss to produce Ir(II) dimers. An equilibrium between the Ir(III)–hydride and its ligand protonated Ir(I) tautomer is proposed as a key step in these reactions. Hydride abstraction from the Ir(III)-hydride complexes was also demonstrated and again involvement of the tautomer is invoked. These unanticipated pathways involving metal-ligand tautomerization provide new directions in our plan to develop aerobic late metal catalysts for olefin epoxidation.

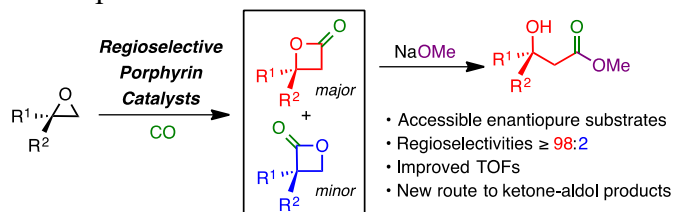
DE-SC0018057: Selective Oxidations Using Molecular Oxygen: Strategies for O-Atom Transfer to Olefins

New Advances in Catalysts for Heterocycle Functionalization

Geoffrey W. Coates
 Department of Chemistry and Chemical Biology, Cornell University

Presentation Abstract

In the current funding period, we reported a highly efficient and regioselective process for the carbonylation of 2,2-disubstituted epoxides using an octaethylporphyrin catalyst, and a tetraphenylporphyrin catalyst. Mechanistic experiments revealed that the turnover limiting step is epoxide ring-opening, an insight that facilitated the development of a faster system using weakly donating, ethereal solvents. With optimized reaction conditions in hand, a large range of alkyl epoxides was carbonylated regioselectively. These epoxide substrates can be prepared in enantiopure form to produce enantiopure ketone-aldol-type products traditionally accessed via Mukaiyama aldol reactions. This sought-after tertiary alcohol functionality remains an important component of various natural products and pharmaceuticals. To the best of our knowledge, this is the first report of a carbonylative approach to the production of difficult-to-access ketone-aldol products. Future work will investigate the properties of polymers derived from these monomers.



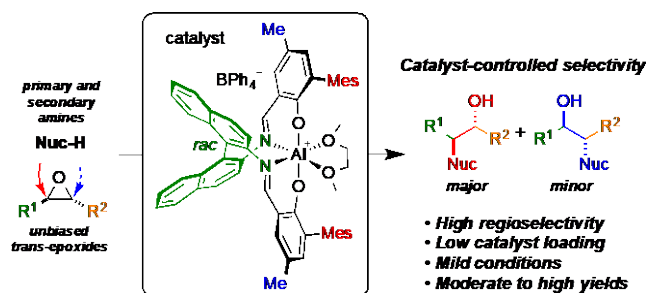
DE-FG02-05ER15687: Bimetallic Catalysts for Heterocycle Transformations: Energy Efficient Routes to Monomers and Chemical Feedstocks

Postdoc(s): Kristine Klimovica

Student(s): Aran Hubbell

RECENT PROGRESS

Lee, M.; Lamb, J. R.; Sanford, M. J.; LaPointe, A. M.; Coates, G. W. *Chem. Commun.* **2018**, 54, 12998–13001.



Publications Acknowledging this Grant in 2015-2018

(IV) Exclusively funded by this grant;

1. Hubbell, A. K.; LaPointe, A. M.; Lamb, J. R.; Coates, G. W. "Regioselective Carbonylation of 2,2-Disubstituted Epoxides: An Alternative Route to Ketone-Based Aldol Products" *J. Am. Chem. Soc.* **2019**, *141*, 2474–2480.
2. Lee, M.; Lamb, J. R.; Sanford, M. J.; LaPointe, A. M.; Coates, G. W. "Nucleophilic ring opening of *trans*-2,3-disubstituted epoxides to β -amino alcohols with catalyst-controlled regioselectivity" *Chem. Commun.* **2018**, *54*, 12998–13001.
3. John, A.; Miranda, M. O.; Ding, K.; Dereli, B.; Ortuño, M. A.; LaPointe, A. M.; Coates, G. W.; Cramer, C. J.; Tolman, W. B. "Nickel Catalysts for the Dehydrative Decarbonylation of Carboxylic Acids to Alkenes" *Organometallics*, **2016**, *35*, 2391–2400.
4. Dunn, E. W.; Lamb, J. L.; LaPointe, A. M.; Coates, G. W. "Carbonylation of Ethylene Oxide to β -Propiolactone: A Facile Route to Poly(3-Hydroxypropionate) and Acrylic Acid" *ACS Catalysis*, **2016**, *6*, 8219–8223.
5. Lamb, J. R.; Jung, Y.; Coates, G. W. "Meinwald-type rearrangement of monosubstituted epoxides to methyl ketones using an [Al porphyrin]⁺[Co(CO)₄]⁻ catalyst" *Org. Chem. Front.* **2015**, *2*, 346–349.
6. Kramer, J. W.; Rowley, J. M.; Coates, G. W. "Ring-Expanding Carbonylation of Epoxides" *Organic Reactions*, **2015**, *86*, 1–103.

(V) Jointly funded by this grant and other grants with leading intellectual contribution from this grant;

(VI) Jointly funded by this grant and other grants with relatively minor intellectual contribution from this grant.

Justin M. Notestein

Understanding oxide catalysis through collaborative science in the Institute for Catalysis in Energy Processes (ICEP)

Justin M Notestein

Chemical and Biological Engineering, Northwestern University, Evanston IL 60208

Presentation Abstract

Oxide-oxide interfaces and small oxide clusters are common motifs for catalytic active sites. Because these interfaces may not be stable thermodynamic minima, the active site structure, and thus catalytic activity, can be influenced by many parameters, including composition, catalyst precursors and pre-treatment history, and synthesis strategy. At one length scale, these tools are deployed to construct supports, reactant binding sites, or catalytic active sites. At one step further, various synthesis strategies can be used to construct tailored nanostructures around an active site, in order to effect multiple reactions in sequence or to control the local environment of an active site. This talk will discuss two research themes that are distributed across several research groups and are supported as part of the Institute for Catalysis in Energy Processes (ICEP) at Northwestern University. The first part will discuss advancements at the first length scale in understanding local oxide structures that give rise to catalytic active sites in selective oxidation. This work combines theory, spectroscopy, and experiment to interrogate metal oxide clusters across several materials sets, including supported oxides and metal organic frameworks. The second part will pull out to larger length scales to synthesize nanostructured environments at oxide-oxide and other interfaces around catalytic active sites. Significant changes to the observed catalytic activity and selectivity arise from these changes to the local environment, even while the active site itself remains largely unchanged. This talk will also highlight other work within ICEP, including two other posters given at this meeting.

This work was supported by the US Department of Energy, Office of Basic Energy Sciences, through a grant (DE-FG02-03ER15457) to the Institute for Catalysis for Energy Processes (ICEP) at Northwestern University.

DE-FG02-03ER15457: Institute for Catalysis in Energy Processes (ICEP)

PI: Justin M. Notestein¹ (lead)

Additional PIs: M. Bedzyk², L. Broadbelt¹, O. Farha³, J. Hupp³, H. Kung¹, M. Kung¹, L. Marks², T. Marks³, S. Nguyen³, K. Poepelmeier³, G. Schatz³, N. Schweitzer¹, R. Snurr¹, P. Stair³, E. Weitz³

Affiliations(s): Northwestern University, Center for Catalysis and Surface Science and

¹Department of Chemical and Biological Engineering or ²Department of Materials Science and Engineering or ³Department of Chemistry

RECENT PROGRESS

Introduction:

The overarching ICEP goal is targeted research to address the inhomogeneity challenge in heterogeneous catalysis. Our vision is to create catalysts with unique types and combinations of active sites and surface phases in an atomistically controlled fashion so that we can move beyond indirect evidence to definitive, hypothesis-driven science. ICEP directly addresses two of the Priority Research Directions (PRDs) to *Design catalysts beyond the binding site* to provide rationally designed catalytically active site environments and selectively control molecular access to the sites and to *Manipulate reaction networks in complex environments to steer catalytic transformations selectively* by positioning multiple catalytic functions in optimal surface architectures.

To achieve these advances, we combine novel catalytic structures and synthesis techniques with atomic-scale structural information and electronic properties. These are coupled to chemical and catalytic reaction experiments that are sensitive and instructive as to these properties. The ICEP team is organized into three complementary and interacting thrusts, as well as cross-cutting strengths in experimental and theoretical methods, and burgeoning efforts in data science and catalyst benchmarking. A few recent achievements of each thrust are briefly described below.

Thrust I: Metal-Oxide Nanoparticle System Design. This thrust designs metal nanoparticle - oxide support interactions using several strategies, to improve our understanding of these catalytic interfaces. This thrust combines ICEP expertise in *in-situ* spectroscopy, theory, integrated catalyst testing facilities, and synthesis of face-controlled supports and oxide overcoats to provide fundamental insight into supported metal catalysis. The thrust is divided into two broad projects, each of which are multi-investigator and use multimodal characterization to obtain the details of the metal/oxide interface structures, including XANES/EXAFS, EELS, aberration-corrected electron microscopy, XRD/XPS/XSW, and *ab-initio* DFT thermodynamics methods. Probe reactions that interrogate the metal-oxide interfaces include CO₂ reduction, CO oxidation, H₂/D₂ exchange, and regioselective arene hydrogenation. In addition to steady state measurements, reactions are followed with techniques such as SSITKA/FTIR. In this thrust, we use these tools to address in detail how the structural, chemical, and electronic details of the metal-oxide interface determine catalytic behavior. The two broad projects within this thrust are T1P1) control of metal

nanoparticle structure via nanocrystalline oxide supports and T1P2) building new oxide interfaces *around* supported metal nanoparticles to tune reactivity.

L. Marks and **Poepelmeier** have synthesized four different LnScO_3 particles suitable for use as catalyst supports. (Figure 1, marked) These rare earth perovskite scandates provide a smoothly varying set of lattice constants on which cube-cube epitaxy controls the structure of metal nanoparticles that are supported thereupon. This will be especially true for Au, Ag, Pd, and Pt nanoparticles that have similar lattice spacings. We expect that across this series there will be systematic and quantifiable structural and electronic changes in the metal nanoparticles, which in turn will lead to systematic changes in their catalytic behavior. Control of water partial pressure during synthesis was found to be essential to correct particle growth of the scandates. The oxide synthesis was reported on, as it is broadly useful inside and outside the catalysis community. Au has been deposited on these supports, characterized with microscopy, and in collaboration with **Notestein**, studies have begun to understand rates of CO oxidation over these materials. Separately, an *in situ* combined XPS/XSW is being brought online at the Advanced Photon Source by **Bedzyk** and is meeting internal progress milestones for startup. This apparatus will allow catalytic oxides and metals supported on crystalline surfaces to be interrogated with unprecedented spatial and oxidation state precision.

In completed studies carried out by **L. Marks**, **Poepelmeier**, **Stair**, **Bedzyk**, and **Schweitzer**, Pd supported on nanocrystalline SrTiO_3 was fully characterized and the oxide termination face (001 or 110) was determined to control the Pd particle morphology, and thus the rates of CO oxidation. The identity of the support facet was found to control the relative rates of nanoparticle nucleation and growth, ultimately controlling catalytic oxidation rates. Similarly, a separate report described changes in acrolein hydrogenation selectivity over Pt as the support – and resulting lattice strain in the Pt – moved across the series $\text{Ba}_x\text{Sr}_{1-x}\text{TiO}_3$.

In T1P2, TiO_2 and Al_2O_3 were deposited *over* supported Pt catalysts. In published work carried out by **Stair**, **L. Marks**, and **Poepelmeier**, acrolein hydrogenation was found to be more selective on the TiO_2 -overcoated material due to specific interactions with the acrolein. (Figure 2)

Through synthesis methods such as this, the buried metal-support interface (needed for metal nanoparticle stability) can be distinct and optimized independently from the three-phase boundary between support, metal, and the fluid phase, which might need to be optimized for interactions

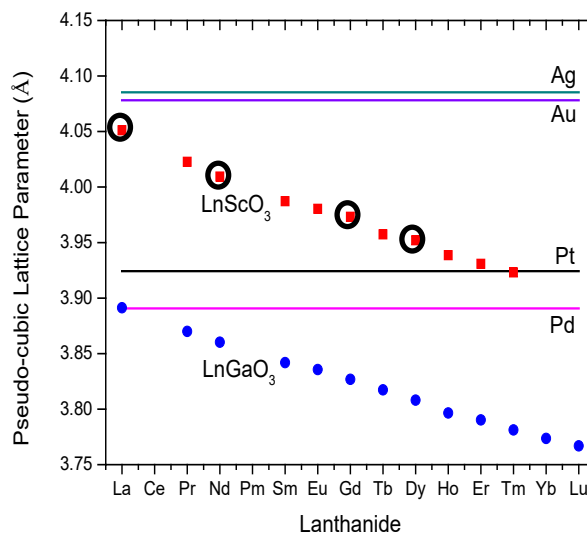


Figure 1. Plot of the pseudo-cubic lattice parameters of the LnScO_3 and LnGaO_3 series compared to the bulk lattice parameters of Ag, Au, Pd and Pt. Circled points have been synthesized and used as supports for Au nanoparticle growth. In those, testing has begun for CO oxidation.

with reactants. In continuing work by **Stair**, the rates and the mechanistic pathways (ER vs LHHW) for CO₂ hydrogenation appear to be controlled by the choice of overcoat in a similar system. Separately, **Notestein** and **Weitz** studied the formation and catalytic relevance of TiOx overcoats on supported Cu for CO₂ hydrogenation. In complementary efforts, **T. Marks, Stair**, and collaborators developed and reported on a controlled route to uniform supported Pd nanoparticles via a surface metal-organic precursor.

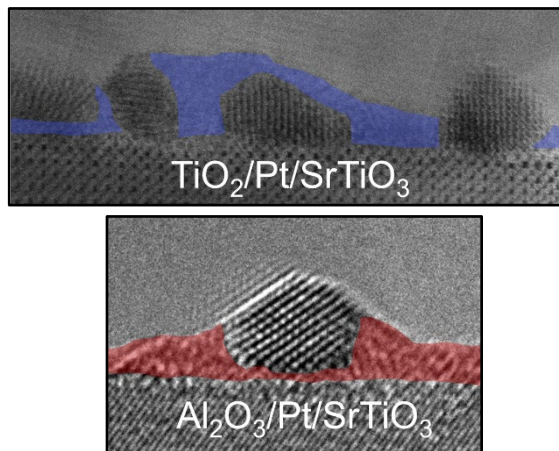


Figure 2. TiOx (blue) and AlOx (red) coatings deposited by ALD over Pt/SrTiO₃ catalysts. These and similar structures control rates and selectivities for CO₂ and acrolein hydrogenation, akin to natural SMSI.

Thrust II: Atom-Scale Control of Critical Oxide-Oxide Interfaces.

This thrust uses several strategies to control supported oxide active sites and the resulting catalytic processes. Structure-function relationships in supported oxides are challenging because of the complexity of the oxide-oxide interface, which leads to many potential active sites and pathways for activating oxidants. This complexity also renders challenging the development of effective design principles. Interconnected efforts in materials synthesis, kinetics, advanced characterization, and computational modeling allow ICEP researchers to make significant progress in understanding supported oxide structures. Multimodal characterization is similar to that of Thrust I. Within this Thrust, two projects are structured around addressing these fundamental catalysis science questions: T2P1 develops probes and materials to interrogate and synthesize active sites at the oxide-oxide interface with improved precision, and T2P2 utilizes oxide nanostructures to investigate oxide active site confinement and related effects.

Thrust II reported on several advances in understanding and synthesizing supported metal oxide catalysts in the last year. Within T2P1, **Notestein, Stair**, and **Snurr** completed a pair of reports on understanding supported CuOx for oxidative dehydrogenation. One finding was that Lewis acidic supports lead to greater pathway selectivity for cyclohexane ODH vs combustion. Support Lewis acidity was readily quantified via a spectrophotometric probe, rather than a textbook value. Lewis acidity was also a weaker predictor of activity and CuOx reducibility. Separately, the structure of CuOx on SiO₂ was examined as a function of loading. (Figure 3) **Stair, Snurr, Notestein**, and **Weitz** collaborated on several projects, including the use of ALD syntheses and characterization by time-resolved FITR to study cyclohexane and cyclohexene oxidation over VOx/CeO₂ and VOx/TiO₂ catalysts. **Farha** advanced the synthesis of alternative supports based on metal organic frameworks, including CeO₂-

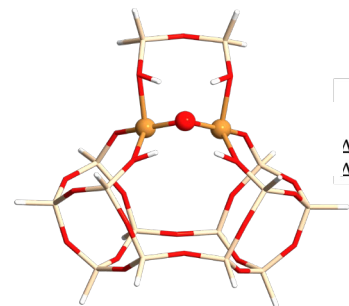


Figure 3. Experimental results indicated a single site for CuOx deposited on SiO₂. EXAFS, UV-vis, Raman and DFT revealed the ODH active site to be a dimer at a specific silica defect, even at very low surface coverage.^z

based clusters, which will be used in future ICEP activities. **Stair, Schatz, and van Duyne** completed a detailed understanding of the surprising complexity of TiO₂ deposition by atomic layer deposition, in which surface enhanced Raman spectroscopy (SERS) was employed to understand the structure of the surface species. Finally, **T. Marks** has expanded investigations into the use of carbon-supported Mo dioxo active sites derived from (dme)MoO₂Cl₂ for selective redox processes. Most recently, it was found that N-oxides and sulfoxides can be reduced catalytically by coupling it to alcohol oxidation.

Within T2P2, **Notestein and Stair** have studied the growth of SiO₂ overcoats around M/SiO₂ active sites and grafted organic species for controlling the heats of adsorption of reactants. In particular, they have demonstrated that certain template and oxide compositions can enhance the adsorption of epoxidation reactants at M/SiO₂ active sites, thus lowering the apparent activation barriers without changing the active site itself. Separately, they are advancing work on understanding the limits on small-molecule templated ALD by looking at selective re-adsorption at the created surface sites.

Thrust III: Understanding-Based Manipulation of Catalytic Environments at Controlled Length-Scales. Thrust III seeks to understand and design cooperativity and tandem reactions between multiple molecular catalytic centers, especially as controlled by a solid interface. It builds upon ICEP's unique synthetic capabilities for both small molecule catalysts and surfaces and draws inspiration from homogeneous organometallic and enzyme catalysis. As in the other two Thrusts, efforts are divided into two projects that share strategies. In T3P1, ICEP researchers study the interactions between molecular active sites and extended surfaces that play a co-catalytic or tandem catalytic role. In T3P2, multiple catalytic entities communicate through fluid-phase intermediates to effect selective oxidation.

In T3P1, **T. Marks** has reported on a supported, single-site organohafnium catalyst with high activity for olefin polymerization. (Figure 4) Hf has not generally been explored for single-site heterogeneous catalysis, and this system is well-positioned to lead to fundamental insights. Separately, work proceeds by **Kung** on developing Au/TiO_x inverse catalysts and siloxane-based cooperative catalysis. These findings are described in an additional abstract.

In T3P2, **Broadbelt and Kung** have reported on the full microkinetic model of selective cyclooctene epoxidation by soluble Au clusters. Building off this achievement, **Broadbelt** is developing more complex models in collaboration with **Notestein and Kung** to address multifunctional limonene selective epoxidation and coupled cyclooctene and ethyl benzene selective oxidation. The microkinetic modeling frameworks being developed for these reaction networks should prove to be broadly applicable for future ICEP projects. Separately, **Nguyen** has reported on the coupling of H₂O₂ synthesis over supported Pd with subsequent H₂O₂ utilization in epoxidation by a molecular Mo catalyst. Undesired crossover between the two catalytic cycles was prevented by entrapping the Pd active site within a microporous material. This system is also being expanded into other selective oxidation reactions such as sulfoxidation.

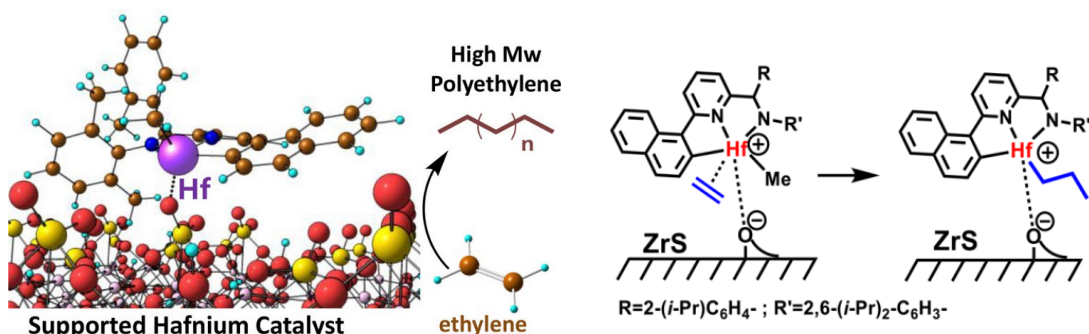


Figure 4. A new single-site supported d^0 organohafnium catalyst exhibits high activity for olefin polymerization/copolymerization while providing critical insights into the reaction mechanism. Hf is an unexplored element in single-site heterogeneous catalysis. This study is a key step in grafting industrially-relevant catalysts with precision control -- generating well-defined catalysts and enabling rational catalyst design and the first in-depth studies of structure-activity relationships over this class of catalyst.

Cross-Cut: New approaches to coupling Data Science, Theory, and Experiment. Efforts here are in direct service of the Catalysis Science PRD 5 and focus on integrating experimental and computational tools across the center and beginning to build experimental and computational data sets amenable to data science approaches.

At the interface of Thrust I and the Cross-cutting efforts, **Schweitzer** has begun routinely collecting H_2/D_2 exchange rates and rates of ethylene hydrogenation to evaluate all supported metal catalysts prepared within ICEP and elsewhere at Northwestern University. The goal is to routinely collect this information as metadata to feed into data science efforts. Likewise, at the interface of Thrust II and the Cross-cutting efforts, a SSITKA/FTIR apparatus was completed. Methanol oxidation is being routinely carried out by **Schweitzer** on oxide catalysts developed within ICEP as part of our benchmarking efforts.

Finally, in a pair of papers, a high-throughput quantum chemical workflow was developed by **Snurr** and **Notestein** to study oxidant activation and subsequent C-H bond activation in hundreds of supported oxide cluster catalysts. (Figure 5) Current efforts are aimed at applying these tools more broadly.

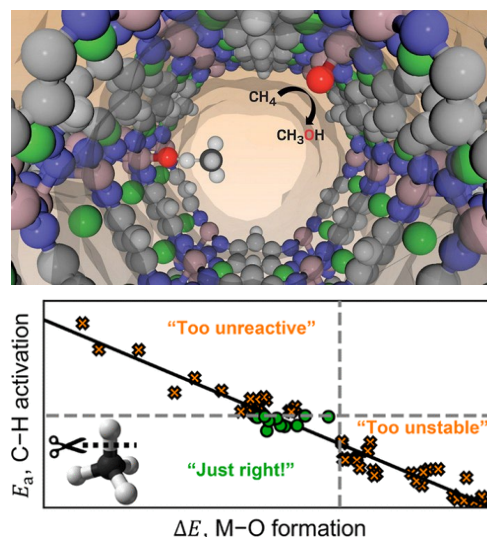


Figure 5. A high throughput quantum chemical workflow was developed to computationally study a class of supported oxide cluster catalysts, resulting in robust rules of thumb to screen large numbers of candidates for oxidizing strong C-H bonds.

Publications Acknowledging this Grant in 2015-2018 (submitted or published)

Sole Support from ICEP.

1. Ardagh, M. A.; Bo, Z. Y.; Nauert, S. L.; Notestein, J. M., Depositing SiO₂ on Al₂O₃: a Route to Tunable Brønsted Acid Catalysts. *ACS Catalysis* **2016**, *6* (9), 6156-6164.
2. Bachrach, M.; Marks, T. J.; Notestein, J. M., Understanding the Hydrodenitrogenation of Heteroaromatics on a Molecular Level. *ACS Catalysis* **2016**, *6* (3), 1455-1476.
3. Bhattacharyya, K.; Wu, W. Q.; Weitz, E.; Vijayan, B. K.; Gray, K. A., Probing Water and CO₂ Interactions at the Surface of Collapsed Titania Nanotubes Using IR Spectroscopy. *Molecules* **2015**, *20* (9), 15469-15487.
4. Brydon, R. R. O.; Broadbelt, L. J., Mechanistic modeling of the partial oxidation of 1,3-propanediol: Comparison of free-radical and concerted mechanisms. *Industrial & Engineering Chemistry Research* **2017**.
5. Brydon, R. R. O.; Peng, A. Y.; Qian, L. P.; Kung, H. H.; Broadbelt, L. J., Microkinetic Modeling of Homogeneous and Gold Nanoparticle-Catalyzed Oxidation of Cyclooctene. *Industrial & Engineering Chemistry Research* **2018**, *57* (14), 4832-4840.
6. Hu, L.; Marks, L. D.; Stair, P. C.; Poepelmeier, K. R., Synthesis and Shape Effect of Perovskite Polyhedron Nanocrystals: A Case of Uniform Supported Heterogeneous Pt Catalyst for CO Oxidation. **2019**, submitted.
7. Hu, L. H.; Wang, C. D.; Kennedy, R. M.; Marks, L. D.; Poepelmeier, K. R., The Role of Oleic Acid: From Synthesis to Assembly of Perovskite Nanocuboid Two-Dimensional Arrays. *Inorganic Chemistry* **2015**, *54* (3), 740-745.
8. Kung, H. H., New Materials for Catalysis and Energy Storage Devices. *Aiche J.* **2016**, *62* (10), 3518-3528.
9. Kwon, S.; Liao, P. L.; Stair, P. C.; Snurr, R. Q., Alkaline-earth metal-oxide overlayers on TiO₂: application toward CO₂ photoreduction. *Catalysis Science & Technology* **2016**, *6* (21), 7885-7895.
10. Liu, S.; Tan, J. M.; Gulec, A.; Crosby, L. A.; Drake, T. L.; Schweitzer, N. M.; Delferro, M.; Marks, L. D.; Marks, T. J.; Stair, P. C., Stabilizing Single-Atom and Small-Domain Platinum via Combining Organometallic Chemisorption and Atomic Layer Deposition. *Organometallics* **2017**, *36* (4), 818-828.
11. Mouat, A. R.; Mane, A. U.; Elam, J. W.; Delferro, M.; Marks, T. J.; Stair, P. C., Volatile Hexavalent Oxo-amidinate Complexes: Molybdenum and Tungsten Precursors for Atomic Layer Deposition. *Chemistry of Materials* **2016**, *28* (6), 1907-1919.
12. Nauert, S. L.; Schax, F.; Limberg, C.; Notestein, J. M., Cyclohexane oxidative dehydrogenation over copper oxide catalysts. *Journal of Catalysis* **2016**, *341*, 180-190.
13. Nauert, S. L.; Savereide, L.; Notestein, J. M., Role of Support Lewis Acid Strength in Copper-Oxide-Catalyzed Oxidative Dehydrogenation of Cyclohexane. *ACS Catalysis* **2018**, *8* (8), 7598-7607.
14. Paull, R. J.; Mansley, Z. R.; Ly, T.; Marks, L. D.; Poepelmeier, K. R., Synthesis of Gadolinium Scandate from a Hydroxide Hydrogel. *Inorganic Chemistry* **2018**, *57* (7), 4104-4108.
15. Qian, L. P.; Wang, Z.; Beletskiy, E. V.; Liu, J. Y.; dos Santos, H. J.; Li, T. H.; Rangel, M. D.; Kung, M. C.; Kung, H. H., Stable and solubilized active Au atom clusters for selective epoxidation of cis-cyclooctene with molecular oxygen. *Nat. Commun.* **2017**, *8*, 8.
16. Stalzer, M. M.; Delferro, M.; Marks, T. J., Supported Single-Site Organometallic Catalysts for the Synthesis of High-Performance Polyolefins. *Catalysis Letters* **2015**, *145* (1), 3-14.

17. Wang, C.; Hu, L.; Lin, Y.; Poeppelmeier, K. R.; Stair, P. C.; Marks, L. D., Controllable ALD synthesis of platinum nanoparticles by tuning different synthesis parameters. *J. Phys. D- Appl. Phys.* **2017**, *50* (41), 9.
 18. Wang, C.; Hu, L.; Poeppelmeier, K. R.; Stair, P. C.; Marks, L. D., Nucleation and growth process of atomic layer deposition platinum nanoparticles on strontium titanate nanocuboids. *Nanotechnology* **2017**, *28* (18), 8.
 19. Wu, W.; Ding, K.; Liu, J.; Drake, T.; Stair, P.; Weitz, E., Methanol Oxidation to Formate on ALD Prepared $\text{VO}_x/\text{Al}_2\text{O}_3$ Catalysts: A Mechanistic Study. *The Journal of Physical Chemistry* **2017**, 40.
 20. Wu, W.; Saveriede, L. M.; Notestein, J. M.; Weitz, E., In-situ IR spectroscopy as a Probe of Oxidation/Reduction of Ce in Nanostructured CeO_2 . *Applied Surface Science* **2018**, *445* (1 July 2018), 548-554.
 21. Wu, Y. Y.; Kung, H. H., Probing properties of the interfacial perimeter sites in $\text{TiO}_x/\text{Au}/\text{SiO}_2$ with 2-propanol decomposition. *Appl. Catal. A-Gen.* **2017**, *548*, 150-163.
- Some Joint Support, but Leading Intellectual Contributions from ICEP**
1. Bachrach, M.; Marks, T. J.; Notestein, J. M., C-N bond hydrogenolysis of aniline and cyclohexylamine over $\text{TaO}_x\text{-Al}_2\text{O}_3$. *New Journal of Chemistry* **2016**, (40), 6001-6004.
 2. Bae, J.; Samek, I. A.; Stair, P. C.; Snurr, R. Q., Investigation of the Hydrophobic Nature of Metal Oxide Surfaces Created by Atomic Layer Deposition. *Langmuir* **2019**, *35* (17), 5762-5769.
 3. Beletskiy, E. V.; Hou, X. L.; Shen, Z. L.; Gallagher, J. R.; Miller, J. T.; Wu, Y. Y.; Li, T. H.; Kung, M. C.; Kung, H. H., Supported Tetrahedral Oxo-Sn Catalyst: Single Site, Two Modes of Catalysis. *Journal of the American Chemical Society* **2016**, *138* (13), 4294-4297.
 4. Bo, Z.; S., A.; Ardagh, M. A.; Schweitzer, N. M.; Canlas, C. P.; Farha, O. K.; Notestein, J. M., Synthesis and Stabilization of Small Pt Nanoparticles on TiO_2 Partially Masked by SiO_2 . *Applied Catalysis A: General* **2017**.
 5. Bo, Z. Y.; Eaton, T. R.; Gallagher, J. R.; Canlas, C. P.; Miller, J. T.; Notestein, J. M., Size-Selective Synthesis and Stabilization of Small Silver Nanoparticles on TiO_2 Partially Masked by SiO_2 . *Chemistry of Materials* **2015**, *27* (4), 1269-1277.
 6. Chen, B.-R.; Crosby, L. A.; George, C.; Kennedy, R. M.; Schweitzer, N. M.; Wen, J.; Van Duyne, R. P.; Stair, P. C.; Poeppelmeier, K. R.; Marks, L. D.; Bedzyk, M. J., Morphology and CO Oxidation Activity of Pd Nanoparticles on SrTiO_3 Nanopolyhedra. *ACS Catalysis* **2018**, *8* (6), 4751-4760.
 7. Chen, B.-R.; George, C.; Lin, Y.; Hu, L.; Crosby, L. A.; Hu, X.; Stair, P. C.; Marks, L. D.; Poeppelmeier, K. R.; Van Duyne, R. P.; Bedzyk, M. J., Morphology and oxidation state of ALD-grown Pd nanoparticles on TiO_2 - and SrO -terminated SrTiO_3 nanocuboids. *Surface Science* **2016**, *648*, 291-298.
 8. Crosby, L.; Enterkin, J.; Rabuffetti, F.; Poeppelmeier, K.; Marks, L., Wulff shape of strontium titanate nanocuboids. *Surface Science* **2015**, *632*, L22-L25.
 9. Crosby, L. A.; Chen, B.-R.; Kennedy, R. M.; Wen, J.; Poeppelmeier, K. R.; Bedzyk, M. J.; Marks, L. D., All Roads Lead to TiO_2 : TiO_2 -Rich Surfaces of Barium and Strontium Titanate Prepared by Hydrothermal Synthesis *Chemistry of Materials* **2018**, *30* (3), 841-846.
 10. Crosby, L. A.; Kennedy, R. M.; Chen, B.-R.; Wen, J.; Poeppelmeier, K. R.; Bedzyk, M. J.; Marks, L. D., Complex surface structure of (110) terminated strontium titanate nanododecahedra. *Nanoscale* **2016**, *8* (37), 16606-16611.
 11. Ding, K.; Gulec, A.; Johnson, A. M.; Schweitzer, N. M.; Stucky, G. D.; Marks, L. D.; Stair,

- P. C., Identification of active sites in CO oxidation and water-gas shift over supported Pt catalysts. *Science* **2015**, *350* (6257), 189-192.
12. Ding, K. L.; Gulec, A.; Johnson, A. M.; Drake, T. L.; Wu, W. Q.; Lin, Y.; Weitz, E.; Marks, L. D.; Stair, P. C., Highly Efficient Activation, Regeneration, and Active Site Identification of Oxide-Based Olefin Metathesis Catalysts. *ACS Catalysis* **2016**, *6* (9), 5740-5746.
 13. Drake, T. L.; Stair, P. C., Vapor deposition of molybdenum oxide using bis(ethylbenzene) molybdenum and water. *Journal of Vacuum Science & Technology A* **2016**, *34* (5), 7.
 14. Drake, T. L.; Stair, P. C., Multiwavelength Raman Spectroscopic Characterization of Alumina-Supported Molybdenum Oxide Prepared by Vapor Deposition. *Topics in Catalysis* **2017**, *60* (19), 1618-1630.
 15. Engelhardt, C. M.; Kennedy, R. M.; Enterkin, J. A.; Poepelmeier, K. R.; Ellis, D. E.; Marshall, C. L.; C., S. P., Structure Sensitivity of Acrolein Hydrogenation by Platinum Nanoparticles on Ba_xSr_{1-x}TiO₃ Nanocuboids. *ChemCatChem* **2018**, *10* (3), 632-641.
 16. Feng, Z.; Ma, Q.; Lu, J.; Feng, H.; Elam, J. W.; Stair, P. C.; Bedzyk, M. J., Atomic-scale cation dynamics in a monolayer VO_x/Fe₂O₃ catalyst. *Rsc Advances* **2015**, *5* (126), 103834-103840.
 17. Galloway, J. M.; Kung, M.; Kung, H. H., Synthesis and characterization of bifunctional surfaces with tunable functional group pairs. *Surface Science* **2016**, *648*, 284-290.
 18. Grosso-Giordano, N. A.; Eaton, T. R.; Bo, Z. Y.; Yacob, S.; Yang, C. C.; Notestein, J. M., Silica support modifications to enhance Pd-catalyzed deoxygenation of stearic acid. *Applied Catalysis B-Environmental* **2016**, *192*, 93-100.
 19. Gu, W. X.; Stalzer, M. M.; Nicholas, C. P.; Bhattacharyya, A.; Motta, A.; Gallagher, J. R.; Zhang, G. H.; Miller, J. T.; Kobayashi, T.; Pruski, M.; Delferro, M.; Marks, T. J., Benzene Selectivity in Competitive Arene Hydrogenation: Effects of Single-Site Catalyst center dot center dot center dot Acidic Oxide Surface Binding Geometry. *Journal of the American Chemical Society* **2015**, *137* (21), 6770-6780.
 20. Hackler, R. A.; Kang, G.; Schatz, G. C.; Stair, P. C.; Van Duyne, R. P., Analysis of TiO₂ Atomic Layer Deposition Surface Chemistry and Evidence of Propene Oligomerization Using Surface-Enhanced Raman Spectroscopy. *Journal of the American Chemical Society* **2019**, *141* (1), 414-422.
 21. Hackler, R. A.; McAnally, M. O.; Schatz, G. C.; Stair, P. C.; Van Duyne, R. P., Identification of Dimeric Methylalumina Surface Species during Atomic Layer Deposition Using Operando Surface-Enhanced Raman Spectroscopy. *Journal of the American Chemical Society* **2017**, *139* (6), 2456-2463.
 22. Kennedy, R. M.; Crosby, L. A.; Ding, K.; Canlas, C. P.; Gulec, A.; Marks, L. D.; Elam, J. W.; Marshall, C. L.; Stair, P. C.; Poepelmeier, K. R., Artificial SMSI Created Via ALD: TiO₂ Overcoats Increase Pt-Catalyzed Acrolein Hydrogenation Selectivity. *Catalysis Letters* **2018**, *148* (8), 2223-2232.
 23. Klet, R. C.; Tussupbayev, S.; Borycz, J.; Gallagher, J. R.; Stalzer, M. M.; Miller, J. T.; Gagliardi, L.; Hupp, J. T.; Marks, T. J.; Cramer, C. J.; Delferro, M.; Farha, O. K., Single-Site Organozirconium Catalyst Embedded in a Metal-Organic Framework. *Journal of the American Chemical Society* **2015**, *137* (50), 15680-15683.
 24. Kwon, S.; Schweitzer, N. M.; Park, S.; Stair, P. C.; Snurr, R. Q., A kinetic study of vapor-phase cyclohexene epoxidation by H₂O₂ over mesoporous TS-1. *Journal of Catalysis* **2015**, *326*, 107-115.
 25. Li, J.; Liu, S.; Lohr, T. L.; Marks, T. J., Efficient Chemoselective Reduction of N-Oxides and

- Sulfoxides using a Carbon-Supported Molybdenum-Dioxo Catalyst and Alcohols. *Chem.Cat.Chem.* **2019**, in press.
26. Limvorapitux, R.; Chen, H. Y.; Mendonca, M. L.; Liu, M. T.; Snurr, R. Q.; Nguyen, S. T., Elucidating the mechanism of the UiO-66-catalyzed sulfide oxidation: activity and selectivity enhancements through changes in the node coordination environment and solvent. *Catalysis Science & Technology* **2019**, *9* (2), 327-335.
 27. Limvorapitux, R.; Chou, L. Y.; Young, A. P.; Tsung, C. K.; Nguyen, S. T., Coupling Molecular and Nanoparticle Catalysts on Single Metal-Organic Framework Microcrystals for the Tandem Reaction of H₂O₂ Generation and Selective Alkene Oxidation. *ACS Catalysis* **2017**, *7* (10), 6691-6698.
 28. Lin, Y.; McCarthy, J. A.; Poeppelmeier, K. R.; Marks, L. D., *Catalysis by Materials with Well-Defined Structures*. 1 ed.; Elsevier: Waltham, MA, 2015; p 392.
 29. Lin, Y. Y.; Wen, J. G.; Hu, L. H.; McCarthy, J. A.; Wang, S. C.; Poeppelmeier, K. R.; Marks, L. D., Electron-induced Ti-rich surface segregation on SrTiO₃ nanoparticles. *Micron* **2015**, *68*, 152-157.
 30. Lin, Y. Y.; Wu, Z. L.; Wen, J. G.; Ding, K. L.; Yang, X. Y.; Poeppelmeier, K. R.; Marks, L. D., Adhesion and Atomic Structures of Gold on Ceria Nanostructures: The Role of Surface Structure and Oxidation State of Ceria Supports. *Nano Letters* **2015**, *15* (8), 5375-5381.
 31. Liu, S.; Li, J.; Jurca, T.; Stair, P. C.; Lohr, T. L.; Marks, T. J., Efficient carbon-supported heterogeneous molybdenum-dioxo catalyst for chemoselective reductive carbonyl coupling. *Catal. Sci. Technol.* **2017**, (7), 2165-2169.
 32. Liu, S.; Tan, J. M.; Gulec, A.; Schweitzer, N. M.; Delferro, M.; Marks, L. D.; Stair, P. C.; Marks, T. J., Direct Synthesis of Low-Coordinate Pd Catalysts Supported on SiO₂ via Surface Organometallic Chemistry. *ACS Catalysis* **2016**, *6* (12), 8380-8388.
 33. Lohr, T. L.; Mouat, A. R.; Schweitzer, N. M.; Stair, P. C.; Delferro, M.; Marks, T. J., Efficient catalytic greenhouse gas-free hydrogen and aldehyde formation from aqueous alcohol solutions. *Energ Environ Sci* **2017**, *10* (7), 1558-1562.
 34. Marks, L. D.; Chiamonti, A. N.; Rahman, S. U.; Castell, M. R., Transition from Order to Configurational Disorder for Surface Reconstructions on SrTiO₃(111). *Physical Review Letters* **2015**, *114* (22), 6.
 35. Masango, S. S.; Hackler, R. A.; Henry, A. I.; McAnally, M. O.; Schatz, G. C.; Stair, P. C.; Van Duyne, R. P., Probing the Chemistry of Alumina Atomic Layer Deposition Using Operando Surface-Enhanced Raman Spectroscopy. *Journal of Physical Chemistry C* **2016**, *120* (7), 3822-3833.
 36. Masango, S. S.; Hackler, R. A.; Large, N.; Henry, A. I.; McAnally, M. O.; Schatz, G. C.; Stair, P. C.; Van Duyne, R. P., High-Resolution Distance Dependence Study of Surface-Enhanced Raman Scattering Enabled by Atomic Layer Deposition. *Nano Letters* **2016**, *16* (7), 4251-4259.
 37. McBriarty, M. E.; Campbell, G. P.; Drake, T. L.; Elam, J. W.; Stair, P. C.; Ellis, D. E.; Bedzyk, M. J., Atomic-Scale View of VO_x-WO_x Coreduction on the alpha-Al₂O₃ (0001) Surface. *Journal of Physical Chemistry C* **2015**, *119* (28), 16179-16187.
 38. Mouat, A. R.; George, C.; Kobayashi, T.; Pruski, M.; van Duyne, R. P.; Marks, T. J.; Stair, P. C., Highly Dispersed SiO_x/Al₂O₃ Catalysts Illuminate the Reactivity of Isolated Silanol Sites. *Angewandte Chemie-International Edition* **2015**, *54* (45), 13346-13351.
 39. Mouat, A. R.; Kobayashi, T.; Pruski, M.; Marks, T. J.; Stair, P. C., Direct Spectroscopic Evidence for Isolated Silanols in SiO_x/Al₂O₃ and Their Formation Mechanism. *Journal of*

- Physical Chemistry C* **2017**, *121* (11), 6060-6064.
40. Mouat, A. R.; Lohr, T. L.; Wegener, E. C.; Miller, J. T.; Delferro, M.; Stair, P. C.; Marks, T. J., Reactivity of a Carbon-Supported Single-Site Molybdenum Dioxo Catalyst for Biodiesel Synthesis. *ACS Catalysis* **2016**, *6* (10), 6762-6769.
 41. Mouat, A. R.; Whitford, C. L.; Chen, B.-R.; Liu, S. S.; Perras, F. A.; Pruski, M.; Bedzyk, M. J.; Delferro, M.; Stair, P. C.; Marks, T. J., Synthesis of Supported Pd⁰ Nanoparticles from a Single-Site Pd²⁺ Surface Complex by Alkene Reduction. *Chemistry of Materials* **2018**, *30* (3), 1032-1044.
 42. Nguyen, H. G. T.; Mao, L.; Peters, A. W.; Audu, C. O.; Brown, Z. J.; Farha, O. K.; Hupp, J. T.; Nguyen, S. T., Comparative study of titanium-functionalized UiO-66: support effect on the oxidation of cyclohexene using hydrogen peroxide. *Catalysis Science & Technology* **2015**, *5* (9), 4444-4451.
 43. Paull, R. J.; Ly, T.; Mansley, Z. R.; Poepfelmeier, K. R.; Marks, L. D., Controlled Two-Step Formation of Faceted Perovskite Rare-Earth Scandate Nanoparticles. *Crystals* **2019**, *9* (4).
 44. Peroff, A. G.; Weitz, E.; Van Duyne, R. P., Mechanistic studies of pyridinium electrochemistry: alternative chemical pathways in the presence of CO₂. *Phys Chem Chem Phys* **2016**, *18* (3), 1578-1586.
 45. Rosen, A. S.; Notestein, J. M.; Snurr, R. Q., Identifying promising metal-organic frameworks for heterogeneous catalysis via high-throughput periodic density functional theory. *Journal of Computational Chemistry* **2019**, *40* (12), 1305-1318.
 46. Rosen, A. S.; Notestein, J. M.; Snurr, R. Q., Structure-Activity Relationships That Identify Metal-Organic Framework Catalysts for Methane Activation. *ACS Catalysis* **2019**, *9* (4), 3576-3587.
 47. Samek, I. A.; Bobbitt, N. S.; Snurr, R. Q.; Stair, P. C., Interactions of VO_x Species with Amorphous TiO₂ Domains on ALD-Derived Alumina-Supported Materials. *The Journal of Physical Chemistry C* **2019**, *123* (13), 7988-7999.
 48. Stalzer, M. M.; Nicholas, C. P.; Bhattacharyya, A.; Motta, A.; Delferro, M.; Marks, T. J., Single-Face/All-cis Arene Hydrogenation by a Supported Single-Site d(0) Organozirconium Catalyst. *Angewandte Chemie-International Edition* **2016**, *55* (17), 5263-5267.
 49. Stoltz, S. E.; Ellis, D. E.; Bedzyk, M. J., Interface of Pt with SrTiO₃(001); A combined theoretical and experimental study. *Surface Science* **2015**, *633*, 8-16.
 50. Wang, C.; Koirala, P.; Stair, P. C.; Marks, L. D., ALD synthesis of platinum nanoparticles on single-crystal SrTiO₃ pretreated with wet chemical etching. *Applied Surface Science* **2017**, *422*, 661-665.
 51. Wang, S.; Xie, H.; Lin, Y.; Poepfelmeier, K. R.; Li, T.; Winans, R. E.; Cui, Y.; Ribeiro, F. H.; Canlas, C. P.; Elam, J. W.; Zhang, H.; Marshall, C. L., High Thermal Stability of La₂O₃- and CeO₂-Stabilized Tetragonal ZrO₂. *Inorganic Chemistry* **2016**, *55* (5), 2413-2420.
 52. Wang, Z.; Beletskiy, E. V.; Lee, S.; Hou, X. L.; Wu, Y. Y.; Li, T. H.; Kung, M. C.; Kung, H. H., Amine-functionalized siloxane oligomer facilitated synthesis of subnanometer colloidal Au particles. *J. Mater. Chem. A* **2015**, *3* (4), 1743-1751.
 53. Wang, Z.; Hou, X.; Wu, Y. Y.; Shen, J.; Li, T.; Fang, C.; Kung, M. C.; Kung, H. H., Controlled Generation of TiO_x-Au Interface Using Titanium Molecular Complex Bearing Pyridyl Anchors: Synthesis, Characterization and Catalysis. *Topics in Catalysis* **2018**, *61* (9), 800-809.
 54. Wen, J.; Lin, Y.; Sheng, H.; Wang, L.; Miller, D. J.; Wu, Z.; Poepfelmeier, K. R.; Marks, L. D., Atomic Surface Structures of Oxide Nanoparticles with Well-defined Shapes. *Microsc.*

Microanal. **2016**, *22* (Suppl 3) 360-361.

55. Zhang, J.; Motta, A.; Cesar, L. G.; Lohr, T. L.; Miller, J. T.; Gao, Y.; Marks, T. J., Molecular-level Control of Olefin Polymerization Reactions with Pyridylamido Hafnium on the Surface of Sulfated Alumina. **2019**, submitted.
56. Zhang, J. L.; Motta, A.; Gao, Y. S.; Stalzer, M. M.; Delferro, M.; Liu, B. P.; Lohr, T. L.; Marks, T. J., Cationic Pyridylamido Adsorbate on Bronsted Acidic Sulfated Zirconia: A Molecular Supported Organohafnium Catalyst for Olefin Homo- and Co-Polymerization. *ACS Catalysis* **2018**, *8* (6), 4893-4901.

Secondary Support from ICEP

1. Adhikari, D.; Miller, A. W.; Baik, M. H.; Nguyen, S. T., Intramolecular ring-opening from a CO₂-derived nucleophile as the origin of selectivity for 5-substituted oxazolidinone from the (salen)Cr-catalyzed aziridine + CO₂ coupling. *Chemical Science* **2015**, *6* (2), 1293-1300.
2. Ashwell, A. P.; Lin, W.; Hofman, M. S.; Yang, Y.; Ratner, M. A.; Koel, B. E.; Schatz, G. C., Hydrogenation of CO to Methanol on Ni(110) through Subsurface Hydrogen. *Journal of the American Chemical Society* **2017**, *139* (48), 17582-17589.
3. Beletskiy, E. V.; Wu, Y. Y.; Kung, M. C.; Kung, H. H., Addition of Sn-O'Pr across a C=C Bond: Unusual Insertion of an Alkene into a Main-Group-Metal-Alkoxide Bond. *Organometallics* **2016**, *35* (3), 301-302.
4. Cardinal, M. F.; Ende, E. V.; Hackler, R. A.; McAnally, M. O.; Stair, P. C.; Schatz, G. C.; Van Duyne, R. P., Expanding applications of SERS through versatile nanomaterials engineering. *Chem. Soc. Rev.* **2017**, *46* (13), 3886-3903.
5. Chen, Y.; Yang, L.; Wu, J.; Wang, G.; Huang, W.; Melkonyan, F. S.; Lu, Z.; Huang, Y.; Marks, T. J.; Facchetti, A., Performance, Morphology, and Charge Recombination Correlations in Ternary Squaraine Solar Cells. *Chemistry of Materials* **2018**, *30* (19), 6810-6820.
6. Cho, S.; Park, W.; Kim, H.; Jokisaari, J. R.; Roth, E. W.; Lee, S.; Klie, R. F.; Lee, B.; Kim, D.-H., Gallstone-Formation-Inspired Bimetallic Supra-nanostructures for Computed-Tomography-Image-Guided Radiation Therapy. *ACS Applied Nano Materials* **2018**, *1* (9), 4602-4611.
7. Cook, S.; Dylla, M. T.; Rosenberg, R. A.; Mansley, Z. R.; Snyder, G. J.; Marks, L. D.; Fong, D. D., The Vacancy-Induced Electronic Structure of the SrTiO_{3-δ} Surface. *Advanced Electronic Materials* **2019**, *5* (1), 1800460.
8. Du, M.; Agrawal, A. M.; Chakraborty, S.; Garibay, S. J.; Limvorapitux, R.; Choi, B.; Madrahimov, S. T.; Nguyen, S. T., Matching the Activity of Homogeneous Sulfonic Acids: The Fructose-to-HMF Conversion Catalyzed by Hierarchically Porous Sulfonic-Acid-Functionalized Porous Organic Polymer (POP) Catalysts. *ACS Sustainable Chemistry & Engineering* **2019**, *7* (9), 8126-8135.
9. Howarth, A. J.; Liu, Y. Y.; Li, P.; Li, Z. Y.; Wang, T. C.; Hupp, J.; Farha, O. K., Chemical, thermal and mechanical stabilities of metal-organic frameworks. *Nat Rev Mater* **2016**, *1* (3).
10. Islamoglu, T.; Goswami, S.; Li, Z. Y.; Howarth, A. J.; Farha, O. K.; Hupp, J. T., Postsynthetic Tuning of Metal-Organic Frameworks for Targeted Applications. *Accounts Chem. Res.* **2017**, *50* (4), 805-813.
11. Jiang, X. F.; Huang, H.; Chai, Y. F.; Lohr, T. L.; Yu, S. Y.; Lai, W. Z.; Pan, Y. J.; Delferro, M.; Marks, T. J., Hydrolytic cleavage of both CS₂ carbon-sulfur bonds by multinuclear Pd(II) complexes at room temperature. *Nature Chemistry* **2017**, *9* (2), 188-193.
12. Jurca, T.; Peters, A. W.; Mouat, A. R.; Farha, O. K.; Hupp, J. T.; Lohr, T. L.; Delferro, M.;

- Marks, T. J., Second-generation hexavalent molybdenum oxo-amidinate precursors for atomic layer deposition. *Dalton Transactions* **2017**, 46 (4), 1172-1178.
13. Karagiari, O.; Vermeulen, N. A.; Klet, R. C.; Wang, T. C.; Moghadam, P. Z.; Al-Juaid, S. S.; Stoddart, J. F.; Hupp, J. T.; Farha, O. K., Functionalized Defects through Solvent-Assisted Linker Exchange: Synthesis, Characterization, and Partial Postsynthesis Elaboration of a Metal-Organic Framework Containing Free Carboxylic Acid Moieties. *Inorganic Chemistry* **2015**, 54 (4), 1785-1790.
 14. Kwon, G.; Jang, H.; Lee, J.-S.; Mane, A.; Mandia, D. J.; Soltau, S. R.; Utschig, L. M.; Martinson, A. B. F.; Tiede, D. M.; Kim, H.; Kim, J., Resolution of Electronic and Structural Factors Underlying Oxygen-Evolving Performance in Amorphous Cobalt Oxide Catalysts. *Journal of the American Chemical Society* **2018**, 140 (34), 10710-10720.
 15. Lin, W.; Schatz, G. C., Mechanisms of Formaldehyde and C₂ Formation from Methylene Reacting with CO₂ Adsorbed on Ni(110). *The Journal of Physical Chemistry C* **2018**, 122 (25), 13827-13833.
 16. McBriarty, M. E.; Ellis, D. E., Cation synergies affect ammonia adsorption over VO_x and (V,W)O_x dispersed on α-Al₂O₃ (0001) and α-Fe₂O₃ (0001). *Surface Science* **2016**, 651, 41-50.
 17. McCullough, L. R.; Cheng, E. S.; Gosavi, A. A.; Kilos, B. A.; Barton, D. G.; Weitz, E.; Kung, H. H.; Notestein, J. M., Gas phase acceptorless dehydrogenative coupling of ethanol over bulk MoS₂ and spectroscopic measurement of structural disorder. *Journal of Catalysis* **2018**, 366, 159-166.
 18. Moreau, L. M.; Jones, M. R.; Roth, E. W.; Wu, J.; Kewalramani, S.; O'Brien, M. N.; Chen, B.-R.; Mirkin, C. A.; Bedzyk, M. J., The Role of Trace Ag in the Synthesis of Au Nanorods. *Nanoscale* **2019**, in press.
 19. Prieto-Centurion, D.; Eaton, T. R.; Roberts, C. A.; Fanson, P. T.; Notestein, J. M., Catalytic reduction of NO with H₂ over redox-cycling Fe on CeO₂. *Applied Catalysis B-Environmental* **2015**, 168, 68-76.
 20. Rimoldi, M.; Howarth, A. J.; DeStefano, M. R.; Lin, L.; Goswami, S.; Li, P.; Hupp, J. T.; Farha, O. K., Catalytic Zirconium/Hafnium-Based Metal-Organic Frameworks. *ACS Catalysis* **2017**, 7 (2), 997-1014.
 21. Savereide, L.; Nauert, S. L.; Roberts, C. A.; Notestein, J. M., The effect of support morphology on CoO_x/CeO₂ catalysts for the reduction of NO by CO. *Journal of Catalysis* **2018**, 366, 150-158.
 22. Wang, Z.; Loon, A.; Subramanian, A.; Gerhold, S.; McDermott, E.; Enterkin, J. A.; Hieckel, M.; Russell, B. C.; Green, R. J.; Moewes, A.; Guo, J.; Blaha, P.; Castell, M. R.; Diebold, U.; Marks, L. D., Transition from Reconstruction toward Thin Film on the (110) Surface of Strontium Titanate. *Nano Letters* **2016**, 16 (4), 2407-2412.
 23. Yacob, S.; Kilos, B. A.; Barton, D. G.; Notestein, J. M., Vapor phase ethanol carbonylation over Rh supported on zeolite 13X. *Applied Catalysis A: General* **2016**, 520, 122-131.
 24. Yacob, S.; Park, S.; Kilos, B. A.; Barton, D. G.; Notestein, J. M., Vapor-phase ethanol carbonylation with heteropolyacid-supported Rh. *Journal of Catalysis* **2015**, 325, 1-8.
 25. Zhang, X.; Yan, P.; Zhao, B.; Liu, K.; Kung, M. C.; Kung, H. H.; Chen, S.; Zhang, Z. C., Selective Hydrodeoxygenation of Guaiacol to Phenolics by Ni/Anatase TiO₂ Catalyst Formed by Cross-Surface Migration of Ni and TiO₂. *ACS Catalysis* **2019**, 9 (4), 3551-3563.

Organofunctionalized Surfaces for Controlling the Behavior of Interfacial Catalysts

Igor I. Slowing, Marek Pruski, Long Qi, Aaron D. Sadow
U.S. DOE Ames Laboratory and Iowa State University, Ames, IA

Presentation Abstract

The collaborative program of the Ames Laboratory combines expertise in homogeneous and heterogeneous catalysis, reaction kinetics and solid-state (SS) NMR to investigate the complex interactions between reactants, active sites and local environment in catalytic conversions at solid-liquid interfaces. The research is aimed at understanding mechanisms of interfacial reactions to enable the design of hierarchical catalysts with molecular-scale control of activity. Key to the design is the pursuit of low temperature and low energy pathways that take advantage of second sphere non-covalent interactions to enable efficient and selective transformations of complex feedstocks. In this presentation we will discuss the surface modification of mesoporous silica nanoparticles with organic moieties including their grafting kinetics, spatial distribution, conformational mobility, and interactions with the surface. We will present hierarchical catalysts where the surface groups act either as organocatalysts in single and tandem conversions, as modulators of the activity of supported catalysts, or as selective adsorbents that enable catalytic separations of complex reaction feeds. We will examine experimental evidence that suggest cooperativity between surface species, solvent, and active sites, and will discuss how surface groups can regulate the dielectric properties at the solid-liquid interface and thereby affect catalyst behavior.

References:

1. Singappuli-Arachchige, D.; Kobayashi, T.; Wang, Z.; Burkhov, S.J.; Smith, E.A.; Pruski, M.; Slowing, I.I. "Interfacial Control of Catalytic Activity in the Aldol Condensation: Combining the Effects of Hydrophobic Environments and Water" *ACS Catal.* **2019**, *9*, 5574-5582.
2. Kobayashi, T.; Singappuli, D.; Wang, Z.; Slowing, I. I.; Pruski, M. "Spatial Distribution of Organic Functional Groups Supported on Mesoporous Silica Nanoparticles: A Study by Conventional and DNP-Enhanced ^{29}Si Solid-State NMR" *Phys. Chem. Chem. Phys.* **2017**, *19*, 1781-1789.
3. Singappuli-Arachchige, D.; Manzano, J.S.; Sherman, L.M.; Slowing, I.I. "Polarity Control at Interfaces: Quantifying Pseudo-solvent Effects in Nano-confined Systems" *ChemPhysChem* **2016**, *17*, 2982-2986.
4. de Lima Batista, A.P.; Zahariev, F.; Slowing, I.I.; Braga, A.A.C.; Ornellas, F.R.; Gordon, M.S. "Silanol-Assisted Carbinolamine Formation in an Amine-Functionalized Mesoporous Silica Surface: Theoretical Investigation by Fragmentation Methods" *J. Chem. Phys. B.* **2016**, *120*, 1660-1669.

Olefination and the Catalytic Monoborylation of Methane by Combining Synthesis, Theory and High-Throughput Optimizations.

Dieter Sorsche, Pavel Zatsepin, and Daniel J. Mindiola*
Department of Chemistry, University of Pennsylvania, Philadelphia, PA 19104

Presentation Abstract

We show how $\text{Cp}^*(\text{Me}_3\text{P})\text{Ir}(\text{CH}_3)(\text{OTf})$, a complex known to reversibly activate CH_4 and other hydrocarbons under mild conditions, reacts with the phosphorus ylide $\text{H}_2\text{C}=\text{P}(\text{Ph})_3$ in THF to afford two major species $[\text{Cp}^*(\text{Me}_3\text{P})(\text{Ph}_3\text{P})\text{Ir}(\text{CH}_2\text{CH}_3)]^+[\text{OTf}]^-$ and $[\text{Cp}^*(\text{Me}_3\text{P})\text{Ir}(\text{H})(\eta^2\text{-CH}_2\text{CH}_2)]^+[\text{OTf}]^-$. Insertion of the ylide methylene group can also occur with $\text{Cp}^*(\text{Me}_3\text{P})\text{Ir}(\text{Ph})(\text{OTf})$ to afford the benzyl $[\text{Cp}^*(\text{Me}_3\text{P})(\text{Ph}_3\text{P})\text{Ir}(\text{CH}_2\text{Ph})]^+[\text{OTf}]^-$ and theoretical studies suggest the intermediacy of an $\text{Ir}(\text{III})=\text{CH}_2$ species after the C-H activation of the alkane and prior to the C-C bond forming step. In addition to this work we also show case progress in the optimization of a catalytic reaction involving the monoborylation of methane by the pre-catalyst $[(\text{COD})\text{Ir}(\text{Cl})_2]_2$ as well as the mono-nuclear phosphine precursors $(\text{COD})(\text{dmpe})\text{Ir}(\text{X})$ ($\text{X}^- = \text{Cl}, \text{CH}_3$). A combination of synthesis, high-throughput and high-pressure screening methods, as well as theory have allowed us to understand the mechanism as well as improve TON and selectivity in the borylation of this parent hydrocarbon.

DEFG02-07ER15893: Synthesis and Exploratory Catalysis of 3d Metals: Atom and Group-Transfer Reactions and the Activation and Functionalization of Small Molecules Including Greenhouse Gases

PI: Lead PI(s) Name(s) (*include only if different from above*)

Postdoc(s): Dieter Sorsche, Maria E. Carroll,

Student(s): Pavel Zatsepin, Lauren N. Grant

Affiliations(s): (*include only if different from above*)

RECENT PROGRESS

Optimizations of a catalyst for the monoborylation of methane. Using high-pressure and high-throughput screening methods we have improved the catalytic monoborylation of methane from 100 to 170 TON with 9:1 selectivity for monoborylation versus diborylation of the parent alkane (Figure 1). Likewise, we have found other solvents with higher-boiling points such as cyclooctane and decaline to be also suitable media for catalytic borylation, and ideally for future kinetic studies. More soluble and well-defined Ir(I) pre-catalysts such as $(\text{COD})(\text{dmpe})\text{Ir}(\text{X})$ ($\text{X}^- = \text{Cl}, \text{CH}_3$) (Figure 1) were also discovered to be effective in the catalytic monoborylation. It was also established that conversion was no higher than 50% due to deactivation of the catalytic via the formation and subsequent accumulation of HBpin. Instead of two cycles being involved in the borylation catalysis (via B_2pin_2 and HBpin), only one is active with HBpin being a catalyst poison and gradually shutting down the catalyst via formation of polyhydrides (Scheme 1). In fact, control reactions established the catalyst to gradually convert to the inactive polyhydride dimer

$[(\text{dmpe})\text{IrH}(\text{Bpin})]_2(\text{COD})_2(\text{H})_2$. It was also found that the chelating and phenylene bridged phosphine $\text{Me}_2\text{PC}_6\text{H}_4\text{PMe}_2$ was also an effective ligand scaffold for catalysis when combined with $[(\text{COD})\text{Ir}(\text{COD})\text{Cl}]_2$. Theoretical studies point to the polarizability of the phosphines being key to lowering the rate-determining step (RDS), which was found to be the oxidative-addition of the C-H bond methane. The boryl group also participates in the RDS by promoting heterolytic splitting of C-H bond enroute to an oxidative-addition involving a transient Ir(V) species. Lastly, preliminary studies in collaboration with Prof. Clark Landis using WiHP-NMR spectroscopy with a gas circulation pump, using precatalyst $(\text{COD})(\text{dmpe})\text{Ir}(\text{CH}_3)$ in decaline at 120°C over several hours reveal the gradual formation H_3CBpin and HBpin along with the consumption of the precatalyst and formation of new species. A background, and summary of prior and current results will be presented and discussed.

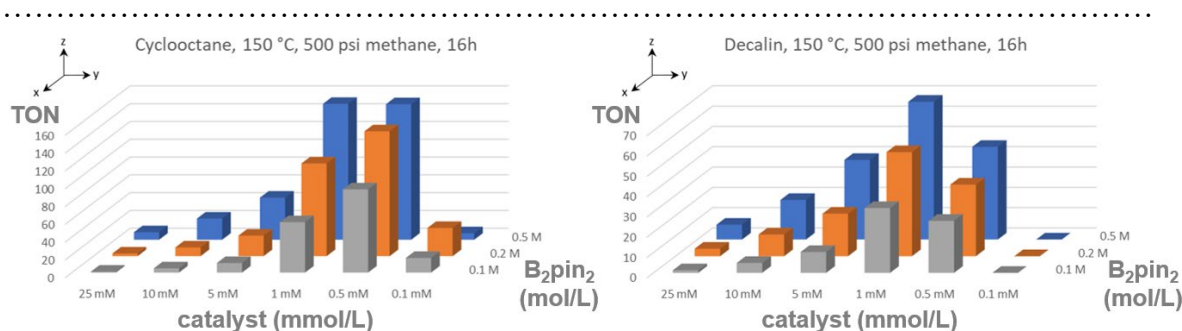


Figure 1. Catalytic reactions using different solvents (cyclooctane, left; decaline, right) along TON, catalyst and B_2pin_2 loadings.

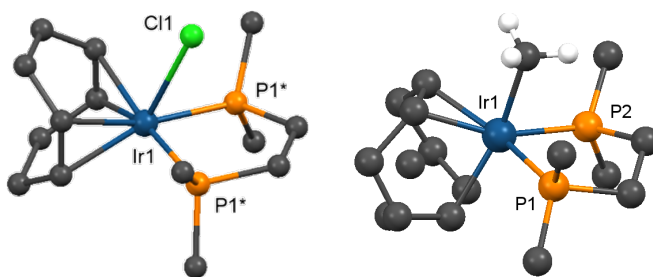
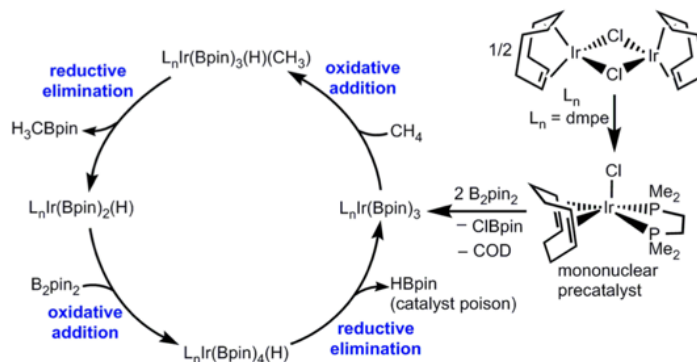


Figure 2. Solid-state structures of the pre-catalyst complexes $(\text{COD})(\text{dmpe})\text{Ir}(\text{Cl})$ (left) and $(\text{COD})(\text{dmpe})\text{Ir}(\text{CH}_3)$ (right).



Scheme 1. Proposed catalytic cycle for the monoborylation of methane using B_2pin_2 .

Publications Acknowledging this Grant in 2015-2018

Please classify your publications into three categories according to the source of support for the work published:

(I) Exclusively funded by this grant;

1. Grant, L. N.; Krzystek, J.; Pinter, B.; Telser, J.; Grützmacher, H.; Mindiola, D. J. Finding a Soft Spot for Vanadium: A P-Bound OCP Ligand. Manuscript accepted to *Chem. Commun.* **2019**.
2. Catalytic Borylation of Methane: Combining Computational and High-Throughput Screening Approaches to Discover A New Catalyst *In Alkane Functionalization* (Ed. Pombeiro, A. J. L.), J. Wiley publisher. Zatsepin, P.; Sorsche, D.; Ahn, S.; Baik, M.-H.; Mindiola, D. J. *In press*.
3. Grant, L. N.; Pinter, B.; Gu, J.; Mindiola, D. J. A Molecular Zirconium Nitride Super Base from a Mononuclear Parent Imide. *J. Am. Chem. Soc.* **2018**, *140*, 17399-17403.
4. Sorsche, D.; Miehllich, M.; Zolnhofer, E. M.; Carroll, P. J.; Manor, B. C.; Meyer, K.; Mindiola, D. J. Metal-Ligand Cooperativity Promoting Sulfur-Atom Transfer in Ferrous Complexes and Isolation of a Sulfurmethylenephosphorane Adduct. *Inorg. Chem.* **2018**, *57*, 11552-11559.
5. Grant, L. N.; Balazs Pinter, B.; Carroll, P. J.; Grützmacher, H.; Mindiola, D. J. A Scandium Stabilized Diisophosphaethynolate Ligand, [OCPPCO]⁴⁻. *Angew. Chem. Int. Ed.* **2018**, *57*, 1049-1052.
6. Grant, L. N.; Miehllich, M.; Meyer, K.; and Mindiola, D. J. Arrested Disproportionation in Trivalent, Mononuclear, and Non-Metallocene Complexes of Zr(III) and Hf(III). *Chem. Commun.* **2018**, *54*, 2052-2055.
7. Grant, L. N.; Pinter, B.; Carroll, P. J.; Suter, R.; Grützmacher, H.; Mindiola, D. J. A Planar Ti₂P₂ Core Assembled by Reductive Decarbonylation of –O–C≡P and P–P Radical Coupling. *Chem. - A Eur. J.* **2017**, *23*, 6272-6276 (hot paper).
8. Grant, L. N.; Ahn, S.; Manor, B. C.; Baik, M.-H.; Mindiola, D. J. Structural Elucidation of a Mononuclear Titanium Methylidene. *Chem. Commun.* (front art cover for issue) **2017**, *53*, 3415-3417.
9. Grant, L. N.; Pinter, B.; Kurogi, T.; Carroll, M. E.; Wu, G.; Carroll, P. J.; Mindiola, D. J. Molecular Titanium Nitrides. Nucleophiles Unleashed. *Chem. Sci.* **2017**, *8*, 1209-1224.
10. Carroll, M. E.; Grant, L. N.; Carroll, P. J.; Mindiola, D. J. An Unusual Cobalt Azide Adduct that Produces a Nitrene Species for C-H Insertion Chemistry. *Inorg. Chem.* **2016**, *55*, 7997-8002.
11. Carroll, M. E.; Pinter, B.; Carroll, P. J.; Mindiola, D. J. A Terminally Bound Nitrido Ligand on Titanium. *J. Am. Chem. Soc.* **2015**, *137*, 8884-8887.
12. Hounjet, L. J.; Adhikari, D.; Pink, M.; Carroll, P. J.; Mindiola, D. J. Synthesis of an Iron(II) Ethyl Complex Accompanied by Formation of an Unusual Dinitrogen-Ligated Iron(I) Hydride. *Zeitschrift für Anorganische und Allgemeine Chemie (ZAAC)*, **2015**, *641*, 45-48 in the special issue "Reactive Nitrogen-Containing Species: Generation, Characterization and Functionalization".
13. Thompson, R.; Tran, B. L.; Chen, C.-H.; Pink, M.; Baik, M.-H.; Mindiola, D. J.

Addition of Si-H and B-H Bonds and Redox Reactivity Involving Low-Coordinate Nitrido Vanadium Complexes. *Inorg. Chem.* **2015**, *54*, 3068-3077.

(VII) *Jointly funded by this grant and other grants with leading intellectual contribution from this grant;*

1. Zatsepin, P.; Ahn, S.; Pudasaini, B.; Gau, M. R.; Baik, M.-H.; Mindiola, D. J. Methane Conversion to Ethylene Using an Iridium Complex and Phosphorus Ylide as a Methylene Transfer Reagent. *Chem. Commun.* **2019**, *55*, 1927-1930.
2. Ahn, S.; Sorsche, D.; Ryu, H.; Berritt, S.; Gau, M. R.; Mindiola, D. J.; Baik, M.-H. Rational Design of a Catalyst for the Selective Monoborylation of Methane. *ACS Catal.* **2018**, *8*, 10021-10031.
3. Mullane, K. C.; Ryu, H.; Cheisson, T.; Grant, L. N.; Park, J. Y.; Manor, B. C.; Carroll, P. J.; Baik, M.-H.; Mindiola, D. J.; Schelter, E. J. C-H Bond Addition Across a Transient Uranium Nitrido and Formation of a Parent Uranium Imido Complex. *J. Am. Chem. Soc.* **2018**, *140*, 11335-11340.
4. Fortier, S.; Wijeratne, G. B.; Chen, C.-H.; Zolnhofer, E. M.; Carroll, P. J.; Grant, L. N.; Meyer, K.; Krzystek, J.; Ozarowski, A.; Jackson, T. A.; Mindiola, D. J.; Telser, J. Electronic Structure and Reactivity of a Well-Defined Mono-nuclear Complex of Ti(II). *Inorg. Chem.* **2015**, *54*, 10380-10397.
5. Pinter, B.; Kyle T. Smith, K. T.; Kamitani, M.; Zolnhofer, E. M.; Tran, B. L.; Fortier, S.; Pink, M.; Wu, G.; Manor, B. C.; Meyer, K.; Baik, M.-H.; Mindiola, D. J. Cyclo-P₃ Complexes of Vanadium: Redox Properties and the Origin of the ³¹P NMR Spectroscopic Chemical Shift. *J. Am. Chem. Soc.* **2015**, *137*, 15247-15261.

Bimetallic Catalysts for Bio-oil Upgrading: A Multi-Scale Modeling Approach

Jacob Bray^a, Neeru Chaudhary^a, Alyssa J. R. Hensley^{a,b}, Megan Rose Hawkins^a, Junnan Shangguan^b, Yong Wang^{a,c}, Cathy Chin^b, Di Wu^a, Jean-Sabin McEwen^{a,c*}

^a*Washington State University, Pullman, WA 99164*

^b*University of Toronto, Toronto, ON M5P 2G8*

^c*Pacific Northwest National Laboratory, Richland, WA 99352*

Presentation Abstract

One aspect crucial to the design of effective catalysts is knowledge of the elementary reaction mechanism, which is difficult to divine from experiment alone. However, first principle modeling techniques can be used to address this knowledge gap. An area currently in need of such fundamental insight is the hydrodeoxygenation (HDO) of bio-oil to create useable biofuels, where precious metal promoted Fe catalysts are effective at selective HDO but the role of the promoter remains elusive. As precious metals increase catalyst cost, the promoter's role in facilitating HDO must be further understood to minimize the use of these costly metals and identify precious metal alternatives. In this work, we predict the cooperative effects and concerted behavior of several facets at the surface of a single Fe catalytic grain when it is exposed to oxygen, hydrogen and oxygenated aromatic compounds. We model these effects on several-crystal Fe facets using a combination of density functional theory (DFT) calculations, and cluster expansion techniques, which can then be compared to the experimental results.

Results indicate that the clustering tendency of precious metal promoters is predictive of their ability to promote HDO. For instance, ground state configurations of Pd over Fe(100) are band-like structures while Rh is more dispersed, protecting more of the Fe surface. These results align closely with experimental results highlighting the superior performance of Rh over Pd. We also investigate C as an earth-abundant alternative to precious metals in the form of Fe carbide, which has a similar HDO activity to metallic Fe surfaces but decreases the selectivity toward phenolic C-O bond cleavage, hinting at a reduction in surface oxophilicity, thus minimizing oxidative deactivation. Finally, we investigate the HDO of phenol and guaiacol under the aqueous environment present in bio-oil. We demonstrate that protic solvents such as water can ionize hydrogen adatoms (H^*), generating protons (H^+) at the solid-liquid interface, which alters the kinetically relevant HDO paths. Our study shows that, by choosing an appropriate pair of solvent and metal, we can manipulate the charge of the reactive hydrogen species and in turn the HDO reactivity and selectivity towards the desired C-O bond cleavage.

DE-SC0014560: Developing Multi-Scale Models for the Effective Design of Bimetallic Catalysts for the Targeted Refinement of Bio-oil to Usable Biofuels

Student(s): Jacob Bray, Neeru Chaudhary, Megan Rose Hawkins

RECENT PROGRESS

Specific Aim 1: Determine the chemical nature of the synergetic properties between the two metals of a bimetallic catalyst and the lateral interactions between the phenolic compounds.

Coverage behavior is being characterized for Pd, Pt, Ru, and Rh promoters alloyed into Fe(100) using lattice gas cluster expansion (LGCE) methods combined with Monte Carlo (MC) approaches. The LGCEs for Pd and Ru are complete, while the LGCEs for Pt and Rh are in development. A MC code is under development within the group and is currently capable of determining equilibrium promoter distributions based on LGCE input. Figure 1 shows the output from the LGCE+MC model for Ru/Fe(100). Figure 1a shows the Ru clusters that contribute most strongly to the ground state configuration of Ru/Fe(100) at 1.0 ML. Figure 1b shows the equilibrium MC configuration at 1.0 ML, forming band-like arrangements, stabilized by the presence of the attractive Ru clusters. This equilibrium MC structure is in good agreement with the 1.0 ML ground state configuration for Ru determined by sampling the configuration space via DFT. Characterization of the precious metal's clustering tendencies is expected to result in a predictive descriptor of the precious metal's catalytic activity observed experimentally.[1]

Additionally, preliminary LGCE models have characterized the lateral interactions of carbon on the Fe(100) facet: a promising earth-abundant alternative to costly precious metals. Results indicate the formation of a $c(2 \times 2)$ ground state structure occurring at $\frac{1}{2}$ ML carbon coverage (Figure 2a) due to the presence of repulsive nearest neighbor and attractive second nearest neighbor interactions (Figure 2b). This correlates well with previous studies for carbon adsorption on Fe surfaces and matches the experimentally-observed low electron energy diffraction structure.[2] These preliminary results set the stage for developing further insights into the effect of carburization on Fe surfaces.

Specific Aim 2: Predict the cooperative effects and concerted behavior on several facets at the surface of a single catalytic grain under hydrodeoxygenation conditions.

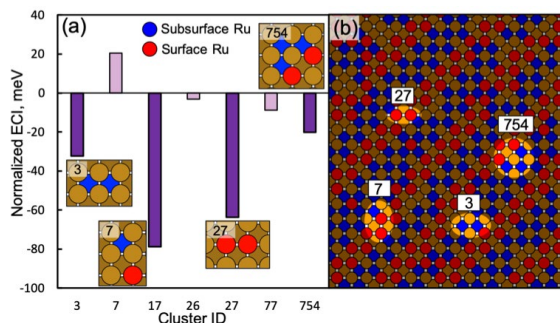


Figure 1: The LGCE+MC model of an Fe(100) facet promoted with 1.0 ML of Ru. (a) The effective cluster interactions (ECI) of clusters present in the ground state configuration at 1.0 ML, where the dark purple bars are the top four most attractive clusters. (b) Equilibrium, canonical Monte Carlo configuration at 500K using the Ru/Fe(100) LGCE, where the highlighted areas reveal the clusters acting to stabilize the configuration.

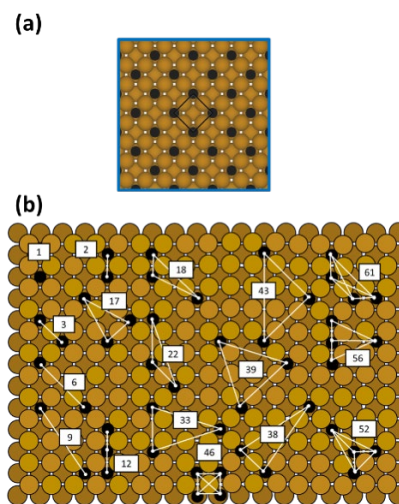


Figure 2: Preliminary LGCE models used to characterize the lateral interactions for carbon on Fe(100). (a) Carbon clusters that make up the LGCE; (b) $c(2 \times 2)$ ground state structure that occurs at 0.5 ML, where cluster 3 is highly attractive and stabilizes the $c(2 \times 2)$ ground state.

We have determined the mean field (MF) coverage dependence on the adsorption energy of phenol (PH) on Ru(0001) and Ru(10-11), along with the effect of the solvent environment on this MF coverage dependence. This study examines PH adsorption over a large coverage range, a sampling of which are shown in Figure 3a. Similar to previous results for benzene and PH on Pt(111) under vapor phase conditions, the vapor phase adsorption energy for PH on Ru(0001) and Ru(10-11) can be adequately described with linear MF models (Figure 3b). The effective lateral interactions from the MF model for PH/Ru(0001), e.g. 4.74 eV/ML (Figure 3c), are nearly identical to benzene/Pt(111), e.g. 4.84 eV/ML, and PH/Pt(111), e.g. 4.76 eV/ML [3], which suggests that the aromatic ring dictates the dominant coverage behavior for phenolics on a transition metal surface. PH binds stronger on the more open, Ru(10-11) facet as compared to Ru(0001). Additionally, the PH-PH effective lateral interactions (Figure 3c) are weaker on Ru(10-11) as compared to Ru(0001) by a factor of ~ 4 . This suggests that the more open and reactive facets (e.g. Ru(10-11)) will see higher PH coverages than the more stable, flat facets (e.g. Ru(0001)) under vapor phase conditions. Furthermore, the MF model we developed for PH adsorption on Pt(111) (Figure 4a and 4b) compares favorably to the

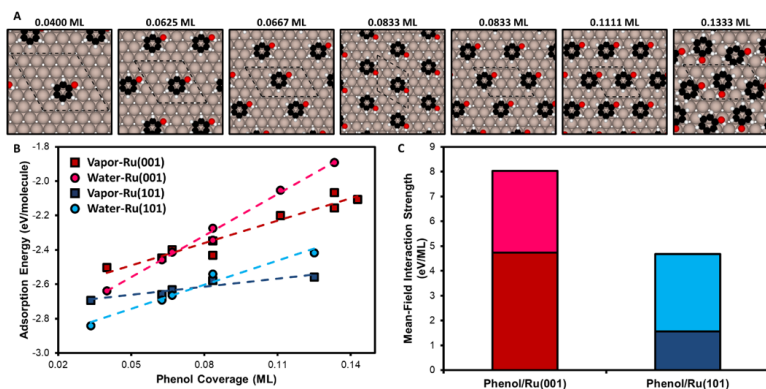


Figure 3: Coverage dependent behavior of phenol on Ru surfaces in the absence and presence of water a solvent. (A) Example configurations for phenol on Ru(0001) (denotes as Ru(001) in the Figure), where the silver, black, red, and white spheres represent Ru, C, O, and H, respectively. (B) Average phenol adsorption energy as a function of coverage on Ru(0001) and Ru(-101) under vapor and water phases calculated with the implicit solvent model, VASPsol. (C) Effective phenol-phenol lateral interaction strength determined here from the mean-field best fit slopes from panel (B).

PH/Ru(0001), e.g. 4.74 eV/ML (Figure 3c), are nearly identical to benzene/Pt(111), e.g. 4.84 eV/ML, and PH/Pt(111), e.g. 4.76 eV/ML [3], which suggests that the aromatic ring dictates the dominant coverage behavior for phenolics on a transition metal surface. PH binds stronger on the more open, Ru(10-11) facet as compared to Ru(0001). Additionally, the PH-PH effective lateral interactions (Figure 3c) are weaker on Ru(10-11) as compared to Ru(0001) by a factor of ~ 4 . This suggests that the more open and reactive facets (e.g. Ru(10-11)) will see higher PH coverages than the more stable, flat facets (e.g. Ru(0001)) under vapor phase conditions. Furthermore, the MF model we developed for PH adsorption on Pt(111) (Figure 4a and 4b) compares favorably to the

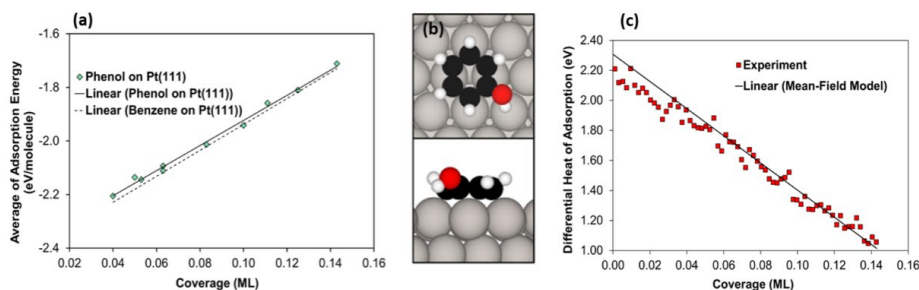


Figure 4: Lateral interaction in phenolics on Pt(111). (a) Construction of a mean-field model using average adsorption energies from each site as a function of coverage for phenol on Pt(111) as well as the mean-field model trendline for benzene on Pt(111). (b) Most favorable configuration for phenol adsorption on Pt(111). (c) Comparison of theoretically calculated and experimentally measured differential heat of adsorption for phenol on Pt(111).

experimentally determined differential heat of adsorption[4], indicating that a MF model can be used to accurately model phenolic compounds (Figure 4c).

The effect of water on the coverage-dependent adsorption energy for PH on Ru(0001) and Ru(10-11) was determined using an implicit solvation model. As shown in Figure 3b, water alters the coverage dependence of PH on both Ru(0001) and Ru(10-11) by increasing the stability of low coverage systems and decreasing the stability of high coverage systems. This results in an increase in the effective, MF PH-PH lateral interactions by a factor of 1.7 for Ru(0001) and 3.0 for Ru(10-11) (Figure 3c). This demonstrates the potential for solvents to mediate adspecies coverage by altering the lateral interactions between adspecies.

Specific Aim 3: Determine the dominant mechanism for the deoxygenation of phenol on Fe-based catalysts in the presence of Pd, Pt, Rh, Ni, Cu and alkali metal promoters with surface oxygen and water.

Preliminary work, in collaboration with the Wang group, has been performed to characterize the vapor phase HDO reaction mechanisms of PH over an Fe carbide surface, Fe₃C(001) (Figure 5a). Results suggest that the overall barrier for PH deoxygenation is similar to PH deoxygenation over a pure Fe surface. However, the carburization of Fe decreases the selectivity for C-O bond cleavage indicating a reduction in surface oxophilicity, minimizing oxidative deactivation (Figure 5b).

We are also currently investigating the selective reduction of propanal (AL) to propanol (OL) over a Ru(0001) surface. AL reduction occurs by hydrogenating the carbonyl group through the Horiuti-Polanyi mechanism via the alkoxy and hydroxy pathway, and agrees well with experimental observations and those reported in literature.[5] We show that CO coverage (used as probing molecule in experiments to control the active sites) does not affect these interpretations. The kinetic experimental isotopic data, obtained from the Chin group at the University of Toronto, indicates that a negatively charged adsorbed H reacts with the positively charged carbon of the adsorbed AL, forming propoxy as the most abundant surface intermediate. Subsequent hydrogenation of the alkoxy group to form OL is the rate limiting step. Corresponding calorimetric studies are being performed by the Wu group to further guide our modeling efforts.

[1] Hong, Y.; Zhang, H.; Sun, J.; Ayman, K.M.; Hensley, A.J.R.; Gu, M.; Engelhard, M.H.; McEwen, J.-S.; Wang, Y. Synergistic Catalysis Between Pd and Fe in Gas Phase Hydrodeoxygenation of m-Cresol, *ACS Catal.*, **2014**, 4, 3335-3345.

[2] D.E. Jiang, E.A. Carter, Carbon Atom Adsorption on and Diffusion into Fe(110) and Fe(100) from First Principles, *Phys. Rev. B*, **2005**, 71, 045402.

[3] Wong, B.; Collinge, G.; Hensley, A. J. R.; Wang, Y.; McEwen, J.-S. Benchmarking the Accuracy of Coverage-Dependent Models: Adsorption and Desorption of Benzene on Pt(111) and

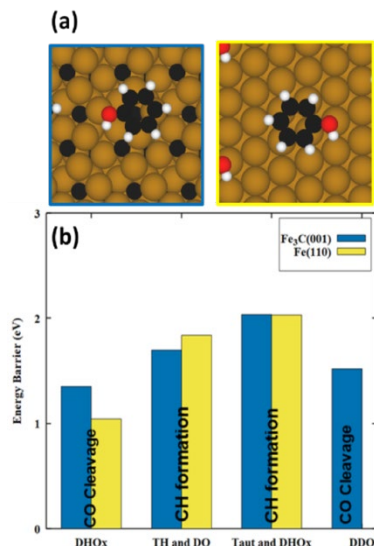


Figure 5: (a) Top view of phenol adsorbed on Fe₃C(001) and Fe(110). (b) Comparison between the activation energies of phenol for several possible HDO mechanisms over Fe₃C(001) and Fe(110). (DHOx = Dehydroxylation, TH and DO = Transhydrogenation & Deoxygenation, Taut and DHO = Tautomerization and Dehydroxylation, DDO = Direct Deoxygenation).

Pt₃Sn(111) from First Principles, *Prog. Surf. Sci.*, **2019**, <http://dx.doi.org/10.1016/j.progsurf.2019.04.001>.

[4] S.J. Carey, W. Zhao, Z. Mao, C.T. Campbell, Energetics of Adsorbed Phenol on Ni (111) and Pt (111) by Calorimetry, *J. Phys. Chem. C*, **2019**, 123, 7627-7632.

[5] Sinha, N. K.; Neurock, M. A First Principles Analysis of the Hydrogenation of C₁-C₄ aldehydes and ketones over Ru(0001), *J. Catal.*, **2012**, 295, 31-44.

Publications Acknowledging this Grant in 2015-2018

(VIII) *Exclusively funded by this grant:*

- 1- Hensley, A. J. R.; Wang, Y.; McEwen, J.-S. The Partial Reduction of Clean and Doped - Fe₂O₃(0001) from First Principles, *Appl. Catal. A: Gen.*, **2019**, 582, 116989.

(IX) *Jointly funded by this grant and other grants with leading intellectual contribution from this grant:*

- 1- Wong, B.; Collinge, G.; Hensley, A. J. R.; Wang, Y.; McEwen, J.-S. Benchmarking the Accuracy of Coverage-Dependent Models: Adsorption and Desorption of Benzene on Pt(111) and Pt₃Sn(111) from First Principles, *Prog. Surf. Sci.*, **2019**, <http://dx.doi.org/10.1016/j.progsurf.2019.04.001>.
- 2- Che, F; Gray, J.; Ha, S.; Kruse, N.; Scott, S. L.; McEwen, J.-S. Elucidating the Roles of the Electric Fields in Catalysis: A Perspective, *ACS Catal.*, **2018**, 8, 5153-5174.
- 3- Hensley, A. J. R; Wöckel, C.; Gleichweit, C.; Gotterbarm, K.; Papp, C.; Steinrueck, H.-P.; Wang, Y; Denecke, R.; McEwen, J.-S. Identifying the Thermal Decomposition Mechanism of Guaiacol on Pt(111): An Integrated X-ray Photoelectron Spectroscopy and Density Functional Theory Study. *J. Phys. Chem. C*, **2018**, 122, 4261-4273.
- 4- Bray, J.; Hensley, A. J. R.; Collinge, G.; Che, J.; Wang, Y.; McEwen, J.-S. Modeling the Adsorbate Coverage Distribution Over a Multi-Faceted Catalytic Grain in the Presence of an Electric Field: O/Fe from First Principles, *Catal. Today*, **2018**, 312, 92-104.
- 5- Bray, J.; Collinge, G.; Stampfl, C.; Wang, Y.; McEwen, J.-S. Predicting the Electric Field Effect on the Lateral Interactions Between Adsorbates: O/Fe(100) from First Principles, *Top. Catal.*, **2018**, 61, 763-775.
- 6- Hensley, A. J. R.; Wang, Y.; Mei, D.; McEwen, J.-S. Mechanistic Effects of Water on the Fe-Catalyzed Hydrodeoxygenation of Phenol - The Role of Bronsted Acid Sites, *ACS Catal.*, **2018**, 8, 2200-2208.
- 7- Hensley, A. J. R.; Ghale, K.; Rieg, C.; Dang, T.; Anderst, E.; Studt, F.; Campbell, C. T.; McEwen, J.-S.; Xu, Y. A DFT-Based Method for More Accurate Adsorption Energies: An Adaptive Sum of Energies from RPBE and vdW Density Functionals, *J. Phys. Chem. C*, **2017**, 121, 4937-4945.

- 8- Hongchun, H.; Hensley, A. J. R.; McEwen, J.-S.; Wang, Y. Perspective on Catalytic Hydrodeoxygenation of Biomass Pyrolysis Oils: Essential Roles of Fe-based Catalysts, *Catal. Lett.* **2016**, 146, 1621-1633.
 - 9- Hensley, A. J. R.; Wang, Y.; McEwen, J.-S. Adsorption of Guaiacol on Fe (110) and Pd (111) from First Principles, *Surf. Sci.* **2016**, 648, 74-83.
 - 10- Hensley, A. J. R.; Schneider, S.; Wang, Y.; McEwen, J.-S. Adsorption of Aromatics on the (111) Surface of PtM and PtM₃ (M = Fe, Ni) Alloys, *RSC Adv.*, **2015**, 5, 85705-85719.
- (X) *Jointly funded by this grant and other grants with relatively minor intellectual contribution from this grant:*
- 1- Hu, S.; Che, F.; Bitá, K.; Mina, J.; Chang Won, Y.; McEwen, J.-S.; Scudiero, L.; Ha, S. Improving the Electrochemical Oxidation of Formic Acid by Tuning the Electronic Properties of Pd-Based Bimetallic Nanoparticles, *Appl. Catal. B: Environ.*, **2019**, 254, 685-692.
 - 2- Smith, M.; Helms, G.; McEwen, J.-S.; Garcia-Perez, M. Effect of Pyrolysis Temperature on Aromatic Cluster Size of Cellulose Char by Quantitative Multi Cross-Polarization ¹³C NMR with Long Range Dipolar Dephasing. *Carbon*, **2017**, 116, 210-222.
 - 3- Smith, M.; Scudiero, L.; Espinal-Lopez, J. F.; McEwen, J.-S.; Garcia-Perez, M. Improving the Deconvolution and Interpretation of XPS Spectra from Chars by ab Initio Calculations. *Carbon*, **2016**, 110, 155-171.

**Catalytic Hydrogenation of Arenes: Evolution of the Conversion of a
Molecular Rh-CAAC Complex to Rh Nanoparticles**

R. Morris Bullock, Ba L. Tran, John L. Fulton, John C. Linehan, and Johannes A. Lercher
Institute for Integrated Catalysis, Pacific Northwest National Laboratory, Richland, WA

Hydrogenation of the arene ring of ethers, amides, and esters occurs at room temperature and low hydrogen pressure, starting from $[(\text{CAAC}^{\text{Cy,Dipp}})\text{Rh}(\text{COD})\text{Cl}]$ (CAAC = cyclic alkyl amino carbene). The site-selective arene hydrogenation catalyzed by this system is under steric control, as shown by competition experiments with derivatives of ethers, amides, and esters bearing different aromatic rings of varying electronic and steric influence. Rh K-edge X-ray absorption fine structure (XAFS) spectroscopy was carried out at the Advanced Photon Source, Argonne National Laboratory. We examined arene hydrogenation of diphenyl ether by a combination of stoichiometric reactions of $[(\text{CAAC}^{\text{Cy,Dipp}})\text{Rh}(\text{COD})\text{Cl}]$ and *operando* XAFS kinetics studies. Our results unequivocally show that Rh nanoparticles generated from the single-site Rh complex catalyze the arene hydrogenation. *Operando* XAFS studies illuminate the role of Ag^+ (for removal of Cl^- from $[(\text{CAAC})\text{Rh}(\text{COD})\text{Cl}]$) on the pre-catalyst reactivity, the effect of increasing H_2 pressure on increasing the catalytic efficiency, the stabilizing influence of Ph_2O on the relative rate of formation of active Rh nanoparticles, and the absence of soluble single-site Rh species that might leach from bulk heterogeneous Rh nanoparticles. We gained insights into the divergent deactivation pathways mediated by sub-stoichiometric benzothiophene and excess KO^tBu toward H_2 activation, which is a key step *en route* to Rh nanoparticles for arene hydrogenation. Excess KO^tBu leads to the formation of a Rh-O^tBu complex that interferes with H_2 activation, precluding the formation of Rh nanoparticles. Benzothiophene does not interfere with the activation of H_2 at Rh in the $\text{CAAC}^{\text{Cy,Dipp}}$ complex while Rh nanoparticles are formed. Once Rh nanoparticles are formed, however, benzothiophene binds irreversibly to the Rh nanoparticles, preventing adsorption of H_2 and hydrogenation of diphenyl ether.

FWP 47319: Transdisciplinary Approaches to Realize Novel Catalytic Pathways to Energy Carriers

PI: Johannes Lercher

NATIONAL LABORATORIES ABSTRACTS

**Catalytic Environments at the Interface: Characterization of Sites and Distributions,
Catalytic Activity and Reaction Mechanisms**

Aaron D. Sadow, Takeshi Kobayashi, Marek Pruski, Frédéric A. Perras, Long Qi, Igor I. Slowing
U.S. DOE Ames Laboratory and Iowa State University, Ames, IA

Presentation Abstract

The overarching goal of this collaborative project is to elucidate the key properties that control catalytic phenomena at liquid-solid interfaces and thereby guide the rational design of selective and efficient heterogeneous catalysts for redox conversions of oxygenated compounds. To this end our research team combines expertise in mesoporous and nanostructured catalyst synthesis, organometallic chemistry, kinetics and mechanisms of catalytic reactions, and solid-state (SS)NMR, including the ultrasensitive dynamic nuclear polarization (DNP) technique. Herein, we report that appropriate surface functionalization, to influence the polarity of the interfacial region in the pores of mesoporous silica nanoparticles (MSN) and create the desired catalytic environment, enhances the activity of catalysts for aldol and related reactions. Binding strength of a propanoic acid derivative are improved in the presence vs absence of phenyl groups in the MSN pores, while binding is diminished with flexible compared to rigid phenyl groups. Such studies inform design principles of catalysts operating in pores. Toward this end, a highly active organolanthanum catalyst catalyzes C–O bond cleavage reactions using pinacol borane. Catalytic properties of immobilized analogue and homogeneous derivative may be compared using NMR kinetics that makes use of emerging magic angle spinning (MAS) NMR techniques. We also describe solid-state NMR advances in methods, making use of the high resolution provided by ultra-fast MAS and the sensitivity enhancement available with dynamic nuclear polarization (DNP) enhanced NMR spectroscopy. These techniques have provided new access to ^{17}O NMR measurement that do not rely on ^1H cross polarization, characterization of the coordination sphere of single-site catalysts immobilized on silica, and determine the spatial distribution of organic groups on the surfaces of functionalized silicas prepared by co-condensation and grafting.

AL-03-380-011: Homogeneous and Interfacial Catalysis in 3D Controlled Environments

Graduate Students: Abhranil Biswas, Walikadage Boteju, Puranjan Chatterjee, Yang-Yun Chu, Pranjali Naik, Smita Patnaik, Nishant Praveen, Austin Thompson, Zhuoran Wang, Dilini Singappuli, Pranjali Naik, Juan Manzano.

Postdoc: Zhicheng Luo

RECENT PROGRESS

Publications Acknowledging this Grant in 2016-2019

Source of support for the work published:

(XI) *Exclusively funded by this grant*¹⁻¹⁵

(XII) *Jointly funded by this grant and other grants leading intellectual contribution from this grant*¹⁶⁻³⁹

(XIII) *Jointly funded by this grant and other grants with relatively minor intellectual contribution from this grant*⁴⁰⁻⁵¹

(1) Controlling water-support interactions enhances catalytic performance in C-C bond forming reactions.

We have previously demonstrated that the catalytic activity of primary amines for the aldol and related reactions is improved upon supporting them on mesoporous silica nanoparticles (MSN). The activity enhancement was due to cooperativity between the amines and surface silanol groups.⁵¹⁻⁵³

We have also shown that in non-polar media aminopropyl-MSN (AP-MSN) catalysts are poisoned by forming stable imine species,⁵² and that the pathways leading to this state can be inhibited by performing the reaction in water. We also determined that increasing the dielectric constant of the solvent is detrimental to the reaction because it favors proton transfer from the acidic silanols to the amines turning the latter into non-nucleophilic ammonium cations.⁵⁴

Thus, to maximize the performance of this catalyst for the aldol and related C-C coupling reactions it is necessary to produce a low polarity environment around the catalytic sites (to minimize ion-pair formation), and at the same time allow the access of water to the reaction center (to prevent the production of inhibitory imines). We have recently demonstrated that immobilizing organic groups on the surface of MSN controls the effective dielectric constant at the solid-liquid interface in aqueous media.¹⁵

Therefore, we hypothesized that suitable functionalization of AP-MSN with non-polar groups could be a way to produce low polarity environments around active sites while allowing contact with water. Indeed, aqueous suspensions of hexyl-modified AP-MSN presented a linear dependence of interfacial dielectric constant on the surface density of hexyl groups (assessed by fluorescence spectroscopy of impregnated solvatochromic probe Prodan). This control of interfacial dielectric constant successfully resulted in an enhancement of catalytic activity for the aldol (**Figure 1**), Henry and vinylogous aldol reactions, and proved consistent with the Eyring-Laidler model for the effect of dielectric media on polar reactions. Structure-activity relationship studies utilizing Hammett parameters further supported the role of interfacial dielectric constant on reactivity of these species. Ultimately, this synergy between the low interfacial polarity and access to water is an example of how the secondary sphere around catalytic sites can be designed to precisely control activity.¹

(2) Controlling reactant-support interactions by tailoring the geometry and mobility of surface phenyl groups in organo-modified mesoporous silicas. Phenyl-functionalized mesoporous silicas were used to explore the role of non-covalent interactions on the desorption of phenyl substituted propionic acid into aqueous media.⁶ Variations in orientation and conformational mobility of the surface phenyl groups were introduced by selecting different structural precursors: 1) use of phenyltrimethoxysilane led to aryl groups with rigid upright orientation relative to the support

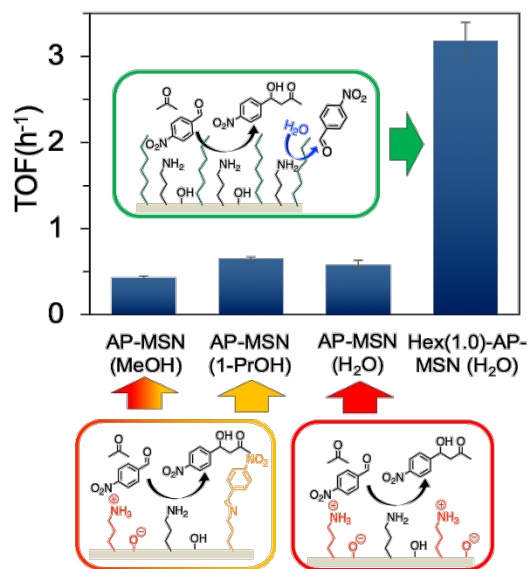


Figure 1. The amine-catalyzed aldol condensation has low activity in polar media (MeOH, 1-PrOH) due to formation of non-nucleophilic ammonium cations and inhibitory imines. Use of water prevents imine formation, but stabilizes ammonium-silanoxy pairs. Combining a hexyl modified (low polarity) surface with water increases dramatically catalytic activity (TOF).

surface (Ph-MSN); 2) phenethyltrimethoxysilane precursor led to mobile aryl groups due to flexible ethylene linkers (PhEt-MSN); 3) bis-(trimethylsilyl)benzene precursors resulted in a periodic mesoporous organosilica with aryl groups co-planar to the surface (Ph-PMO). The desorption profiles of 2-(4-isobutylphenyl)propanoic acid from these materials and non-functionalized MSN into aqueous media were analyzed using an adsorption-diffusion model developed by Zeng, et al.⁵⁵ The model provided kinetic and thermodynamic parameters that evidenced fundamental differences in the interaction of the modified surfaces with the probe molecule. All phenyl-bearing materials showed lower initial desorption rates than bare MSN. Interestingly, conformationally locked Ph-MSN and Ph-PMO presented stronger interactions with the probe (negative ΔG_{ads}) than the flexible PhEt-MSN and bare MSN (positive ΔG_{ads}). These differences were consistent with the relative binding energies obtained from DFT calculations. B3LYP-D3-optimized models showed that π - π interactions contribute more to probe adsorption than H-bonding between carboxy and silanol groups (**Figure 2**). These results highlight the relevance of surface functionalization for controlling the geometry and strength of interactions between reactants and catalyst supports, and should serve as a guide to design new hierarchical materials with precise control over the mode and strength of reactant binding.

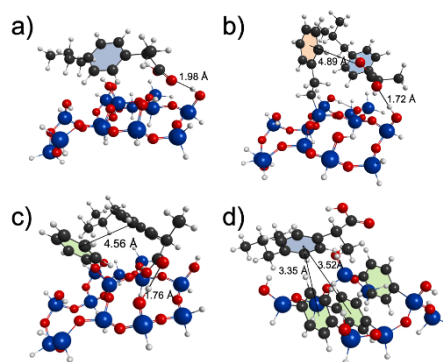


Figure 2. B3LYP-D3-optimized geometries of 2-(4-isobutylphenyl)propionic acid interacting with fragments of a) MSN, b) PhEt-MSN, c) Ph-MSN and d) Ph-PMO surfaces illustrate differences between the strength of adsorption of the probe molecule and varying configurations of aryl surface groups.

(3) Catalytic hydroboration of esters and epoxides. New methods for breaking C–O bonds under reducing conditions are important for conversions of oxidized organic materials. In fact, hydroboration of esters and epoxides are limited to only a few examples with magnesium and molybdenum catalysts. Previously, we had reported zirconium amide-based catalysts for hydroboration of aldehydes and ketones. That study compared the performance of homogeneous, soluble $\text{Zr}(\text{NMe}_2)_4$ with that of mesoporous silica nanoparticle (MSN) supported $\text{Zr}(\text{NMe}_2)_3@MSN$.⁵⁶ The supported catalyst was highly recyclable and could be reactivated after exposure to air and moisture with HBpin; however, the reaction rates of supported catalyst were diminished compared to the soluble analogue. In addition, these zirconium catalysts were not effective for less electrophilic substrates, such as esters, and did not break C–O bonds. Instead, we turned to the organolanthanide complex $\text{Ln}\{\text{C}(\text{SiHMe}_2)_3\}_3$ recently reported in our group,⁵⁷ which might graft onto MSN similarly to $\text{Zr}(\text{NMe}_2)_4$ and also could give effective hydroboration catalysis for C–O bond cleavage. In this first part of the study, we have demonstrated that $\text{La}\{\text{C}(\text{SiHMe}_2)_3\}_3$ is an

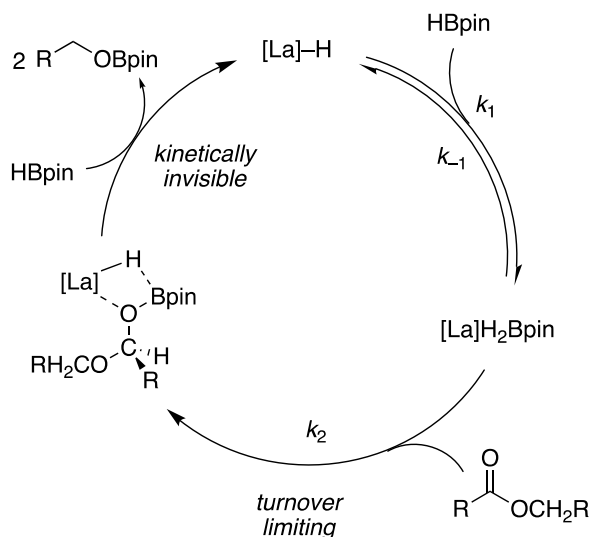


Figure 3. Proposed catalytic cycle for alkyl-lanthanum-catalyzed hydroboration and C–O bond cleavage of esters. The mechanism is proposed based on kinetic studies and because esters are not reduced by $[\text{La}]\text{-H}$ in independent experiments.

effective precatalyst for the hydroboration of both esters and epoxides with pinacolborane (HBpin), giving borate ester products at room temperature.³ For example, hydroboration of ethyl acetate occurs with an initial TOF of 7120 h⁻¹, and TON reach 10,000. The precatalyst reacts with HBpin to form lanthanum hydride species and a carbon-boron bond in (Me₂HSi)₃C-Bpin. The lanthanum hydride reacts with ketones to give alkoxides, but lanthanum hydride species does not appear to react with esters. Kinetic studies provide a ternary rate law, as well as saturation behavior under conditions with large excesses of either ester or HBpin. These results are consistent with a two-step mechanism in which lanthanum hydride reversibly forms an adduct with HBpin to generate a species that is competent for reducing esters (**Figure 3**). A related “HBpin-first” pathway is also likely operative in epoxide ring-opening, which shows a related rate law. Current efforts involve grafting La{C(SiHMe₂)₃}₃ onto silica for a comparison of catalytic performance to this homogeneous analogue; however, the kinetic studies in hand already suggest that such a comparison will be complicated by the nonlinear effects of concentration on rate.

(4) *In situ* MAS-NMR study of interfacial hydroboration. We have developed *in situ* and *operando* MAS-NMR capability in our lab to directly study reaction mechanism and kinetics of triphasic catalytic systems.¹⁷ The technique allows *in situ* quantitative analysis of reactants and products at high pressure/temperature. One of the exemplary applications is the *in situ* study of hydroboration of methyl anisate catalyzed by La{C(SiHMe₂)₃}₂@MSN. The arrays of alternating ¹¹B and ¹H NMR spectra were acquired with variation of catalyst loading. The air-sensitive HBpin and silica-grafted La catalyst are well kept in the air-tight rotor under nitrogen. The ¹¹B NMR spectra in **Figure 4** clearly shows the conversion of HBpin (a doublet at 28.1 ppm) and formation of methyl and p-anisyl borates (singlets at 22.3 ppm). In complementary, ¹H NMR can provide conversion of methyl anisate and formation of p-anisyl borate. The 2nd-order rate constant can be directly obtained by curvefitting the concentration profiles extracted from quantitative spectra of high quality.

The rotor can hold vapors generated from solvents and other low-boiling reaction species under heating. Besides, gases (up to 100 bar) can be pre-charged into the rotor; particularly in the case of dihydrogen, the study of hydrogenation, hydrogenolysis, and hydrodeoxygenation chemistry can thus be achieved. As a phase-sensitive technique, the MAS-NMR can be applied under catalysis-relevant conditions to study the sorption of gas and liquid species by the 3D catalysts as a result of solvent and confinement effect. NMR parameters, including chemical shift, line width, and relaxation time, can be used to assign signals in different phases and understand chemical environment inside micro- and meso- pores. New NMR methodology is also under development to obtain information of more challenging nuclei (like ¹⁵N) and dynamics of molecules at the solid-liquid interface at elevated temperature.

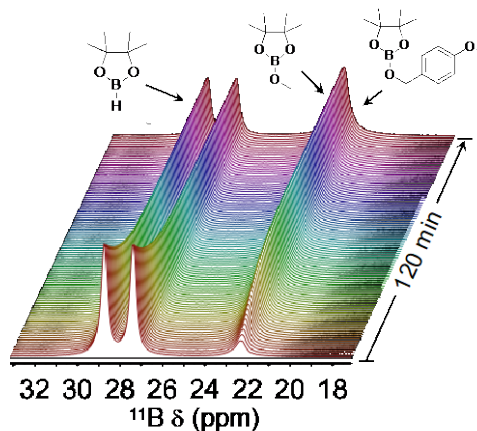


Figure 4. *In situ* array of direct polarization ¹¹B MAS-NMR spectra for La{C(SiHMe₂)₃}₂@MSN catalyzed hydroboration of methyl anisate with

(5) Tris(oxazolanyl)borate-supported first-row metal complexes in oxidations. Single-site heterogeneous catalysts, with designed coordination spheres distributed uniformly in heterogeneous environments, would enable selective catalytic conversions. Toward this goal, we have been developing tris(oxazolanyl)borate compounds for surface attachment strategies (through the boron center) that should not affect the catalytic site's coordination sphere upon immobilization. The coordination sphere provided by To^M provides steric protection from redistribution reactions but remains sufficiently open to allow chemical reactivity. For example, To^MFeBr is more stable than To^M_2Fe and $FeBr_2$, which contrasts the established chemistry of Tp^*FeBr ($Tp^* = HB(N_2C_3HMe_2)_3$) that redistributes to the more stable Tp^*_2Fe (**Figure 5**).⁴ In order to compare homogeneous and supported sites, we have been developing oxidative conversions catalyzed by phenyl tris(oxazolanyl)borato cobalt (To^MCo^{II}) complexes.³⁹

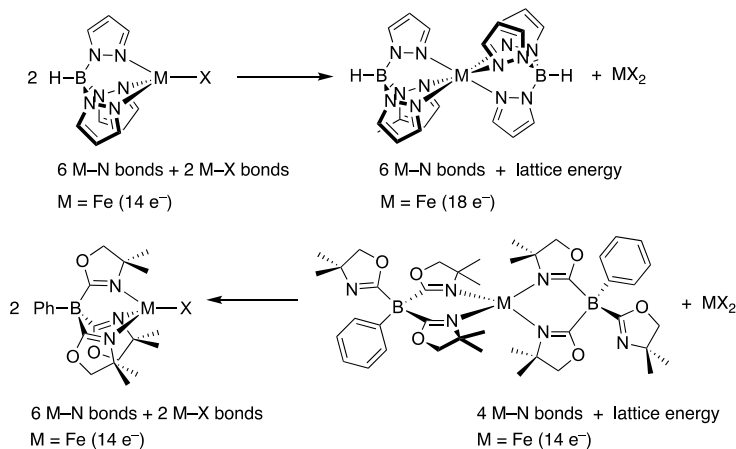
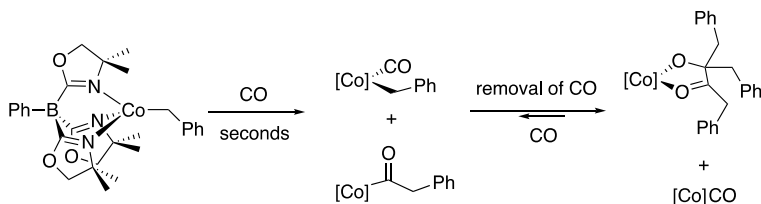


Figure 5. Contrasting stabilities of Tp^*_2Fe and To^MFeBr with respect to redistribution.

Related methylcobalt compounds give acetyl upon treatment with CO, and acetate upon oxidation.³² Recently, we discovered that To^MCoBn reacts with CO to give β -alkoxyketone involving carbon-carbon bond formation.²⁴ NMR and EPR, as well as IR, spectroscopic features of molecular To^MCoX and To^MFeX compounds are required for comparison to surface-supported and pore-localized analogues. These will be used to mimic enzymatic sites and develop catalytic carbon-carbon bond formations.



(6) Solid-state NMR studies of structure, spatial distribution, and dynamics of catalysts. In concert with the work being done into the design of well-ordered 3D-structured heterogeneous catalysts with well-defined catalytic active sites, SSNMR methods are extensively being developed to gain new insights into the structure and function of these catalysts. The central goal of these methods development is to enable the characterization of the structure and dynamics of the catalysts on the length scales that are of relevance to the chemistry. Namely, we are interested in determining the 3D structure of the active sites of our heterogeneous catalysts with atomistic precision, something that cannot at present be achieved by any other means. Moving beyond the active site, we are additionally concerned with determining the nature of the environment around a particular functional group situated at the solid-liquid interface. The SSNMR methods mainly take advantage of two recent instrumental breakthroughs that have revolutionized the study of structure at interfaces, particularly in the case of heterogeneous catalysts. The first of these is ultrafast magic-angle-spinning (MAS) which, enables unprecedented resolution to be obtained,

something that is crucial in the study of complex structures. The second is dynamic nuclear polarization (DNP). DNP can routinely yield sensitivity improvements of >100, and time savings of 4 or 5 orders of magnitude, which uniquely allows for the acquisition of previously unfeasible experiments. This is particularly important when studying dilute catalytically-active species on material surfaces.

Single-site heterogeneous catalysts generally rely on a very precise structure to yield targeted and controlled catalytic activity in a way that mirrors that which is achieved in well-structured homogeneous catalysts. This structure is nevertheless difficult to determine. For instance, it is important to determine what is the topology of the complex as this affects the metal center's charge as well as its number of available coordination sites. We must also determine which ligands survived the grafting process and which were expelled. Lastly, in determining the ordering of the ligands on the metal center we can rule out which catalytic mechanisms are spatially reasonable. To address these points we have applied DNP for the first time to the direct detection of the catalytically-active metal center.^{38, 45} This enabled us to determine that the Pt(IV) center was coordinated in a bipodal fashion to the surface and rule out the possibility of reaction mechanisms involving a platinum dihydride.³⁵ Simultaneously, we have developed direct ¹⁷O DNP methods that allowed us to detect the oxygen bridge that links the metal center to the support.¹⁹ This method should notably allow us to probe non-covalent metal-support interactions. We have additionally applied multidimensional fast-MAS as well as DNP methods to probe the ligands in the catalysts.^{1, 9, 43, 45-47, 56} In particular, in a recent study, inter-ligand through-space ¹H-¹³C correlations have enabled for the ordering of three ligands on an Ir(III) single-site catalyst to be determined.¹ We found that the large pincer-type ligand rested away from the surface, thus limiting the potential number of adjacent coordination sites on the metal.

Aside from the precise structure near the active site, the spatial distribution of functional groups on the surfaces of our 3D structured materials also has a large influence on the catalytic activity due to their abilities in creating microenvironments,¹⁵ or to promote cooperativity. To date, there were, however, no good methods to probe the spatial distribution of functional groups on surfaces. To this aim we have applied DNP to sensitize natural abundance ²⁹Si-²⁹Si double-quantum-single-quantum correlation experiments and probe T-T correlations which can only occur from a clustering of functional groups at the silica surface.¹¹ We found that significant functional group clustering occurred when using co-condensation methods and that grafting led to a better site isolation; in contrast to the preceding belief in the community. Given that this method is insensitive to the nature of the individual functional groups we were interested in applying ¹³C-¹³C correlation experiments to probe the proximity of the functional groups themselves directly. This is nevertheless an incredibly insensitive technique, with each carbon only having a 1.1% chance of being the NMR-active ¹³C isotope and as such the application of DNP was critical. Crucial to the success of this work, however, was the development of a CHHC method that filters the uncorrelated magnetization enabling the detection of extremely dilute spin pairs.¹³ Using this method we could prove that two functional groups were intermixed at the silica surface and did not form isolated domains. Lastly, probing the proximity between like functional groups is challenging since intra-group correlations typically outweigh the inter-group ones. To counter this we have applied multiple-quantum spectroscopy to only detect correlations involving a minimum of like spins that exceeds its total in the functional group. For example, using triple-quantum spectroscopy to probe CH₂-CH₂ proximities.² In doing so we were able to not only observe these inter-group proximities but also discover that they are unaffected by the concentration of the functional groups on the surface, therefore proving that these have a high propensity for clustering.

References.

1. Singappuli-Arachchige, D.; Kobayashi, T.; Wang, Z.; Burkhaw, S. J.; Smith, E. A.; Pruski, M.; Slowing, I. I., Interfacial Control of Catalytic Activity in the Aldol Condensation: Combining the Effects of Hydrophobic Environments and Water. *ACS Catal.* **2019**, *9* (6), 5574-5582.
2. Kobayashi, T.; Pruski, M., Spatial Distribution of Silica-Bound Catalytic Functional Groups Can Now Be Revealed by Conventional and DNP-enhanced Methods. *ACS Catal.* **2019**.
3. Patnaik, S.; Sadow, A. D., Interconverting Lanthanum Hydride and Borohydride Catalysts for C=O Reduction and C–O Bond Cleavage. *Angew. Chem. Int. Ed.* **2019**, *58* (8), 2505-2509.
4. Reinig, R. R.; Ellern, A.; Sadow, A. D., Heteroleptic Four-Coordinate Tris(oxazolinyl)borato Iron(II) Compounds. *Inorg. Chem.* **2019**, *58* (9), 6044-6051.
5. Biswas, A.; Ellern, A.; Sadow, A. D., CO Displacement in an Oxidative Addition of Primary Silanes to Rhodium(I). *Inorg. Chem.* **2019**, *58* (6), 3815-3824.
6. Manzano, S. J.; Singappuli-Arachchige, D.; Parikh, B. L.; Slowing, I. I., Fine-tuning the Release of Molecular Guests from Mesoporous Silicas by Controlling the Orientation and Mobility of Surface Phenyl Substituents. *Chem. Eng. J.* **2018**, *340*, 73-80.
7. Wang, Z.; Opembe, N.; Kobayashi, T.; Nelson, N. C.; Slowing, I. I.; Pruski, M., Quantitative Atomic-scale Structure Characterization of Ordered Mesoporous Carbon Materials by Solid State NMR. *Carbon* **2018**, *131*, 102-110.
8. Nelson, N. C.; Wang, Z.; Naik, P.; Manzano, J. S.; Pruski, M.; Slowing, I. I., Phosphate Modified Ceria as a Bronsted Acidic/Redox Multifunctional Catalyst. *J. Mater. Chem. A* **2017**, *5* (9), 4455-4466.
9. Eedugurala, N.; Wang, Z.; Yan, K.; Boteju, K. C.; Chaudhary, U.; Kobayashi, T.; Ellern, A.; Slowing, I. I.; Pruski, M.; Sadow, A. D., β -SiH-Containing Tris(silazido) Rare-Earth Complexes as Homogeneous and Grafted Single-Site Catalyst Precursors for Hydroamination. *Organometallics* **2017**, *36* (6), 1142-1153.
10. Boteju, K. C.; Ellern, A.; Sadow, A. D., Homoleptic Organolanthanide Compounds Supported by the Bis(dimethylsilyl)benzyl Ligand. *Chem. Commun.* **2017**, *53* (4), 716-719.
11. Kobayashi, T.; Singappuli-Arachchige, D.; Wang, Z.; Slowing, I. I.; Pruski, M., Spatial Distribution of Organic Functional Groups Supported on Mesoporous Silica Nanoparticles: A Study by Conventional and DNP-enhanced ^{29}Si Solid-state NMR. *Phys. Chem. Chem. Phys.* **2017**, *19* (3), 1781-1789.
12. Perras, F. A.; Wang, Z.; Naik, P.; Slowing, I. I.; Pruski, M., Natural Abundance ^{17}O DNP NMR Provides Precise O–H Distances and Insights into the Brønsted Acidity of Heterogeneous Catalysts. *Angew. Chem. Int. Ed.* **2017**, *56* (31), 9165-9169.
13. Kobayashi, T.; Slowing, II; Pruski, M., Measuring Long-Range C-13-C-13 Correlations on a Surface under Natural Abundance Using Dynamic Nuclear Polarization-Enhanced Solid-State Nuclear Magnetic Resonance. *J. Phys. Chem. C* **2017**, *121* (44), 24687-24691.
14. Nelson, N. C.; Manzano, J. S.; Slowing, II, Deactivation of Ceria Supported Palladium through C-C Scission during Transfer Hydrogenation of Phenol with Alcohols. *J. Phys. Chem. C* **2016**, *120* (49), 28067-28073.
15. Singappuli-Arachchige, D.; Manzano, J. S.; Sherman, L. M.; Slowing, I. I., Polarity Control at Interfaces: Quantifying Pseudo-solvent Effects in Nano-confined Systems. *ChemPhysChem* **2016**, *17* (19), 2982-2986.

16. Kobayashi, T.; Wang, Z.; Pruski, M., Homonuclear Dipolar Recoupling of Arbitrary Pairs in Multi-spin Systems Under Magic Angle Spinning: A Double-Frequency-selective ZQ-SEASHORE Experiment. *Solid State Nucl. Magn. Reson.* **2019**.
17. Chamas, A.; Qi, L.; Mehta, H. S.; Sears, J. A.; Scott, S. L.; Walter, E. D.; Hoyt, D. W., High temperature/pressure MAS-NMR for the study of dynamic processes in mixed phase systems. *Magnetic Resonance Imaging* **2019**, *56*, 37-44.
18. Perras, F. A.; Wang, J. S.; Manzano, J. S.; Chaudhary, U.; Opembe, N.; Johnson, D. D.; Slowing, I. I.; Pruski, M., Optimal Sample Formulations for DNP SENS: The Importance of Radical-Surface Interactions. *Curr. Opin. Colloid Interface Sci.* **2018**, *33*, 9-18.
19. Perras, F. A.; Boteju, K. C.; Slowing, I. I.; Sadow, A. D.; Pruski, M., Direct ¹⁷O Dynamic Nuclear Polarization of Single-site Heterogeneous Catalysts. *Chem. Commun.* **2018**, *54* (28), 3472-3475.
20. Kobayashi, T.; Nishiyama, Y.; Pruski, M., Heteronuclear Correlation SSNMR Spectroscopy with Indirect Detection under Fast Magic Angle Spinning. In *New Developments in Solid-State NMR, No. 15, 'Modern Methods in Solid-State NMR: A practitioner's guide'*, Hodgkinson, P., Ed. Royal Society of Chemistry: London, 2018.
21. Perras, F. A.; Kobayashi, T.; Pruski, M., Growing Signals from the Noise: Challenging Nuclei in Materials DNP. In *Encyclopedia of Magnetic Resonance*, 2018; p in press.
22. Maluta, J. R.; Machado, S. A. S.; Chaudhary, U.; Manzano, J. S.; Kubota, L. T.; Slowing, I. I., Development of a Semigraphitic Sulfur-doped Ordered Mesoporous Carbon Material for Electroanalytical Applications. *Sensors and Actuators B: Chemical* **2018**, *257*, 347-353.
23. Boteju, K. C.; Wan, S.; Venkatesh, A.; Ellern, A.; Rossini, A. J.; Sadow, A. D., Rare Earth Arylsilazido Compounds with Inequivalent Secondary Interactions. *Chem. Commun.* **2018**, *54* (53), 7318-7321.
24. Reinig, R. R.; Fought, E. L.; Ellern, A.; Windus, T. L.; Sadow, A. D., Cobalt(II) Acyl Intermediates in Carbon-Carbon Bond Formation and Oxygenation. *Dalton Trans.* **2018**, *47* (35), 12147-12161.
25. Perras, F. A.; Padmos, J. D.; Johnson, R. L.; Wang, L.-L.; Schwartz, T. J.; Kobayashi, T.; Horton, J. H.; Dumesic, J. A.; Shanks, B. H.; Johnson, D. D.; Pruski, M., Characterizing Substrate-Surface Interactions on Alumina-Supported Metal Catalysts by Dynamic Nuclear Polarization-Enhanced Double-Resonance NMR Spectroscopy. *J. Am. Chem. Soc.* **2017**, *139* (7), 2702-2709.
26. Mouat, A. R.; Kobayashi, T.; Pruski, M.; Marks, T. J.; Stair, P. C., Direct Spectroscopic Evidence for Isolated Silanols in SiO_x/Al₂O₃ and Their Formation Mechanism. *J. Phys. Chem. C* **2017**, *121* (11), 6060-6064.
27. Perras, F. A.; Luo, H.; Zhang, X.; Mosier, N. S.; Pruski, M.; Abu-Omar, M. M., Atomic-Level Structure Characterization of Biomass Pre- and Post-Lignin Treatment by Dynamic Nuclear Polarization-Enhanced Solid-State NMR. *The Journal of Physical Chemistry A* **2017**, *121* (3), 623-630.
28. Perras, F. A.; Venkatesh, A.; Hanrahan, M. P.; Goh, T. W.; Huang, W.; Rossini, A. J.; Pruski, M., Indirect Detection of Infinite-speed MAS Solid-state NMR Spectra. *J. Magn. Reson.* **2017**, *276*, 95-102.
29. Kobayashi, T.; Perras, F. A.; Murphy, A.; Yao, Y.; Catalano, J.; Centeno, S. A.; Dybowski, C.; Zumbulyadis, N.; Pruski, M., DNP-enhanced Ultrawideline ²⁰⁷Pb Solid-state NMR Spectroscopy: An Application to Cultural Heritage Science. *Dalton Trans.* **2017**, *46* (11), 3535-3540.

30. Kobayashi, T.; Perras, F. A.; Chaudhary, U.; Slowing, I. I.; Huang, W.; Sadow, A. D.; Pruski, M., Improved strategies for DNP-enhanced 2D 1H-X heteronuclear correlation spectroscopy of surfaces. *Solid State Nucl. Magn. Reson.* **2017**, *87* (Supplement C), 38-44.
31. Egner, T. K.; Naik, P.; Nelson, N. C.; Slowing, I. I.; Venditti, V., Mechanistic Insight into Nanoparticle Surface Adsorption by Solution NMR Spectroscopy in an Aqueous Gel. *Angew. Chem. Int. Ed.* **2017**, *56* (33), 9802-9806.
32. Reinig, R. R.; Fought, E. L.; Ellern, A.; Windus, T. L.; Sadow, A. D., Rapid and Ordered Carbonylation and Oxygenation of a Cobalt(II) Methyl. *Chem. Commun.* **2017**, *53* (80), 11020-11023.
33. Manzano, J. S.; Weinstein, Z. B.; Sadow, A. D.; Slowing, I. I., Direct 3D Printing of Catalytically Active Structures. *ACS Catal.* **2017**, *7*, 7567-7577.
34. Nelson, N. C.; Boote, B. W.; Naik, P.; Rossini, A. J.; Smith, E. A.; Slowing, I. I., Transfer Hydrogenation over Sodium-modified Ceria: Enrichment of Redox Sites Active for Alcohol Dehydrogenation. *J. Catal.* **2017**, *346*, 180-187.
35. Johnson, R. L.; Perras, F. A.; Kobayashi, T.; Schwartz, T. J.; Dumesic, J. A.; Shanks, B. H.; Pruski, M., Identifying Low-coverage Surface Species on Supported Noble Metal Nanoparticle Catalysts by DNP-NMR. *Chem. Commun.* **2016**, *52* (9), 1859-1862.
36. Perras, F. A.; Chaudhary, U.; Slowing, I. I.; Pruski, M., Probing Surface Hydrogen Bonding and Dynamics by Natural Abundance, Multidimensional, O-17 DNP-NMR Spectroscopy. *J. Phys. Chem. C* **2016**, *120* (21), 11535-11544.
37. Perras, F. A.; Kobayashi, T.; Pruski, M., Magnetic Resonance Imaging of DNP Enhancements in a Rotor Spinning at the Magic Angle. *J. Magn. Reson.* **2016**, *264*, 125-130.
38. Kobayashi, T.; Perras, F. A.; Goh, T. W.; Metz, T. L.; Huang, W. Y.; Pruski, M., DNP-Enhanced Ultrawideband Solid-State NMR Spectroscopy: Studies of Platinum in Metal-Organic Frameworks. *J. Phys. Chem. Lett.* **2016**, *7* (13), 2322-2327.
39. Reinig, R. R.; Mukherjee, D.; Weinstein, Z. B.; Xie, W.; Albright, T.; Baird, B.; Gray, T. S.; Ellern, A.; Miller, G. J.; Winter, A. H.; Bud'ko, S. L.; Sadow, A. D., Synthesis and Oxidation Catalysis of [Tris(oxazoliny)borato]cobalt(II) Scorpionates. *Eur. J. Inorg. Chem.* **2016**, *2016* (15-16), 2486-2494.
40. Syed, Z. H.; Kaphan, D. M.; Perras, F. A.; Pruski, M.; Ferrandon, M. S.; Wegener, E. C.; Celik, G.; Wen, J.; Liu, C.; Dogan, F.; Goldberg, K. I.; Delferro, M., Electrophilic Organoiridium(III) Pincer Complexes on Sulfated Zirconia for Hydrocarbon Activation and Functionalization. *J. Am. Chem. Soc.* **2019**, *141* (15), 6325-6337.
41. Huang, X.-M.; Perras, F. A.; Manzano, J. S.; Slowing, I. I.; McNabb, A.; Pruski, M., The Anomalous Solidification of Concrete Grindings from Acid Treatment. *Cem. Concr. Res.* **2019**, *116*, 65-69.
42. Carnahan, S. L.; Lampkin, B. J.; Naik, P.; Hanrahan, M. P.; Slowing, I. I.; VanVeller, B.; Wu, G.; Rossini, A. J., Probing O-H Bonding through Proton Detected 1H-17O Double Resonance Solid-State NMR Spectroscopy. *J. Am. Chem. Soc.* **2019**, *141* (1), 441-450.
43. Mouat, A. R.; Whitford, C. L.; Chen, B. R.; Liu, S. S.; Perras, F. A.; Pruski, M.; Bedzyk, M. J.; Delferro, M.; Stair, P. C.; Marks, T. J., Synthesis of Supported Pd-0 Nanoparticles from a Single-Site Pd²⁺ Surface Complex by Alkene Reduction. *Chem. Mater.* **2018**, *30* (3), 1032-1044.
44. Khazdozian, H. A.; Manzano, J. S.; Gandha, K.; Slowing, I. I.; Nlebedim, I. C., Recycled Sm-Co Bonded Magnet Filaments for 3D Printing of Magnets. *AIP Advances* **2018**, *8* (5), 056722.

45. Camacho-Bunquin, J.; Ferrandon, M.; Sohn, H.; Yang, D. L.; Liu, C.; Ignacio-de Leon, P. A.; Perras, F. A.; Pruski, M.; Stair, P. C.; Delferro, M., Chemoselective Hydrogenation with Supported Organoplatinum(IV) Catalyst on Zn(II)-Modified Silica. *J. Am. Chem. Soc.* **2018**, *140* (11), 3940-3951.
46. Kaphan, C.; Klet, R. C.; Perras, F. A.; Pruski, M.; Yang, C.; Kropf, A. J.; Delferro, M., Surface Organometallic Chemistry of Supported Iridium(III) as a Probe for Metal-Support Interactions in C-H Activation. *ACS Catal.* **2018**, *8*, 5363-5373.
47. Klet, R. C.; Kaphan, D. M.; Liu, C.; Yang, C.; Kropf, A. J.; Perras, F. A.; Pruski, M.; Hock, A. S.; Delferro, M., Evidence for Redox Mechanisms in Organometallic Chemisorption and Reactivity on Sulfated Metal Oxides. *J. Am. Chem. Soc.* **2018**, *140* (20), 6308-6316.
48. Garcia, A.; Evans, J. W.; Slowing Igor, I., Pore Diameter Dependence of Catalytic Activity: p-Nitrobenzaldehyde Conversion to an Aldol Product in Amine-Functionalized Mesoporous Silica. *J. Chem. Phys.* **2018**, *Accepted*.
49. Alammari, T.; Slowing, I.; Anderegg, J.; Mudring, A. V., Ionic-Liquid-Assisted Microwave Synthesis of Solid Solutions of Sr_{1-x}Ba_xSnO₃ Perovskite for Photocatalytic Applications. *ChemSusChem* **2017**, *10* (17), 3387-3401.
50. Dairo, T. O.; Nelson, N. C.; Slowing, I.; Angelici, R. J.; Woo, L. K., Aerobic Oxidation of Cyclic Amines to Lactams Catalyzed by Ceria-Supported Nanogold. *Catal. Lett.* **2016**, *146* (11), 2278-2291.
51. de Lima Batista, A. P.; Zahariev, F.; Slowing, I. I.; Braga, A. A. C.; Ornellas, F. R.; Gordon, M. S., Silanol-Assisted Carbinolamine Formation in an Amine-Functionalized Mesoporous Silica Surface: Theoretical Investigation by Fragmentation Methods. *J. Phys. Chem. B* **2016**, *120* (8), 1660-1669.
52. Kandel, K.; Peerapattit, C.; Trewyn, B. G.; Pruski, M.; Slowing, I. I., Enzyme-Mesoporous Silica Nanocomposites for Upgrading the Carbon Content of Bio-ethanol. *Preprint Papers - American Chemical Society, Division of Petroleum Chemistry* **2012**, *57* (1), 202-204.
53. Garcia, A.; Slowing, I. I.; Evans, J. W., Pore diameter dependence of catalytic activity: p-nitrobenzaldehyde conversion to an aldol product in amine-functionalized mesoporous silica. *The Journal of Chemical Physics* **2018**, *149* (2), 024101.
54. Kandel, K.; Althaus, S. M.; Peerapattit, C.; Kobayashi, T.; Trewyn, B. G.; Pruski, M.; Slowing, I. I., Solvent-Induced Reversal of Activities between Two Closely Related Heterogeneous Catalysts in the Aldol Reaction. *ACS Catalysis* **2013**, *3* (2), 265-271.
55. Zeng, L.; An, L.; Wu, X., Modeling Drug-Carrier Interaction in the Drug Release from Nanocarriers. *J. Drug Delivery* **2011**, *2011*, 370308.
56. Eedugurala, N.; Wang, Z.; Chaudhary, U.; Nelson, N.; Kandel, K.; Kobayashi, T.; Slowing, I. I.; Pruski, M.; Sadow, A. D., Mesoporous Silica-Supported Amidozirconium-Catalyzed Carbonyl Hydroboration. *ACS Catal.* **2015**, *5*, 7399-7414.
57. Pindwal, A.; Yan, K.; Patnaik, S.; Schmidt, B. M.; Ellern, A.; Slowing, I. I.; Bae, C.; Sadow, A. D., Homoleptic Trivalent Tris(alkyl) Rare Earth Compounds. *J. Am. Chem. Soc.* **2017**, *139* (46), 16862-16874.

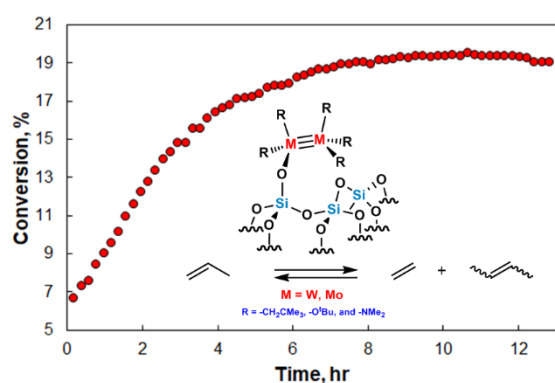
Electronic Cooperativity in Supported Organometallic Catalysts for Low Temperature Upgrading of Light Alkenes

Alon Chapovetsky,¹ Gokhan Celik,¹ Ryan R. Langeslay,² Frédéric A. Perras,² Marek Pruski,² Magali S. Ferrandon,¹ Evan C. Wegener,¹ Hacksung Kim,¹ Jacob White,³ Laura Gagliardi,³ Alfred P. Sattelberger,¹ David M. Kaphan,¹ Massimiliano Delferro¹

¹Chemical Sciences and Engineering Division, Argonne National Laboratory, ²Ames Laboratory, ³Department of Chemistry, University of Minnesota

Presentation Abstract

The catalytic formation of C-C bonds has received significant attention in recent decades due to its commercial relevance. Industrially, these transformations are performed using heterogeneous catalysts due to their stability, recyclability, and cost. However, homogeneous catalysts for C-C bond activation offer some advantages, such as higher selectivity, over their heterogeneous counterparts. Supported organometallic catalysts on solid inorganic or organic substrates are making an important contribution to heterogeneous catalysis. The large majority of supports currently used in industry are inorganic materials (SiO₂, Al₂O₃, MgCl₂), with silica being the most important. Single-site supported catalysts are most commonly prepared by molecular-level anchoring/chemisorption, in which a molecular precursor undergoes reaction with the surface while maintaining most of the ligand sphere of the parent molecule. Herein, we present the catalytic olefin metathesis properties of a series of dimers of the form M₂L₆ (where M = W, Mo; and L = alkyl, oxide, amide) grafted on a partially dehydroxylated silica surface through surface organometallic chemistry. The structure of the site-isolated organometallic Mo and W dimer sites have been fully elucidated through a series of spectroscopic surface characterization techniques, which include solution-phase ¹H NMR spectroscopy, DNP solid-state NMR spectroscopy, diffuse



reflectance infrared Fourier transform spectroscopy (DRIFTS), UV-Raman, and X-ray adsorption spectroscopy (XAS). Low temperature liquid- (1-nonene) and gas-phase (disproportionation of propylene to butenes) metathesis of alkenes were carried out using both [M₂X₅@SiO₂] and the homogeneous analogues. The supported Mo³⁺- and W³⁺-based catalysts exhibit high activity without any pre-activation with H₂, while the organometallic catalyst controls are completely unreactive. Moreover, the reactivity depends on the ancillary

ligands, with the activity for the metathesis of olefin following the order –neopentyl > -O^tBu > and -NMe₂. These results suggest the formation of a metal-methylidene active species enabled by a synergistic interaction between the metal complexes and the surface.

FWP50966: Electronic Cooperativity in Supported Single- and Multinuclear-Sites for Catalytic C-C and C-H Bonds Functionalization

Principal Investigators: Massimiliano Delferro (Lead PI), David M. Kaphan, Cong Liu, A. Jeremy Kropf

Argonne Staff members: Magali Ferrandon

Postdocs: Gokhan Celik, Alon Chapovetsky, Evan Wegener, Ryan R. Langeslay

Affiliations: Chemical Sciences and Engineering Division, Argonne National Laboratory, Lemont, IL 60439

RECENT PROGRESS

Goals

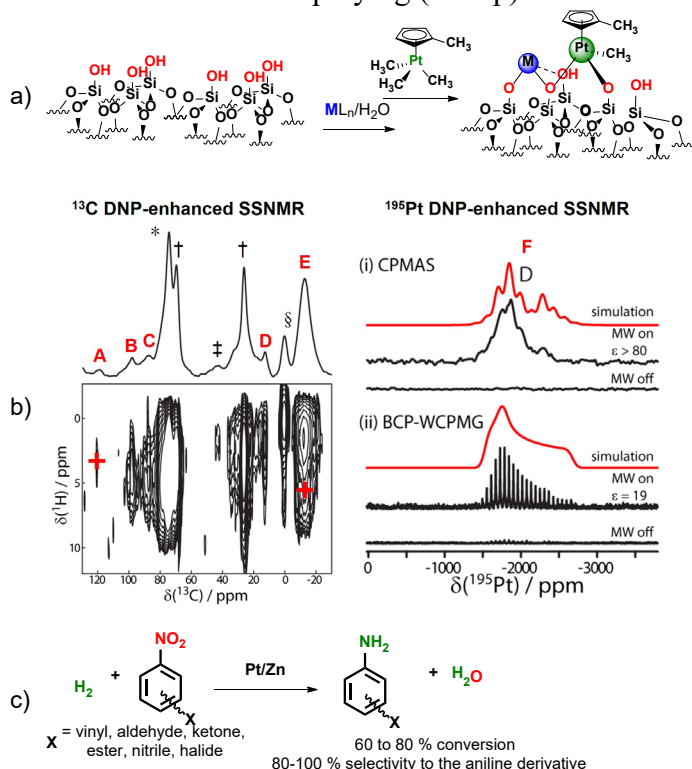
The long-term goals of our efforts are to understand and manipulate isolated, “homogeneous-in-function” supported single-site catalysts for low-temperature transformations (e.g., alkane C–H activation and functionalization) and elucidation of operant mechanisms in these systems. Our group recently developed synthetic control of isolated, single-site catalysts on metal oxide supports (i.e. SiO₂) employing the tools of surface organometallic chemistry (SOMC) and atomic layer deposition (ALD). The nature of these active site support platforms provides efficient and general routes to isolated, single-site surface species that exhibit catalytic activity, selectivity and stability, notably under reaction conditions where their molecular analogs are largely unstable and/or unreactive.

Description of the Results

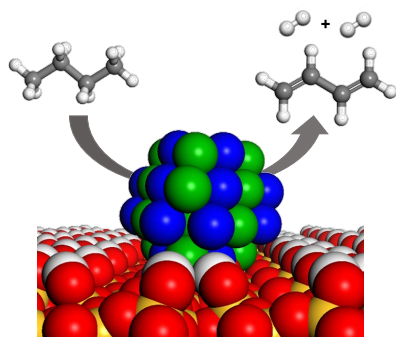
Our group achieved successes in two major project thrusts in FY16-19. The first project thrust has been focused on control of the reactivity and stability of sensitive single-atom catalysts supported on *tailored metallo-ligand environments/surfaces*. By employing stepwise synthesis of multicomponent catalyst scaffolds, we successfully developed site-isolated organometallic catalysts on surfaces equipped with metal anchoring sites/promoter ions. In parallel, we have developed *rational design via well-defined, single-site catalysts* on support platforms for controlled hydrocarbon transformations such as non-oxidative dehydrogenation of alkanes to alkenes and its microscopic reverse, alkene hydrogenation. Our recent achievements cover advances in the (1) synthesis of well-defined, supported organometallic sites using state-of-the-art synthetic techniques (e.g., ALD, surface organometallic synthesis), (2) development of spectroscopic strategies to elucidate operant reaction mechanisms and (3) computationally guided development of supported single-atom catalytic sites.

Promoter and Anchoring Site Effects in Single-Site Catalysts. Single-ion catalysts based on highly reducible noble metals (e.g., Pt) remains challenging due to their susceptibility to sintering. To date, two notable strategies have been shown effective in stabilizing single-ion or pseudo-single-ion noble metal catalysts on solid supports, which include (1) nucleation on defect sites on bulk oxides and (2) support on carbonaceous surfaces where the surface hydroxyl concentrations are low. Air-stable, well-defined, isolated organoplatinum(IV) precatalysts were deposited on ALD-Zn²⁺(submonolayer)/SiO₂ surfaces, employing solution-phase synthesis conditions under which SiO₂ is largely unreactive (Figure 1). The straightforward deposition of the trimethyl(methylcyclopentadienyl)platinum(IV) [(MeCp)PtMe₃] precursor is attributed to the increased acidity of surface silanols associated to Zn²⁺ cations. DFT modeling of the platination reaction suggests that the metalation of Zn²⁺-bound silanols is thermodynamically more favorable ($\Delta G = -12.4$ kcal/mol) than with silanols of non-modified SiO₂. The results of a combination of

spectroscopic (e.g., XAS, SS ^1H , ^{13}C , and ^{195}Pt NMR, DRIFTS, DR-UV-Vis) and surface characterization (e.g., TPR) techniques are consistent with the presence of site-isolated Pt^{4+} sites. The Pt^{4+} sites deposited via solution-phase synthesis ((MeCp)PtMe/Zn/SiO₂) are stabilized by a methylcyclopentadienyl ligand, one unreacted methyl group, and an anionic siloxy group, as confirmed by advanced solid state DNP NMR (in collaboration with DOE Ames Lab/Dr. M. Pruski). Solution-phase, chemoselective hydrogenation of a series of functionalized nitroaryls to the corresponding anilines was achieved under mild conditions employing (MeCp)PtMe/Zn/SiO₂ with excellent tolerance of other hydrogenation-sensitive functionalities (e.g., vinyl, aldehyde, ketone, esters, nitriles and halides). On the other hand, Pt(NP)/SiO₂ (NP = nanoparticles) fully hydrogenated the $-\text{NH}_2$ group and other unsaturated functionalities (i.e., alkene and carbonyl groups). TPR, variable-temperature DRIFTS, and *in situ* XAS experiments under H₂ provided important insights into the precatalyst activation mechanism. In particular for (MeCp)PtMe/Zn/SiO₂, at the reaction temperature of 135 °C, the Pt-CH₃ group undergoes hydrogenolysis to yield a Pt^{4+} -H species, identified via *in situ* DRIFTS, while the CpMe ligand is not cleaved. This suggests that the ancillary ligand is necessary for the observed chemoselectivity.



The atomic-level control achieved in the stepwise ALD or SOMC synthesis of the site-isolated organoplatinum(IV) catalysts offers a promising general strategy for accessing multi-metallic sites where the promoter/anchoring site can be varied, allowing for the tuning of active site electronic and steric properties. Multimetallic nanoclusters (<1 nm) exhibit notable orthogonal catalytic reactivity as compared to their monometallic analogues. The addition of a second metal imparts a change in electron density (ligand effects) and/or a blocking of undesired reactive sites (ensemble effects), which in turn influence the catalytic properties, such as activity, selectivity, and stability. In preliminary experiments, we have shown that a supported PtZn alloy on silica, obtained via stepwise ALD or

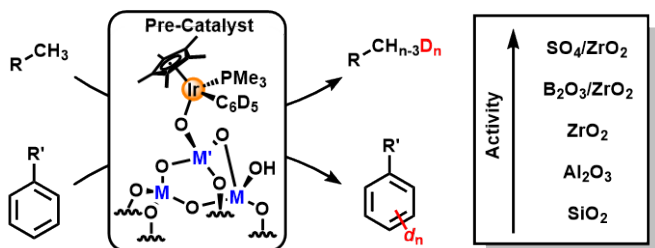


and followed by activation under H₂ at 550 °C, gives rise to an efficient and selective nanocluster catalyst of particle size ~ 1 nm for the non-oxidative dehydrogenation (equilibrium conditions > 500 °C) of *n*-butane to 1,3-butadiene (BDE), a valuable precursor for synthetic rubber and fine chemicals production (*n*-butane conversion = 80%, theoretical 83.8%; BDE yield = 10%). The formation of the nanocluster alloy catalyst was confirmed employing a set of characterization tools, including XAS, XPS, and scanning transmission electron microscopy-energy dispersive X-ray (STEM-EDX). Note that a

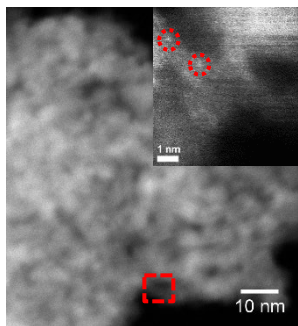
Pt/SiO₂ catalyst is mainly selective to butenes (*n*-butane conversion = 20%; BDE yield = 4 %) and is prone to deactivation and fouling since the desired product, BDE, is a potent coke precursor. The high conversion and selectivity towards the diene formation is attributed to a combination of geometrical (particle size; via STEM) and electronic effects (bimetallic vs monometallic; via XAS, XPS, XRD, and pair distribution function (PDF)). Comparison of the activity of various PtZn/SiO₂ catalysts with different particle sizes (from single-atom to 5 nm particles) reveals the profound effects of the synthesis method on 1,3-butadiene production and long-term stability. Subnanometer clusters (<1 nm) of PtZn/SiO₂ outperform their larger counterparts (> 2 nm), suggesting a possible quantum effect for particles smaller than 1 nm.

Rational Design of Supported Single-Site Catalysts. Rational Design of Supported Single-Site Catalysts.

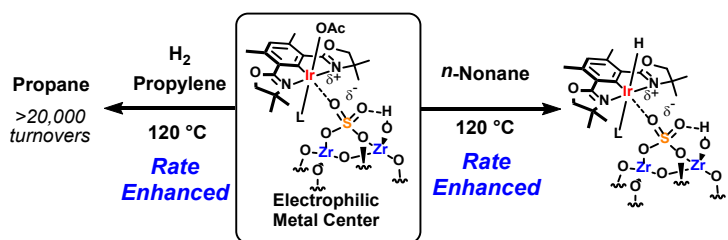
Systematic study of the interactions between organometallic catalysts and metal oxide support materials is critical for the realization of rational design in heterogeneous catalysis. The stoichiometric and catalytic chemistry of a [Cp*(PMe₃)Ir(III)] complex chemisorbed on a variety of acidic metal oxides was studied as a multifaceted probe for stereoelectronic communication between the support and organometallic center. Electrophilic bond activation was explored in the context of stoichiometric hydrogenolysis as well as catalytic H/D exchange. Further information was obtained from the observation of processes related to dynamic exchange between grafted organometallic species and those in solution. The supported organometallic species were characterized by a variety of



spectroscopic techniques including DNP solid-state NMR spectroscopy, DRIFT, and XAS. Strongly acidic modified metal oxides such as sulfated zirconia engender high levels of activity toward electrophilic bond activation of both sp² and sp³ C–H bonds, including the rapid deuteration of methane at room temperature; however, the global trend for the supports studied here does not suggest a direct correlation between activity and surface Brønsted acidity, and more complex metal surface interactions are at play. One such interaction was identified as an unexpected redox event between the organometallic species and the modified oxide surfaces. Evidence of oxidative mechanism was provided by studying the analogous homogeneous reactivity of the organometallic precursors toward [Ph₃C]⁺, a Lewis acid known to effect formal hydride abstraction by one electron oxidation followed by hydrogen atom abstraction. Organometallic deuterium incorporation, a result of the surface redox process, was found to be correlated with surface sulfate concentration, as well as the extent of dehydration under thermal activation conditions of sulfated alumina and sulfated zirconia supports. Surface sulfate concentration dependence, in conjunction with a computational study of surface electron affinity, indicates an electron deficient pyrosulfate species as the redox active moiety. These results provide further evidence for the ability of sulfated metal oxides to participate in redox chemistry not only toward organometallic complexes, but also in the larger context of their application as catalysts for the transformation of light alkanes. Having found that sulfated oxides could act as solid non-coordinating counterions in the context of IrCp* complexes, imbuing activity in C–H bond insertion reactions reminiscent of homogeneous counterions such as triflate, we sought to translate this capability to a catalyst platform active in the hydrogenation and dehydrogenation of light hydrocarbons. The (^{dm}Phebox)Ir(III) pincer complex has garnered recent attention in the field for its ability to activate and functionalize alkanes,



however, dehydrogenation could only be achieved in a formal catalytic cycle, as the elevated temperatures required for C-H activation and β -hydride elimination interfered with the remaining elementary steps to regenerate the active species. Previous computational and experimental results from the groups of Cundari and Goldman suggest that withdrawing electron density from the iridium center might lower the barrier to these troublesome steps. By chemisorbing (dm Phebox)Ir(III)(OAc)₂(OH₂) on sulfated zirconia, we envisioned that in the heterogenization, we would simultaneously increase electrophilicity at the iridium center and facilitate the bond activation and elimination process. Indeed, cationic character was imparted to the iridium center by its grafting onto sulfated zirconia, with alkane activation and β -hydride elimination to form the corresponding olefin and iridium-hydride on a reasonable timescale at 120 °C for the supported complex, compared to 200 °C for the molecular bis-acetate complex. While the detection of catalytic turnover in the dehydrogenation proved elusive, the microscopic reverse of this process, olefin hydrogenation, was highly efficient with this supported complex, with over 20,000 turnovers observed in 50 hours on stream and little evidence of deactivation. In contrast, the homologous complex supported on silica was inactive, and eventually decomposed to iridium nanoparticles. Spectroscopic methods such as diffuse reflectance infrared Fourier transformation spectroscopy, dynamic nuclear polarization enhanced solid-state nuclear magnetic resonance spectroscopy, and X-ray absorption spectroscopy were used to characterize the supported species, and DFT calculations based on a cluster model for the sulfated surface underscored the role of the surface as a non-coordinating counterion by *in silico* comparison to the triflate analogue. Tetrabutylammonium acetate was found to remove the organometallic species from the surface, enabling solution-phase analytical techniques in conjunction with traditional surface methods.



Publications funded by this FWP in 2016-2019

1. Syed, Z. H.; Kaphan, D. M.; Perras, F. A.; Pruski, M.; Ferrandon, M. S.; Wegener, E. C.; Celik, G.; Wen, J.; Liu, C.; Dogan, F.; Goldberg, K. I.; Delferro, M. Electrophilic Organoiridium(III) Pincer Complexes on Sulfated Zirconia for Hydrocarbon Activation and Functionalization. *J. Am. Chem. Soc.* **2019**, *141*, 6325-6337.
2. Langeslay, R. R.; Kaphan, D. M.; Marshall, C. L.; Stair, P. C.; Sattelberger, A. P.; Delferro, M. Catalytic Applications of Vanadium: A Mechanistic Perspective. *Chem. Rev.* **2019**, *119*, 2128-2191.
3. Plascencia, C.; Curtiss, L. A.; Liu, C. Hydrogen Activation by Silica-Supported Metal Ion Catalysts: Catalytic Properties of Metals and Performance of DFT Functionals. *J. Phys. Chem. A* **2019**, *123*, 171-186
4. Camacho-Bunquin, J.; Ferrandon, M. S.; Sohn, H.; Kropf, A. J.; Yang, C.; Wen, J.; Hackler, R. A.; Liu, C.; Celik, G.; Marshall, C. L.; Stair, P. C.; Delferro, M. Atomically Precise Strategy

- to a PtZn Alloy Nanocluster Catalyst for the Deep Dehydrogenation of n-Butane to 1,3-Butadiene. *ACS Catal.* **2018**, 10058-10063.
- Langeslay, R. R.; Sohn, H.; Hu, B.; Mohar, J. S.; Ferrandon, M.; Liu, C.; Kim, H.; Niklas, J.; Poluektov, O. G.; Alp, E. E.; Sattelberger, A. P.; Hock, A. S.; Delferro, M. Nuclearity Effects in Supported, Single-Site Fe(II) Hydrogenation Catalysts. *Dalton Trans.* **2018**, 47, 10842-10846.
 - Klet, R. C.; Kaphan, D. M.; Liu, C.; Yang, C.; Kropf, A. J.; Perras, F. A.; Pruski, M.; Hock, A. S.; Delferro, M., Evidence for Redox Mechanisms in Organometallic Chemisorption and Reactivity on Sulfated Metal Oxides. *J. Am. Chem. Soc.* **2018**, 140, 6308-6316 (JACS May 23, 2018 Cover and JACS Spotlights).
 - Kaphan, D. M.; Klet, R. C.; Perras, F. A.; Pruski, M.; Yang, C.; Kropf, A. J.; Delferro, M. Surface Organometallic Chemistry of Supported Iridium(III) as a Probe for Organotransition Metal-Support Interactions in C-H Activation. *ACS Catal.* **2018**, 8, 5363-5373
 - Camacho-Bunquin, J.; Ferrandon, M.; Sohn, H.; Yang, D.; Liu, C.; Ignacio-de Leon, P. A.; Perras, F. A.; Pruski, M.; Stair, P. C.; Delferro, M. Chemo-Selective Hydrogenation of Nitro Compounds with Supported Organoplatinum(IV) on Zn(II)/SiO₂ Catalyst. *J. Am. Chem. Soc.* **2018**, 140, 3940-3951.
 - Liu, C.; Camacho-Bunquin, J.; Ferrandon, M.; Savara, A.; Sohn, H.; Yang, D.; Kaphan, D. M.; Langeslay, R. R.; Ignacio-de Leon, P. A.; Liu, S.; Das, U.; Yang, B.; Hock, A. S.; Stair, P. C.; Curtiss, L. A.; Delferro, M. Development of Activity-Descriptor Relationship in Supported Metal Ion Hydrogenation Catalysts on Silica. *Polyhedron* **2018**, 152, 73-83 (Invited contribution)
 - Zhao, Y.; Sohn, H.; Hu, B.; Niklas, J.; Poluektov, O. G.; Tian, J.; Delferro, M.; Hock, A. S. Zirconium Modification Promotes Catalytic Activity of a Single-Site Cobalt Heterogeneous Catalyst for Propane Dehydrogenation. *ACS Omega* **2018**, 3, 11117-11127.
 - Sohn, H.; Camacho-Bunquin, J.; Langeslay, R. R.; Ignacio-de Leon, P. A.; Niklas, J.; Poluektov, O. G.; Liu, C.; Connell, J. G.; Yang, D.; Kropf, J.; Kim, H.; Stair, P. C.; Ferrandon, M.; Delferro, M. Supported Single-Site Organo-Vanadium(III) Catalyst on Silica for Hydrogenation of Alkenes and Alkynes. *Chem. Commun.* **2017**, 53, 7325-7328 (invited for special issue: ChemComm Emerging Investigators Issue 2017).
 - Camacho-Bunquin, J.; Ferrandon, M.; Das, U.; Dogan, F.; Liu, C.; Larsen, C.; Platero-Prats, A. E.; Curtiss, L. A.; Hock, A. S.; Miller, J. T.; Nguyen, S. T.; Marshall, C. L.; Delferro, M.; Stair, P. C. Supported Aluminum Catalysts for Olefin Hydrogenation. *ACS Catal.* **2017**, 7, 689-694.
 - Getsoian A.; Hu B.; Miller J. T.; Hock A. S. Supported Single-Site Sc and Y Alkyl Catalysts for Olefin Hydrogenation. *Organometallics*, **2017**, 36, 3677-3685.
 - Camacho-Bunquin, J.; Aich, P.; Ferrandon, M.; Getsoian, A.; Das, U.; Dogan, F.; Curtiss, L.; Miller, J. T.; Marshall, C. L.; Hock, A. S.; Stair, P. C. Single-Site Zinc on Silica Catalysts for

Propylene Hydrogenation and Propane Dehydrogenation. Synthesis and Reactivity Evaluation through Integrated Atomic Layer Deposition-Catalysis Experimentation. *J. Catal.* **2017**, *345*, 170-182 (Editor's Choice).

15. Getsoian, A.; Das, U.; Camacho-Bunquin, J.; Zhang, G.; Gallagher, J. Hu, B.; Schaidle, J.; Ruddy, D. A.; Kraft, S. J.; Henley, J.; Curtiss, L. A.; Miller, J. T.; Hock, A.S. Organometallic model complexes elucidate the active gallium species in alkane dehydrogenation catalysts based on ligand effects in Ga K-edge XANES. *Catal. Sci. Technol.* **2016**, *6*, 6339-6353.
16. Das, U.; Zhang, G.; Hu, B.; Hock, A. S.; Redfern, P. C.; Miller, J. T.; Curtiss, L. A. Effect of Siloxane Ring Strain and Cation Charge Density on the Formation of Coordinately Unsaturated Metal Sites on Silica: Insights from Density Functional Theory (DFT) Studies. *ACS Catal.* **2016**, *5*, 7177-7185.

Submitted/In preparation:

17. Kaphan, D. M.; Langeslay, R. R.; Ferrandon, M.; Liu, C.; Wegner, E.; Kropf, A. J.; Delferro, M. Mechanistic Aspects of a Surface Organovanadium(III) Catalyst for Hydrocarbon Hydrogenation and Dehydrogenation. *ChemRxiv*, **2019**

Patents

18. Multimetallic catalysts for selective hydrogenation of dienes. Camacho-Bunquin, J.; Ferrandon, M.; Delferro, M. U.S. Patent Application Number: 15/484,928.
19. Multimetallic catalysts. Camacho-Bunquin, J.; Ferrandon, M.; Delferro, M.; Stair, P. C. U.S. Patent Application Number: 62/402,218.
20. Multimetallic catalysts for alkane dehydrogenation and synthesis thereof. Stair, P. C.; Camacho-Bunquin, J.; Marshall, C. L.; Hock A. S. U.S. Patent Application Number: 15/157,109.

Publications jointly funded by this FWP and other grants with leading intellectual contribution from this FWP in 2016-2019

21. Jang, J. H.; Sohn, H.; Camacho-Bunquin, J.; Yang, D.; Park, C.; Delferro, M.; Abu-Omar, M. M., Deoxydehydration (DODH) of Biomass-Derived Polyols with a Reusable Unsupported Rhenium Nanoparticles Catalyst. *ACS Sustainable Chem. Eng.* **2019**, DOI: 10.1021/acssuschemeng.9b01253.
22. Zhong, H.; Friedfeld, M. R.; Camacho-Bunquin, J.; Sohn, H.; Yang, C.; Delferro, M.; Chirik, P. J., Exploring the Alcohol Stability of Bis(phosphine) Cobalt Dialkyl Precatalysts in Asymmetric Alkene Hydrogenation. *Organometallics* **2019**, *38*, 149-156
23. Pang, H.; Gallou, F.; Sohn, H.; Bunquin, J. C.; Delferro, M.; Lipshutz B. H. Synergistic effects in Fe nanoparticles doped with ppm levels of (Pd + Ni). A new catalyst for sustainable nitro group reductions. *Green Chem.* **2018**, *20*, 130-135
24. Huang, Z.; Liu, D.; Camacho-Bunquin, J.; Zhang, G.; Yang, D.; López-Encarnación, J. M.; Jellinek, J.; Xu, Y.; Ferrandon, M.; Lei, A.; Bunel, E. E.; Delferro, M. Supported Single-Site

Ti(IV) on a Metal–Organic Framework for the Hydroboration of Carbonyl Compounds. *Organometallics* **2017**, *36*, 3921-3930

25. Cybulskis, V. J.; Pradhan, S. U.; Lovón-Quintana, J. J.; Hock, A. S.; Hu, B.; Zhang, G.; Delgass, W. N.; Ribeiro, F. H.; Miller J. T. The Nature of the Isolated Gallium Active Center for Propane Dehydrogenation on Ga/SiO₂. *Catal. Lett.* **2017**, *147*, 1252-1262.
26. Martynowycz, M. W.; Hu, B.; Kuzmenko, I.; Bu, W.; Hock, A.; Gidalevitz, D. Monomolecular Siloxane Film as a Model of Single-Site Catalysts *J. Am. Chem. Soc.* **2016**, *138*, 12432-12439.

Jointly funded by this FWP and other grants with relatively minor intellectual contribution from this FWP in 2016-2019

27. Jung, D.; Saleh, L. M. A.; Berkson, Z. J.; El-Kady, M. F.; Hwang, J. Y.; Mohamed, N.; Wixtrom, A. I.; Titarenko, E.; Shao, Y.; McCarthy, K.; Guo, J.; Martini, I. B.; Kraemer, S.; Wegener, E. C.; Saint-Cricq, P.; Ruehle, B.; Langeslay, R. R.; Delferro, M.; Brosmer, J. L.; Hendon, C. H.; Gallagher-Jones, M.; Rodriguez, J.; Chapman, K. W.; Miller, J. T.; Duan, X.; Kaner, R. B.; Zink, J. I.; Chmelka, B. F.; Spokoyny, A. M., A molecular cross-linking approach for hybrid metal oxides. *Nature Mater.* **2018**, *17*, 341-348.
28. Halder, A.; Liu, C.; Liu, Z.; Emery, J. D.; Pellin, M. J.; Curtiss, L. A.; Zapol, P.; Vajda, S.; Martinson, A. B. F. Water Oxidation Catalysis via Size-Selected Iridium Clusters. *J. Phys. Chem. C* **2018**, *122*, 9965-9972.
29. Canossa, S.; Bellè, E.; Delferro, M.; Predieri, G.; Graiff, C. Structural motifs in heteroleptic copper and cadmium selenites *Inorg. Chim. Acta* **2018**, *470*, 206-212.
30. Yang, B.; Liu, C.; Halder, A.; Tyo, E.; Martinson, A. B. F.; Seifert, S.; Zapol, P.; Curtiss, L. A.; Vajda, S. Copper Cluster Size Effect in Methanol Synthesis from CO₂. *J. Phys. Chem. C* **2017**, *121*, 10406-10412.

**In-situ Studies for the Conversion of C-O Bonds
on Complex Metal-Oxide and Metal-Carbide Interfaces**

José A. Rodriguez, Ping Liu, Sanjaya D. Senanayake and Michael G. White
Brookhaven National Laboratory, Chemistry Department

Presentation Abstract

In the area of C1 Chemistry, the oxidation of carbon monoxide ($\text{CO} + 0.5\text{O}_2 \rightarrow \text{CO}_2$), the water-gas shift reaction (WGS: $\text{CO} + \text{H}_2\text{O} \leftrightarrow \text{H}_2 + \text{CO}_2$) and the hydrogenation of CO_2 to methanol ($\text{CO}_2 + 3\text{H}_2 \rightarrow \text{CH}_3\text{OH} + \text{H}_2\text{O}$) are important processes which involve the formation or cleavage of C-O bonds. Complex metal-oxide interfaces play a fundamental role in materials used to catalyze these processes. Fundamental studies have been performed to investigate the chemistry associated with CO oxidation, the WGS reaction and CO_2 hydrogenation on a series of model and powder catalysts which contain metal-oxide and metal-carbide interfaces. Several *in-situ* techniques {X-ray diffraction (XRD), pair-distribution function analysis (PDF), X-ray absorption spectroscopy (XAS), environmental scanning tunneling spectroscopy (ESTM), infrared spectroscopy (IR) and ambient-pressure X-ray photoelectron spectroscopy (AP-XPS)} and theoretical calculations {Density Functional Theory and kinetic Monte Carlo} were used to characterize the properties of the active phase in the catalysts and the reaction mechanism. The active phase in these catalysts involved metallic elements (Cu, Au, Pt) in contact with oxide and carbide supports. The *in-situ* studies indicate that metal-oxide interfaces useful for the WGS and CO_2 hydrogenation are dynamic entities which change with reaction conditions. In many cases cooperative interactions between the metal and carbide or oxide lead to high catalytic activity or selectivity. In general, the highly active WGS and CO_2 hydrogenation catalysts are bifunctional with the metal and oxide or carbide catalyzing different parts of the reactions. The complexity of metal-oxide interfaces can be modified by the controlled use of alkali metals. The alkali-modified metal-oxide interfaces display an enhanced activity for the WGS reaction and a shift in selectivity from methanol to higher alcohols during the hydrogenation of CO_2 .

FWP-BNL-CO040: Catalysis for Advanced Fuel Synthesis and Energy

Co-PIs: Ping Liu, Sanjaya Senanayake, and Michael G. White

Postdoc(s): Zongyuan Liu, Robert Palomino, David Grinter, Mausumi Mahapatra,
Juan Pablo Simonovis, Siyu Yao, Lili Lin

Student(s): Si Luo, Zongyuan Liu, Fang Xu, Dimitriy Vovchok, Zhijun Zuo, Pamela Carrillo, Kenneth Goodman, Rebecca Hamlyn, Yilin Ma, Jason Wang, Meng Xue, Feng Zhang, Jindong Kang, Kaixi Deng.

Affiliations(s): All students are from SUNY Stony Brook, Department of Chemistry

RECENT PROGRESS

C1 chemistry involves the conversion of molecules that contain one carbon atom into valuable products. C1 chemistry is expected to become a major area of interest for the transportation fuel and chemical industries in the relatively near future. In general, the feedstocks for C1 chemistry include natural gas (mostly methane), carbon monoxide, carbon dioxide, methanol and synthesis gas (a mixture of carbon monoxide and hydrogen). Thus, a fundamental understanding of the conversion of C-O and C-H bonds is essential for controlling C1 chemistry. The Catalysis Group at BNL has been quite active in this area. In the period 2016-2019, sixty-six papers have been published in peer-reviewed journals (Science, Angewandte Chemie, Journal of the American Chemical Society).¹⁻⁶⁶ Sixteen of them were exclusively funded by this grant and for the other fifty this grant made the major intellectual contribution. The reactions investigated included the oxidation of CO, the water-gas shift, the hydrogenation of CO₂ and the activation of methane and its dry reforming. Experimental and theoretical studies have been performed exploring correlations between the structure and reactivity of typical metal catalysts or catalysts that contain oxides and carbides. Work was done with high-surface area powders and model catalysts. In the last three years, major research achievements within this program have been:

- Identification of the inverse ZnO/Cu system as an active catalyst for C1 chemistry.^{47,57,60}
- Discovery of the essential role that complex metal-oxide and metal-carbide interfaces play in the catalysis associated with C1 chemistry.^{7,9,35,43,48,56,66}
- Detailed proof through *operando* studies that metal/oxide catalysts are dynamic entities that change as a function of reaction conditions during the water-gas shift, CO₂ hydrogenation and methane dry reforming.^{14,15,38,53,59}
- Discovery of the importance of metal-support interactions in active catalysts for C1 chemistry.^{17,18,19,22,36,66}
- Discovery of the high surface mobility of K as a promoter of the activity of catalysts used for CO oxidation, the water-gas shift and CO₂ hydrogenation.^{29,49}
- Identification of M-CeO₂ (M= Co, Ni, Fe, Pt, Ru) as active systems for the low-temperature activation of methane.^{53,59}

These are examples of the research done during the 2018-2019 years:

A. Catalytic properties of inverse ZnO/Cu catalysts: C-O bond conversion

Mixtures of CuO-ZnO are frequently used as catalysts for the WGS and the synthesis of methanol. A recent transmission electron microscopy (TEM) study has revealed that strong metal-support interactions between Cu and ZnO lead to the formation of a ZnO overlayer on top of the Cu particles in an industrial Cu/ZnO/Al₂O₃ catalyst under reaction conditions [Lunkenbein et al, *Angew Chem Int Ed* **2015**, 54, 4544] Such formation of an oxide overlayer on Cu could create a catalytically active metal-oxide interface. The ZnO detected on the TEM study has a graphitic-like structure. We have performed a systematic study investigating the growth mode of ZnO on Cu(111) under different reaction conditions using scanning tunneling microscopy (STM).^{57,60} Different grow modes were identified as a function of temperature and deposition conditions (see Figure 1).

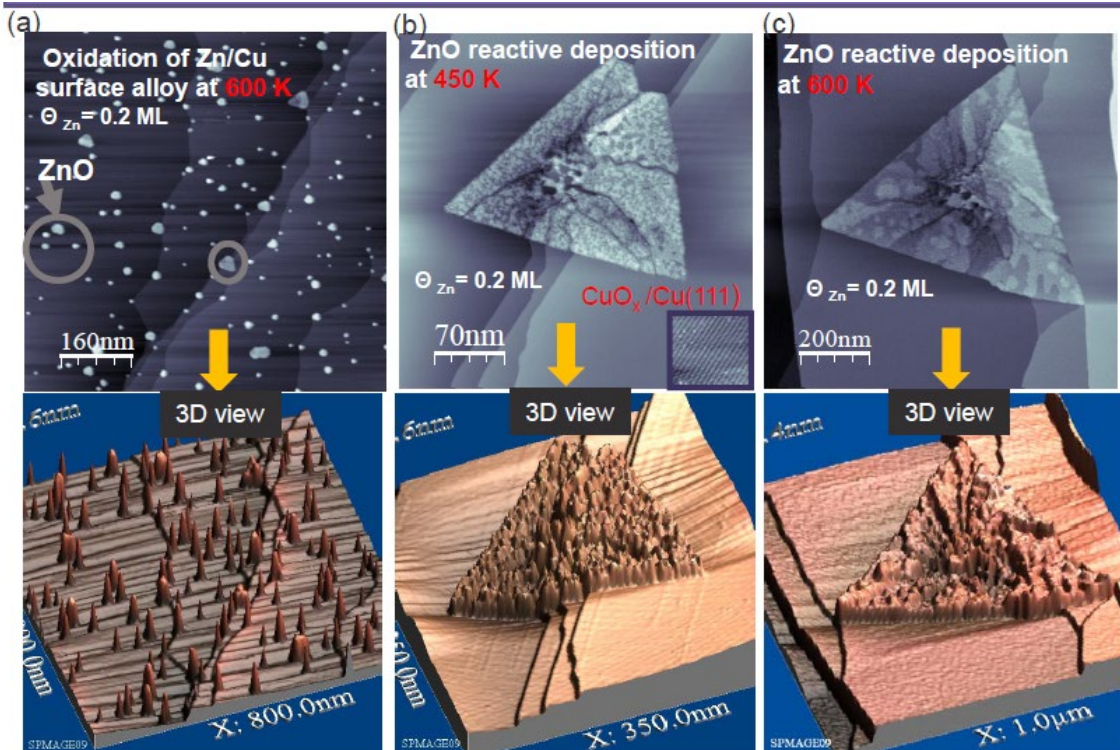


Figure 1 Growth modes for ZnO on Cu(111) at different temperatures and without (a) and with O₂ gas in the background during the deposition of zinc.⁶⁰ A layer of ZnO is formed between the ZnO and the Cu(111) substrate.

In a set of experiments, Zn was deposited on Cu(111) or CuO_x/Cu(111) surfaces at 300 K with subsequent exposure to O₂ at higher temperatures (400-550 K) which exhibited small particles of ZnO (< 20 nm in size) on the surface.^{57,60} The deposition of Zn onto CuO_x/Cu(111) at elevated temperatures (450-600 K) in an oxygen ambient produced large ZnO islands (300-650 nm in size) which were very rough and spread over several terraces of Cu(111).⁶⁰ XPS/Auger spectra showed that all the preparation conditions stated above led to the formation ZnO/CuO_x/Cu(111) surfaces where the oxidation state of zinc was uniform. The large diameter of the ZnO islands in Figure 1 indicates that, at high temperatures, a critical size nuclei is necessary to stabilize the Zn on the surface rather than diffusing into the Cu bulk. The edges of the ZnO_x islands coincide with the Cu(111) lattice direction. High-resolution images revealed that the bare surfaces surrounding the triangular islands are a CuO_x-44 structure (shown in the inset in Figure 1b) as expected. It has been observed that the majority of the triangular islands grow near step edges although there are some instances where they grow on flat terraces. The shape of the triangles varies; it can be a perfect isosceles triangle, or a triangle with truncated edges as shown in Figure 1b. However, all the triangular islands have some common features: they tend to have depressions in the center, rugged morphology, contain several layers, and are very porous in nature. Figure 1b and 1c display a zoomed in 3D view clearly showing a rough morphology and depressions inside the islands.⁶⁰

It has been observed that a majority of the triangular islands grow across multiple step edges (as shown in Figure 1b) in the so-called carpet mode.⁶⁰ The step edges which occupy the islands are heavily kinked (compare to the smooth step edges observed on Cu(111)), which suggest

that the step edges change to accommodate the growing ZnO islands. The growth mechanism of the triangular islands across the step edges can be a result of the seeding and growth process as explained in the case carpet growth mode of graphene on Ru(0001).⁶⁰ We need to carry out further investigation but it can be speculated that when a growing ZnO island meets a descending step edge, some of the surface Cu atoms underneath the ZnO island has been removed at some localized spot. At these spots the ZnO island attaches to the lower terrace and provides the seed for the growth of the island in the lower terrace.

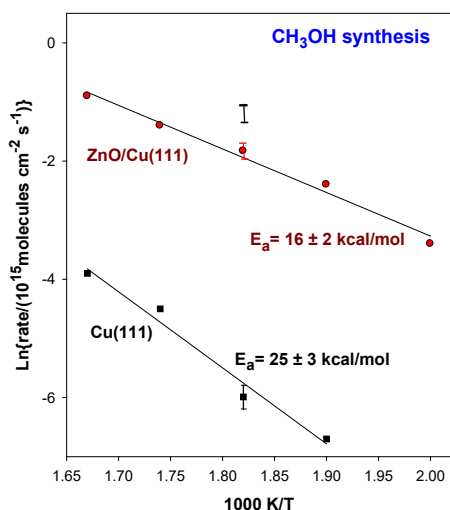


Figure 2: Methanol synthesis on clean Cu(111) and on a copper surface pre-covered with 0.3 ML of ZnO.⁴⁷

All the ZnO/CuO_x/Cu(111) structures displayed in Figure 1 exhibited catalytic activity for CO oxidation, the WGS reaction and CO₂ hydrogenation but only the systems prepared at 600 K displayed long term stability under reaction conditions.^{47,60} As mentioned above, a HR-TEEM study revealed that the active phase of ZnO-Cu based catalysts under CO₂ hydrogenation reaction conditions consists of Cu particles encapsulated by a ZnO overlayer with a graphite-like structure [Lunkenbein et al, *Angew Chem Int Ed* **2015**, *54*, 4544]. In our studies, we did not see graphite-like structures as seen for the powder catalyst under reaction conditions. However, in catalytic tests, we found that our ZnO/CuO_x/Cu(111) systems were much more active for CO₂ hydrogenation than Cu(111). Figure 2 compares the catalytic activity of a system where ~ 30% of the copper substrate was covered with ZnO. The ZnO overlayer was prepared at 600 K to induce the formation of big ZnO islands. The addition of ZnO to the copper

substrate enhanced the catalytic activity by two-three orders of magnitude. For this sample, the measured line shape for the Zn LMM Auger spectra pointed to the presence of ZnO on the copper surface during reaction.

In a set of experiments, ambient-pressure XPS was used to compare the surface chemistry for CO₂ hydrogenation on Cu(111) and ZnO/Cu(111) surfaces.⁴⁷ The C 1s XPS data shown in Figure 3 indicate that on Cu(111) there is only a small amount of adsorbed CO₂^{δ-} and carbon formed by the dissociation of CO₂ on defect sites. On the other hand, on the ZnO/Cu(111) system, there are strong signals for CO₂^{δ-} and HCOO species.⁴⁷ The formation of a stable ZnO-copper interface opens the door for new chemistry that enhances the rate of formation of methanol. The experimental studies with the model system agree with the results of theoretical studies which show a much larger rate for the formation of methanol on ZnO/Cu(111) than on CuZn(111)¹⁹ and with the TEM data for Cu/ZnO/Al₂O₃.

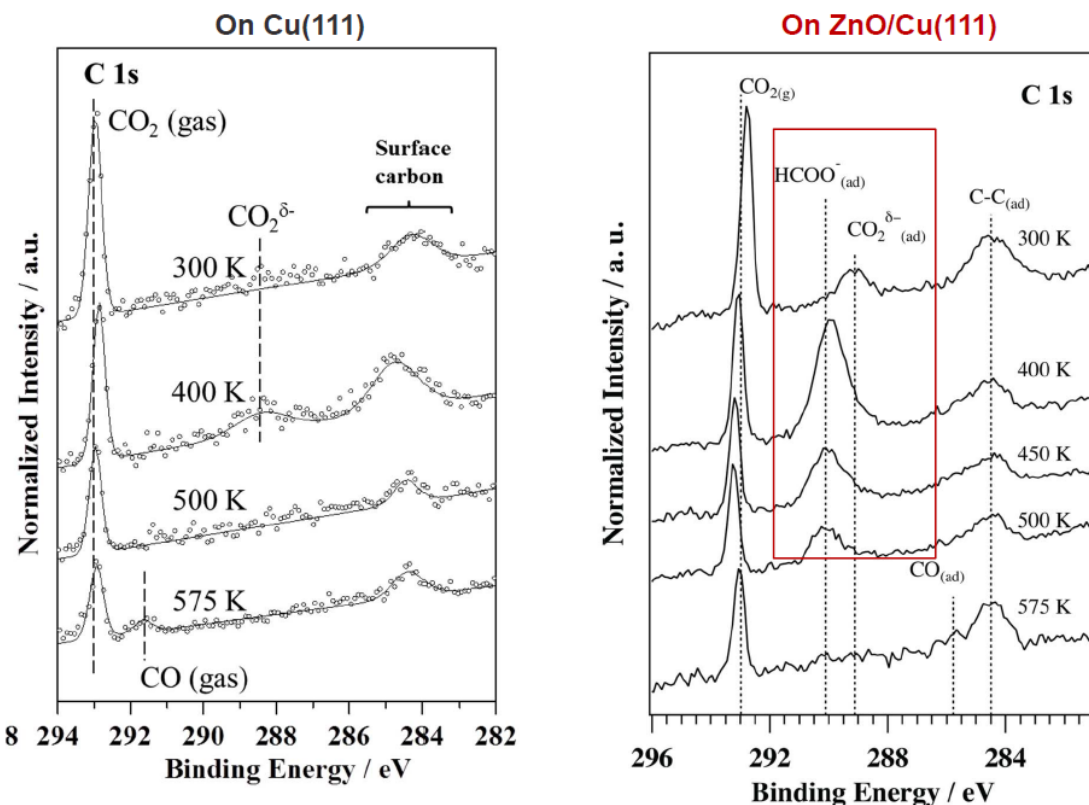


Figure 3 C 1s AP-XPS spectra collected while exposing Cu(111), left-side panel), and a ZnO/Cu(111) surface, right-side panel, to 50 mTorr of CO₂ and 200 mTorr of H₂.⁴⁷

B. Novel metal/nitride catalysts for CO₂ hydrogenation

Strong bonding interactions between a transition metal substrate or support is one of the most effective strategies to immobilize sub-nm scale clusters or atoms in heterogeneous catalysis. In a recent study, we showed that such a type of phenomenon can take place on a Mo₂N surface. Combined experimental and theoretical studies have confirmed that strong metal-support interactions between face-centered cubic (fcc) structured γ -Mo₂N and cobalt is an effective approach to anchor sub-nm Co clusters and prevent their aggregation. The results of XANES, AP-XPS and DFT revealed electronic perturbations in the nitride-bonded cobalt not seen on a strongly active oxide such as CeO₂. A charge transfer from Co to Mo₂N was observed with a significant stabilization of the Co 3d levels which prevents the full decomposition of CO₂. The sub-nm Co loaded on γ -Mo₂N catalysts exhibited very high selectivity to the product CO, while the undesirable methanation activity, typically inevitable on traditional Co/oxide catalysts, was successfully suppressed. As a consequence of the electronic perturbations induced by the nitride, the cobalt was not able to fully dissociate the CO₂ molecule to generate C or CH_x fragments necessary for methane production. Under reaction conditions the strong bonding between Co and γ -Mo₂N maintained the sub-nm geometry of Co, leading to remarkable selectivity and stability.

C. Novel metal/carbide catalysts for C1 chemistry

The hydrogenation of CO₂, the water-gas shift reaction, and the activation of methane were investigated on novel catalysts generated by the deposition of metals on carbide surfaces.^{20,21,28,33,36} For small Cu and Au clusters supported on TiC or MoC, strong admetal ↔ C_{surface} interactions induce charge polarization over the surface.²⁸ As a result, there is a significant enhancement in the catalytic activity when going from metal bulk surfaces to carbide-supported small clusters, and systems such as Au/MoC and Au/TiC display a high catalytic activity for the low-temperature water-gas shift reaction.⁴³

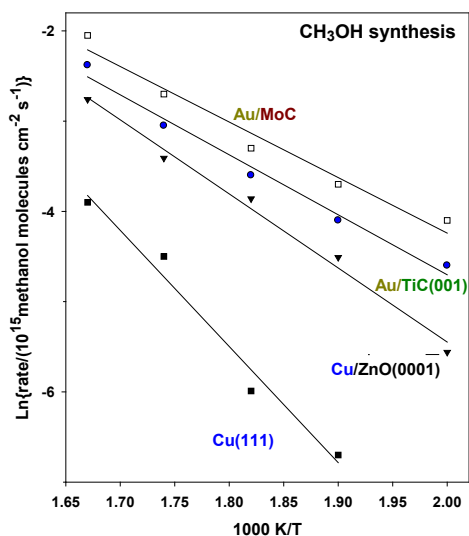


Figure 4: Methanol synthesis on clean Cu(111) and on a surfaces generated by depositing gold on carbides..²⁸

Carbon dioxide does not interact with gold at all, but when nanoparticles of the noble metal are deposited on surfaces of carbides, Figure 4 one obtains very good catalysts for the conversion of CO₂ to methanol or CO.^{28,43} For these systems, the highest catalytic activity is found for small two-dimensional particles or clusters of the gold in close contact with TiC(001) or polycrystalline MoC.²⁸ DFT calculations have shown that a charge polarization induced by the Au-C interaction enhances the CO₂ adoption via a η²-C,O bonding configuration on Au/TiC(001), and therefore the production of methanol probably involves the hydrogenation of a HCOO intermediate or of the CO generated by the reverse WGS.⁴³

Methane is an extremely stable molecule, a major component of natural gas, and also one of the most powerful greenhouse gases contributing to global warming. A major research goal is to find systems that can activate methane even at low temperature. Combining experiments followed by X-ray photoemission and accurate DFT based calculations, we have shown that small Ni clusters dispersed on TiC(001) are able to capture and dissociate methane at room temperature.⁶⁶ In DFT calculations, a small energy barrier of 0.18 eV is predicted for CH₄ dissociation into adsorbed methyl and hydrogen atom species. In addition, the calculated reaction free energy profile at 300 K and 1 atm of CH₄ shows no effective energy barriers in the system. A comparison to other reported systems which activate methane at room temperature, including oxide and zeolite-based materials, indicates that a different chemistry takes place on the metal/carbide system.⁶⁶ The discovery of a carbide-based surface able to activate methane at low temperatures paves the road for the design of new types of catalysts towards an efficient conversion of this hydrocarbon into other added-value chemicals, with implications in climate change mitigation.⁶⁶

More details on the work of the BNL Catalysis group on methane activation and conversion will be included in the presentations of Dr. Ping Liu and Dr. Sanjaya Senanayake.

Publications Acknowledging this Grant in 2015-2018

*** Exclusively funded by this grant*

2016:

1. Liu, S.; White, M.G.; Liu, P. Mechanism of Oxygen Reduction Reaction on Pt(111) in Alkaline Solution: Importance of Chemisorbed Water on Surface”, *J. Phys. Chem. C* **2016**, *120*, 15288-15298.
2. An, W.; Liu, P. Complex behavior of Pd₇ cluster supported on TiO₂(110) during CO oxidation: adsorbate-driven promoting effect, *Phys. Chem. Chem. Phys.: Communication* **2016**, *18*, 30881-31340. **(Cover art)**
3. Liu, Z.; Senanayake, S.D.; Rodriguez, J.A. Elucidating the Interaction between Ni and CeOx in Ethanol Steam Reforming Catalysts: A Perspective of Recent Studies over Model and Powder Systems, *Applied Catal. B: Environmental*, **2016**, *197*, 184-199 **(Invited)**.
4. Hoffmann, F.M.; Hrbek, J.; Ma, S. et al. Enhancing the Reactivity of Gold: Nanostructured Au(111) Adsorbs CO, *Surf. Sci.* **2016**, *650*, 17-32.
5. Magee, J. W.; Palomino, R. M.; White, M. G. Infrared Spectroscopy Investigation of Fe-Promoted Rh Catalysts Supported on Titania and Ceria for CO Hydrogenation, *Catal. Lett.* **2016**, *146*, 1771-1779.
6. Pruski, M.; Sadow, A.D.; Slowing, I.I. et al, Virtual Special Issue on Catalysis at the US Department of Energy National Laboratories, *ACS Catal.* **2016**, *6*, 3227.

2017:

7. Rodriguez, J.A.; Grinter, D.C.; Liu, Z.; Palomino, R.M.; Senanayake, S.D. Ceria-based Model Catalysts: Fundamental Studies on the Importance of the Metal-Ceria Interface in CO oxidation, the Water-gas Shift, CO₂ Hydrogenation, and Methane and Alcohol reforming, *Chem. Soc. Reviews* **2017**, *46*, 1824-1833. **(Invited)**
8. Palomino, R.M.; Hamlyn, R.; Liu, Z.; Grinter, D.C.; Waluyo, I.; Rodriguez, J.A.; Senanayake, S.D. Interfaces in Heterogeneous Catalytic Reactions: Ambient Pressure XPS as a Tool to Unravel Surface Chemistry, *J. Electron Spectros. & Related Phen*, **2017**, *221*, 28-43 **(Invited)**.
9. Liu, Z.; Senanayake, S.D.; Rodriguez, J.A. Catalysts for the steam reforming of ethanol and other alcohols”, in *Ethanol: Science and Engineering* (Elsevier) - Editors: Angelo Basile, Adolfo Iulianelli, Nejat T. Veziroglu, April (2017) **(Invited)**

2018:

10. Liu, S.; White, M.G.; Liu, P. Oxygen Reduction Reaction on Ag(111) in Alkaline Solution: A Combined Density Functional Theory and Kinetic Monte Carlo Study, *ChemCatChem* **2018**, *10*, 540-549. **(Cover art)**
11. Liu, S.; Liu, P. Optimized Pt-based Catalysts for Oxygen Reduction Reaction in Alkaline Solution: A First Principle Study, *J. Electrochem. Soc.* **2018**, *165*, J3090-J3094 (Invited).

12. Hamlyn, R.; Mahapatra, M.; Grinter, D.; Xu, F.; Luo, S.; Palomino, R.; Kattel, S.; Waluyo, I.; Liu, P.; Stacchiola, D.; Senanayake, S.; Rodriguez, J. A. "Imaging the Ordering of a Weakly Adsorbed Two-dimensional condensate: ambient-pressure microscopy and spectroscopy of CO₂ molecules on rutile TiO₂(110)", *Phys. Chem. Chem. Phys.* 2018, 20, 13122-13126.

13. Carrillo, P.; Shi, R. ; Teeluck, K.; Senanayake, S. D.; White, M. G.; Nano-Fe₂O₃ as Support and Promoter for Rh Catalysts for Ethanol Synthesis from Syngas Conversion, *ACS Catal.* 2018, in press, doi.org/10.1021/acscatal.8b02235.

2019:

14. Liu, Z.; Senanayake, S. D.; Rodriguez, J. A. Chapter 5 - Catalysts for the Steam Reforming of Ethanol and Other Alcohols. In *Ethanol*; Basile, A., Iulianelli, A., Dalena, F., Veziroğlu, T. N., Eds.; Elsevier, 2019; pp 133–158 (**invited**).

15. Rodriguez, J. A.; Zhang, F.; Liu, Z.; Senanayake, S. D. Methane Activation and Conversion on Well-Defined Metal-Oxide Surfaces: In Situ Studies with Synchrotron-Based Techniques. In *Catalysis: Volume 31*; The Royal Society of Chemistry, 2019; Vol. 31, pp 198–215 (**invited**).

16. Senanayake, S. D.; Liu, P.; Rodriguez, J. A. Preface: Virtual Special Issue in Honor of Dr. Jan Hrbek. *Surf. Sci.* 2019, 680, A1. <https://doi.org/10.1016/j.susc.2018.11.008>.

*** Jointly funded by this grant and other grants with leading intellectual contribution from this grant:*

2016

17. Grinter, D.C.; Park, J.B.; Agnoli, S. et al, Water-gas Shift Reaction over Gold Nanoparticles Dispersed on Nanostructured CeO_x-TiO₂(110) Surfaces: Effects of High Ceria Coverage, *Surf. Sci.* **2016**, 650, 34-46.

18. Senanayake, S.D.; Pappoe, N.A.; Nguyen-Phan, T.D. et al, Interfacial Cu⁺ Promoted Surface Reactivity: Carbon Monoxide Oxidation Reaction over Polycrystalline Copper-Titania Catalysts, *Surf. Sci.* **2016**, 652, 206-218.

19. Senanayake, S.D.; Ramírez, P.J.; Waluyo, I. et al, Hydrogenation of CO₂ to Methanol on CeO_x/Cu(111) and ZnO/Cu(111) Catalysts: Role of the Metal-Oxide Interface and Importance of Ce³⁺ Sites, *J. Phys. Chem. C*, **2016**, 120, 1778-1784.

20. Posada-Pérez, S.; Ramírez, P.J.; Gutiérrez, R.A. et al, The Conversion of CO₂ to Methanol on orthorhombic β-Mo₂C and Cu/β-Mo₂C Catalysts: Mechanism for Admetal-induced Change in the Selectivity and Activity, *Catal. Sci. & Tech.* **2016**, 6, 6766-6772.

21. Jimenez-Orozco, C.; Florez, E.; Moreno, A.; Liu, P.; Rodriguez, J.A. Systematic Theoretical Study of Ethylene Adsorption on δ-MoC(001), TiC(001), and ZrC(001) Surfaces, *J. Phys. Chem. C*, **2016**, 120, 13531-13536.

22. Liu, Z.; Grinter, D.C.; Lustemberg, P. et al. Dry Reforming of Methane on a Highly-Active Ni-CeO₂ Catalyst: Effects of Metal-Support Interactions on C–H Bond Breaking, *Angew. Chem. Int. Ed.* **2016**, 55, 7455-7459.

- 23.** Rodriguez, J.A.; Rousseau, R.; Stacchiola, D. et al, Catalytic Chemistry of Oxide Nanostructures, in: *Oxide Materials at the Two Dimensional Limit*, First ed.; F. Netzer, Fortunelli, A., Eds. Springer International: New York, 2016; pp 251-280. **(Invited)**
- 24.** Liu, Z.; Duchon, T.; Wang, H.R. et al, Ambient pressure XPS and IRRAS investigation of ethanol steam reforming on Ni- CeO₂(111) catalysts: an in situ study of C-C and O-H bond scission, *Phys. Chem. Chem. Phys.* **2016**, *18*, 16621-16625.
- 25.** Mudiyansele, K.; Luo, S.; Kim, H.Y. et al, How to Stabilize Highly Active Cu⁺ Cations in a Mixed-oxide Catalyst. *Catal. Today* **2016**, *263*, 4-17.
- 26.** Nguyen-Phan, T.; Baber, A.E.; Rodriguez, J.A.; Senanayake, S.D. Au and Pt Nanoparticle Supported Catalysts Tailored for H₂ Production: From Models to Powder Catalysts, *Applied Catalysis A: Gen.* **2016**, *518*, 18-32.
- 27.** Plata, J.J.; Graciani, J.; Evans, J.; Rodriguez, J.A.; Fernandez-Sanz, J. Cu Deposited on CeO_x-Modified TiO₂(110): Synergistic Effects at the Metal– Oxide Interface and the Mechanism of the WGS Reaction. *ACS Catal.* **2016**, *6*, 4608.
- 28.** Posada-Pérez, S.; Ramírez, P.J.; Evans, J.; Viñes, F.; Liu, P.; Illas, F.; Rodriguez, J. A. Highly Active Au/ δ -MoC and Cu/ δ -MoC Catalysts for the Conversion of CO₂: The Metal/C Ratio as a Key Factor Defining Activity, Selectivity, and Stability, *J. Am. Chem. Soc.* **2016**, *138*, 8269-8274.
- 29.** Grinter, D.; Remensal, E.R.; Luo, S. et al. Potassium and Water Co-Adsorption on TiO₂(110): OH-Induced Anchoring of Potassium and the Generation of Single-Site Catalysts, *J. Phys. Chem. Lett.* **2016**, *7*, 3866-3870.
- 30.** Zuo, Z.; Ramirez, P.J.; Senanayake, S.D.; Liu, P.; Rodriguez, J.A. The Low-temperature Conversion of Methane to Methanol on CeO_x/Cu₂O Catalysts: Water Controlled Activation of the C-H Bond, *J. Am. Chem. Soc.* **2016**, *138*, 13810-13814.
- 31.** Lustemberg, P.; Ramirez, P.J.; Liu, Z. et al, Room Temperature Activation of Methane and Dry Reforming with CO₂ on Ni-CeO₂(111) Surfaces: Effect of Ce³⁺ Sites and Metal-Support Interactions on C-H bond Cleavage, *ACS Catal.* **2016**, *6*, 8184-8189.

2017

- 32.** Xue, M.; Nakayama, M.; Liu, P.; White, M.G. Electronic Interactions of Size-Selected Oxide Clusters on Metallic and Thin Film Oxide Supports, *J. Phys. Chem. C*, **2017**, *121*, 22234–22247.
- 33.** Posada-Pérez, S.; Viñes, F.; Valero, R.; Rodriguez, J.A.; Illas, F. Adsorption and dissociation of molecular hydrogen on orthorhombic β -Mo₂C and cubic α -MoC(001) surfaces, *Surf. Sci.* **2017**, *656*, 24-29.
- 34.** Luo, S.; Barrio, L; Nguyen-Phan, T.-D. et al, Importance of Low Dimensional CeO_x Nanostructures in Pt/CeO_x-TiO₂Catalysts for the Water–Gas Shift Reaction, *J. Phys. Chem. C*, **2017**, *121*, 6635-6640.
- 35.** Jimenez-Orozco, C.; Florez, E.; Moreno, A.; Liu, P.; Rodriguez, J.A. Acetylene Adsorption on δ -MoC(001), TiC(001) and ZrC(001) Surfaces: A Comprehensive Periodic DFT Study, *Phys. Chem. Chem. Phys.* **2017**, *19*, 1571-1576.

36. Posada-Perez, S.; Ramirez, P.J.; Gutierrez R.A. et al, The Conversion of CO₂ to Methanol on Orthorhombic β -Mo₂C and Cu/ β -Mo₂C Catalysts: Mechanism for Admetal Induced Change in the Selectivity and Activity, *Catal. Sci. & Technol.* **2016**, *6*, 6766-6774.
37. Rodriguez, J.A.; Ramirez, P.J.; Gutierrez, R.A. Highly Active Pt/MoC and Pt/TiC Catalysts for the Low-Temperature Water-gas Shift Reaction: Effects of the Carbide Metal/Carbon Ratio on the Catalyst Performance, *Catal. Today* 2017, *289*, 47-58.
38. Guild, C.J.; Vovchok, D.; Kriz, D.A. et al, Water-Gas-Shift over Metal-Free Nanocrystalline Ceria: An Experimental and Theoretical Study, *Chem. Cat. Chem.* **2017**, *9*, 1373.
39. Palomino, R.; Stavitski, E.; Waluyo, I. et al, New In-Situ and Operando Facilities for Catalysis Science at NSLS-II: The Deployment of Real-Time, Chemical, and Structure-Sensitive X-ray Probes, *Synchrotron Radiation News*, **2017**, *30*, 30-44 (**Invited**).
40. Vovchok, D.; Guild, C.J.; Llorca, J. et al, Cu Supported on Mesoporous Ceria: Water-gas Shift Activity at Low Cu Loadings through Metal-Support Interactions, *Phys. Chem. Chem. Phys.* *2017*, *19*, 17708-17713.
41. Yao, S.; Zhang, X.; Xhou, W. et al, Atomic layered Au clusters on α -MoC as catalyst for the low temperature water gas shift reaction, *Science*, **2017**, *357*, 389-393.
42. Liu, Z.; Lustemberg, P.; Gutierrez, R.A. et al, In-situ Investigation of Methane Dry Reforming on M-CeO₂(111) {M= Co, Ni, Cu} Surfaces: Metal-Support Interactions and the activation of C-H bonds at Low Temperature, *Angew. Chem. Int. Ed.* **2017**, *56*, 13041-13045.
43. Posada-Pérez, S.; Gutiérrez, R.A.; Zuo, Z. et al, Highly active Au/ δ -MoC and Au/ β -Mo₂C catalysts for the Low-temperature Water Gas Shift Reaction: Effects of the Carbide Metal/Carbon Ratio on the Catalyst Performance, *Catal. Sci. & Technol.* 2017, *7*, 5332-5339.
44. An, W.; Men, Y.; Wang, J.; Liu, P. Interfacial and Alloying Effects on Activation of Ethanol from First Principles, *J. Phys. Chem. C*, **2017**, *121*, 5603–5611.
45. Lu, F.; Zhang, Y.; Liu, S. et al, Surface Proton Transfer Promotes Four-Electron Oxygen Reduction on Gold Nanocrystal Surfaces in Alkaline Solution, *J. Am. Chem. Soc.* **2017**, *139*, 7310–7317.
46. Vukmirovic, M.B.; Teeluck, K.M.; Liu, P.; Adzic R.R. Single Platinum Atoms Electrocatalysts: Oxygen Reduction and Hydrogen Oxidation Reactions, *Croatica Chemica Acta*, **2017**, *90*, 1-6.

2018

47. Palomino, R.M.; Ramirez, P.J.; Liu, Z. et al, Hydrogenation of CO₂ on ZnO/Cu(100) and ZnO/Cu(111) Catalysts: Role of Copper Structure and Metal-Oxide Interface in Methanol Synthesis, *J. Phys. Chem. B*, **2018**, *122*, 794-798.
48. Jimenez-Orozco, C.; Florez, E.; Moreno, A.; Liu P.; Rodriguez, J.A. Acetylene and Ethylene Adsorption on a β -Mo₂C(100) Surface: A Periodic DFT Study on the Role of C- and Mo-terminations for Bonding and Hydrogenation Reactions, *J. Phys. Chem. C*, **2017**, *121*, 19786-19791.

49. Rodriguez, J.A.; Grinter, D.C.; Ramírez, P.J. et al, High Activity of Au/K/TiO₂(110) for CO Oxidation: Alkali Enhanced Dispersion of Au and Bonding of CO, *J. Phys. Chem. C*, **2018**, *122*, 4324-4328.
50. Hamlyn, R.C.E.; Mahapatra, M.; Grinter, D.C. et al, Imaging the Ordering of a Weakly Adsorbed Two-Dimensional Condensate: Ambient-Pressure Microscopy and Spectroscopy of CO₂ Molecules on Rutile TiO₂(110), *Phys. Chem. Chem. Phys.* **2018**, *20*, 13122-13126.
51. Kunkel, C.; Viñes, F.; Ramírez, P.J.; Rodriguez, J.A.; Illas, F. Combining Theory and Experiment for Multitechnique Characterization of Activated CO₂ on Transition Metal Carbide (001) Surfaces, *J. Phys. Chem. C*, **2018**, *123*, 7567-7576.
52. Vovchok, D.; Guild, C.; Senanayake, S.D. et al, Characterization of Mesoporous Co/CeO₂ Catalysts for the High Temperature Water-Gas Shift, *J. Phys. Chem. C*, **2018**, *122*, 8998-9008.
53. Zhang, F.; Liu, Z.; Zhang, S. et al, *In-situ* Elucidation of the Active State of Co-CeO₂ Catalysts in the Dry Reforming of Methane: The Important Role of the Reducible Oxide Support and Interactions with Cobalt, *ACS Catal.* **2018**, *8*, 3550-3560.
54. Lin, L.; Yao, S.; Liu, Z. et al, *In-situ* Characterization of Cu/CeO₂ Nanocatalysts for CO₂ Hydrogenation: Morphological Effects of Nanostructured Ceria on the Catalytic Activity, *J. Phys. Chem. C*, **2018**, *122*, 12934-12943.
55. Ma, Z.; Zhang, Y.; Liu, S. et al, Reaction Mechanism for Oxygen Evolution on RuO₂, IrO₂, and RuO₂@IrO₂ Core-shell Nanocatalysts, *J. Electroanal. Chem.* **2018**, *819*, 296-305.
56. Zuo, Z.; Liu, S.; Wang, Z.; Liu, C.; Huang, W.; Huang, J.; Liu, P. “Dry reforming of Methane on single site Ni/MgO catalysts: importance of site confinement”, *ACS Catalysis*, **2018**, *8*, 9821–9835.
57. Mahapatra, M.; Gutiérrez, R. A.; Kang, J.; Rui, N.; Hamlyn, R.; Liu, Z.; Orozco, I.; Ramírez, P. J.; Senanayake, S. D.; Rodriguez, J. A. The Behavior of Inverse Oxide/Metal Catalysts: CO Oxidation and Water-Gas Shift Reactions over ZnO/Cu(111) Surfaces. *Surf. Sci.* **2018**, *681*, 116–121.
58. Vovchok, D.; Guild, C. J.; Llorca, J.; Palomino, R. M.; Waluyo, I.; Rodriguez, J. A.; Suib, S. L.; Senanayake, S. D. Structural and Chemical State of Doped and Impregnated Mesoporous Ni/CeO₂ Catalysts for the Water-Gas Shift. *Appl. Catal. A Gen.* **2018**, *567*, 1–11.
59. Zhang, F.; Yao, S.; Liu, Z.; Gutiérrez, R. A.; Vovchok, D.; Cen, J.; Xu, W.; Ramírez, P. J.; Kim, T.; Senanayake, S. D.; et al. Reaction of Methane with MO_x/CeO₂ (M = Fe, Ni, and Cu) Catalysts: In Situ Studies with Time-Resolved X-Ray Diffraction. *J. Phys. Chem. C* **2018**, *122*, 28739–28747.
60. Mahapatra, M.; Kang, J.; Ramírez, P. J.; Hamlyn, R.; Rui, N.; Liu, Z.; Orozco, I.; Senanayake, S. D.; Rodriguez, J. A. Growth, Structure, and Catalytic Properties of ZnO_x Grown on CuO_x/Cu(111) Surfaces. *J. Phys. Chem. C* **2018**, *122*, 26554–26562.

2019

61. Waluyo, I.; Mudiyanse, K.; Xu, F.; An, W.; Liu, P.; Boscoboinik, J. A.; Rodriguez, J. A.; Stacchiola, D. J. “Potassium-Promoted Reduction of Cu₂O/Cu(111) by CO”, *J. Phys. Chem. C* **2019**, *123*, 8057-8066

62. Zhang, H. T.; Liu, C.; Liu, P.; Hu, Y. H. “Mo₆S₈-Based Single-Metal-Atom Catalysts for Direct Methane to Methanol Conversion”, *J. Chem. Phys.*, doi: 10.1063/1.5110875. (Invited)
63. Flege, J. I.; Hocker, J.; Sadowski, J. T.; Senanayake, S. D.; Falta, J. Nucleation, Morphology, and Structure of Sub-Nm Thin Ceria Islands on Rh(111). *Surf. Interface Anal.* **2019**, *51*, 110–114.
64. Simonovis, J. P.; Hunt, A.; Senanayake, S. D.; Waluyo, I. Subtle and Reversible Interactions of Ambient Pressure H₂ with Pt/Cu(111) Single-Atom Alloy Surfaces. *Surf. Sci.* **2019**, *679*, 207–213.
65. Lin, L.; Yao, S.; Rui, N.; Han, L.; Zhang, F.; Gerlak, C. A.; Liu, Z.; Cen, J.; Song, L.; Senanayake, S. D.; et al. Conversion of CO₂ on a Highly Active and Stable Cu/FeO_x/CeO₂ Catalyst: Tuning Catalytic Performance by Oxide-Oxide Interactions. *Catal. Sci. Technol.* **2019**, in press, <https://doi.org/10.1039/C9CY00722A>.
66. Prats, H.; Gutierrez, R.A.; Piñero, J.J.; Viñes, F.; Bromley, S.T.; Ramirez, P.J.; Rodriguez, J.A.; Illas, F. R. Room Temperature Methane Capture and Activation by Ni Clusters Supported on TiC(001): Effects of Metal–Carbide Interactions on the Cleavage of the C–H Bond. *J. Am. Chem. Soc.* **2019**, *141*, 5303-5313.

Simon R. Bare

The Consortium for Operando and Advanced Catalyst Characterization via Electronic Spectroscopy and Structure (Co-ACCESS) at SSRL

Simon R. Bare

Chemical Science Division, Energy Sciences Directorate, and SSRL, SLAC National Accelerator Laboratory

Presentation Abstract

The application of synchrotron-based techniques for catalyst characterization is an essential component of many catalysis research programs, mainly due to *in-situ/operando* methodology, which allows determination of the structure of the catalyst in the working state, and it is often the only way to determine this information. The Synchrotron Catalysis Consortium (SCC), initially at NSLS, demonstrated the enhanced impact that such research could have by using a consortium model to “promote the utilization of synchrotron techniques to perform cutting-edge catalysis nano-science research under in-situ conditions”. This talk will provide an update on the Consortium for Operando and Advanced Catalyst Characterization via Electronic Spectroscopy and Structure (Co-ACCESS) at SSRL. Co-ACCESS was formally initiated in FY19 as is based on the concept that creating a collaborative research environment in catalysis characterization at SSRL will lead to a more integrated and capable catalysis research community. The talk will focus on the equipment, techniques, and capabilities that have been implemented, our methodology of interacting with user groups, and some of the recent science that has resulted. The talk will also show that our success is due in part by being closely integrated into SSRL and SLAC. Our future plans will be presented, with the ultimate goal of the researcher leaving the beamline with knowledge and not just data.

Grant or FWP: DE-AC02-76SF00515, 100462 Consortium for Operando and Advanced Catalyst Characterization via Electronic Spectroscopy and Structure

Postdoc(s): Adam Hoffman, Alexey Boubnov

RECENT PROGRESS

There are several key areas in catalysis science research that are driving the prioritization and implementation of capabilities of Co-ACCESS capabilities at SSRL. One such focal area has been on single atom and single atom alloy catalysis, a topic that is receiving significant attention from the catalysis community. In these catalysts XAS has proven to be a critical characterization technique, providing information on the binding geometry of the single metal atom on the support under catalytic conditions. Often the metal concentration in these single atom catalysts is low, e.g. <0.1 wt%, and the use of wiggler beamlines, coupled with the 100-element Ge detector, and the use of high energy resolution fluorescence detection (HERFD) XAS are needed. We have thus utilized both of these capabilities, by designing, fabricating, and installing the necessary hardware to allow the catalyst to be treated in-situ so that it is in its catalytically active state. A second focal

area has been to develop capabilities in the time domain. Here we have focused on two extremes: (i) providing capability for insight into the causes of long-term catalyst deactivation over many days, and (ii) developing capabilities to study kinetic phenomena that occur on the timescale of second. This has been exemplified by a study of the ligand exchange kinetics on a supported molecular catalyst.

In light of these scientific drivers, the focus in FY19 has been on: (i) Growing the catalysis user base at SSRL, (ii) Developing the equipment and capabilities that are available to the users, (iii) Improving our operations, (iv) Making our laboratory at SSRL functional for catalysis users, (v) Communicating to the greater catalysis community, and (vi) Planning future developments.

While the major focus of the FWP has been on growing the catalysis user base at SSRL, with an emphasis on groups in the Western half of the United States, in reality we have attracted users from throughout the US (and abroad). Through outreach efforts during visits to universities, attending conferences (e.g. Gordon Conference on Catalysis), attending the Catalysis PI meeting, organizing a workshop, and word of mouth, we are on a good track to attract some excellent catalysis research to SSRL. Our growth is illustrated in Figure 1. Over a 3-year period we have grown from 7 unique proposals to 30, and the amount of beamtime awarded to these proposals has

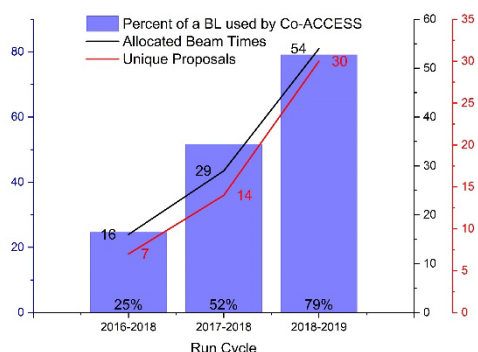


Figure 2. Growth of users collaborating with Co-ACCESS

grown from 15% of a beamline equivalent to almost 80%. Our involvement has included: (i) Working with the collaborators to write the beamtime proposal, (ii) Planning for the beamtime, (iii) Providing the equipment necessary for the experiment, (iv) Assisting during the data collection, (v) Assisting and advising during the data analysis and interpretation, and (vi) Contributing to the resulting manuscript. Through this hands-on interaction with the many user groups we have learned the type of catalyst and catalysis research that is of most importance, and thus been able to use this information to help prioritize our work processes.

Regarding the development of the equipment and capabilities available to the catalysis user, our emphasis in FY19 has been on designing, fabricating and implementing equipment necessary for safe operations of *in-situ/operando* gas phase heterogeneous catalysis experiments. At beamline (BL) 2-2 the equipment for high pressure *in-situ* catalysis studies is fully functional. The hardware in the gas cabinet was modified to safely supply either high pressure (80 bar) or ambient pressure gases (e.g. CO, H₂) to the hutch. A patch panel was designed, fabricated, and installed in the hutch. This panel enables gas lines from the gas cabinet to be permanently installed and thus leak-free, and readily available to the user.

The construction of two “Pilot Plant on Wheels” were completed and fully implemented. This capability allows *in-situ/operando* gas-phase catalysis research to be conducted across beamlines at SSRL. One system is designed for operation at high pressure (80 bar), and was implemented, for example, for both Fischer-Tropsch synthesis experiments and higher alcohol synthesis from syngas XAS experiments. It allows control of three gases (e.g. CO, H₂ and inert) at flow rates 2-120 sccm. The second systems is designed for ambient pressure operations, controlling up to 6 gases that can be combined in any combination, and a bypass loop to allow the feed to be analyzed in addition to the product. With these LabView-controlled modular pieces of equipment we have demonstrated that a user can be safely and fully functional for catalysis experiments within

approximately two hours of arriving at the beamline. This results in greater efficiency of user operations. Additionally, we have designed and constructed a modular flow board to allow modulation excitation XAS experiments to be conducted.

We have also continued to develop our suite of *in-situ* cells for catalysis research. We collaborated with a user groups to: (i) Develop an *in-situ* cell for aqueous electrocatalysis experiments, (ii) Expand the capability of the capillary cell to high temperature (1100°C), and (iii) Allow the safe handling of extremely air sensitive catalysts. For these developments we seek input from the user community to ensure that we can conduct the experiments that meet the user demand.

There are many aspects to a successful *in-situ* catalysis experiment at a beamline, and one of these aspects is access to the ancillary equipment that the user might have in their home institution. This equipment could be used for everything from catalyst synthesis to sample preparation to confirming the integrity of the sample. One capability that we now have available is an *in-situ* FTIR spectrometer, using diffuse reflectance infrared spectroscopy. This instrument is now fully functional and its capability was demonstrated on two different catalyst research projects in collaboration with a research group at Stanford University. The spectrometer is connected to a Brooks-controlled gas manifold to allow a variety of gases to be safely utilized. The construction of a transmission FTIR cell was initiated. The whole laboratory where the FTIR resides is now fully functional and is used to support the many catalysis users at SSRL. The laboratory incorporates two fume hoods that have permanently plumbed gas lines, a FTIR spectrometer, an argon glove box, two gas cabinets, appropriate ancillary equipment (furnaces, drying oven, balances, etc), and bench space for catalyst sample preparation.

In catalysis research there are many different time domains that are relevant to further our understanding. At Co-ACCESS we have developed capabilities that now allow the user to explore these time domains, from the slow deactivation of a catalyst over many days to measuring the kinetics of ligand exchange in a supported complex that occurs in seconds. The study of the fast ligand exchange was the first *in-situ* quick XAS catalysis experiment conducted using the cam-shaft QXAS monochromator in BL2-2. This experiment followed the ligand exchange kinetics of a supported atomically-dispersed catalyst as a function of reaction temperature. These experiments proved the concept of the utility of QXAS for novel spectro-kinetics measurements and allows for future planning. The longer term catalyst deactivation was accomplished by testing the capability to schedule two experiments simultaneously so that the beamline was utilized efficiently.

Outreach is a key component of our program, and provides much needed feedback to us, and allows us to fulfill our goal of educating the students. As such, we organized a workshop at the SSRL/LCLS Annual Users Meeting on “Catalysis by Single Atoms: What is all the fuss about?” A synopsis of the meeting was published in Synchrotron Radiation News. We held our first hands-on EXAFS analysis boot camp in December 2018. It was attended by graduate students from UCLA, UCSB and Univ. New Mexico. This boot camp led to two of the groups forming a collaboration from this interaction, making Co-ACCESS not just a resource but also a facilitator and a conduit to collaboration. In June 2019, we organized a workshop on “Time- and Space-Resolved X-ray Absorption Spectroscopy (XAS) at SSRL: Analysis of Large Data Sets”, as a forward looking workshop on the planned development of quick scanning XAS at SSRL.

Our sub-contract with the University of Washington for DFT/FEFF XANES calculations (Prof. Fernando Vila) has recently been fully executed and we have begun collaborative discussions.

Publications Acknowledging this Grant in 2016-2019

Please classify your publications into three categories according to the source of support for the work published:

(XIV) Exclusively funded by this grant;

None

(XV) Jointly funded by this grant and other grants with leading intellectual contribution from this grant;

1. Hoffman, A.S.; Azzam, S.; Zhang, K.; Xu, Y.; Liu, Y.; Bare, S.R.; Simonetti D.A. Direct Observation of the Kinetics of Gas-Solid Reactions using In-situ Kinetic and Spectroscopic Techniques. *Reaction Chemistry & Engineering* **2018**, *3*, 668 – 675; DOI: 10.1039/c8re00020d
2. Lu, Y.; Wang, J.; Yu, L.; Kovarik, L.; Zhang, X.; Hoffman, A.S.; Gallo, A.; Bare, S.R.; Sokaras, D.; Kroll, D.; Dagle, V.; Xin, H.; Karim, A.M. Identification of the Active Complex for CO Oxidation over Single Atom Ir-on-MgAl₂O₄ Catalysts . *Nature Catalysis* **2019** *2* 149-156; DOI: 10.1038/s41929-018-0192-4.
3. Hoffman, A.S.; Singh, J.A.; Bent, S.F.; Bare, S.R. In-situ Observation of Phase Changes of a Silica Supported Cobalt Catalyst for the Fischer-Tropsch Process by the Development of a Synchrotron-Compatible In-situ/Operando Powder X-ray Diffraction Cell. *Journal of Synchrotron Radiation*, **2018**, *25*, 1673-1682; DOI: 10.1107/S1600577518013942.
4. Singh, J.A.; Hoffman, A.S.; Schumann, J.; Boubnov A.; Asundi, A.S.; Nathan, S.S.; Nørskov, J.; Bare, S.R.; Bent, S.F. Role of Co₂C in ZnO-promoted Co Catalysts for Alcohol Synthesis from Syngas. *ChemCatChem*, **2019**, *11*, 799-809; DOI: 10.1002/cctc.201801724.
5. Wrasman, C.J.; Boubnov, A.; Riscoe, A.R.; Hoffman, A.S.; Bare, S.R.; Cargnello, M. Synthesis of Colloidal Pd/Au Dilute Alloy Nanocrystals and Their Potential for Selective Catalytic Oxidations. *Journal of the American Chemical Society*, **2018**, *140* 12930-12939; DOI: 10.1021/jacs.8b07515.
6. Aitbekova, A.; Wu, L.; Wrasman, C.J.; Boubnov, A.; Hoffman, A.S.; Goodman, E.D.; Bare, S.R.; Cargnello, M. Low-temperature restructuring of CeO₂-supported Ru nanocrystals determines selectivity in CO₂ catalytic reduction. *Journal of the American Chemical Society*, **2018**, *140* 13736-13745; DOI: 10.1021/jacs.8b07615.
7. Babucci, M.; Fang, C-Y.; Perez-Aguilar, J.E.; Hoffman, A.S.; Boubnov, A.; Guan, E.; Bare, S.R.; Gates, B.C.; Uzun, A. Controlling catalytic activity and selectivity for partial hydrogenation by tuning the environment around active sites in iridium complexes bonded to supports. *Chemical Science* **2019**, *10*, 2623-2632; DOI: 10.1039/c8sc05287e.

8. Boubnov, A.; Timoshenko, J.; Wrasman, C.J.; Hoffman, A.S.; Cargnello, M.; Frenkel, A.I.; Bare, S.R. Advanced modeling of EXAFS data from Pd-Au nanoparticle catalyst libraries: Comparison of data from SSRL and the APS. *Radiation Physics and Chemistry* **2019**, 10.1016/j.radphyschem.2019.04.054.
9. DeRita, L.; Resasco, J.; Dai, S.; Boubnov, A.; Thang, H.V.; Hoffman, A.S.; Ro, I.; Graham, G.W.; Bare, S.R.; Pacchioni, G.; Pan, X.; Christopher, P. Structure-function relationships during the dynamic evolution of TiO₂ supported Pt single atom catalysts. *Nature Materials*, **2019**, DOI: 10.1038/s41563-019-0349-9.
10. Riscoe, A.R.; Wrasman, C.J.; Herzing, A.A.; Hoffman, A.S.; Menon, A.; Boubnov, A.; Vargas, M.; Bare, S.R.; Cargnello, M. Transition State and Product Diffusion Control by Polymer-Nanocrystal Hybrid Catalysts. *Nature Catalysis*, **2019**, accepted.

(XVI) *Jointly funded by this grant and other grants with relatively minor intellectual contribution from this grant*

1. Grosso-Giordano, N.A.; Hoffman, A.S.; Boubnov, A.; Small, D.W.; Bare, S.R.; Zones, S.I.; Katz, A. Dynamic reorganization and confinement of TiIV active sites controls olefin epoxidation catalysis on two-dimensional zeotypes. *Journal of the American Chemical Society*, **2019**, *141*, 7090-7106; DOI: 10.1021/jacs.9b02160.
2. Timoshenko, J.; Wrasman, C.J.; Luneau, M.; Shirman, T.; Cargnello, M.; Bare, S.R.; Aizenberg, J.; Friend, C.M.; Frenkel, A.I. Probing atomic distributions in mono- and bimetallic nanoparticles by supervised machine learning. *Nano Letters* **2019**, *19*, 520–529; DOI: 10.1021/acs.nanolett.8b04461.

Harnessing Complexity for Catalytic Efficiency

Presentation Abstract:

The overarching goal of the Catalysis Program at Lawrence Berkeley National Laboratory is to reveal new concepts that enable the design and synthesis of new catalysts, the understanding and design of new catalytic mechanisms, and the realization of new catalytic transformations. New concepts are needed to move the field of catalysis from empiricism to design and to advance the current design of catalysts to structures that enable new classes of reactions and make existing reactions more practical. The types of catalysts and the types of catalytic reactions studied by the Berkeley Catalysis Program, and the classes of mechanisms by which the catalysts react, are broad in scope but converge on several themes, which have been the focal point of investigations over the past several years. The three themes focus on the discovery and development new catalysts and catalytic processes involving multifunctional active sites, conducting catalysis in confined environments that alter the interactions of the substrate and catalyst, and integrated catalysis that combines two or more of homogeneous catalysis, heterogeneous catalysis, biocatalysis, and even informatics.

The theme on multidimensional catalysis focuses on processes like the selective reactions at typically unreactive bonds (such as C-H bonds, C-C bonds, C=C bonds of unactivated alkenes, and the C=O bonds of carbon dioxide) and the selective conversion of alcohols derived from biomass. A majority of the transformations are being addressed by using multiple catalysts in multi-step processes, multiple catalytic sites in a single solid catalyst, multiple metals held by ligands designed to juxtapose two metals, and allosteric triggering of one metal by coordination of another to a distal atom of a ligand. Studies on single metal sites provide the foundation for this work on more complex catalytic systems. The theme on catalysis in confined environment was initiated by work focusing on catalysis within a supramolecular nanovessel, and success in this program has motivated research on a broader range of confined spaces, such as alternative supramolecular cages, zeolites, the pores of metal-organic frameworks (MOFs), the active sites of artificial enzymes, and whole cells. The third theme, termed “Integrated Catalysis” builds upon successes with catalysis in confined spaces, a growing capability of this Catalysis Program in biocatalysis, a long-standing strength of LBNL in combining materials science with catalysis and new capabilities in the combination of catalysis and data science. Research on this theme encompasses the creation of artificial metalloenzymes that integrate molecular catalysts with chemical biology methods to enable selectivities difficult to achieve with small-molecule catalysts and the use of high-throughput experimentation with novel approaches to manage large data sets to discover new catalytic systems.

Highlights from selected projects within these topics are described below.

Recent Results on Subtask 1: Multifunctional Catalytic Active Sites: New Systems, New Reactions, and New Operando Methods for Monitoring the Reactivity of Such Catalysts

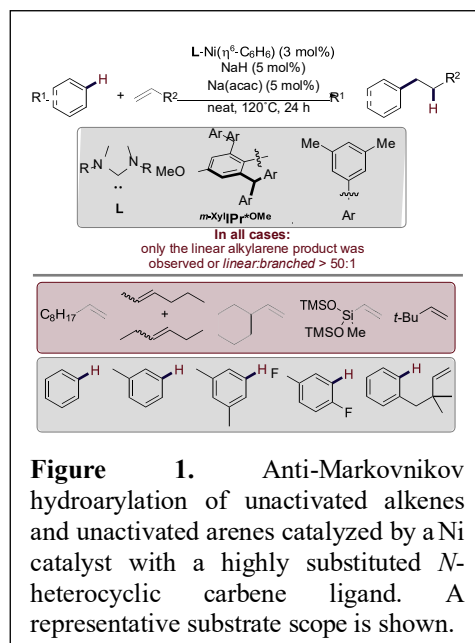
Nickel-Catalyzed Anti-Markovnikov Hydroarylation of Unactivated Alkenes with Unactivated Arenes Facilitated by non-Covalent Interactions

A cross-cutting theme of the LBNL catalysis program is the exploitation of interactions in the second coordination sphere to control the activity and selectivity of catalytic systems. By exploiting these interactions, Hartwig and coworkers have developed a catalyst for the anti-Markovnikov hydroarylation of alkenes. Anti-Markovnikov additions to alkenes have been a longstanding goal of catalysis, and anti-Markovnikov addition of arenes to alkenes would produce alkylarenes that are distinct from those formed by acid-catalyzed processes. Existing hydroarylations are either directed or occur with low reactivity and low regioselectivities for the linear alkylarene. They developed a catalyst system for the first anti-Markovnikov hydroarylation of unactivated alkenes with unactivated arenes that occurs with high regioselectivity. This reaction also occurs in good yield in many cases with turnover numbers an order of magnitude higher than prior homogeneous catalysts.

The reaction occurs with a Ni catalyst ligated by an oversized *N*-heterocyclic carbene ligand containing dimesitylmethyl groups at the 2,6 positions of the *N*-aryl groups of an *N*-heterocyclic carbene (Figure 1). Catalytically relevant arene- and alkene-bound Ni complexes have been characterized, and the rate-limiting step was shown to be reductive elimination to form the C-C bond. Although one might expect the extreme steric hindrance of the ligand to promote the catalytic process by enhancing the rate of the reductive elimination, a detailed computational analysis of the process using the ligand-substrate interaction model pioneered by Houk and the second-generation absolutely-localized molecular orbital energy decomposition analysis (ALMO-EDA) developed by Head-Gordon (Figure 4b) showed that attractive, non-covalent interactions enhance the rate of this step. The multiple aryl groups give rise to favorable electrostatic interactions and the peripheral methyl groups give rise to favorable London dispersion interactions that lead to the lower barrier for this step and the overall catalytic process than for reactions catalyzed by complexes of less hindered NHC analogs.

Reference:

“Nickel-Catalyzed Anti-Markovnikov Hydroarylation of Unactivated Alkenes with Unactivated Arenes Facilitated by non-Covalent Interactions” Saper, N.I.; Ohgi, A.; Small, D. Semba, K.; Nakao, Y.; Hartwig,



J.F. Submitted and deposited into chemrxiv: https://chemrxiv.org/articles/Nickel-Catalyzed_Anti-Markovnikov_Hydroarylation_of_Unactivated_Alkenes_with_Unactivated_Arenes_Facilitated_by_non-Covalent_Interactions/7825844 under the DOI 10.26434/chemrxiv.7825844.

Stabilization of reactive Co₄O₄ cubane oxygen- evolution catalysts within porous frameworks

A major challenge to the implementation of artificial photosynthesis, in which fuels are produced from abundant materials (water and carbon dioxide) in an electrochemical cell through the action of sunlight, is the discovery of active, inexpensive, safe, and stable catalysts for the oxygen evolution reaction (OER). Multimetallic molecular catalysts, inspired by the natural photosynthetic enzyme, can provide important guidance for catalyst design but the necessary mechanistic understanding has been elusive. In particular, fundamental transformations for reactive intermediates are difficult to observe, and well-defined molecular models of such species are highly prone to decomposition by intermolecular aggregation. A general strategy for stabilization of the molecular cobalt-oxo cubane core (Co₄O₄) followed by Tilley and coworkers is immobilization as part of metal-organic frameworks, thus preventing intermolecular pathways of catalyst decomposition (Figure 2). The material they prepared retain the OER activity and mechanism of the molecular Co₄O₄ analogue, yet demonstrate unprecedented long-term stability at pH 14. The organic linkers of the framework allow for chemical fine-tuning of activity and stability and, perhaps most importantly, provide “matrix isolation” that allows for observation and stabilization of intermediates in the water-splitting pathway. The identification of its molecular structure allows a confident assignment of the protonation states of oxygen ligands that lead to O–O bond formation. Also, the electrocatalytic activity of a reactive intermediate was verified over many turnovers, and analysis of electrochemical kinetics allowed establishment of firm parallels between molecular models and bulk cobalt oxide OER catalysts. This work involved collaborators from LBNL, Columbia University, SLAC National Accelerator Laboratory, Rensselaer Polytechnic Institute and Brookhaven National Laboratory.

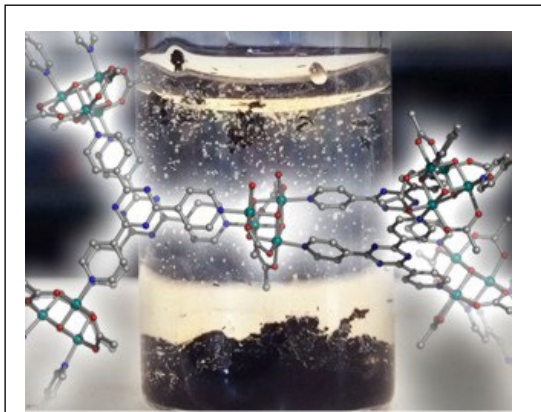


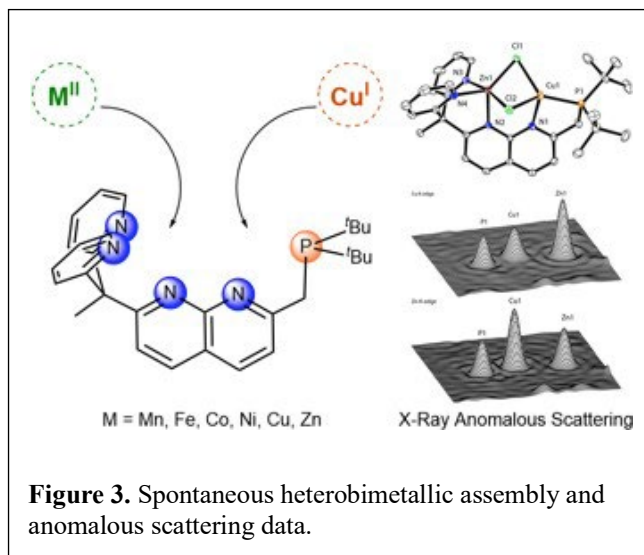
Figure 2. An overlay of the atomistic model of the cubane framework OER catalysts on a photograph showing O₂ evolving from the material. The model was constructed from X-ray absorption spectroscopy and scattering data.

Reference: "Stabilization of reactive Co₄O₄ cubane oxygen-evolution catalysts within porous frameworks." A. I. Nguyen, K. M. Van Allsburg, M. W. Terban, M. Bajdich, J. Oktawiec, M. S. Ziegler, J.

P. Dombrowski, K. V. Lakshmi, W. S. Drisdell, J. Yano, S. J. L. Billinge and T. D. Tilley, *Proc. Nat. Acad. Sci.* 2019, in press. DOI: [10.1073/pnas.1815013116](https://doi.org/10.1073/pnas.1815013116)

Selective synthesis of heterobimetallic complexes for studies on metal-metal cooperation.

Metal-metal cooperation is integral to the function of many enzymes and synthetic catalysts, and model complexes hold enormous potential for providing insights into the capabilities of analogous multimetallic cores. However, the selective synthesis of heterobimetallic complexes remains a significant challenge, especially for systems that hold the metals in close proximity and feature open or reactive coordination sites for both metals. To address this issue, Tilley has built complexes from a rigid, naphthyridine-based dinucleating ligand featuring distinct binding environments was synthesized (Figure 3). This ligand enables the selective synthesis of a series of $M^{\text{II}}\text{Cu}^{\text{I}}$ bimetallic complexes ($M = \text{Mn, Fe, Co, Ni, Cu, Zn}$), in which each metal center exclusively occupies its preferred binding pocket, from simple chloride salts. The precision of this selectivity is evident from various characterizations, including anomalous X-ray diffraction experiments conducted at the ALS, Lawrence Berkeley National Laboratory. Current investigations are exploring the chemical conversions and catalysis associated with various heterobimetallic combinations.



Reference: "Selective Synthesis of a Series of Isostructural $M^{\text{II}}\text{Cu}^{\text{I}}$ Heterobimetallic Complexes Spontaneously Assembled by an Unsymmetrical Naphthyridine-Based Ligand." A. Nicolay and T. D. Tilley. *Chem. Eur. J.* **2018**, *41*, 10329-10333. DOI: 10.1002/chem.201802623

Identifying the active Cu active sites in the electrocatalytic conversion of aqueous CO₂ to C₂₊ products

The electrocatalytic conversion of aqueous CO₂ to value-added chemicals and fuels presents an opportunity to use renewably-generated electricity to recycle CO₂ and close the carbon cycle.¹ A critical challenge for the field is to understand what defines a catalytically active surface for C-C bond formation in such conditions.² To this end, Yang and his coworkers have recently identified an *in situ* formed, structurally dynamic Cu-based catalyst that converts CO₂ to multi-carbon products (C₂₊) with >50% faradaic efficiency at relatively low overpotential (-0.8 V vs. RHE).³ The structural transformation of this system under CO₂ reducing conditions is striking, with an ensemble of uniform 7 nm spherical Cu nanoparticles evolving into sharp cuboidal features of 10-20 nm (Figure 4). Using a battery of *in situ* and *ex situ* characterization techniques, his group has sought to unveil the structural origin of the lowered activation barrier towards C-C bond formation in this system, given its unique structural dynamics.⁴

Conventional *ex situ* characterization suggests that the cubic evolved structures are single-crystal Cu₂O, which is correlated to high electrocatalytic activity for multicarbon formation. However, a

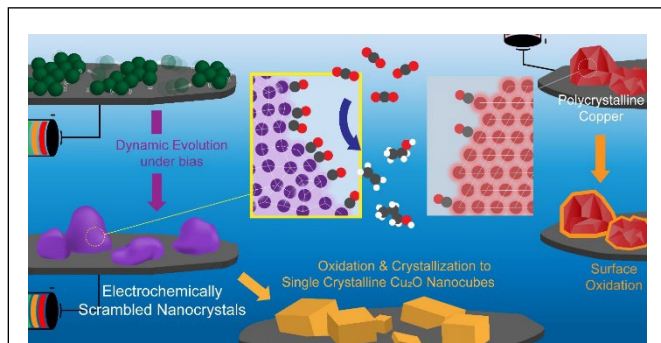


Figure 4. An ensemble of 7 nm copper nanoparticles demonstrates high mobility under CO₂ electroreducing conditions as measured by *in situ* electrochemical STEM. These fuse into uniquely disordered copper structures that rapidly crystallize into single crystal oxide cubes, but can be passivated from oxidation and investigated by EXAFS. The unique structural dynamics of this system are hypothesized to give way to its high activity for CO₂-to-C₂₊ conversion, in contrast with polycrystalline copper nanostructures that exhibit neither.

series of passivation and *in situ* experiments demonstrate that the true catalyst is metallic Cu. EXAFS and HRTEM on the passivated catalyst reveal disorder to be a unique quality of the active evolved catalyst. They posit that this disorder significantly enhances C-C coupling on the undercoordinated surface, while being highly susceptible to rapid crystallization into Cu₂O, in contrast with typical polycrystalline copper surfaces (summarized in Fig 4). They furthermore employed *in situ* electrochemical liquid cell STEM to illustrate that the mobility of the nanoparticle system plays a large role in the catalyst structure ultimately evolved. They found that 7 nm nanoparticles exhibit high mobility and rapidly fuse into the active structure, whereas 20 nm nanoparticles are relatively immobile under the same conditions and are similarly inactive for

CO₂-to-C₂₊ conversion. Thus, they illustrate that the disorder as measured through EXAFS is an important parameter correlated with C₂₊ activity and that the mobility of nanostructures under operating conditions is necessary for such an active structure to evolve. Through this work, they hope to identify active sites for CO₂-to-C₂₊ electroconversion, as well as demonstrate avenues for advanced catalyst characterization critical for a full understanding of catalysts under operating conditions, such as catalyst passivation and *in situ* XAS and TEM.

References:

1. Ross, M.B.; Luna, P.D.; Li, Y.; Dinh, C.T.; Kim, D.; Yang, P.; Sargent, E.H. Designing materials for electrochemical carbon dioxide recycling. *Nature Catalysis*. **2019**, *In press*.
2. Gao, D.; Aran-Ais, R.; Jeon, H.; Cuenya, B. Rational catalyst and electrolyte design for CO₂ electroreduction towards multicarbon products. *Nature Catalysis*. **2019**, *2*, 198-210.
3. Kim, D.; Kley, C. S.; Li, Y.; Yang, P. Copper nanoparticle ensembles for selective electroreduction of CO₂ to C₂–C₃ products. *Proc. Natl. Acad. Sci.* **2017**, *114*, 10560–10565.
4. Li, Y.*; Kim, D.*; Louisia, S.; Xie, C.; Kong, Q.; Yu, S.; Lin, T.; Aloni, S.; Yang, P. Electrochemically scrambled nanocrystals are catalytically active for CO₂-to-multicarbon. *In review*.

Cooperative reactivity of acidic sites in catalysts alcohol and ketone dehydrative coupling

Alexis T. Bell and Dean Toste are establishing detailed relationships between the composition and structure of active sites and their catalytic activity for the targeted formation of C-C, C-O, and C-N bonds that are involved in processes for the formation of fuels and chemicals. This work provides guidance for achieving high catalyst activity together with high selectivity to desired products and reveals the importance of cooperative action of Brønsted- and Lewis-acid sites. A portion of their recent efforts have focused on the mechanism and kinetics of alcohol etherification on tungstated zirconia. A high selectivity for alcohol etherification relative to dehydration was achieved on this catalyst, and investigations of the mechanism and kinetics of these reactions indicate that cooperation between Brønsted- and Lewis-acid sites on tungstated zirconia promotes bimolecular ether formation relative to unimolecular alcohol dehydration. In addition, Aldol

condensation of acetone to MIBK was investigated over hydroxyapatite. The activity of this catalyst

can be maximized by surface cation exchange of Ca^{2+} by Sr^{2+} . Again, DFT calculations reveal that a proper balance between Lewis acidity/basicity is required. Cations that are too large (Ba^{2+}) or too small (Mg^{2+}) adversely affect reaction rates due to excessive stabilization of intermediate species. The Sr^{2+} -substituted hydroxyapatite catalyst is highly active because it catalyzes α -proton abstraction and C-O bond cleavage of diacetone alcohol efficiently.

References:

1. Rorrer, J.; He, Y.; Toste, F. D.; Bell, A. T. Mechanism and Kinetics of 1-Dodecanol Etherification over Tungstated Zirconia. *J. Catal.* **2017**, *354*, 13-23.
2. Rorrer, J.; Pindi, S.; Toste, F. D.; Bell, A. T. Effect of Alcohol Structure on the Kinetics of Etherification and Dehydration over Tungstated Zirconia. *ChemSusChem* **2018**, *11*, 3104-3111.

New Methods for Operando Studies of Catalytic Processes: The nature of active sites for CO oxidation on PdCo and PtCo bimetallic catalysts: a new look to the strong metal- support interaction

Multi-component catalysts can exhibit superior activity and selectivity compared with single-components. To investigate the origin of the catalytic activity of CoPd bimetallic catalysts Salmeron and Somorjai followed the composition and structural evolution of CoPd nanoparticles (NPs) during CO oxidation using ambient pressure XPS (APXPS), and transmission electron microscopy (TEM). They found that the reaction induces a reconstruction of the NPs by which CoO segregates forming a shell around the Pd-rich core. Synergy between Pd and CoO_x promotes the catalytic activity and could be optimized by tuning the Co/Pd ratio to reach a maximum near $\text{Co}_{0.26}\text{Pd}_{0.74}$, (Fig. 5, curve #3) which exhibits the lowest temperature for complete CO conversion. At this composition Co segregates to form a CoO monolayer covering the NP as shown by TEM (Fig. 5) by APXPS.

To explore the possible generality of this phenomenon, they are currently studying PtCo and AuCo as catalysts for the same reaction. In this case, CoO is deposited on flat Pt and Au(111) crystals, which allows Scanning Tunneling Microscopy to be used for atomic scale imaging at the reaction pressures. Together with APXPS experiments, they have found that reduction of a CoO monolayer via $\text{CoO} + 1/2\text{O}_2 \rightarrow \text{Co}^0 + \text{CO}_2$ occurs at room temperature, but requires higher temperatures for thicker CoO films.

Structure of Copper-Cobalt Surface Alloys in Equilibrium with CO gas

Somorjai and Salmeron studied the structure of the copper-cobalt (CuCo) surface alloy, formed by Co deposition on Cu(110), in dynamic equilibrium with CO. Using scanning tunneling microscopy (STM), we found that, in vacuum at room temperature and at low Co coverage, clusters of a few Co atoms substituting Cu atoms form at the surface. At CO pressures in the Torr range,

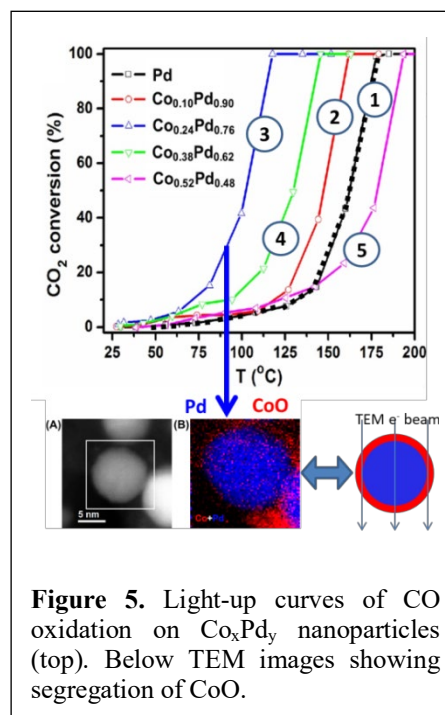


Figure 5. Light-up curves of CO oxidation on Co_xPd_y nanoparticles (top). Below TEM images showing segregation of CoO.

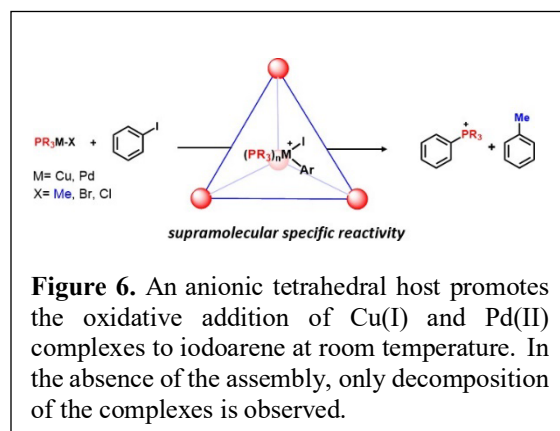
they found that up to 2.5 CO molecules can bind on a single Co atom, in carbonyl-like configurations. Based on high-resolution STM images, together with density functional theory calculations, they determined that the most stable CuCo cluster structures formed with bound CO. Such carbonyl-like formation manifests in shifts in the binding energy of the Co core-level peaks in X-ray photoelectron spectra, as well as shifts in the vibrational modes of adsorbed CO in infrared reflection absorption spectra. The multiple CO adsorption on a Co site weakens the Co–CO bond and thus reduces the C–O bond scission probability. These results may explain the different product distribution, including higher selectivity toward alcohol formation, when bimetallic CuCo catalysts are used compared to pure Co.

Reference: Structure of Copper-Cobalt Surface Alloys in Equilibrium with Carbon Monoxide Gas. Baran Eren, Daniel Torres, Osman Karşlıoğlu, Zongyuan Liu, Cheng Hao Wu, Dario Stacchiola, Hendrik Bluhm, Gabor Somorjai, Miquel Salmeron. *J. Am. Chem. Soc.*, **140**, 6575-6581 (2018).

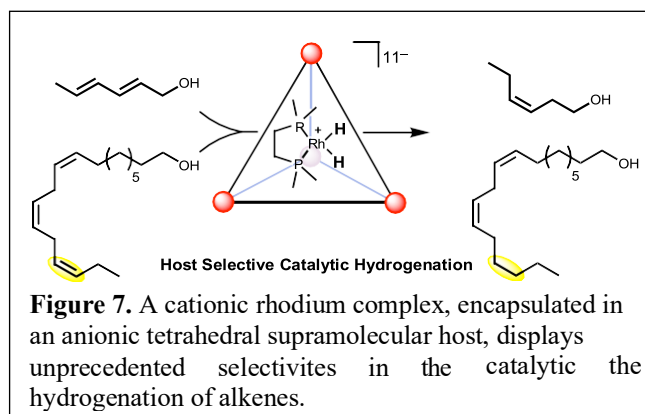
Subtask 2: Catalysis in Confined Spaces

Supramolecular control over selectivity of organometallic catalysts

Supramolecular hosts offer defined microenvironments that facilitate selective host-guest interactions, enabling reactivity that would otherwise be challenging in bulk solution. While impressive rate enhancements and selectivities have been previously reported, examples of reaction in which the host not only accelerates, but alters the lowest energy reaction pathway from that in bulk solution, remain rare. Toste, Raymond and Bergman recently showed that a supramolecular host stabilizes reactive cationic organometallic complexes in the presence of a well encapsulated iodoarene guest and that subsequent oxidative addition occurs under mild conditions (Figure 6). Alternative reaction trajectories (typically decomposition) resulted under host free reaction conditions, indicating that the observed selectivities and conversions are exclusively host dependent. These observations suggest that supramolecular cages can provide access to host-selective reaction pathways.



Performing selective transformations on complex substrates, particularly in the presence of similar functional groups at multiple sites, remains a challenge in catalysis. They recently discovered a supramolecular strategy by which encapsulation of a homogeneous cationic transition metal hydrogenation catalyst enables selective olefin hydrogenation, even in the presence of multiple sites of unsaturation (Figure 7). While the reaction requires at least one sterically non-demanding alkene substituent, the rate of hydrogenation is not sensitive to the distance between



the alkene and the functional group, including a carboxylate, distal to the alkene. This observation indicates that the double bond alone needs to be encapsulated to effect hydrogenation. The high size- and site-selectivity, as well as the lack of requirement for full encapsulation of the substrate, suggest that this strategy is promising for performing precise transformation on complex substrates.

References:

1. “Supramolecular Host-Specific Activation of Iodoarenes by Encapsulated Organometallics.” Bender, T. A.; Morimoto, M.; Bergman, R. G.; Raymond, K. N.; Toste, F. D. *J. Am. Chem. Soc.* **2019**, *141*, 1701- 1706.
2. “A Supramolecular Strategy for Selective Catalytic Hydrogenation Independent of Remote Chain Length.” Bender, T. A.; Bergman, R. G.; Raymond, K. N.; Toste, F. D. *submitted*.

Using Catalyst Supramolecular Structure to Control Product Selectivity for the Oxygen Reduction Reaction

The oxygen reduction reaction is of great importance for understanding biological processes and developing new energy technologies. One of the primary challenges for systems that catalyze oxygen reduction is controlling the product selectivity between the 2-electron/2-proton reduction to form H₂O₂ and the 4-electron/4-proton reduction to form H₂O. Recently, C. Chang’s laboratory has been investigating various methods to enhance the activity of molecular electrocatalysts, and a supramolecular strategy was developed wherein porosity is designed into a molecular catalyst resulting in enhanced substrate and charge transport within the heterogeneous catalyst film (Figure 8). This supramolecular catalyst platform is composed of six metalloporphyrins connected through covalent imine bonds to form a porphyrin box.

They hypothesized that the supramolecular arrangement of the six individual active sites in each porphyrin box could provide an opportunity to control the extent of active site isolation.

Reference: Smith, P. T.; Benke, B. P.; Cao, Z.; Kim, Y.; Nichols, E. M.; Kim, K.; Chang, C. J., Iron Porphyrins Embedded into a Supramolecular Porous Organic Cage for Electrochemical CO₂ Reduction in Water. *Angew. Chem. Int. Ed.* **2018**, *57* (31), 9684-9688.

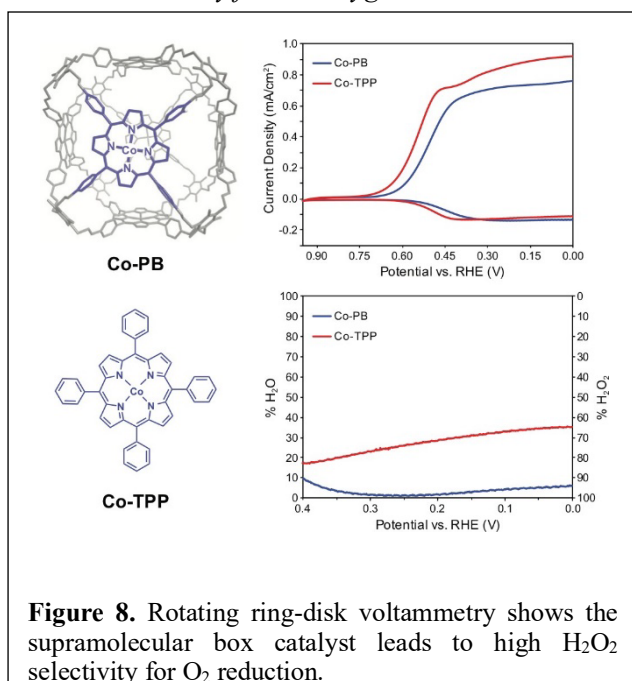


Figure 8. Rotating ring-disk voltammetry shows the supramolecular box catalyst leads to high H₂O₂ selectivity for O₂ reduction.

Understanding the Origins of Chemoselectivity from a Confined Protein Space.

The selective modification of unactivated sp^3 C–H bonds is a challenging problem because it requires the identification of catalysts that are sufficiently powerful to activate these bonds while maintaining selectivity. Remarkably, living systems evolved a set of non-heme Fe^{II}/α -ketoglutarate (Fe^{II}/α KG)-dependent enzymes that use a high-valent metal-oxo intermediate that can activate these bonds. Upon rebound with either the hydroxyl group formed upon H atom abstraction or a bound halide ligand, these enzymes can carry out either hydroxylation or halogenation respectively (Figure 1). While there are a large number of hydroxylases known, only a handful of these radical halogenases have been characterized to date, comprising two families with limited set of substrates. The SyrB2 family has been found to maintain a strict requirement for carrier-protein tethered substrates, whereas the WelO5 family halogenates late-stage indole alkaloid natural products. Since these types of intermediates are not readily modified using downstream enzymatic pathways, the discovery of new enzymes that act on simple and modular building blocks would greatly expand the potential of radical halogenation for biotransformation.

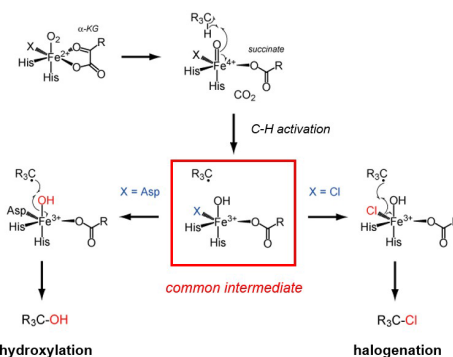
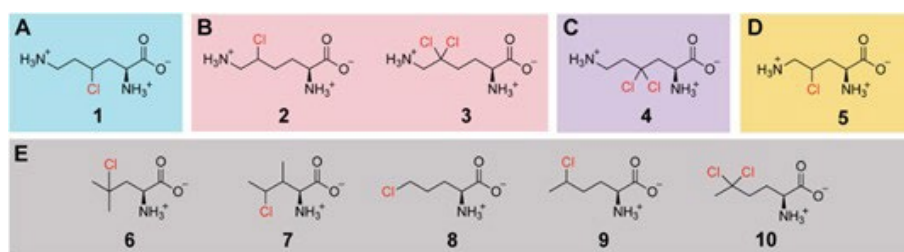


Figure 9. Reaction partitioning between Fe/α KG hydroxylases and halogenases



M. Chang recently discovered a radical halogenase, BesD, which chlorinates the free amino acid lysine, making it the first of the α KG-dependent radical halogenases reported to chlorinate an amino acid without the requirement for a carrier protein.¹ Not only are these substrates more amenable for engineering, they are also simpler targets for mechanistic studies. By investigating the unexplored sequence space around BesD, they have discovered new members of the BesD family that chlorinate different polar and nonpolar amino acids with varied regioselectivity (Figure 9).² In this project, they are investigating the origins of the partitioning between $Fe(II)$ -Cl vs $Fe(III)$ -OH rebound because both are possible in radical halogenases. This new family will be a target for studying how one pathway is favored over another using spectroscopic and biochemical approaches.

References

1. J. A. Marchand, M. E. Neugebauer, M. C. Ing, C.-I. Lin, J. G. Pelton, M. C. Y. Chang, "Discovery of a pathway for terminal-alkyne amino acid biosynthesis", *Nature* **2019**, 567, 420-424.
2. M. E. Neugebauer, K. H. Sumida,² J. G. Pelton, J. L. McMurry, J. A. Marchand, M. C. Y. Chang, "A new family of radical halogenases for the engineering of amino acid-based products", *Nat. Chem. Biol.* **2019**, accepted for publication.

Integration of Catalytic Processes

Two research areas that integrate disparate areas of catalysis have been pursued in the program. One topic focuses on the integration of molecular organometallic systems with protein hosts to create artificial metalloenzymes that catalyze abiotic reactions with high regioselectivity. As second topic focuses on integrating soluble molecular metal or acid catalysts with metal-organic frameworks to create heterogeneous systems with molecular-level control.

Abiological Catalysis Artificial Haem Proteins Containing Noble Metals in Place of Iron Having the Kinetics of Natural Enzymes

During the past several years, Hartwig, in collaboration with Clark, have created a series of artificial metalloenzymes that catalyze the formation of C-C and C-N bonds. These enzymes are created by combining the active site of P450 enzymes with an organometallic cofactors containing a noble metal that leads to high, inherent activity of the catalytic site. Most recently, they have sought to assess the potential of these enzymes to catalyze the reactions with selectivities that would be difficult or impossible to achieve with a small-molecule catalyst. On the basis of their prior observation of intermolecular insertion of acceptor-only carbenes into the C-H bonds of the symmetrical molecule phthalan (R=H in Figure 10), they sought to evolve two enzymes that could react selectively with either or the two methylene C-H bonds of a 4-substituted phthalan in which the two sets of methylene C-H bonds are inequivalent but nearly identical in steric and electronic properties. Indeed, they showed that one mutant of CYP119 containing an iridium cofactor catalyzed reactions selectively at the C-H bonds para to the substituent while a second mutant catalyzed reactions at the C-H bond meta to the substituent. These results show how the supramolecular interactions of the enzyme active site can control the reactivity of an organometallic active site.

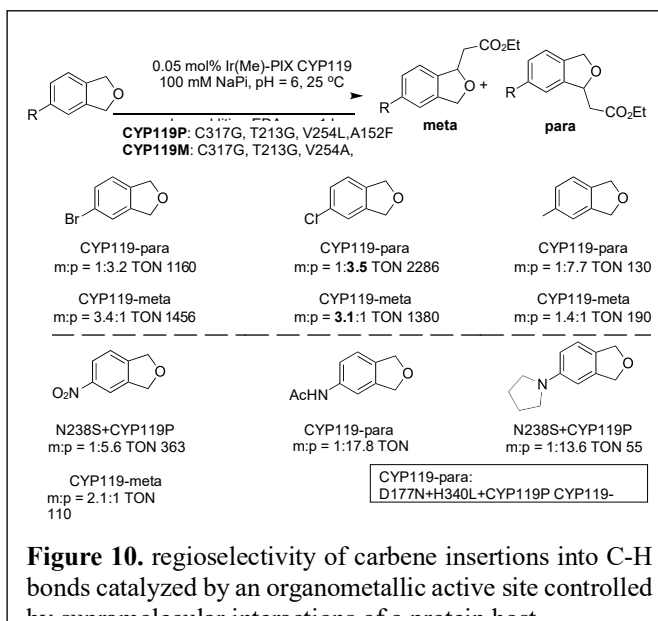


Figure 10. regioselectivity of carbene insertions into C-H bonds catalyzed by an organometallic active site controlled

Reference: Gu, Y; Natoli, Sean, N.; Liu, Z.; Clark, D.S.; Hartwig, J.F. “Site-Selective Functionalization of (sp³)C–H Bonds Catalyzed by Artificial Metalloenzymes Containing an Iridium-Porphyrin Cofactor” submitted.

Oligomerization of light olefins catalyzed by Bronsted acid MOF-808

Sulfated Metal-Organic Framework-808 (S-MOF-808) exhibits strong Brønsted-acidic character which makes it a potential candidate for the heterogeneous acid catalysis. Here, Somorjai studied the isomerization and oligomerization reactions of light olefins (C₃-C₆) over S-MOF-808 at relatively low temperatures and ambient pressure. Different products (dimers, isomers and heavier oligomers) were obtained for different olefins, and effective C-C coupling was observed between isobutene and iso-pentene. Among the substrates investigated, facile oligomerization occurred very specifically for the structures with an α -double bond and two substituents at the second carbon

atom of the main carbon chain. The possible oligomerization mechanism of light olefins was discussed based on the reactivity and selectivity trends. Moreover, the deactivation and regeneration of S-MOF-808 were investigated. The catalyst deactivates via two mechanisms which predominance depends on the substrate and reaction conditions.

Above 110 °C, a loss of acidic sites was observed due to water desorption, and the deactivated catalyst could be re-generated by a simple treatment with water vapor. For C5 substrates and unsaturated ethers, the oligomers with increased molecular weight caused deactivation via blocking of the active sites, which could not be readily reversed. These findings offer the first systematic report on carbocation-mediated olefin coupling within MOFs in which the Brønsted acidity is associated with the secondary building units of the MOF itself and is not related to any guest substance hosted within its pore system.

Reference: Oligomerization of light olefins catalyzed by Brønsted-acidic MetalOrganic Framework-808. Ping Liu, Evgeniy Redekop, Xiang Gao, Wenchi Liu, Unni Olsbye and Gabor A. Somorjai. *J. Am. Chem. Soc.*, 2019, just accepted DOI:10.1021/jacs.9b03867

Identification of the strong Brønsted acid site in a metal–organic framework solid acid catalyst

It is difficult to understand the surface of solid acid catalysts at the molecular level, despite their importance for industrial catalytic applications. A sulfated zirconium-based metal–organic framework, MOF-808-SO₄, (Figure 12) was previously shown to be a strong solid Brønsted acid material. More recently Somorjai and Yaghi probed the origin of its acidity through an array of spectroscopic, crystallographic and computational characterization techniques. The strongest Brønsted acid site is shown to consist of a specific arrangement of adsorbed water and sulfate moieties on the zirconium clusters. When a water molecule adsorbs to one zirconium atom, it participates in a hydrogen bond with a sulfate moiety that is chelated to a neighboring zirconium atom; this motif, in turn, results in the presence of a strongly acidic proton. On dehydration, the material loses its acidity. The hydrated sulfated MOF catalyzes the dimerization of isobutene (2-methyl-1-propene), and achieves a 100% selectivity for C₈ products with a good conversion efficiency.

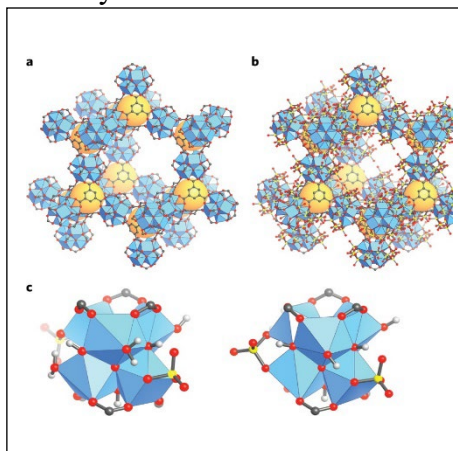


Figure 12a, Pristine MOF-808 comprises six connected zirconium-based metal clusters that contain five formate groups and are linked by BTC into the depicted spn topology framework. **b**, These formates may be substituted with sulfate anions, which coordinate in a bidentate fashion to zirconium, either in a chelating mode to a single zirconium atom, or in a bridging mode to two zirconium atoms. Sulfate is predominantly in the bridging mode in the solvated MOF, and converts exclusively to the chelating mode after activation by heating under a dynamic vacuum. **c**, Two representations of the modelled zirconium clusters, with BTC linkers omitted beyond the coordinating carboxylate group, highlight the differences in molecular decoration between different clusters in the overall structure. A similar stoichiometry of hydroxide, water and sulfate groups are present on each cluster, but the local arrangement and apportionment of these groups differ. Zr-based clusters (Zr₆O₄(OH)₄), blue polyhedra; O, red; C, grey; S, yellow; H, white; pores, large yellow spheres. In **a** and **b**, hydrogen atoms are omitted for clarity. a.u., arbitrary units.

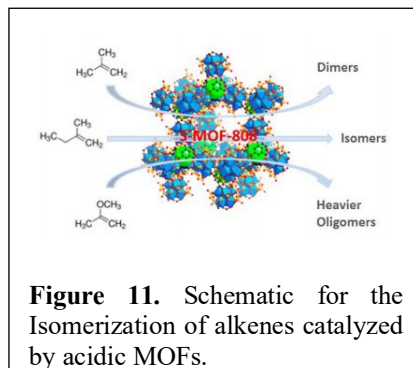
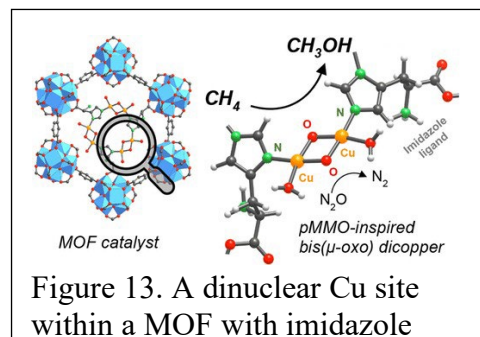


Figure 11. Schematic for the Isomerization of alkenes catalyzed by acidic MOFs.

Reference: Identification of the Bronsted Acid Catalytic Site in Sulfated MOF-808. Christopher A. Trickett, Thomas M. Osborn Popp, Ji Su,^{1,2} Chang Yan, Jonathan Weisberg, Ashfia Huq, Philipp Urban, Juncong Jiang, Markus J. Kalmutzki, Qingni Liu, Jayeon Baek, Martin P. Head-Gordon, Gabor A. Somorjai,¹ Jeffrey A. Reimer, and Omar M. Yaghi. *Nature Chem.*, **2018**, DOI: 10.1038/s41557-018-0171-z

Bioinspired MOF Catalysts for Selective Methane Oxidation to Methanol

Particulate methane monooxygenase (pMMO) is an enzyme that oxidizes methane to methanol with high activity and selectivity. Limited success has been achieved in incorporating biologically relevant ligands for the formation of such active site in a synthetic system. Somorjai and Yaghi also reported the design and synthesis of metal-organic framework (MOF) catalysts inspired by pMMO for selective methane oxidation to methanol. By judicious selection of a framework with appropriate topology and chemical functionality, MOF-808 was used to postsynthetically install ligands bearing imidazole units for subsequent metalation with Cu(I) in the presence of dioxygen (Figure 13). The catalysts show high selectivity for the oxidation of methane to methanol under isothermal conditions at 150 °C.



Reference: Bioinspired Metal-Organic Framework Catalysts for Selective Methane Oxidation to Methanol. Jayeon Baek, Bunyarat Rungtaweivoranit, Xiaokun Pei, Myeongkee Park, Sirine C. Fakra, Yi-Sheng Liu, Roc Matheu, Sultan A. Alshimiri, Saeed Alshehri, Christopher A. Trickett, Gabor A. Somorjai and Omar M. Yaghi. *J. Am. Chem. Soc.*, **2018**, *140*, 18208-18216.

Catalysis Program Publications 2015–2017

2016

1. Brown, C. J.; Kokai, A.; Miller, G. M.; Bergman, R. G.; Raymond, K. N., Improved Scope and Diastereoselectivity of C-H Activation in an Expanded Supramolecular Host. *Supramol. Chem.*, **2016**, *28*, 188–191. DOI: 10.1080/10610278.2015.1122196.
2. Cao, Z.; Kim, D.; Yu, Y.; Xu, J.; Lin, S.; Wen, X.; Nichols, E. M.; Jeong, K.; Reimer, J. A.; Yang, P.; Chang, C. J., A Molecular Surface Functionalization Approach to Tuning Nanoparticle Electrocatalysts for Carbon Dioxide Reduction, *J. Am. Chem. Soc.*, **2016**, *138*, 8120–8125. DOI: 10.1021/jacs.6b02878.
3. Carencio, S.; Capucine Sassoie; Marco Faustini; Pierre Eloy; Damien P. Debecker; Hendrik Bluhm; Miquel Salmeron., The Active State of Supported Ruthenium Oxide Nanoparticles during Carbon Dioxide Methanation. *J. Phys. Chem. C*, **2016**, *120* (28), 15354–15361. DOI: 10.1021/acs.jpcc.6b06313.
4. Dombrowski, J. P.; Johnson, G. R.; Bell, A. T.; Tilley, T. D., Ga[OSi(O^tBu)₃]₃•THF, A Thermolytic Molecular Precursor for High Surface Area Gallium-Containing Silica Materials of Controlled Dispersion and Stoichiometry. *Dalton Trans.*, **2016**, *45*, 11025–11034. DOI: 10.1039/C6DT01676F.
5. Dong, Y.; Lipschutz, M. I.; Tilley, T. D. Regioselective, Transition Metal-Free C–O Coupling

- Reactions involving Aryne Intermediates. *Org. Lett.*, **2016**, *18*, 1530–1533. DOI: 10.1021/acs.orglett.6b00183.
- Goulas, K. A.; Sreekumar, S.; Song, Y.; Kharidehal, P.; Gunbas, G.; Dietrich, P. J.; Johnson, G. R.; Wang, Y. C.; Grippo, A. M.; Grabow, L. C.; Gokhale, A. A.; Toste, F. D., Synergistic Effects in Bimetallic Palladium-Copper Catalysts Improve Selectivity in Oxygenate Coupling Reactions. *J. Am. Chem. Soc.*, **2016**, *138*, 6805. DOI: 10.1021/jacs.6b02247.
 - Ho, C.; Shylesh, S.; Bell, A. T., Mechanism and Kinetics of Ethanol Coupling to Butanol over Hydroxyapatite. *ACS Catal.*, **2016**, *6*, 938–949. DOI: 10.1021/acscatal.5b02672.
 - Howell, J.; Li, Y.-P.; Bell, A. T., Propene Metathesis over Supported Tungsten Oxide Catalysts: A Study of Active Site Formation. *ACS Catal.*, **2016**, DOI: 10.1021/acscatal.6b01842.
 - Johnson, G. R.; Bell, A. T., Effects of Lewis Acidity of Metal-Oxide Promoters on the Activity and Selectivity of Co-Based Fischer-Tropsch Catalysts. *J. Catal.*, **2016**, *338*, 250–264. DOI: 10.1016/j.jcat.2016.03.022.
 - Landry, A.M.; Iglesia, E., Synthesis of Bimetallic AuPt Clusters with Clean Surfaces via Sequential Displacement-Reduction Processes. *Chem. Mater.*, **2016**, *28*, 2872–5886. DOI: 10.1021/acs.chemmater.6b02346.
 - Landry, A.M.; Iglesia, E., Displacement-reduction Routes to PtPd Clusters and Mechanistic Inferences for the Synthesis of other Bimetallic Compositions. *J. Cat.*, **2016**, *344*, 389–400. DOI: 10.1016/j.jcat.2016.10.007.
 - Liberman-Martin, A.L.; Levine, D.S.; Liu, W.; Bergman, R.G.; Tilley, T.D., Biaryl Reductive Elimination is Dramatically Accelerated by a Remote Lewis Acid Chemical Switch: Evidence for an Unusual Bidentate Ligand Dissociation Mechanism. *Organometallics*, **2016**, *35*, 1064–1069. DOI: 10.1021/acs.organomet.5b01003.
 - Liberman-Martin, A.L.; Levine, D.S.; Ziegler, M.S.; Bergman, R.G.; Tilley, T.D., Lewis Acid-Base Interactions between Platinum(II) Diaryl Complexes and Bis(perfluorophenyl)zinc: Strongly Accelerated Reductive Elimination Induced by a Z-type Ligand. *Chem. Comm.*, **2016**, *52*, 7039–7042. DOI: 10.1039/c6cc02433e
 - Liberman-Martin, A.L.; Ziegler, M.S.; DiPasquale, A.G.; Bergman, R.G.; Tilley, T.D., Functionalization of an Iridium–Diamidocarbene Complex by Ligand-Based Reactions with Titanocene and Zirconocene Sources. *Polyhedron*, **2016**, *116*, 111–115. DOI: 10.1016/j.poly.2016.03.044.
 - Licht, R.B.; Vogt, D.; Bell, A.T., The Mechanism and Kinetics of Propene Ammoxidation over α -Bismuth Molybdate. *J. Catal.*, **2016**, *339*, 228–241. DOI: 10.1016/j.jcat.2016.04.012.
 - Licht, R.B.; Getsoian, A.B.; Bell, A.T. Identifying the Unique Properties of α -Bi₂Mo₃O₁₂ for the Activation of Propene. *J. Phys. Chem. C*, **2016**, *120*, 29233–29247. DOI: 10.1021/acs.jpcc.6b09949.
 - Melaet, G.; Ralston, W.; Liu, W.C.; Somorjai, G., Product Distribution Change in the Early Stages of Carbon Monoxide Hydrogenation over Cobalt Magnesium Fischer-Tropsch Catalyst. *Catalysis Today*, **2016**, *272*, 69–73. DOI: 10.1016/j.cattod.2016.03.027.
 - Na, K.; Yoon, Y.; Somorjai, G.A., Control of Model Catalytic Conversion Reaction over Pt

- Nanoparticle Supported Mesoporous BEA Zeolite Catalysts. *Catalysis Today*, **2016**, *265*, 225–230. DOI: 10.1016/j.cattod.2015.08.058.
19. Park, J.Y.; Somorjai, G.A., Hot Electron Surface Chemistry at Oxide-Metal Interfaces: Foundation of Acid-Base Catalysis. *Cat. Lett.*, **2016**, *146*, 1–11. DOI: 10.1007/s10562-015-1657-6.
 20. Su, J.; Xie, C.; Chen, C.; Yu, Y.; Kennedy, G.; Somorjai, G.A.; Yang, P., Insights into the Mechanism of Tandem Alkene Hydroformylation over Nanocrystalline Catalyst with Multiple Interfaces. *J. Am. Chem. Soc.*, **2016**, *138*, 11568–11574.
 21. Niu, Z.; Becknell, N.; Yu, Y.; Kim, D.; Chen, C.; Kornienko, N.; Somorjai, G.A.; Yang, P., Anisotropic Phase Segregation and Migration of Pt in Nanocrystals en route to Nanoframe Catalysts. *Nature Materials*, **2016**, *15*, 1188–1194.
 22. Palla, K.S.; Hurlburt, T.J.; Buyanin, A.M.; Somorjai, G.A.; Francis, M.B., Site-selective Oxidative Coupling Reactions for the Attachment of Enzymes to Glass Surfaces through DNA Directed Immobilization. *J. Am. Chem. Soc.* **2016**, *139*, 1967–1974.
 23. Kennedy, G.; Melaet, G.; Han, H.-L.; Ralston, W.T.; Somorjai, G.A., *In situ* Spectroscopic Investigation into the Active Sites for Crotonaldehyde Hydrogenation at the Pt Nanoparticle-CO₃O₄ Interface. *ACS Catal.*, **2016**, *6*, 7140–7147. DOI: 10.1021/acscatal.6b01640.
 24. Sgarlata, C.; Raymond, K.N., Untangling the Diverse Interior and Multiple Exterior Guest Interactions of a Supramolecular Host by the Simultaneous Analysis of Complementary Observables. *Anal. Chem.*, **2016**, *88*, 6923–6929. DOI: 10.1021/acs.analchem.6b01684.
 25. Xi, Y.; Butcher, T.W.; Zhang, J.; Hartwig, J.F., Regioselective, Asymmetric Formal Hydroamination of Unactivated Internal Alkenes. *Angew. Chem. Int. Ed.*, **2016**, *55*, 776–780. DOI: 10.1002/anie.201509235.
 26. Xi, Y.; Hartwig, J.F., Diverse Asymmetric Hydrofunctionalization of Aliphatic Internal Alkenes through Catalytic Regioselective Hydroboration. *J. Am. Chem. Soc.*, **2016**, *138*, 6703–6706. DOI: 10.1021/jacs.6b02478.
 27. Ye, R.; Hurlburt, T.; Sabyrov, K.; Alayoglu, S.; Somorjai, G. A., Molecular Catalysis Science: Perspective on Unifying the Fields of Catalysis. *PNAS*, **2016**, *113*, 5159–5166. DOI: 10.1073/pnas.1601766113.
 28. Ye, R.; Yuan, B.; Zhao, J.; Ralston, W.; Wu, C.Y.; Barin, E.U.; Toste, D.F.; Somorjai, G.A., Metal Nanoparticles Catalyzed Selective Carbon-Carbon Bond Activation in the Liquid Phase. *J. Am. Chem. Soc.*, **2016**, *138*, 8533–8537. DOI: 10.1021/jacs.6b03977.
 29. Zhai, S.; Wütschert, M.; Licht, R. B.; Bell, A. T., Effects of Catalyst Structure on the Oxidation of Propene to Acrolein. *Catal. Today*, **2016**, *261*, 146–153. DOI: 10.1016/j.cattod.2015.06.011.
 30. Dydio, P.; Key, H.M.; Nazarenko, A.; Rha, J.Y.-E.; Seyedkazemi, V.; Clark, D.S.; Hartwig, J.F., An Artificial Metalloenzyme with the Kinetics of Native Enzymes. *Science*, **2016**, *330*, 102–106. DOI: 10.1126/science.124427.
 31. Key, H.M.; Dydio, P.; Clark, D.S.; Hartwig, J.F., Abiological Catalysis by Artificial Haem Proteins Containing Noble Metals in Place of Iron. *Nature*, **2016**, *534*, 534–537. DOI: 10.1038/nature17968.
 32. Axelson, J.C.; Gonzalez, M.I.; Meihaus, K.R.; Chang, C. J.; Long, J.R., Synthesis and

Characterization of a Tetrapodal NO₄⁴⁻ Ligand and Its Transition Metal Complexes. *Inorg. Chem.* **2016**, *55*, 7527–7534. DOI: 10.1021/acs.inorgchem.6b00908. *Efforts by C.J.C. laboratory involve direction the synthesis and structural characterization of first-row transition metal complexes with pentadentate ligands.*

33. Levin, M.; Kaphan, D.; Hong, C.; Bergman, R.G.; Raymond, K.; Toste, F.D., Scope and Mechanism of Cooperativity at the Intersection of Organometallic and Supramolecular Catalysis. *J. Am. Chem. Soc.*, **2016**, *138*, 9682–9693. DOI: 10.1021/jacs.6b05442. *Fellowship support from NIH General Medical Sciences.*
34. Liu, H.-J.; Cai, I.C.; Fedorov, A.; Ziegler, M.S.; Copéret, C.; Tilley, T.D., Tricoordinate Organochromium(III) Complexes Supported by Bulky Silylamido Ligands Produce Ultra-High-Molecular Weight Polyethylene in the Absence of Activators. *Helv. Chim. Acta*, **2016**, *99*, 859–867. DOI: 10.1002/hlca.201600199. *This DOE program supported the synthesis, characterization and reactivity studies of the 3-coordinate Cr alkyl complexes. The polymerization studies were carried out at the ETH.*
35. Ziegler, M.S.; Lakshmi, K.V.; Tilley, T.D., Aryl Group Transfer from Tetraarylborato Anions to an Electrophilic Dicopper(I) Center and a Mixed-Valence *m*-Aryl Dicopper(I,II) Complex. *J. Am. Chem. Soc.*, **2016**, *138*, 6484–6491. DOI: 10.1021/jacs.6b00802. *This work is almost entirely supported by this DOE program; our collaborator Lakshmi obtained the EPR spectra.*
36. Kashif, M.K.; Milhuisen, R.A.; Nippe, M.; Hellerstedt, J.; Zee, D.Z.; Duffy, N.W.; Halstead, B.; De Angelis, F.; Fantacci, S.; Fuhrer, M. S.; Chang, C. J.; Cheng, Y.-B.; Long, J. R.; Spiccia, L.; Bach, U., Cobalt Polypyridyl Complexes as Transparent Solution-Processable Solid-State Charge Transport Materials. *Adv. Energy Mater.* **2016**, 1600874. DOI: 10.1002/aenm.201600874.
37. Zhang, J.; Shrestha, R.; Hartwig, J.F.; Zhao, P. A Decarboxylative Approach for Regioselective Hydroarylation of Alkynes. *Nature Chem.* **2016**, *8*, 1444. DOI: 10.1038/NCHEM.2602. *The high-throughput catalyst discovery and development was conducted at UC Berkeley and was supported by this DOE program. Work at NDSU was supported by NSF.*
38. Lee, S.Y.; Hartwig, J.F. Palladium-Catalyzed, Site-Selective Direct Allylation of Aryl C-H Bonds by Silver-Mediated C-H Activation: A Synthetic and Mechanistic Investigation. *J. Am. Chem. Soc.* **2016**, *138*, 15278–15284. DOI: 10.1021/jacs.6b10220. *SYL is supported by an NIH postdoctoral fellowship; her supplies and operating expenses were supported by this DOE program.*

2017

1. Carenco, S.; Liu, Z.; Salmeron, M., The Birth of Nickel Phosphides Catalysts: Monitoring Phosphorus Insertion into Nickel. *ChemCatChem.*, **2017**, DOI: 10.1002/cctc.201601526R1.
2. Choi, K.-M.; Kim, D.; Rungtaweeworanit, B.; Trickett, C.A.; Barmanbek, J.T.D.; Alshammari, A.S.; Yang, P.; Yaghi, O.M., Plasmon-Enhanced Photocatalytic CO₂ Conversion within Metal-Organic Frameworks Under Visible Light, *J. Am. Chem. Soc.*, **2017**, *139*, 356–362. DOI: 10.1021/jacs.6b11027.
3. Deraedt, C.; Melaet, G.; Ralston, W.; Ye, R.; Somorjai, G.A., Platinum and Other Transition Metal Nanoclusters (Pd, Rh) Stabilized by PAMAM Dendrimer as Excellent Heterogeneous

- Catalysts: Application to the MethylCyclopentane (MCP) Hydrogenative Isomerization. *Nano Letters.*, **2017**, *17*, 1853–1862. DOI: 10.1021/acs.nanolett.6b05156.
4. Dydio, P.; Key, H.M.; Hayashi, H.; Clark, D.S.; Hartwig, J.F., Chemoselective, Enzymatic C-H Bond Amination Catalyzed by a Cytochrome P450 Containing an Ir(Me)-PIX Cofactor. *J. Am. Chem. Soc.*, **2017**, *139*, 1750–1753. DOI: 10.1021/jacs.6b11410.
 5. Guillo, P.; Lipschutz, M. I.; Fasulo, M. E.; Tilley, T. D., Tantalum-Polyhedral Oligosilsesquioxane (POSS) Complexes as Structural Models and Functional Catalysts for Epoxidation. *ACS Catal.*, **2017**, *7*, 2303–2312. DOI: 10.1021/acscatal.7b00020.
 6. Hong, C.M.; Kaphan, D.M.; Bergman, R.G. Raymond, K.N.; Toste, F.D., Conformation Selection as the Mechanism of Guest Binding in a Flexible Supramolecular Host. *J. Am. Chem. Soc.*, **2017**, *139*, in press.
 7. Key, H.M.; Dydio, P.; Liu, Z.; Rha, J.Y-E.; Nazarenko, A.; Seyedkazemi, V.; Clark, D.S.; Hartwig, J.F. Beyond Fe: Iridium-Containing P450 Enzymes for Selective Cyclopropanations of Structurally Diverse Alkenes. *ACS Cent. Sci.* **2017**, *3*, 302–308. DOI:10.1021/acscentsci.6b00391.
 8. Kim, D.; Becknell, N.; Yu, Y.; Yang, P., Room-Temperature Dynamics of Vanishing Copper Nanoparticles Supported on Silica, *Nano Letters*, **2017**, in press.
 9. Levine, D.S.; Tilley, T.D.; Andersen, R.A., Evidence for the Existence of Group 3 Terminal Methylidene Complexes. *Organometallics*, **2017**, *36*, 80–88. DOI: 10.1021/acs.organomet.6b00394.
 10. Li, Y.; Cui, F.; Ross, M.B.; Kim, D.; Sun, Y.; Yang, P., Structure-sensitive CO₂ Electroreduction to Hydrocarbons on Ultrathin Five-Fold Twinned Copper Nanowires, *Nano Letters*, **2017**, *17*, 1312–17. DOI: 10.1021/acs.nanolett.6b05287.
 11. Licht, R.B.; Bell, A.T., A DFT Investigation of the Mechanism of Propene Ammoxidation over \square -Bismuth Molybdate. *ACS Catalysis*, **2017**, *7*, 161–176. DOI: 10.1021/acscatal.6b02523. Lin, S.; Yang, X.; Jia, S.; Weeks, A.M.; Hornsby, M.; Lee, P.S.; Nichiporuk, R.V.; Iavarone, A.T.; Wells, J.A.; Toste, F.D.; Chang, C.J., Redox-Based Reagents for Chemoselective Methionine Bioconjugation. *Science*, **2017**, *355*, 597–602. DOI: 10.1126/science.aal3316.
 12. Lipke, M.C.; Liberman-Martin, A.; Tilley, T.D., Electrophilic Activation of Silicon-Hydrogen Bonds in Catalytic Hydrosilations. (review article) *Angew. Chem. Int. Ed.*, **2017**, *56*, 2260–2294. DOI: 10.1002/anie.201605198.
 13. Nguyen, A. I.; Suess, D. L. M.; Darago, L. E.; Oyala, P. H.; Levine, D. S.; Ziegler, M. S.; Britt, R. D.; Tilley, T. D., Manganese-Cobalt Oxido Cubanes Relevant to Manganese-Doped Water Oxidation Catalysts. *J. Am. Chem. Soc.*, **2017**, *139*, 5579–5587. DOI: 10.1021/jacs.7b01792.
 14. Nguyen, A. I.; Wang, J.; Levine, D. S.; Ziegler, M. S.; Tilley, T. D., Control and Empirical Prediction of Redox Potentials for Co₄O₄ Cubanes over a 1400 mV Range: Implications for the Feasibility of a Co(V)-Oxo Species. *Chem. Sci.*, **2017**, Advance Article. DOI: 10.1039/C7SC00627F.
 15. Ralston, W.T.; Melaet, G.; Saephan, T.; Somorjai, G.A.; Evidence of Structure Sensitivity in the Fischer-Tropsch Research on Model Cobalt Nanoparticles by Time-Resolved Chemical Transient Kinetics. *Angewandte Chemie*, **2017**, accepted.
 16. Sabyrov, K.; Musselwhite, N.; Melaet, G.; Somorjai, G.A., Hydroisomerization of *n*-

Hexadecane: Remarkable Selectivity of Platinum Nanoparticles Supported on Mesoporous Silica Post-Synthetically Modified with Aluminum. *Catal. Sci. Technol.*, **2017**, *7*, 1756–1765. DOI: 10.1039/C7CY00203C.

17. Sakimoto, K.K.; Kornienko, N.; Yang, P.D., Cyborgian Material Design for Solar Fuel Production: The Emerging Photosynthetic Biohybrid Systems, *Acc. Chem. Res.*, **2017**, *50*, 476–481. DOI: 10.1021/acs.accounts.6b00483.
18. Suslick, B.A.; Liberman-Martin, A.L.; Wambach, T.C.; Tilley, T.D., Olefin Hydroarylation Catalyzed by (Pyridyl-Indolate)Pt(II) Complexes: Catalytic Efficiencies and Mechanistic Aspects. *ACS Catal.*, accepted. DOI: 10.1021/acscatal.7b01560.
19. Tatsumi, H.; Liu, F.; Han, H.-L.; Carl, L.M.; Sapi, A.; Somorjai, G.A., Alcohol Oxidation at Platinum-Gas and Platinum-Liquid Interfaces: The Effect of Platinum Nanoparticle Size, Water Coadsorption, and Alcohol Concentration. *J. Phys. Chem. C*, **2017**, *121*, 7365–7371. DOI: 10.1021/acs.jpcc.7b01432.
20. Troshin, K.; Hartwig, J.F., Snap Deconvolution: an Informatics Approach to High Throughput Discovery of Catalytic Reactions. *Science*, **2017**, accepted.
21. Wu, C.-H.; Eren, B.; Bluhm, H.; Salmeron, M.B., An Ambient-Pressure X-ray Photoelectron Spectroscopy Study of Cobalt Foil Model Catalyst under CO, H₂, and their Mixtures. *ACS Catal.*, **2017**, *7*, 1150–1157. DOI: 10.1021/acscatal.6b02835.
22. Wu, C.-Y.; Wolf, W.J.; Levratovsky, Y.; Bechtel, H.A.; Martin, M.C.; Toste, F.D.; Gross, E., High Spatial Resolution Mapping of Catalytic Reactivity on Pt Nanoparticles. *Nature*, **2017**, *541*, 511–515. DOI: 10.1038/nature20795.
23. Ye, Q.; Ziegler, M. S.; Lakshmi K. V.; Tilley, T. D., Titanium Imido Complexes by Displacement of –SiMe₃ and C–H Bond Activation in a Ti^{III} Amido Complex, Promoted by a Cyclic (Alkyl)(Amino) Carbene (cAAC) *Eur. J. Inorg. Chem.*, **2017**, 2484–2487. DOI: 10.1002/ejic.201700295.
24. Ye, R.; Zhao, J.; Yuan, B.; Liu, W.-C.; De Araujo, J. R.; Fuacher, F. F.; Chang, M.; Toste, F.D.; Somorjai, G.A., New Insights into Aldol Reactions Catalyzed by Heterogenized Homogeneous Catalysts. *Nano. Lett.*, **2017**, *17*, 584–589. DOI: 10.1021/acs.nanolett.6b04827.
25. Yun, Y.; Araujo, J.R.; Melaet, G.; Baek, J.; Archanjo, B.S.; Oh, M.-H.; Alivisatos, A.P.; Somorjai, G.A., Activation of Tungsten Oxide for Propane Dehydrogenation and Its High Catalytic Activity and Selectivity. *Catal. Lett.*, **2017**, *147*, 622. DOI: 10.1007/s10562-016-1915-2.
26. Zhao, J.; Nguyen, S.C.; Ye, R.; Ye, B.; Weller, H.; Somorjai, G.A.; Alivisatos, A.P.; Toste, F.D., A Comparison of Photocatalytic Activities and of Gold Nanoparticles Following Plasmonic and Interband Excitation and a Strategy for Harnessing Interband Hot Carriers for Solution Phase Oxidative Photo-catalysis. *ACS Central. Sci.*, **2017**, *3*, in press.
27. Ziegler, M.S.; Lakshmi, K.V.; Tilley, T.D., Dicopper Cu(I)Cu(I) and Cu(I)Cu(II) Complexes in Copper-Catalyzed Azide-Alkyne Cycloaddition, *J. Am. Chem. Soc.* **2017**, *139*, 5378–5386. DOI: 10.1021/jacs.6b13261.

2018

1. Aubrey, M. L.; Wiers, B. M.; Andrews, S. C.; Sakurai, T.; Reyes-Lillo, S. E.; Hamed, S. M.; Yu, C. J.; Darago, L. E.; Mason, J. A.; Baeg, J. O.; Grandjean, F.; Long, G. J.; Seki, S.; Neaton, J. B.; Yang, P. D.; Long, J. R., Electron delocalization and charge mobility as a function of reduction in a metal-organic framework. *Nat. Mater.* **2018**, *17*, 625-+.
2. Baek, J.; Rungtaweevoranit, B.; Pei, X. K.; Park, M.; Fakra, S. C.; Liu, Y. S.; Matheu, R.; Alshimri, S. A.; Alshehri, S.; Trickett, C. A.; Somorjai, G. A.; Yaghi, O. M., Bioinspired Metal-Organic Framework Catalysts for Selective Methane Oxidation to Methanol. *J. Am. Chem. Soc.* **2018**, *140*, 18208-18216.
3. Bekenstein, Y.; Dahl, J. C.; Huang, J. M.; Osowiecki, W. T.; Swabeck, J. K.; Chan, E. M.; Yang, P. D.; Alivisatos, A. P., The Making and Breaking of Lead-Free Double Perovskite Nanocrystals of Cesium Silver-Bismuth Halide Compositions. *Nano Lett.* **2018**, *18*, 3502-3508.
4. Bischak, C. G.; Wong, A. B.; Lin, E.; Limmer, D. T.; Yang, P. D.; Ginsberg, N. S., Tunable Polaron Distortions Control the Extent of Halide Demixing in Lead Halide Perovskites. *Journal of Physical Chemistry Letters* **2018**, *9*, 3998-4005.
5. Cao, Z.; Derrick, J. S.; Xu, J.; Gao, R.; Gong, M.; Nichols, E. M.; Smith, P. T.; Liu, X.; Wen, X.; Coperet, C.; Chang, C. J., Chelating N-Heterocyclic Carbene Ligands Enable Tuning of Electrocatalytic CO₂ Reduction to Formate and Carbon Monoxide through Surface Organometallic Chemistry. *Angew. Chem. Int. Ed.* **2018**, *57*, 4981-4985.
6. Cestellos-Blanco, S.; Yang, P. D., Semiconductor-Microorganism Catalytic Biohybrid Systems for Artificial Photosynthesis. **2018**, *15*, 031002.
7. De Luna, P.; Quintero-Bermudez, R.; Dinh, C. T.; Ross, M. B.; Bushuyev, O. S.; Todorovic, P.; Regier, T.; Kelley, S. O.; Yang, P. D.; Sargent, E. H., Catalyst electro-redeposition controls morphology and oxidation state for selective carbon dioxide reduction. *Nat. Catal.* **2018**, *1*, 103-110.
8. Dery, S.; Kim, S.; Haddad, D.; Cossaro, A.; Verdini, A.; Floreano, L.; Toste, F. D.; Gross, E., Identifying site-dependent reactivity in oxidation reactions on single Pt particles. *Chem. Sci.* **2018**, *9*, 6523-6531.
9. Diercks, C. S.; Lin, S.; Komienko, N.; Kapustin, E. A.; Nichols, E. M.; Zhu, C. H.; Zhao, Y. B.; Chang, C. J.; Yaghi, O. M., Reticular Electronic Tuning of Porphyrin Active Sites in Covalent Organic Frameworks for Electrocatalytic Carbon Dioxide Reduction. *J. Am. Chem. Soc.* **2018**, *140*, 1116-1122.
10. Durrbeck, S.; Shi, X. R.; Samadashvili, M.; Redinger, J.; Bertel, E.; Salmeron, M., Complex reactions on a convertible catalyst surface: A study of the S-O-Cu system. *Surf. Sci.* **2018**, *678*, 228-233.
11. Eren, B.; Kersell, H.; Weatherup, R. S.; Heine, C.; Crumlin, E. J.; Friend, C. M.; Salmeron, M. B., Structure of the Clean and Oxygen-Covered Cu(100) Surface at Room Temperature in the Presence of Methanol Vapor in the 10-200 mTorr Pressure Range. *J. Phys. Chem. B* **2018**, *122*, 548-554.
12. Eren, B.; Torres, D.; Karslioglu, O.; Liu, Z. Y.; Wu, C. H.; Stacchiola, D.; Bluhm, H.; Somorjai, G. A.; Salmeron, M., Structure of Copper-Cobalt Surface Alloys in Equilibrium with Carbon Monoxide Gas. *J. Am. Chem. Soc.* **2018**, *140*, 6575-6581.
13. Hong, C. M.; Morimoto, M.; Kapustin, E. A.; Alzakhem, N.; Bergman, R. G.; Raymond, K. N.; Toste, F. D., Deconvoluting the Role of Charge in a Supramolecular Catalyst. *J. Am. Chem. Soc.* **2018**, *140*, 6591-6595.

14. Hurlburt, T. J.; Liu, W. C.; Ye, R.; Somorjai, G. A., Surface Science Approach to the Molecular Level Integration of the Principles in Heterogeneous, Homogeneous, and Enzymatic Catalysis. *Top. Catal.* **2018**, *61*, 1210-1217.
15. Kiel, G. R.; Samkian, A. E.; Nicolay, A.; Witzke, R. J.; Tilley, T. D., Titanocene-Mediated Dinitrile Coupling: A Divergent Route to Nitrogen-Containing Polycyclic Aromatic Hydrocarbons. *J. Am. Chem. Soc.* **2018**, *140*, 2450-2454.
16. Kim, H. W.; Ross, M. B.; Kornienko, N.; Zhang, L.; Guo, J. H.; Yang, P. D.; McCloskey, B. D., Efficient hydrogen peroxide generation using reduced graphene oxide-based oxygen reduction electrocatalysts. *Nature Catalysis* **2018**, *1*, 282-290.
17. Kornienko, N.; Zhang, J. Z.; Sakimoto, K. K.; Yang, P. D.; Reisner, E., Interfacing nature's catalytic machinery with synthetic materials for semi-artificial photosynthesis. *Nat. Nanotechnol.* **2018**, *13*, 890-899.
18. Lechner, B. A. J.; Feng, X. F.; Feibelman, P. J.; Cerda, J. I.; Salmeron, M., Scanning Tunneling Microscopy Study of the Structure and Interaction between Carbon Monoxide and Hydrogen on the Ru(0001) Surface. *J. Phys. Chem. B* **2018**, *122*, 649-656.
19. Lee, H.; Ko, J. H.; Song, H. C.; Salmeron, M.; Kim, Y. H.; Park, J. Y., Isotope- and Thickness- Dependent Friction of Water Layers Intercalated Between Graphene and Mica. *Tribol. Lett.* **2018**, *66*.
20. Liu, F. D.; Wang, H. L.; Sapi, A.; Tatsumi, H.; Zhrebetsky, D.; Han, H. L.; Carl, L. M.; Somorjai, G. A., Molecular Orientations Change Reaction Kinetics and Mechanism: A Review on Catalytic Alcohol Oxidation in Gas Phase and Liquid Phase on Size-Controlled Pt Nanoparticles. *Catalysts* **2018**, *8*.
21. Lu, X. W.; Khatib, O.; Du, X. T.; Duan, J. H.; Wei, W.; Liu, X. L.; Bechtel, H. A.; D'Apuzzo, F.; Yan, M. T.; Buyanin, A.; Fu, Q.; Chen, J. N.; Salmeron, M.; Zeng, J.; Raschke, M. B.; Jiang, P.; Bao, X. H., Nanoimaging of Electronic Heterogeneity in Bi₂Se₃ and Sb₂Te₃ Nanocrystals. *Advanced Electronic Materials* **2018**, *4*.
22. Mann, V. R.; Powers, A. S.; Tilley, D. C.; Sack, J. T.; Cohen, B. E., Azide-Alkyne Click Conjugation on Quantum Dots by Selective Copper Coordination. *ACS Nano* **2018**, *12*, 4469-4477.
23. Melaet, G.; Stavila, V.; Klebanoff, L.; Somorjai, G. A., The effect of aluminum and platinum additives on hydrogen adsorption on mesoporous silicates. *Phys. Chem. Chem. Phys.* **2018**, *20*, 12075-12083.
24. Nguyen, A.I.; Darago, L.; Balcells, D.; Tilley, T.D. "Influence of a "Dangling" Co(II) Ion Bound to a [MnCo₃O₄] Oxo Cubane" *J. Am. Chem. Soc.* 2018, *140*, 9030-9033. DOI: 10.1021/jacs.8b04065.
25. Nichols, E. M.; Derrick, J. S.; Nistanaki, S. K.; Smith, P. T.; Chang, C. J., Positional effects of second-sphere amide pendants on electrochemical CO₂ reduction catalyzed by iron porphyrins. *Chem. Sci.* **2018**, *9*, 2952-2960.
26. Nicolay, A.; Tilley, T. D., Selective Synthesis of a Series of Isostructural (MCuI)-Cu-II Heterobimetallic Complexes Spontaneously Assembled by an Unsymmetrical Naphthyridine-Based Ligand. *Chem. Eur. J.* **2018**, *24*, 10329-10333.
27. Olshansky, L.; Huerta-Lavorie, R.; Nguyen, A.I.; Vallapurackal, J.; Furst, A.; Tilley, T.D.; Borovik, A.S. "Artificial Metalloproteins Containing Co₄O₄ Active Sites" *J. Am. Chem. Soc.* **2018**, *140*, 2739– 2742. DOI: 10.1021/jacs.7b13052.
28. Park, M.; Neukirch, A. J.; Reyes-Lillo, S. E.; Lai, M. L.; Ellis, S. R.; Dietze, D.; Neaton, J. B.; Yang, P. D.; Tretiak, S.; Mathies, R. A., Excited-state vibrational dynamics toward the

- polaron in methylammonium lead iodide perovskite. *Nat. Commun.* **2018**, *9*.
29. Rorrer, J.; Pindi, S.; Toste, F. D.; Bell, A. T., Effect of Alcohol Structure on the Kinetics of Etherification and Dehydration over Tungstated Zirconia. *Chemsuschem* **2018**, *11*, 3104-3111.
 30. Sacha, G. M.; Verdaguer, A.; Salmeron, M., A Model for the Characterization of the Polarizability of Thin Films Independently of the Thickness of the Film. *J. Phys. Chem. B* **2018**, *122*, 904-909.
 31. Sakimoto, K. K.; Kornienko, N.; Cestellos-Blanco, S.; Lim, J.; Liu, C.; Yang, P. D., Physical Biology of the Materials-Microorganism Interface. *J. Am. Chem. Soc.* **2018**, *140*, 1978-1985.
 32. Salmeron, M., From Surfaces to Interfaces: Ambient Pressure XPS and Beyond. *Top. Catal.* **2018**, *61*, 2044-2051.
 33. Shimizu, T. K.; Maier, S.; Verdaguer, A.; Velasco-Velez, J. J.; Salmeron, M., Water at surfaces and interfaces: From molecules to ice and bulk liquid. *Prog. Surf. Sci.* **2018**, *93*, 87-107.
 34. Smith, P. T.; Benke, B. P.; Cao, Z.; Kim, Y.; Nichols, E. M.; Kim, K.; Chang, C. J. Iron Porphyrins Embedded into a Supramolecular Porous Organic Cage for Electrochemical CO₂ Reduction in Water. *Angew. Chem. Int. Ed.* **2018**, *57*, 9684-9688.
 35. Wang, H. X.; Wu, C. H.; Weatherup, R. S.; Feng, B. M.; Ye, Y. F.; Liu, Y. S.; Glans, P. A.; Guo, J. H.; Fang, H. T.; Salmeron, M. B., X-ray-Induced Fragmentation of Imidazolium-Based Ionic Liquids Studied by Soft X-ray Absorption Spectroscopy. *J. Phys. Chem. Lett.* **2018**, *9*, 785-790.
 36. Wang, J. Y.; Strom, A. E.; Hartwig, J. F., Mechanistic Studies of Palladium-Catalyzed Aminocarbonylation of Aryl Chlorides with Carbon Monoxide and Ammonia. *J. Am. Chem. Soc.* **2018**, *140*, 7979-7993.
 37. Weatherup, R. S.; Wu, C. H.; Escudero, C.; Perez-Dieste, V.; Salmeron, M. B., Environment-Dependent Radiation Damage in Atmospheric Pressure X-ray Spectroscopy. *J. Phys. Chem. B* **2018**, *122*, 737-744.
 38. Wu, C. H.; Pascal, T. A.; Baskin, A.; Wang, H. X.; Fang, H. T.; Liu, Y. S.; Lu, Y. H.; Guo, J. H.; Prendergast, D.; Salmeron, M. B., Molecular-Scale Structure of Electrode-Electrolyte Interfaces: The Case of Platinum in Aqueous Sulfuric Acid. *J. Am. Chem. Soc.* **2018**, *140*, 16237-16244.
 39. Wu, L. P.; Gokhale, A.; Goulas, K. A.; Myers, J. E.; Toste, F. D.; Scown, C. D., Hybrid Biological- Chemical Approach Offers Flexibility and Reduces the Carbon Footprint of Biobased Plastics, Rubbers, and Fuels. *ACS Sus. Chem. Eng.* **2018**, *6*, 14523-14532.
 40. Yim, C. M.; Chen, J.; Zhan, Y.; Shaw, B. J.; Pang, C. L.; Grinter, D. C.; Bluhm, H.; Salmeron, M.; Murny, C. A.; Michaelides, A.; Thornton, G., Visualization of Water-Induced Surface Segregation of Polarons on Rutile TiO₂(110). *J. Phys. Chem. Lett.* **2018**, *9*, 4865-4871.
 41. Zhang, H.; Liu, H.; Tian, Z. Q.; Lu, D.; Yu, Y.; Cestellos-Blanco, S.; Sakimoto, K. K.; Yang, P. D., Bacteria photosensitized by intracellular gold nanoclusters for solar fuel production. *Nat. Nanotechnol.* **2018**, *13*, 900-+.
 42. Ziegler, M. S.; Torquato, N. A.; Levine, D. S.; Nicolay, A.; Celik, H.; Tilley, T. D., Dicopper Alkyl Complexes: Synthesis, Structure, and Unexpected Persistence. *Organometallics* **2018**, *37*, 2807- 2823.

2019

1. Bender, T. A.; Morimoto, M.; Bergman, R. G.; Raymond, K. N.; Toste, F. D., Supramolecular Host- Selective Activation of Iodoarenes by Encapsulated Organometallics. *J. Am. Chem. Soc.* **2019**, *141*, 1701-1706..
2. Cai, I. C.; Ziegler, M. S.; Bunting, P. C.; Nicolay, A.; Levine, D. S.; Kalendra, V.; Smith, P. W.; Lakshmi, K. V.; Tilley, T. D., Monomeric, Divalent Vanadium Bis(arylamido) Complexes: Linkage Isomerism and Reactivity. *Organometallics* **2019**, *38*, 1648-1663
3. Eren, B.; Salmeron, M., Predicting Surface Clustering at Ambient Conditions from Thermodynamic Data. *J. Phys. Chem. C* **2019**, *123*, 8171-8176.
4. Jia, S.; He, D.; Chang, C. J., Bioinspired Thiophosphorodichloridate Reagents for Chemospecific Histidine Bioconjugation. *J. Am. Chem. Soc.* **2019**, *141*, 7294-7301.
5. Liu, F. D.; Han, H. L.; Carl, L. M.; Zhrebetsky, D.; An, K.; Wang, L. W.; Somorjai, G. A., Catalytic 1-Propanol Oxidation on Size-Controlled Platinum Nanoparticles at Solid-Gas and Solid- Liquid Interfaces: Significant Differences in Kinetics and Mechanisms. *J. Phys. Chem. C* **2019**, *123*, 7577-7583.
6. Natoli, S. N.; Hartwig, J. F., Noble-Metal Substitution in Hemoproteins: An Emerging Strategy for Abiological Catalysis. *Acc. Chem. Res.* **2019**, *52*, 326-335.
7. Nguyen, A. I.; Van Allsburg, K. M.; Terban, M. W.; Bajdich, M.; Oktawiec, J.; Ziegler, M. S.; Dombrowski, J. P.; Lakshmi, K. V.; Drisdell, W. S.; Yano, J.; Billinge, S. J. L.; Tilley, T. D. "Stabilization of reactive Co₄O₄ cubane oxygen-evolution catalysts within porous frameworks" *Proc. Nat. Acad. Sci.* 2019, in press. DOI: [10.1073/pnas.1815013116](https://doi.org/10.1073/pnas.1815013116).
8. Nichols, E. M.; Chang, C. J., Urea-Based Multipoint Hydrogen-Bond Donor Additive Promotes Electrochemical CO₂ Reduction Catalyzed by Nickel Cyclam. *Organometallics* **2019**, *38*, 1213-1218.
9. Ross, M. B.; Li, Y. F.; De Luna, P.; Kim, D.; Sargent, E. H.; Yang, P. D., Electrocatalytic Rate Alignment Enhances Syngas Generation. *Joule* **2019**, *3*, 257-264.
10. Ross, M. B.; De Luna, P.; Li, Y.; Dinh, C. T.; Kim, D.; Yang, P. D.; Sargent, E.H., Designing materials for electrochemical carbon dioxide recycling. *Nat. Catal.* **2019**, *In press*
11. Smith, P. W.; Ellis, S. R.; Handford, R. C.; Tilley, T. D., An Anionic Ruthenium Dihydride Cp*((Pr₂MeP)-Pr-i)RuH₂ (-) and Its Conversion to Heterobimetallic Ru(μ-H)(2)M (M = Ir or Cu) Complexes. *Organometallics* **2019**, *38*, 336-342.
12. Trickett, C. A.; Popp, T. M. O.; Su, J.; Yan, C.; Weisberg, J.; Huq, A.; Urban, P.; Jiang, J. C.; Kalmutzki, M. J.; Liu, Q. N.; Baek, J.; Head-Gordon, M. P.; Somorjai, G. A.; Reimer, J. A.; Yaghi, O. M., Identification of the strong Bronsted acid site in a metal-organic framework solid acid catalyst. *Nat. Chem.* **2019**, *11*, 170-176.
13. van Spronsen, M. A.; Daunmu, K.; O'Connor, C. R.; Egle, T.; Kersell, H.; Oliver-Meseguer, J.; Salmeron, M. B.; Madix, R. J.; Sautet, P.; Friend, C. M., Dynamics of Surface Alloys: Rearrangement of Pd/Ag(111) Induced by CO and O₂. *J. Phys. Chem. C* **2019**, *123*, 8312-8323.
14. Wu, C. H.; Liu, C.; Su, D.; Xin, H. L. L.; Fang, H. T.; Erens, B.; Zhang, S.; Murray, C. B.; Salmeron, M. B., Bimetallic synergy in cobalt-palladium nanocatalysts for CO oxidation. *Nat. Catal.* **2019**, *2*, 78-85.

FWP ERKCC96: Fundamentals of Catalysis and Chemical Transformations

PIs: Zili Wu, Miaofang Chi, Sheng Dai, De-en Jiang (UC-Riverside), Stephan Irle, Felipe Pologaron, Aditya (Ashi) Savara

Postdoc(s): Zhenghong Bao, Bo Chen, Hao Chen, Jisue Moon, Yifan Sun

Student(s): Ka Huang Lee (UTK), Francis Okejiri (UTK), Victor Fung, Kristen Wang (UC-Riverside)

Affiliation (s): Oak Ridge National Laboratory

RECENT PROGRESS

The overarching goal of this project is to understand how to control reaction pathways through tuning synergism in multi-functional catalysts with well-defined structures. The vision of our research is that by fundamentally understanding the composition, structure and interaction of catalytic sites and the reaction pathways, we will be able to precisely assemble different catalytic sites/entities into a synergistic catalyst to achieve the desired level of selectivity and activity. Specifically, we will elucidate the synergism among site geometry, surface and bulk composition, acid-base and redox sites, and metal-support interactions in controlling reactivity, selectivity and stability in reactions catalyzed by oxide surfaces and supported metal particles. We summarize here our recent progress along these lines. To understand the catalytic consequence of composition and structure of oxides, we choose perovskites as the model ternary oxides because of the wide tunability of the A and B cations in ABO_3 perovskites that can result in tunable catalytic chemistry. One of the foci of our research is to understand surface reconstruction behaviors of complex oxides by investigating both model single crystal, thin film surfaces and nanoshaped particles of perovskites. From these studies, we learned about the importance of the synergy among different surface sites and between surface and subsurface in catalyzing acid-base and redox reactions and how to take advantage of surface reconstruction to achieve the synergism. We have also investigated how to tune the synergism at the interface between metal and support to stabilize metal particles and enhance their catalytic reactivity. These include utilizing perovskites and high entropy oxides as supports to stabilize single atoms, core-shell structures to enhance metal-support interactions and visualizing interfacial charge distribution in perovskite supported metal nanoparticles.

Composition and structure effect in oxide catalysis

The goal of this part of work is to achieve a fundamental understanding of how acid-base and redox sites on oxide surfaces work synergistically to control reaction pathways and catalytic selectivity. We hypothesize that this can be achieved via tuning the surface structure and composition of oxides and probed by studying the adsorption and reaction of oxygenates and hydrocarbons over ternary oxides including perovskites and mixed oxides where both surface and bulk structure and composition can be widely tuned. We have used the comparison of oriented film vs shaped nanocrystals to probe structure-function relationships in oxide catalysis. A key focus was to understand the impact of *surface reconstruction* of complex oxides on both acid-base and redox reactions. For nanoshaped particles, reactions were studied via reaction kinetic measurements, DRIFTS/Raman, microcalorimetry, and inelastic neutron scattering (INS). We probed the surface species over thin film surfaces with ambient pressure x-ray photoelectron spectroscopy (AP-XPS) and the desorption products in TPD. DFT has enhanced our understanding

of the reaction mechanism, the surface structure and composition of perovskites and provided predictive catalytic descriptors. Together these studies have led to a detailed description of reaction pathways of model oxygenates and understanding of the synergism among various catalytic sites over complex oxides where surface reconstruction cannot be underestimated.

Embrace surface reconstruction of perovskites to understand reactivity trend. Taking advantage of our understanding of surface reconstruction behavior of perovskites from acid-base catalysis, we investigated the impact that the reconstruction of surface and subsurface monolayers of perovskite catalysts has on redox reactions including methane combustion (Polo-Garzon *et al.*)²⁷ and oxidative coupling (OCM) (Bai *et al.*)³² using SrTiO₃ (STO) as a model perovskite. Several STO samples obtained through different synthesis methods and subjected to different post-synthesis-treatments were tested for methane combustion and OCM. Through top surface characterization, kinetic experiments (including isotope labelling experiments) and density functional theory (DFT) calculations, it is shown that both surface segregation of Sr and creation of step-surfaces of STO can impact the rate of methane conversion in both reactions over an order of magnitude (**Figure 1**). The relative density of basic sites, which is correlated with the surface segregation of Sr, is found as a potential reactivity descriptor for CH₄ activation and conversion (combustion and OCM) in general. Furthermore, the subsurface structure (co-existence of Sr-O-Ti moiety) of the catalysts when compared to SrO supported on TiO₂ is believed to play an important role in determining the reaction rate and selectivity. This work highlights the possibility of utilizing and tuning the surface reconstruction of perovskites for efficient methane activation and conversion.

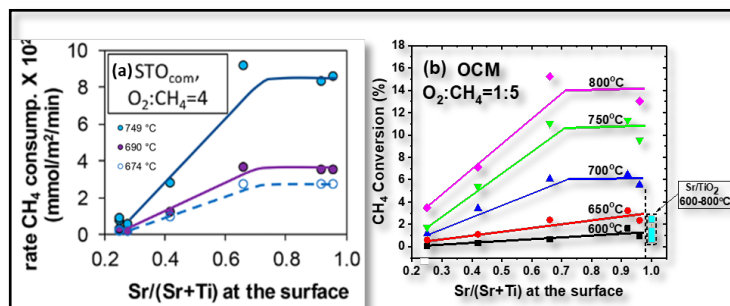


Figure 1. Impact of surface composition of STO surfaces on the rate of methane combustion and OCM.

Uncover the nature of active sites on faceted perovskites for acid-base reactions. Shape-controlled nanocrystals of oxides have shown to be good models for understanding oxide catalysis because they display specific crystallographic faces. However, the surface reconstruction of perovskites complicates the straightforward correlation of the surface structure with catalytic performance over complex oxides, as we showed previously for ethanol conversion over shaped STO particles where ethanol turnover rate is not directly correlated to the percentage of either surface facet ((001) or (110)) (Foo *et al.*)¹⁸ Instead, the reaction rate is found to increase with the strength of acid sites but decrease with the strength of base sites. Inspired by the role of step sites in methane activation and conversion in our recent work, we hypothesize that these step sites originated from surface reconstruction of STO are also the active centers for alcohol conversion. To test this hypothesis, we used

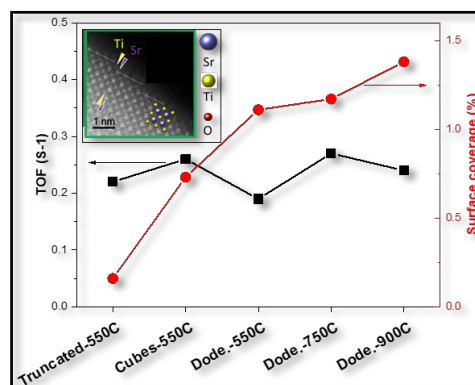


Figure 2. TOF of acetone formation and surface coverage of intermediates to acetone over different STO nanoshapes derived from SSITKA analysis. Inset shows the image of the step sites as the proposed active sites. (Bao *et al.*, in preparation, 2019)

three STO nanoshapes, cubes (dominated by (001)), truncated cubes ((001) + (110)) and dodecahedra (dominated by (110)) that are treated at different temperatures and tested for isopropanol (IPA) conversion. The main product is acetone via the dehydrogenation pathway catalyzed by surface basic sites on STO. Although there is no correlation between the areal rate of acetone formation and the facet of STO, the turnover frequency (TOF) derived from steady state isotopic transient kinetic analysis (SSITKA) is very similar across the different STO samples (**Figure 2**), indicating similar active sites present on the various STO. DFT calculation confirmed that the step sites terminated with Sr are the most active center for IPA conversion to acetone. The difference in areal rate is explained by the difference in the number of such step sites as inferred from the calculated surface coverage of intermediates from SSITKA. The SSITKA result obtained under reaction condition suggests that the role of surface facet of STO is to control the degree of surface reconstruction and thus the density of active step sites. The less stable (110) facet tends to undergo reconstruction more readily than the stable (001) facet, thus the STO dodecahedra give higher reaction rate than the cubes. The finding here underscores the importance of characterizing the top surface compositions and sites properties under reaction conditions using approaches such as transient kinetic analysis when assessing the catalytic performance of shape-controlled complex oxides such as perovskites.

Effect of substitution on the catalytic behavior of perovskite thin films. Compositional tuning is one effective way to control the catalysis of complex oxides, for example moving from SrTiO₃ to LaMnO₃ and other perovskites can greatly impact the surface properties and thus chemistry. Doping an additional *A*-cation (*A'*) into the perovskite lattice can further alter the catalytic behavior of the non-doped perovskite by altering the strain of the lattice, changing the oxidation state of *B* or introducing *O*-vacancies if *A* and *A'* have different oxidation states, or through different compositional terminations at the surface. We explored this effect by synthesizing a series Sr-doped La_{1-x}Sr_xMnO₃(001) (*x* = 0, 0.3, 0.7) (LSMO) thin films. The catalytic conversion of acetic acid was characterized by temperature programmed desorption / decomposition (TPD) and temperature programmed reaction (TPR) in an ultrahigh vacuum environment (Zhang *et al.*).³⁹ The main products observed in both types of experiments were CO, CO₂, H₂O, acetaldehyde, and ketene (ethenone) (**Figure 3**). Both the reactivity and ketene/acetaldehyde ratio decrease with increasing Sr doping, ascribed to the surface enrichment of Sr due to surface reconstruction as probed by energy dependent XPS analysis. The results are consistent with ketene being formed by a dehydration mechanism, a pathway suppressed with surface oxygen vacancies. The work shows that vacancy tuning via doping is an effective to control the activity and selectivity in perovskite catalysis. We have taken this information in further studying the effects of Sr substitution and oxygen vacancies over La(Sr)MnO₃ for the selectivity in the conversion of small alcohols (isopropyl alcohol, ethanol, and methanol). Our recent results indicate that dehydration of ethanol to ethene is promoted by increasing surface oxygen vacancies via reductive treatment while isopropanol dehydration to propene is inhibited by increase bulk vacancies via Sr-doping. Future work will attempt to elucidate the sources of these differences.

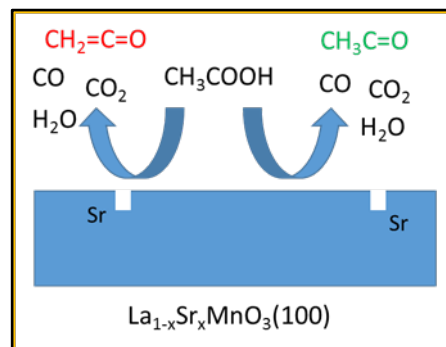


Figure 3. Product distribution of acetic acid reaction over La_{1-x}Sr_xMnO₃(001).

Predictive descriptors for adsorbate interactions with perovskite surfaces from DFT. A new model of bonding between radical adsorbates including H, CH₃, NH₂, and SH and lattice oxygens

is proposed that considers both the adsorbate-oxygen bonding and the weakening of the metal-oxygen bonds. Density-functional calculations of SrMO₃ perovskites for M being 3d, 4d, and 5d transition metals are used to correlate the bulk electronic structure with the surface-oxygen reactivity. Occupation of the metal-oxygen antibonding states, examined via the crystal orbital Hamilton population (COHP), is found to be a useful *bulk descriptor* that correlates with the vacancy formation energy of the lattice oxygen and its hydrogen adsorption energy (**Figure 4**) (Fung *et al.*).²⁰ Analysis of density-of-states and COHP indicates that H adsorption energy is a combined result of formation of the O-H bond and the weakening of the surface metal-oxygen bond due to occupation of the metal-oxygen antibonding states by the electron from H. This approach has been further used to understand the effect of hydrogen-induced surface metallization of perovskites upon hydrogen chemisorption (Gao *et al.*).³⁴ This new theoretical model provides a more comprehensive understanding of surface adsorption trends of radical intermediates such as H and CH₃ from methane activation on perovskites and transition-metal oxides in general and allows the use of a bulk descriptor to correlate to surface reactivity.

Mechanistic insights into C-C coupling over oxide surface from DFT. It is highly desirable to convert bioethanol to value-added chemicals such as propene. Zr-doped In₂O₃ has shown promising catalytic performance for ethanol-to-propene (ETP) conversion, but the detailed surface chemistry has been unclear. We have used density functional theory to investigate the detailed reaction pathways from ethanol to propene via important intermediates including acetaldehyde, acetate, and acetone on the In₂O₃ (110) surface (Huang *et al.*).³⁵ We find that the ETP reactions proceed through three major stages: ethanol to acetaldehyde, acetaldehyde to acetone, and acetone to propene. The ethanol-to-acetaldehyde step is kinetically facile. Comparing the two pathways from acetaldehyde to acetone, we show that the aldol reaction pathway via direct coupling of two acetaldehyde is more favorable than the acetate-ketonization pathway. The acetone-to-propene process is found to be the rate-limiting step of the overall reaction. This work provides a detailed mechanistic view of the ETP chemistry on In₂O₃(110) that paves the way for understanding the Zr-doping effect on the selectivity and catalyst stability, which is currently experimentally investigated.

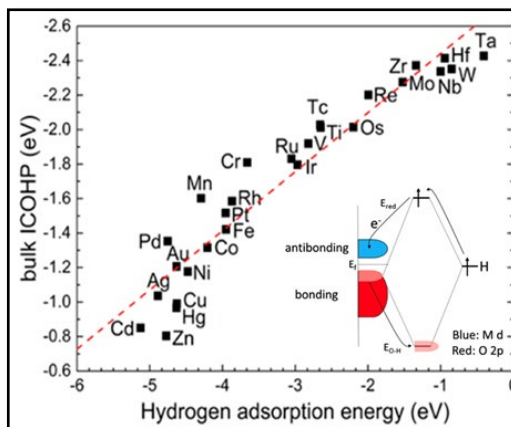


Figure 4. Correlation plots for perovskite SrMO₃(100) M-terminated surfaces with M being the transition metals between hydrogen adsorption energy on the lattice oxygen and bulk integrated crystal orbital Hamilton population (ICOHP) ($R^2 = 0.91$). Inset is a Diagram of the O-H bonding involving O 2p nonbonding states (pink) and one-electron reduction into the M-O antibonding states (blue).

Neutron spectroscopy of surface chemistry during hydrogenation reactions over oxide catalysts. In the conversion of hydrocarbon and oxygenates over oxide surfaces, hydrogen transfer is commonly involved in the dehydration, hydrogenation, dehydrogenation and oxidation reactions. To understand how an oxide manages surface hydrogen, we studied CO₂ hydrogenation – reverse water gas shift reaction (RWGS) over a commercial CuCrFeOx catalyst and acetylene hydrogenation over CeO₂ with various *in situ* spectroscopy including neutron spectroscopy (INS), IR and AP-XPS. The reaction mechanism of high temperature (HT) WGS over CuCrFeOx remains unclear and has no spectroscopic support for either redox or associative pathways (via formate

HCOO or COOH intermediate). AP-XPS evidenced the surface reconstruction under reaction conditions that Cu dissolves out of the mixed oxide to form Cu nanoparticles. Neither *in situ* IR nor INS experiments detected formate-like surface species under reaction conditions. Temperature programmed surface reaction (TPSR) experiments showed that the kinetic evolution of products for WGS over CuCrFeO_x greatly differ from the kinetic evolution during formic acid decomposition (molecule mimicking the associative mechanism) over the same catalyst, thus supporting a redox mechanism. SSITKA using CO + H₂¹⁶O → CO + H₂¹⁸O evidenced intense scrambling of oxygen atoms with the surface, characteristic of a redox mechanism. Finally, activation energies computed via DFT showed that the redox mechanism is favored over the associative mechanism. The multi-modal characterization of this catalytic system clearly points at the redox mechanism, not the associative mechanism (Polo-Garzon *et al.*).³⁷ This fundamental understanding sets the ground for rational optimization of this important catalytic reaction.

Our previous INS study showed for the first time the presence of Ce-H species upon H₂ interaction with CeO₂ at high temperatures (Wu *et al.*).¹⁵ The role of the surface hydrogen species, Ce-H and OH, was recently investigated for acetylene hydrogenation via both *in situ* INS and IR. INS spectra clearly showed the reactivity of Ce-H with acetylene and the production of C₂ surface species. *In situ* IR study of CeO₂ treated under oxidative and reductive conditions showed that the OH groups are also active for acetylene hydrogenation but more selective than Ce-H species. This work provides vital insights into the design of more active and selective ceria-based hydrogenation catalysts.

Tuning metal-support interface for enhanced stability and catalysis

The goal of this part of work is to understand how synergism can be tailored at the metal-support interface to control catalytic activity, selectivity and stability. Our hypothesis is the long-range synergism arising from the chemical and electronic interactions between metal nanoparticles and oxides can provide an amplification of catalytic activity, selectivity and/or stability of the supported metal centers. In the past year, we have explored various ways to tailor the interfacial structure and electronic property to achieve highly stable metal single atoms and nanoparticles (NPs) with enhanced catalytic reactivity and selectivity.

Stabilization of single metal sites through high entropy oxide. In addition to perovskite support, we also explored new strategy to stabilize active metal centers. Our hypothesis was that introduction of noble metals into an appropriate mixed metal oxide solid solution such as high entropy (HE) oxides would afford a randomly dispersed, homogeneous system of single atoms which are entropically stabilized at elevated temperatures. Up to now, HE concept has been only restricted to hard materials, such as high-entropy alloys and ceramics. Recently, we report the mechanochemical synthesis of noble metal atoms incorporated into HE metal oxides (NiMgCuZnCo)O under ambient condition (**Figure 5**) (Chen *et al.*).⁶⁴ The advantage of this approach was demonstrated by the introduction of up to 5 wt % noble metal into (NiMgCuZnCo)O, as single atoms or nanoclusters,

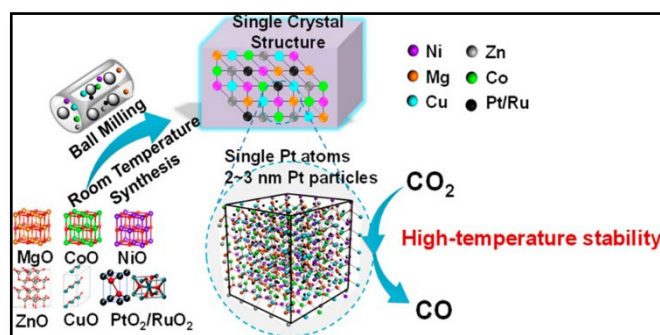


Figure 5. Scheme of the formation of 0.3 wt% PtNiMgCuZnCoO_x entropy-stabilized metal oxide solid solution.

The advantage of this approach was demonstrated by the introduction of up to 5 wt % noble metal into (NiMgCuZnCo)O, as single atoms or nanoclusters,

which showed good stability at high temperature (773 K) and produced a high catalytic activity in the hydrogenation of atmospheric CO₂ to CO. The HE concept was also applied to multi-metal alloy such as PtAuPdRhRu alloy which showed prominent electrocatalytic hydrogen evolution activity (Liu *et al.*),⁶⁷ also to polymetallic zeolitic imidazolate framework (ZIF-8) that showed enhanced catalytic conversion of CO₂ into carbonate compared with ZIF-8 presumably a result of the synergistic effect of the five metal ions as Lewis acid in epoxide activation (Xu *et al.*).⁷² We expect that this exciting new synthetic approach will hold great promise for the development of stabilized single atom materials for high temperature reactions such as methane reforming which is currently under study.

Taming the stability of Pd active phases through a compartmentalizing strategy toward

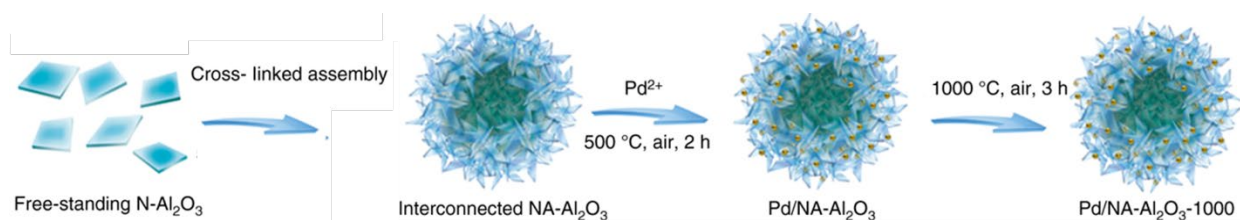


Figure 5. Scheme for the synthesis of NA-Al₂O₃ and the stabilization of Pd particles at high temperatures.

nanostructured catalyst supports. Tuning the local coordination status of the oxide support is an effective approach to stabilize metal particles such as in the case of pentacoordinated Al³⁺ (Al_{penta}³⁺) sites in Al₂O₃. Herein, we demonstrate a compartmentalization strategy (**Figure 6**) for designing robust nanocatalysts by taking advantage of both sintering-resistant Al₂O₃ nanosheet and abundance of Al_{penta}³⁺ centers (Yang *et al.*).⁷³ Ultrafine palladium active phases can be highly dispersed and thermally stabilized by nanosheet-assembled □-Al₂O₃ (NA-Al₂O₃) architectures. The NA-Al₂O₃ architectures with unique flowerlike morphologies not only efficiently suppress the lamellar aggregation and irreversible phase transformation of □-Al₂O₃ nanosheets at elevated temperatures to avoid the sintering and encapsulation of metal phases, but also exhibit significant structural advantages for heterogeneous reactions, such as fast mass transport and easy access to active sites. The Pd/NA-Al₂O₃ catalysts showed excellent low temperature methane oxidation activity as well as high temperature stability. This is a facile stabilization strategy that can be further extended to improve the thermal stability of other Al₂O₃-supported nanocatalysts for industrial catalytic applications, in particular for those involving high-temperature reactions.

Predictive structure of metal – support system via DFTB.

Overcoming the limitation of DFT in handling catalytic systems of sub-nanometer size, density-functional tight-binding (DFTB) can handle thousands of atoms (**Figure 6**) with reasonable accuracy in geometry and energy comparable to DFT. A starting goal of our DFTB effort is the simulation of surface transformations and dynamic structural evolutions of metal clusters on oxide supports such as model Pt/TiO₂ system. We developed a general-purpose Pt-Pt DFTB parameter for Pt clusters as well as bulk, using a genetic algorithm (GA) to automatize the parameterization effort. We analyzed the performance

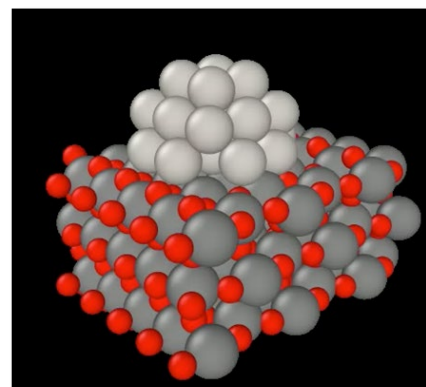


Figure 6. large Pt/TiO₂ systems to be modeled with DFTB method.

of our two DFTB Pt-Pt parameter sets against DFT as well as earlier DFTB Pt-Pt parameters (Lee *et al.*).³⁶ Our study shed light on the role of both repulsive and electronic parameters with regards to DFTB performance and allowing us to obtain a generalized set of Pt parameters for both Pt bulk and Pt nanoparticles. Given Pt's prominence in both heterogeneous and homogeneous catalysis, having DFTB parameters for the element would allow researchers the ability to compute system sizes or dynamical properties typically limited by DFT's high computational cost. Currently we are working on the parameterization of C, H, O, N, Ti and Sr. This is the first step toward DFTB-based studies of surface dynamic evolution processes occurring at Pt-clusters on TiO₂ and SrTiO₃ active support interfaces, paving the way for the design of new metal catalysts on active supports

Visualize the charge distribution at metal – support interface via 4D STEM. Among the various tunable parameters for metal – support interactions, charge transfer is currently the least understood, despite it is believed to strongly modify the catalytic function. This is largely due to challenges in directly measuring it with its inherently sub-nanometer length scale. Recently, we utilized four-dimensional scanning transmission electron microscopy (4D-STEM)-based phase contrast imaging to directly probe the charge distribution at a metal – oxide support interface (Au/STO) down to the atomic scale, revealing the nature of charge transfer in this system (**Figure 7**). By combining the experimental results with DFT calculations, we provide new insights into the origins and characteristics of the charge transfer at the atomic scale, as well as the possible origin of highly active boundaries between the metal and support. This work provides a method for directly studying charge transfer in heterogeneous catalysts, opening new opportunities to better understand catalytic reaction mechanisms and design more efficient catalysts.

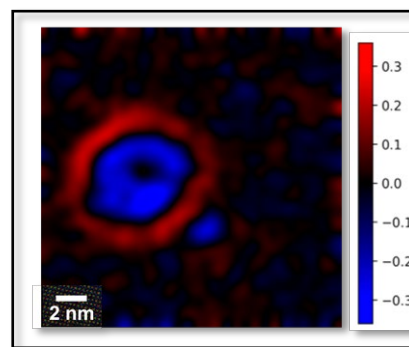


Figure 7. Atomic-scale charge density map showing the charge distribution at the Au-STO interface. (Chi *et al.*, in preparation, 2019)

Publications Acknowledging this Grant in the past three years (July 2016 – June 2019)

(XVII) Exclusively funded by this grant:

1. Mullins, D. R., The interaction of carbon monoxide with rhodium on potassium-modified CeO₂(111). *Surface Science* **2016**, *652*, 238-246.
2. Poutsma, M. L., Extension of Structure–Reactivity Correlations for the Hydrogen Abstraction Reaction to the Methyl Radical and Comparison to the Chlorine Atom, Bromine Atom, and Hydroxyl Radical. *The Journal of Physical Chemistry A* **2016**, *120* (26), 4447-4454.
3. Savara, A., Simulation and fitting of complex reaction network TPR: The key is the objective function. *Surface Science* **2016**, *653*, 169-180.
4. Savara, A., Comment on "Equilibrium Constants and Rate Constants for Adsorbates: Two-Dimensional (2D) Ideal Gas, 2D Ideal Lattice Gas, and Ideal Hindered Translator Models". *J Phys Chem C* **2016**, *120* (36), 20478-20480.
5. Tian, C. C.; Zhu, X.; Abney, C. W.; Tian, Z. Q.; Jiang, D. E.; Han, K. S.; Mahurin, S. M.; Washton, N. M.; Dai, S., Use of steric encumbrance to develop conjugated nanoporous polymers for metal-free catalytic hydrogenation. *Chemical Communications* **2016**, *52* (80), 11919-11922.

6. Wu, Z.; Hu, G.; Jiang, D.-e.; Mullins, D. R.; Zhang, Q.-F.; Allard, L. F.; Wang, L.-S.; Overbury, S. H., Diphosphine-Protected Au₂₂ Nanoclusters on Oxide Supports Are Active for Gas-Phase Catalysis without Ligand Removal. *Nano Letters* **2016**, *16* (10), 6560-6567.
7. Beste, A., Methanol Adsorption and Dissociation on LaMnO₃ and Sr Doped LaMnO₃ (001) Surfaces. *Surface Science* **2017**, *664*, 155-161.
8. Foo, G. S.; Hu, G.; Hood, Z. D.; Li, M.; Jiang, D.-e.; Wu, Z., Kinetics and Mechanism of Methanol Conversion over Anatase Titania Nanoshapes. *ACS Catalysis* **2017**, *7* (8), 5345-5356.
9. Foo, G. S.; Polo-Garzon, F.; Fung, V.; Jiang, D.-e.; Overbury, S. H.; Wu, Z., Acid-Base Reactivity of Perovskite Catalysts Probed via Conversion of 2-Propanol over Titanates and Zirconates. *ACS Catalysis* **2017**, *7*, 4423-4434.
10. Fung, V.; Jiang, D.-e., Exploring Structural Diversity and Fluxionality of Ptn (n = 10–13) Clusters from First-Principles. *The Journal of Physical Chemistry C* **2017**, *121* (20), 10796-10802.
11. Gill, L.; Beste, A.; Chen, B.; Li, M.; Mann, A. K. P.; Overbury, S. H.; Hagaman, E. W., Fast MAS 1H NMR Study of Water Adsorption and Dissociation on the (100) Surface of Ceria Nanocubes: A Fully Hydroxylated, Hydrophobic Ceria Surface. *The Journal of Physical Chemistry C* **2017**, *121* (13), 7450-7465.
12. Hu, G.; Tang, Q.; Lee, D.; Wu, Z.; Jiang, D.-e., Metallic Hydrogen in Atomically Precise Gold Nanoclusters. *Chemistry of Materials* **2017**, *29* (11), 4840-4847.
13. Polo-Garzon, F.; Yang, S.-Z.; Fung, V.; Foo, G. S.; Bickel, E. E.; Chisholm, M. F.; Jiang, D.-e.; Wu, Z., Controlling Reaction Selectivity via Surface Termination of Perovskite Catalysts. *Angewandte Chemie International Edition* **2017**, *56* (33), 9820-9824.
14. Tian, C.; Zhu, X.; Abney, C. W.; Liu, X.; Foo, G. S.; Wu, Z.; Li, M.; Meyer, H. M.; Brown, S.; Mahurin, S. M.; Wu, S.; Yang, S.-Z.; Liu, J.; Dai, S., Toward the Design of a Hierarchical Perovskite Support: Ultra-Sintering-Resistant Gold Nanocatalysts for CO Oxidation. *ACS Catalysis* **2017**, *7* (5), 3388-3393.
15. Wu, Z.; Cheng, Y.; Tao, F.; Daemen, L.; Foo, G. S.; Nguyen, L.; Zhang, X.; Beste, A.; Ramirez-Cuesta, A. J., Direct Neutron Spectroscopy Observation of Cerium Hydride Species on a Cerium Oxide Catalyst. *Journal of the American Chemical Society* **2017**, *139* (28), 9721-9727.
16. Zhang, Y.; Savara, A.; Mullins, D. R., Ambient-Pressure XPS Studies of Reactions of Alcohols on SrTiO₃(100). *The Journal of Physical Chemistry C* **2017**, *121* (42), 23436-23445.
17. Chen, H.; Fu, J.; Zhang, P.; Peng, H.; Abney, C. W.; Jie, K.; Liu, X.; Chi, M.; Dai, S., Entropy-stabilized metal oxide solid solutions as CO oxidation catalysts with high-temperature stability. *Journal of Materials Chemistry A* **2018**, *6*, 11129-11133
18. Foo, G. S.; Hood, Z. D.; Wu, Z., Shape Effect Undermined by Surface Reconstruction: Ethanol Dehydrogenation over Shape-Controlled SrTiO₃ Nanocrystals. *ACS Catalysis* **2018**, *8* (1), 555-565.
19. Fung, V.; Polo-Garzon, F.; Wu, Z.; Jiang, D.-e., Exploring perovskites for methane activation from first principles. *Catalysis Science & Technology* **2018**, *8* (3), 702-709.
20. Fung, V.; Wu, Z.; Jiang, D.-e., New Bonding Model of Radical Adsorbate on Lattice Oxygen of Perovskites. *The Journal of Physical Chemistry Letters* **2018**, *9* (21), 6321-6325.
21. Hu, G.; Wu, Z.; Dai, S.; Jiang, D.-e., Interface Engineering of Earth-Abundant Transition Metals by Boron Nitride for Selective Electroreduction of CO₂. *ACS Applied Materials & Interfaces* **2018**, *10* (7), 6694-6700.
22. Hu, G.; Wu, Z.; Jiang, D.-e., First Principles Insight into H₂ Activation and Hydride Species on TiO₂ Surfaces. *The Journal of Physical Chemistry C* **2018**, *122* (35), 20323-20328.

23. Hu, G.; Wu, Z.; Jiang, D.-e., Stronger-than-Pt hydrogen adsorption in a Au₂₂ nanocluster for the hydrogen evolution reaction. *Journal of Materials Chemistry A* **2018**, *6*, 7532-7537.
24. Huang, R.; Fung, V.; Zhang, Y.; Mullins, D. R.; Wu, Z.; Jiang, D.-e., Understanding Methanol Coupling on SrTiO₃ from First Principles. *The Journal of Physical Chemistry C* **2018**, *122* (13), 7210-7216.
25. Lukosi, M.; Tian, C.; Li, X.; Mahurin, S. M.; Meyer, H. M.; Foo, G. S.; Dai, S., Tuning the Core–Shell Structure of Au₁₄₄@Fe₂O₃ for Optimal Catalytic Activity for CO Oxidation. *Catalysis Letters* **2018**, *148* (8), 2315-2324.
26. Mullins, D. R., Variations in the surface chemistry of methanol with CeO₂(100) at low and elevated pressures. *Surf. Interface Anal.* **2018**, *50* (10), 913-920.
27. Polo-Garzon, F.; Fung, V.; Liu, X.; Hood, Z. D.; Bickel, E. E.; Bai, L.; Tian, H.; Foo, G. S.; Chi, M.; Jiang, D.-e.; Wu, Z., Understanding the Impact of Surface Reconstruction of Perovskite Catalysts on CH₄ Activation and Combustion. *ACS Catalysis* **2018**, *9*, 10306-10315.
28. Polo-Garzon, F.; Wu, Z., Acid-base catalysis over perovskites: a review. *Journal of Materials Chemistry A* **2018**, *6* (7), 2877-2894.
29. Prati, L.; Villa, A.; Jouve, A.; Beck, A.; Evangelisti, C.; Savara, A., Gold as modifier of metal nanoparticles: effect on structure and catalysis. *Faraday Discussions* **2018**, *208*, 395-407.
30. Tang, Q.; Hu, G.; Fung, V.; Jiang, D.-e., Insights into Interfaces, Stability, Electronic Properties, and Catalytic Activities of Atomically Precise Metal Nanoclusters from First Principles. *Accounts of Chemical Research* **2018**, *51* (11), 2793-2802.
31. Wu, Z.; Mullins, D. R.; Allard, L. F.; Zhang, Q.; Wang, L., CO oxidation over ceria supported Au₂₂ nanoclusters: Shape effect of the support. *Chinese Chemical Letters* **2018**, *29* (6), 795-799.
32. Bai, L.; Polo-Garzon, F.; Bao, Z.; Luo, S.; Moskowitz, B. M.; Tian, H.; Wu, Z., Impact of Surface Composition of SrTiO₃ Catalysts for Oxidative Coupling of Methane. *ChemCatChem* **2019**, *11* (8), 2107-2117.
33. Chen, H.; Yang, Z.; Zhang, Z.; Chen, Z.; Chi, M.; Wang, S.; Fu, J.; Dai, S., A Strategy for Construction of a Nanoporous Highly Crystalline Hexagonal Boron Nitride from an Amorphous Precursor. *Angewandte Chemie International Edition* **2019**, DOI: 10.1002/anie.201904996.
34. Gao, Y.; Huang, R.; Wang, J.; Wu, Z.; Jiang, D.-e., Effect of Hydrogen-Induced Metallization on Chemisorption. *The Journal of Physical Chemistry C* **2019**, *123* (24), 15171-15175.
35. Huang, R.; Fung, V.; Wu, Z.; Jiang, D.-e., Understanding the conversion of ethanol to propene on In₂O₃ from first principles. *Catalysis Today* **2019**, 10.1016/j.cattod.2019.05.035.
36. Lee, K. H.; Vuong, V. Q.; Fung, V.; Jiang, D. E.; Irle, S., Density-Functional Tight-Binding for Platinum Clusters and Bulk: Electronic vs Repulsive Parameters. *MRS Advances* **2019**, *1*, Just accepted (June 13, 2019).
37. Polo-Garzon, F.; Fung, V.; Nguyen, L.; Tang, Y.; Tao, F.; Cheng, Y.; Daemen, L. L.; Ramirez-Cuesta, A. J.; Foo, G. S.; Zhu, M.; Wachs, I. E.; Jiang, D.-e.; Wu, Z., Elucidation of the Reaction Mechanism for High-Temperature Water Gas Shift over an Industrial-Type Copper–Chromium–Iron Oxide Catalyst. *Journal of the American Chemical Society* **2019**, *141* (19), 7990-7999.
38. Polo-Garzon, F.; Luo, S.; Cheng, Y.; Page, K. L.; Ramirez-Cuesta, A. J.; Britt, P. F.; Wu, Z., Neutron Scattering Investigations of Hydride Species in Heterogeneous Catalysis. *ChemSusChem* **2019**, *12* (1), 93-103.

39. Zhang, Y.; Mullins, D. R.; Savara, A., Effect of Sr Substitution in LaMnO₃(100) on Catalytic Conversion of Acetic Acid to Ketene and Combustion-Like Products. *The Journal of Physical Chemistry C* **2019**, *123* (7), 4148-4157.

(XVIII) Jointly funded by this grant and other grants with leading intellectual contribution from this grant:

40. D'Angelo, A. M.; Wu, Z.; Overbury, S. H.; Chaffee, A. L., Cu-Enhanced Surface Defects and Lattice Mobility of Pr-CeO₂ Mixed Oxides. *The Journal of Physical Chemistry C* **2016**, *120* (49), 27996-28008.

41. Liu, F. J.; Liu, C.; Kong, W. P.; Qi, C. Z.; Zheng, A. M.; Dai, S., Design and synthesis of micro-meso-macroporous polymers with versatile active sites and excellent activities in the production of biofuels and fine chemicals. *Green Chemistry* **2016**, *18* (24), 6536-6544.

42. Liu, F. J.; Wu, Q.; Liu, C.; Qi, C. Z.; Huang, K.; Zheng, A. M.; Dai, S., Ordered Mesoporous Polymers for Biomass Conversions and Cross-Coupling Reactions. *ChemSuschem* **2016**, *9* (17), 2496-2504.

43. Savara, A.; Rossetti, I.; Chan-Thaw, C. E.; Prati, L.; Villa, A., Microkinetic Modeling of Benzyl Alcohol Oxidation on Carbon-Supported Palladium Nanoparticles. *Chemcatchem* **2016**, *8* (15), 2482-2491.

44. Yue, Y.; Li, Y.; Bridges, C. A.; Rother, G.; Zhang, J.; Chen, J.; Hensley, D. K.; Kidder, M. K.; Richardson, B. C.; Parans Paranthaman, M.; Dai, S., Hierarchically Superstructured Metal Sulfides: Facile Perturbation-Assisted Nanofusion Synthesis and Visible Light Photocatalytic Characterizations. *ChemNanoMat* **2016**, *2* (12), 1104-1110.

45. Zhan, W. C.; He, Q.; Liu, X. F.; Guo, Y. L.; Wang, Y. Q.; Wang, L.; Guo, Y.; Borisevich, A. Y.; Zhang, J. S.; Lu, G. Z.; Dai, S., A Sacrificial Coating Strategy Toward Enhancement of Metal-Support Interaction for Ultrastable Au Nanocatalysts. *Journal of the American Chemical Society* **2016**, *138* (49), 16130-16139.

46. Zhu, W.; Gao, X.; Li, Q.; Li, H.; Chao, Y.; Li, M.; Mahurin, S. M.; Li, H.; Zhu, H.; Dai, S., Controlled Gas Exfoliation of Boron Nitride into Few-Layered Nanosheets. *Angewandte Chemie International Edition* **2016**, *55* (36), 10766-10770.

47. Doughty, B.; Goverapet Srinivasan, S.; Bryantsev, V. S.; Lee, D.; Lee, H. N.; Ma, Y.-Z.; Lutterman, D. A., Absolute Molecular Orientation of Isopropanol at Ceria (100) Surfaces: Insight into Catalytic Selectivity from Interfacial Structure. *The Journal of Physical Chemistry C* **2017**, *121* (26), 14137-14146.

48. Savara, A.; Chan-Thaw, C. E.; Sutton, J. E.; Wang, D.; Prati, L.; Villa, A., Molecular Origin of the Selectivity Differences between Palladium and Gold-Palladium in Benzyl Alcohol Oxidation: Different Oxygen Adsorption Properties. *ChemCatChem* **2017**, *9* (2), 253-257.

49. Tan, S.; Gray, M. B.; Kidder, M. K.; Cheng, Y.; Daemen, L. L.; Lee, D.; Lee, H. N.; Ma, Y.-Z.; Doughty, B.; Lutterman, D. A., Insight into the Selectivity of Isopropanol Conversion at Strontium Titanate (100) Surfaces: A Combination Kinetic and Spectroscopic Study. *ACS Catalysis* **2017**, *7* (12), 8118-8129.

50. Wang, T.; Zhang, P.; Sun, Y.; Liu, B.; Liu, Y.; Qiao, Z.-A.; Huo, Q.; Dai, S., New Polymer Colloidal and Carbon Nanospheres: Stabilizing Ultrasmall Metal Nanoparticles for Solvent-Free Catalysis. *Chemistry of Materials* **2017**, *29* (9), 4044-4051.

51. Zhan, W.; Shu, Y.; Sheng, Y.; Zhu, H.; Guo, Y.; Wang, L.; Guo, Y.; Zhang, J.; Lu, G.; Dai, S., Surfactant-Assisted Stabilization of Au Colloids on Solids for Heterogeneous Catalysis. *Angewandte Chemie International Edition* **2017**, *56* (16), 4494-4498.
52. Zhan, W.; Wang, J.; Wang, H.; Zhang, J.; Liu, X.; Zhang, P.; Chi, M.; Guo, Y.; Guo, Y.; Lu, G.; Sun, S.; Dai, S.; Zhu, H., Crystal Structural Effect of AuCu Alloy Nanoparticles on Catalytic CO Oxidation. *Journal of the American Chemical Society* **2017**, *139* (26), 8846-8854.
53. Zhan, W.; Yang, S.; Zhang, P.; Guo, Y.; Lu, G.; Chisholm, M. F.; Dai, S., Incorporating Rich Mesoporosity into a Ceria-Based Catalyst via Mechanochemistry. *Chemistry of Materials* **2017**, *29* (17), 7323-7329.
54. Zhu, W.; Wu, Z.; Foo, G. S.; Gao, X.; Zhou, M.; Liu, B.; Veith, G. M.; Wu, P.; Browning, K. L.; Lee, H. N.; Li, H.; Dai, S.; Zhu, H., Taming interfacial electronic properties of platinum nanoparticles on vacancy-abundant boron nitride nanosheets for enhanced catalysis. *Nature Communications* **2017**, *8*, 15291.
55. Chan-Thaw, C.; Savara, A.; Villa, A., Selective Benzyl Alcohol Oxidation over Pd Catalysts. *Catalysts* **2018**, *8* (10), 431.
56. Ding, S.; Tian, C.; Zhu, X.; Wang, H.; Wang, H.; Abney, C. W.; Zhang, N.; Dai, S., Engineering nanoporous organic frameworks to stabilize naked Au clusters: a charge modulation approach. *Chemical Communications* **2018**, *54* (40), 5058-5061.
57. Dong, H.; Li, Y.; Jiang, D.-e., First-Principles Insight into Electrocatalytic Reduction of CO₂ to CH₄ on a Copper Nanoparticle. *The Journal of Physical Chemistry C* **2018**, *122* (21), 11392-11398.
58. Huang, K.; Zhang, J.-Y.; Liu, F.; Dai, S., Synthesis of Porous Polymeric Catalysts for the Conversion of Carbon Dioxide. *ACS Catalysis* **2018**, *8* (10), 9079-9102.
59. Huang, W.; Wu, Z.; Tang, J.; Wei, W. D.; Guo, X., Surface chemistry connecting heterogeneous catalysis, photocatalysis and plasmonic catalysis. *Chinese Chemical Letters* **2018**, *29* (6), 725-726.
60. Peng, H.; Rao, C.; Zhang, N.; Wang, X.; Liu, W.; Mao, W.; Han, L.; Zhang, P.; Dai, S., Confined Ultrathin Pd-Ce Nanowires with Outstanding Moisture and SO₂ Tolerance in Methane Combustion. *Angewandte Chemie International Edition* **2018**, *57* (29), 8953-8957.
61. Xiao, W.; Yang, S.; Zhang, P.; Li, P.; Wu, P.; Li, M.; Chen, N.; Jie, K.; Huang, C.; Zhang, N.; Dai, S., Facile Synthesis of Highly Porous Metal Oxides by Mechanochemical Nanocasting. *Chemistry of Materials* **2018**, *30* (9), 2924-2929.
62. Zhang, P.; Chen, N.; Chen, D.; Yang, S.; Liu, X.; Wang, L.; Wu, P.; Phillip, N.; Yang, G.; Dai, S., Ultra-Stable and High-Cobalt-Loaded Cobalt@Ordered Mesoporous Carbon Catalysts: All-in-One Deoxygenation of Ketone into Alkylbenzene. *ChemCatChem* **2018**, *10* (15), 3299-3304.
63. Zhu, X.; Tian, C.; Wu, H.; He, Y.; He, L.; Wang, H.; Zhuang, X.; Liu, H.; Xia, C.; Dai, S., Pyrolyzed Triazine-Based Nanoporous Frameworks Enable Electrochemical CO₂ Reduction in Water. *ACS Applied Materials & Interfaces* **2018**, *10* (50), 43588-43594.
64. Chen, H.; Lin, W.; Zhang, Z.; Jie, K.; Mullins, D. R.; Sang, X.; Yang, S.-Z.; Jafta, C. J.; Bridges, C. A.; Hu, X.; Unocic, R. R.; Fu, J.; Zhang, P.; Dai, S., Mechanochemical Synthesis of High Entropy Oxide Materials under Ambient Conditions: Dispersion of Catalysts via Entropy Maximization. *ACS Materials Letters* **2019**, *1*, 83-88.
65. Hou, S.; Chen, N.; Zhang, P.; Dai, S., Heterogeneous viologen catalysts for metal-free and selective oxidations. *Green Chemistry* **2019**, *21* (6), 1455-1460.

66. Leng, Y.; Jiang, Y.; Peng, H.; Zhang, Z.; Liu, M.; Jie, K.; Zhang, P.; Dai, S., Heterogeneity of polyoxometalates by confining within ordered mesopores: toward efficient oxidation of benzene to phenol. *Catalysis Science & Technology* **2019**, *9* (9), 2173-2179.
67. Liu, M.; Zhang, Z.; Okejiri, F.; Yang, S.; Zhou, S.; Dai, S., Entropy-Maximized Synthesis of Multimetallic Nanoparticle Catalysts via a Ultrasonication-Assisted Wet Chemistry Method under Ambient Conditions. *Adv. Mater. Interfaces* **2019**, *6* (0), 1900015.
68. Liu, X.; Hood, Z. D.; Zheng, Q.; Jin, T.; Foo, G. S.; Wu, Z.; Tian, C.; Guo, Y.; Dai, S.; Zhan, W.; Zhu, H.; Chi, M., Optimizing the structural configuration of FePt-FeOx nanoparticles at the atomic scale by tuning the post-synthetic conditions. *Nano Energy* **2019**, *55*, 441-446.
69. Matera, S.; Schneider, W. F.; Heyden, A.; Savara, A., Progress in Accurate Chemical Kinetic Modeling, Simulations, and Parameter Estimation for Heterogeneous Catalysis. *ACS Catalysis* **2019**, DOI: 10.1021/acscatal.9b01234.
70. Peng, H.; Dong, T.; Zhang, L.; Wang, C.; Liu, W.; Bao, J.; Wang, X.; Zhang, N.; Wang, Z.; Wu, P.; Zhang, P.; Dai, S., Active and stable Pt-Ceria nanowires@silica shell catalyst: Design, formation mechanism and total oxidation of CO and toluene. *Applied Catalysis B: Environmental* **2019**, *256* (5), 117807.
71. Polo-Garzon, F.; Bao, Z.; Zhang, X.; Huang, W.; Wu, Z., Surface Reconstructions of Metal Oxides and the Consequences on Catalytic Chemistry. *ACS Catalysis* **2019**, *9* (6), 5692-5707.
72. Xu, W.; Chen, H.; Jie, K.; Yang, Z.; Li, T.; Dai, S., Entropy-Driven Mechanochemical Synthesis of Polymetallic Zeolitic Imidazolate Frameworks for CO₂ Fixation. *Angew. Chem* **2019**, *131* (15), 5072-5076.
73. Yang, X.; Li, Q.; Lu, E.; Wang, Z.; Gong, X.; Yu, Z.; Guo, Y.; Wang, L.; Guo, Y.; Zhan, W.; Zhang, J.; Dai, S., Taming the stability of Pd active phases through a compartmentalizing strategy toward nanostructured catalyst supports. *Nature Communications* **2019**, *10* (1), 1611.
74. Zhao, C.; Watt, C.; Kent, P. R.; Overbury, S. H.; Mullins, D. R.; Calaza, F. C.; Savara, A.; Xu, Y., Coupling of Acetaldehyde to Crotonaldehyde on CeO_{2-x}(111): Bifunctional Mechanism and Role of Oxygen Vacancies. *The Journal of Physical Chemistry C* **2019**, *123* (13), 8273-8286.

(XIX) *Jointly funded by this grant and other grants with relatively minor intellectual contribution from this grant:*

75. Moon, J.-W.; Phelps, T. J.; Fitzgerald Jr, C. L.; Lind, R. F.; Elkins, J. G.; Jang, G. G.; Joshi, P. C.; Kidder, M.; Armstrong, B. L.; Watkins, T. R.; Ivanov, I. N.; Graham, D. E., Manufacturing demonstration of microbially mediated zinc sulfide nanoparticles in pilot-plant scale reactors. *Applied Microbiology and Biotechnology* **2016**, *100* (18), 7921-7931.
76. Wen, J.; Lin, Y.; Sheng, H.; Wang, L.; Miller, D. J.; Wu, Z.; Poeppelmeier, K. R.; Marks, L. D., Atomic Surface Structures of Oxide Nanoparticles with Well-defined Shapes. *Microscopy and Microanalysis* **2016**, *22* (S3), 360-361.
77. Zhang, Y.; Kidder, M.; Ruther, R. E.; Nanda, J.; Foo, G. S.; Wu, Z.; Narula, C. K., Promotional Effects of In on Non-Oxidative Methane Transformation Over Mo-ZSM-5. *Catalysis Letters* **2016**, *146* (10), 1903-1909.
78. Abney, C. W.; Patterson, J. T.; Gilhula, J. C.; Wang, L.; Hensley, D. K.; Chen, J.; Foo, G. S.; Wu, Z.; Dai, S., Controlling interfacial properties in supported metal oxide catalysts through

metal-organic framework templating. *Journal of Materials Chemistry A* **2017**, *5* (26), 13565-13572.

79. Bugnet, M.; Overbury, S.; Wu, Z.; Aires, F.; Epicier, T., Atomic scale environmental transmission electron microscopy study of the surface mobility of ceria nanocubes. *Microscopy and Microanalysis* **2017**, *23* (S1), 898-899.

80. Bugnet, M.; Overbury, S. H.; Wu, Z. L.; Epicier, T., Direct Visualization and Control of Atomic Mobility at {100} Surfaces of Ceria in the Environmental Transmission Electron Microscope. *Nano Letters* **2017**, *17* (12), 7652-7658.

81. Ding, S.; Tian, C.; Zhu, X.; Abney, C. W.; Tian, Z.; Chen, B.; Li, M.; Jiang, D.-e.; Zhang, N.; Dai, S., Pd-Metalated Conjugated Nanoporous Polycarbazoles for Additive-Free Cyanation of Aryl Halides: Boosting Catalytic Efficiency through Spatial Modulation. *ChemSuschem* **2017**, *10* (11), 2348-2351.

82. Kwak, K.; Choi, W.; Tang, Q.; Kim, M.; Lee, Y.; Jiang, D.-e.; Lee, D., A molecule-like PtAu₂₄(SC₆H₁₃)₁₈ nanocluster as an electrocatalyst for hydrogen production. *Nature Communications* **2017**, *8*, 14723.

83. Lepore, A. W.; Li, Z.; Davison, B. H.; Foo, G. S.; Wu, Z.; Narula, C. K., Catalytic Dehydration of Biomass Derived 1-Propanol to Propene over M-ZSM-5 (M = H, V, Cu, or Zn). *Industrial & Engineering Chemistry Research* **2017**, *56* (15), 4302-4308.

84. Li, Z.; Lepore, A. W.; Salazar, M. F.; Foo, G. S.; Davison, B. H.; Wu, Z.; Narula, C. K., Selective conversion of bio-derived ethanol to renewable BTX over Ga-ZSM-5. *Green Chemistry* **2017**, *19* (18), 4344-4352.

85. Liu, J.; Olds, D.; Peng, R.; Yu, L.; Foo, G. S.; Qian, S.; Keum, J.; Guiton, B. S.; Wu, Z.; Page, K., Quantitative analysis of the morphology of {101} and {001} faceted anatase TiO₂ nanocrystals and its implication on photocatalytic activity. *Chemistry of Materials* **2017**, *29* (13), 5591-5604.

86. Narula, C. K.; Allard, L. F.; Wu, Z., Ab Initio Density Functional Calculations and Infra-Red Study of CO Interaction with Pd Atoms on θ -Al₂O₃ (010) Surface. *Scientific Reports* **2017**, *7* (1), 6231.

87. Sutton, J. E.; Danielson, T.; Beste, A.; Savara, A., Below-Room-Temperature C-H Bond Breaking on an Inexpensive Metal Oxide: Methanol to Formaldehyde on CeO₂(111). *The Journal of Physical Chemistry Letters* **2017**, *8* (23), 5810-5814.

88. Wang, B.; Di, J.; Zhang, P.; Xia, J.; Dai, S.; Li, H., Ionic liquid-induced strategy for porous perovskite-like PbBiO₂Br photocatalysts with enhanced photocatalytic activity and mechanism insight. *Applied Catalysis B: Environmental* **2017**, *206*, 127-135.

89. Wu, P.; Yang, S.; Zhu, W.; Li, H.; Chao, Y.; Zhu, H.; Li, H.; Dai, S., Tailoring N-Terminated Defective Edges of Porous Boron Nitride for Enhanced Aerobic Catalysis. *Small* **2017**, *13* (44), 1701857.

90. Yao, Q.; Feng, Y.; Fung, V.; Yu, Y.; Jiang, D.-e.; Yang, J.; Xie, J., Precise control of alloying sites of bimetallic nanoclusters via surface motif exchange reaction. *Nature Communications* **2017**, *8* (1), 1555.

91. Yao, Q.; Yuan, X.; Fung, V.; Yu, Y.; Leong, D. T.; Jiang, D.-e.; Xie, J., Understanding seed-mediated growth of gold nanoclusters at molecular level. *Nature Communications* **2017**, *8* (1), 927.

92. Zhang, P.; Wang, L.; Yang, S.; Schott, J. A.; Liu, X.; Mahurin, S. M.; Huang, C.; Zhang, Y.; Fulvio, P. F.; Chisholm, M. F.; Dai, S., Solid-state synthesis of ordered mesoporous

carbon catalysts via a mechanochemical assembly through coordination cross-linking. *Nature Communications* **2017**, *8*, 15020.

93. Artyushkova, K.; Mullins, D. R.; Gregoratti, L.; Yu, X. Y., Foreword to special section on “Near Ambient and Synchrotron Surface Analysis (NAXPS)”. *Surface and Interface Analysis* **2018**, *0* (0), doi:10.1002/sia.6383.

94. Bugnet, M.; Overbury, S. H.; Wu, Z.; Aires, F. J. C. S.; Meunier, F.; Epicier, T., Visualizing and Quantifying the Cationic Mobility at {100} Surfaces of Ceria: Application to CO₂ Adsorption/Desorption Phenomena in the Environmental Transmission Electron Microscope. *Microscopy and Microanalysis* **2018**, *24* (S1), 1940-1941.

95. Chen, H.; Shi, X.; Liu, J.; Jie, K.; Zhang, Z.; Hu, X.; Zhu, Y.; Lu, X.; Fu, J.; Huang, H.; Dai, S., Controlled synthesis of hierarchical ZSM-5 for catalytic fast pyrolysis of cellulose to aromatics. *Journal of Materials Chemistry A* **2018**, *6* (42), 21178-21185.

96. Chen, T.; Fung, V.; Yao, Q.; Luo, Z.; Jiang, D.-e.; Xie, J., Synthesis of Water-Soluble [Au₂₅(SR)₁₈]- Using a Stoichiometric Amount of NaBH₄. *Journal of the American Chemical Society* **2018**, *140* (36), 11370-11377.

97. Choi, W.; Hu, G.; Kwak, K.; Kim, M.; Jiang, D.-e.; Choi, J.-P.; Lee, D., Effects of Metal-Doping on Hydrogen Evolution Reaction Catalyzed by MAu₂₄ and M₂Au₃₆ Nanoclusters (M = Pt, Pd). *ACS Applied Materials & Interfaces* **2018**, *10* (51), 44645-44653.

98. Duchesne, P. N.; Li, Z. Y.; Deming, C. P.; Fung, V.; Zhao, X.; Yuan, J.; Regier, T.; Aldalbahi, A.; Almarhoon, Z.; Chen, S.; Jiang, D.-e.; Zheng, N.; Zhang, P., Golden single-atomic-site platinum electrocatalysts. *Nature Materials* **2018**, *17*, 1033-1039.

99. Hossain, S.; Ono, T.; Yoshioka, M.; Hu, G.; Hosoi, M.; Chen, Z.; Nair, L. V.; Niihori, Y.; Kurashige, W.; Jiang, D.-e.; Negishi, Y., Thiolate-Protected Trimetallic Au~20Ag~4Pd and Au~20Ag~4Pt Alloy Clusters with Controlled Chemical Composition and Metal Positions. *The Journal of Physical Chemistry Letters* **2018**, *9* (10), 2590-2594.

100. Kim, M.; Tang, Q.; Narendra Kumar, A. V.; Kwak, K.; Choi, W.; Jiang, D.-e.; Lee, D., Dopant-Dependent Electronic Structures Observed for M₂Au₃₆(SC₆H₁₃)₂₄ Clusters (M = Pt, Pd). *The Journal of Physical Chemistry Letters* **2018**, *9* (5), 982-989.

101. Leng, Y.; Zhang, C.; Liu, B.; Liu, M.; Jiang, P.; Dai, S., Synergistic Activation of Palladium Nanoparticles by Polyoxometalate-Attached Melem for Boosting Formic Acid Dehydrogenation Efficiency. *ChemSusChem* **2018**, *11* (19), 3396-3401.

102. Li, W.; He, D.; Hu, G.; Li, X.; Banerjee, G.; Li, J.; Lee, S. H.; Dong, Q.; Gao, T.; Brudvig, G. W.; Waegle, M. M.; Jiang, D.-e.; Wang, D., Selective CO Production by Photoelectrochemical Methane Oxidation on TiO₂. *ACS Central Science* **2018**, *4* (5), 631-637.

103. Liu, C.; Camacho-Bunquin, J.; Ferrandon, M.; Savara, A.; Sohn, H.; Yang, D.; Kaphan, D. M.; Langeslay, R. R.; Ignacio-de Leon, P. A.; Liu, S.; Das, U.; Yang, B.; Hock, A. S.; Stair, P. C.; Curtiss, L. A.; Delferro, M., Development of activity-descriptor relationships for supported metal ion hydrogenation catalysts on silica. *Polyhedron* **2018**, *152*, 73-83.

104. Liu, F.; Huang, K.; Zheng, A.; Xiao, F.-S.; Dai, S., Hydrophobic Solid Acids and Their Catalytic Applications in Green and Sustainable Chemistry. *ACS Catalysis* **2018**, *8* (1), 372-391.

105. Liu, Y.; Zhang, P.; Liu, J.; Wang, T.; Huo, Q.; Yang, L.; Sun, L.; Qiao, Z.-A.; Dai, S., Gold Cluster-CeO₂ Nanostructured Hybrid Architectures as Catalysts for Selective Oxidation of Inert Hydrocarbons. *Chemistry of Materials* **2018**, *30* (23), 8579-8586.

106. Lu, M.; Lepore, A. W.; Choi, J.-S.; Li, Z.; Wu, Z.; Polo-Garzon, F.; Hu, M. Z., Acetic Acid/Propionic Acid Conversion on Metal Doped Molybdenum Carbide Catalyst Beads for Catalytic Hot Gas Filtration. *Catalysts* **2018**, *8* (12), 643.

107. Nair, L. V.; Hossain, S.; Takagi, S.; Imai, Y.; Hu, G.; Wakayama, S.; Kumar, B.; Kurashige, W.; Jiang, D.-e.; Negishi, Y., Hetero-biicosahedral $[\text{Au}_{24}\text{Pd}(\text{PPh}_3)_{10}(\text{SC}_2\text{H}_4\text{Ph})_5\text{Cl}_2]^+$ nanocluster: selective synthesis and optical and electrochemical properties. *Nanoscale* **2018**, *10* (40), 18969-18979.
108. Wu, H.; Zeng, M.; Zhu, X.; Tian, C.; Mei, B.; Song, Y.; Du, X.-L.; Jiang, Z.; He, L.; Xia, C.; Dai, S., Defect Engineering in Polymeric Cobalt Phthalocyanine Networks for Enhanced Electrochemical CO_2 Reduction. *ChemElectroChem* **2018**, *5* (19), 2717-2721.
109. Yao, Q.; Fung, V.; Sun, C.; Huang, S.; Chen, T.; Jiang, D.-e.; Lee, J. Y.; Xie, J., Revealing isoelectronic size conversion dynamics of metal nanoclusters by a noncrystallization approach. *Nature Communications* **2018**, *9* (1), 1979.
110. You, B.; Zhang, Y.; Yin, P.; Jiang, D.-e.; Sun, Y., Universal molecular-confined synthesis of interconnected porous metal oxides-N-C frameworks for electrocatalytic water splitting. *Nano Energy* **2018**, *48*, 600-606.
111. Di, J.; Zhu, H.; Xia, J.; Bao, J.; Zhang, P.; Yang, S.-Z.; Li, H.; Dai, S., High-performance electrolytic oxygen evolution with a seamless armor core-shell FeCoNi oxynitride. *Nanoscale* **2019**, *11* (15), 7239-7246.
112. Dong, H.; Liu, C.; Li, Y.; Jiang, D.-e., Computational screening of M/Cu core/shell nanoparticles and their applications for the electro-chemical reduction of CO_2 and CO. *Nanoscale* **2019**, *11* (23), 11351-11359.
113. Hülsey, M. J.; Zhang, B.; Ma, Z.; Asakura, H.; Do, D. A.; Chen, W.; Tanaka, T.; Zhang, P.; Wu, Z.; Yan, N., In situ spectroscopy-guided engineering of rhodium single-atom catalysts for CO oxidation. *Nature Communications* **2019**, *10* (1), 1330.
114. Kong, L.; Zhao, J.; Han, S.; Zhang, T.; He, L.; Zhang, P.; Dai, S., Facile Synthesis of Copper Containing Ordered Mesoporous Polymers via Aqueous Coordination Self-Assembly for Aerobic Oxidation of Alcohols. *Industrial & Engineering Chemistry Research* **2019**, *58* (16), 6438-6445.
115. Liu, D.; Dai, L.; Lin, X.; Chen, J.-F.; Zhang, J.; Feng, X.; Müllen, K.; Zhu, X.; Dai, S., Chemical Approaches to Carbon-Based Metal-Free Catalysts. *Advanced Materials* **2019**, *31* (0), 1804863.
116. Mefford, J. T.; Kurilovich, A.; Saunders, J.; Hardin, W. G.; Abakumov, A.; Forslund, R.; Bonnefont, A.; Dai, S.; Johnston, K. P.; Stevenson, K., Decoupling the Roles of Carbon and Metal Oxides on the Electrocatalytic Reduction of Oxygen on $\text{La}_{1-x}\text{Sr}_x\text{CoO}_{3-\delta}$ Perovskite Composite Electrodes. *Physical Chemistry Chemical Physics* **2019**, *21*, 3327-3338.
117. Shi, R.; Tian, C.; Zhu, X.; Peng, C.-Y.; Mei, B.; He, L.; Du, X.; Jiang, Z.; Chen, Y.; Dai, S., Achieving an Exceptionally High Loading of Isolated Cobalt Single Atoms on Porous Carbon Matrix for Efficient Visible-Light-Driven Photocatalytic Hydrogen Production. *Chemical Science* **2019**, *10*, 2585-2591.
118. Wu, H.; Zeng, M.; Li, Z.; Zhu, X.; Tian, C.; Xia, C.; He, L.; Dai, S., Coupling FeNi alloys and hollow nitrogen-enriched carbon frameworks leads to high-performance oxygen electrocatalysts for rechargeable zinc-air batteries. *Sustainable Energy & Fuels* **2019**, *3* (1), 136-141.
119. Yan, Y.; Zhang, Z.; Bak, S.-M.; Yao, S.; Hu, X.; Shadik, Z.; Do-Thanh, C.-L.; Zhang, F.; Chen, H.; Lyu, X.; Chen, K.; Zhu, Y.; Lu, X.; Ouyang, P.; Fu, J.; Dai, S., Confinement of Ultrasmall Cobalt Oxide Clusters within Silicalite-1 Crystals for Efficient Conversion of Fructose into Methyl Lactate. *ACS Catalysis* **2019**, *9* (3), 1923-1930.

120. Ye, J.; Bai, L.; Liu, B.; Tian, H.; Hu, J.; Polo-Garzon, F.; Mayes, R. T.; Wu, Z.; Fang, Y.-X., Fabrication of Pillared ZSM-5 Framework for Shape Selectivity of Ethane Dehydroaromatization. *Industrial & Engineering Chemistry Research* **2019**, *58* (17), 7094-7106.
121. Yusuf, S.; Neal, L.; Bao, Z.; Wu, Z.; Li, F., Effects of Sodium and Tungsten Promoters on Mg₆MnO₈-Based Core-Shell Redox Catalysts for Chemical Looping—Oxidative Dehydrogenation of Ethane. *ACS Catalysis* **2019**, *9* (4), 3174-3186.
122. Zhou, M.; Higaki, T.; Hu, G.; Sfeir, M. Y.; Chen, Y.; Jiang, D.-e.; Jin, R., Three-orders-of-magnitude variation of carrier lifetimes with crystal phase of gold nanoclusters. *Science* **2019**, *364* (6437), 279-282.

Johannes Lercher

Self-Organization Around Active Centers Influencing Catalytic Rates for Brønsted Acid Catalyzed Reactions

Johannes Lercher,^{a,b} Oliver Gutiérrez,^a Don Camaioni,^a Wang Meng,^a John Fulton,^a Jian Zhi Hu,^a Yue Liu,^b Huamin Wang,^a Manish Shetty,^a Andreas Jentys^b

^a Pacific Northwest National Laboratory, Physical and Computational Sciences Directorate and Institute for Integrated Catalysis

^b Technical University Munich, Department of Chemistry

Presentation Abstract

The chemical and steric environment around the active center stabilizes the ground and transition states of reacting molecules directing selective reaction pathways. Such effects are rather subtle for gas-phase reactions catalyzed by solid catalysts, but begin to be highly important for reactions in the condensed phase. The poster will address the chemical consequences of such an environment for sorption and catalysis. It will be shown how water and protic solvent molecules self-organize in this environment and how they impact the thermodynamic state of the sorbed and reacting molecules. It will also be shown that the interactions can be designed and controlled via direct synthesis (changing pore sizes and concentration of sites), as well as via the addition of cations, oxidic clusters or organic fragments. As examples for catalytic transformations, the poster will compare elimination reactions of alcohols and alkylation of aromatic molecules in protic and aprotic solvents of varying polarity. Experimental methods to define the state of the reacting molecules combined with detailed kinetic analysis and theory will be used to explain the principal contributions of the interactions and the confinement to determine reaction rates. It will be discussed, how reaction rates and pathways are influenced and potentially can be tailored using the space available for a transition state and the chemical constituents around the active center.

FWP 47319: Transdisciplinary Approaches to Realize Novel Catalytic Pathways to Energy Carriers

PI: Johannes Lercher

Subtask PI's: Aaron M. Appel, Zdenek Dohnálek, Johannes A. Lercher, Roger Rousseau, János Szanyi

Co-PIs and Key Personnel: S. Thomas Autrey, R. Morris Bullock, David A. Dixon, John L. Fulton, Feng Gao, Bojana Ginovska, Vassiliki-Alexandra Glezakou, Oliver Gutiérrez- Tinoco, Jian Zhi Hu, Enrique Iglesia, Andreas Jentys, Abhijeet Karkamkar, Bruce D. Kay, Greg A. Kimmel, Libor Kovarik, John C. Linehan, Nikolay G. Petrik, Gregory K. Schenter, Wendy J. Shaw, Huamin Wang, Yong Wang, Eric S. Wiedner

RECENT PROGRESS

The central goal of this BES Catalysis Sciences research program, “Transdisciplinary approaches to enhancing rates and selectivities in catalytic pathways,” is to develop insight into novel approaches for designing catalytic centers and their environments. We aim to catalyze C-C and C-H bond formation and C-O bond cleavage on acid-base and hydrogenation sites with rates that exceed the current state-of-the-art by at least an order of magnitude and with selectivities that match the best currently known. We target the fundamental catalysis of these reactions because high rates for these reactions at mild reaction conditions coupled with high selectivity is one of the keys for more flexible production of fuels and chemicals.

We are convinced that in order to enhance the rates and selectivity of acid-base catalyzed C-C coupling and metal-catalyzed hydrogen addition to C-O bonds, the nature of active sites has to be understood at a level of complexity that markedly exceeds the current state. We will acquire and use new insights for the design of active sites by placing specific emphasis on both (1) the nature, nuclearity, and local environment of active centers; and (2) the extended chemical and structural environment around the active center to support suitable self-organization of reactants and solvents and to stabilize transition states. Our work will be rooted in the knowledge that the nature of the active center (its electronic properties, spatial arrangement, and nuclearity) determines the chemical specificity and intrinsic reactivity. It will be guided by the fundamental hypothesis of this proposal that activity along selected pathways for metal and acid-base catalyzed reactions can be markedly enhanced by (i) positioning of functional groups around the active center, (ii) adjusting the available space around the active center to match that of the rate-limiting transition state, and (iii) self-organization of solvent and reactant molecules around the active center. This environment can have the form of a void (maximizing van der Waals contacts with minimal distortions of the host and the guest in the transition state), a functional group aiding the stabilization of reactants along the reaction path, and solvent/reactant molecules engulfing the active center.

To achieve our goal of enhancing rates and selectivities for our target reactions, the program is organized into two thrusts that focus on “Tailoring acid-base sites for controlled C-C bond formation” and “Enhancing H₂ addition rates by designing the metal center and its environment.” To gain molecular level insight into catalysis on both types of sites, computational catalysis is integrated in the crosscutting subtask, “Novel theoretical approaches to describe catalysts and catalysis,” and will support, enhance, and guide experimental efforts. The first thrust explores the impact of the geometric and electronic properties of Lewis and Brønsted acid-base sites on C-C bond formation by combining precision synthesis of homotopic active sites of chosen nuclearity and the stabilization of such sites in homogeneous catalysts, inert substrates, faceted oxides, mesoporous solids, and zeolites. Spectroscopic characterization of these sites and the catalytic transformations allow for directed cross-coupling of the obtained insights. The second thrust addresses the fundamentals of hydrogen addition to CO groups in molecules such as CO₂, alcohols, aldehydes, ketones, and carboxylic acids. We will exploit novel, highly active sites comprised of single metal atoms and small clusters of defined nuclearity supported on homogeneous scaffolds of increasing complexity and heterogeneous supports, such as graphene and faceted oxides, as well as in micropores. We designed our program structure to promote cross-disciplinary collaborations within and across thrusts and subtasks. The structure-activity relationships dominated by the acid-base or metal center are highlighted in the first subtasks in each thrust, while the second subtasks feature the impact of the environment (ligands, confinement, solvent, and reactant molecules).

Examples of Recent Results

Adsorption and Dissociation of Methanol on Anatase TiO₂(101) Single Crystals and Faceted Nanoparticles. We employ a cross-disciplinary approach to study the adsorption and dissociation of methanol on the anatase TiO₂(101) surfaces of single crystals (SCs) and faceted nanoparticles (F-NPs). While scanning tunneling microscopy (STM) is used to follow the spatial distribution of adsorbed methanol molecules and methoxy and hydroxy species on SCs, temperature programmed desorption and infrared reflection spectroscopy results are compared on both SC and F-NP surfaces. We find that molecular methanol adsorbed at 80 K on SC TiO₂(101) clusters along the titania rows. These clusters are metastable and fall apart upon annealing due to the repulsion of neighboring molecules. Further, we find that on SC TiO₂(101) methanol deprotonates to produce neighboring methoxy and hydroxyl groups at high coverages following annealing to 290 K (Figure 3). The coverage of methoxy and hydroxyl groups can be increased with repeated adsorption and annealing cycles, and the annealing above 290 K leads to the recombinative desorption of methanol. On F-NP TiO₂(101) we find that at higher pressures methanol adsorbs both molecularly and dissociatively at 290 K. With increasing temperature, molecularly adsorbed methanol gradually converts to methoxy. Therefore, close correlations and complementary information are found in adsorption and surface reaction on single crystal and nanoparticle surfaces.

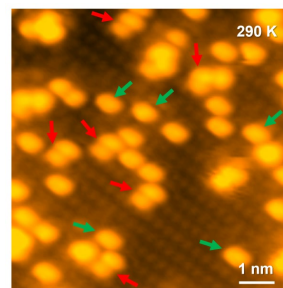


Figure 3. The STM image of anatase TiO₂(101) with molecularly (green) and dissociatively (red) bound methanol.

Alkanol Dehydration on Single-Facet Dominant Anatase TiO₂(101) and (001) Model Catalysts.

Two anatase titania model catalysts, with preferential exposure of (101) and (001) facets, were synthesized and studied for 2-propanol dehydration. A series of microscopic and spectroscopic techniques including X-ray diffraction, scanning electron microscopy, transmission electron microscopy, ammonia temperature program desorption (NH₃-TPD), diffuse reflectance infrared Fourier transform spectroscopy (DRIFTS) and chemical titration were employed to correlate the structure properties of the model catalysts to their catalytic performances. Based on selective site poisoning titration using 2,6-di-tert-butyl pyridine, surface Lewis acid sites were found to be active for 2-propanol dehydration. The higher activity for TiO₂(101) catalyst was ascribed to its higher strength of acid sites compared with TiO₂(001) facets. Surface species present during steady-state reaction were probed using temperature-dependent DRIFTS. Density functional theory (DFT) was

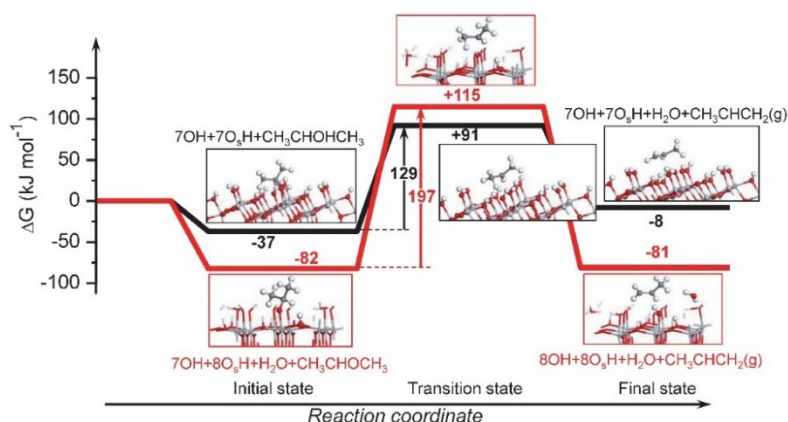


Figure 4. 2-propanol dehydration on hydroxylated anatase TiO₂(101) and (001) surfaces via the E2 mechanism.

subsequently used to to determine the elementary steps of 2-propanol dehydration. On both anatase surfaces, 2-propanol was found to dehydrate via concerted E2 elimination pathways, but with different initial states and thus also different intrinsic activation barriers (Figure 4). Molecular 2-propanol dehydration dominates on TiO₂(101) while on TiO₂(001), 2-propanol simultaneously

converts to more stable 2-propoxide before dehydration, which then requires higher activation energies for E2 elimination.

Understanding and Quantifying the Influence of Hydronium Ions in Zeolites on Sorption. The presence of reactive binding sites and unreactive domains in the three-dimensional space of catalysts lead to a local organization of molecules during catalysis. Zeolites serve as examples of such a three-dimensional space, having non-reactive channel walls and Brønsted acidic OH groups or Lewis acid sites. When used in the presence of water, hydrated hydronium ions ($\text{H}_3\text{O}^+_{\text{hydr}}$) are formed in locally constrained environments from Brønsted acid sites (Figure 5). For a medium-pore zeolite, such as MFI depicted in Figure 5, the hydrated hydronium ions consist of eight water molecules (0.24 nm^3); the space between these hydrated hydronium ions remains empty under normal conditions. The zeolite forms a dynamically rearranging quasi-solid electrolyte. Organic molecules adsorb in this space. Thus, the available pore volume for organic molecules decreases proportionally to the concentration of the hydronium ions. The higher charge density (increasing ionic strength) resulting from the increasing concentration of hydronium ions leads to an increase in the activity coefficients of adsorbed molecules. In turn, this translates to weaker sorbate-sorbent interactions and higher free energy of the sorbed molecules. The presence of the water cluster, however, also enhances the interactions with polar groups of sorbed molecules, allowing in this way to direct interactions and reaction pathways. While it has been developed here for a particular set of zeolites, it can be directly applied for related materials such as silicoaluminophosphates and metal-organic frameworks as well as for organic polymers and biopolymers containing ion pairs.

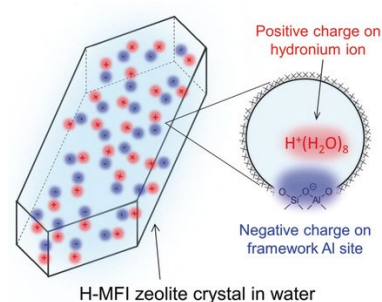


Figure 5. Schematic illustration of positively charged hydronium ions and negatively charged framework Al sites in H-MFI zeolite crystal in water.

Genesis and Stability of Hydronium Ions in Zeolite Channels. As outlined above, Brønsted acidic zeolite are profoundly altered by the presence of water leading to the formation of hydrated hydronium ions. Combining high-resolution solid-state NMR spectroscopy and theory, the elementary steps of water interacting with zeolite Brønsted acid sites and their conversion to hydrated hydronium ions was elucidated. The signal at 9 ppm in ^1H NMR (Figure 6), observed at loadings of 2–9 water molecules per Brønsted acid site, has been successfully assigned to the hydrated hydronium ions on the basis of chemical shift calculations, and the direct comparison with HClO_4 in water. The variation in the intensity of ^1H - ^{29}Si cross-polarization signal indicates that hydrogen bonds between water molecules and the tetrahedrally coordinated aluminum in the zeolite lattice weaken with the formation of hydronium ion–water clusters and increase the mobility of protons. DFT-based ab initio molecular dynamics studies support this conclusion. Above $140 \text{ }^\circ\text{C}$, however, fast proton exchange between bridging hydroxyl groups and water occurs even in the presence of only one water molecule per acid site.

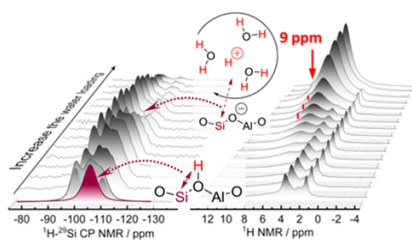


Figure 6. ^1H - ^{29}Si CP and ^1H NMR spectra as the concentration of water in the zeolite pores increases. The transition from a framework Brønsted site to a hydronium ion is indicated by the signal at 9 ppm.

Phosphines Not Needed. In going beyond phosphine-containing complexes, we have determined the thermodynamics and kinetics of a unique ruthenium-1,8-diazabicyclo[5.4.0]undec-7-ene (DBU) catalyst that catalyzes the hydrogenation of CO₂ to formate at room temperature. While DBU is not usually considered a good ligand, it is integral to produce an

active catalyst in these systems. We have observed that [CpRu(CH₃CN)₃]⁺ catalyzes the reduction of CO₂ at room temperature in the presence of DBU. No other base, either weaker or stronger, affords catalysis. Through careful thermodynamic and kinetic studies, we have found that two DBUs must bind to the ruthenium center to generate the active catalyst. The complex pre-equilibrium is shown in Figure 7 in which the first DBU binds favorably with $\Delta G = -2.4$ kcal mol⁻¹, while the second DBU binding is mildly unfavorable, $\Delta G = 0.7$ kcal mol⁻¹. The hydrogenation of CO₂ to formate proceeds at a TOF of 300 h⁻¹ at 20 °C. These results demonstrate that (1) active catalysts without phosphine ligands can be produced and (2) one must be very careful in assigning the identity of the actual catalyst, especially in studies in which “cocktails” of catalyst precursors are mixed prior to catalysis.

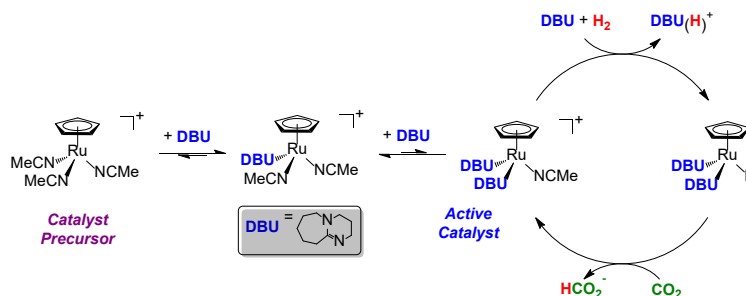


Figure 7. Proposed mechanism for CO₂ hydrogenation to formate by CpRu(NCMe)₃⁺ and DBU.

Carboxyl Route in Reverse Water-Gas Shift Reaction. A series of isothermal, *stoichiometric* surface reactions (H₂ → H₂(t) → CO₂) provide convincing evidence for the carboxyl intermediate in the WGS reaction. Figure 8a depicts the carbonyl coverage (θ_{CO}) as a function of CO₂ exposure time on the H₂-treated catalyst. The individual data sets signify the He purge duration prior to the introduction of CO₂. As anticipated, the carbonyl formation rate (θ_{CO} min⁻¹) depends on the He purge time, i.e. the amount of hydrogen adsorbed on the catalyst. More compelling was the *absence* of formate for He purge times above 5 min (Figure 8b). These results have several inferences. First, the formate (HCOO) pathway is not operative during the *stoichiometric* reaction since we observe carbonyl in the absence of formate. The associative redox pathway is also not operative

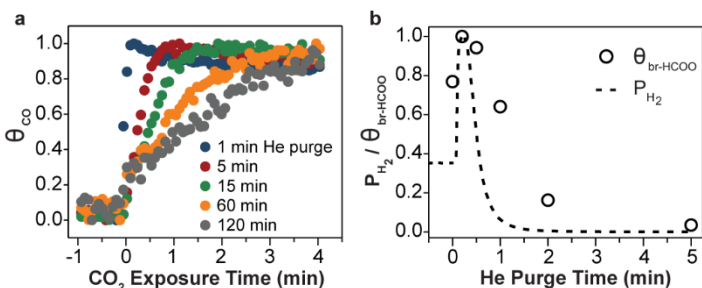


Figure 8. (a) Normalized carbonyl absorbance at 1890 cm⁻¹ (θ_{CO}) as a function of CO₂ exposure time. (b) Normalized formate IR absorbance and normalized H₂ partial pressure (P_{H_2}) profile as a function of He purge time.

since CO₂ does not dissociate on Pd; thus, the results in Figure 8a are only consistent with the carboxyl (COOH) pathway. Second, at least two different active sites exist distinguished by their regioselective H-addition to CO₂ (HCOO vs. COOH). Third, the hydrogen desorption rate for the two distinct active sites differ markedly during the He purge: The site-selective to formate formation contains adsorbed H only in the presence of gas-phase H₂, indicating fast recombinative desorption. In contrast, the site-selective to carboxyl formation contains adsorbed H even after a 2 h He purge at 300 °C, indicating slow recombinative desorption.

The Impact of Solvent in the Design of Catalysts. The solvent can have a huge impact on the favorability of individual steps in catalytic hydrogenation of CO₂. In a Minireview, we described recent and emerging studies on the impact of solvent on the mechanisms for hydrogenation of CO₂ by molecular catalysts. The solvent can affect the thermodynamics and kinetics for hydride transfer from the catalyst to CO₂ and, in some cases, switching between solvents can reverse the direction of hydride transfer. The speciation of CO₂ into carbonate species, both inorganic and organic, is also affected by the solvent and allows the possibility of multiple hydride transfer pathways. Additionally, the solvent can be used to lower the thermodynamic barrier for hydrogenation of CO₂ to formic acid, as well as enable the subsequent formation of methanol by activating formic acid to accept more hydride equivalents from the catalyst. In particular, we established a thermodynamic cycle to describe the hydride acceptor ability of formic acid as a function of its protonation state (Figure 9). These solvent effects provide a basis for using the solvent as a key parameter to rationally control catalyst performance.

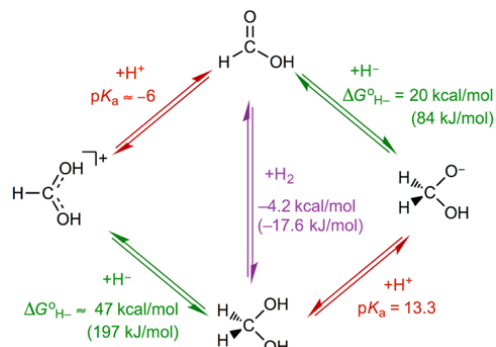


Figure 9. Reduction of challenging intermediates will be greatly benefited by thermodynamic insight into the free energies for H⁺ and H⁻ transfer reactions, as illustrated with the net hydrogenation of formic acid.

Palladium-Catalyzed Reductive Insertion of Alcohols into Aryl Ether Bonds. Building upon our recently reported mechanism for the selective hydrolytic cleavage of the arene-oxygen bond in aromatic ethers, the question arose as to whether alcohols could also cleave such ether bonds and thereby could be used for transesterification. In the presence of water, the aromatic C-O bond is cleaved by insertion of water upon the partial hydrogenation of the arene ring to an enol ether. Water rapidly adds to the enol ether to form a hemi-ketal, which undergoes elimination to cyclohexanone and phenol/alkanol. In our most recent study focused on the corresponding alcoholysis, we found that indeed Pd/C catalyzes C-O bond cleavage of aryl ethers (diphenyl ether and cyclohexyl phenyl ether) by alcohol in the presence of H₂. Figure 10 illustrates the competing hydrogenation and solvolysis occurring in methanol. The aromatic C-O bond is cleaved by reductive methanolysis, which is initiated by Pd-catalyzed partial hydrogenation of one phenyl ring to form an enol ether. The enol ether reacts rapidly with methanol to form a ketal, which generates methoxycyclohexene by eliminating phenol or an alkanol. Subsequent hydrogenation leads to methoxycyclohexane.

We also demonstrated that this solvolysis mechanism applies to a variety of alcohols in the presence of H₂. The attack of an alcohol, however, is slower than attack by water; thus, the selectivity to alcoholysis is lower than for hydrolysis under comparable conditions. The selectivity toward reductive alcoholysis is inversely proportional to the carbon number of the alcohol. The selectivity of the different metals to catalyze hydrogenation of the enol ether is a feature that remains to be explored in greater detail.

Heterolytic H₂ Cleavage on Fe₃O₄(001) Supported Single Palladium Atoms. We employ a combination of STM and DFT and demonstrate that on a model single atom catalyst (SAC)

comprised of single Pd atoms on $\text{Fe}_3\text{O}_4(001)$, H_2 dissociates heterolytically between Pd and surface oxygen. The efficient hydrogen spillover allows for continuous hydrogenation to high coverages which ultimately leads to the lifting of Fe_3O_4 reconstruction and Pd reduction and destabilization. The reducibility of Fe_3O_4 is critical for continuous H_2 activation. We find that water plays an important role in reducing the hydrogen diffusion barrier, thereby facilitating the redistribution of hydroxyls away from Pd. We further establish how the oxidation state and stability of Pd change with the increasing level of hydrogenation. Annealing of the hydrogenated surfaces leads to water formation and one layer deep pits on the terraces due to lattice oxygen extraction. Our study demonstrates a distinct H_2 activation mechanism on single Pd atoms and corroborates the importance of charge transport on reducible supports away from the active sites. The DFT calculations further allow us to predict the differences in H_2 activation on single atoms of different metals as shown in Figure 11.

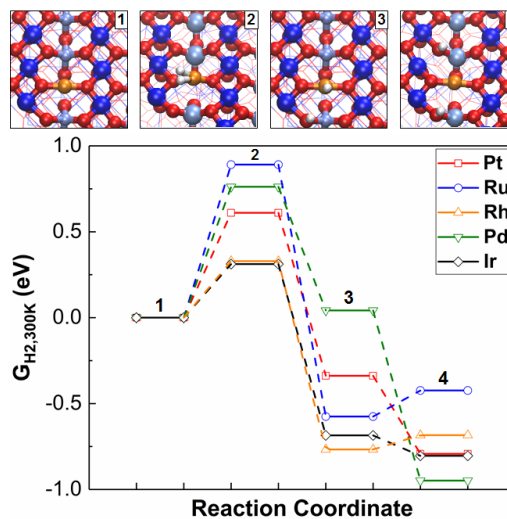


Figure 11. DFT-predicted energy pathway of H_2 dissociation mechanism on a single metal (Pt, Ru, Rh, Pd, and Ir) atom on $\text{Fe}_3\text{O}_4(001)$.

Targeted Theory Development for Modeling Catalysis in Complex Environments. In addition to direct collaborations with concurrent experiments on our core BES catalysis program, the theory cross-cutting subtask engages in targeted development of theory and simulation capabilities to address the needs of modeling reactivity in complex environments. For instance, in collaboration

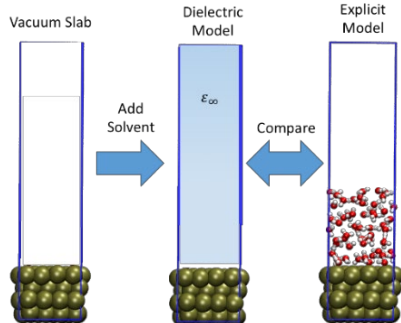


Figure 12. We use experimental measurands of reactivity and AIMD simulations of solid-liquid interfaces to guide the construction of continuum models of solvation that can accelerate research of catalysis in liquids.

with the group of Prof. Chris K. Skylaris (U. Southampton UK), we are using state of the art explicit solvent AIMD simulations and kinetic measurements of reactivity and adsorption at solid-liquid interfaces to help guide the construction of implicit solvent models. Recently we have developed a model based on Fiscaro's soft sphere solvation cavities that can faithfully capture the electronic structure changes of metal surfaces in contact with liquids as well as quantitative changes in solvation free energetics. In collaboration with Prof. Michele Parrinello (ETH Zurich, Switzerland) we are investigating the development and use of advanced collective variables (CVs) for use in free energy simulations which capture the appreciable effects on the reaction free energy from complex chemical environments such as flexible extended coordination spheres and confined spaces. In our recent work, we have adapted a set of CVs able to access the acid-base properties of complex catalysts irrespective of the number of acid-base species simultaneously present, nature of reactants and kind of solvent. This has allowed us to understand the evolution of acid/base properties inside of zeolite pores as a function of the pore size/shape and number of water molecules present. We find that it is a delicate balance between enthalpic and entropic forces that determine the protonation state in zeolites with the preferred state being a protonated water cluster whose size is dependent upon the size of the zeolite pore in which the water is confined.

Publications Acknowledging this Grant in 2016-2019

Publications exclusively funded by this grant

2016

1. Baylon, R. A. L.; Sun, J.; Martin, K. J.; Venkitasubramanian, P.; Wang, Y., Beyond Ketonization: Selective Conversion of Carboxylic Acids to Olefins over Balanced Lewis Acid-base Pairs. *Chem. Commun.* **2016**, *52*, 4975-4978. <http://dx.doi.org/10.1039/C5CC10528E>.
2. Baylon, R. A. L.; Sun, J.; Wang, Y., Conversion of Ethanol to 1,3-butadiene over Na Doped $Zn_xZr_yO_z$ Mixed Metal Oxides. *Catal. Today* **2016**, *259, Part 2*, 446-452. <http://dx.doi.org/10.1016/j.cattod.2015.04.010>.
3. Chen, L.; Smith, R. S.; Kay, B. D.; Dohnálek, Z., Adsorption of Small Hydrocarbons on Rutile $TiO_2(110)$. *Surf. Sci.* **2016**, *650*, 83-92. <http://dx.doi.org/10.1016/j.susc.2015.11.002>.
4. Deshlahra, P.; Iglesia, E., Toward More Complete Descriptors of Reactivity in Catalysis by Solid Acids. *ACS Catal.* **2016**, *6*, 5386-5392. <http://dx.doi.org/10.1021/acscatal.6b01402>.
5. Deshlahra, P.; Iglesia, E., Reactivity and Selectivity Descriptors for the Activation of C-H Bonds in Hydrocarbons and Oxygenates on Metal Oxides. *J. Phys. Chem. C* **2016**, *120*, 16741-16760. <http://dx.doi.org/10.1021/acs.jpcc.6b04604>.
6. Fang, Z.; Zetterholm, P.; Dixon, D. A., 1,2-Ethandiol and 1,3-Propanediol Conversions over $(MO_3)_3$ (M = Mo, W) Nanoclusters: A Computational Study. *J. Phys. Chem. A* **2016**, *120*, 1897-1907. <http://dx.doi.org/10.1021/acs.jpca.6b00158>.
7. Henderson, M. A.; Dahal, A.; Dohnálek, Z.; Lyubinetsky, I., Strong Temperature Dependence in the Reactivity of H_2 on $RuO_2(110)$. *J. Phys. Chem. Lett.* **2016**, *7*, 2967-2970. <http://dx.doi.org/10.1021/acs.jpcclett.6b01307>.
8. Henderson, M. A.; Mu, R.; Dahal, A.; Lyubinetsky, I.; Dohnálek, Z.; Glezakou, V.-A.; Rousseau, R., Light Makes a Surface Banana-Bond Split: Photodesorption of Molecular Hydrogen from $RuO_2(110)$. *J. Am. Chem. Soc.* **2016**, *138*, 8714-8717. <http://dx.doi.org/10.1021/jacs.6b05083>.
9. Hu, J. Z.; Xu, S.; Kwak, J. H.; Hu, M. Y.; Wan, C.; Zhao, Z.; Szanyi, J.; Bao, X.; Han, X.; Wang, Y.; Peden, C. H. F., High Field ^{27}Al MAS NMR and TPD Studies of Active Sites in Ethanol Dehydration using Thermally Treated Transitional Aluminas as Catalysts. *J. Catal.* **2016**, *336*, 85-93. <http://dx.doi.org/10.1016/j.jcat.2016.01.006>.
10. Knaeble, W.; Iglesia, E., Acid Strength and Metal-acid Proximity Effects on Methylcyclohexane Ring Contraction Turnover Rates and Selectivities. *J. Catal.* **2016**, *344*, 817-830. <http://dx.doi.org/10.1016/j.jcat.2016.08.007>.
11. Knaeble, W.; Iglesia, E., Kinetic and Theoretical Insights into the Mechanism of Alkanol Dehydration on Solid Brønsted Acid Catalysts. *J. Phys. Chem. C* **2016**, *120*, 3371-3389. <http://dx.doi.org/10.1021/acs.jpcc.5b11127>.

12. Novotny, Z.; Netzer, F. P.; Dohnálek, Z., Ceria Nanoclusters on Graphene/Ru(0001): A New Model Catalyst System. *Surf. Sci.* **2016**, *652*, 230-237. <http://dx.doi.org/10.1016/j.susc.2016.03.020>.
13. Petrik, N. G.; Kimmel, G. A.; Shen, M.; Henderson, M. A., Quenching of electron transfer reactions through coadsorption: A study of oxygen photodesorption from TiO₂(110). *Surf. Sci.* **2016**, *652*, 183-188. <http://dx.doi.org/10.1016/j.susc.2015.12.038>.
14. Rahman, M. M.; Davidson, S. D.; Sun, J. M.; Wang, Y., Effect of Water on Ethanol Conversion over ZnO. *Top. Catal.* **2016**, *59*, 37-45. <http://dx.doi.org/10.1007/s11244-015-0503-9>.
15. Ramasamy, K. K.; Gray, M.; Job, H.; Santosa, D.; Li, X. S.; Devaraj, A.; Karkamkar, A.; Wang, Y., Role of Calcination Temperature on the Hydrotalcite Derived MgO-Al₂O₃ in Converting Ethanol to Butanol. *Top. Catal.* **2016**, *59*, 46-54. <http://dx.doi.org/10.1007/s11244-015-0504-8>.
16. Robinson, S. J.; Zall, C. M.; Miller, D. L.; Linehan, J. C.; Appel, A. M., Solvent influence on the thermodynamics for hydride transfer from bis(diphosphine) complexes of nickel. *Dalton. Trans.* **2016**, *45*, 10017-10023. <http://dx.doi.org/10.1039/c6dt00309e>.
17. Sun, J.; Baylon, R. A. L.; Liu, C.; Mei, D.; Martin, K. J.; Venkitasubramanian, P.; Wang, Y., Key Roles of Lewis Acid-Base Pairs on Zn_xZr_yO_z in Direct Ethanol/Acetone to Isobutene Conversion. *J. Am. Chem. Soc.* **2016**, *138*, 507-517. <http://dx.doi.org/10.1021/jacs.5b07401>.
18. Wan, C.; Hu, M. Y.; Jaegers, N. R.; Shi, D.; Wang, H.; Gao, F.; Qin, Z.; Wang, Y.; Hu, J. Z., Investigating the Surface Structure of γ -Al₂O₃ Supported WO_x Catalysts by High Field ²⁷Al MAS NMR and Electronic Structure Calculations. *J. Phys. Chem. C* **2016**, *120*, 23093-23103. <http://dx.doi.org/10.1021/acs.jpcc.6b09060>.
19. Wang, H.; Wang, Y., Characterization of Deactivated Bio-oil Hydrotreating Catalysts. *Top. Catal.* **2016**, *59*, 65-72. <http://dx.doi.org/10.1007/s11244-015-0506-6>.
20. Wang, X.; Hong, Y. C.; Shi, H.; Szanyi, J., Kinetic modeling and transient DRIFTS-MS studies of CO₂ methanation over Ru/Al₂O₃ catalysts. *J. Catal.* **2016**, *343*, 185-195. <http://dx.doi.org/10.1016/j.jcat.2016.02.001>.
21. Wang, Y. G.; Cantu, D. C.; Lee, M. S.; Li, J.; Glezakou, V. A.; Rousseau, R., CO Oxidation on Au/TiO₂: Condition-Dependent Active Sites and Mechanistic Pathways. *J. Am. Chem. Soc.* **2016**, *138*, 10467-10476. <http://dx.doi.org/10.1021/jacs.6b04187>.
22. Yi, C. W.; Szanyi, J., Pd overlayer on oxygen pre-covered graphene/Ru(0001): Thermal stability. *Surf. Sci.* **2016**, *648*, 271-277. <http://dx.doi.org/10.1016/j.susc.2015.12.018>.
23. Zall, C. M.; Linehan, J. C.; Appel, A. M., Triphosphine-Ligated Copper Hydrides for CO₂ Hydrogenation: Structure, Reactivity, and Thermodynamic Studies. *J. Am. Chem. Soc.* **2016**, *138*, 9968-9977. <http://dx.doi.org/10.1021/jacs.6b05349>.
24. Zhao, Z.; Xu, S.; Hu, M. Y.; Bao, X.; Hu, J. Z., In Situ High Temperature High Pressure MAS NMR Study on the Crystallization of AlPO₄₋₅. *J. Phys. Chem. C* **2016**, *120*, 1701-1708. <http://dx.doi.org/10.1021/acs.jpcc.5b11294>.

2017

25. Boralugodage, N. P.; Arachchige, R. J.; Dutta, A.; Buchko, G. W.; Shaw, W. J., Evaluating the role of acidic, basic, and polar amino acids and dipeptides on a molecular electrocatalyst for H₂ oxidation. *Catal. Sci. Technol.* **2017**, *7*, 1108-1121. <http://dx.doi.org/10.1039/c6cy02579j>.
26. Burgess, S. A.; Appel, A. M.; Linehan, J. C.; Wiedner, E. S., Changing the Mechanism for CO₂ Hydrogenation Using Solvent-Dependent Thermodynamics. *Angew. Chem.* **2017**, *129*, 15198-15201. <http://dx.doi.org/10.1002/ange.201709319>.
27. Burgess, S. A.; Grubel, K.; Appel, A. M.; Wiedner, E. S.; Linehan, J. C., Hydrogenation of CO₂ at Room Temperature and Low Pressure with a Cobalt Tetrakisphosphine Catalyst. *Inorg. Chem.* **2017**, *56*, 8580-8589. <http://dx.doi.org/10.1021/acs.inorgchem.7b01391>.
28. Chen, J.; Sun, J.; Wang, Y., Catalysts for Steam Reforming of Bio-oil: A Review. *Ind. Eng. Chem. Res.* **2017**, *56*, 4627-4637. <http://dx.doi.org/10.1021/acs.iecr.7b00600>.
29. Chen, L.; Smith, R. S.; Kay, B. D.; Dohnalek, Z., Direct Deoxygenation of Phenylmethanol to Methylbenzene and Benzyl Radicals on Rutile TiO₂(110). *ACS Catal.* **2017**, *7*, 2002-2006. <http://dx.doi.org/10.1021/acscatal.6b03225>.
30. Dahal, A.; Dohnálek, Z., Formation of Metastable Water Chains on Anatase TiO₂(101). *J. Phys. Chem. C* **2017**, *121*, 20413-20418. <http://dx.doi.org/10.1021/acs.jpcc.7b08122>.
31. Fang, Z.; Outlaw, M. A.; Dixon, D. A., Electronic Structures of Small (RuO₂)_n (n = 1–4) Nanoclusters and Their Anions and the Hydrolysis Reactions with Water. *J. Phys. Chem. A* **2017**, *121*, 7726-7744. <http://dx.doi.org/10.1021/acs.jpca.7b07226>.
32. Glezakou, V.-A.; Rousseau, R.; Elbert, S. T.; Franz, J. A., Trends in Homolytic Bond Dissociation Energies of Five- and Six-Coordinate Hydrides of Group 9 Transition Metals: Co, Rh, Ir. *J. Phys. Chem. A* **2017**, *121*, 1993-2000. <http://dx.doi.org/10.1021/acs.jpca.6b11655>.
33. Henderson, M. A.; Shen, M. M., Electron-Scavenging Chemistry of Benzoquinone on TiO₂(110). *Top. Catal.* **2017**, *60*, 440-445. <http://dx.doi.org/10.1007/s11244-016-0707-7>. (Henderson, Michael A. Shen, Mingmin)
34. Hong, Y.; Wang, Y., Elucidation of Reaction Mechanism for m-cresol Hydrodeoxygenation over Fe Based Catalysts: A Kinetic Study. *Catal. Commun.* **2017**, *100*, 43-47. <http://dx.doi.org/10.1016/j.catcom.2017.06.028>.
35. Hong, Y.; Zhang, S.; Tao, F.; Wang, Y., Stabilization of Iron-based Catalysts against Oxidation: An in situ Ambient Pressure XPS Study. *ACS Catal.* **2017**, *7*, 3639-3643. <http://dx.doi.org/10.1021/acscatal.7b00636>.
36. Houghton, A. Y.; Autrey, T., Calorimetric Study of the Activation of Hydrogen by Tris(pentafluorophenyl)borane and Trimesitylphosphine. *J. Phys. Chem. A* **2017**, *121*, 8785-8790. <http://dx.doi.org/10.1021/acs.jpca.7b08582>.
37. Hu, J. Z.; Wan, C.; Vjunov, A.; Wang, M.; Zhao, Z.; Hu, M. Y.; Camaioni, D. M.; Lercher, J. A., ²⁷Al MAS NMR Studies of HBEA Zeolite at Low to High Magnetic Fields. *J. Phys. Chem. C* **2017**, *121*, 12849-12854. <http://dx.doi.org/10.1021/acs.jpcc.7b03517>.

38. Jaegers, N. R.; Hu, M. Y.; Hoyt, D. W.; Wang, Y.; Hu, J. Z. *Development and Application of In Situ High-Temperature, High-Pressure Magic Angle Spinning NMR in Modern Magnetic Resonance*; Webb, G. A., Ed.; Springer International Publishing: Cham, 2017; pp 1-19.
39. Jaegers, N. R.; Wan, C.; Hu, M. Y.; Vasiliu, M.; Dixon, D. A.; Walter, E.; Wachs, I. E.; Wang, Y.; Hu, J. Z., Investigation of Silica-Supported Vanadium Oxide Catalysts by High Field V-51 Magic-Angle Spinning NMR. *J. Phys. Chem. C* **2017**, *121*, 6246-6254. <http://dx.doi.org/10.1021/acs.jpcc.7b01658>.
40. Li, W.-Z.; Nie, L.; Cheng, Y.; Kovarik, L.; Liu, J.; Wang, Y., Surface Enrichment of Pt in Stable Pt-Ir Nano-alloy Particles on MgAl₂O₄ Spinel in Oxidizing Atmosphere. *Catal. Commun.* **2017**, *93*, 57-61. <http://dx.doi.org/10.1016/j.catcom.2017.01.012>.
41. Liu, Y. S.; Vjunov, A.; Shi, H.; Eckstein, S.; Camaioni, D. M.; Mei, D. H.; Barath, E.; Lercher, J. A., Enhancing the Catalytic Activity of Hydronium Ions through Constrained Environments. *Nat. Commun.* **2017**, *8*, 14113. <http://dx.doi.org/10.1038/ncomms14113>.
42. Mei, D. H.; Lercher, J. A., Mechanistic insights into aqueous phase propanol dehydration in H-ZSM-5 zeolite. *AIChE J.* **2017**, *63*, 172-184. <http://dx.doi.org/10.1002/aic.15517>.
43. Mu, R.; Dahal, A.; Wang, Z.-T.; Dohnálek, Z.; Kimmel, G. A.; Petrik, N. G.; Lyubinetsky, I., Adsorption and Photodesorption of CO from Charged Point Defects on TiO₂(110). *J. Phys. Chem. Lett.* **2017**, *8*, 4565-4572. <http://dx.doi.org/10.1021/acs.jpcclett.7b02052>.
44. Nguyen, M.-T.; Mu, R.; Cantu, D. C.; Lyubinetsky, I.; Glezakou, V.-A.; Dohnálek, Z.; Rousseau, R., Dynamics, Stability, and Adsorption States of Water on Oxidized RuO₂(110). *J. Phys. Chem. C* **2017**, *121*, 18505-18515. <http://dx.doi.org/10.1021/acs.jpcc.7b03280>.
45. Shi, H.; Eckstein, S.; Vjunov, A.; Camaioni, D. M.; Lercher, J. A., Tailoring nanoscopic confines to maximize catalytic activity of hydronium ions. *Nat. Commun.* **2017**, *8*, 15442. <http://dx.doi.org/10.1038/ncomms15442>.
46. Vasiliu, M.; Peterson, K. A.; Arduengo, A. J.; Dixon, D. A., Characterization of Carbenes via Hydrogenation Energies, Stability, and Reactivity: What's in a Name? *Chem. Eur. J.* **2017**, *23*, 17556-17565. <http://dx.doi.org/10.1002/chem.201703539>.
47. Wang, M.; Shi, H.; Camaioni, D. M.; Lercher, J. A., Palladium-Catalyzed Hydrolytic Cleavage of Aromatic C-O Bonds. *Angew. Chem., Int. Ed.* **2017**, *56*, 2110-2114. <http://dx.doi.org/10.1002/anie.201611076>.
48. Wang, X.; Shi, H.; Szanyi, J., Controlling selectivities in CO₂ reduction through mechanistic understanding. *Nat. Commun.* **2017**, *8*, 513. <http://dx.doi.org/10.1038/s41467-017-00558-9>.
49. Wang, Z. T.; Wang, Y. G.; Mu, R.; Yoon, Y. H.; Dahal, A.; Schenter, G. K.; Glezakou, V. A.; Rousseau, R.; Lyubinetsky, I.; Dohnalek, Z., Probing Equilibrium of Molecular and Deprotonated Water on TiO₂(110). *Proc. Natl. Acad. Sci. U. S. A.* **2017**, *114*, 1801-1805. <http://dx.doi.org/10.1073/pnas.1613756114>.

50. Zhang, S.; Appel, A. M.; Bullock, R. M., Reversible Heterolytic Cleavage of the H–H Bond by Molybdenum Complexes: Controlling the Dynamics of Exchange Between Proton and Hydride. *J. Am. Chem. Soc.* **2017**, *139*, 7376-7387. <http://dx.doi.org/10.1021/jacs.7b03053>.
51. Zhao, Z.; Shi, H.; Wan, C.; Hu, M. Y.; Liu, Y.; Mei, D.; Camaioni, D. M.; Hu, J. Z.; Lercher, J. A., Mechanism of Phenol Alkylation in Zeolite H-BEA Using In Situ Solid-State NMR Spectroscopy. *J. Am. Chem. Soc.* **2017**, *139*, 9178-9185. <http://dx.doi.org/10.1021/jacs.7b02153>.

2018

52. Andrews, L.; Cho, H.-G.; Fang, Z.; Vasiliu, M.; Dixon, D. A., Tungsten Hydride Phosphorus- and Arsenic-Bearing Molecules with Double and Triple W–P and W–As Bonds. *Inorg. Chem.* **2018**, *57*, 5320-5332. <http://dx.doi.org/10.1021/acs.inorgchem.8b00348>.
53. Baxter, A. F.; Schaab, J.; Hegge, J.; Saal, T.; Vasiliu, M.; Dixon, D. A.; Haiges, R.; Christe, K. O., α -Fluoroalcohols: Synthesis and Characterization of Perfluorinated Methanol, Ethanol and n-Propanol, and their Oxonium Salts. *Chem. Eur. J.* **2018**, *24*, 16737-16742. <http://dx.doi.org/10.1002/chem.201804306>.
54. Baylon, R. A. L.; Sun, J.; Kovarik, L.; Engelhard, M.; Li, H.; Winkelman, A. D.; Martin, K. J.; Wang, Y., Structural Identification of $Zn_xZr_yO_z$ Catalysts for Cascade Aldolization and Self-Deoxygenation Reactions. *Appl. Catal. B* **2018**, *234*, 337-346. <http://dx.doi.org/10.1016/j.apcatb.2018.04.051>.
55. Cassidy, S. J.; Brettell-Adams, I.; McNamara, L. E.; Smith, M. F.; Bautista, M.; Cao, H.; Vasiliu, M.; Gerlach, D. L.; Qu, F.; Hammer, N. I.; Dixon, D. A.; Rupar, P. A., Boranes with Ultra-High Stokes Shift Fluorescence. *Organometallics* **2018**, *37*, 3732-3741. <http://dx.doi.org/10.1021/acs.organomet.8b00460>.
56. Dahal, A.; Mu, R.; Lyubinetsky, I.; Dohnálek, Z., Hydrogen adsorption and reaction on $RuO_2(110)$. *Surf. Sci.* **2018**, *677*, 264-270. <http://dx.doi.org/10.1016/j.susc.2018.07.014>.
57. Eric, W.; John, L., Making a Splash in Homogeneous CO_2 Hydrogenation: Elucidating the Impact of Solvent on Catalytic Mechanisms. *Chem. Eur. J.* **2018**. <http://dx.doi.org/doi:10.1002/chem.201801759>.
58. Fang, Z.; Vasiliu, M.; Peterson, K. A.; Dixon, D. A., Computational Study of Molecular Hydrogen Adsorption over Small $(MO_2)_n$ Nanoclusters (M = Ti, Zr, Hf; n = 1 to 4). *J. Phys. Chem. A* **2018**, *122*, 4338-4349. <http://dx.doi.org/10.1021/acs.jpca.7b12634>. (Computational work and writing of manuscript by Fang, Vasiliu, and Dixon supported by this project.)
59. Glezakou, V.-A.; Rousseau, R., Shedding light on black titania. *Nat. Mater.* **2018**, *17*, 856-857. <http://dx.doi.org/10.1038/s41563-018-0150-1>.
60. Hoffman, A. S.; Debeve, L. M.; Zhang, S.; Perez-Aguilar, J. E.; Conley, E. T.; Justl, K. R.; Arslan, I.; Dixon, D. A.; Gates, B. C., Beating Heterogeneity of Single-Site Catalysts: MgO-Supported Iridium Complexes. *ACS Catal.* **2018**, *8*, 3489-3498. <http://dx.doi.org/10.1021/acscatal.8b00143>. (Computational work and writing of manuscript by Zhang and Dixon supported by this project.)

61. Junk, C. P.; He, Y.; Zhang, Y.; Smith, J. R.; Dixon, D. A.; Vasiliu, M.; Lemal, D. M., Chemistry of the Highly Strained Alkene Perfluorobicyclo[2.2.0]hex-1(4)-ene. *European Journal of Organic Chemistry* **2018**, 2018, 3167-3179. <http://dx.doi.org/10.1002/ejoc.201800058>.
62. Kwon, S.; Deshlahra, P.; Iglesia, E., Dioxygen activation routes in Mars-van Krevelen redox cycles catalyzed by metal oxides. *J. Catal.* **2018**, 364, 228-247. <http://dx.doi.org/10.1016/j.jcat.2018.05.016>.
63. Liu, Y.; Baráth, E.; Shi, H.; Hu, J.; Camaioni, D. M.; Lercher, J. A., Solvent-determined mechanistic pathways in zeolite-H-BEA-catalysed phenol alkylation. *Nat. Catal.* **2018**, 1, 141-147. <http://dx.doi.org/10.1038/s41929-017-0015-z>.
64. Novotny, Z.; Nguyen, M.-T.; Netzer, F. P.; Glezakou, V.-A.; Rousseau, R.; Dohnálek, Z., Formation of Supported Graphene Oxide: Evidence for Enolate Species. *J. Am. Chem. Soc.* **2018**, 140, 5102-5109. <http://dx.doi.org/10.1021/jacs.7b12791>.
65. Shi, D.; Wang, H.; Kovarik, L.; Gao, F.; Wan, C.; Hu, J. Z.; Wang, Y., WO_x supported on γ -Al₂O₃ with different morphologies as model catalysts for alkanol dehydration. *J. Catal.* **2018**, 363, 1-8. <http://dx.doi.org/10.1016/j.jcat.2018.04.004>.
66. Tran, B. L.; Fulton, J. L.; Linehan, J. C.; Lercher, J. A.; Bullock, R. M., Rh(CAAC)-Catalyzed Arene Hydrogenation: Evidence for Nanocatalysis and Sterically Controlled Site-Selective Hydrogenation. *ACS Catal.* **2018**, 8, 8441-8449. <http://dx.doi.org/10.1021/acscatal.8b02589>.
67. Wang, M.; Gutierrez, O. Y.; Camaioni, D. M.; Lercher, J. A., Palladium catalyzed reductive insertion of alcohols in aryl ether bonds. *Angew. Chem., Int. Ed.* **2018**, 57, 3747-3751. <http://dx.doi.org/10.1002/anie.201709445>.
68. Yun, D.; Wang, Y.; Herrera, J., 1-Ethanol partial oxidation over VO_x/TiO₂ catalysts: the role of titania surface oxygen on the vanadia reoxidation in the Mars-van Krevelen mechanism. *ACS Catal.* **2018**, 8, 4681-4693. <http://dx.doi.org/10.1021/acscatal.7b03327>
- 2019**
69. Dutta, A.; Shaw, W. J., Chemical Method for Evaluating Catalytic Turnover Frequencies (TOF) of Moderate to Slow H₂ Oxidation Electrocatalysts. *Organometallics* **2019**, 38, 1311-1316. <http://dx.doi.org/10.1021/acs.organomet.8b00580>.
70. Eckstein, S.; Hintermeier, P. H.; Zhao, R.; Barath, E.; Shi, H.; Liu, Y.; Lercher, J. A., Influence of Hydronium Ions in Zeolites on Sorption. *Angew Chem Int Ed Engl* **2019**, 58, 3450-3455. <http://dx.doi.org/10.1002/anie.201812184>.
71. Li, H.; Sun, J.; Wang, Y., Surface acetone reactions on Zn_xZr_yO_z: A DRIFTS-MS study. *Appl. Catal. A* **2019**, 573, 22-31. <http://dx.doi.org/10.1016/j.apcata.2019.01.007>.
72. Tran, B. L.; Fulton, J. L.; Linehan, J. C.; Balasubramanian, M.; Lercher, J. A.; Bullock, R. M., Operando XAFS Studies on Rh(CAAC)-Catalyzed Arene Hydrogenation. *ACS Catal.* **2019**, 4106-4114. <http://dx.doi.org/10.1021/acscatal.8b04929>.
73. Wang, M.; Jaegers, N. R.; Lee, M.-S.; Wan, C.; Hu, J. Z.; Shi, H.; Mei, D.; Burton, S. D.; Camaioni, D. M.; Gutierrez, O. Y.; Glezakou, V. A.; Rousseau, R.; Wang, Y.; Lercher, J.

- A., Genesis and Stability of Hydronium Ions in Zeolite Channels. *J. Am. Chem. Soc.* **2019**, *141*, 3444-3455. <http://dx.doi.org/10.1021/jacs.8b07969>.
74. Yu, N.; Rahman, M. M.; Chen, J.; Sun, J.; Engelhard, M.; Hernandez, X. I. P.; Wang, Y., Steam reforming of simulated bio-oil on K-Ni-Cu-Mg-Ce-O/Al₂O₃: The effect of K. *Catal. Today* **2019**, *323*, 183-190. <http://dx.doi.org/https://doi.org/10.1016/j.cattod.2018.04.010>.

Publications jointly funded by this grant and other grants with leading intellectual contribution from this grant

2016

75. Alexopoulos, K.; Lee, M.-S.; Liu, Y.; Zhi, Y.; Liu, Y.; Reyniers, M.-F.; Marin, G. B.; Glezakou, V.-A.; Rousseau, R.; Lercher, J. A., Anharmonicity and Confinement in Zeolites: Structure, Spectroscopy, and Adsorption Free Energy of Ethanol in H-ZSM-5. *J. Phys. Chem. C* **2016**, *120*, 7172-7182. <http://dx.doi.org/10.1021/acs.jpcc.6b00923>. (MS Lee, VA Glezakou, R Rousseau, and JA Lercher were supported by the BES project. MSL and VAG performed calculations. RR and JAL participated in the interpretation of the results, in the postulation of hypotheses, and in the drafting of the manuscript.)
76. Asthagiri, A.; Dixon, D. A.; Dohnálek, Z.; Kay, B. D.; Rodriguez, J. A.; Rousseau, R.; Stachiola, D. J.; Weaver, J. F. *Catalytic Chemistry on Oxide Nanostructures in Oxide Materials at the Two-Dimensional Limit*; Netzer, P. F., Fortunelli, A., Eds.; Springer International Publishing: Cham, 2016; pp 251-280.
77. Cardenas, A. J. P.; Ginovska, B.; Kumar, N.; Hou, J.; Raugei, S.; Helm, M. L.; Appel, A. M.; Bullock, R. M.; O'Hagan, M., Controlling Proton Delivery through Catalyst Structural Dynamics. *Angew. Chem., Int. Ed.* **2016**, *55*, 13509-13513. <http://dx.doi.org/10.1002/anie.201607460>. (BB. Ginovska was supported by this program for doing MD simulations and manuscript preparation.)
78. Comish, A. J.; Ginovska, B.; Thelen, A.; da Silva, J. C. S.; Soares, T. A.; Raugei, S.; Dupuis, M.; Shaw, W. J.; Hegg, E. L., Single-Amino Acid Modifications Reveal Additional Controls on the Proton Pathway of FeFe -Hydrogenase. *Biochemistry* **2016**, *55*, 3165-3173. <http://dx.doi.org/10.1021/acs.biochem.5b01044>. (Single-Amino Acid Modifications Reveal Additional Controls on the Proton Pathway of FeFe -Hydrogenase.)
79. Dutta, A.; Ginovska, B.; Raugei, S.; Roberts, J. A.; Shaw, W. J., Optimizing conditions for utilization of an H₂ oxidation catalyst with outer coordination sphere functionalities. *Dalton Trans* **2016**, *45*, 9786-93. <http://dx.doi.org/10.1039/c6dt00280c>. (AD, BG, WS designed and performed the experiments, analyzed and interpreted data and wrote the paper.)
80. Fang, Z.; Thanthiriwatte, K. S.; Dixon, D. A.; Andrews, L.; Wang, X., Properties of Cerium Hydroxides from Matrix Infrared Spectra and Electronic Structure Calculations. *Inorg. Chem.* **2016**, *55*, 1702-1714. <http://dx.doi.org/10.1021/acs.inorgchem.5b02619>. (DA Dixon and Z. Fang supported by this program for computational work on Ce compounds and writing the manuscript.)

81. Fang, Z. T.; Both, J.; Li, S. G.; Yue, S. W.; Apra, E.; Keceli, M.; Wagner, A. F.; Dixon, D. A., Benchmark Calculations of Energetic Properties of Groups 4 and 6 Transition Metal Oxide Nanoclusters Including Comparison to Density Functional Theory. *J. Chem. Theory Comput.* **2016**, *12*, 3689-3710. <http://dx.doi.org/10.1021/acs.jctc.6b00464>. (DA Dixon Z. Fang, and J. Both supported by this program for most of the computational work and writing the manuscript.)
82. Fang, Z. T.; Lee, Z.; Peterson, K. A.; Dixon, D. A., Use of Improved Orbitals for CCSD(T) Calculations for Predicting Heats of Formation of Group IV and Group VI Metal Oxide Monomers and Dimers and UCl₆. *J. Chem. Theory Comput.* **2016**, *12*, 3583-3592. <http://dx.doi.org/10.1021/acs.jctc.6b00327>. (DA Dixon and Z. Fang supported by this program for computational work on Group 4 and 6 compounds and writing the manuscript.)
83. Feller, D.; Peterson, K. A.; Dixon, D. A. The Impact of Larger Basis Sets and Explicitly Correlated Coupled Cluster Theory on the Feller-Peterson-Dixon Composite Method in Annual Reports in Computational Chemistry; Dixon, D. A., Ed.; Elsevier: Amsterdam, 2016; Vol. 12.
84. Finney, B.; Fang, Z.; Francisco, J. S.; Dixon, D. A., Energetic Properties and Electronic Structure of [Si,N,S] and [Si,P,S] Isomers. *J. Phys. Chem. A* **2016**, *120*, 1691-1697. <http://dx.doi.org/10.1021/acs.jpca.6b00918>. (DA Dixon and Z. Fang supported by this program for computational work on title compounds and writing the manuscript.)
85. Ginovska, B.; Raugei, S.; Shaw, W. J. Molecular Dynamics Studies of Proton Transport in Hydrogenase and Hydrogenase Mimics in Computational Approaches for Studying Enzyme Mechanism, Pt B; Voth, G. A., Ed., 2016; Vol. 578; pp 73-101.
86. Haiges, R.; Vasiliu, M.; Dixon, D. A.; Christe, K. O., The niobium oxoazides [NbO(N3)3], [NbO(N3)3.2CH3CN], [(bipy)NbO(N3)3], Cs₂[NbO(N3)5] and [PPh₄]₂[NbO(N3)5]. *Dalton Trans* **2016**, *45*, 10523-9. <http://dx.doi.org/10.1039/c6dt01479h>. (DA Dixon and M. Vasiliu supported by this program for all computational work and writing the manuscript.)
87. Henderson, M. A.; Chen, J. G.; Dohnálek, Z., Editorial: Insights into Surface Phenomena: In Honor of John T. Yates Jr. *Surf. Sci.* **2016**, *652*, 1. <http://dx.doi.org/10.1016/j.susc.2016.06.017>. (Z Dohnálek and MA Henderson were funded by this FWP to prepare this Editorial.)
88. Kelley, S. P.; McCrary, P. D.; Flores, L.; Garner, E. B.; Dixon, D. A.; Rogers, R. D., Structural and Theoretical Study of Salts of the B₉H₁₄⁻ Ion: Isolation of Multiple Isomers and Implications for Energy Storage. *Chempluschem* **2016**, *81*, 922-925. <http://dx.doi.org/10.1002/cplu.201600270>. (DA Dixon, L Flores, and EB Garner supported by this program for all computational work and writing the manuscript.)
89. Kwak, J. H.; Lee, J.; Szanyi, J.; Peden, C. H. F., Modification of the acid/base properties of γ -Al₂O₃ by oxide additives: An ethanol TPD investigation. *Catal. Today* **2016**, *265*, 240-244. <http://dx.doi.org/10.1016/j.cattod.2015.07.042>. (J.Szanyi was supported by this program to participate in the experimental design, data interpretation and in the preparation of the manuscript.)
90. Laminack, W.; Gole, J. L.; White, M. G.; Ozdemir, S.; Ogden, A. G.; Martin, H. J.; Fang, Z.; Wang, T.-H.; Dixon, D. A., Synthesis of nanoscale silicon oxide oxidation state

- distributions: The transformation from hydrophilicity to hydrophobicity. *Chem. Phys. Lett.* **2016**, *653*, 137-143. <http://dx.doi.org/10.1016/j.cplett.2016.04.079>. (DA Dixon, TH Wang and Z. Fang supported by this program for all computational work and writing the manuscript.)
91. Lao, D. B.; Galan, B. R.; Linehan, J. C.; Heldebrant, D. J., The steps of activating a prospective CO₂ hydrogenation catalyst with combined CO₂ capture and reduction. *Green Chem.* **2016**, *18*, 4871-4874. <http://dx.doi.org/10.1039/c6gc01800a>. (JC Linehan and BR Galan were supported by this program to perform operando catalysis studies and interpret the corresponding data.)
 92. Lee, M. S.; Um, W.; Wang, G.; Kruger, A. A.; Lukens, W. W.; Rousseau, R.; Glezakou, V. A., Impeding (⁹⁹Tc(IV) mobility in novel waste forms. *Nat. Commun.* **2016**, *7*, 12067. <http://dx.doi.org/10.1038/ncomms12067>. (M.-S.L. contributed to the planning and executed the simulations and analysed the data, W.U., G.W. and W.W.L. performed the experiments and related data analysis. R.R. provided pseudopotentials for the calculations and contributed to the analysis of the data. V.-A.G. planned and supervised the research. M.-S.L., R.R. and V.-A.G. jointly wrote the manuscript with input from all authors.)
 93. Peroni, M.; Mancino, G.; Baráth, E.; Gutiérrez, O. Y.; Lercher, J. A., Bulk and γ -Al₂O₃-supported Ni₂P and MoP for hydrodeoxygenation of palmitic acid. *Appl. Catal. B* **2016**, *180*, 301-311. <http://dx.doi.org/10.1016/j.apcatb.2015.06.042>. (Supported by the BES project, JA Lercher participated in the interpretation of the results, in the postulation of hypotheses, and in the drafting of the manuscript.)
 94. Priyadarshani, N.; Dutta, A.; Ginovska, B.; Buchko, G. W.; O'Hagan, M.; Raugei, S.; Shaw, W. J., Achieving Reversible H₂/H⁺ Interconversion at Room Temperature with Enzyme-Inspired Molecular Complexes: A Mechanistic Study. *ACS Catal.* **2016**, *6*, 6037-6049. <http://dx.doi.org/10.1021/acscatal.6b01433>. (NP, AD, BG,GB, WS designed and performed the experiments, analyzed and interpreted data and wrote the paper.)
 95. Proding, S.; Derewinski, M. A.; Vjunov, A.; Burton, S. D.; Arslan, I.; Lercher, J. A., Improving Stability of Zeolites in Aqueous Phase via Selective Removal of Structural Defects. *J. Am. Chem. Soc.* **2016**, *138*, 4408-4415. <http://dx.doi.org/10.1021/jacs.5b12785>. (A Vjunov, SA Burton, I Arslan and J ALercher were supported by this program. SAB contribute to NMR measurements, AV participated in the preparation of the manuscript, IA carried our TEM measurements and JAL participate in data evaluation and manuscript preparation.)
 96. Pruski, M.; Sadow, A. D.; Slowing, I. I.; Marshall, C. L.; Stair, P.; Rodriguez, J.; Harris, A.; Somorjai, G. A.; Biener, J.; Matranga, C.; Wang, C.; Schaidle, J. A.; Beckham, G. T.; Ruddy, D. A.; Deutsch, T.; Alia, S. M.; Narula, C.; Overbury, S.; Toops, T.; Bullock, R. M.; Peden, C. H. F.; Wang, Y.; Allendorf, M. D.; Nørskov, J.; Bligaard, T., Virtual Special Issue on Catalysis at the U.S. Department of Energy's National Laboratories. *ACS Catal.* **2016**, *6*, 3227-3235. <http://dx.doi.org/10.1021/acscatal.6b00823>.
 97. Reback, M. L.; Ginovska, B.; Buchko, G. W.; Dutta, A.; Priyadarshani, N.; Kier, B. L.; Helm, M. L.; Raugei, S.; Shaw, W. J., Investigating the role of chain and linker length on the catalytic activity of an H₂ production catalyst containing beta-hairpin peptide. *J. Coord. Chem.* **2016**, *69*, 1730-1747. <http://dx.doi.org/10.1080/00958972.2016.1188924>. (BG, GB,

- AD, NP, WS designed and performed the calculations and supporting experiments, analyzed and interpreted data and wrote the paper.)
98. Rodriguez-Macia, P.; Priyadarshani, N.; Dutta, A.; Weidenthaler, C.; Lubitz, W.; Shaw, W. J.; Rudiger, O., Covalent Attachment of the Water-insoluble Ni(P^{Cy2}N^{Phe2})₂ Electrocatalyst to Electrodes Showing Reversible Catalysis in Aqueous Solution. *Electroanalysis* **2016**, *28*, 2452-2458. <http://dx.doi.org/10.1002/elan.201600306>. (AD and WS provided the molecular complex, assisted in interpreting data and co-wrote the paper.)
 99. Schreiber, M. W.; Rodriguez-Nino, D.; Gutierrez, O. Y.; Lercher, J. A., Hydrodeoxygenation of fatty acid esters catalyzed by Ni on nano-sized MFI type zeolites. *Catal. Sci. Technol.* **2016**, *6*, 7976-7984. <http://dx.doi.org/10.1039/c6cy01598k>. (Funded by this BES project, JA Lercher participated in the interpretation of the results, in the postulation of hypotheses, and in the drafting of the manuscript.)
 100. Song, W.; Liu, Y.; Baráth, E.; Wang, L. L.; Zhao, C.; Mei, D.; Lercher, J. A., Dehydration of 1-Octadecanol over H-BEA: A Combined Experimental and Computational Study. *ACS Catal.* **2016**, *6*, 878-889. <http://dx.doi.org/10.1021/acscatal.5b01217>. (LL Wang, D Mei, and JA Lercher were supported by the BES project. LLW and DM performed first-principle computations. JAL participated in the interpretation of the results, in the postulation of hypotheses, and in the drafting of the manuscript.)
 101. Song, Y.; Gutiérrez, O. Y.; Herranz, J.; Lercher, J. A., Aqueous phase electrocatalysis and thermal catalysis for the hydrogenation of phenol at mild conditions. *Appl. Catal. B* **2016**, *182*, 236-246. <http://dx.doi.org/https://doi.org/10.1016/j.apcatb.2015.09.027>. (Supported by this project, JA Lercher participated in the interpretation of the results, in the postulation of hypotheses, and in the drafting of the manuscript.)
 102. Wang, W. Y.; Wu, K.; Liu, P. L.; Li, L.; Yang, Y. Q.; Wang, Y., Hydrodeoxygenation of p-Cresol over Pt/Al₂O₃ Catalyst Promoted by ZrO₂, CeO₂, and CeO₂-ZrO₂. *Ind. Eng. Chem. Res.* **2016**, *55*, 7598-7603. <http://dx.doi.org/10.1021/acs.iecr.6b00515>. (Y.Wang participated in the interpretation of results and writing the paper.)
 103. Wiedner, E. S.; Chambers, M. B.; Pitman, C. L.; Bullock, R. M.; Miller, A. J. M.; Appel, A. M., Thermodynamic Hydricity of Transition Metal Hydrides. *Chem. Rev.* **2016**, *116*, 8655-8692. <http://dx.doi.org/10.1021/acs.chemrev.6b00168>. (ES Wiedner and AM Appel were supported by this program to tabulate thermochemical values and participate in the manuscript preparation.)
 104. Xu, S.; Zhao, Z.; Hu, M. Y.; Han, X.; Hu, J. Z.; Bao, X., Investigation of water assisted phase transformation process from AlPO₄-5 to AlPO₄-tridymite. *Microporous Mesoporous Mat.* **2016**, *223*, 241-246. <http://dx.doi.org/10.1016/j.micromeso.2015.10.039>. (J. Z. Hu , S. Xu, Z. Zhao and M. Hu were supported by this program for conducting the NMR experiments and participate in the preparation of the manuscript. In particular J. Z. Hu provided the NMR mentorship to S. Xu.)
 105. Yu, X. J.; Zhang, Z. R.; Yang, C. W.; Bebensee, F.; Heissler, S.; Nefedov, A.; Tang, M. R.; Ge, Q. F.; Chen, L.; Kay, B. D.; Dohnalek, Z.; Wang, Y. M.; Woll, C., Interaction of Formaldehyde with the Rutile TiO₂(110) Surface: A Combined Experimental and Theoretical Study. *J. Phys. Chem. C* **2016**, *120*, 12626-12636.

- <http://dx.doi.org/10.1021/acs.jpcc.6b03689>. (L Cheng, BD Kay, and Z Dohnalek were funded by this FWP. LC carried out the TPD measurements, BDK and ZD guided TPD experiments, put forward data interpretations, and contributed to the manuscript preparation.)
106. Zhang, S. G.; Li, H. X.; Appel, A. M.; Hall, M. B.; Bullock, R. M., Facile P-C/C-H Bond-Cleavage Reactivity of Nickel Bis(diphosphine) Complexes. *Chem.-Eur. J.* **2016**, *22*, 9493-9497. <http://dx.doi.org/10.1002/chem.201601469>. (SG Zhang, AM Appel, and RM Bullock were supported by this project to perform and interpret all experimental data, as well as prepare the manuscript.)
- 2017**
107. Agirrezabal-Telleria, I.; Iglesia, E., Stabilization of active, selective, and regenerable Ni-based dimerization catalysts by condensation of ethene within ordered mesopores. *J. Catal.* **2017**, *352*, 505-514. <http://dx.doi.org/10.1016/j.jcat.2017.06.025>. (IA stipend was covered by a Marie Curie Fellowship. Most of the materials expenses and all of EI time were covered by this project.)
108. Burgess, S. A.; Kendall, A. J.; Tyler, D. R.; Linehan, J. C.; Appel, A. M., Hydrogenation of CO₂ in Water Using a Bis(diphosphine) Ni-H Complex. *ACS Catal.* **2017**, *7*, 3089-3096. <http://dx.doi.org/10.1021/acscatal.7b00350>. (SA Burgess, JC Linehan, and AM Appel were supported by this project to perform and interpret all catalytic and thermodynamic data, as well as prepare the manuscript.)
109. Chen, M.; Dixon, D. A., Modeling the formation of TiO₂ ultra-small nanoparticles. *Nanoscale* **2017**, *9*, 7143-7162. <http://dx.doi.org/10.1039/C7NR01749A>. (DA Dixon supported by this program for data analysis and writing the manuscript.)
110. Christe, K. O.; Haiges, R.; Rahm, M.; Dixon, D. A.; Vasiliu, M., Misconceptions on fluoronium ions and hypervalent fluorine cations. *J. Fluorine Chem.* **2017**, *204*, 6-10. <http://dx.doi.org/10.1016/j.jfluchem.2017.09.011>. (DA Dixon and M. Vasiliu supported by this program for most of the computational work and writing the manuscript.)
111. Christe, K. O.; Haiges, R.; Vasiliu, M.; Dixon, D. A., Formation Mechanism of NF₄⁺ Salts and Extraordinary Enhancement of the Oxidizing Power of Fluorine by Strong Lewis Acids. *Angew. Chem., Int. Ed.* **2017**. <http://dx.doi.org/10.1002/anie.201701784>. (DA Dixon and M. Vasiliu supported by this program for all computational work and writing the manuscript.)
112. Eckstein, S.; Hintermeier, P. H.; Olarte, M. V.; Liu, Y.; Baráth, E.; Lercher, J. A., Elementary steps and reaction pathways in the aqueous phase alkylation of phenol with ethanol. *J. Catal.* **2017**, *352*, 329-336. <http://dx.doi.org/10.1016/j.jcat.2017.06.002>. (Funded by this BES project, JA Lercher contributed to the interpretation of the data and manuscript preparation.)
113. Fang, Z. T.; Vasiliu, M.; Peterson, K. A.; Dixon, D. A., Prediction of Bond Dissociation Energies/Heats of Formation for Diatomic Transition Metal Compounds: CCSD(T) Works. *J. Chem. Theory Comput.* **2017**, *13*, 1057-1066. <http://dx.doi.org/10.1021/acs.jctc.6b00971>. (DA Dixon and M. Vasiliu supported by this program for all computational work and writing the manuscript.)

114. Feng, R. L.; Vasiliu, M.; Peterson, K. A.; Dixon, D. A., Acidity of $M(VI)O_2(OH)_2$ for $M =$ Group 6, 16, and U as Central Atoms. *J. Phys. Chem. A* **2017**, *121*, 1041-1050. <http://dx.doi.org/10.1021/acs.jpca.6b11889>. (DA Dixon and M. Vasiliu supported by this program for computational work on Group 6 and 16 and writing the manuscript.)
115. Foraita, S.; Liu, Y.; Haller, G. L.; Barath, E.; Zhao, C.; Lercher, J. A., Controlling Hydrodeoxygenation of Stearic Acid to n-Heptadecane and n-Octadecane by Adjusting the Chemical Properties of Ni/SiO₂-ZrO₂ Catalyst. *Chemcatchem* **2017**, *9*, 195-203. <http://dx.doi.org/10.1002/cctc.201601162>. (Supported by this project to explore oxidic supports for deoxygenation, JA Lercher participated in the interpretation of the results, in the postulation of hypotheses, and in the drafting of the manuscript.)
116. Gentil, S.; Lalaoui, N.; Dutta, A.; Nedellec, Y.; Cosnier, S.; Shaw, W. J.; Artero, V.; Le Goff, A., Carbon-Nanotube-Supported Bio-Inspired Nickel Catalyst and Its Integration in Hybrid Hydrogen/Air Fuel Cells. *Angew. Chem., Int. Ed.* **2017**, *56*, 1845-1849. <http://dx.doi.org/10.1002/anie.201611532>. (AD and WS provided the molecular complex, assisted in interpreting data and co-wrote the paper.)
117. Hintermeier, P. H.; Eckstein, S.; Mei, D.; Olarte, M. V.; Camaioni, D. M.; Baráth, E.; Lercher, J. A., Hydronium-Ion-Catalyzed Elimination Pathways of Substituted Cyclohexanols in Zeolite H-ZSM5. *ACS Catal.* **2017**, *7*, 7822-7829. <http://dx.doi.org/10.1021/acscatal.7b01582>. (Supported by this project, JA Lercher participated in the interpretation of the results, in the postulation of hypotheses, and in the drafting of the manuscript.)
118. Hoffman, A. S.; Sokaras, D.; Zhang, S.; Debeve, L. M.; Fang, C.-Y.; Gallo, A.; Kroll, T.; Dixon, D. A.; Bare, S. R.; Gates, B. C., High-Energy-Resolution X-ray Absorption Spectroscopy for Identification of Reactive Surface Species on Supported Single-Site Iridium Catalysts. *Chem. Eur. J.* **2017**, *23*, 14760-14768. <http://dx.doi.org/10.1002/chem.201701459>. (Computational work and writing of manuscript by Zhang and Dixon supported by this project.)
119. Jeletic, M. S.; Hulley, E. B.; Helm, M. L.; Mock, M. T.; Appel, A. M.; Wiedner, E. S.; Linehan, J. C., Understanding the Relationship Between Kinetics and Thermodynamics in CO₂ Hydrogenation Catalysis. *ACS Catal.* **2017**, *7*, 6008-6017. <http://dx.doi.org/10.1021/acscatal.7b01673>. (MS Jeletic, AM Appel, ES Wiedner, and JC Linehan were supported by this program to perform catalysis and thermodynamic measurements, and to prepare the manuscript.)
120. Li, W. Z.; Kovarik, L.; Cheng, Y. W.; Nie, L.; Bowden, M. E.; Liu, J.; Wang, Y., Stabilization and transformation of Pt nanocrystals supported on ZnAl₂O₄ spinel. *Rsc Advances* **2017**, *7*, 3282-3286. <http://dx.doi.org/10.1039/c6ra26159k>. (W.Li performed most experimental studies, Y.Wang and J.Liu participated in the interpretation of the results and drafting the manuscript.)
121. Mu, R.; Zhao, Z.-j.; Dohnalek, Z.; Gong, J., Structural motifs of water on metal oxide surfaces. *Chem. Soc. Rev.* **2017**, *46*, 1785-1806. <http://dx.doi.org/10.1039/C6CS00864J>. (Z Dohnálek was funded by this FWP to contribute to this Review.)
122. Nie, L.; Mei, D.; Xiong, H.; Peng, B.; Ren, Z.; Isidro Pereira Hernandez, X.; DeLaRiva, A.; Wang, M.; Engelhard, M.; Kovarik, L.; Datye, A.; Wang, Y., Activation of surface

- lattice oxygen in single-atom Pt/CeO₂ for low-temperature CO oxidation. *Science* **2017**, 358, 1419-1423. <http://dx.doi.org/10.1126/science.aao2109>. (D.MeI performed DFT calculations and Y.Wang participated in the interpretation of results.)
123. Novotny, Z.; Zhang, Z.; Dohnálek, Z., Imaging Chemical Reactions One Molecule at a Time. *Reference Module in Chemistry, Molecular Sciences and Chemical Engineering* **2017**. <http://dx.doi.org/10.1016/B978-0-12-409547-2.12844-6>. (Z Dohnálek was funded by this FWP to contribute to this Review.)
124. Peroni, M.; Lee, I.; Huang, X.; Baráth, E.; Gutiérrez, O. Y.; Lercher, J. A., Deoxygenation of Palmitic Acid on Unsupported Transition-Metal Phosphides. *ACS Catal.* **2017**, 7, 6331-6341. <http://dx.doi.org/10.1021/acscatal.7b01294>. (Supported by this project to explore nonoxidic supports for deoxygenation, JA Lercher participated in the interpretation of the results, in the postulation of hypotheses, and in the drafting of the manuscript.)
125. Proding, S.; Shi, H.; Eckstein, S.; Hu, J. Z.; Olarte, M. V.; Camaioni, D. M.; Derewinski, M. A.; Lercher, J. A., Stability of Zeolites in Aqueous Phase Reactions. *Chem. Mater.* **2017**, 29, 7255-7262. <http://dx.doi.org/10.1021/acs.chemmater.7b01847>. (S Hui, H Eckstein, JZ Hu, M V Olarte D M Camaioni and J A Lercher were supported by this program for exploring acidic supports for deoxygenation reactions and NMR experiments. SH participate in catalytic tests, HE contribute to measurement of sorption properties, JZH participated in the NMR measurements, MVO was involved in catalytic measurements and JAL in data interpretation and preparation of the manuscript.)
126. Resende, K. A.; Hori, C. E.; Noronha, F. B.; Shi, H.; Gutierrez, O. Y.; Camaioni, D. M.; Lercher, J. A., Aqueous phase hydrogenation of phenol catalyzed by Pd and PdAg on ZrO₂. *Applied Catalysis. A, General* **2017**, Medium: X; Size: p. 128-135. <http://dx.doi.org/10.1016/j.apcata.2017.08.005>. (H.S., O.Y.G., D.M.C. and J.A.L were supported by this program and participated in the interpretation of the results, in the postulation of hypotheses ultimately confirmed, and in the drafting of the manuscript. K.A.R. and C.E.H. were supported by the National Council for Scientific and Technological Development (CNPq, Conselho Nacional de Desenvolvimento Científico e Tecnológico) of the Brazilian federal government under the Ministry of Science and Technology.)
127. Vasiliu, M.; Peterson, K. A.; Dixon, D. A., Benchmark-Quality Atomization Energies for BeH and BeH₂. *J. Chem. Theory Comput.* **2017**, 13, 649-653. <http://dx.doi.org/10.1021/acs.jctc.6b01154>. (DA Dixon and M. Vasiliu supported by this program for most of the computational work and writing the manuscript.)
128. Vjunov, A.; Wang, M.; Govind, N.; Huthwelker, T.; Shi, H.; Mei, D.; Fulton, J. L.; Lercher, J. A., Tracking the Chemical Transformations at the Brønsted Acid Site upon Water-Induced Deprotonation in a Zeolite Pore. *Chem. Mater.* **2017**, 29, 9030-9042. <http://dx.doi.org/10.1021/acs.chemmater.7b02133>. (A Vjunov, JL Fulton, D Mei, H Shi and JA Lercher were supported by the BES project. AV and JAL performed X-ray absorption spectroscopy measurements. AV performed Infrared spectroscopy measurements. DM performed first principle calculations. JAL and JLF contributed to the interpretation of the results, in the postulation of hypotheses, and in the drafting of the manuscript.)

129. Wagenhofer, M. F.; Barath, E.; Gutierrez, O. Y.; Lercher, J. A., Carbon-Carbon Bond Scission Pathways in the Deoxygenation of Fatty Acids on Transition-Metal Sulfides. *ACS Catal.* **2017**, *7*, 1068-1076. <http://dx.doi.org/10.1021/acscatal.6b02753>. (JAL was supported by this program. MFW, EB, OYG were support by the German Federal Ministry of Food and Agriculture.)
130. Wei, R.; Li, Q.; Gong, Y.; Andrews, L.; Fang, Z.; Thanthiriwatte, K. S.; Vasiliu, M.; Dixon, D. A., Infrared Spectroscopic and Theoretical Studies on the OMF₂ and OMF (M = Cr, Mo, W) Molecules in Solid Argon. *J. Phys. Chem. A* **2017**, *121*, 7603-7612. <http://dx.doi.org/10.1021/acs.jpca.7b08088>. (DA Dixon KS Thanthiriwatte, and M Vasiliu supported by this program for all computational work and writing the manuscript.)
131. Xu, C.-Q.; Lee, M.-S.; Wang, Y.-G.; Cantu, D. C.; Li, J.; Glezakou, V.-A.; Rousseau, R., Structural Rearrangement of Au–Pd Nanoparticles under Reaction Conditions: An ab Initio Molecular Dynamics Study. *ACS Nano* **2017**. <http://dx.doi.org/10.1021/acsnano.6b07409>. (The authors M.S.L., Y.G.W., D.C.C., V.A.G., and R.R. were supported by this program. C.Q.X. and J.L. were financially sponsored by NSFC and NKBRFSF of China.)
132. Yang, D.; Zhang, S.; Xu, P.; Browning, N. D.; Dixon, D. A.; Gates, B. C., Single-Site Osmium Catalysts on MgO: Reactivity and Catalysis of CO Oxidation. *Chem. Eur. J.* **2017**, *23*, 2532-2536. <http://dx.doi.org/10.1002/chem.201605131>. (Computational work and writing of manuscript by Zhang and Dixon supported by this project.)
133. Zhang, S.; Foyle, S. D.; Okrut, A.; Solovyov, A.; Katz, A.; Gates, B. C.; Dixon, D. A., Role of N-Heterocyclic Carbenes as Ligands in Iridium Carbonyl Clusters. *J. Phys. Chem. A* **2017**, *121*, 5029-5044. <http://dx.doi.org/10.1021/acs.jpca.7b04161>. (Computational work and writing of manuscript by Zhang and Dixon supported by this project.)

2018

134. Burks, D. B.; Vasiliu, M.; Dixon, D. A.; Papish, E. T., Thermodynamic Acidity Studies of 6,6'-Dihydroxy-2,2'-bipyridine: A Combined Experimental and Computational Approach. *J. Phys. Chem. A* **2018**, *122*, 2221-2231. <http://dx.doi.org/10.1021/acs.jpca.7b11441>. (DA Dixon and M. Vasiliu supported by this program for all of the computational work and writing the manuscript.)
135. Dutta, A.; Appel, A. M.; Shaw, W. J., Designing electrochemically reversible H₂ oxidation and production catalysts. *Nat. Rev. Chem.* **2018**, *2*, 244-252. <http://dx.doi.org/10.1038/s41570-018-0032-8>. (All authors contributed equally to the preparation of this review which was supported by both EFRC (Appel) and BES (Shaw) funding.)
136. Feller, D.; Dixon, D. A., Density Functional Theory and the Basis Set Truncation Problem with Correlation Consistent Basis Sets: Elephant in the Room or Mouse in the Closet? *J. Phys. Chem. A* **2018**, *122*, 2598-2603. <http://dx.doi.org/10.1021/acs.jpca.8b00392>. (DA Dixon supported by this program for writing the manuscript.)
137. Frederick, R. T.; Novotny, Z.; Netzer, F. P.; Herman, G. S.; Dohnálek, Z., Growth and Stability of Titanium Dioxide Nanoclusters on Graphene/Ru(0001). *J. Phys. Chem. B* **2018**, *122*, 640-648. <http://dx.doi.org/10.1021/acs.jpcc.7b05518>. (Z Novotny and Z Dohnalek were funded by this FWP. ZN took part in the STM measurements, ZD guided the experiments and contributed to the manuscript preparation.)

138. Hensley, A. J. R.; Wang, Y.; Mei, D.; McEwen, J.-S., Mechanistic Effects of Water on the Fe-Catalyzed Hydrodeoxygenation of Phenol. The Role of Brønsted Acid Sites. *ACS Catal.* **2018**, *8*, 2200-2208. <http://dx.doi.org/10.1021/acscatal.7b02576>. (D.MeI performed DFT calculations and Y.Wang participated in the interpretation of results and writing the manuscript.)
139. Maestri, M.; Iglesia, E., First-principles theoretical assessment of catalysis by confinement: NO–O₂ reactions within voids of molecular dimensions in siliceous crystalline frameworks. *Phys. Chem. Chem. Phys.* **2018**, *20*, 15725-15735. <http://dx.doi.org/10.1039/C8CP01615A>. (This publication is based on previous work supported by this grant. Iglesia's contributions were exclusively funded by this grant. Maestri contributions were supported by his own funding at the Politecnico of Milano)
140. Oughli, A. A.; Ruff, A.; Boralugodage, N. P.; Rodríguez-Maciá, P.; Plumeré, N.; Lubitz, W.; Shaw, W. J.; Schuhmann, W.; Rüdiger, O., Dual properties of a hydrogen oxidation Ni-catalyst entrapped within a polymer promote self-defense against oxygen. *Nat. Commun.* **2018**, *9*, 864. <http://dx.doi.org/10.1038/s41467-018-03011-7>. (Shaw was funded by this FWP to help design experiments, interpret data, and write the manuscript. Boralugodage was funded by this FWP to provide complexes.)
141. Prodinge, S.; Shi, H.; Wang, H.; Derewinski, M. A.; Lercher, J. A., Impact of structural defects and hydronium ion concentration on the stability of zeolite BEA in aqueous phase. *Appl. Catal. B* **2018**, *237*, 996-1002. <http://dx.doi.org/10.1016/j.apcatb.2018.06.065>. (JA Lercher was supported by this program as science lead and for writing the manuscript.)
142. Prodinge, S.; Vjunov, A.; Hu, J. Z.; Fulton, J. L.; Camaioni, D. M.; Derewinski, M. A.; Lercher, J. A., Elementary Steps of Faujasite Formation Followed by in Situ Spectroscopy. *Chem. Mater.* **2018**, *30*, 888-897. <http://dx.doi.org/10.1021/acs.chemmater.7b04554>. (A Vjunov and JL Fulton were supported by this program to perform XAFS measurements and contributed to the interpretation of the data, JZ Hu participated in NMR measurements and data evaluation, JL Camaioni and JA Lercher were supported by this program and participated in the evaluation of the data and manuscript preparation.)
143. Xue, N.; Vjunov, A.; Schallmoser, S.; Fulton, J. L.; Sanchez-Sanchez, M.; Hu, J. Z.; Mei, D.; Lercher, J. A., Hydrolysis of zeolite framework aluminum and its impact on acid catalyzed alkane reactions. *J. Catal.* **2018**, *365*, 359-366. <http://dx.doi.org/10.1016/j.jcat.2018.07.015>. (A Vjunov, JL Fulton, JZ Hu, D Mei and JA Lercher were funded by this FWP. A Vjunov, JL Fulton, and JZ Hu perform experimental, X-ray and NMR experiments, respectively. D Mei was supported by this program for the computational work. JA Lercher was supported by this program as science lead and for writing the manuscript.)
144. Yu, Z.; Wang, Y.; Liu, S.; Yao, Y.; Sun, Z.; Li, X.; Liu, Y.; Wang, W.; Wang, A.; Camaioni, D. M.; Lercher, J. A., Aqueous Phase Hydrodeoxygenation of Phenol over Ni₃P-CePO₄ Catalysts. *Ind. Eng. Chem. Res.* **2018**, *57*, 10216-10225. <http://dx.doi.org/10.1021/acs.iecr.8b01606>. (DM Camaioni and JA Lercher were funded by this FWP. DM Camaioni was supported by this program for writing the manuscript and scientific advisor. JA Lercher was supported by this program as science lead and for writing the manuscript.)

145. Yu, Z.; Wang, Y.; Sun, Z.; Li, X.; Wang, A.; Camaioni, D. M.; Lercher, J. A., Ni₃P as a high-performance catalytic phase for the hydrodeoxygenation of phenolic compounds. *Green Chem.* **2018**, *20*, 609-619. <http://dx.doi.org/10.1039/C7GC03262E>. (Supported by this project to explore nonoxidic supports for deoxygenation, J A Lercher and DM Camaioni participated in the interpretation of the results, in the postulation of hypotheses, and in the drafting of the manuscript.)

2019

146. Christe, K. O.; Dixon, D. A.; Vasiliu, M.; Haiges, R.; Hu, B., How Energetic are cyclo-Pentazolates? *Propellants, Explosives, Pyrotechnics* **2019**, *44*, 263-266. <http://dx.doi.org/10.1002/prop.201800351>. (Effort and computational work and writing of manuscript by Vasiliu and Dixon supported by this project.)
147. Denk, C.; Foraita, S.; Kovarik, L.; Stoerzinger, K. A.; Liu, Y.; Barath, E.; Lercher, J. A., Rate enhancement by Cu in Ni_xCu_{1-x}/ZrO₂ bimetallic catalysts for hydrodeoxygenation of stearic acid. *Catal. Sci. Technol.* **2019**. <http://dx.doi.org/10.1039/C9CY00181E>. (C Denk was supported for experimental work. L Kovarik was supported for microscopy characterization. KA Stoerzinger was supported for XPS characterization. JA Lercher was supported as science lead and for writing the manuscript.)
148. Kovarik, L.; Bowden, M.; Shi, D.; Szanyi, J.; Peden, C. H. F., Structural Intergrowth in δ -Al₂O₃. *J. Phys. Chem. C* **2019**, *123*, 9454-9460. <http://dx.doi.org/10.1021/acs.jpcc.8b10135>. (L. Kovarik and J. Szanyi was funded by this program. L. Kovarik designed and carried out all the TEM experiments. J. Szanyi supervised the experimental work and continued to writing the manuscript.)
149. Persaud, R. R.; Chen, M.; Peterson, K. A.; Dixon, D. A., Potential Energy Surface of Group 11 Trimers (Cu, Ag, Au): Bond Angle Isomerism in Au₃. *J. Phys. Chem. A* **2019**, *123*, 1198-1207. <http://dx.doi.org/10.1021/acs.jpca.8b11219>. (Computational work and writing of manuscript by Persaud and Dixon supported by this project.)
150. Walsh, A. P.; Laureanti, J. A.; Katipamula, S.; Chambers, Geoffrey M.; Priyadarshani, N.; Lense, S.; Bays, J. T.; Linehan, J. C.; Shaw, W. J., Evaluating the impacts of amino acids in the second and outer coordination spheres of Rh-bis(diphosphine) complexes for CO₂ hydrogenation. *Faraday Discuss.* **2019**. <http://dx.doi.org/10.1039/C8FD00164B>. (All authors were supported by this FWP, with the exception of Chambers, who provided a ligand and was supported by the EFRC.)
151. Yu, Z.; Wang, A.; Liu, S.; Yao, Y.; Sun, Z.; Li, X.; Liu, Y.; Wang, Y.; Camaioni, D. M.; Lercher, J. A., Hydrodeoxygenation of phenolic compounds to cycloalkanes over supported nickel phosphides. *Catal. Today* **2019**, *319*, 48-56. <http://dx.doi.org/10.1016/j.cattod.2018.05.012>. (DM Camaioni and JA Lercher were funded by this FWP. DM Camaioni was supported by this program for writing the manuscript and scientific advisor. JA Lercher was supported by this program as science lead and for writing the manuscript.)

Publications jointly funded by this grant and other grants with relatively minor intellectual contribution from this grant

2016

152. Bligaard, T.; Bullock, R. M.; Campbell, C. T.; Chen, J. G. G.; Gates, B. C.; Gorte, R. J.; Jones, C. W.; Jones, W. D.; Kitchin, J. R.; Scott, S. L., Toward Benchmarking in Catalysis Science: Best Practices, Challenges, and Opportunities. *ACS Catal.* **2016**, *6*, 2590-2602. <http://dx.doi.org/10.1021/acscatal.6b00183>. (RM Bullock was supported by this program and participated in writing and revising the article, which resulted from discussions at a Catalysis Science PI meeting (DOE-BES).)
153. Callini, E.; Atakli, Z. O. K.; Hauback, B. C.; Orimo, S.; Jensen, C.; Dornheim, M.; Grant, D.; Cho, Y. W.; Chen, P.; Hjorvarsson, B.; de Jongh, P.; Weidenthaler, C.; Baricco, M.; Paskevicius, M.; Jensen, T. R.; Bowden, M. E.; Autrey, T. S.; Zuttel, A., Complex and liquid hydrides for energy storage. *Appl. Phys. A-Mater. Sci. Process.* **2016**, *122*. <http://dx.doi.org/10.1007/s00339-016-9881-5>. (T Autrey contributed to section of complex hydrides for this review article.)
154. Deokar, P.; Leitz, D.; Stein, T. H.; Vasiliu, M.; Dixon, D. A.; Christe, K. O.; Haiges, R., Preparation and Characterization of Antimony and Arsenic Tricyanide and Their 2,2'-Bipyridine Adducts. *Chem.-Eur. J.* **2016**, *22*, 13251-13257. <http://dx.doi.org/10.1002/chem.201602436>. (DA Dixon, TH Stein, and M. Vasiliu supported by this program for all computational work and writing the manuscript.)
155. Deokar, P.; Vasiliu, M.; Dixon, D. A.; Christe, K. O.; Haiges, R., The Binary Group 4 Azides [PPh₄]₂[Zr(N₃)₆] and [PPh₄]₂[Hf(N₃)₆]. *Angew. Chem., Int. Ed.* **2016**, *55*, 14348-14352. <http://dx.doi.org/10.1002/anie.201609195>. (DA Dixon, TH Stein, and M. Vasiliu supported by this program for all computational work and writing the manuscript.)
156. Du, Y.; Li, G.; Peterson, E. W.; Zhou, J.; Zhang, X.; Mu, R.; Dohnalek, Z.; Bowden, M.; Lyubinetsky, I.; Chambers, S. A., Iso-oriented monolayer α -MoO₃(010) films epitaxially grown on SrTiO₃(001). *Nanoscale* **2016**, *8*, 3119-3124. <http://dx.doi.org/10.1039/C5NR07745A>. (R Mu, I Lyubinetsky, and Z Dohnalek were funded by this FWP. RM took part in the STM measurements, IL and ZD contributed to the manuscript preparation.)
157. Kaneza, N.; Zhang, J.; Liu, H.; Archana, P. S.; Shan, Z.; Vasiliu, M.; Polansky, S. H.; Dixon, D. A.; Adams, R. E.; Schmehl, R. H.; Gupta, A.; Pan, S., Electrochemical and Spectroscopic Properties of Boron Dipyrromethene–Thiophene–Triphenylamine-Based Dyes for Dye-Sensitized Solar Cells. *J. Phys. Chem. C* **2016**, *120*, 9068-9080. <http://dx.doi.org/10.1021/acs.jpcc.6b01611>. (DA Dixon, SH Polansky, and M. Vasiliu supported by this program for all computational work and writing the manuscript.)
158. Kim, B.; Dohnálek, Z.; Szanyi, J.; Kay, B. D.; Kim, Y. K., Temperature-programmed desorption study of NO reactions on rutile TiO₂(110)-1 × 1. *Surf. Sci.* **2016**, *652*, 148-155. <http://dx.doi.org/10.1016/j.susc.2016.01.032>. (J.Szanyi was supported by this program to participate in the data interpretation and in the preparation of the manuscript.)
159. Liu, X. G.; Zhang, Y. Z.; Li, B.; Zakharov, L. N.; Vasiliu, M.; Dixon, D. A.; Liu, S. Y., A Modular Synthetic Approach to Monocyclic 1,4-Azaborines. *Angew. Chem., Int. Ed.* **2016**,

- 55, 8333-8337. <http://dx.doi.org/10.1002/anie.201602840>. (DA Dixon and M. Vasiliu supported by this program for all computational work and writing the manuscript.)
160. Matthiesen, J. E.; Carraher, J. M.; Vasiliu, M.; Dixon, D. A.; Tessonnier, J. P., Electrochemical Conversion of Muconic Acid to Biobased Diacid Monomers. *ACS Sustain. Chem. Eng.* **2016**, *4*, 3575-3585. <http://dx.doi.org/10.1021/acssuschemeng.6b00679>. (DA Dixon and M. Vasiliu supported by this program for all computational work and writing the manuscript.)
161. Smith, M. F.; Cassidy, S. J.; Adams, I. A.; Vasiliu, M.; Gerlach, D. L.; Dixon, D. A.; Rugar, P. A., Substituent Effects on the Properties of Borafluorenes. *Organometallics* **2016**, *35*, 3182-3191. <http://dx.doi.org/10.1021/acs.organomet.6b00537>. (DA Dixon and M. Vasiliu supported by this program for all computational work and writing the manuscript.)
162. Sun, J.; Cai, Q. X.; Wan, Y.; Wan, S. L.; Wang, L.; Lin, J. D.; Mei, D. H.; Wang, Y., Promotional Effects of Cesium Promoter on Higher Alcohol Synthesis from Syngas over Cesium-Promoted Cu/ZnO/Al₂O₃ Catalysts. *ACS Catal.* **2016**, *6*, 5771-5785. <http://dx.doi.org/10.1021/acscatal.6b00935>. (D.Mei performed DFT calculations and Y.Wang participated in the interpretation of results and writing the manuscript.)
163. Tapu, D.; Buckner, O. J.; Boudreaux, C. M.; Norvell, B.; Vasiliu, M.; Dixon, D. A.; McMillen, C. D., A benzothiadiazole-supported N-heterocyclic carbene and its rhodium and iridium complexes. *J. Organomet. Chem.* **2016**, *823*, 40-49. <http://dx.doi.org/https://doi.org/10.1016/j.jorganchem.2016.09.016>. (DA Dixon and M. Vasiliu supported by this program for all computational work and writing the manuscript.)
164. Whittemore, S. M.; Bowden, M.; Karkamkar, A.; Parab, K.; Neiner, D.; Autrey, T.; Ishibashi, J. S. A.; Chen, G.; Liu, S. Y.; Dixon, D. A., Blending materials composed of boron, nitrogen and carbon to transform approaches to liquid hydrogen stores. *Dalton. Trans.* **2016**, *45*, 6196-6203. <http://dx.doi.org/10.1039/c5dt04276c>. (DA Dixon supported by this program for all computational work and writing the manuscript.)
- 2017**
165. Cammarota, R. C.; Vollmer, M. V.; Xie, J.; Ye, J.; Linehan, J. C.; Burgess, S. A.; Appel, A. M.; Gagliardi, L.; Lu, C. C., A Bimetallic Nickel–Gallium Complex Catalyzes CO₂ Hydrogenation via the Intermediacy of an Anionic d¹⁰ Nickel Hydride. *J. Am. Chem. Soc.* **2017**, *139*, 14244-14250. <http://dx.doi.org/10.1021/jacs.7b07911>. (JC Linehan, SA Burgess, and AM Appel were supported by this project to help collect and interpret high pressure NMR spectroscopy data.)
166. Gates, B. C.; Flytzani-Stephanopoulos, M.; Dixon, D. A.; Katz, A., Atomically dispersed supported metal catalysts: perspectives and suggestions for future research. *Catal. Sci. Technol.* **2017**, *7*, 4259-4275. <http://dx.doi.org/10.1039/C7CY00881C>. (DA Dixon supported by this program for writing this review.)
167. Goldberg, J. M.; Goldberg, K. I.; Heinekey, D. M.; Burgess, S. A.; Lao, D. B.; Linehan, J. C., Detection of an Iridium–Dihydrogen Complex: A Proposed Intermediate in Ionic Hydrogenation. *J. Am. Chem. Soc.* **2017**, *139*, 12638-12646. <http://dx.doi.org/10.1021/jacs.7b06480>. (JC Linehan and SA Burgess were supported by this project for the high pressure NMR spectroscopy and corresponding mechanistic studies.)

168. Iglesia, E.; Wang, S.; Agirrezabal-Telleria, I.; Bhan, A.; Simonetti, D.; Takanabe, K., Catalysis for Fuels Introductory Lecture: Catalytic routes to fuels from C₁ and oxygenate molecules. *Faraday Discuss.* **2017**. <http://dx.doi.org/10.1039/C7FD00018A>. (This is a review paper that includes as one of the examples, the IA work on intrapore liquid effects on transition state stability.)
169. Lee, J.; Szanyi, J.; Kwak, J. H., Ethanol dehydration on γ -Al₂O₃: Effects of partial pressure and temperature. *Mol. Catal.* **2017**, *434*, 39-48. <http://dx.doi.org/10.1016/j.mcat.2016.12.013>. (J. Szanyi participated in the interpretation of the data and in writing the manuscript.)
170. Li, Z.; Yang, X.; Tsumori, N.; Liu, Z.; Himeda, Y.; Autrey, T.; Xu, Q., Tandem Nitrogen Functionalization of Porous Carbon: Toward Immobilizing Highly Active Palladium Nanoclusters for Dehydrogenation of Formic Acid. *ACS Catal.* **2017**, *7*, 2720-2724. <http://dx.doi.org/10.1021/acscatal.7b00053>. (T Autrey contributed to analysis of the results and writing of this paper.)
171. Liu, Z.; Ishibashi, J. S. A.; Darrigan, C.; Dargelos, A.; Chrostowska, A.; Li, B.; Vasiliu, M.; Dixon, D. A.; Liu, S.-Y., The Least Stable Isomer of BN Naphthalene: Toward Predictive Trends for the Optoelectronic Properties of BN Acenes. *J. Am. Chem. Soc.* **2017**, *139*, 6082-6085. <http://dx.doi.org/10.1021/jacs.7b02661>. (DA Dixon and M. Vasiliu supported by this program for most of the computational work and writing the manuscript.)
172. Prodinge, S.; Derewinski, M. A.; Wang, Y. L.; Washton, N. M.; Walter, E. D.; Szanyi, J.; Gao, F.; Wang, Y.; Peden, C. H. F., Sub-micron Cu/SSZ-13: Synthesis and application as selective catalytic reduction (SCR) catalysts. *Appl. Catal. B* **2017**, *201*, 461-469. <http://dx.doi.org/10.1016/j.apcatb.2016.08.053>. (S. P and M. A. D acknowledge support by the Materials Synthesis and Simulation Across Scales (MS3 Initiative) conducted under the Laboratory Directed Research & Development Program at PNNL.)

2018

173. Andrella, N. O.; Liu, K.; Gabidullin, B.; Vasiliu, M.; Dixon, D. A.; Baker, R. T., Metal Heptafluoroisopropyl (M-hfip) Complexes for Use as hfip Transfer Agents. *Organometallics* **2018**, *37*, 422-432. <http://dx.doi.org/10.1021/acs.organomet.7b00837>. (DA Dixon and M. Vasiliu supported by this program for all of the computational work and writing the manuscript.)
174. Chen, J. G.; Crooks, R. M.; Seefeldt, L. C.; Bren, K. L.; Bullock, R. M.; Darensbourg, M. Y.; Holland, P. L.; Hoffman, B.; Janik, M. J.; Jones, A. K.; Kanatzidis, M. G.; King, P.; Lancaster, K. M.; Lymar, S. V.; Pfromm, P.; Schneider, W. F.; Schrock, R. R., Beyond fossil fuel-driven nitrogen transformations. *Science* **2018**, *360*, eaar6611. <http://dx.doi.org/10.1126/science.aar6611>. (RM Bullock participated in the discussion at the DOE-BES workshop and helped write the paper, which contained intellectual contributions from all participants at the workshop)
175. Lee, M.-S.; McGrail, B. P.; Rousseau, R.; Glezakou, V.-A., Molecular Level Investigation of CH₄ and CO₂ Adsorption in Hydrated Calcium-Montmorillonite. *J. Phys. Chem. C* **2018**, *122*, 1125-1134. <http://dx.doi.org/10.1021/acs.jpcc.7b05364>. (This work was supported by the US Department of Energy, Office of Fossil Energy (M.-S.L., B.P.M. and V.-A.G.) and the Office of Basic Energy Science, Division of Chemical Sciences (R.R.)

176. Nguyen, M.-T.; Wang, Z.; Rod, K. A.; Childers, M. I.; Fernandez, C.; Koech, P. K.; Bennett, W. D.; Rousseau, R.; Glezakou, V.-A., Atomic Origins of the Self-Healing Function in Cement–Polymer Composites. *ACS Appl. Mater. Interfaces* **2018**, *10*, 3011-3019. <http://dx.doi.org/10.1021/acsami.7b13309>. (R Rousseau and V-A Glezakou provided technical input on the analysis of the results of the polymer/surface interactions)
177. Yun, D.; Wang, Y.; Herrera, J., Ethanol partial oxidation over VO_x/TiO₂ catalysts: the role of titania surface oxygen on the vanadia reoxidation in the Mars-van Krevelen mechanism. *ACS Catal.* **2018**, *8*, 4681-4693. <http://dx.doi.org/10.1021/acscatal.7b03327>. (Y.Wang was supported by this program for the interpretation of results and writing the manuscript.)

2019

178. Clark, J. A.; Murray, A.; Lee, J.-m.; Autrey, T. S.; Collord, A. D.; Hillhouse, H. W., Complexation Chemistry in N,N-Dimethylformamide-Based Molecular Inks for Chalcogenide Semiconductors and Photovoltaic Devices. *J. Am. Chem. Soc.* **2019**, *141*, 298-308. <http://dx.doi.org/10.1021/jacs.8b09966>. (T Autrey was supported by this grant to direct the calorimetry experiments, assist with analysis of data and writing the manuscript)
179. Lee, M.-S.; Glezakou, V.-A.; Rousseau, R.; McGrail, B. P., Molecular Simulation of the Catalytic Regeneration of nBuLi through a Hydrometalation Route. *Inorg. Chem.* **2019**, *58*, 3033-3040. <http://dx.doi.org/10.1021/acs.inorgchem.8b02910>. (R Rousseau and V-A Glezakou provided guidance on the planning, execution and analysis of the liquid phase catalysis simulations)

Thomas F. Jaramillo

**Fundamental Understanding and Catalyst Development for Electrochemical Processes
Involving H₂O, H₂, O₂, and H₂O₂**

McKenzie Hubert, Zhihua Chen, Shuchung Chen, Alaina Strickler, Yi Cui,
Frank Abild-Pedersen, Christopher Hahn, Drew Higgins, Laurie A. King,
Samira Siahrostami, Zhenan Bao, Jens K. Nørskov, Thomas F. Jaramillo

SLAC National Accelerator Laboratory & Stanford University

Presentation Abstract

Fundamental understanding of catalysis is essential to designing and developing new catalyst systems and processes for improved chemical transformations. A major driver is the use of renewable energy sources to power processes that conventionally require fossil fuels. This poster will describe efforts within SUNCAT-FWP that focus on a range of key catalytic processes for the production and use of fuels and chemicals that utilize renewable electricity as the input energy source. This poster will describe recent efforts in understanding and developing catalysts for three particular electrochemical reactions of interest: H₂O₂ production by means of the 2 e⁻ oxygen reduction reaction (ORR), the oxygen evolution reaction (OER), and the hydrogen evolution reaction (HER).

For the electrochemical production of H₂O₂, we are developing novel carbon-based catalysts that can selectively favor the 2 e⁻ pathway for the ORR over the 4 e⁻ pathway. The combination of computational and experimental approaches has been critical to producing the fundamental understanding needed to design and develop catalyst systems with high activity and selectivity. For the OER, we are studying various compositions and morphologies of iridium-based materials, particularly targeting catalyst systems with potential to provide both activity and stability in acidic conditions while lowering precious metal content. For the HER, we have recently been working on fundamental studies of catalyst translation, taking catalysts designed and developed in SUNCAT-FWP to operate under conditions more relevant to commercial technology. Our future research efforts will continue to focus on understanding reaction mechanisms and improving catalyst design for the production of renewable fuels and chemicals.

FWP10049 SUNCAT Center for Interface Science and Catalysis

RECENT PROGRESS

The primary focus of the SUNCAT-FWP is to develop an understanding of heterogeneous catalysis to arrive at a set of catalyst design principles. Our approach is to combine computational and experimental investigations to develop a theory of heterogeneous catalysis. The theory we aim for is a set of concepts that makes it possible to identify the catalyst properties that are most important in determining catalytic properties (rate, selectivity, stability). We do this by extensive use of computational chemistry methods to understand phenomena and to establish trends in surface chemistry. We also rely on detailed experimental investigations of catalysts and reactions

to provide and test ideas. Our goal is the ability to design new catalysts based on insight, something that is not possible without the combination of theory and experiment.

Task 1: Catalysis Data Science and Computational Infrastructure

We have developed the concept of “active learning” for a range of applications relevant for simulating catalysts and catalytic reactions. A sketch of how one can simply apply the concept is shown in Figure 1. Many aspects of catalysis simulations require global optimization, and often each iteration is computationally very expensive. One first makes a few “expensive” calculations (or utilize suitable existing data). These initial observations are used to fit a surrogate machine learning model. One then proceeds to carry out the global search in the cheap-to-evaluate surrogate machine learning model rather than using the original expensive model. If the surrogate model is accurate (which is of course initially highly unlikely if it is based on only a few observations) then the global search within the surrogate model converges to a very good approximation to a global optimum. If the surrogate model is not yet accurate, the global search in the surrogate model will converge to a point believed in the surrogate model to optimal, but which the accurate expensive model finds less than optimal. The surrogate model has thus selected a point which is extremely relevant to learn from, and the point is introduced in the training set for a new and more accurate surrogate model. When iterating this procedure, computational resources are spent on either something

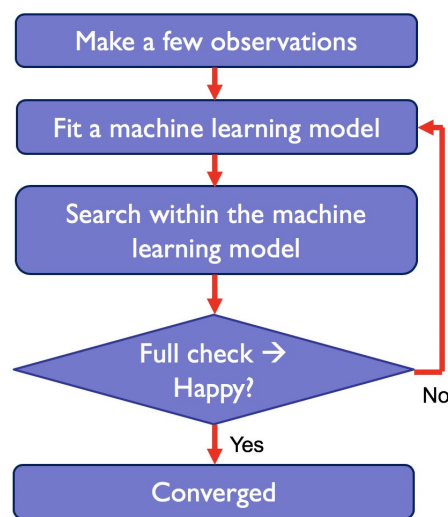


Figure 1. Surrogate machine learning model accelerated global search.

relevant as a solution, or something relevant for learning.

We have for example utilized surrogate machine learning model accelerated search for exploring reaction networks, for accelerating genetic algorithms for structural search, for accelerating the Nudged Elastic Band (NEB) method for simulating activation energies, and for searching for novel catalysts for the ethane dehydrogenation process (See Fig. 2).

In order to enable access to accurate machine learning models for catalysis relevant properties, we are establishing large databases of catalytically relevant properties. One such database is the “Surface Reaction” app found under Catalysis-hub.org. Here we make more than 100,000 surface reaction energies available online, with access to the structural data from the simulations, such that users can establish their own

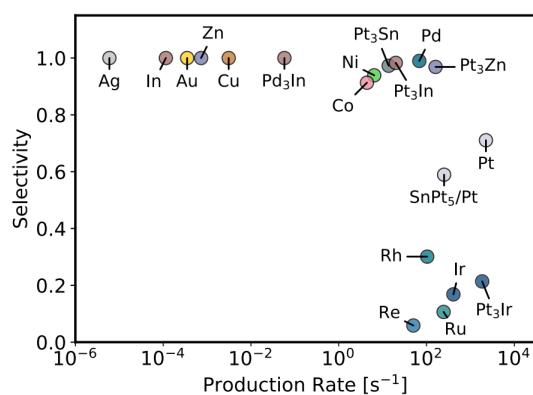


Figure 2. Activity vs. selectivity towards C₂H₄ (g) predicted by the descriptor-based micro-kinetic model. Pt₅Sn/Pt denotes a Pt(111) 3x2 super-cell, where a single Pt atom has been substituted for Sn in the outer layer. They were calculated at 873 K, 0.2 bar C₂H₆ (g), 0.6 bar H₂, 2·10⁻⁴ bar C₂H₄ (0.1% carbon conversion), 10⁻⁶ bar CH₄ and 10⁻⁹ bar C₂H₂.

feature representation for machine learning models. Ultimately, we aim to share all calculations at SUNCAT with the public by including all new adsorption calculations in this database. We also provide our machine learning toolkit “CatLearn”, and our surface analysis/generator code “CatKit” as open source.

Task 2: Fundamentals of Electrochemistry

In recent years there has been substantial progress in understanding and developing electrocatalysts for sustainable energy conversion reactions. There also remain significant challenges. In addition to making a number of scientific advances in this domain during this funding period, we also provided context to the field by means of two perspective articles, published in *Nature Materials* and *Science*, that describe recent milestones and remaining challenges in electrocatalysis. The first outlines the key scientific challenges remaining in this field; technoeconomics, semiconductor materials development, catalyst design and system integration. The second article showcases the systematic framework of coupling theoretical and experimental studies towards developing advanced electrocatalysts for sustainable energy conversion and storage applications, and thus, highlights the core missions and strategies of SUNCAT (Figure 3).

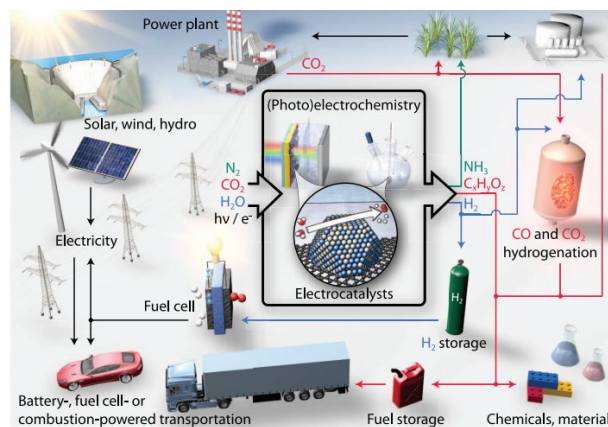


Figure 3. Role of electrocatalysis in the sustainable energy future.

Catalyst development for the hydrogen evolution reaction (HER)

Prior funding in SUNCAT has led substantial progress towards the development and characterization of highly active NPG catalysts for the hydrogen evolution reaction (HER). During this funding phase at SUNCAT, we built on our expertise in fundamental catalyst development (SUNCAT FWP) to work together with Proton Onsite (SBIR-DoD project) to scale-up a SUNCAT cobalt phosphide catalyst to an 86 cm² commercial-scale polymer electrolyte membrane (PEM) electrolyzer. As shown in Figure 4, the CoP catalyst was found to be active and stable, operating at 1.86 A.cm⁻² for >1700 h of continuous H₂ production (Figure 4) while providing substantial material cost savings relative to Pt. This work highlights the practical relevance of NPG catalyst development that has been a core part of SUNCAT FWP research.

We have also investigated various strategies towards enhancing the activity of NPG catalysts: designing catalyst-support electronic interactions that tune the hydrogen binding energy of thiomolybdate nanoclusters, and engineering highly active S-vacancies on MoS₂ basal planes. Additionally, we reported, two-dimensional layered transition metal carbides, MXenes, as electrocatalysts for the HER. Towards understanding the role of pH on activity of Pt, we have identified intrinsically lower barriers for the HER with respect to hydronium mediated mechanism as opposed to water mediated mechanism as the cause of favorable kinetics for acidic media over alkaline.

Water oxidation catalysis

Beyond water splitting, OER is important in other energy conversion systems, e.g. metal-air batteries, and the complementary half-reaction for the electrochemical reduction of N_2 or CO_2 . However, the high overpotentials associated with the OER make it a significant bottleneck. Furthermore, in acidic media, precious metal based materials (iridium and ruthenium) remain the only viable catalysts for the OER. This has motivated our work to design and characterize lower-precious metal content OER catalysts. In the prior funding period we reported a highly active and stable $IrO_x/SrIrO_3$ OER catalyst. Intriguingly, the high activity of this catalyst was shown to form *in situ* via Sr leaching. Grown epitaxially as thin films by pulsed laser deposition, this highly promising catalyst motivated us to study higher surface area Sr-Ir-Ox particulate catalysts. Micron-sized Sr_4IrO_6 , Sr_2IrO_4 and $SrIrO_3$ catalysts were thus synthesized by solid-state thermochemical methods. The Sr_2IrO_4 demonstrated superior activity and stability compared to commercial Ir/C (Premetek) nanoparticles, requiring 286 mV overpotential to reach $10\text{ mA cm}^{-2}_{\text{geo}}$. Ir-alloy thin films have also offered an interesting platform for modifying the electronic and geometric properties of electrocatalysts. Prepared by physical vapor deposition (PVD), we have synthesized thin films of Ir, $IrSn_2$, $IrCr$, $IrTi$, and $IrNi$. $IrCr$ demonstrated significant intrinsic activity enhancement over Ir. Our DFT calculations suggest that this enhancement is due to near-surface Cr doping. We have also studied the OER process extensively in alkaline media.

Oxygen Reduction Reaction: understanding selectivity of 2-electron vs 4-electron

Catalyst design for highly selective oxygen reduction reaction (ORR) catalysts is extremely important for both fuel cell technologies (four-electron) and electrochemical hydrogen peroxide production (two-electron). Thus, SUNCAT has focused efforts on steering selectivity appropriately, in particular to identify reaction mechanisms for the electrochemical production of H_2O_2 .

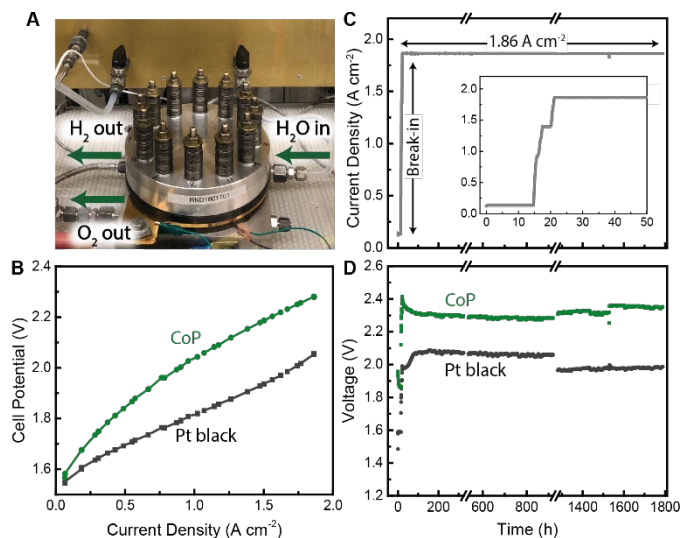


Figure 4 (a) Photograph of the 86 cm² electrolyzer test station. (b) Polarization curve. (c) Current density durability protocol. The inset shows the break-in period. (d) Durability voltage-time plots for the PEM electrolyzer. 1.0 mg.cm⁻² CoP loading, 50 °C and 400 psi.

Heteroatom co-doping offers an attractive strategy to modifying the electronic and surface structures of carbon-based materials and thus tuning catalytic activity. Recently at SUNCAT, we have designed a systematic investigation to uncover the nature of B-C-N materials. Synthetically, we prepared B,N doped carbon materials and investigated their selectivity to either 4-electron or 2-electron ORR which were found to be >80 % selective (Figure 5d) to H_2O_2 , with promising overpotentials (Figure 5c, <100 mV). X-ray absorption spectroscopy at SSRL was coupled to other spectroscopic and microscopic techniques to fully characterize *h*-BN domains of these materials. Our DFT calculations demonstrate that the interface between *h*-BN domains and the graphene host lattice preferentially drives 2-electron ORR and thus, the work highlights insights for designing further improved carbon catalysts. We have also explored fundamental questions involving scalable syntheses as well as catalysts functioning within the context of small-scale reactors for decentralized H_2O_2 production.

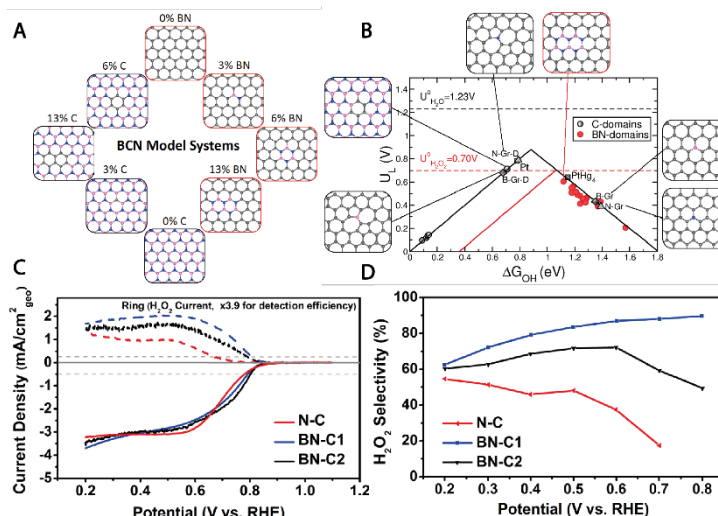


Figure 5 (a) Schematic of the BCN configuration models examined in this study: C, gray; N, blue; B, pink. (b) Theoretical activity volcano maps for 2e⁻ (red) and 4e⁻ (black) ORR. (c) RRDE voltammograms of N-C, BN-C1, and BN-C2 at 1600 rpm in 0.1 M KOH electrolyte. (d) H_2O_2 selectivity as a function of the applied potential.

Task 3: Fundamentals of Thermal Catalysis

Syngas chemistry: advances in our mechanistic understanding of selectivity

Syngas ($\text{CO} + \text{H}_2$) conversion into higher oxygenates ($\text{C}_{2+\text{oxy}}$) and methanol synthesis from CO_2 and H_2 are both highly desirable routes for alternative and sustainable supplies of commodity chemicals and transportation fuels. During the past funding period, we have advanced our field by contributing a detailed mechanistic understanding of $\text{C}_{2+\text{oxy}}$ synthesis by improving the mechanism of syngas formation at low temperatures on Ru-based materials, and by identifying promising candidates for methanol synthesis from CO/CO_2 and H_2 , in all cases through theory and experiment. In addition, we were able to shed light on CO hydrogenation, an important step in these reactions, through modeling metal/oxide interfaces and by observing the electronic states of transient species using X-ray free electron laser capabilities.

We investigated close-packed transition metal surfaces and step-blocking strategies for $\text{C}_{2+\text{oxy}}$ synthesis. We obtained theory-based production rate volcanoes on close-packed transition metal surfaces, which led us to understand selectivity patterns for $\text{C}_{2+\text{oxy}}$ synthesis, identify favorable catalyst adsorption properties and unveil the step-blocking function of promoter oxides

added to Fischer-Tropsch and Rh-based catalysts. Building on these insights, we synthesized Rh catalysts having step sites passivated by varying coverage of Na. Although displaying decreased rates, these catalysts were effective at preserving C-C bonds leading to high C₂+oxy selectivity. In a different approach, we improved selectivity and rates by creating bifunctional sites at metal-oxide interfaces: Using atomic layer deposition (ALD), we modified Rh nanoparticles with a MnO promoter and found that C₂+oxy production could be enhanced at Rh-MnO interface sites, which facilitate CO dissociation, stabilize the key transition state for C₂+oxy, and block step sites on Rh. We also developed methodology and equipment to characterize catalysts *operando* using both synchrotron X-ray diffraction (XRD) and X-ray absorption spectroscopy (XAS).

For methanol synthesis, we identified several promising catalysts, including transition metal phosphides (MoP, Ru_xP), metal/oxide interfaces (Rh/MoO₃) and intermetallics (Co-Ga, Au-Ni-Ga, In-Pd). MoP is a highly active catalyst over a wide range of CO/CO₂/H₂ feed compositions (Figure 6) due to its unique ability to stabilize formate in a mono-dentate configuration, instead of the bi-dentate geometry observed on transition metals.

Dynamics and stability of catalysts: modeling sintering and SMSI

Deactivation mechanisms like sintering and strong metal/support interaction (SMSI) decrease active site densities, which in turn, impacts reactivity and selectivity. We obtained a comprehensive understanding of catalyst deactivation by combining theoretical simulations, phase diagrams, stochastic/mean-field kinetic models, and experiments. We also provided the field with an up-to-date perspective on sintering mechanisms and strategies for their mitigation.

DFT derived sintering models integrating particle migration (PM) and Ostwald ripening (OR) quantitatively reproduce both Wulff constructed nanoparticle structures, and experimental dependencies of particle size distributions as a function of temperature and pressure for Pt/SiO₂. These simulations indicate that OR mediated by PtO₂ (g) moieties is the predominant sintering mechanism at higher temperatures and under more oxidizing environments with PM becoming increasingly relevant in reducing environments.

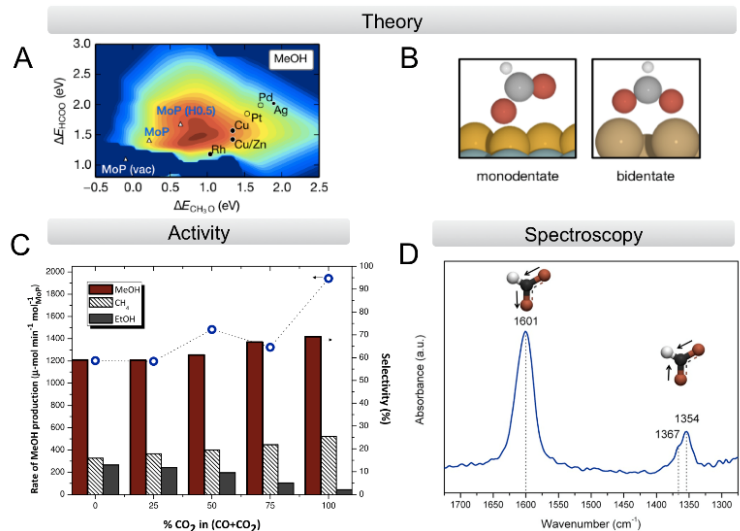


Figure 6. (A) Qualitative theoretical activity map showing deviation of MoP catalysts from formate scaling relationships observed on transition metal catalysts (B) m-HCOO⁻ on MoP and b-HCOO⁻ on Cu (C) Feed switching study showing robust methanol synthesis activity of MoP in a range of CO/CO₂/H₂ conditions at 31 bar and 230°C. (D) in-situ DRIFT spectrum showing m-HCOO⁻ on MoP during CO₂ hydrogenation at 10 bar and 230°C.

We uncovered a novel deactivation mechanism for Pd/Al₂O₃ catalysts and that was surprisingly found to be dependent on metal particle density (or loading). Active sites of metal NPs can also be lost through encapsulation through the SMSI process. We thus undertook rigorous TEM characterization coupled with DFT-derived phase diagrams to elucidate the formation of crystallographically-defined titania overlayers on Pd NPs under reducing conditions (Figure 7).

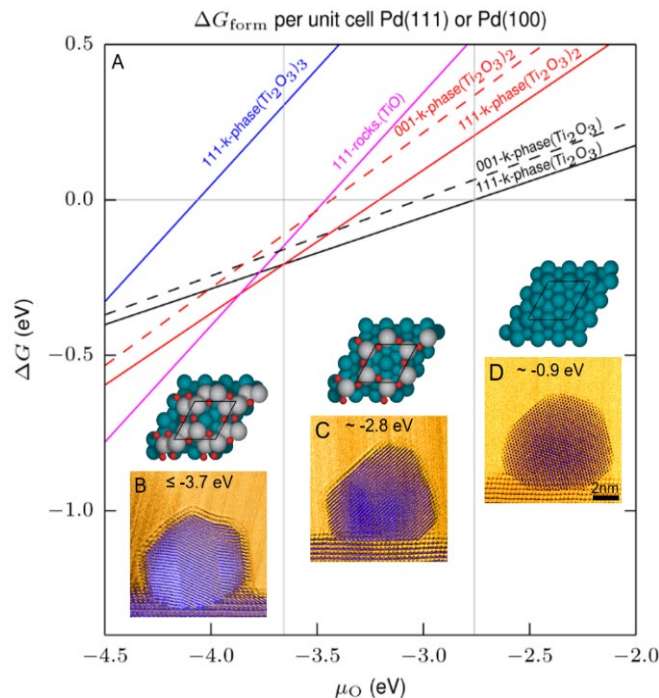


Figure 7. (A) Theoretical calculations of free energy G for different TiO_x phases on Pd(111) or Pd(100) surfaces as a function of oxygen chemical potential μ_{O} , verified experimentally under different μ_{O} in an atmospheric TEM (B, C, D).

Publications Acknowledging this Grant in 2016-2019

(I)

1. Garcia-Pintos D, Voss J, Jensen AD, Studt F. Hydrodeoxygenation of Phenol to Benzene and Cyclohexane on Rh(111) and Rh(211) Surfaces: Insights from Density Functional Theory. *J Phys Chem C*. 2016;120(33):18529–37.
2. Luntz AC, Beck RD. Review Article: Dynamics of methane dissociation on transition metals. *J Vac Sci Technol A Vacuum, Surfaces, Film* [Internet]. 2017;35(5):05C201.
3. Stegmaier S, Voss J, Reuter K, Luntz AC. Li+Defects in a Solid-State Li Ion Battery: Theoretical Insights with a Li3OCl Electrolyte. *Chem Mater*. 2017;29(10):4330–40.
4. Luntz AC, McCloskey BD. Li-air batteries: Importance of singlet oxygen. *Nat Energy* [Internet]. 2017;2(5):1–2.
5. Sharada SM, Bligaard T, Luntz AC, Kroes G-J, Norskov JK. SBH10: A Benchmark Database of Barrier Heights on Transition Metal Surfaces. *J Phys Chem C*. 2017 Sep;121(36):19807–15.
6. Jane Bukas V, Won Kim H, Sengpiel R, Knudsen KB, Voss J, McCloskey BD, et al. Combining Experiment and Theory to Unravel the Mechanism of Two-Electron Oxygen Reduction at a Selective and Active Co-Catalyst. 2018
7. Chakraborty D, Damsgaard CD, Silva H, Conradsen C, Olsen JL, Carvalho HWP, et al. Bottom-Up Design of a Copper–Ruthenium Nanoparticulate Catalyst for Low-Temperature Ammonia Oxidation. *Angew Chemie - Int Ed*. 2017;56(30).

8. Ulissi ZW, Medford AJ, Bligaard T, Nørskov JK. To address surface reaction network complexity using scaling relations machine learning and DFT calculations. *Nat Commun.* 2017;8.
9. Zhang L, Qiao L, Bligaard T, Su Y. A first-principle study of H adsorption and absorption under the influence of coverage. *Appl Surf Sci.* 2018;457.
10. De Wispelaere K, Martínez-Espín JS, Hoffmann MJ, Svelle S, Olsbye U, Bligaard T. Understanding zeolite-catalyzed benzene methylation reactions by methanol and dimethyl ether at operating conditions from first principle microkinetic modeling and experiments. *Catal Today.* 2018;312.
11. Hoffmann MJ, Bligaard T. A Lattice Kinetic Monte Carlo Solver for First-Principles Microkinetic Trend Studies. *J Chem Theory Comput.* 2018;14(3).
12. Jennings PC, Hummelshøj JS, Bligaard T, Lysgaard S, Vegge T. Machine Learning Accelerated Genetic Algorithms for Computational Materials Search. Submitted. 2018;1–5.
13. Torres JAG, Jennings PC, Hansen MH, Boes JR, Bligaard T. Low-Scaling Algorithm for Nudged Elastic Band Calculations Using a Surrogate Machine Learning Model. Submitted. 2019;1–11.
14. Hansen MH, Bligaard T, Nørskov J. First Principles Micro-kinetic Model of Catalytic Non-oxidative Dehydrogenation of Ethane over Close-packed Metallic Facets. Submitted. 2019;1–36.
15. Hansen MH, Jennings PC, Boes JR, Mamun OG, Bligaard T. Active Learning Surrogate Model Algorithm for Screening in Catalysis. Submitted. 2019;1–17.
16. Winther KT, Hoffmann MJ, Mamun O, Boes JR, Nørskov JK, Bajdich M, et al. Catalysis-Hub . org : An Open Electronic Structure Database for Surface Reactions. Submitted. 2019;
17. Boes J, Mamun O, Winther K, Bligaard T. Graph Theory Approach to High-Throughput Surface Adsorption Structure Generation. Submitted 2019;
18. Jennings PC, Hansen MH, Torres JAG, Wang Z, Boes JR, Hummelshøj JS, et al. CatLearn - An Atomistic Machine Learning Package for Surface Science and Catalysis. Submitted. 2019;1–32.
19. Montoya, J. H.; Seitz, L. C.; Chakthranont, P.; Vojvodic, A.; Jaramillo, T. F.; Nørskov, J. K. Materials for Solar Fuels and Chemicals. *Nat. Mater.* **2016**, *16* (1), 70–81.
20. She, Z. W.; Kibsgaard, J.; Dickens, C. F.; Chorkendorff, I.; Nørskov, J. K.; Jaramillo, T. F. Combining Theory and Experiment in Electrocatalysis: Insights into Materials Design. *Science (80-.)*. **2017**, *355* (6321). <https://doi.org/10.1126/science.aad4998>.
21. Tsai, C.; Li, H.; Park, S.; Park, J.; Han, H. S.; Nørskov, J. K.; Zheng, X.; Abild-Pedersen, F. Electrochemical Generation of Sulfur Vacancies in the Basal Plane of MoS₂ for Hydrogen Evolution. *Nat. Commun.* 2017, 8.
22. Seh, Z. W.; Fredrickson, K. D.; Anasori, B.; Kibsgaard, J.; Strickler, A. L.; Lukatskaya, M. R.; Gogotsi, Y.; Jaramillo, T. F.; Vojvodic, A. Two-Dimensional Molybdenum Carbide (MXene) as an Efficient Electrocatalyst for Hydrogen Evolution. *ACS Energy Lett.* 2016, *1* (3), 589–594.
23. Schlexer, P.; Singh, A. R.; Liu, X.; Chan, K. PH Effects on Hydrogen Evolution and Oxidation over Pt(111): Insights from First Principle, *Submitted*, **2019**
24. Strickler, A. L.; Jaramillo, T. F. Synthesis and Electrocatalytic Investigation of SrxIryOz Catalysts for Oxygen Evolution. *Submitted*, **2019**

25. Dickens, C. F.; Nørskov, J. K. A Theoretical Investigation into the Role of Surface Defects for Oxygen Evolution on RuO₂. *J. Phys. Chem. C*, **2017**, *121* (34), 18516–18524.
26. Ng, J. W. D.; García-Melchor, M.; Bajdich, M.; Chakthranont, P.; Kirk, C.; Vojvodic, A.; Jaramillo, T. F. Gold-Supported Cerium-Doped NiO_x Catalysts for Water Oxidation. *Nat. Energy* **2016**, *1*, 16053.
27. Chakthranont, P.; Kibsgaard, J.; Gallo, A.; Park, J.; Mitani, M.; Sokaras, D.; Kroll, T.; Sinclair, R.; Mogensen, M. B.; Jaramillo, T. F. Effects of Gold Substrates on the Intrinsic and Extrinsic Activity of High-Loading Nickel-Based Oxyhydroxide Oxygen Evolution Catalysts. *ACS Catal.* **2017**, *7* (8), 5399–5409.
28. Strickler, A. L.; Escudero-Escribano, M.; Jaramillo, T. F. Core-Shell Au@Metal-Oxide Nanoparticle Electrocatalysts for Enhanced Oxygen Evolution. *Nano Lett.* **2017**, *17* (10), 6040–6046.
29. Fester, J.; Bajdich, M.; Walton, A. S.; Sun, Z.; Plessow, P. N.; Vojvodic, A.; Lauritsen, J. V. Comparative Analysis of Cobalt Oxide Nanoisland Stability and Edge Structures on Three Related Noble Metal Surfaces: Au(111), Pt(111) and Ag(111). *Top. Catal.* **2017**, *60* (6–7), 503–512.
30. Zhang, B.; Zheng, X.; Voznyy, O.; Comin, R.; Bajdich, M.; García-Melchor, M.; Han, L.; Xu, J.; Liu, M.; Zheng, L.; et al. Homogeneously Dispersed Multimetal Oxygen-Evolving Catalysts. *Science* (80-.). **2016**, *352* (6283), 333–337.
31. Lu, Z.; Chen, G.; Li, Y.; Wang, H.; Xie, J.; Liao, L.; Liu, C.; Liu, Y.; Wu, T.; Li, Y.; et al. Identifying the Active Surfaces of Electrochemically Tuned LiCoO₂ for Oxygen Evolution Reaction. *J. Am. Chem. Soc.* **2017**, *139* (17), 6270–6276.
32. Doyle, A. D.; Bajdich, M.; Vojvodic, A. Theoretical Insights to Bulk Activity Towards Oxygen Evolution in Oxyhydroxides. *Catal. Letters* **2017**, *147* (6), 1533–1539.
33. Baker, J. G.; Schneider, Joel, R.; Garrido Torres, J. A. .; Singh, J. A. .; MacKus, A. J. M. .; Bajdich, M.; Bent, S. F. The Role of Aluminum in Promoting Ni Fe OOH Electrocatalysts for the Oxygen Evolution Reaction. *Submitted*, **2019**
34. Fester, J.; García-Melchor, M.; Walton, A. S.; Bajdich, M.; Li, Z.; Lammich, L.; Vojvodic, A.; Lauritsen, J. V. Edge Reactivity and Water-Assisted Dissociation on Cobalt Oxide Nanoislands. *Nat. Commun.* **2017**, *8*, 14169.
35. Fester, J.; Bajdich, M.; Walton, A. S.; Sun, Z.; Plessow, P. N.; Vojvodic, A.; Lauritsen, J. V. Comparative Analysis of Cobalt Oxide Nanoisland Stability and Edge Structures on Three Related Noble Metal Surfaces: Au(111), Pt(111) and Ag(111). *Top. Catal.* **2017**, *60* (6–7), 503–512.
36. Dickens, C. F.; Montoya, J. H.; Kulkarni, A. R.; Bajdich, M.; Nørskov, J. K. An Electronic Structure Descriptor for Oxygen Reactivity at Metal and Metal-Oxide Surfaces. *Surf. Sci.* **2019**, *681*, 122–129.
37. Montoya, J. H.; Doyle, A. D.; Nørskov, J. K.; Vojvodic, A. Trends in Adsorption of Electrocatalytic Water Splitting Intermediates on Cubic ABO₃ oxides. *Phys. Chem. Chem. Phys.* **2018**, *20* (5), 3813–3818.
38. Zhao, Z.; Schlexer, P.; Kulkarni, A. R. .; Bajdich, M. Electrochemical OER and ORR Activities of Layered Transition Metal (Oxy)(Hydro)Oxides: Trends and Descriptor Analysis. *Submitted*, **2019**
39. Shi, X.; Siahrostami, S.; Li, G. L.; Zhang, Y.; Chakthranont, P.; Studt, F.; Jaramillo, T. F.; Zheng, X.; Nørskov, J. K. Understanding Activity Trends in Electrochemical Water Oxidation to Form Hydrogen Peroxide. *Nat. Commun.* **2017**, *8* (1).

40. Siahrostami, S.; Li, G.-L.; Viswanathan, V.; Nørskov, J. K. One- or Two-Electron Water Oxidation, Hydroxyl Radical, or H₂O₂ Evolution. *J. Phys. Chem. Lett.* **2017**, *8* (6), 1157–1160.
41. Chen, S.; Chen, Z.; Siahrostami, S.; Higgins, D.; Nordlund, D.; Sokaras, D.; Kim, T. R.; Liu, Y.; Yan, X.; Nilsson, E.; et al. Designing Boron Nitride Islands in Carbon Materials for Efficient Electrochemical Synthesis of Hydrogen Peroxide. *J. Am. Chem. Soc.* **2018**, *140* (25), 7851–7859.
42. Chen, S.; Chen, Z.; Siahrostami, S.; Kim, T. R.; Nordlund, D.; Sokaras, D.; Nowak, S.; To, J. W. F.; Higgins, D.; Sinclair, R.; et al. Defective Carbon-Based Materials for the Electrochemical Synthesis of Hydrogen Peroxide. *ACS Sustain. Chem. Eng.* **2018**, *6* (1), 311–317.
43. Ulissi, Z. W.; Singh, A. R.; Tsai, C.; Nørskov, J. K. Automated Discovery and Construction of Surface Phase Diagrams Using Machine Learning. *J. Phys. Chem. Lett.* **2016**, *7* (19), 3931–3935.
44. To, J. W. F.; Ng, J. W. D.; Siahrostami, S.; Koh, A. L.; Lee, Y.; Chen, Z.; Fong, K. D.; Chen, S.; He, J.; Bae, W.-G.; et al. High-Performance Oxygen Reduction and Evolution Carbon Catalysis: From Mechanistic Studies to Device Integration. *Nano Res.* **2017**, *10* (4), 1163–1177.
45. Chen, S.; Koshy, D. M.; Tsao, Y.; Pfattner, R.; Yan, X.; Feng, D.; Bao, Z. Highly Tunable and Facile Synthesis of Uniform Carbon Flower Particles. *J. Am. Chem. Soc.* **2018**, *140* (32), 10297–10304.
46. Park, Z.; Chen, Z.; Jaramillo, T. F.; Bao, Z. Development of Ni-HAB Metal-Organic Frameworks for Electrochemical Oxygen Reduction. *In preparation* **2019**
47. Chen, Z.; Chen, S.; Siahrostami, S.; Chakthranont, P.; Hahn, C.; Nordlund, D.; Dimosthenis, S.; Nørskov, J. K.; Bao, Z.; Jaramillo, T. F. Development of a Reactor with Carbon Catalysts for Modular-Scale, Low-Cost Electrochemical Generation of H₂O₂. *React. Chem. Eng.* **2017**, *2* (2), 239–245.
48. Higgins, D.; Wette, M.; Gibbons, B. M.; Siahrostami, S.; Hahn, C.; Escudero-Escribano, M.; García-Melchor, M.; Ulissi, Z.; Davis, R. C.; Mehta, A.; et al. Copper Silver Thin Films with Metastable Miscibility for Oxygen Reduction Electrocatalysis in Alkaline Electrolytes. *ACS Appl. Energy Mater.* **2018**, *1* (5), 1990–1999.
49. **2019**
50. Strickler, A. L.; Jackson, A.; Jaramillo, T. F. Active and Stable Ir@Pt Core-Shell Catalysts for Electrochemical Oxygen Reduction. *ACS Energy Lett.* **2017**, *2* (1), 244–249.
51. Jackson, A.; Strickler, A.; Higgins, D.; Jaramillo, T. Engineering Ru@Pt Core-Shell Catalysts for Enhanced Electrochemical Oxygen Reduction Mass Activity and Stability. *Nanomaterials* **2018**, *8* (1), 38.
52. Singh, A. R.; Rohr, B. A.; Schwalbe, J. A.; Cargnello, M.; Chan, K.; Jaramillo, T. F.; Chorkendorff, I.; Nørskov, J. K. Electrochemical Ammonia Synthesis - The Selectivity Challenge. *ACS Catal.* **2017**, *7* (1), 706–709.
53. Boyd, M.; Latimer, A. A.; Dickens, C. F. ; Hahn, C.; Higgins, D. C.; Jaramillo, T. F. Understanding Methane Activation and Adsorption Trends on Pt Surfaces. *Submitted* **2019**
54. Chan, K.; Nørskov, J. K. Electrochemical Barriers Made Simple. *J. Phys. Chem. Lett.* **2015**, *6* (14), 2663–2668.
55. Chan, K.; Nørskov, J. K. Potential Dependence of Electrochemical Barriers from Ab Initio Calculations. *J. Phys. Chem. Lett.* **2016**, *7* (9), 1686–1690.

56. Chen, L. D.; Bajdich, M.; Martirez, J. M. P.; Krauter, C. M.; Gauthier, J. A.; Carter, E. A.; Luntz, A. C.; Chan, K.; Nørskov, J. K. Understanding the Apparent Fractional Charge of Protons in the Aqueous Electrochemical Double Layer. *Nat. Commun.* **2018**, *9* (1), 3202.
57. Dickens, C. F. .; Kirk, C. S.; Nørskov, J. K. First Principles Determination of Barriers and Microkinetic Modeling of Rates for Oxygen Evolution and Oxygen Reduction Reaction on Rutile and Metal Surfaces. *Submitted*, **2019**.
58. Chen, L. D.; Urushihara, M.; Chan, K.; Nørskov, J. K. Electric Field Effects in Electrochemical CO₂ Reduction. *ACS Catal.* **2016**, *6* (10), 7133–7139.
59. Gauthier, J. A.; Dickens, C. F.; Chen, L. D.; Doyle, A. D.; Nørskov, J. K. Solvation Effects for Oxygen Evolution Reaction Catalysis on IrO₂(110). *J. Phys. Chem. C* **2017**, *121* (21), 11455–11463.
60. Ji, Y.; Nørskov, J. K.; Chan, K. Scaling Relations on Basal Plane Vacancies of Transition Metal Dichalcogenides for CO₂ Reduction. *Submitted*, **2019**.
61. Ludwig, T.; Gauthier, J. A.; Brown, K. S.; Ringe, S.; Nørskov, J. K.; Chan, K. Solvent-Adsorbate Interactions and Adsorbate-Specific Solvent Structure in Carbon Dioxide Reduction on a Stepped Cu Surface. *JPCC, Submitted*, **2019**.
62. Willis, J. J.; Goodman, E. D.; Wu, L.; Riscoe, A. R.; Martins, P.; Tassone, C. J.; Cargnello, M. “Systematic Identification of Promoters for Methane Oxidation Catalysts by Using Size- and Composition-Controlled Pd-based Bimetallic Nanocrystals.”, *J. Am. Chem. Soc.* **2017**, *139*, 11989-11997.
63. Willis, J. J.; Gallo, A.; Sokaras, D.; Aljama, H.; Nowak, S. H.; Goodman, E. D.; Wu, L.; Tassone, C. J.; Jaramillo, T. F.; Abild-Pedersen, F.; Cargnello, M. “Systematic Structure-Property Relationship Studies in Palladium-Catalyzed Methane Complete Combustion.”, *ACS Catal.* **2017**, *7*, 7810-7821.
64. Goodman, E.; Latimer, A.; Yang, A.-C.; Wu, L.; Tahsini, N.; Abild-Pedersen, F.; Cargnello, M. “Low-Temperature Methane Partial Oxidation to Syngas with Modular Nanocrystal Catalysts.”, *ACS Appl. Nano Mat.* **2018**, *1*, 5258-5267.
65. Schumann, J.; Medford, A. J.; Yoo, J. S.; Zhao, Z.-J.; Bothra, P.; Cao, A.; Studt, F.; Abild-Pedersen, F.; Nørskov, J. K. Selectivity of Synthesis Gas Conversion to C₂+ Oxygenates on Fcc(111) Transition-Metal Surfaces. *ACS Catal.* **2018**, *8* (4), 3447–3453.
66. Yang, N.; Yoo, J. S.; Schumann, J.; Bothra, P.; Singh, J. A.; Valle, E.; Abild-Pedersen, F.; Nørskov, J. K.; Bent, S. F. Rh-MnO Interface Sites Formed by Atomic Layer Deposition Promote Syngas Conversion to Higher Oxygenates. *ACS Catal.* **2017**, *7* (9), 5746–5757.
67. Yang, N.; Liu, X.; Asundi, A. S.; Nørskov, J. K.; Bent, S. F. The Role of Sodium in Tuning Product Distribution in Syngas Conversion by Rh Catalysts. *Catal. Letters* **2018**, *148* (1), 289–297.
68. Cao, A.; Schumann, J.; Wang, T.; Zhang, L.; Xiao, J.; Bothra, P.; Liu, Y.; Abild-Pedersen, F.; Nørskov, J. K. Mechanistic Insights into the Synthesis of Higher Alcohols from Syngas on CuCo Alloys. *ACS Catal.* **2018**, *8* (11), 10148–10155.
69. Goodman, E. D.; Latimer, A. A.; Yang, A.-C.; Wu, L.; Tahsini, N.; Abild-Pedersen, F.; Cargnello, M. Low-Temperature Methane Partial Oxidation to Syngas with Modular Nanocrystal Catalysts. *ACS Appl. Nano Mater.* **2018**, acsanm.8b01256.

70. Duyar, M.; Tsai, C.; Snider, J. L.; Singh, J. A.; Gallo, A.; Yoo, J. S.; Medford, A. J.; Abild-Pedersen, F.; Studt, F.; Kibsgaard, J.; et al. Discovery of a Highly Active Molybdenum Phosphide Catalyst for Methanol Synthesis from CO and CO₂. *Angew. Chemie Int. Ed.* **2018**, *57* (46), 15045.
71. Singh, J. A.; Cao, A.; Schumann, J.; Wang, T.; Nørskov, J. K.; Abild-Pedersen, F.; Bent, S. F. Theoretical and Experimental Studies of CoGa Catalysts for the Hydrogenation of CO₂ to Methanol. *Catal. Letters* **2018**, *148* (12), 3583–3591.
72. Sandberg, R. B.; Hansen, M. H.; Nørskov, J. K.; Abild-Pedersen, F.; Bajdich, M. Strongly Modified Scaling of CO Hydrogenation in Metal Supported TiO Nanostripes. *ACS Catal.* **2018**, *8* (11), 10555–10563.
73. Gallo, A.; Snider, J. L.; Sokaras, D.; Nordlund, D.; Ogasawara, H.; Kovarik, L.; Duyar, M. S.; Jaramillo, T. F. Ni₅Ga₃ Catalysts for CO₂ Reduction to Methanol: Exploring the Role of Ga Surface Oxidation/Reductions on Catalytic Activity. *Submitt. Appl. Catal. B* **2018**.
74. Hoffman, A. S.; Singh, J. A.; Bent, S. F.; Bare, S. R. In Situ Observation of Phase Changes of a Silica-Supported Cobalt Catalyst for the Fischer–Tropsch Process by the Development of a Synchrotron-Compatible in Situ/Operando Powder X-Ray Diffraction Cell. *J. Synchrotron Radiat.* **2018**, *25* (6).
75. Singh, J.; Hoffman, A. S.; Schumann, J.; Boubnov, A.; Asundi, A.; Nørskov, J.; Bare, S. R.; Bent, S. F. Role of Co₂C in ZnO-Promoted Co Catalysts for Alcohol Synthesis from Syngas. *ChemCatChem* **2018**, *0* (ja).
76. Duyar, M. S.; Gallo, A.; Snider, J. L.; Singh, J.; Bothra, P.; Valle, E.; Regli, S. K.; McEnaney, J.; Abild-Pedersen, F.; Ronning, M.; et al. Zirconia Supported MoP Nanoparticles with Exceptional Catalytic Activity for CO₂ Hydrogenation to Methanol. *Prep.* **2018**.
77. Duyar, M. S.; Gallo, A.; Snider, J. L.; Jaramillo, T. F. Low Pressure Methanol Synthesis from CO₂ over Promoted Ni-Ga Catalysts. *Prep.* **2019**.
78. Snider, J. L.; Gallo, A.; Streibel, V.; Hubert, M. A.; Choksi, T. S.; Valle, E.; Upham, D. C.; Duyar, M. S.; Abild-Pedersen, F.; Jaramillo, T. F. Revealing the Synergy between Oxide and Alloy Phases on the Performance of Bimetallic In-Pd Catalysts for CO₂ Hydrogenation to Methanol. *Prep.* **2018**.
79. Singh, J. A.; Cao, A.; Schumann, J.; Wang, T.; Nørskov, J. K.; Pedersen, F. A.; Bent, S. F. Theoretical and Experimental Studies of CoGa Catalysts for the Hydrogenation of CO₂ to Methanol. *Catal. Letters* **2018**, *0* (0), 1–9.
80. ten Have, I. C.; Valle, E.; Gallo, A.; Snider, J. L.; Duyar, M. S.; Jaramillo, T. F. Development of MoP Catalysts for Higher Alcohol Synthesis from Syngas by Exploiting Support and Promoter Effects. *Prep.* **2018**.
81. Orazov, M.; Upham, D. C.; Duyar, M. S.; Jaramillo, T. F. No Title. *Prep.* **2018**.
82. Goodman, E. D.; Schwalbe, J. A.; Cargnello, M. Mechanistic Understanding and the Rational Design of Sinter-Resistant Heterogeneous Catalysts. *ACS Catal.* **2017**, *7* (10), 7156–7173.
83. Dietze, E. M.; Abild-Pedersen, F.; Plessow, P. N. Comparison of Sintering by Particle Migration and Ripening through First Principles Based Simulations. *J. Phys. Chem. C* **2018**
84. Li, L.; Plessow, P. N.; Rieger, M.; Sauer, S.; Sánchez-Carrera, R. S.; Schaefer, A.; Abild-Pedersen, F. Modeling the Migration of Platinum Nanoparticles on Surfaces Using a Kinetic

- Monte Carlo Approach. *J. Phys. Chem. C* **2017**, *121* (8), 4261–4269.
85. Plessow, P. N.; Abild-Pedersen, F. Sintering of Pt Nanoparticles via Volatile PtO₂: Simulation and Comparison with Experiments. *ACS Catal.* **2016**, *6* (10), 7098–7108.
 86. Goodman, Emmett, D.; Johnston-Peck, A. C.; Dietze, E. M.; Wrasman, C. J.; Hoffman, A. S.; Abild-Pedersen, F.; Bare, S. R.; Plessow, P. N.; Cargnello, M. Density-Dependent Deactivation Mechanism in Supported Catalysts by High-Temperature Decomposition of Particles into Single Atoms. *Rev. Nat.* **2018**.
 87. Plessow, P. N.; Sánchez-Carrera, R. S.; Li, L.; Rieger, M.; Sauer, S.; Schaefer, A.; Abild-Pedersen, F. Modeling the Interface of Platinum and α -Quartz(001): Implications for Sintering. *J. Phys. Chem. C* **2016**, *120* (19), 10340–10350.
 88. Plessow, P. N.; Bajdich, M.; Greene, J.; Vojvodic, A.; Abild-Pedersen, F. Trends in the Thermodynamic Stability of Ultrathin Supported Oxide Films. *J. Phys. Chem. C* **2016**, *120* (19), 10351–10360.
 89. Roling, L. T.; Li, L.; Abild-Pedersen, F. Configurational Energies of Nanoparticles Based on Metal-Metal Coordination. *J. Phys. Chem. C* **2017**, *121* (41), 23002–23010.
 90. Roling, L. T.; Choksi, T. S.; Abild-Pedersen, F. A Coordination-Based Model for Transition Metal Alloy Nanoparticles. *Rev.* **2018**.
 91. Roling, L. T.; Abild-Pedersen, F. Structure-Sensitive Scaling Relations: Adsorption Energies from Surface Site Stability. *ChemCatChem* **2018**, *10* (7), 1643–1650.
 92. Choksi, T. S.; Roling, L. T.; Streibel, V.; Abild-Pedersen, F. Predicting Adsorption Properties of Bimetallic Alloys as a Function of Their Morphology and Local Composition. *Prep.* **2018**.
 93. Choksi, T. S.; Roling, L. T.; Streibel, V.; Abild-Pedersen, F. Predicting Adsorption Properties of Bimetallic Alloys as a Function of Their Morphology and Local Composition. *to be Submitt.* **2018**.
 94. Yu, L.; Abild-Pedersen, F. Bond Order Conservation Strategies in Catalysis Applied to the NH₃Decomposition Reaction. *ACS Catal.* **2017**, *7* (1), 864–871.
 95. Yu, L.; Vilella, L.; Abild-Pedersen, F. Generic Approach to Access Barriers in Dehydrogenation Reactions. *Commun. Chem.* **2018**, *1* (1), 2.
 96. Aljama, H.; Abild-Pedersen, F. Efficient Computational Method for Calculating C-C Transition State Energy. *Prep.* **2018**.
 97. Fields, M.; Tsai, C.; Chen, L. D.; Abild-Pedersen, F.; Nørskov, J. K.; Chan, K. Scaling Relations for Adsorption Energies on Doped Molybdenum Phosphide Surfaces. *ACS Catal.* **2017**, *7* (4), 2528–2534.
 98. Siahrostami, S.; Falsig, H.; Beato, P.; Moses, P. G.; Nørskov, J. K.; Studt, F. Exploring Scaling Relations for Chemisorption Energies on Transition-Metal-Exchanged Zeolites ZSM-22 and ZSM-5. *ChemCatChem* **2016**, *8* (4), 767–772.
 99. Kakekhani, A.; Roling, L. T.; Kulkarni, A.; Latimer, A. A.; Abroshan, H.; Schumann, J.; Aljama, H.; Siahrostami, S.; Ismail-Beigi, S.; Abild-Pedersen, F.; et al. Nature of Lone-Pair-Surface Bonds and Their Scaling Relations. *Inorg. Chem.* **2018**, *57* (12), 7222–7238.
 100. Singh, A. R.; Montoya, J. H.; Rohr, B. A.; Tsai, C.; Vojvodic, A.; Nørskov, J. K. Computational Design of Active Site Structures with Improved Transition-State Scaling for Ammonia Synthesis. *ACS Catal.* **2018**, *8* (5), 4017–4024.

101. Wrasman, C. J.; Boubnov, A.; Riscoe, A. R.; Hoffman, A. S.; Bare, S. R.; Cargnello, M. Synthesis of Colloidal Pd/Au Dilute Alloy Nanocrystals and Their Potential for Selective Catalytic Oxidations. *J. Am. Chem. Soc.* **2018**, *140* (40), 12930–12939.
102. Kulkarni, A. R.; Zhao, Z. J.; Siahrostami, S.; Nørskov, J. K.; Studt, F. Monocopper Active Site for Partial Methane Oxidation in Cu-Exchanged 8MR Zeolites. *ACS Catal.* **2016**, *6* (10), 6531–6536.
103. Zhao, Z. J.; Kulkarni, A.; Vilella, L.; Nørskov, J. K.; Studt, F. Theoretical Insights into the Selective Oxidation of Methane to Methanol in Copper-Exchanged Mordenite. *ACS Catal.* **2016**, *6* (6), 3760–3766.
104. Latimer, A. A.; Aljama, H.; Kakekhani, A.; Yoo, J. S.; Kulkarni, A.; Tsai, C.; Garcia-Melchor, M.; Abild-Pedersen, F.; Nørskov, J. K. Mechanistic Insights into Heterogeneous Methane Activation. *Phys. Chem. Chem. Phys.* **2017**, *19* (5), 3575–3581.
105. Latimer, A. A.; Kulkarni, A. R.; Aljama, H.; Montoya, J. H.; Yoo, J. S.; Tsai, C.; Abild-Pedersen, F.; Studt, F.; Nørskov, J. K. Understanding Trends in C-H Bond Activation in Heterogeneous Catalysis. *Nat. Mater.* **2017**, *16* (2), 225–229.
106. Aljama, H.; Nørskov, J. K.; Abild-Pedersen, F. Theoretical Insights into Methane C-H Bond Activation on Alkaline Metal Oxides. *J. Phys. Chem. C* **2017**, *121* (30), 16440–16446.
107. Aljama, H.; Nørskov, J. K.; Abild-Pedersen, F. Tuning Methane Activation Chemistry on Alkaline Earth Metal Oxides by Doping. *J. Phys. Chem. C* **2018**.
108. Willis, J. J.; Gallo, A.; Sokaras, D.; Aljama, H.; Nowak, S. H.; Goodman, E. D.; Wu, L.; Tassone, C. J.; Jaramillo, T. F.; Abild-Pedersen, F.; et al. Systematic Structure-Property Relationship Studies in Palladium-Catalyzed Methane Complete Combustion. *ACS Catal.* **2017**, *7* (11), 7810–7821.
109. Willis, J. J.; Goodman, E. D.; Wu, L.; Riscoe, A. R.; Martins, P.; Tassone, C. J.; Cargnello, M. Systematic Identification of Promoters for Methane Oxidation Catalysts Using Size- and Composition-Controlled Pd-Based Bimetallic Nanocrystals. *J. Am. Chem. Soc.* **2017**, *139* (34), 11989–11997.
110. Latimer, A. A.; Abild-Pedersen, F.; Nørskov, J. K. A Theoretical Study of Methanol Oxidation on RuO₂(110): Bridging the Pressure Gap. *ACS Catal.* **2017**, *7* (7), 4527–4534.
111. Aljama, H.; Yoo, J. S.; Nørskov, J. K.; Abild-Pedersen, F.; Studt, F. Methanol Partial Oxidation on Ag(1 1 1) from First Principles. *ChemCatChem* **2016**, *8* (23), 3621–3625.
112. Latimer, A. A.; Kakekhani, A.; Kulkarni, A. R.; Nørskov, J. K. Direct Methane to Methanol: The Selectivity-Conversion Limit and Design Strategies. *ACS Catal.* **2018**, *8* (8), 6894–6907.

(II)

113. Reinecke BN, Kuhl KP, Ogasawara H, Li L, Voss J, Abild-Pedersen F, et al. Elucidating the electronic structure of supported gold nanoparticles and its relevance to catalysis by means of hard X-ray photoelectron spectroscopy. *Surf Sci* 2016;650:24–33.
114. Pruski M, Sadow AD, Slowing II, Marshall CL, Stair P, Rodriguez J, et al. Virtual Special Issue on Catalysis at the U.S. Department of Energy's National Laboratories. *ACS Catal.* 2016;6(5).

115. Bligaard T, Bullock RM, Campbell CT, Chen JG, Gates BC, Gorte RJ, et al. Toward Benchmarking in Catalysis Science: Best Practices, Challenges, and Opportunities. *ACS Catal.* 2016;6(4).
116. Lu Z, Chen G, Li Y, Wang H, Xie J, Liao L, et al. Identifying the Active Surfaces of Electrochemically Tuned LiCoO₂ for Oxygen Evolution Reaction. *J Am Chem Soc.* 2017;139(17):6270–6
117. Papp JK, Forster JD, Burke CM, Kim HW, Luntz AC, Shelby RM, et al. Poly(vinylidene fluoride) (PVDF) Binder Degradation in Li-O₂ Batteries: A Consideration for the Characterization of Lithium Superoxide. *J Phys Chem Lett.* 2017;8(6):1169–74.
118. Chen LD, Bajdich M, Martirez JMP, Krauter CM, Gauthier JA, Carter EA, et al. Understanding the apparent fractional charge of protons in the aqueous electrochemical double layer. *Nat Commun [Internet].* 2018;9(1):1–8.
119. Ulissi, Z. W.; Singh, A. R.; Tsai, C.; Nørskov, J. K. Automated Discovery and Construction of Surface Phase Diagrams Using Machine Learning. *J. Phys. Chem. Lett.* **2016**, 7 (19), 3931–3935.
120. King, L. A.; Hubert, M. A.; Capuano, C.; Manco, J.; Danilovic, N.; Valle, E.; Hellstern, T. R.; Ayers, K. E.; Jaramillo, T. F. Integrating a Non-Precious Metal Hydrogen Evolution Catalyst in a Commercial Polymer Electrolyte Membrane Electrolyser. *Submitted.* **2018**.
121. Hellstern, T. R.; Kibsgaard, J.; Tsai, C.; Palm, D. W.; King, L. A.; Abild-Pedersen, F.; Jaramillo, T. F. Investigating Catalyst-Support Interactions to Improve the Hydrogen Evolution Reaction Activity of Thiomolybdate [Mo₃S₁₃]₂-Nanoclusters. *ACS Catal.* **2017**, 7 (10), 7126–7130.
122. Frydendal, R.; Seitz, L. C.; Sokaras, D.; Weng, T. C.; Nordlund, D.; Chorkendorff, I.; Stephens, I. E. L.; Jaramillo, T. F. Operando Investigation of Au-MnO_x Thin Films with Improved Activity for the Oxygen Evolution Reaction. *Electrochim. Acta* **2017**, 230, 22–28.
123. Seitz, L. C.; Nordlund, D.; Gallo, A.; Jaramillo, T. F. Tuning Composition and Activity of Cobalt Titanium Oxide Catalysts for the Oxygen Evolution Reaction. *Electrochim. Acta* **2016**, 193, 240–245.
124. Zhou, D.; Cai, Z.; Bi, Y.; Tian, W.; Luo, M.; Zhang, Q.; Xie, Q.; Wang, J.; Li, Y.; Kuang, Y.; et al. Effects of Redox-Active Interlayer Anions on the Oxygen Evolution Reactivity of NiFe-Layered Double Hydroxide Nanosheets. *Nano Res.* **2018**, 11 (3), 1358–1368.
125. Lu, Z.; Chen, G.; Siahrostami, S.; Chen, Z.; Liu, K.; Xie, J.; Liao, L.; Wu, T.; Lin, D.; Liu, Y.; et al. High-Efficiency Oxygen Reduction to Hydrogen Peroxide Catalysed by Oxidized Carbon Materials. *Nat. Catal.* **2018**.
126. Park, J.; Hinckley, A. C.; Huang, Z.; Feng, D.; Yakovenko, A.; Lee, M.; Chen, S.; Zou, X.; Bao, Z. Synthetic Routes for a 2D Semiconductive Copper Hexahydroxybenzene Metal–Organic Framework. *J. Am. Chem. Soc.* **2018**, 140, jacs.8b06666.
127. Feng, D.; Lei, T.; Lukatskaya, M. R.; Park, J.; Huang, Z.; Lee, M.; Shaw, L.; Chen, S.; Yakovenko, A. A.; Kulkarni, A.; et al. Robust and Conductive Two-Dimensional Metal–Organic Frameworks with Exceptionally High Volumetric and Areal Capacitance. *Nat. Energy* **2018**, 3 (1), 30–36.

128. Hedström, S.; Dos Santos, E. C.; Liu, C.; Chan, K.; Abild-Pedersen, F.; Pettersson, L. G. M. Spin Uncoupling in Chemisorbed OCCO and CO₂: Two High-Energy Intermediates in Catalytic CO₂ Reduction. *J. Phys. Chem. C* **2018**, *122* (23), 12251–12258.
129. Zhao, W.; Bajdich, M.; Carey, S.; Vojvodic, A.; Nørskov, J. K.; Campbell, C. T. Water Dissociative Adsorption on NiO(111): Energetics and Structure of the Hydroxylated Surface. *ACS Catal.* **2016**, *6* (11), 7377–7384.
130. Zhao, W.; Doyle, A. D.; Morgan, S. E.; Bajdich, M.; Nørskov, J. K.; Campbell, C. T. Formic Acid Dissociative Adsorption on NiO(111): Energetics and Structure of Adsorbed Formate. *J. Phys. Chem. C* **2017**, *121* (50), 28001–28006.
131. Hellstern, T. R.; Palm, D. W.; Carter, J.; Deangelis, A.; Horsley, K.; Weinhardt, L.; Yang, W.; Blum, M.; Gaillard, N.; Heske, C.; et al. Molybdenum Disulfide Catalytic Coatings with Atomic Layer Deposition for Solar Hydrogen Production from Copper Gallium Diselenide Photocathodes. *ACS Appl. Energy Mater.* **2019**, Accepted.
132. Wu, L.; Lian, H.; Willis, J. J.; Goodman, E. D.; McKay, I. S.; Qin, J.; Tassone, C. J.; Cargnello, M. “Tuning Precursor Reactivity towards Nanometer-Size Control in Palladium Nanoparticles Studied by in-Situ Small Angle X-ray Scattering.”, *Chem. Mater.* **2018**, *30*, 1127-1135.
133. Wu, L.; Fournier, A. P.; Willis, J. J.; Cargnello, M.; Tassone, C. J. “In Situ X-ray Scattering Guides the Synthesis of Uniform PtSn Nanocrystals.”, *Nano Lett.* **2018**, *6*, 4053-4057.
134. Wrasman, C. J.; Boubnov, A.; Riscoe, A. R.; Hoffman, A. S.; Bare, S. R.; Cargnello, M. “Synthesis of Colloidal Pd/Au Dilute Alloy Nanocrystals and Their Potential for Selective Catalytic Oxidations.”, *J. Am. Chem. Soc.* **2018**, *140*, 12930-12939.
135. Timoshenko, T.; Wrasman, C. J.; Luneau, M.; Shirman, T.; Cargnello, M.; Bare, S. R.; Aizenberg, J.; Friend, C. M.; Frenkel, A. I. Probing Atomic Distributions in Mono- and Bimetallic Nanoparticles by Supervised Machine Learning. *Nano Lett.* **2019**, *19*, 520-529.
136. Aitbekova, A.; Wu, L.; Wrasman, C. J.; Boubnov, A.; Hoffman, A. S.; Goodman, E. D.; Bare, S. R.; Cargnello, M. Low-Temperature Restructuring of CeO₂-Supported Ru Nanoparticles Determines Selectivity in CO₂ Catalytic Reduction. *J. Am. Chem. Soc.* **2018**, *140*, 13736-13745.
137. Huang, W.; Goodman, E. D.; Losch, P.; Cargnello, M. Deconvoluting Transient Water Effects on the Activity of Pd Methane Combustion Catalysts. *Ind. Eng. Chem. Res.* **2018**, *57*, 10261-10268.
138. Beck, A.; Yang, A.-C.; Leland, A. R.; Riscoe, A. R.; Lopez, F. A.; Goodman, E. D.; Cargnello, M. Understanding the preferential oxidation of carbon monoxide (PrOx) using size-controlled Au nanocrystal catalyst. *AIChE J.* **2018**, *64*, 3159-3167.
139. LaRue, J.; Krejčí, O.; Yu, L.; Beye, M.; Ng, M. L.; Öberg, H.; Xin, H.; Mercurio, G.; Moeller, S.; Turner, J. J.; et al. Real-Time Elucidation of Catalytic Pathways in CO Hydrogenation on Ru. *J. Phys. Chem. Lett.* **2017**, *8* (16), 3820–3825.
140. Nilsson, A.; LaRue, J.; Öberg, H.; Ogasawara, H.; Dell’Angela, M.; Beye, M.; Öström, H.; Gladh, J.; Nørskov, J. K.; Wurth, W.; et al. Catalysis in Real Time Using X-Ray Lasers. *Chem. Phys. Lett.* **2017**, *675*, 145–173.

141. Beye, M.; Öberg, H.; Xin, H.; Dakovski, G. L.; Dell'Angela, M.; Föhlisch, A.; Gladh, J.; Hantschmann, M.; Hieke, F.; Kaya, S.; et al. Chemical Bond Activation Observed with an X-Ray Laser. *J. Phys. Chem. Lett.* **2016**, *7* (18), 3647–3651.
142. Zhang, S.; Plessow, P. N.; Willis, J. J.; Dai, S.; Xu, M.; Graham, G. W.; Cargnello, M.; Abild-Pedersen, F.; Pan, X. Dynamical Observation and Detailed Description of Catalysts under Strong Metal-Support Interaction. *Nano Lett.* **2016**, *16* (7), 4528–4534.

POSTER PRESENTATION ABSTRACTS

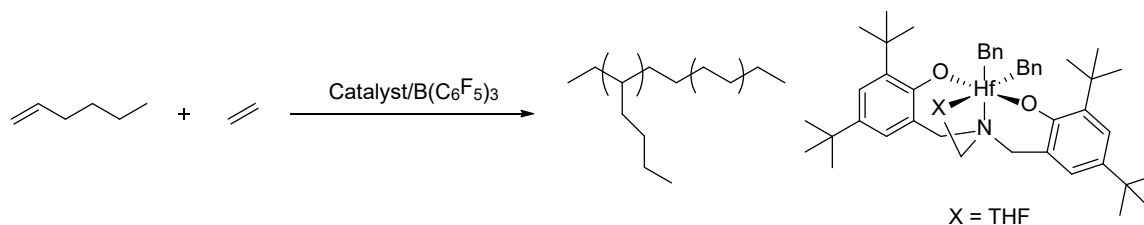
Kinetics of ethylene and 1-hexene co-oligomerization/co-polymerization

Chan Y. Park,^a Joshua Speer,^a Jeffrey Switzer,^b Grigori Medvedev,^b James M. Caruthers,^b and Mahdi M. Abu-Omar^a

^aDepartment of Chemistry and Biochemistry, University of California, Santa Barbara, California 93106. ^bSchool of Chemical Engineering, Purdue University, West Lafayette, Indiana 47907

Presentation Abstract

Our research group has developed an ethylene/1-hexene co-oligomerization/co-polymerization kinetics methodology and kinetic modeling using Zr or Hf-amine bis(phenolate) catalysts, $M[tBu-ON^XO]Bn_2$ (where X = THF activated by $B(C_6F_5)_3$). The incorporation of each olefinic monomer was calculated by ^{13}C NMR to obtain triad content in the resulting oligomer/polymer. The effects of reaction time, olefin concentration and catalyst concentration on the composition of copolymer were investigated. In-situ 1H NMR experiments show that the observed rate constant of ethylene consumption in the presence of α -olefin (1-hexene) is approximately 5x times faster than the observed rate constant of ethylene homo-polymerization. The experimental tools and kinetic methodology for obtaining comprehensive and sensitive multi-response data are described. Progress in kinetic modeling for obtaining elementary reactions rate constants for ethylene insertion into 1-hexene and vice versa will be discussed.



DE-SC0019161: Mechanism based oligomerization catalysis for upgrading α -olefins to produce specialty fuels and chemicals

Postdocs: Dr. Jeffrey Switzer

Students: Chan Y. Park and Joshua Speer

RECENT PROGRESS

The increased production of unconventional natural gas to light olefins presents an opportunity for using catalytic chemistry to convert light α -olefins to specialty fuels and higher hydrocarbons (chemicals). The most direct chemistry with 100% atom economy to do this transformation is single-site olefin oligomerization catalysis. The challenge, however, is to precisely control ethylene versus α -olefin insertion and introduce branching. To achieve this objective one must know the operative mechanism and pertinent elementary reaction rate constants that determine the outcome of a complex catalytic system. Our research program is developing the

methods to obtain multi-response kinetic data and comprehensive modeling of the kinetics enabling determination of mechanism and the corresponding elementary reactions rate constants, which in turn are used to design new systems and experiments. This iterative process leads to the determination of structure-function relationships illuminating the field of catalyst design.

Ethylene/1-hexene co-insertion under batch conditions

In toluene under 1 atm of ethylene and different concentrations of 1-hexene at 25 °C, pre-catalyst Hf[tBu-ON^{THF}O]Bn₂ is added followed by activator B(C₆F₅)₃. The products ranged in M_n from 15 to 29 kg mol⁻¹ and \bar{D} of 1.3-1.5, indicative of single site behavior and co-insertion of ethylene and 1-hexene because one uniform product was formed rather than two polymers/oligomers. Depending on the concentration of 1-hexene and extent of reaction, the % ethylene content varies (Table 1). By reducing the initial concentration of 1-hexene from 3.0 M to 0.5 M, the percent ethylene in the copolymers decreases (Entry 1-3). However, increasing reaction time from 10 to 70 min results in an increase in the percent of ethylene incorporation by a significant 13% (Entry 3 versus 4). The effect of reaction time on ethylene incorporation at higher 1-hexene concentration is not as significant (Entry 2 and 5).

Table 1. Batch ethylene/1-hexene copolymerization catalyzed by Hf[tBu-ON^{THF}O]Bn₂/B(C₆F₅)₃ at 25 °C.

Entry ^a	Time (min)	Initial [H] (M) ^c	Δ [H] (M) ^c	Hexene Conv. (%) ^c	Product yield (g)	% E ^d
1	10	3.0	0.357	12.1	0.455	17
2	10	1.5	0.259	17.7	0.255	23
3	10	0.5	0.076	14.9	0.090	26
4	70	0.5	0.278	55.5	0.275	39
5	30	1.5	0.513	34.3	0.407	19
6 ^b	30	1.5	0.464	31.0	0.458	23

^a Conditions: In toluene; volume of liquid phase = 10 mL; [cat.] = 3.00 mM; [act.] = 1.1 eq; ethylene pressure = 1 bar; temp = 25 °C; all reactions are stirred. ^b [cat.] = 5.00 mM ^c[H] was determined by ¹H NMR. ^d Percent ethylene in the copolymer was determined by ¹³C NMR.

The reaction is quenched with MeOD and product copolymer purified. ¹³C NMR is collected and regions selected following the Hsieh and Randall method.⁴ The triad distributions are calculated and summarized in Table 2. As the initial 1-hexene concentration is decreased, HHH decreases notably but EEE and EEH remain constant (Entries 1-3). The unexpected increases in EHE, HEH, and EHH will require insight from kinetic modeling to reconcile this experimental observation. As the reaction time increases from 10 to 70 min, HHH decreases and all other triads except EEE increase significantly (Entries 3 and 4). However, this trend appears to be quite sensitive to initial 1-hexene concentration. At high 1-hexene concentration of 1.5 M the trend is opposite of what is observed at lower concentration (Entries 2 and 5). These trends indicate a kinetic phenomenon and

the interplay of the rate constants from kinetic modeling should begin to provide explanations that can continue to hold or be refuted with further kinetic experiments that modeling can guide.

Table 2. Quantitative determination of triads of ethylene/1-hexene in copolymer products

Entry ^a	Initial [H] (M) ^c	Reaction time (min)	% E ^d	EEE ^e	EEH ^e	EHE ^e	HEH ^e	EHH ^e	HHH ^e
1	3.0	10	17	0.9	6.9	1.4	10.2	24.4	64.0
2	1.5	10	23	1.2	9.5	4.1	15.2	31.7	49.1
3	0.5	10	26	1.3	7.8	4.3	17.5	34.1	44.1
4	0.5	70	39	1.8	27.5	11.0	20.2	45.9	23.0
5	1.5	30	19	1.7	4.17	2.81	15.0	28.5	53.7
6 ^b	1.5	30	26	< 0.2	12.7	4.9	16.6	36.1	42.4

^a Conditions: In toluene; liquid volume = 10 mL; [cat.] = 3.00 mM; [act.] = 1.1 eq; ethylene pressure = 1 bar; temp = 25 °C; all reactions are stirred. ^b [cat.] = 5.00 mM. ^c [H] was determined by ¹H NMR. ^d Percent ethylene in the copolymer was determined by ¹³C NMR. ^e Percent triads calculation by ¹³C NMR.

In situ NMR studies

In situ NMR reactions without stirring are used to monitor the consumptions of ethylene and 1-hexene in real time. The kinetic profiles of both 1-hexene and ethylene consumption follow first-order kinetics and k_{obs} values are summarized in Table 3. Interestingly, k_{obs} of ethylene/1-hexene copolymerization was 4.4 times faster than k_{obs} of ethylene homo-polymerization.

Kinetic modeling

The sequence of olefin insertion to make carbon-carbon bonds on a catalyst site is a result of the rate of insertion of each olefin type, in our case ethylene versus α -olefin (1-hexene). An accurate record of the monomer sequence is therefore key in determining reaction rate constants for monomer insertion. In practice, while entire chain sequences are not available, the concentration of short monomer sequences can be collected through ¹³C NMR spectroscopy. We have collected monomer triad concentrations for ethylene–hexene copolymerization (Table 2 above) and used the data to examine potential chemical mechanisms for the reactions.

In the course of the project, we have developed a computational modeling code that will produce triad and monomer concentrations as functions of reaction time given an input chemical mechanism, initial monomer and catalyst concentrations, and rate constants. The modeling code allows us to compare hypothetical reaction schemes with actual chemical data, eliminating reactions that do not reproduce the observations. Furthermore, the modeling script provides the opportunity to distinguish between two or more potential mechanisms that both fit the chemical data. Each viable mechanism will contain differences that become pronounced for a certain set of

reaction conditions (e.g. different catalyst concentrations). The code allows us to explore these differences virtually, which guides experiment selection. In principle, only one model will fit all experimental data. The triad concentrations show dependence on initial 1-hexene concentration, where a higher value produces a higher concentration of HHH triads.

Table 3. NMR ethylene/1-hexene copolymerization by $\text{Hf}[\text{tBu-ON}^{\text{THF}}\text{O}]\text{Bn}_2/\text{B}(\text{C}_6\text{F}_5)_3$ at 25 °C.^a

Entry	[E] ₀ / M	[H] ₀ / M	[H]/[E] Ratio	k_{obs}^H/s^{-1}	k_{obs}^E/s^{-1}
1	0.0317	1.066	34	6.9×10^{-4}	25×10^{-4}
2	0.0377	0.141	4	8.3×10^{-4}	26×10^{-4}
3	0.0339	0	–	–	5.8×10^{-4}

^a Conditions: In deuterio toluene at 25 °C; liquid reaction volume = 2.75 mL; [cat.] = 5.00 mM; [act.] = 1.1 equivalent relative to catalyst. Concentration of H and E was monitored by ¹H NMR and kinetic profiles fitted to 1st order rate law equation.

Much of the modeling results are ongoing. One modeling result thus far is that the rate constant for the insertion of ethylene into hexene chain is as fast as or faster than the rate constant for the insertion of ethylene into another ethylene. This result is somewhat surprising because the conventional wisdom for olefin insertion is that a less sterically demanding alkyl chain would allow for faster olefin insertion.

Publications Acknowledging this Grant in 2015-2018

(XX) *Exclusively funded by this grant;*

(1) Gunasekara, T.; Preston, A. Z.; Zeng, M.; Abu-Omar, M. M. Highly Regioselective α -olefin Dimerization Using Zirconium and Hafnium Amine Bis(phenolate) Complexes. *Organometallics* **2017**, *36*, 2934-2939.

(2) Gunasekara, T.; Kim, J.; Xiong, S.; Preston, A.; Steelman, D. K.; Medvedev, G. A.; Delgass, W. N.; Caruthers, J. M.; Abu-Omar, M. M. Interaction between Two Active Sites of the Same Catalyst for Macromonomer Enchained Olefin Polymerization. *Macromolecules* **2017**, *50*, 9151-9161.

(3) Switzer, J. M.; Pletcher, P. D.; Steelman, D. K.; Kim, J.; Medvedev, G. A.; Abu-Omar, M. M.; Caruthers, J. M.; Delgass, W. N. Quantitative Modeling of the Temperature Dependence of the Kinetic Parameters for Zirconium Amine Bis (Phenolate) Catalysts for 1-Hexene Polymerization. *ACS Catalysis* **2018**, *8*, 10407-10418.

(XXI) *Jointly funded by this grant and other grants with leading intellectual contribution from this grant;*

(1) Pletcher, P. D.; Switzer, J. M.; Steelman, D. K.; Medvedev, G. A.; Delgass, W. N.; Caruthers, J. M.; Abu-Omar, M. M. Quantitative Comparative Kinetics of 1-Hexene Polymerization across Group IV Bis-Phenolate Catalysts. *ACS Catalysis* **2016**, *6*, 5138-5145.

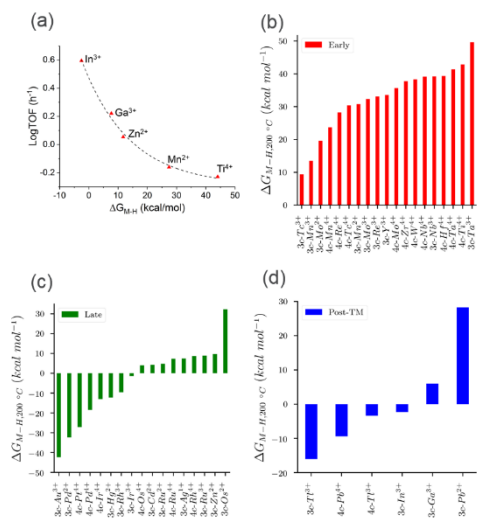
(2) Preston, A. Z.; Kim, J.; Medvedev, G. A.; Delgass, W. N.; Caruthers, J. M.; Abu-Omar, M. M. Steric and solvation effects on polymerization kinetics, dormancy, and tacticity of Zr-salan catalysts. *Organometallics* **2017**, *36*, 2237-2244.

(3) Gunasekara, T.; Kim, J.; Preston, A.; Steelman, D. K.; Medvedev, G. A.; Delgass, W. N.; Sydora, O. L.; Caruthers, J. M.; Abu-Omar, M. M. Mechanistic Insights into Chromium-Catalyzed Ethylene Trimerization. *ACS Catalysis* **2018**, *8*, 6810-6819.

Development of Silica Supported Single-Site Metal Ion Catalysts for Alkenes Hydrogenation and Alkanes Dehydrogenation

Cong Liu, Magali Ferrandon, A. Jeremy Kropf, David M. Kaphan, Massimiliano Delferro
Chemical Sciences and Engineering Division, Argonne National Laboratory

With the increasing attention on single-site heterogeneous catalysts on account of their unique catalytic properties and well-defined catalytic sites, more effective design strategies are necessary to fully leverage the potential of these this class of catalyst. We demonstrate a computationally guided active-site design strategy for the development of silica-supported metal ion catalysts (M/SiO₂) for olefin hydrogenation. Propylene hydrogenation was used as a probe reaction to establish an activity-descriptor relationship, which correlates the computational activity descriptor (reaction free energy of the metal hydride formation) with the experimental reaction rate, as a function of silica-supported metal ion catalyst (i.e., Ga³⁺, Zn²⁺, Mn²⁺ and Ti⁴⁺/SiO₂). This relationship was then used to predict the trend of activities of a variety of M/SiO₂ systems, and an In³⁺/SiO₂ catalyst was identified as the most promising candidate based on its predicted activity and synthetic feasibility. The monodisperse In³⁺/SiO₂ catalyst was then synthesized, for the first time, and showed higher propylene hydrogenation activity than the other four single-site heterogeneous catalysts, as predicted. Furthermore, more detailed computational studies were carried out on a larger set of potential single site catalyst structures to investigate the reactivity of these catalysts with H₂ as well as to evaluate the performance of density functional theory (DFT) methods in conjunction with triple- ζ quality basis sets (i.e., cc-pVTZ) on reaction energetics. The ions considered include 4*d* and 5*d* metals as well as several post-transition metal ions. ONIOM calculations (CCSD(T)//MP2) are used to assess the accuracy and reliability of the MP2 results and it is found that MP2 is a suitable level of theory for gauging the performance of DFT functionals. The performance of various DFT functionals is assessed relative to MP2 results and it is found that the wB97xd and PBE0 functionals have the lowest standard deviation (STD) values. The B3LYP functional is shown to have the similar MAD and STD values as the top performing functionals. Potential active catalytic sites for exergonic hydrogen activation predicted in this study include mostly late and post transition metal ions, i.e., Au³⁺, Pd²⁺, Pt⁴⁺, Pd⁴⁺, Ir⁴⁺, Hg²⁺, Rh³⁺, Pb⁴⁺, Tl³⁺, In³⁺, Ir³⁺, Os⁴⁺, Cd²⁺, Ru²⁺, and Ga³⁺. This study provides important guidance to future computational studies of such catalyst systems.

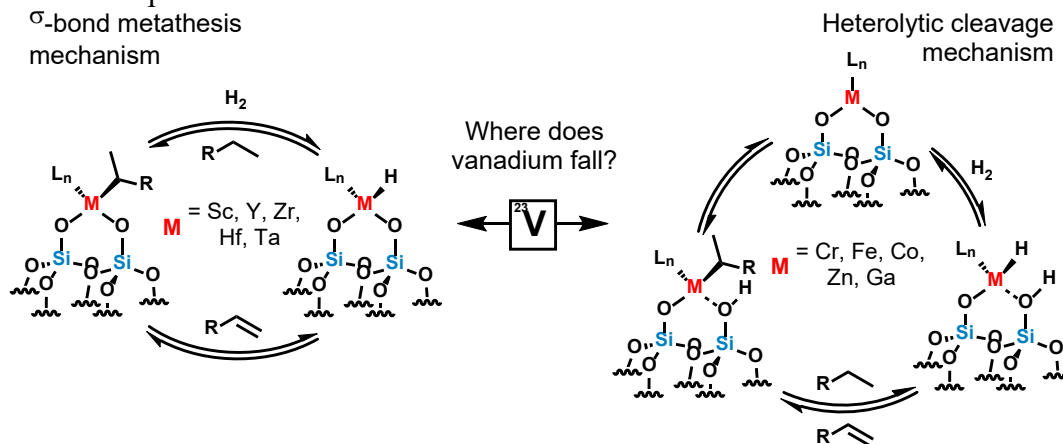


FWP50966: Electronic Cooperativity in Supported Single- and Multinuclear-Sites for Catalytic C-C and C-H Bonds Functionalization

Mechanistic Aspects of a Surface Organovanadium(III) Catalyst for Hydrocarbon Hydrogenation and Dehydrogenation

David M. Kaphan, Magali S. Ferrandon, Ryan R. Langeslay, Gokhan Celik, Evan C. Wegener, Cong Liu, Jens Niklas, Oleg G. Poluektov, Massimiliano Delferro
Chemical Sciences and Engineering Division, Argonne National Laboratory

Understanding the mechanisms of action for base metal catalysis of transformations typically associated with precious metals is essential for the design of new technologies for a sustainable energy economy. Isolated transition metal and post-transition metal catalysts on oxides such as silica are generally proposed to effect hydrogenation and dehydrogenation by a mechanism featuring either σ -bond metathesis or heterolytic bond cleavage as the key bond activation step. In this work an organovanadium(III) complex on silica, which is a precatalyst for both olefin hydrogenation and alkane dehydrogenation, is interrogated by a series of reaction kinetics and isotopic labeling studies in order to shed light on the operant mechanism for hydrogenation. Upon exposure to dihydrogen, spectroscopic evidence including EPR and X-ray absorption spectroscopy are consistent with the formation of a persistent surface vanadium(III) hydride. This structural assignment is further supported by study of ethylene oligomerization activity for both the hydrogenolyzed and as prepared material. The putative vanadium hydride was highly active for oligomerization at room temperature, however, the as prepared material also effected this transformation unexpectedly, after ethylene insertion into the vanadium-mesityl bond and β -hydride elimination to generate the vanadium hydride *in situ*. The kinetic dependencies of the reaction components of the hydrogenation process are potentially consistent with both the σ -bond metathesis and the heterolytic bond activation mechanisms, however, a key deuterium incorporation experiment definitively excludes the simple σ -bond metathesis mechanism. Alternatively a two electron redox cycle, rarely invoked for homologous catalyst systems, is also consistent with experimental observations.



FWP50966: Electronic Cooperativity in Supported Single- and Multinuclear-Sites for Catalytic C-C and C-H Bonds Functionalization

Heterogeneous Catalysts for Strategic Formation of C-C, C-O, and C-N Bonds

Chemical Sciences Division, Lawrence Berkeley National Laboratory, Berkeley, CA

Presentation Abstract

The objectives of this program are to establish detailed relationships between the composition and structure of active sites and their catalytic activity for the targeted formation of C-C, C-O, and C-N bonds that are involved in processes for the formation of fuels and chemicals. This work provides guidance for achieving high catalyst activity together with high selectivity to desired products. Recent efforts have focused on the mechanism and kinetics of alcohol etherification over tungstated zirconia, the synthesis of isobutene from ethanol over zirconia-supported ZnO, the amination of propanol over HAP, and the reductive amination of isobutene over zeolites. These studies have provided fundamental insights into the roles of Lewis acid and Lewis/Brønsted base sites in promoting these reactions.

FWP Number: CH03201

Grant Title: Catalysis Program*

*This work is part of the Chemical Sciences Division Catalysis Program at LBNL

Student(s): Lance Bettison, Christopher Ho, Branden Leonhardt

RECENT PROGRESS

Mechanism and Kinetics of Alcohol Etherification over Tungstated Zirconia

Growing interest in finding renewable alternatives to conventional fossil fuels and petroleum-derived specialty chemicals has motivated the investigation of biomass-derived alcohols to make ethers as diesel additives or lubricants (see Fig. 1). To optimize the direct etherification of long chain alcohols in the liquid phase, it is necessary to develop an understanding of the kinetics and mechanism of etherification and dehydration reactions. Our work has focused on tungstated zirconia, a highly active and selective solid-acid

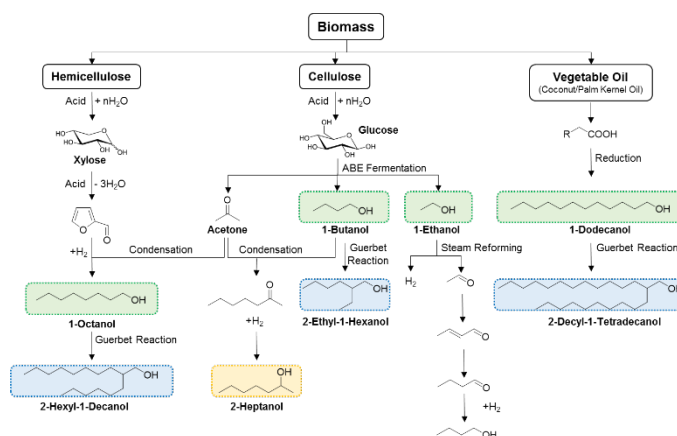


Fig. 1 Pathways to the formation of linear and branched alcohols derived from biomass

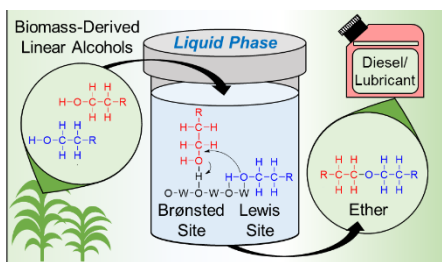


Fig. 2. Schematic illustrating the roles of Brønsted- and Lewis-acid sites in the conversion of biomass-derived alcohols to ethers over tungstated zirconia

catalyst for the liquid-phase etherification of 1-dodecanol and other alcohols. Investigations of the mechanism and kinetics of this reaction suggest that cooperation between Brønsted- and Lewis-acid sites on tungstated zirconia enhances the selectivity to ether by increasing the surface concentration of adsorbed alcohol, thereby promoting bimolecular ether formation relative to unimolecular alcohol dehydration. As shown in Fig. 2, the rate-limiting step for etherification is the formation of a C-O bond between two adsorbed alcohol molecules, and the suggested rate-limiting step for dehydration is the cleavage of the C-H bond of the β -carbon atom in an adsorbed alcohol. Measurements of the

kinetic isotope effects for etherification and dehydration support the proposed mechanism. A microkinetic model based on the proposed mechanism for dodecanol etherification and dehydration over tungstated zirconia accurately describes the observed effects of alcohol concentration and product inhibition.

We have also undertaken a comprehensive investigation of the effect of alcohol structure on the kinetics of liquid phase etherification over tungstated zirconia. For direct etherification of primary alcohols in the liquid phase, ether selectivities of $>94\%$ for C_6 - C_{12} linear alcohol coupling at 393 K, even though at this temperature dehydration to alkenes is thermodynamically preferred. We examined the influence of alcohol chain length, position of carbon chain branches, and length of carbon chain branches on both etherification and dehydration. The length of linear primary alcohols (C_6 - C_{12}) has a negligible effect on apparent activation energies for etherification and dehydration, demonstrating the possibility to produce both symmetrical and asymmetrical linear ethers. Reactions over a series of C_6 alcohols with varying methyl branch positions indicated that substituted alcohols (2° , 3°) and alcohols with branches on the β -carbon readily undergo dehydration, but alcohols with branches at least 3 carbons away from the $-OH$ group are highly selective to ether. Trends in the effects of alcohol structure on selectivity are consistent with previously proposed mechanisms for etherification and dehydration, and elucidate possible pathways for the selective formation of ethers from biomass-derived alcohols.

Acetone Condensation over Cation-exchanged Hydroxyapatite Catalysts

We have investigated the mechanism and site requirements for acetone coupling to methyl isobutyl ketone over hydroxyapatite. The reaction proceeds by consecutive aldol addition, dehydration, and hydrogenation. Product distributions from diacetone alcohol and mesityl oxide feeds reveal that aldol addition is rapid and reversible, and that the subsequent dehydration is rate-limiting. *In-situ* pyridine and CO_2 titration studies show that aldol dehydration occurs mainly over basic sites via an E_{1cB} mechanism. A series of cation-substituted hydroxyapatite samples were prepared by ion-exchange to investigate further the role of acid-base strength on catalytic performance. Characterization of these samples by PXRD, BET, ICP-OES, XPS, CO_2 -TPD, and Raman spectroscopy show that the exchange procedure does not affect the bulk properties of hydroxyapatite. DFT calculations reveal that in addition to Lewis acidity/basicity, the size of the cation plays a big role in the chemistry: cations that are too large (Ba^{2+}) or too small (Mg^{2+}) adversely affect reaction rates due to excessive stabilization of intermediate species. Strontium-

substituted hydroxyapatite catalyst is the most active because it catalyzes α -proton abstraction and C-O bond cleavage of diacetone alcohol efficiently.

Dehydromination of propanol and hydroamination of isobutene

We have investigated Ni-supported hydroxyapatite catalyst (Ni/HAP) for propanol amination to propylamine at 423 K. The reaction proceeds via dehydromination, a process that involves sequential dehydrogenation, condensation, and hydrogenation. Kinetic and isotopic studies indicate that α -H abstraction from propoxide species limits the rate of the dehydrogenation step, and hence the overall rate of reaction (see Fig. 2). The rate of propanol dehydrogenation depends on the composition of the support and on the concentration of Ni sites located at the interface between the Ni nanoparticles and the support. Ni/HAP is an order of magnitude more active than Ni/SiO₂ and displays a higher selectivity towards primary amine. The superior performance of Ni/HAP results from the high density of basic sites HAP, which are responsible for stabilizing alkoxide intermediates and suppressing the disproportionation and secondary amination of amines.

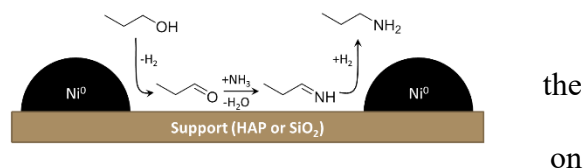


Fig. 3. Mechanism for the dehydroamination of propanol

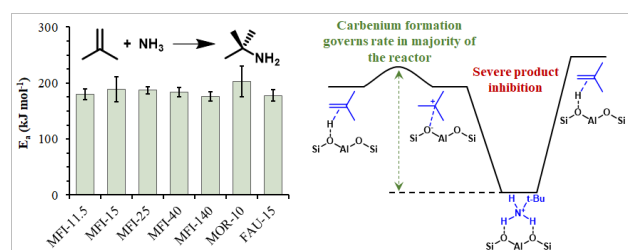


Fig. 4. Effects of zeolite structure on the TOF for the mechanism of isobutene hydroamination

In more recent work, we investigated the hydroamination of isobutene with NH₃ over Brønsted acidic zeolites at 1 atm and 453-483 K. To compare catalytic activities over different zeolites, the measured reaction rates are normalized by the number of active sites determined by tert-butylamine TPD. Small- and medium-pore zeolites with one-dimensional channels exhibit low activity due to pore blockage by adsorbed tert-

butylammonium ions. However, turnover frequencies and activation energies are not sensitive to framework identity, as long as the active site is accessible to isobutene and tert-butylamine (see Fig. 4). Kinetic measurements and FTIR spectroscopy reveal that the Brønsted acid sites in MFI are covered predominantly with tert-butylammonium ions under reaction conditions. Desorption of tert-butylamine is assisted by the concurrent adsorption of isobutene. DFT simulations show that at very low tert-butylamine partial pressures, e.g., at the inlet to the reactor, tert-butylamine desorption is rate-limiting (see Fig. 4). However, at sufficiently high tert-butylamine partial pressures (> 0.03 kPa), protonation of isobutene to the corresponding carbenium ion limits the rate of amination.

Publications Acknowledging this Grant in 2015-2018

1. Johnson, G. R.; Werner, S.; Bell, A. T. An Investigation into the Effects of Mn Promotion on the Activity and Selectivity of Co/SiO₂ for Fischer-Tropsch Synthesis: Evidence for Enhanced CO Adsorption and Dissociation. *ACS Catal.*, **2015**, *5*, 5888-5903.
2. Johnson, G. R.; Bell, A. T. Role of ZrO₂ in Promoting the Activity and Selectivity of Co-

- Based Fischer–Tropsch. *ACS Catal.*, **2015**, *6*, 100-114.
3. Zhai, S.; Wütschert, M.; Licht, R. B.; Bell, A. T. Effects of Catalyst Structure on the Oxidation of Propene to Acrolein. *Catal. Today*, **2016**, *261*, 146-153.
 4. Ho, C.; Shylesh, S.; Bell, A. T.; Mechanism and Kinetics of Ethanol Coupling to Butanol over Hydroxyapatite. *ACS Catal.*, **2016**, *6*, 938-949.
 5. Johnson, G. R.; Bell, A. T. Effects of Lewis Acidity of Metal-Oxide Promoters on the Activity and Selectivity of Co-Based Fischer-Tropsch Catalysts. *J. Catal.*, **2016**, *338*, 250-264.
 6. Licht, R. B.; Vogt, D.; Bell, A. T. The Mechanism and Kinetics of Propene Ammoxidation over α -Bismuth Molybdate. *J. Catal.*, **2016**, *339*, 228-241.
 7. Dombrowski, J.; Bell, A. T.; Tilley, T. D. Ga[OSi(O(t)Bu)₃]₃·THF, a Thermolytic Molecular Precursor for High Surface Area Gallium-Containing Silica Materials of Controlled Dispersion and Stoichiometry. *Dalton Trans.*, **2016**, *45*, 11025-11034.
 8. Howell, J.; Li, Y.-P.; Bell, A. T. Propene Metathesis over Supported Tungsten Oxide Catalysts: A Study of Active Site Formation. *ACS Catal.*, **2016**, *6*, 7728–7738.
 9. Licht, R. B.; Getsoian, A. B.; Bell, A. T. The Role of Local Site Geometry on the Hydrogen Abstraction Ability of Scheelite Mixed Metal Molybdates. *J. Phys. Chem.*, **2016**, *120*, 29233–29247.
 10. Licht, R. B.; Bell, A. T.; A DFT Investigation of the Mechanisms of Propene Ammoxidation over α -Bismuth Molybdate. *ACS Catal.*, **2017**, *7*, 161-176.
 11. Rorrer, J.; He, Y.; Toste, F. D.; Bell, A. T. Mechanism and Kinetics of 1-Dodecanol Etherification over Tungstated Zirconia. *J. Catal.* **2017**, *354*, 13-23.
 12. Shylesh, S.; Gokhale, A. A.; Ho, C. .; Bell, A.T. Novel Strategies for the Production of Fuels, Lubricants, and Chemicals from Biomass. *Acc. Chem. Res.* **2017**, *50*, 2589-2597.
 13. Rorrer, J.; Pindi, S.; Toste, F. D.; Bell, A. T. Effect of Alcohol Structure on the Kinetics of Etherification and Dehydration over Tungstated Zirconia. *ChemSusChem* **2018**, *11*, 3104-3111.
 14. Ho, C. R.; Zheng, S.; Sylesh, S.; Bell, A. T. The mechanism and kinetics of methyl isobutyl ketone synthesis from acetone from hydroxyapatite. *J. Catal.* **2018**, *365*, 174-183.

Lewis Acid and Solvent Effects on Carbon Dioxide Insertion and Valorization Processes

Nilay Hazari¹ and Wesley H. Bernskoetter²
 Yale University¹ and University of Missouri²

Presentation Abstract

The worldwide dependence on non-renewable energy sources and chemical feedstocks is detrimental to the environment, while the fluctuating cost and availability of these finite resources creates economic uncertainty. As a result, there are significant benefits associated with transitioning to renewable resources in order to meet our global energy and commodity chemical demands. Carbon dioxide (CO₂) is an especially appealing renewable C₁ feedstock for the production of fuels and commodity chemicals due to its low cost, abundance, and relative lack of toxicity. This poster summarizes our project's latest advances in understanding the catalytic transformations associated with CO₂ valorization. These include: (1) Kinetic studies elucidating the respective influences of solvent, Lewis acids and metal-ligand identity on the rate of CO₂ insertion reactions; and (2) the application of pincer supported iron catalysts for (de)hydrogenative reactions relevant to hydrogen storage and commercial chemical syntheses.

DE-SC0018222: Elucidating the Role of Lewis Acid Co-Catalysts in Base Metal Promoted CO₂ Hydrogenation and Related Processes

Postdoc(s): Name(s) Upul Jayarathne (Missouri); Danielle Chirdon (Missouri)

Student(s): Julia Curley (Yale); Jessica E. Heimann (Yale); Nicholas E. Smith (Yale)

RECENT PROGRESS

Research progress towards the design of more efficient catalysts for reversible base metal catalyzed CO₂ hydrogenation and related reactions is summarized below for selected areas.

Examine the precise role of Lewis Acids (LAs) in the (de)insertion of carbon dioxide into metal hydrides and related ligands.

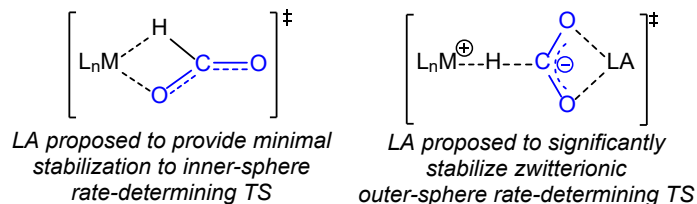


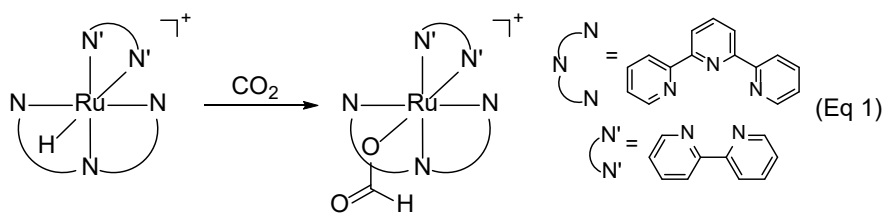
Figure 1. Rate limiting transition structures for CO₂ insertion into metal-hydrides.

undergo CO₂ insertion reactions, there are relatively few experimental, mechanistic studies about CO₂ insertion and even fewer in which the kinetics of insertion are measured. Thus, the factors

The insertion of CO₂ into a transition metal hydride bond is a key step in many catalytic transformations involving CO₂. For example, in the hydrogenation of CO₂ to formic acid or methanol, the insertion of CO₂ into a metal hydride is proposed to be crucial. However, while a plethora of well-defined systems

that are important in determining the rate of CO₂ insertion are unclear. Recently, we started using a stopped-flow instrument with a UV-Vis detector to determine the kinetics of CO₂ insertion into metal hydrides. We have studied the insertion of CO₂ into [(^tBuPCP)NiH] (^tBuPCP = 2,6-C₆H₃-(CH₂P^tBu)₂) to form [(^tBuPCP)Ni-OC(O)H], and [(ⁱPrPN^HP)IrH₃] (ⁱPrPN^HP = HN{CH₂CH₂(PⁱPr)₂})₂) to form *trans*-[(ⁱPrPN^HP)IrH₂OC(O)H]. The former is proposed to insert CO₂ via an inner-sphere pathway, which has a direct interaction between CO₂ and the metal in the rate-determining transition state (TS). The latter, meanwhile, is postulated to react via an outer-sphere pathway, which proceeds with no interaction between CO₂ and the metal in the rate-determining TS (Figure 1). In our preliminary work, we determined the rate law, activation parameters, and solvent effect for both of these systems. For our inner-sphere Ni system, we demonstrated that the rate of CO₂ insertion increases as the ancillary ligand becomes more electron rich or less sterically bulky. Analysis of solvent effects for both systems revealed that contrary to a previous report, there is almost no correlation between the dielectric constant of the solvent and the rate of CO₂ insertion. Instead, the acceptor number (AN; a measure of the Lewis acidity of the solvent) is the best predictor of the rate of CO₂ insertion for a given solvent. The solvent effect is significantly larger for [(ⁱPrPN^HP)IrH₃] as compared to [(^tBuPCP)NiH], suggesting that it may be possible to use solvent effects to make predictions about the mechanism of CO₂ insertion. Furthermore, the addition of 20 equivalents of a Lewis acid (LA) such as LiPF₆ increases the rate of CO₂ insertion into [(ⁱPrPN^HP)IrH₃] by up to a factor of almost 100, whereas there is no LA effect on the rate of insertion into [(^tBuPCP)NiH]. These results are rationalized on the basis that a LA or solvent with a higher AN provides stabilization for the zwitterionic rate-determining TS in an outer-sphere process. Conversely, for an inner-sphere process, this zwitterionic state is not rate-determining, so its stabilization by LA or solvent does not affect the overall rate of reaction.

The complex [(ⁱPrPN^HP)IrH₃] is only soluble in non-polar organic solvents where the speciation and dissociation constants of alkali metal salts are often unclear. This causes difficulties in understanding LA effects in CO₂ insertion from alkali metals, as it is possible that ion pairing may reduce the effective concentration of a LA in solution. In contrast, the Ru complex [(terpy)(bipy)RuH]⁺ (terpy = 2,2':6',2''-terpyridine; bipy = 2,2'-bipyridine) is known to undergo CO₂ insertion in a range of more polar solvents, such as ACN, ⁱPrOH, and MeOH, where the speciation of LAs is well understood. We have used stopped-flow to measure the kinetics of CO₂ insertion into [(terpy)(bipy)RuH]⁺ in a range of different solvents both in the presence and absence

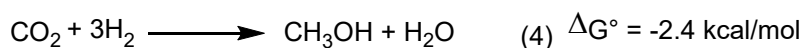
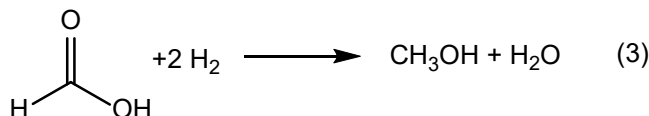
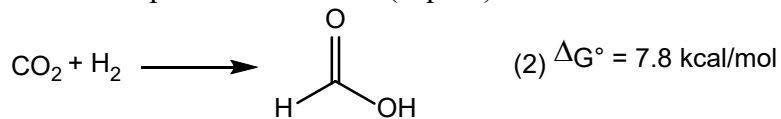


of LAs (Eq 1). Our main findings are: (i) The enhancement in the rate of CO₂ insertion is solvent dependent with alkali metal LAs, such as Li⁺. Some solvents

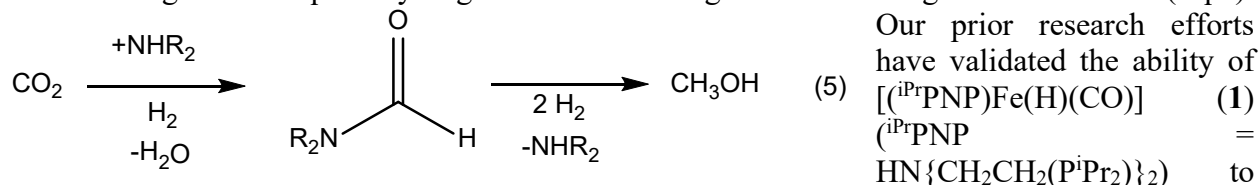
display large LA enhancements, whereas others display no enhancement. In general, solvents that can coordinate strongly to Li⁺, such as DMSO, display no LA effect. (ii) In solvents where there is an enhancement in the rate of CO₂ insertion, such as ACN, the identity of the anion associated with the alkali metal Lewis acid does not matter. For example, LiOTf, LiNTf, and LiBPh₄ all give the same enhancement in the rate of CO₂ insertion. (iii) For alkali metal cations in ACN, the smaller cations provide more stabilization to the TS and the order of enhancement is Li⁺ >> Na⁺ > K⁺ >> Rb⁺. This work is currently being prepared for publication.

Sequential hydrogenation of CO₂ to methanol

The hydrogenation of CO₂ to methanol is a key target of this project, and one which has the potential to influence renewable energy storage and commodity chemical production. The most common approach to this critical hydrogenation involves reduction of CO₂ with one equivalent of H₂ to give intermediate formic acid (or formate) and then, hydrogenation of the formic acid with 2 additional equivalents of H₂ to produce methanol (Eq 2-4).



However, while the overall process is thermodynamically favorable, the intermediate production of formic acid is uphill energetically. To circumvent this problem, our project has targeted methods which trap the intermediate formic acid (or formate) in a more stable form and hydrogenate that trapped species to ultimately yield methanol and reform the trapping agent. Our primary trapping agents have been secondary amines. These undergo initial N-formylation with CO₂ allowing for subsequent hydrogenation of resulting formamides to generate methanol (Eq 5).



mediate both steps of the proposed amine assisted CO₂-to-MeOH conversion (Figure 2). However, despite the promising precedent suggesting catalyst **1** could conduct both steps of the conversion in a single setup, we have only successfully obtained methanol when completing this reaction as two separate steps. The system achieves TONs as high as 590 for methanol production using a morpholine

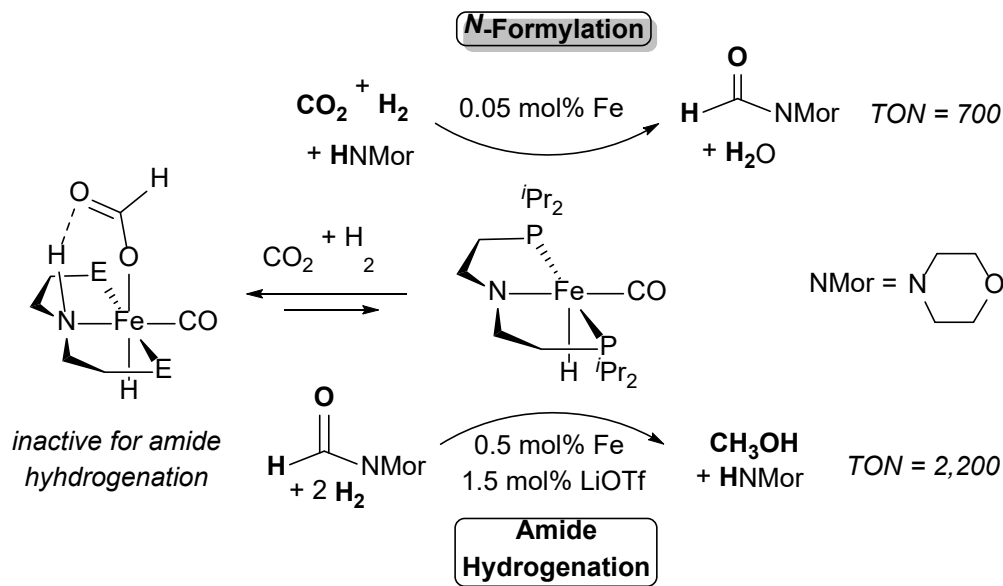
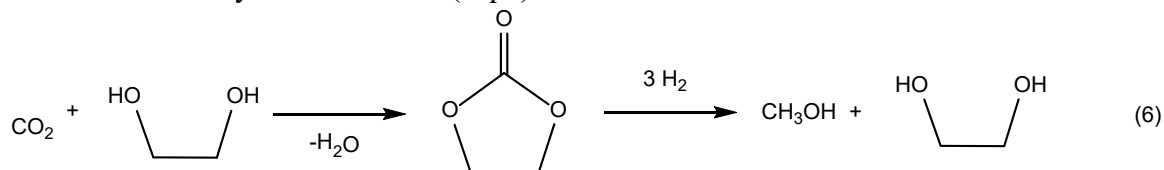


Figure 2. Two component reactions of proposed amine assisted CO₂-to-MeOH conversion.

assisted path, but the need for a sequential process originates from the formation of an overly stable iron formate complex, [(ⁱPr^HP)^NFeH(CO){OC(O)H}] (Figure 2). Strong bases can be added to activate the iron formate species for further methanol production, but the need for such bases is incompatible with a single stage catalytic process. Our current efforts for enabling a single step CO₂-to-methanol conversion focus on replacing amines with diols to trap formate/formic acid intermediates as cyclic carbonates (Eq 6).



Preliminary investigations indicate that catalyst **1** affords promising activity for ethylene carbonate reduction, achieving over 8,000 turnovers with respect to carbonate consumption (Figure 3). The yield of methanol is slightly less (~6,000) due to a build-up of intermediate aldehydes likely produced via reaction of alcohols with transient formaldehyde. Additional optimization of this reaction should allow for development of an alternative CO₂-to-methanol pathway possibly allowing for all-in-one conversion.

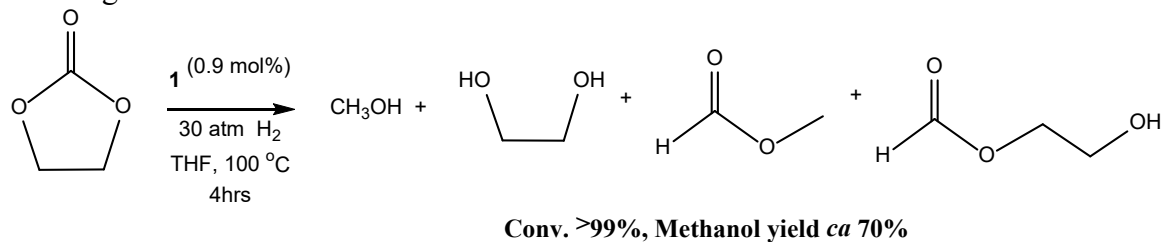


Figure 3. Catalytic hydrogenation of ethylene carbonate.

Publications Acknowledging this Grant in 2016-2019

(I) Exclusively funded by this grant;

Jayarathne, U.; Hazari, N.; Bernskoetter, W. H. "Selective Iron-Catalyzed N- Formylation of Amines using Dihydrogen and Carbon Dioxide" *ACS Catal.* **2018**, *8*, 1338-1345.

Lane, E. M.; Hazari, N.; Bernskoetter, W. H. "Iron-catalyzed Urea Synthesis: Dehydrogenative Coupling of Methanol and Amines" *Chem. Sci.* **2018**, *9*, 4003-4008.

Heimann, J. E.; Bernskoetter, W.H.; Guthrie, J.A.; Hazari, N.; Mayer, J.M. "Effect of Nucleophilicity on the Kinetics of CO₂ Insertion into Pincer-Supported Nickel Complexes" *Organometallics*, **2018**, *37*, 3649-3653.

Heimann, J. E.; Bernskoetter; Hazari, N. "Understanding the Individual and Combined Effects of Solvent and Lewis Acid on CO₂ Insertion into a Metal Hydride." *J. Am. Chem. Soc.* **2019**, *online ASAP*.

(II) Jointly funded by this grant and other grants with leading intellectual contribution from this grant;

Curley, J. B.; Smith, N. E.; Bernskoetter, W. H.; Hazari, N.; Mercado, B. Q. "Catalytic Formic Acid Dehydrogenation and CO₂ Hydrogenation Using Iron PN^RP Pincer Complexes with Isonitrile Ligands" *Organometallics*, **2018**, *37*, 3846-3853.

Suárez, L. A.; Culakova, Z.; Balcells, D.; Bernskoetter, W. H.; Eisenstein, O.; Goldberg, K.I.; Hazari, N.; Tilset, M.; Nova, A. "The Key Role of the Hemiaminal Intermediate in the Iron-Catalyzed Deaminative Hydrogenation of Amides" *ACS Catal.* **2018**, *8*, 8781-8762.

Heimann, J. E.; Bernskoetter; W.H. Hazari, N.; Mayer, J.M. "Acceleration of CO₂ Insertion into Metal Hydrides: Ligand, Lewis Acid and Solvent Effects on Reaction Kinetics" *Chem. Sci.* **2018**, *9*, 6629-6638.

Clusters as catalysts for small molecule activation

Amy Marie M. Bartholomew, Justin J. Teesdale, Brian J. Malbrecht
Harvard University, 12 Oxford Street, Cambridge, MA 02138

Presentation Abstract

Current state of the art small molecule activation catalyst design has not directly targeted transition metal complexes capable of mediating the multi-electron redox processes necessary to reduce the overpotential (energy loss) required to achieve efficient activation of small molecule substrates. In this vein, a new strategy has been developed for the assembly of polynuclear architectures; allowing for the construction of tunable polymetallic centers that assemble easily within a pre-organized template (conferring stability, selectivity and tunability) that can effect multi-electron redox processes for reactions. Catalyst development has commenced with the following target design elements: (1) catalysts featuring multiple transition metal ions in the same reaction space to greatly expand accessible molecular redox capabilities; (2) catalysts are assembled in a polynucleating ligand framework that permits control over the cluster morphology as well as the local steric and electronic environment of the transition metal ions within the cluster. The high-tunability of the catalyst composition (metal content) and geometric flexibility has permitted a rigorous assessment of electronic-structure-to-function relationship to be developed, further guiding synthetic efforts to realize more potent catalysts.

Grant or FWP Number: Catalyst design for small molecule activation of energy consequence

PI: Theodore A. Betley

Student(s): Amy Marie M. Bartholomew, Justin J. Teesdale, Brian J. Malbrecht

RECENT PROGRESS

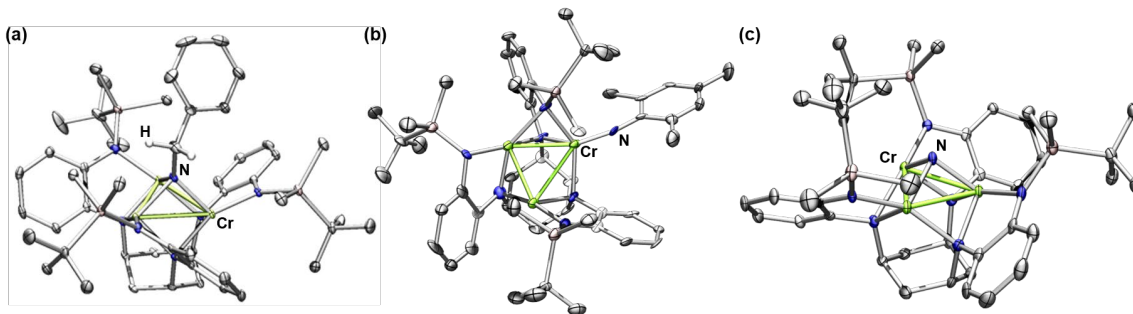
Multi-electron reactivity of a trichromium cluster

Figure 1. Solid-state molecular structures (a) $(^{tbs}L)Cr_3(\mu^3-NBn)$, (b) $(^{tbs}L)Cr_3(\mu^1-NMes)$, and (c) $(^{tbs}L)Cr_3(\mu^3-N)$ at 100 K with 50% (a,c) or 35% (b) probability ellipsoids. Solvent molecules and most hydrogen atoms omitted for clarity.

Publications Acknowledging this Grant in 2018-2019

(II) Publications jointly funded

Bartholomew, A. M.; Teesdale, J. J.; Hernández Sánchez, R.; Malbrecht, B. J.; Juda, C. E.; Menard, G.; Bu, W.; Iovan, D. A.; Mikhailine, A. A.; Zheng, S.-L.; Sarangi, R.; Wang, S. G.; Chen, Y.-S.; Betley, T. A. “Resolving redox inequivalence within isovalent clusters: exposing the inadequacy of redox formalisms.” *Proc. Nat. Acad. Sci.* **2019**, *In Press*.

Bartholomew, A. M.; Juda, C. E.; Nessralla, J. N.; Lin, B.; Wang, S.Y. G.; Chen, Y.-S.; Betley, T. A. “Ligand-based control of single-site vs multi-site reactivity by a trichromium cluster.” *Angew. Chem. Int. Ed.*, **2019**, *58*, 5687-5691.

Hernández Sánchez, R.; Betley, T. A. “Thermally persistent high spin ground states in octahedral iron clusters.” *J. Am. Chem. Soc.* **2018**, *140*, 16792-16806.

Polyfunctional Catalysis for C₁ conversion: Appraisal and circumvention of thermodynamic limits in non-oxidative methane dehydroaromatization

Neil K. Razdan, Anurag Kumar, Aditya Bhan
Chemical Engineering and Materials Science
University of Minnesota

Presentation Abstract

Carbide forms of molybdenum encapsulated in medium-pore MFI zeolites (Mo/ZSM-5) catalyze non-oxidative methane dehydroaromatization (DHA) with high benzene selectivity (~70%) at conversions near the thermodynamic limit (~10% at 973 K and 1 atmosphere pressure). Congruence between conversion versus contact time curves obtained for a partially deactivated catalyst bed and a fresh catalyst bed at identical contact times enables us to establish that Mo/ZSM-5 catalysts undergo nonselective deactivation and to identify that DHA involves sequential $\text{CH}_4 \leftrightarrow \text{C}_2\text{H}_6 \leftrightarrow \text{C}_2\text{H}_4 \leftrightarrow \text{C}_2\text{H}_2 \leftrightarrow \text{C}_6\text{H}_6$ reactions with ethane as the only primary carbon-containing product. Appraisal of reversibility of the individual steps reveals that the kinetically relevant step in this series network is a function of conversion when rigorous averaging of rates and reversibility are accomplished. Hydrogen removal is the kinetically relevant step at methane conversions exceeding 3% and the addition of zirconium as a hydrogen absorbent serves to alleviate thermodynamic limits to DHA by forming a bulk metal hydride that can be regenerated in inert flow. Proximity requirements in polyfunctional Mo/ZSM-5 + Zr formulations can be described by a reaction-transport model that synthesizes interplay of kinetic, diffusive, and convective length- and time-scales captured by Péclet and Dämmkohler number to predict influence of catalyst-absorbent proximity on DHA rates.

DE-SC0019028: Polyfunctional catalysis for upgrading C1 feedstocks

Student(s): Anurag Kumar, Neil K. Razdan

RECENT PROGRESS

Strong, apolar C-H bonds in methane confer formidable kinetic challenges and thermodynamic limits in non-oxidative methane dehydroaromatization (DHA). We quantitatively distinguish these kinetic and thermodynamic barriers by elucidation of a series reaction network ($\text{CH}_4 \leftrightarrow \text{C}_2\text{H}_6 \leftrightarrow \text{C}_2\text{H}_4 \leftrightarrow \text{C}_2\text{H}_2 \leftrightarrow \text{C}_6\text{H}_6$) and rigorous affinity- and length-averaging of net methane aromatization rates. Deconvolution of thermodynamic and kinetic influence on DHA reactions reveals forward synthesis rates are invariant beyond 2% methane conversion and are largely controlled by steps involving acetylene. Identification of acetylene as a key intermediate in methane DHA is critical in de-conflating net and forward reaction rates by application of De Donder relations and concepts of microscopic reversibility.

Figures 1 and 2 show results from DHA reactions as a function of methane conversion. Coincidence of conversion-selectivity profiles of all products across several deactivating samples

demonstrates deactivation is non-selective, or occurs without modification of intrinsic active site chemistry. Change of methane conversion by extent of catalyst deactivation is therefore equivalent to conventional steady-state contact-time variation experiments and permits elucidation of the DHA reaction network by examination of product selectivities and reversibilities as a function of methane conversion on partially deactivated catalyst beds.

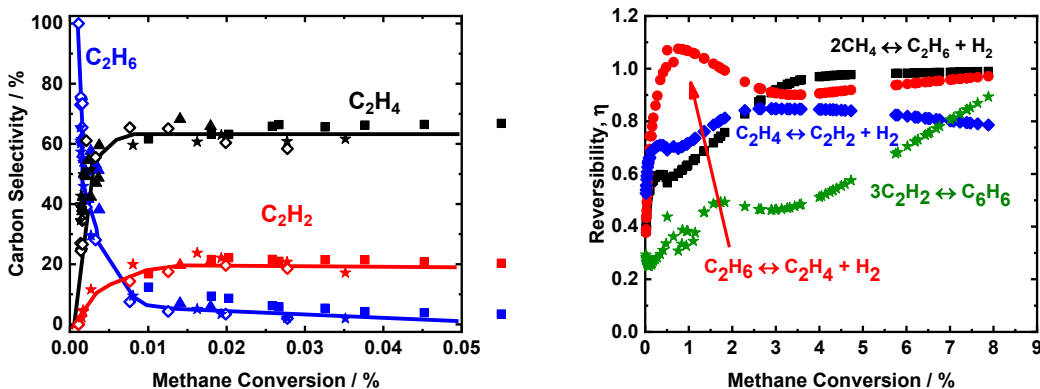


Figure 1: Carbon selectivity of C_2 products as a function of methane conversion on four deactivating catalyst samples. Reactions performed at 973 K, atmospheric pressure, $130 \text{ cm}^3 \text{ min}^{-1}$ total flow of 90 kPa CH_4 , 10 kPa Ar. Catalyst loadings: 25-250 mg

Figure 2: Approach to equilibrium of intervening DHA reactions as a function of methane conversion collated from several deactivating catalyst samples. Reactions performed at 973 K, atmospheric pressure, $13\text{-}130 \text{ cm}^3 \text{ min}^{-1}$ total flow of 90 kPa CH_4 , 10 kPa Ar, 0.025-1.2 g Mo/H-ZSM-5 (mesh 40-80 $\text{Mo}/\text{Al}_F = 0.25$, $\text{Si}/\text{Al} = 11.5$)

The asymptotic approach of C_2H_6 selectivity to 100% as methane conversion approaches zero in Fig. 1 reveals ethane is the sole primary stable gas-phase product of methane DHA; ethylene and acetylene are necessarily sequential pyrolysis products formed from dehydrogenation of ethane. The rank of ethane dehydrogenation products is evident in Fig. 2 which shows reversibility (or approach to equilibrium), η , of interconversion between C_2 hydrocarbons and benzene. Approach to equilibrium for each reaction is calculated as shown in Eq. 1:

$$\eta = \frac{1}{K_{\text{eq}}} \prod_j P_j^{v_j} \quad (1)$$

$\eta < 1$ for $C_2H_4 \leftrightarrow C_2H_2 + H_2$ demonstrates acetylene is a dehydrogenation product of ethylene and evinces a series \leftrightarrow reaction pathway wherein methane activation to C_2H_6 is followed by sequential dehydrogenation to C_2H_4 and then C_2H_2 which aromatizes to C_6H_6 .

The elucidation of DHA as a single-path, sequential reaction network motivates use of De Donder relations to quantitatively assess the influence of intrinsic thermodynamic constraints to effect suppression of net benzene synthesis rates as methane conversion approaches the 10% equilibrium limit. De Donder relations show, for a series reaction pathway, the forward rate of the overall reaction, \vec{r} , is related to the net rate, r , by

$$\vec{r} = \frac{r}{1 - \eta^{1/\sigma}} \quad (2)$$

where

$$\bar{\sigma} = \frac{\sum_i \sigma_i \ln(\eta_i)}{\sum_i \ln(\eta_i)} \quad (3)$$

is the affinity-averaged stoichiometric number and σ_i is the stoichiometric number of each intervening step. Calculation of $\bar{\sigma}$ permits quantitative evaluation of the extent to which each step controls the reversibility, \bar{r}/\bar{r} , of the overall DHA reaction sequence and therefore allows calculation of \bar{r} from measured net rates. Exit streams in flow reactors reflect spatially-averaged rates, but only effluent, or instantaneous, η . Use of Eq. (2) from flow reactor data requires affinity-averaging of η by use of Eq. (3) and numerical integration of η along the catalyst bed (i.e. length-averaging). The effluent flow rate of a product in a PFR normalized by the total number of active sites, F , is

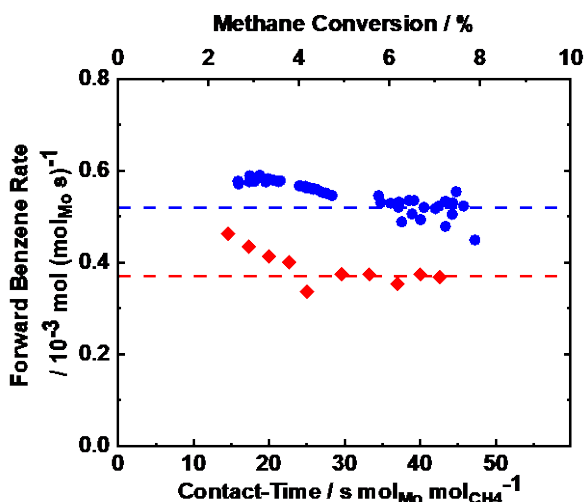


Figure 3: Overall forward rate of benzene formation as a function of methane conversion and contact-time per *active* Mo atom calculated by Eq. (2)-(5) from collation of data from deactivating samples (blue circles) at 973 K and steady-state contact-time variation (red diamonds) at 950 K.

$$F = \frac{\int_0^X r dx}{\int_0^X dx} = \langle r \rangle \quad (4)$$

where x is the axial coordinate along the catalyst bed and X is the total catalyst loading. The pseudo-steady-state hypothesis (PSSH) for all adsorbed species requires that the overall forward rate is constant along the catalyst bed. Thus,

$$\bar{r} = \frac{F \cdot X}{\int_0^X 1 - \eta^{1/\bar{\sigma}} dx} \quad (5)$$

which is a function of exclusively measurable quantities: effluent flow rates (F), effluent $\eta^{1/\bar{\sigma}}$, and catalyst loading.

Fig. 3 shows \bar{r} calculated by Eq. (5) for contact-time varied either at steady-state or by extent of catalyst deactivation. The invariance of overall forward rates of methane DHA evinces the validity

of PSSH and the De Donder equation and demonstrates the sole inhibiting effect of H₂ liberated in DHA reactions is thermodynamic in nature.

Thermodynamic barriers set by endothermicity of methane pyrolysis can be overcome by in-situ removal of H₂ formed during rate-controlling dehydrogenation events. Polyfunctional configurations of Mo/H-ZSM-5 and Zr metal, a known hydrogen absorbent, in the form of staged beds and interpellet physical mixtures are virtuous in alleviating thermodynamic constraints to DHA and producing aromatic hydrocarbons at supra-equilibrium yields (Fig. 4a) while concentrating H₂ in bulk zirconium hydride, ZrH_{1.75}, as evinced by X-ray diffraction and thermal desorption studies.

Proximity effects in polyfunctional catalyst-absorbent mixtures can be rigorously described by hydrodynamic bed-scale packed-bed reactor models that consider characteristic diffusive and convective length-scales which dictate efficacy of H₂ transport to couple catalytic and absorptive functions at sites separate in function and spatial location. Eq. (6) represent a highly redacted version of the reaction-transport model that captures key elements of computational efforts

$$0 = \frac{1}{Pe} \frac{\partial^2 P_j}{\partial x^2} - \frac{\partial P_j}{\partial x} + P_{CH_4}^{0.7} \sum_i v_{ij} Da_i (1 - \eta_i^{1/\bar{\sigma}_i}) \quad (6)$$

Péclet number, Pe, near unity in axially dispersed polyfunctional configurations permits motility of H₂ to Zr in layered configurations and demands application of Danckwerts boundary conditions which confer mixing between staged catalyst and absorbent beds. Fig.4b shows simulation of Eq. (6) and demonstrates addition of Zr in either interpellet mixtures or staged beds effectively abstracts H₂, reflected in reversibility, $\eta \sim P_{H_2}^{3/2}$, lifting equilibrium constraints and enhancing benzene and naphthalene yield, as confirmed by experimental kinetic studies.

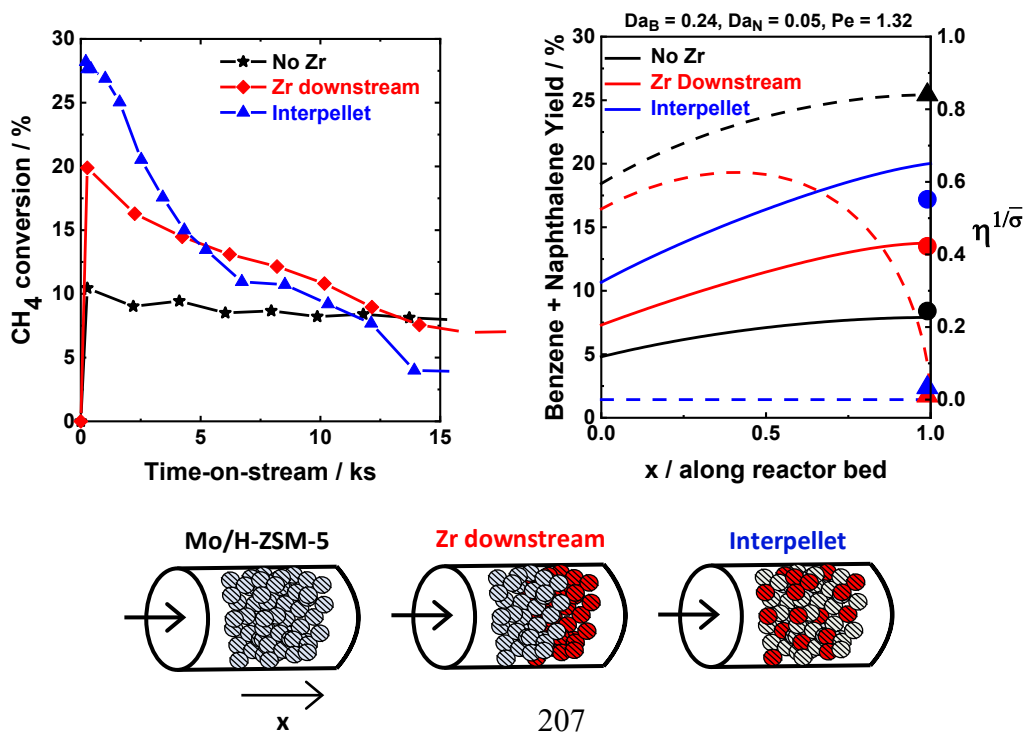


Figure 4a: Experimentally-measured methane conversion as a function of time-on-stream. **Figure 4b:** Axial profiles of benzene + naphthalene yield (solid lines; left) and reversibility for benzene production (dashed lines; right) per simulation of the reaction transport model, shown in redacted form in Eq. (6). Solid circles and triangles are experimentally-observed effluent B+N yield and $\eta^{1/\bar{\sigma}}$, respectively.

P_j	dimensionless partial pressure of j	u	linear velocity [m/s]
x	dimensionless length along reactor	L	length catalyst bed [m]
D_{eff}	effective diffusivity [$\text{m}^2 \text{s}^{-1}$]	ν_{ij}	stoichiometric coefficient of component j in reaction i
k_i	rate constant for reaction i [s^{-1}]	Pe	$= uL/D_{\text{eff}} = \text{Péclet number}$
$K_{\text{eq},i}$	equilibrium constant of reaction i	Da	$= kL/u = \text{Damköhler number}$

Publications Acknowledging this Grant in 2015-2018

(I) *Exclusively funded by this grant:*

1. Razdan, N. K.; Kumar, A.; Bhan, A. Controlling kinetic and diffusive length-scales during absorptive hydrogen removal in methane dehydroaromatization on $\text{MoC}_x/\text{H-ZSM-5}$ catalysts. *J. Catal.* **2019**, *372*, 370-381.

(II) *Jointly funded by this grant and other grants with leading intellectual contribution from this grant:*

4. Kumar, A.; Song, K.; Liu, L.; Han, Y.; Bhan, A. Absorptive hydrogen scavenging for enhanced aromatics yield during non-oxidative dehydroaromatization on $\text{Mo}/\text{H-ZSM-5}$ Catalysts. *Angew. Chem. Int. Ed.* **2018**, *57*, 15577-15582.

Elizabeth J. Biddinger

Interplay of Electrochemical Hydrogenation and Hydrogenolysis of Furfural on Copper with Undesired Side Reactions

Elizabeth J. Biddinger, Andrew May, Sungyup Jung

Department of Chemical Engineering, The City College of New York, CUNY, New York

Presentation Abstract

Electrochemical reduction, paired with renewable electricity, offers opportunities for upgrading biomass-derived species at the biorefinery without the need for externally-supplied hydrogen gas, high temperature or high pressure. Furfural, a biomass-derived platform chemical, can be upgraded to furfuryl alcohol, a fine chemical intermediate, and 2-methyl furan, a biofuel candidate, by electrochemical hydrogenation and hydrogenolysis (ECH). The electrochemical reaction conditions used significantly influences the reaction rate, selectivity, and formation of side products such as hydrogen and humins. The influence of pH, reaction potential, and initial concentration of furfural on the reaction over copper catalysts, known for their ability to produce 2-methyl furan, will be presented. Each of these parameters has a significant influence on the reaction rate, product selectivity and side product formation. Highly acidic electrolytes are necessary to produce 2-methyl furan. These highly acidic electrolytes also promote the formation of undesired humins and hydrogen. At low overpotentials, less hydrogen is produced, though reaction rates towards ECH are also slow. The initial concentration of furfural has to be balanced so that enough furfural is available to react and suppress hydrogen evolution, but yet not so much is present that the electrode surface gets fouled by the biomass-derived species.

DE - SC0019134: Reaction Mechanism and Kinetics for Electrochemical Hydrogenation and Hydrogenolysis of Biomass-Derived Species

PI: Elizabeth J. Biddinger¹

Postdoc(s): N/A

Student(s): Andrew May¹, Leo Gordon¹, Srija Balachandran^{1,2}

Affiliations(s): ¹Department of Chemical Engineering, The City College of New York, CUNY, New York 10031 USA; ²Department of Chemical Engineering, KTH Royal Institute of Technology, Stockholm, Sweden

RECENT PROGRESS

Major efforts on the project in the first year included hiring and training a PhD student intern and a PhD graduate research assistant, and establishing the protocols for future studies.

Modification of Electrochemical Reaction System for Analysis of Products and Reactants at Low Conversions

Bulk electrolysis allows for reaction products to be produced at significant quantities because reaction conditions are held constant for a period of time. Analytical electrochemical methods such as cyclic voltammetry does not traditionally allow for products to be identified. Previously, we have used bulk electrolysis to monitor product selectivity and yield, reactant conversion, and formation of side products over the timeframe of minutes to hours. To better perform kinetic analyses of electrochemical hydrogenation and hydrogenolysis while minimizing homogeneous side reactions, analyses in the seconds to few minute timespans need to be performed. This requires the reaction solution analysis methods to be modified to detect very low concentrations. The analytical workup of the reaction solutions was modified to concentrate the products as was the conditions used in the gas chromatograph-mass spectrometer to be able to detect smaller concentrations of species.

Design of an in-situ Surface Enhanced InfraRed Spectroscopy (SEIRAS) Electrochemical Cell for Electrochemical Hydrogenation and Hydrogenolysis Studies.

In situ electrochemical studies can be performed using two main methods – utilizing external reflection and utilizing internal reflection of the IR beam. Both methods use an electrochemical cell seated above an Attenuated Total Reflectance (ATR) crystal. In the external reflection mode, the working electrode is placed just above the ATR crystal, keeping a thin film of electrolyte between the working electrode and the crystal. In the internal reflection mode, the working electrode is coated onto the ATR crystal. Depending upon the working electrode material, surface enhancement can be achieved. Our preliminary work in the group started with external reflection methods. We were able to observe bulk furfural, however, we were not able to observe adsorbed furfuryl alcohol or 2-methyl furan products using external reflection mode. We have modified the *in situ* electrochemical cell for internal reflection mode and are currently developing the methods for coating the ATR crystal with copper for the working electrode. Copper is surface active, so the experimental setup will be using SEIRAS.

Publications Acknowledging this Grant in 2015-2018

N/A

Thomas Bligaard

Machine Learning Accelerated Catalysis Simulations

Thomas Bligaard
SLAC National Accelerator Laboratory, Energy Sciences Division

Presentation Abstract

The development of novel catalysts and catalytic processes will be key to mitigating climate change over the next century. Computational atomic-scale simulations hold the promise to help achieving this target. Accelerating simulations of catalytic processes could speed up progress significantly. I will discuss a general framework for accelerating various aspects of atomic-scale catalysis simulations through the application of surrogate machine learning models. We have implemented this methodology and integrated it with the Catalysis-hub.org web service in such a way that the DFT simulations from surrogate machine learning model accelerated search can be displayed through a web-service.

FWP 10049: SUNCAT Center for Interface Science and Catalysis

R. Morris Bullock

Catalytic Hydrogenation of Arenes: Evolution of the Conversion of a Molecular Rh-CAAC Complex to Rh Nanoparticles

R. Morris Bullock, Ba L. Tran, John L. Fulton, John C. Linehan, and Johannes A. Lercher
Institute for Integrated Catalysis, Pacific Northwest National Laboratory, Richland, WA

Hydrogenation of the arene ring of ethers, amides, and esters occurs at room temperature and low hydrogen pressure, starting from $[(\text{CAAC}^{\text{Cy,Dipp}})\text{Rh}(\text{COD})\text{Cl}]$ (CAAC = cyclic alkyl amino carbene). The site-selective arene hydrogenation catalyzed by this system is under steric control, as shown by competition experiments with derivatives of ethers, amides, and esters bearing different aromatic rings of varying electronic and steric influence. Rh K-edge X-ray absorption fine structure (XAFS) spectroscopy was carried out at the Advanced Photon Source, Argonne National Laboratory. We examined arene hydrogenation of diphenyl ether by a combination of stoichiometric reactions of $[(\text{CAAC}^{\text{Cy,Dipp}})\text{Rh}(\text{COD})\text{Cl}]$ and *operando* XAFS kinetics studies. Our results unequivocally show that Rh nanoparticles generated from the single-site Rh complex catalyze the arene hydrogenation. *Operando* XAFS studies illuminate the role of Ag^+ (for removal of Cl^- from $[(\text{CAAC})\text{Rh}(\text{COD})\text{Cl}]$) on the pre-catalyst reactivity, the effect of increasing H_2 pressure on increasing the catalytic efficiency, the stabilizing influence of Ph_2O on the relative rate of formation of active Rh nanoparticles, and the absence of soluble single-site Rh species that might leach from bulk heterogeneous Rh nanoparticles. We gained insights into the divergent deactivation pathways mediated by sub-stoichiometric benzothiophene and excess KO^tBu toward H_2 activation, which is a key step *en route* to Rh nanoparticles for arene hydrogenation. Excess KO^tBu leads to the formation of a Rh-O^tBu complex that interferes with H_2 activation, precluding the formation of Rh nanoparticles. Benzothiophene does not interfere with the activation of H_2 at Rh in the $\text{CAAC}^{\text{Cy,Dipp}}$ complex while Rh nanoparticles are formed. Once Rh nanoparticles are formed, however, benzothiophene binds irreversibly to the Rh nanoparticles, preventing adsorption of H_2 and hydrogenation of diphenyl ether.

FWP 47319: Transdisciplinary Approaches to Realize Novel Catalytic Pathways to Energy Carriers

PI: Johannes Lercher

Transition Metal Catalysts Encapsulated in a Metal-Organic Framework for the Autocatalytic Conversion of CO₂ to Methanol

Jeffery A. Byers, Chia-Kuang “Frank” Tsung, Zhehui Li, Thomas M. Rayder, Adam T. Benschel, Enric Adillon, Noella D’Souza
Department of Chemistry, Boston College

Presentation Abstract

The hydrogenation of CO₂ to methanol is reported that is enabled through a cascade of chemical reactions that capitalizes on at least one transition metal complex being encapsulated in a metal-organic framework (MOF). Encapsulation of (^tBuPNP)RuHCl(CO) in the metal-organic framework UiO-66 was achieved using the “aperture-opening” method for incorporating transition metal catalysts in MOFs previously developed in our groups. The known catalytic activity of (^tBuPNP)RuHCl(CO) for the hydrogenation of CO₂ to formic acid was combined with the Lewis acidity of UiO-66 and a second ruthenium-based catalyst (^tBuPNN)RuHCl(CO) to further convert formic acid to methanol via a formate ester intermediate. The strategy is highly selective for the formation of methanol and leads to some of the highest turnover numbers observed for the hydrogenation of CO₂ to methanol at a temperature (70 °C) lower than ever before reported. The system benefits from three different catalytically active species operating simultaneously, which can be tuned independently to maximize catalyst performance. Moreover, because all three reactions are carried out in the same reaction vessel, an autocatalytic capability of the transformation has been realized that allows for the reaction to proceed with the addition of substoichiometric amounts of alcohol additives. The features of the autocatalysis along with the sensitivity of the reaction to the encapsulation of one or both transition metal catalysts will also be discussed.

DOE-BES DE-SC0019055: Organometallic Catalysis from Molecular Catalysts Non-Covalently Confined in Metal-Organic Frameworks

Co-PI: Chia-Kuang “Frank” Tsung

Postdoc(s): none

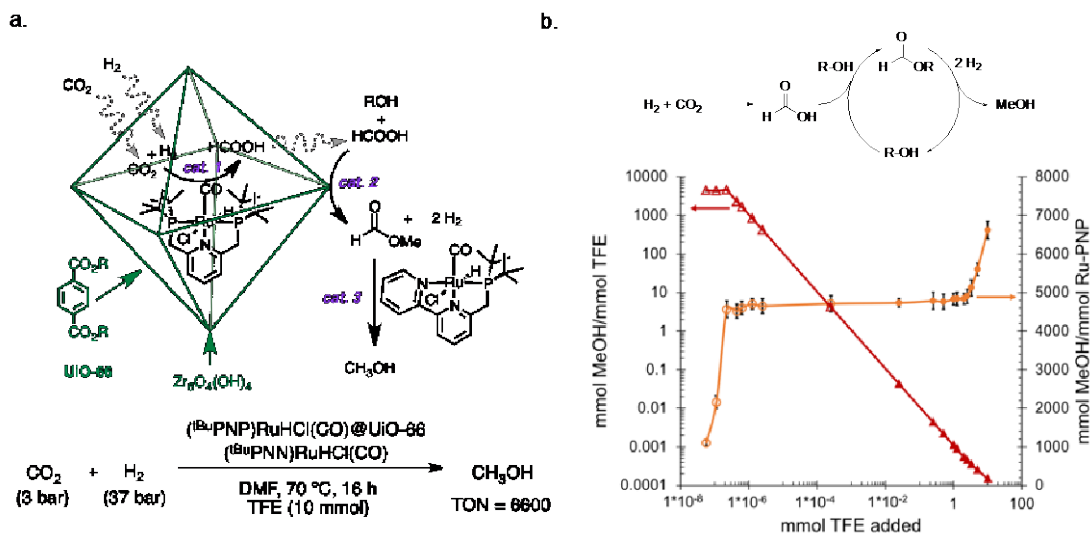
Student(s): Zhehui Li, Thomas R. Rayder, Adam Benschel, Enric Adillon (undergraduate), Noella D’Souza (undergraduate)

RECENT PROGRESS

1. Develop a tandem catalyst system that benefits from the cooperation of multiple catalytically active species for the hydrogenation of CO₂ to methanol.

Significant progress has been made towards achieving this goal in this reporting period. A transition metal catalyst (^tBuPNP)RuHCl(CO) (**1**) that was previously encapsulated in the metal-

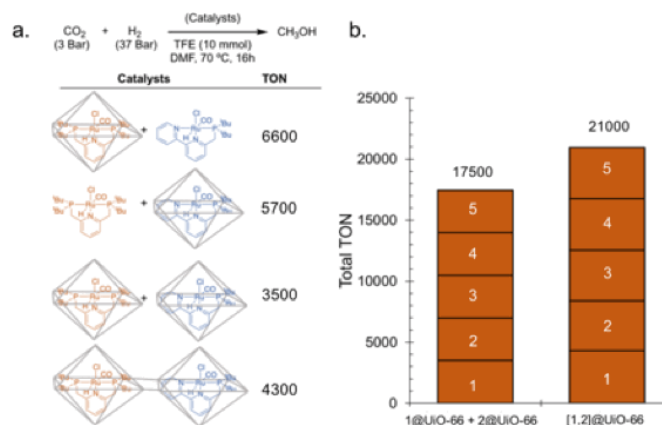
Figure 1. a) Hydrogenation of CO₂ to methanol using a three-component catalytic reaction made possible by encapsulating a transition metal complex into a MOF. b) Dependence of CO₂ hydrogenation on the amount of TFE added to the reaction.



organic framework (MOF) UiO-66 was coupled with the zirconium nodes of UiO-66 and (^tBuPNN)RuHCl(CO) (**2**) external to the encapsulated catalyst to carry out the hydrogenation of CO₂ to methanol that occurs via an ester intermediate (Figure 1a). Significant improvement in catalytic turnover was observed by decreasing the temperature of the reaction and also by using trifluoroethanol (TFE) as an additive. The turnover observed (6600) rivals the highest turnover reported for a well-defined catalyst at a temperature lower than reported previously. Moreover, by decreasing the amount of TFE additive, autocatalytic behavior was observed, which allowed for the additive to be present in substoichiometric quantities (open symbols, Figure 1b). To the best of our knowledge, no one has ever reported autocatalytic behavior in CO₂ hydrogenation reactions.

Finally, we were successful in encapsulating **2** in UiO-66 by a similar aperture opening process that we previously reported for **1** (*J. Am Chem. Soc.*, **2018**, 140(26), 8082-8085) and also developed a procedure for the sequential encapsulation of **1** and **2** in the same UiO-66 to create fully heterogeneous catalysts, **1**@UiO-66+**2**@UiO-66 and [**1,2**]@UiO-66. While these constructs were not as active as catalysis carried out with either **1** or **2** in solution (Figure 2a), they were readily recyclable up to five times without loss in catalytic activity or metal content in the MOF material (Figure 2b). The cumulative TON observed from the recycling process for **1**@UiO-66+**2**@UiO-66 and [**1,2**]@UiO-66 was 21,000, respectively, which is promising for further investigations under more

Figure 2. a) Catalytic activity of different transition metal complexes encapsulated or co-encapsulated in UiO-66 for the hydrogenation of CO₂ to methanol. b) Recycling studies for fully heterogenized catalysts used for the hydrogenation of CO₂ to methanol.



industrially relevant conditions using flow reactors. A manuscript describing these results was recently submitted for publication.

2. Utilize non-covalent interactions between the host and guest to modulate chemical reactivity.

Work in this area during this funding period has predominately focused on developing a physical description for fluorescent dyes that we have encapsulated in variously functionalized UiO-66 variants, which we have attributed to significant second sphere interactions that alter the fluorescent properties of the dye (Figure 3). The research activities centered on explaining our preliminary discoveries that we disclosed in our proposal: 1) the fluorescence of rhodamine-6G dyes encapsulated in UiO-66 was significantly more solvatochromic compared to rhodamine-6G dyes in solution, and 2) fluorescence of the rhodamine-6G dye could be altered by changing the functionality installed in the linker of the UiO-66. To do so, we have carried out linear free energy relationship studies, which revealed that the solvatochromism observed for the encapsulated dyes involves significant synergistic effects between the identity of the solvent (i.e. protic versus aprotic solvents) and the identity of the linker installed on the MOF (both steric and electronic factors were found to be important). A manuscript describing the culmination of this work is currently in its final phases of revision and will be submitted for publication in the next few weeks.

To complement this work, we have begun to investigate the reactivity of **1** encapsulated in variously functionalized UiO-66 (i.e. **1@UiO-66-X**) in CO₂ hydrogenation reactions. In preliminary investigations, we have found that there is little influence on the catalytic activity for the conversion of CO₂ to formic acid when different UiO-66 variants were explored. However, significant changes in activity was observed for the hydrogenation of CO₂ to methanol using the tandem **1@UiO-66-X/2** catalyst described above (Figure 4). We are still trying to optimize these exciting preliminary results as well as positively identify the origin of these effects, but these initial results are encouraging for achieving the primary objective of this goal by the end of the next funding period.

Figure 4. CO₂ hydrogenation to methanol using various substituted UiO-66-X host materials.

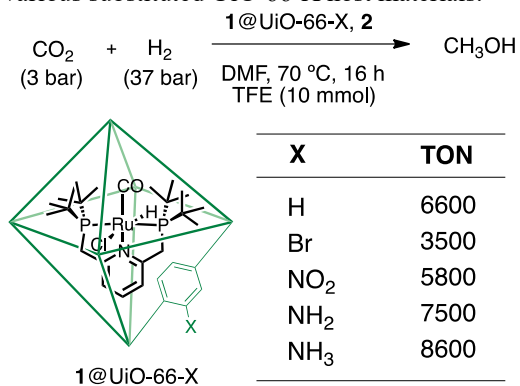
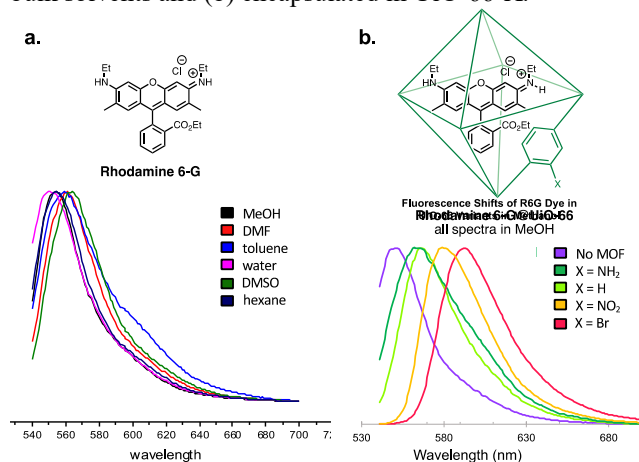


Figure 3. Fluorescence spectra for rhodamine-6G in (a) bulk solvents and (b) encapsulated in UiO-66-X.



3. Stabilize reactive intermediates through their encapsulation in the confined structures in MOFs.

Compared to the first two goals of the project, relatively little has been done to achieve this goal of the project. In an effort to extend our encapsulation method to complexes that are less stable than the ruthenium-based complexes described above, we have begun a collaboration with Nilay Hazari (Yale) and Wesley Bernskoetter (Missouri), whose iron-based catalyst for CO₂ hydrogenation to formic acid is one of the most active non-noble metal catalysts for the process known. Unfortunately, this complex suffers from bimolecular catalyst decomposition. As a first step to investigate whether our encapsulation process will be amenable to encapsulating less stable catalyst precursors, we hypothesized that our encapsulation method would be beneficial to increase catalyst turnover and/or recyclability for the Hazari/Bernskoetter system. As a result, the Hazari/Bernskoetter groups have provided us with a variety of iron-based catalyst precursors that we are currently investigating in aperture-opening encapsulation reactions as well as CO₂ hydrogenation reactions. Results from these initial efforts are too preliminary to report at this time, but we expect that by the end of the next reporting period we will have a better understanding about how to carry out aperture-opening encapsulating reactions involving less stable metal-based precursors. Such understanding will be critical as we move to more challenging metal precursors.

Publications Acknowledging this Grant in 2015-2018

(XXII) Exclusively funded by this grant:

a. none

(XXIII) Jointly funded by this grant and other grants with leading intellectual contribution from this grant:

a. none

(XXIV) Jointly funded by this grant and other grants with relatively minor intellectual contribution from this grant

a. none

Metal Nodes in Bimetallic Metal-Organic Frameworks as Isolated Sites for Hydrogenation Reactions

Donna A. Chen¹, Natalia B. Shustova¹, and Konstantinos Vogiatzis²

¹Department of Chemistry and Biochemistry, University of South Carolina

²Department of Chemistry, University of Tennessee

Presentation Abstract

We report the first study of a gas-phase reaction catalyzed by isolated, highly dispersed sites at the metal nodes of a crystalline metal-organic framework (MOF). The ability to tailor the geometry and ensemble size of the metal nodes in MOFs allows for unprecedented control of the active sites and could lead to significant advances in rational catalyst design. $(\text{Cu}_x\text{Rh}_{1-x})_3(\text{BTC})_2$ (abbreviated CuRhBTC, where BTC^{3-} =benzenetricarboxylate) is prepared from Rh^{3+} and CuBTC (HKUST-1) by post-synthetic ion-exchange. The oxidation state of Rh in CuRhBTC is identified as $2+$, which is a Rh oxidation state that has not previously been observed for crystalline MOF metal nodes. These Rh^{2+} sites are active for the catalytic hydrogenation of propylene to propane at room temperature, and the MOF structure stabilizes the Rh^{2+} oxidation state under reaction conditions. Density functional theory calculations suggest a mechanism in which H_2 dissociation and propylene adsorption occur at the Rh^{2+} sites.

DE-SC0019360: Multimetallic Metal-Organic Frameworks as Tunable Multifunctional Catalysts for Gas Phase Hydroformylation and Hydrogenation Reactions

Postdoc: Thayalan Rajeshkumar

Students: Deependra M. Shakya, Otega Ejegbavwo, Sharfa Farzandh, and Narayan Acharya

RECENT PROGRESS

Propylene hydrogenation activity

Propylene hydrogenation experiments were carried out on the monometallic CuBTC and NiBTC MOFs, as well as a variety of Cu-containing bimetallic MOFs $((\text{Cu}_x\text{M}_{1-x})_3(\text{BTC})_2)$ where $\text{M}=\text{Rh}, \text{Co}, \text{Ni}, \text{Ir}$ and Ru , as shown in Figure 1a. However, only the CuRhBTC exhibited significant activity for propane production at 20 °C. Specifically, the pure CuBTC MOF showed no activity under the same reaction conditions, indicating that the Cu^{2+} ions are not active for propylene hydrogenation. The activity of the CuRh(33%)BTC catalyst is also stable over a 24 period online (Figure 1b). Furthermore, CuRhBTC with a lower bulk concentration of Rh (18%) has 45% of the activity of the CuRh(33%)BTC, which indicates that activity scales linearly with Rh concentration and implies that the Rh ions are the active sites for reaction. The apparent activation energy for propylene hydrogenation on CuRhBTC was determined to be 6.3 kcal/mol based on data collected at 20-50 °C.

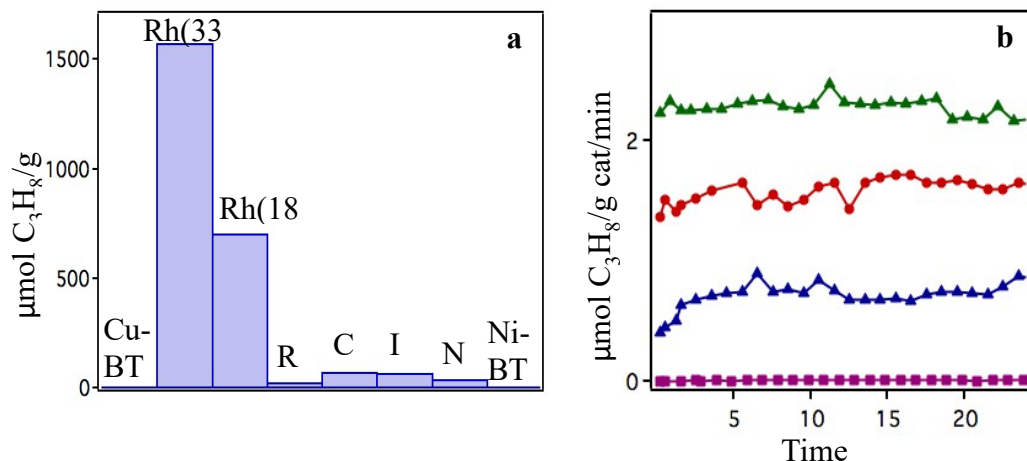


Figure 1. a) Average propylene hydrogenation activity for the following CuMBTC and pure MBTC MOFs: CuBTC, CuRh(33%)BTC, CuRh(18%)BTC, CuRu(6%)BTC; CuCo(50%)BTC; CuIr(5%); CuNi(6%)BTC and NiBTC; and b) activity for propylene hydrogenation as a function of time online over CuRhBTC with the following Rh concentrations: 18% Rh at 20 °C (blue triangles) and 50 °C (green triangles); 33% Rh at 20 °C (red circles); and 0% Rh (pure CuBTC) at 20 °C (pink squares).

Identification of Rh oxidation state

X-ray photoelectron spectroscopy (XPS) experiments address the oxidation state of the Rh ions in CuRhBTC. For the as-received sample, the Rh(3d_{5/2}) peak has a binding energy of 309.2 eV. The spectrum of Rh₂(OAc)₄ provides a standard for the relatively uncommon Rh²⁺ oxidation state, which appears at 308.9 eV for Rh₂(OAc)₄ and is similar to the value observed for CuRhBTC. In contrast, Rh³⁺ in RhCl₃ appears at 310.1 eV, which is consistent with Rh³⁺ oxidation states reported in the literature, whereas Rh¹⁺ is expected at 308.0-308.4 eV. There is no evidence for metallic Rh at 307.0-307.4 eV in the spectrum of CuRhBTC. Ambient pressure XPS studies establish that the Rh oxidation state in CuRhBTC does not change during exposure to the reactant gases at room temperature or during exposure to H₂ only.

Density functional theory-based calculations

The first step in the reaction mechanism is the coordination of propylene at the open site of the Rh²⁺ cation via π -backbonding. After propylene adsorption, Rh can be considered as a hexacoordinated metal after accounting for a weak bond with the Cu²⁺ cation, and therefore the mechanism for H₂ dissociation is not obvious. Several possible mechanisms were considered, including H₂ dissociation on pentacoordinated Rh²⁺ and direct H-transfer to propylene for the formation of a propyl radical. However, the lowest energy pathway for H₂ dissociation involves cleavage of the Rh-O bond to create a second vacant site in the coordination sphere of Rh²⁺ for the binding of H₂. Although this step has a relatively high activation energy of 15.4 kcal/mol, the decoordinated oxygen atom facilitates H₂ dissociation in the next step via the formation of OH. Furthermore, the reaction barrier for H₂ dissociation is only 0.5 kcal/mol and leads to a thermodynamically more stable intermediate. After the H₂ bond is cleaved, a Rh monohydride

and a hydroxyl group are formed. Next, the hydrogen atom of the Rh-hydride is transferred to propylene to form the Rh-propyl intermediate. Finally, a second hydrogen atom from the hydroxyl group is transferred to the propyl radical for the formation of the final product.

Publications Acknowledging this Grant in 2018-2019

(I) Exclusively funded by this grant

1. Shakya, D. M.; Ejegbavwo, O.; Rajeshkumar, T.; Farzandh, S.; Brandt, A. J.; Acharya, N.; Rui, N.; Senanayake, S. D.; Ebrahim, A.; Frenkel, A. I.; Tate, G.; Monnier, J. R.; Vogiatzis, K. D.; Shutova, N. B. and Chen, D. A., to be submitted to *Angewandte Chemie*.

**Dedicated Beamline Facilities for Catalytic Research –
Synchrotron Catalysis Consortium (SCC)**

Jingguang G. Chen, Anatoly I. Frenkel, Jose A. Rodriguez
Columbia University & Brookhaven National Laboratory

Presentation Abstract

The mission of the Synchrotron Catalysis Consortium (SCC), which was established in 2005 and was the first of its kind in the US, is to promote the utilization of synchrotron techniques for cutting-edge catalytic research under in-situ conditions. These tasks are performed by a consortium consisting of PIs and co-PIs from academic, national, and industrial laboratories. The PIs and co-PIs have extensive experience in the areas of catalysis, electrocatalysis and synchrotron techniques. The beamlines and supporting facilities that SCC members acquired and built are located in the National Synchrotron Light Source (NSLS during 2005-2015 and NSLS II after 2017) at Brookhaven National Laboratories. The primary goal of the SCC team is to provide assistance and to develop new sciences/techniques to the catalysis community through the following concerted efforts: (1) developing, setting up, commissioning and testing catalysis facilities and supporting catalysis operations at the two XAFS beamlines at NSLS-II: QAS and TES; (2) assisting the experimental set-up and safety training of catalysis users; and (3) offering training courses for graduate students and postdoctoral fellows on XAFS techniques and data analysis. The availability of well-maintained, user-friendly, and state-of-the-art synchrotron facilities, as provided by SCC, will help a large number of catalysis and electrocatalysis groups in their efforts to perform in-situ measurements. The SCC also provides an efficient model for operating synchrotron facilities; such model demonstrates a closer interaction between funding agencies, beamline scientists and external researchers. The closer interaction will lead to the more efficient utilization of the synchrotron facilities, which ultimately benefits the nation as a whole by increasing the return on the investments made in our national laboratory system. The current consortium represents a critical step for the catalysis community in the United States to remain competitive in catalytic and electrocatalytic research using synchrotron techniques.

Grant or FWP Number: DE-SC0012653

PI: Jinguang G. Chen

Co-PIs: Anatoly I. Frenkel, Jose A. Rodriguez

Research Staff: Nebojsa Marinkovic

RECENT PROGRESS

SCC Partner User Activities at Spectroscopy beamlines at NSLS II (TES and QAS):

SCC has Partner User Agreements with the TES and QAS beamlines of NSLS-II. The Tender-energy spatially resolved and In Situ X-ray Absorption Spectroscopy (TES) beamline is a high performance and in-situ X-ray absorption spectroscopy for spatially-resolved XAS and elemental imaging of heterogeneous or structured materials; it is optimized for the “tender” energy range from 2-6 keV (reaching up to 8 keV) in a helium environment. The end-station is optimized

for user-tunable microbeam (3 x 3 to 15 x 25 μm in size) EXAFS and X-ray fluorescence imaging and in-situ fuel-cell and battery measurements. Fast on-the-fly scanning of the stage and monochromator enables rapid imaging and XAS of dynamic systems, and the EXAFS capability has been recently enabled as well. SCC staff and PIs are involved in designing science commissioning experiments. The first set of such experiments was performed in February 2018. Because of the low energy range, the special reactor systems of interest for catalysis experiments are being designed.

Investigation included structural investigation by XAS on phosphorus K-edge of metal-organic that play essential roles in small molecule activation and catalysis. Fresh-prepared and spent zeolites were mapped on Si-fluorescence to correlate the catalytic properties with their micro-crystal structures. Electrochemically active Pt-based catalysts for oxidation of small organic molecules were mapped on Pt M7-edge together with fluorescence signals of other metals to better understand the micro-structure and overlapping of the metallic particles and correlate to their activity. Transition metal phosphides of importance for photo-electrocatalytic hydrogen evolution reaction were studied on P K-edge to better understand their multiple metal-phosphorus stoichiometry and characterize the local environment of the constituent atoms.

The Quick X-ray Absorption and Scattering (QAS) beamline has come online in the first cycle of 2018 and ran first science commissioning experiments in the May-August 2018, cycle. It will enable in-situ and operando studies of complex nanoscale systems undergoing real-time transformations; synchronous measurements of catalysts by complementary techniques including IR, XAS, XRD, and mass spectrometry; and complex interactions in nanoscale systems at the time scale from tens of ms to hours and length scale from \AA to μm in the energy range 5-31 keV. QAS beamline will utilize all reactor systems SCC transferred from the SSRL BL2-2. For heterogeneous metal-gas catalysis, SCC has designed and implemented a gas delivery system - gas cart with lecture bottles of CO, CO₂, C_xH_y, H₂, O₂ and the carrier/dilution gas (He), as well as the special system for gas exhaust that dilutes poisonous and flammable gases to the safe level before releasing them into the environment. For the analysis of the gases, a residual gas analysis (RGA) system is added to characterize the inlet and outlet gas mixtures.

The QAS station has two hutches – hutch B for the portable catalysis using the reactor systems used earlier (also transported from SSRL) and XRD, and the other (hutch C) for future upgrades. In the next period, Diffuse reflectance infrared FT spectroscopy combined with x-ray absorption study and a Raman spectrometer will be stationed in the hutch C for simultaneous XAS-DRIFTS and XAS-Raman studies. Because both RGA and the gas cart are transportable, they can be moved from one to the other hutch. SCC staff is also involved in implementing the quick-EXAFS and helping in the design of the program to integrate XRD signals into the data acquisition.

Catalyst Users Assisted by SCC at TES and OAS Beamlines at NSLS II:

The SCC team provided help in organizing and executing beamtime during science commissioning in February 2018, and the first PU time in June 2018. In the past year the SCC team has assisted over 30 research groups on the TES and OAS Beamlines.

Workshop and Training Courses

In order to promote the utilization of synchrotron facilities in the catalysis and electrocatalysis communities, it is critical to train graduate students, postdoctoral fellows, and young research staff on data collection and data analysis. The SCC PIs and staff have provided training to new catalysis users. Dr.

Frenkel gave on-site help 2-3 days a week, and consulted visiting groups on issues ranging from data analysis to planning XAFS experiments. In the past 14 years SCC members have organized several training courses and workshops, *which were over-subscribed and received very positive feedback*. The main formal training course in 2018 was held on Nov. 6-8 at BNL, with a title of “**Introduction to X-ray Absorption Spectroscopy**”. This short course in X-ray absorption fine-structure (XAFS) spectroscopy, organized by Dr. Frenkel, was geared toward participants with advanced knowledge of XAFS and its applications. The course was useful for those scientists who wanted to acquire basic knowledge about XAFS technique and its many applications to fundamental and applied sciences. The course included lectures, software demonstrations, and data analysis sessions. X-ray spectroscopy is one of the main techniques of the DOE light sources, and the course supports the DOE mission by educating new users in the applications of this technique. Course instructors used examples from their research during presentations. The topics covered included Introduction and overview of XAFS, theory of XAFS, introduction to synchrotrons and beamlines, XAFS data processing methods, FEFF9 code and its applications to XANES and EXAFS analyses, static and dynamic bond length disorder, basics of sample preparation and detectors, EXAFS data analysis and modeling, advanced topics in XANES and EXAFS data analyses, and XAFS and complementary methods: in situ/operando modes. On the last day of the workshop, the participants worked in the data analysis practicum, solving problems of their own research and sample projects provided by the participants. There were 45 registered participants and 20 auditors in the course.

Tasks during Next Funding Cycle

Transition of NSLS-based catalysis research to NSLS-II in the next cycle of the SCC operations (8/15/2019-8/14/2020) will be complete. The last phase involves testing, commissioning and introduction to the QAS beamline user program the combined instruments, developed by SCC scientists: the DRIFTS-XAS, XRD-XAS and Raman-XAS instruments. In addition, QEXAFS monochromator and software will be commissioned and tested by SCC staff. TES beamline will be used in a micro-spectroscopy mode, utilizing operando micro-reactor (the first tests will be run in May 23-26, 2019). Multi-technique characterization at these beamlines with simultaneous reaction product analysis will remain the main focus of SCC operations at NSLS-II. The SCC team will continue to play a leadership role to ensure that the needs of the catalysis community will be adequately addressed in the NSLS-II facilities.

During the period of 2017-2019, the SCC helped NSLS-II enable growth of catalysis community at NSLS-II. The SCC team will continue to work closely with BNL Photon Sciences Directorate scientists at the Spectroscopy suite beamlines to continue enabling and growing the NSLS-II catalysis community in the next period.

Selected Publications Acknowledging SCC Assistance in 2015-2018:

- P. Huang, J. Huang, S. Pantovich, A. Carl, T. Fenton, C. Caputo, R. Grimm, A. Frenkel, G. Li, Selective CO₂ Reduction Catalyzed by Single Cobalt Sites on Carbon Nitride under Visible-Light Irradiation, *J. Am. Chem. Soc.*, **140**, 16042–16047 (2018).
- T. Wolf, S. Kumar, H. Singh, T. Chakrabarty, F. Aussenac, A. Frenkel, D. Major, M. Leskes, Endogenous Dynamic Nuclear Polarization for Natural Abundance ¹⁷O and Lithium NMR in the Bulk of Inorganic Solids, *J. Am. Chem. Soc.*, **141**, 451-462 (2019).
- D. Vovchok, C. J. Guild, S. Dissanayake, J. Llorca, E. Stavitski, Z. Liu, R.M. Palomino, I. Waluyo, Y. Li, A.I. Frenkel, J.A. Rodriguez, S.L. Suib, S.D. Senanayake, In Situ Characterization of Mesoporous Co/CeO₂ Catalysts for the High-Temperature Water-Gas Shift, *J. Phys. Chem. C* **122**, 8998-9008 (2018).

B. Yan, S. Yao, S. Kattel, Q. Wu, Z. Xie, E. Gomez, P. Liu, D. Su and J.G. Chen, "Active Sites for Tandem Reactions of CO₂ Reduction and Ethane Dehydrogenation", **Proc. Natl. Acad. Sci. USA** **115**, 8278 (2018).

E. Gomez, S. Kattel, B. Yan, S. Yao, P. Liu and J.G. Chen, "Combining CO₂ Reduction with Propane Oxidative Dehydrogenation over Bimetallic Catalysts", **Nat. Commun.** **9**, 1398 (2018).

S. Zhang, Y. Tang, L. Nguyen, Y.-F. Zhao, Z. Wu, T. W. Goh, J. Liu, Y. Li, T. Zhu, W. Huang, A. I. Frenkel, J. Li, F. Tao, Catalysis on singly dispersed Rh atoms anchored on an inert support, *ACS Catal.*, **8**, 110-121 (2018).

Q. Jia, Z. Zhao, L. Cao, J. Li, S. Ghoshal, V. Davies, E. Stavitski, K. Attenkofer, Z. Liu, M. Li, X Duan, S. Mukerjee, T. Mueller and Y. Huang, Roles of Mo Surface Dopants in Enhancing the ORR Performance of Octahedral PtNi Nanoparticles, *Nano Lett.* **18**, 798 (2018).

N.S. Marinkovic, K. Sasaki, R.R. Adzic, "Determination of Single- and Multi-Component Nanoparticle Sizes by X-Ray Absorption Spectroscopy", *J. Electrochem. Soc.* **165**, J3222 (2018).

K. Strickland, R. Pavlicek, E. Miner, Q. Jia, I. Zoller, S. Ghoshal, W. Liang and S. Mukerjee, "Anion Resistant Oxygen Reduction Electrocatalyst in Phosphoric Acid Fuel Cell", **ACS Catal.** **8**, 3833 (2018).

C. Okoli, K. A. Kuttiyiel, K. Sasaki, D. Su, D. Kuila, D. Mahajan and R. R. Adzic, "Highly Dispersed Carbon Supported PdNiMo Core with Pt Monolayer Shell Electrocatalysts for Oxygen Reduction Reaction", **ECS Trans.** **85**, 67 (2018).

J. Masa, I. Sinev, H. Mistry, E. Ventosa, M. de la Mata, J. Arbiol, M. Muhler, B.R. Cuenya and W. Schuhmann, Ultrathin High Surface Area Nickel Boride (Ni₃B) Nanosheets as Highly Efficient Electrocatalyst for Oxygen Evolution, *Adv. Eng. Mater.*, **7**, 1700381 (2017).

R. Palomino, E. Stavitski, I. Waluyo, Y. Chen-Wiegart, M. Abeykoon, J. Sadowski, J. Rodriguez, A. Frenkel, S. Senanayake, New In-Situ and Operando Facilities for Catalysis Science at NSLS-II: The Deployment of Real-Time, Chemical, and Structure-Sensitive X-ray Probes, *Synch. Rad. News*, **30**, 30-37 (2017).

Emerging Electron Microscopy for Heterogeneous Catalysis Research

Miaofang Chi,¹ Michael Zachman¹, Wenpei Gao³, Ahmed O. Elnabawy⁴, Victor Fung¹, Felipe Polo Garzon², Luke T. Roling⁴, De-en Jiang⁵, Younan Xia⁶, Manos Mavrikakis⁴, Zili Wu^{1,2}

¹Center for Nanophase Materials Sciences, ²Chemical Sciences Division, Oak Ridge National Laboratory; ³Department of Materials Science and Engineering, University of California–Irvine;

⁴Department of Chemical and Biological Engineering, University of Wisconsin–Madison;

⁵Department of Chemistry, University of California–Riverside; ⁶Department of Biomedical Engineering, Georgia Institute of Technology

An aim of our BES program titled “Fundamentals of Catalysis and Chemical Transformations (ERKCC96)” is to fundamentally understand how synergism can be tailored at the metal-oxide interface to control catalytic activity and selectivity in heterogeneous catalysts. Various interactions can occur at a metal-oxide interface, e.g., interfacial anchoring via vacancies, impurities, and/or elemental inter-diffusion, formation of interfacial interphases, encapsulation of NPs by the support material, atomic structural rearrangement at the interfaces and surfaces, and/or charge transfer between the NP and support, each of which impacts reactivity and selectivity. These interfacial interactions are sensitive not only to the selection of metal and oxides, but also to their contacting surface atomic arrangements. Our work is to provide mechanistic insight into the role of interfaces in heterogeneous catalysts at the single atom and electron levels for the design of more efficient catalysts.

Scanning transmission electron microscopy (STEM) has long been a primary imaging tool for interface research in catalysis because of its exceptional spatial resolution and simultaneous chemical analysis with single-atom sensitivity. In this talk, we will go beyond atomic-resolution imaging and chemical analysis, and introduce two emerging STEM techniques. We will discuss how these new techniques can benefit heterogeneous catalysis research, especially understanding of the formation and function of interfaces through two examples. The first example features the use of four-dimensional (4-D STEM) –based differential phase contrast (DPC) imaging to probe charge transfer at an interface of Au-SrTiO₃, a prototype metal catalyst–oxide support system. Among the various tunable interaction parameters, charge transfer is the least understood, largely because there is no reliable technique to directly probe charge distribution at the inherent sub-nanometer length scale. Herein, we directly probe the charge distribution at Au-SrTiO₃ interfaces down to the atomic scale, revealing the nature of the charge transfer in this system. Further, by combining the experimental results with density functional theory calculations, we provide new insights into the origins and characteristics of charge transfer at the atomic scale. The second example focuses on understanding the formation mechanism of core-shell nanoparticles using *in situ* liquid cell STEM imaging. Syntheses of core-shell nanoparticles are generally realized through liquid phase deposition of shell atoms on core seed particles. However, synthesizing core-shell particles with atomic precision has not yet been accessible, because of our limited knowledge of the deposition mechanism at sufficient spatial and time resolution. In this work, we observe the dynamic process of depositing individual platinum (Pt) atoms onto palladium (Pd) nanocube seeds at atomic scale. The dynamic interplay between the deposited Pt atoms and the surface of the Pd cube is revealed. The role of the synthesis parameters—e.g., precursor concentration and capping

agent, that dictate the deposition kinetics and surface energy of evolving core-shell particles are elucidated. These examples demonstrate how new STEM imaging techniques allow us to access information regarding catalyst interfaces that before was not possible.

Grant or FWP Number: ERKCC96: Fundamentals of Catalysis and Chemical Transformations. For a full description of recent progress see Extended Abstract for ERKCC96.

Modeling of Catalytic Processes for More Efficient Utilization of Hydrocarbon Resources

Thomas R. Cundari

Department of Chemistry, Center for Advanced Scientific Computing and Modeling (CASCaM),
University of North Texas, Denton, TX 76201

Presentation Abstract

Density functional theory (DFT) and multi-configuration SCF (MCSCF) indicate that nitride/nitridyl complexes of Earth-abundant middle-late 3d metals (notably Co and Ni) are worthy candidates for activation and functionalization of light alkane C–H bonds. Calculations further suggest that imide – and even the amide – intermediates generated by initial and subsequent activation events have sufficient activity to carry out further transformations. The MNH_x ($x = 0, 1, 2$) complexes have very complicated electronic structures, necessitating advanced methods to model the correct balance of nitride/nitridyl, imide/imidyl and amide/aminyl character. Calculations suggest that metal-nitrogen σ -bond strengths and basicity/nucleophilicity and radical character of the N-based actor ligand are key elements in identifying systems that can activate aliphatic C–H bonds. Independent experiments support the predictions put forth in our computational research.

DE-FG02-03ER15387: Modeling of Catalytic Processes for More Efficient Utilization of Hydrocarbon Resources

PI: Thomas R. Cundari

Recent Student Researchers on DE-FG02-03ER15387: Mr. (now Dr.) Bruce Prince (faculty, Texas Southern U.), Mr. (now Dr.) Yavuz Ceylan (postdoc, Brandeis U.), Mr. (now Dr.) Quan Jiang (postdoc, Michigan State U.), Ms. Catherine Moulder (NSF Fellow, UNT), Mr. Zhicheng Daniel Sun (PhD student, UNT).

RECENT PROGRESS

For the past grant period, we have focused on several profitable research thrusts – coinage metal catalysis, redox non-innocence in catalysis by Earth-abundant 3d metals, and the reactivity of unsaturated (both in terms of coordination number and the presence of metal-element multiple bonds) nitrogen complexes. The presentation and this extended abstract will focus on the latter. Research for grant **DE-FG02-03ER15387** in area of multiply bonded metal element complexes has focused on the potential utility of nitride and nitridyl complexes for effecting the activation of aliphatic C–H bonds. Calculations – both density functional theory (DFT) and multi-configuration SCF (MCSCF) – by UNT PhD candidate Zhicheng Daniel Sun indicate that nitridyl complexes of the Earth-abundant middle-late 3d metals (most notably Co and Ni) are worthy candidates for activation and functionalization of light alkane C–H bonds. Mr. Sun was assisted in these calculation by a former NSF-REU summer scholar, Olivia Hull, who is now a PhD student at Kansas State University. These complexes have sufficient activity to activate methane with reasonable free energy barriers ($\Delta G^\ddagger \sim 30$ kcal/mol), **Figure 1**.

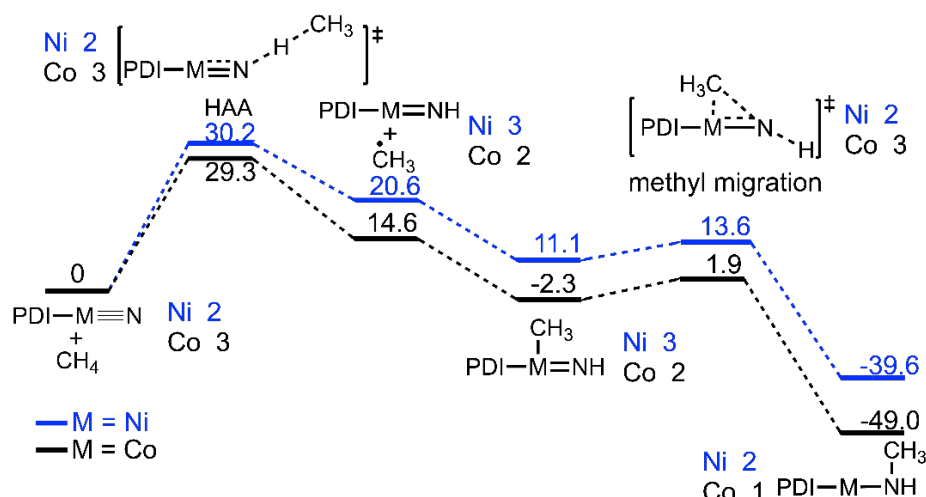


Figure 1. Free energy (in kcal/mol) profile for activation of methane by PDI-M-N complex, M = Co, Ni. Lowest energy spin states are indicated.

Methane Activation by 3d Metal Nitridyl Complexes

Activation proceeds by H-atom abstraction/radical rebound (HAA/RR), although [2+2] and direct insertion mechanisms can be close in energy depending on metal and supporting ligands. Calculations further suggest that imide – and even the amide – intermediates generated by the initial and subsequent activation events have sufficient activity to carry out further transformations. These MNH_xMe_{2-x} ($x = 0 - 2$) complexes have complicated electronic structures, necessitating analysis in cases by MCSCF methods to model the correct balance of nitride ($L_nM\equiv N$)/nitridyl ($L_nM=N^*$), imide ($L_nM=NR$)/imidyl ($L_nM\equiv NR^*$) and amide (L_nM-NR_2)/aminyl ($L_nM\cdots N^*R_2$) character, **Figure 2**.

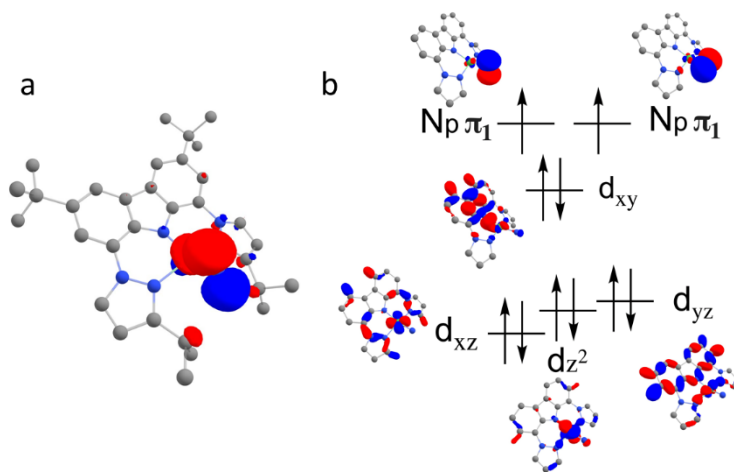


Figure 2. a. Mulliken spin density of Ni nitridyl (**B**) triplet; b. MCSCF (CAS(12, 12)) calculated Ni nitridyl orbitals.

Role of Actor Ligand Basicity and Radical Character

Calculations in our lab by then-undergraduate Catherine Moulder (now an NSF Graduate Research Fellow in our lab) and Mr. Sun suggest that the metal-nitrogen pi-bond strengths and how this modulates the basicity/nucleophilicity of the N-based actor ligand as well as its radical character are key elements in identifying systems that can activate and functionalize aliphatic C—

H bonds. Independent experiments by the Tomson (Co) and Lee (Ni) support the predictions put forth in our papers. We have formed a strategic collaboration with the Lee group to further investigate the chemistry of promising 3d-metal nitridyl complexes, **Figure 3**.

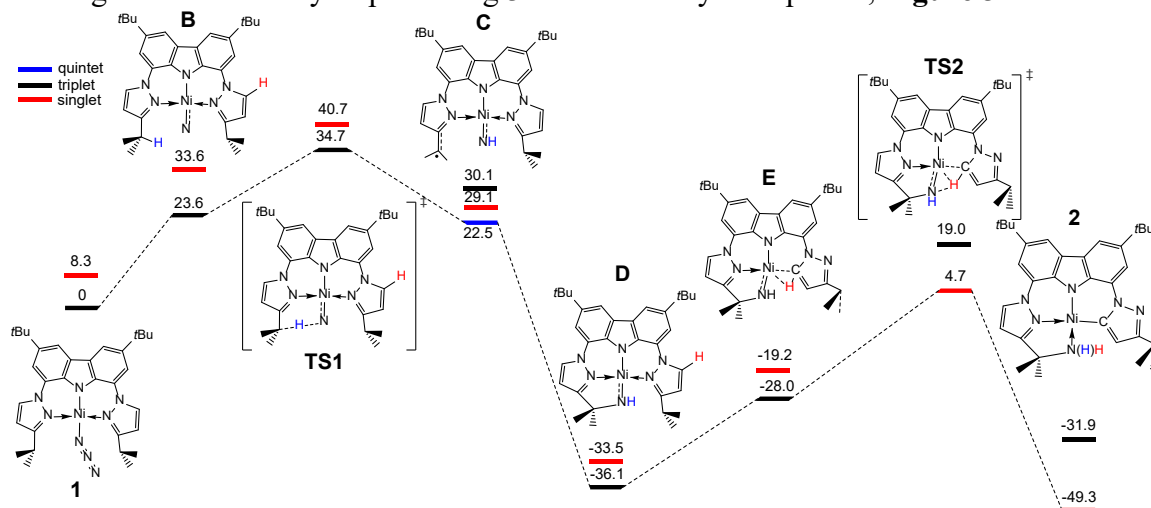


Figure 3. Proposed reaction pathway for the formation of **2** based on DFT calculations (B3LYP). Free energies are reported in kcal/mol at 298.15 K and 1 atm.

Publications Acknowledging this Grant (33 in total; due to space limitations only those since 2017 are shown). All publications are Category II, as they utilized the High-Performance Computing resource @ UNT, funded through grants from the NSF:

1. “Mechanistic Studies of Single-Step Styrene Production Using a Rhodium(I) Catalyst;” B. A. Vaughan, S. K. Khani, J. B. Gary, J. D. Kammert, M. S. Webster-Gardiner, B. A. McKeown, R. J. Davis, T. R. Cundari, T. B. Gunnoe *J. Am. Chem. Soc.* **2017**, *139*, 1486 - 1498.
2. “Redox non-innocence permits catalytic nitrene carbonylation by (dadi)Ti=NAd (Ad = adamantyl);” S. P. Heins, P. T. Wolczanski, T. R. Cundari, S. N. MacMillan *Chem. Sci.* **2017**, *8*, 3410 - 3418.
3. “Elusive Terminal Copper Arylnitrene Intermediates;” A. Bakhoda, Q. Jiang, J. A. Bertke, T. R. Cundari, T. H. Warren *Angew. Chem.* **2017**, *56*, 6426 – 6430 (comm.).
4. “Effect of Ancillary Ligands on Oxidative Addition of CH₄ to Re(III) Complexes: A = B, Al, CH, SiH, N, P Using MP2, CCSD(T) and MCSCF Methods;” R. Parveen, T. R. Cundari *J. Phys. Chem. A* **2017**, *121*, 5341 – 5351. .
5. “Heterolytic H-H and H-B Bond Cleavage Reactions of {(IPr)Ni(μ-S)}₂;” F. F. Olechnowicz, G. L. Hillhouse, T. R. Cundari, R. F. Jordan *Inorg. Chem.* **2017**, *56*, 9922 – 9930.
6. “Comparison of Pd^{II} vs Rh^I-catalyzed Catalytic Cycle for Styrene Production;” Y. S. Ceylan, T. R. Cundari *Comp. Theor. Chem.* **2017**, *1115*, 313 – 322.
7. “Rare Examples of Fe(IV) Alkyl-imide Migratory Insertions: Impact of Fe-C Covalency in (Me₂IPr)Fe(=NAd)R₂ (R = neoPe, 1-nor);” B. P. Jacobs, P. T. Wolczanski, Q. Jiang, T. R. Cundari, S. N. MacMillan *J. Am. Chem. Soc.* **2017**, *139*, 12145 – 12148. (comm.).

8. "Methane Manifesto: A Theorist's Perspective on Light Alkane Functionalization;" *Comm. Inorg. Chem.* T. R. Cundari **2017**, *37*, 219 - 237. (invited)
9. "Studies of the Decomposition of the Ethylene Hydrophenylation Catalyst $\text{TpRu}(\text{CO})(\text{NCMe})\text{Ph}$;" E. E. Joslin, B. A. McKeown, T. R. Cundari, T. B. Gunnoe *J. Organomet. Chem.* **2017**, *847*, 289 - 293. Invited (Gladysz special issue).
10. "Heterobimetallic Ag-Iron Complexes involving $\text{Fe}(\text{CO})_5$ ligands;" G. Wang, Y. S. Ceylan, T. R. Cundari, H. V. R. Dias *J. Am. Chem. Soc.* **2017**, *139*, 14292 - 14301.
11. "Computational Study of Methane C–H Activation by Earth-Abundant Metal-Amide/Aminyl Complexes;" B. M. Prince, T. R. Cundari *Organometallics* **2017**, *36*, 4987 – 3994.
12. "A DFT Survey of the Effects of d-Electron Count and Metal Identity on the Activation and Functionalization of C-H bonds for Mid to Late Transition Metals;" C. A. Moulder, T. R. Cundari *Israel J. Chem.* **2017**, *57*, 1023 - 1031. (invited).
13. "Hydrophenylation of Ethylene Using a Cationic Ru(II) Catalyst: Change in Selectivity Based on an Auxiliary Ligand;" X. Jia, J. B. Gary, B. A. McKeown, S. Gu., T. R. Cundari, T. B. Gunnoe - *Israel J. Chem.* **2017**, *57*, 1037 – 1046. (invited).
14. "Cooperative Metal+Ligand Oxidative Addition and Sigma-Bond Metathesis: A DFT Study;" K. G. Lopez, T. R. Cundari, J. B. Gary *Organometallics* **2018**, *37*, 309 – 313.
15. "Computational Analysis of Potential Transition Metal-Terminal Boride Complexes;" Y. S. Ceylan, T. R. Cundari *J. Phys. Chem. A* **2017**, *121*, 9358 – 9368.
16. "Dispersion Forces Play a Role in $(\text{Me}_2\text{IPr})\text{Fe}(=\text{NAd})\text{R}_2$ (Ad = adamantyl; R = neoPe, 1-nor) Insertions and BDEs;" T. R. Cundari, B. P. Jacobs, S. N. MacMillan, P. T. Wolczanski *J. Chem. Soc., Dalton* **2018**, *47*, 6025 – 6030. (invited).
17. "Computational Study of Methane C–H Activation by Diiminopyridine Nitride Complexes;" Z. Sun, T. R. Cundari *Inorg. Chem.* **2018**, *57*, 6807 – 6815.
18. "Comparative Nitrene-Transfer Chemistry to Olefinic Substrates Mediated by a Library of Anionic Mn(II) Triphenylamido-Amine Reagents and M(II) Congeners (M = Fe, Co, Ni) Favoring Aromatic over Aliphatic Alkenes" V. Bagchi, A. Kalra, P. Das, P. Paraskevopoulou, S. Gorla, L. Ai, Q. Wang, S. Mohapatra, A. Choudhury, Z. Sun, T. R. Cundari, P. Stavropoulos *ACS Cat.* **2018**, *8*, 9183 – 9206.
19. "Complexes of $[(\text{dadi})\text{Ti}(\text{L}/\text{X})]_m$ that Reveal Redox Non-innocence, and a Stepwise Carbene Insertion into a Carbon-carbon Bond;" Heins, S. P.; Morris, W. D.; Cundari, T. R.; MacMillan, S. N.; Lobkovsky, E. B.; Livezey, N.; Wolczanski, P. T. *Organometallics* **2018**, *37*, 3488 – 3501.
20. "Synthesis, photophysical properties, and computational analysis of di- and tetra-nuclear alkyne complexes of copper(I) supported by a highly fluorinated pyrazolate;" D. Parasar, R. Almotawa, N. Jayaratna, Y. S. Ceylan, T. R. Cundari, M. A. Omary, H. V. R. Dias. *Organometallics* **2018**, *37*, 4105 - 4118.

21. "Copper Catalyzed sp^3 C-H Amidation: Sterically Driven 1° and 2° C-H Site-Selectivity;" A. Bakhoda, Q. Jiang, Y. M. Badiei, J. A. Bertke, T. R. Cundari, T. H. Warren *Angew. Chem.* **2019**, *131*, 3459 – 3463.
22. "Direct Anti-Markovnikov Addition of Water to Olefin to Synthesize Primary Alcohols;" Y. S. Ceylan, T. R. Cundari *J. Phys. Chem. A* **2019**, *123*, 958 – 965.
23. "Oxidative Additions to Ti(IV) in $[(\text{dadi})^4]\text{Ti}^{\text{IV}}(\text{THF})$ Involve C-C Bond Formation and Redox Non-innocent Behavior;" Heins, S. P.; Zhang, B.; MacMillan, S. N.; Cundari, T. R.; Wolczanski, P. T. *Organometallics* **2019**, *38*, 1502 – 1515.
24. "Intramolecular C-H functionalization followed by a $[2_\sigma+2_\pi]$ -addition via an Intermediate Nickel Nitridyl;" J. Ghannam, Z. Sun, T. R. Cundari, M. Zeller, A. Lugosan, C. M. Stanek, W-T. Lee *Inorg. Chem.* **2019**, *58*, 7131 – 7135. (comm.).

Tailoring Boron Nitride for Catalysis Applications

Hao Chen,¹ Zhenzhen Yang,¹ Miaofang Chi,¹ De-en Jiang,² Zili Wu,¹ and Sheng Dai¹
¹Oak Ridge National Laboratory and ²University of California Riverside

Hexagonal boron nitride (h-BN), a representative graphene-analogous 2D material, has drawn significant interests in catalysis applications because of its high-temperature stabilities and diverse edge and basal sites. In catalysis, it is essential to have abilities to control both surface areas and interfacial structures for h-BN. Herein, we present three strategies toward the precision synthesis of high-surface area h-BN materials for controlling catalysis processes.¹⁻⁴ Firstly, a scalable synthesis of few-layered h-BN nanosheets (h-BNNS) using a novel gas exfoliation of bulk h-BN in liquid N₂ has been developed. The produced h-BNNS can be utilized to enhance an interfacial electronic effect on Pt nanocrystals through N-vacancies and B-vacancies for superior CO oxidation catalysis. Secondly, a crystallization strategy for the conversion of high-surface area amorphous h-BN to highly crystalline h-BNNS through a successive dissolution-precipitation/crystallization process in the presence of molten Mg has been recently developed. The fabricated h-BNNS exhibited high crystallinity, high porosity, high purity, and enhanced thermal stability. An improved catalytic performance of crystalline h-BNNS was evidenced by its much higher catalytic efficiency in the dehydrogenation of dodecahydro-N-ethylcarbazole. Thirdly, an ionothermal approach for the fabrication of mesoporous h-BN with high yield, high purity and high crystallinity using NaNH₂ and NaBH₄ as precursor materials was developed. The unique properties of inorganic metal salts and strong electrostatic interactions with mesoporous carbon (MC) substrates render this strategy suitable for production of homogeneous h-BN/MC heterostructures with high crystallinity, high h-BN dispersity, and strong interfacial effect.

Publications Acknowledging this Grant in 2016-2019

- (1) Zhu, W. S.; Gao, X.; Li, Q.; Li, H. P.; Chao, Y. H.; Li, M. J.; Mahurin, S. M.; Li, H. M.; Zhu, H. Y.; Dai, S. Controlled Gas Exfoliation of Boron Nitride into Few-Layered Nanosheets. *Angew. Chem.-Int. Edit.* **2016**, *55*, 10766-10770. 10.1002/anie.201605515
- (2) Zhu, W. S.; Wu, Z. L.; Foo, G. S.; Gao, X.; Zhou, M. X.; Liu, B.; Veith, G. M.; Wu, P. W.; Browning, K. L.; Lee, H. N.; Li, H. M.; Dai, S.; Zhu, H. Y. Taming interfacial electronic properties of platinum nanoparticles on vacancy-abundant boron nitride nanosheets for enhanced catalysis. *Nat. Commun.* **2017**, *8* 15291. DOI: 10.1038
- (3) Wu, P. W.; Yang, S. Z.; Zhu, W. S.; Li, H. P.; Chao, Y. H.; Zhu, H. Y.; Li, H. M.; Dai, S. Tailoring N-Terminated Defective Edges of Porous Boron Nitride for Enhanced Aerobic Catalysis. *Small* **2017**, *13*. 10.1002/smll.201701857
- (4) Chen, H.; Yang, Z. Z.; Zhang, Z. H.; Chen, Z. T.; Chi, M. F.; Wang, S.; Fu, J.; Dai, S. Construction of a Nanoporous Highly Crystalline Hexagonal Boron Nitride from an Amorphous Precursor for Catalytic Dehydrogenation. *Angew. Chem.-Int. Edit.* **2019**, in press.

Sub Nanometer Sized Clusters for Heterogeneous Catalysis

Abhaya Datye¹ and Yong Wang²

¹University of New Mexico and ²Washington State University

Presentation Abstract

The focus of this project is the synthesis, characterization and reactivity of transition metal moieties ranging from single atoms to clusters of about 1 nm in diameter that are present on high surface area supports. A major barrier in the utilization of sub-nm clusters is that they are subject to Ostwald ripening, leading to growth in size to form nanoparticles. Our recent work suggests that trapping single atoms on the support could help to slow the rates of ripening. Hence, one of the goals of this project is the understanding of anchoring sites on high surface area catalyst supports. Conventional (non-reducible) oxide supports provide only limited number of sites to anchor ionic species. Reducible oxides, such as ceria provide many more sites for anchoring due to the presence of defects. But reducible oxides are often not available in high surface area form, and they may not be as robust (can react to form carbonates, for example, or sinter easily) compared to the commonly-used high surface area supports such as silica, alumina, or carbon. Increasing atomic trapping sites on conventional catalyst supports is therefore important for improving the stability of sub-nm metal clusters on a supported catalyst. Another goal of this project is to expand the applicability of single atom catalysts to a broader class of catalyzed reactions. Transition metals in ionic form are perfectly situated for further manipulation of their catalytic activity by use of ligands, as in homogeneous catalysis. Understanding the principles that help in the design of robust single atom catalysts is one of the research challenges that is addressed in this project.

Grant No.: DE-FG02-05ER15712

Sub Nanometer Sized Clusters for Heterogeneous Catalysis

Post-docs: Andrew DeLaRiva and Haifeng Xiong (UNM), Junming Sun (WSU)

Graduate Students: Chris Riley (UNM), Deepak Kunwar (UNM), Xavier Isidro Pereira Hernández, Jianghao Zhang & Hannah Kim (WSU)

RECENT PROGRESS

Over the past year we have demonstrated that high loadings of single atoms of Pt can be stabilized on ceria supports (ACS Catalysis, cover page, 2019). When the deposited Pt is activated in CO at 275 °C, a remarkably active CO oxidation catalyst is obtained (Nature Communications, 2019). The high reactivity was shown to be due to the activation of the ceria support for facile oxygen transfer at low temperatures. Our research has also demonstrated the facile and reversible conversion of nanoparticles into single atoms. The ceria support is also shown to facilitate the

formation of sub-nm clusters that are stable under reducing conditions, such as those used in alkane dehydrogenation.

Stabilizing High Metal Loadings of Thermally Stable Platinum Single Atoms on an Industrial Catalyst Support

Scientific Achievement

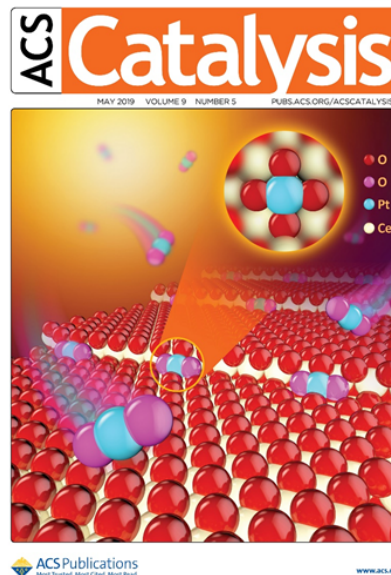
Single atom catalysts enable high atom efficiency and reactivity. Here we demonstrate that up to 3 wt% of Pt in single atom form on an industrial catalyst support can be achieved using high-temperature vapor-phase synthesis.

Significance and Impact

The mobility of single atoms hinders the industrial application of single atom catalysts. Strong binding of Pt ions improves thermal stability of catalysts and allows for facile catalyst regeneration.

Research Details

- High-temperature vapor-phase synthesis (800 °C in air) allows ceria to trap ionic Pt at step edge sites on ceria (see cover for ACS Catalysis).
- The conceptual advance is the recognition that under-coordinated Ce³⁺ at step edges can react with mobile PtO₂ and transform to Ce⁴⁺ while Pt⁴⁺ gets converted to Pt²⁺. This reaction allows formation of covalent bonds between Pt ions and the support.
- This binding is responsible for the facile regeneration of atomically dispersed Pt catalysts on ceria.



Kunwar, D.; Zhou, S.; DeLaRiva, A.; Peterson, E. J.; Xiong, H.; Pereira-Hernández, X. I.; Purdy, S. C.; ter Veen, R.; Brongersma, H. H.; Miller, J. T.; Hashiguchi, H.; Kovarik, L.; Lin, S.; Guo, H.; Wang, Y.; Datye, A. K., Stabilizing High Metal Loadings of Thermally Stable Platinum Single Atoms on an Industrial Catalyst Support. ACS Catal. 2019, 9, 3978-3990 DOI: 10.1021/acscatal.8b04885.



Office of
Science

DE-FG02-05ER15712



Tuning Pt-CeO₂ interactions by high-temperature vapor-phase synthesis for improved reducibility of lattice oxygen

Scientific Achievement

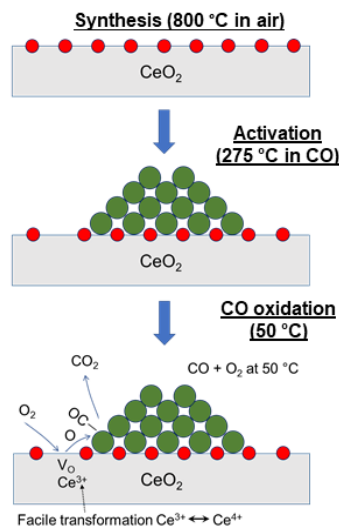
CO oxidation reactivity at low temperatures is hindered by the poisoning of Pt sites by CO. Here we demonstrate that the facile transfer of oxygen from ceria plays a decisive role in achieving CO oxidation at 50 °C.

Significance and Impact

A catalyst that meets the durability requirements of the DOE accelerated aging protocol (800 °C in air) and achieves CO oxidation performance at near room temperature could have a major impact on emission control technologies.

Research Details

- High-temperature vapor-phase synthesis (800 °C in air) allows ceria to trap ionic Pt at defect sites on ceria preventing ceria & Pt sintering (top figure).
- Reduction in CO at 275 °C transforms part of the ionic single-atom Pt species into Pt nanoparticles, creating an active CeO₂ surface (middle figure).
- The reversible conversion from Ce³⁺ to Ce⁴⁺ in the vicinity of the Pt nanoparticles allows activation of oxygen and its transfer to the Pt sites (bottom figure), leading to CO oxidation at near room temperature.



Xavier Isidro Pereira-Hernández, Berlin Sudduth, Mark Engelhard, Libor Kovarik, Yong Wang* (WSU/PNNL); Andrew DeLaRiva, Deepak Kunwar, Haifeng Xiong, Abhaya Datye* (UNM), Valery Muravev, Emiel J.M. Hensen* (TU/e) *Nature Comm*, 2019, Mar 25;10(1):1358, DOI:10.1038/s41467-019-09308-5



Office of
Science

DE-FG02-05ER15712



We also studied the doping of ceria via nickel using a sol-gel synthesis developed in our labs. This doped ceria was shown to be active for selective acetylene hydrogenation (JACS, 2019). Other publications from our group were focused on the synthesis of catalysts for biomass conversion and on synthesis of single atom catalysts.

Highlights from some of the most significant publications from this grant were submitted to the DOE BES Catalysis program. These highlights are included in this abstract since they best describe the progress on this project.

Design of Effective Catalysts for Selective Alkyne Hydrogenation by Doping of Ceria with a Single-Atom Promotor

Scientific Achievement

In this work we propose, based on density functional theory (DFT) investigations, a mechanism that involves the heterolytic dissociation of H₂ at oxygen vacancies of CeO₂(111), facilitated by frustrated Lewis pairs consisting of spatially separated O and Ce sites.

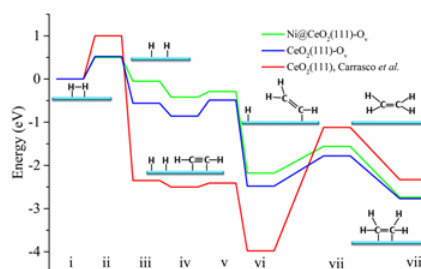
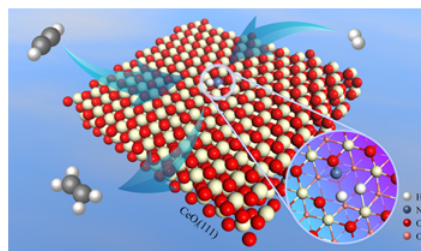
Significance and Impact

We demonstrate that Ni atoms doped into ceria help create vacancies, which then help catalyze selective hydrogenation of acetylene to ethylene. Hydrogenation is generally carried out by metallic surfaces, here we show how an oxide can carry out this reaction.

Research Details

- Ni was doped into ceria using a sol-gel method developed at UNM.
- The doping of ceria by Ni creates oxygen vacancies. The Ni dopant is not directly involved in the catalytic cycle, it serves as a single-atom promotor.
- The combined results from DFT calculations and experiment provide a basis to further develop selective hydrogenation catalysts based on earth abundant materials.

C. Riley, S. Zhou, D. Kunwar, A. De La Riva, E. Peterson, R. Payne, L. Gao, S. Lin, H. Guo, and A. Datye, Design of Effective Catalysts for Selective Alkyne Hydrogenation by Doping of Ceria with a Single-Atom Promotor *Journal of the American Chemical Society* 140 (40) (2018) 12964-12973 DOI: 10.1021/jacs.8b07789.



U.S. DEPARTMENT OF
ENERGY

Office of
Science

DE-FG02-05ER15712



Publications Acknowledging this Grant in 2015-2019

(XXV) Exclusively funded by this grant (24);

1. Sun, J.; Karim, A. M.; Mei, D.; Engelhard, M.; Bao, X.; Wang, Y., New insights into reaction mechanisms of ethanol steam reforming on Co-ZrO₂. *Applied Catalysis B-Environmental* **2015**, 162, 141-148.
2. Sun, J. M.; Karim, A. M.; Mei, D. H.; Engelhard, M.; Bao, X. H.; Wang, Y., New insights into reaction mechanisms of ethanol steam reforming on Co-ZrO₂. *Applied Catalysis B-Environmental* **2015**, 162, 141-148.
3. Sun, J. M.; Zhang, H.; Yu, N.; Davidson, S.; Wang, Y., Effect of Cobalt Particle Size on Acetone Steam Reforming. *ChemCatChem* **2015**, 7 (18), 2932-2936.
4. Wei, Z.; Karim, A. M.; Li, Y.; King, D. L.; Wang, Y., Elucidation of the roles of Re in steam reforming of glycerol over Pt-Re/C catalysts. *Journal of Catalysis* **2015**, 322, 49-59.
5. Wei, Z. H.; Karim, A.; Li, Y.; Wang, Y., Elucidation of the Roles of Re in Aqueous-Phase Reforming of Glycerol over Pt-Re/C Catalysts. *ACS Catalysis* **2015**, 5 (12), 7312-7320.
6. Wei, Z. H.; Karim, A. M.; Li, Y.; King, D. L.; Wang, Y., Elucidation of the roles of Re in steam reforming of glycerol over Pt-Re/C catalysts. *Journal of Catalysis* **2015**, 322, 49-59.
7. Xiong, H. F.; DeLaRiva, A.; Wang, Y.; Datye, A. K., Low-temperature aqueous-phase reforming of ethanol on bimetallic PdZn catalysts. *Catalysis Science & Technology* **2015**, 5 (1), 254-263.

8. Zhang, H.; Sun, J. M.; Liu, C. J.; Wang, Y., Distinct water activation on polar/non-polar facets of ZnO nanoparticles. *Journal of Catalysis* **2015**, 331, 57-62.
9. Davidson, S. D.; Sun, J. M.; Wang, Y., The effect of ZnO addition on H₂O activation over Co/ZrO₂ catalysts. *Catalysis Today* **2016**, 269, 140-147.
10. Hong, Y. C.; Hensley, A.; McEwen, J. S.; Wang, Y., Perspective on Catalytic Hydrodeoxygenation of Biomass Pyrolysis Oils: Essential Roles of Fe-Based Catalysts. *Catalysis Letters* **2016**, 146 (9), 1621-1633.
11. Liu, C. J.; Sun, J. M.; Brown, H. M.; Marin-Flores, O. G.; Bays, J. T.; Karim, A. M.; Wang, Y., Aqueous phase hydrodeoxygenation of polyols over Pd/WO₃-ZrO₂: Role of Pd-WO₃ interaction and hydrodeoxygenation pathway. *Catalysis Today* **2016**, 269, 103-109.
12. Pham, H. N.; Sattler, J. J. H. B.; Weckhuysen, B. M.; Datye, A. K., Role of Sn in the Regeneration of Pt/ γ -Al₂O₃ Light Alkane Dehydrogenation Catalysts. *ACS Catalysis* **2016**, 6 (4), 2257-2264.
13. Wang, W. Y.; Wu, K.; Liu, P. L.; Li, L.; Yang, Y. Q.; Wang, Y., Hydrodeoxygenation of p-Cresol over Pt/Al₂O₃ Catalyst Promoted by ZrO₂, CeO₂, and CeO₂-ZrO₂. *Industrial & Engineering Chemistry Research* **2016**, 55 (28), 7598-7603.
14. Yu, N.; Zhang, H.; Davidson, S. D.; Sun, J. M.; Wang, Y., Effect of ZnO facet on ethanol steam reforming over Co/ZnO. *Catalysis Communications* **2016**, 73, 93-97.
15. Chen, J. X.; Sun, J. M.; Wang, Y., Catalysts for Steam Reforming of Bio-oil: A Review. *Industrial & Engineering Chemistry Research* **2017**, 56 (16), 4627-4637.
16. Hong, Y. C.; Wang, Y., Elucidation of reaction mechanism for m-cresol hydrodeoxygenation over Fe based catalysts: A kinetic study. *Catalysis Communications* **2017**, 100, 43-47.
17. Hong, Y. C.; Zhang, S. R.; Tao, F. F.; Wang, Y., Stabilization of Iron-Based Catalysts against Oxidation: An In Situ Ambient-Pressure X-ray Photoelectron Spectroscopy (AP-XPS) Study. *ACS Catalysis* **2017**, 7 (5), 3639-3643.
18. Nie, L.; Mei, D. H.; Xiong, H. F.; Peng, B.; Ken, Z. B.; Hernandez, X. I. P.; DeLariva, A.; Wang, M.; Engelhard, M. H.; Kovarik, L.; Datye, A. K.; Wang, Y., Activation of surface lattice oxygen in single-atom Pt/CeO(2) for low-temperature CO oxidation. *Science* **2017**, 358 (6369), 1419-+.
19. Spezzati, G.; Su, Y. Q.; Hofmann, J. P.; Benavidez, A. D.; DeLaRiva, A. T.; McCabe, J.; Datye, A. K.; Hensen, E. J. M., Atomically Dispersed Pd-O Species on CeO(2)(111) as Highly Active Sites for Low-Temperature CO Oxidation. *ACS Catalysis* **2017**, 7 (10), 6887-6891.
20. Xiong, H. F.; Lin, S.; Goetze, J.; Pletcher, P.; Guo, H.; Kovarik, L.; Artyushkova, K.; Weckhuysen, B. M.; Datye, A. K., Thermally Stable and Regenerable Platinum-Tin Clusters for Propane Dehydrogenation Prepared by Atom Trapping on Ceria. *Angewandte Chemie-International Edition* **2017**, 56 (31), 8986-8991.
21. Hensley, A. J. R.; Wang, Y.; Mei, D. H.; McEwen, J. S., Mechanistic Effects of Water on the Fe-Catalyzed Hydrodeoxygenation of Phenol. The Role of Bronsted Acid Sites. *ACS Catalysis* **2018**, 8 (3), 2200-2208.
22. Yu, N.; Rahman, M. M.; Chen, J.; Sun, J.; Engelhard, M.; Hernandez, X. I. P.; Wang, Y., Steam reforming of simulated bio-oil on K-Ni-Cu-Mg-Ce-O/Al₂O₃: The effect of K. *Catalysis Today* **2018**.
23. Datye, A.; Wang, Y., Atom trapping: a novel approach to generate thermally stable and regenerable single-atom catalysts. *National Science Review* **2018**, 5 (5), 630-632.

24. Spezzati, G.; Benavidez, A. D.; DeLaRiva, A. T.; Su, Y. Q.; Hofmann, J. P.; Asahina, S.; Olivier, E. J.; Neethling, J. H.; Miller, J. T.; Datye, A. K.; Hensen, E. J. M., CO oxidation by Pd supported on CeO₂(100) and CeO₂(111) facets. *Applied Catalysis B-Environmental* **2019**, *243*, 36-46.

(XXVI) Jointly funded by this grant and other grants with leading intellectual contribution from this grant (17);

1. Xiong, H.; DeLaRiva, A.; Wang, Y.; Datye, A. K., Low-temperature aqueous-phase reforming of ethanol on bimetallic PdZn catalysts. *Catalysis Science & Technology* **2015**, *5* (1), 254-263.
2. Jones, J.; Xiong, H. F.; Delariva, A. T.; Peterson, E. J.; Pham, H.; Challa, S. R.; Qi, G. S.; Oh, S.; Wiebenga, M. H.; Hernandez, X. I. P.; Wang, Y.; Datye, A. K., Thermally stable single-atom platinum-on-ceria catalysts via atom trapping. *Science* **2016**, *353* (6295), 150-154.
3. Rahman, M. M.; Davidson, S. D.; Sun, J. M.; Wang, Y., Effect of Water on Ethanol Conversion over ZnO. *Topics in Catalysis* **2016**, *59* (1), 37-45.
4. Bossola, F.; Pereira-Hernandez, X. I.; Evangelisti, C.; Wang, Y.; Dal Santo, V., Investigation of the promoting effect of Mn on a Pt/C catalyst for the steam and aqueous phase reforming of glycerol. *Journal of Catalysis* **2017**, *349*, 75-83.
5. Carrillo, C.; Xiong, H.; DeLaRiva, A. T.; Kunwar, D.; Peterson, E. J.; Challa, S. R.; Qi, G.; Oh, S.; Wiebenga, M. H.; Hernandez, X. I. P.; Wang, Y.; Datye, A. K., Designing Catalysts for Meeting the DOE 150 °C Challenge for Exhaust Emissions. *Microscopy and Microanalysis* **2017**, *23* (S1), 2028-2029.
6. Xiong, H.; Wiebenga, M. H.; Carrillo, C.; Gaudet, J. R.; Pham, H. N.; Kunwar, D.; Oh, S. H.; Qi, G.; Kim, C. H.; Datye, A. K., Design considerations for low-temperature hydrocarbon oxidation reactions on Pd based catalysts. *Applied Catalysis B: Environmental* **2018**, *236*, 436-444.
7. Hensley, A. J. R.; Zhang, J. H.; Vincon, I.; Hernandez, X. P.; Tranca, D.; Seifert, G.; McEwen, J. S.; Wang, Y., Mechanistic understanding of methanol carbonylation: Interfacing homogeneous and heterogeneous catalysis via carbon supported Ir-La. *Journal of Catalysis* **2018**, *361*, 414-422.
8. Riley, C.; De La Riva, A.; Zhou, S.; Wan, Q.; Peterson, E.; Artyushkova, K.; Farahani, M. D.; Friedrich, H. B.; Burkemper, L.; Atudorei, N.-V.; Lin, S.; Guo, H.; Datye, A., Synthesis of Nickel-Doped Ceria Catalysts for Selective Acetylene Hydrogenation. *ChemCatChem* **2019**, *11* (5), 1526-1533.
9. Riley, C.; De La Riva, A.; Zhou, S.; Wan, Q.; Peterson, E.; Artyushkova, K.; Farahani, M. D.; Friedrich, H. B.; Burkemper, L.; Atudorei, N.-V.; Lin, S.; Guo, H.; Datye, A., Synthesis of Nickel-Doped Ceria Catalysts for Selective Acetylene Hydrogenation. *ChemCatChem* **2019**, *11* (5), 1526-1533.
10. Pereira-Hernández, X. I.; DeLaRiva, A.; Muravev, V.; Kunwar, D.; Xiong, H.; Sudduth, B.; Engelhard, M.; Kovarik, L.; Hensen, E. J. M.; Wang, Y.; Datye, A. K., Tuning Pt-CeO₂ interactions by high-temperature vapor-phase synthesis for improved reducibility of lattice oxygen. *Nature Communications* **2019**, *10* (1), 1358.

11. Kunwar, D.; Zhou, S.; DeLaRiva, A.; Peterson, E. J.; Xiong, H.; Pereira-Hernández, X. I.; Purdy, S. C.; ter Veen, R.; Brongersma, H. H.; Miller, J. T.; Hashiguchi, H.; Kovarik, L.; Lin, S.; Guo, H.; Wang, Y.; Datye, A. K., Stabilizing High Metal Loadings of Thermally Stable Platinum Single Atoms on an Industrial Catalyst Support. *ACS Catalysis* **2019**, *9*, 3978-3990.
12. Yu, N.; Rahman, M. M.; Chen, J.; Sun, J.; Engelhard, M.; Hernandez, X. I. P.; Wang, Y., Steam reforming of simulated bio-oil on K-Ni-Cu-Mg-Ce-O/Al₂O₃: The effect of K. *Catalysis Today* **2018**.
13. Xiong, H. F.; Wiebenga, M. H.; Carrillo, C.; Gaudet, J. R.; Pham, H. N.; Kunwar, D.; Oh, S. H.; Qi, G. S.; Kim, C. H.; Datye, A. K., Design considerations for low-temperature hydrocarbon oxidation reactions on Pd based catalysts. *Applied Catalysis B-Environmental* **2018**, *236*, 436-444.
14. Xiong, H.; Wiebenga, M. H.; Carrillo, C.; Gaudet, J. R.; Pham, H. N.; Kunwar, D.; Oh, S. H.; Qi, G.; Kim, C. H.; Datye, A. K., Design considerations for low-temperature hydrocarbon oxidation reactions on Pd based catalysts. *Applied Catalysis B: Environmental* **2018**, *236*, 436-444.
15. Riley, C.; Zhou, S.; Kunwar, D.; De La Riva, A.; Peterson, E.; Payne, R.; Gao, L.; Lin, S.; Guo, H.; Datye, A., Design of Effective Catalysts for Selective Alkyne Hydrogenation by Doping of Ceria with a Single-Atom Promotor. *Journal of the American Chemical Society* **2018**, *140* (40), 12964-12973.
16. Hensley, A. J. R.; Zhang, J. H.; Vincon, I.; Hernandez, X. P.; Tranca, D.; Seifert, G.; McEwen, J. S.; Wang, Y., Mechanistic understanding of methanol carbonylation: Interfacing homogeneous and heterogeneous catalysis via carbon supported Ir-La. *Journal of Catalysis* **2018**, *361*, 414-422.
17. Feng, Y. X.; Wang, Q.; Xiong, H. F.; Zhou, S. L.; Chen, X.; Hernandez, X. I. P.; Wang, Y.; Lin, S.; Datye, A. K.; Guo, H., Correlating DFT Calculations with CO Oxidation Reactivity on Ga-Doped Pt/CeO₂ Single-Atom Catalysts. *Journal of Physical Chemistry C* **2018**, *122* (39), 22460-22468.

(XXVII) *Jointly funded by this grant and other grants with relatively minor intellectual contribution from this grant(6);*

1. Hensley, A. J. R.; Schneider, S.; Wang, Y.; McEwen, J. S., Adsorption of aromatics on the (111) surface of PtM and PtM₃ (M = Fe, Ni) alloys. *RSC Advances* **2015**, *5* (104), 85705-85719.
2. Hensley, A. J. R.; Wang, Y.; McEwen, J. S., Phenol Deoxygenation Mechanisms on Fe(110) and Pd(111). *ACS Catalysis* **2015**, *5* (2), 523-536.
3. Sun, J. M.; Karim, A. M.; Li, X. S.; Rainbolt, J.; Kovarik, L.; Shin, Y.; Wang, Y., Hierarchically structured catalysts for cascade and selective steam reforming/hydrodeoxygenation reactions. *Chemical Communications* **2015**, *51* (93), 16617-16620.
4. Hensley, A. J. R.; Wang, Y.; McEwen, J. S., Adsorption of guaiacol on Fe (110) and Pd (111) from first principles. *Surface Science* **2016**, *648*, 227-235.

5. Karim, A. M.; Al Hasan, N.; Ivanov, S.; Siefert, S.; Kelly, R. T.; Hallfors, N. G.; Benavidez, A.; Kovarik, L.; Jenkins, A.; Winans, R. E.; Datye, A. K., Synthesis of 1 nm Pd Nanoparticles in a Microfluidic Reactor: Insights from in Situ X-ray Absorption Fine Structure Spectroscopy and Small-Angle X-ray Scattering. *Journal of Physical Chemistry C* **2015**, 119 (23), 13257-13267.
6. Hensley, A. J. R.; Wang, Y.; Mei, D. H.; McEwen, J. S., Mechanistic Effects of Water on the Fe-Catalyzed Hydrodeoxygenation of Phenol. The Role of Bronsted Acid Sites. *ACS Catalysis* **2018**, 8 (3), 2200-2208.

**Conversion of Ethanol to Butanol and Butadiene over
Bifunctional Acid-Base Catalysts**

Robert J. Davis, Sabra Hanspal, Naomi Miyake, J. Tyler Prillaman, Zachary Young
Department of Chemical Engineering, University of Virginia
Charlottesville, VA 22904

Presentation Abstract

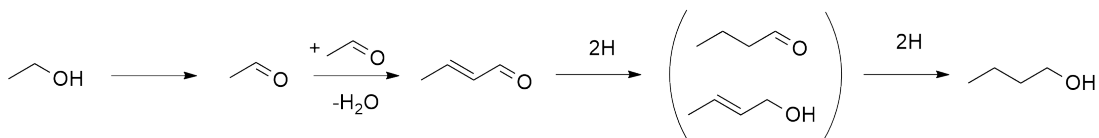
Although much progress has been made over the last few decades in understanding the features of active sites needed to catalyze individual elementary steps, many important chemical transformations often occur through a complex cascade of reactions involving multiple types of active sites present on the catalyst. A catalyst must interact with and subsequently convert many different reaction intermediates throughout the reaction cascade without degrading those same intermediates. This research explores the active site requirements for the Guerbet and Lebedev reactions, which are complex cascade reactions that convert ethanol to butanol and butadiene, respectively. As the catalytically active sites for the Guerbet and Lebedev reactions are thought to involve finely tuned acid-base site pairs on the catalyst surfaces, the objectives of the research involve synthesis of acid-base bifunctional solids, characterization of their surfaces, and evaluation of catalyst reactivity in steady-state and transient reactions involving alcohol dehydrogenation, alcohol dehydration, hydrogen transfer, and C-C coupling. Results from this work could be used to design new catalytic materials for chemical transformations involved in energy storage and conversion as well as chemicals production, particularly relevant to the future biorefinery.

DE-FG02-95ER14549: Acid-Base Bifunctional Catalysts for Cascade Reactions of Alcohols

Student(s): Sabra Hanspal, Nayomi Miyake, J. Tyler Prillaman, Zachary Young

RECENT PROGRESS

Our previous work on the aldol condensation of acetaldehyde over hydroxyapatite (HAP) and magnesia (MgO) showed that surface reactions such as enolate formation are very rapid while the adsorption of acetaldehyde as well as product desorption are kinetically relevant (see publications list). However, the role of hydrogenation and dehydrogenation reactions during Guerbet coupling over HAP and MgO are much less understood, despite being critical steps in the initial dehydrogenation of ethanol to acetaldehyde as well as the final hydrogenation reactions of crotonaldehyde to butanol. We therefore studied various reactions involving hydrogen transfer on catalysts for Guerbet coupling. The most recent efforts have focused on the modification of catalyst acidity to allow for dehydration of products from C-C coupling to produce butadiene without significantly dehydrating the reactant ethanol



Scheme 1. Commonly accepted reaction network in Guerbet coupling of ethanol to butanol. The final two steps in the cascade reaction involve hydrogen transfer.

Exploration of Hydrogen Transfer Reactions on Guerbet Coupling Catalysts

In an effort to understand how the hydrogen transfer reactions occur during Guerbet coupling of ethanol (see Scheme 1), the dehydrogenation of benzyl alcohol at 633 K and the hydrogenation of ethene and acetone at 473 K using both H₂ and ethanol as a hydrogen source were studied over HAP and MgO. The H₂-D₂ exchange reaction at room temperature and the Guerbet coupling of ethanol at 613-673 K in the presence of D₂ were also performed. Although there was no consequence of adding D₂ to the Guerbet coupling of ethanol in terms of rate or selectivity, incorporation of deuterium into product butanol was only observed over MgO. This was attributed to the rapid exchange of H₂-D₂ that can occur over MgO but not over HAP. Hydrogenation of acetone occurred with ethanol as a sacrificial hydrogen donor via a Meerwein-Ponndorf-Verley (MPV)-like reaction whereas hydrogenation with H₂ was not observed. Hydrogenation of ethene with H₂ or ethanol was not observed above background. Comparing the rate of benzyl alcohol dehydrogenation to the rate of ethanol coupling over HAP and MgO suggests that the MPV-like hydrogen transfer reaction over HAP is mostly responsible for generating intermediate acetaldehyde during the Guerbet reaction instead of direct dehydrogenation.

Modification of Hydroxyapatite by Composition, Thermal Treatment and Zirconia

In an effort to shift the selectivity of the Guerbet coupling reaction from butanol to butadiene, some level of acidity is required to catalyze dehydration of the C₄ products. Three strategies were used to vary the acid function of hydroxyapatite. First, we adjusted the composition of the hydroxyapatite $Ca_{(10-x)}(HPO_4)_x(PO_4)_{(6-x)}OH_{(2-x)}$ from our standard Guerbet coupling catalyst ($x=0$), to one having a Brønsted acid site ($x=1$). Then, thermal activation treatments from 873 to 1173 K were used to remove atmospheric adsorbates, to dehydroxylate/dehydrate the material, and to change the crystal structure. Starting with Ca₉(HPO₄)(PO₄)₅(OH) (a hydroxyapatite structure), the catalyst evolves into Ca₃(PO₄)₂ upon thermal treatment between 923 and 973 K, as verified by X-ray diffraction. When this particular composition is in the hydroxyapatite form, the catalyst converts ethanol to light hydrocarbons (ethane and ethane) and diethyl ether, presumably because of the Brønsted acid sites associated with the surface phosphate groups.

The phase transition to calcium phosphate following thermal treatment substantially reduced the surface acidity associated with the hydroxyapatite phase, which in turn affected performance in the catalytic conversion of ethanol. The high temperature treated calcium phosphate catalyzed primarily ethanol coupling reactions to form C₄ oxygenates. We have also added Ca phosphate to zirconia, which has resulted in 20% selectivity to butadiene at 22% conversion of ethanol, but we still observe 33% selectivity to undesired ethane, ethane and diethyl ether. Evidently, the acidity of the added zirconia was not effectively lowered

by addition of the Ca phosphate. Thus, subsequent work has focused on the modification of amphoteric zirconia in the absence of Ca phosphate.

Silver-promoted ZrO₂-SiO₂ Catalysts for Ethanol Coupling to Butadiene

Crystalline ZrO₂ is an amphoteric oxide, exhibiting both acid and basic surface sites, but it is too acidic for ethanol coupling, producing 80% diethyl ether at low ethanol conversion. Dispersing zirconia onto silica substantially lowers the acid character of the crystalline zirconia so that other reactions, such as ethanol dehydrogenation to acetaldehyde, become significant. Adding Ag particles to the catalyst as a dehydrogenating agent (facilitating ethanol dehydrogenation to acetaldehyde – see Scheme 1) allows for lower reaction temperatures to be used and a 1wt%Ag/4 wt%ZrO₂/SiO₂ catalyst in our lab produces butadiene at 623 K with selectivities of >60% and conversions >70%. The Ag component can be physically mixed with the ZrO₂/SiO₂ catalyst to achieve excellent performance, which enable us to explore the influences of zirconia domain size and synthesis method on the final acid-base properties of the mixed oxide without the complication of the silver component.

Publications Acknowledging this Grant in 2015-2018

(XXVIII) Exclusively funded by this grant;

1. Young, Z.D.; Davis, R.J. Hydrogen Transfer Reactions Relevant to Guerbet Coupling of Alcohols over Hydroxyapatite and Magnesium Oxide Catalysts. *Catal. Sci. Technol.* **2018**, *8*, 1722-1729.
2. Hanspal, S.; Young, Z.D.; Prillaman, J.T.; Davis, R.J. Influence of Surface Acid and Base Sites on the Guerbet Coupling of Ethanol to Butanol over Metal Phosphate Catalysts. *J. Catal.* **2017**, *352*, 182-190.
3. Young, Z.D.; Hanspal, S.; Davis, R.J. Aldol Condensation of Acetaldehyde over Titania, Hydroxyapatite and Magnesia. *ACS Catal.* **2016**, *6*, 3193-3202.
4. Hanspal, S.; Young, Z.D.; Shou, H.; Davis, R.J. Multi-product Steady-State Isotopic Transient Kinetic Analysis of the Ethanol Coupling Reaction over Hydroxyapatite and Magnesia. *ACS Catal.* **2015**, *5*, 1737-1746.
5. Hill, I.M.; Hanspal, S.; Young, Z.D.; Davis, R.J. DRIFTS of Probe Molecules Adsorbed on Magnesia, Zirconia and Hydroxyapatite Catalysts. *J. Phys. Chem. C* **2015**, *119*, 9186-9197.

(XXIX) Jointly funded by this grant and other grants with leading intellectual contribution from this grant;

1. Pacheco, H.P.; de Souza, E.F.; Landi, S.M.; David, M.V.; Prillaman, J.T.; Davis, R.J.; Toniolo, F.S. Ru promoted MgO and Al-modified MgO for Ethanol Upgrading. *Top. Catal.* in press.
2. Davis, R.J. Turnover Rates on Complex Heterogeneous Catalysts. *AIChE J.* **2018**, *64*, 3778-3785.

(XXX) Jointly funded by this grant and other grants with relatively minor intellectual contribution from this grant; None

Theory, Simulation, and Design of High-Oxidation State Main-Group Metal Catalysts for Hydrocarbon C-H Functionalization

Daniel H. Ess

Department of Chemistry and Biochemistry, Brigham Young University, Provo, UT 84602

Poster Abstract

This poster will describe our use and development of standard and non-standard density functional theory (DFT) calculations to investigate 5th-row and 6th-row high-oxidation state p-block, main-group compounds as catalysts for alkane and arene C-H functionalization reactions. This poster will feature studies on: i) Quantitative assessment and prediction of C-H activation and functionalization reactions by 5th-row and 6th-row p-block metal carboxylate complexes, which led to the identification and experimental synthesis of Sb(TFA)₅ (TFA = trifluoroacetate) that functionalizes methane and ethane. ii) New mechanistic insights into methane CO functionalization by SbF₅. iii) Development of computational protocols and use for examination of main-group C-H activation and metal-alkyl functionalization reactions in explicit/continuum and explicit carboxylic acid solvent. iv) Computational investigation of the reaction mechanism for methane nitrogen functionalization by Hg(NTf₂)₂ (Tf = SO₂CF₃).

Grant Number: DE-SC0018329 (Theory of Main-Group, p-Block Hydrocarbon Functionalization Reactions)

PI: Daniel H. Ess

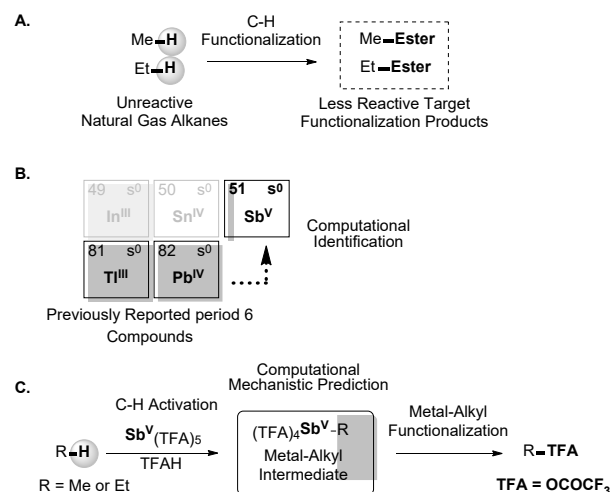
Postdocs: Samantha Gustafson, Madhu Samolia

Students: Clinton King (graduate student), Josh Wheeler (graduate student), Nick Rollins (undergraduate student), Ashley Holdaway (undergraduate student), Ernest Puletasi (visiting undergraduate), Lorna Suaava (visiting undergraduate).

RECENT PROGRESS

Assessment and Design of High-Oxidation State Main-Group Metal-Ligand Complexes for Alkane C-H Activation and Functionalization Reactions

High-oxidation state main-group metal complexes are potential alternatives to transition metals for electrophilic alkane C-H functionalization reactions. However, there is little known about how selection of the p-block, main-group metal and ligand impact alkane C-H activation and functionalization thermodynamics and reactivity. Therefore, we completed the analysis of reactivity across a broad range of high-oxidation state main group metals with several acetate ligands and solvents. The major conclusions from this study were: i) While the main-group metal influences the C-H activation barrier height in a periodic manner, the carboxylate ligand has a much larger quantitative impact on C-H activation with stabilized carboxylate anions inducing the lowest barriers. ii) For metal-methyl functionalization reactions, the main-group metal



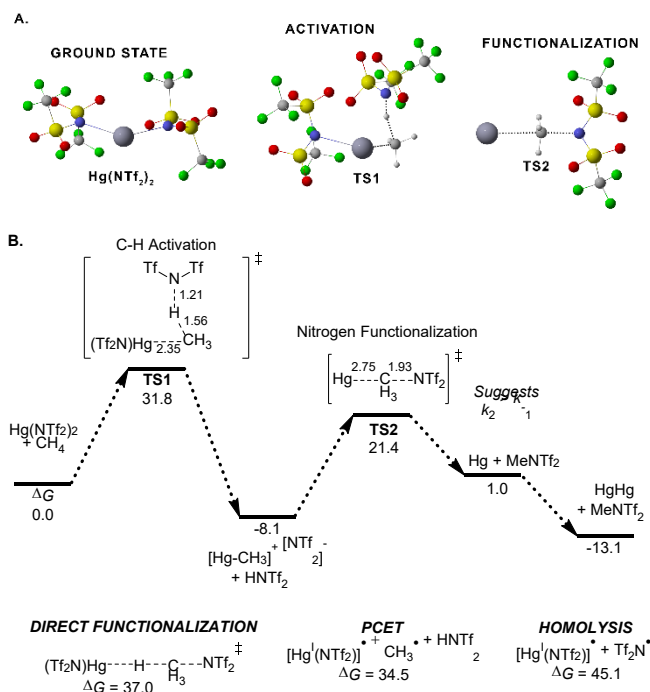
dramatically influences the barrier heights. This was correlated to reaction thermodynamics and bond heterolysis energies as a model two-electron reduction energies.

These two conclusions were critical to set the stage for the computational identification/prediction, and experimental synthesis and testing of an active Sb^{V} carboxylate complex. Based on this computational work, the Periana group at Scripps-Florida experimentally synthesized the $\text{Sb}^{\text{V}}(\text{TFA})_5$ (TFA = trifluoroacetate) complex. Testing of this complex showed that it selectively functionalized methane and ethane C-

H bonds to the corresponding mono and/or diol trifluoroacetate esters at 110-180 °C. Our complete mechanistic DFT calculations provided evidence supporting a C-H activation and Sb-alkyl functionalization mechanism for methane, however, for ethane, it is possible that hydride transfer competes with C-H activation, and therefore a major current thrust is understanding the mechanism and selectivity of ethane C-H functionalization by $\text{Sb}^{\text{V}}(\text{TFA})_5$.

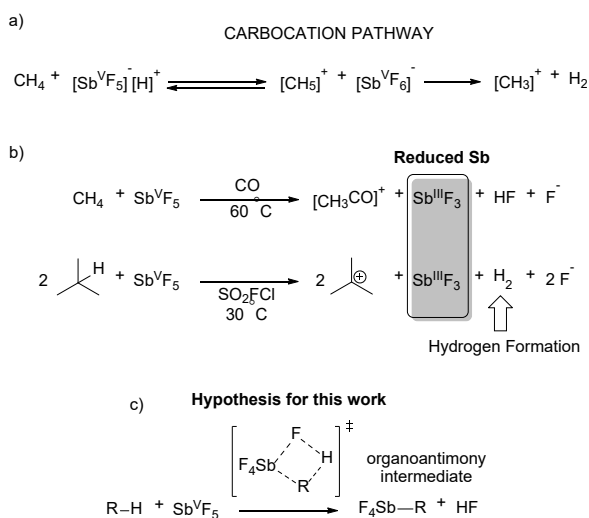
Mechanisms of Main-Group Metal-Alkyl Functionalization Reactions

We used DFT to study $\text{Hg}(\text{NTf}_2)_2$ mediated methane C-H amination. Experimentally, the Periana group at Scripps-Florida discovered that $\text{Hg}(\text{NTf}_2)_2$ induces C-H functionalization of methane to the corresponding alkyl amine. Our DFT study using a combination of continuum and explicit/continuum HNTf_2 solvent models examined a variety of mechanisms, including radical fragmentation, electron transfer, proton-coupled electron transfer, and hydride abstraction. None of these mechanisms are as viable as C-H activation and metal-alkyl amino functionalization (see the Scheme to the right, part B). Our study also explains the selective monofunctionalization preference over difunctionalization for ethane.



Reaction of methane with $\text{Sb}^{\text{V}}\text{F}_5$, especially in the presence of a Brønsted acid (e.g. HF or HSO_3F), is assumed to induce reversible formation of methanium ($[\text{CH}_5]^+$) that fragments to H_2 and methyl cation (Scheme 1a), which can further react leading to alkane oligomerization. For methane, the first step of this superacid-induced reaction pathway is supported by the experimental observation of hydrogen/deuterium (H/D) exchange. The second step in the methanium to methyl cation pathway is tenuous because H_2 is generally not observed. There are several reasons to explore possible alternative mechanisms for reaction of methane with $\text{Sb}^{\text{V}}\text{F}_5$, in particular for conditions without excess Brønsted acid. It was reported multiple times that the reaction of methane with neat $\text{Sb}^{\text{V}}\text{F}_5$ in the presence of CO at 60-80 °C led to formation of $[\text{CH}_3\text{CO}]^+$, reduced Sb, and no observation of H_2 (Scheme part b). Experiments also showed that while H_2 is capable of reducing Sb^{V} to Sb^{III} , under these conditions the rate of reduction is inconsistent with its formation and rapid reaction without observation. This suggests that the carbocation pathway outlined in Scheme a is an unlikely route to $[\text{CH}_3\text{CO}]^+$. In contrast to the methane reaction, it was reported that for the reaction of isobutane with neat $\text{Sb}^{\text{V}}\text{F}_5$ results in $\text{Sb}^{\text{III}}\text{F}_3$ with observation of both H_2 and *tert*-butyl cation.

While previous DFT studies examined reaction pathways for H/D exchange by $\text{Sb}^{\text{V}}\text{F}_5$ superacids, there has been no computational consideration of mechanisms involving C-H activation/metalation (Scheme c) or hydride transfer that provide a route for Sb^{V} to Sb^{III} reduction. We have nearly completed DFT calculations that compare C-H activation, hydride transfer, and protonation pathways for oxidation of methane and isobutane with $\text{Sb}^{\text{V}}\text{F}_5$. We found that the $\text{Sb}^{\text{V}}\text{F}_5$ -mediated C-H activation pathway is viable and results in an Sb^{V} -Me intermediate, which can be functionalized by CO resulting in $[\text{CH}_3\text{CO}]^+$ and Sb^{III} . Because methyl cation is very unstable, this C-H activation pathway is lower in energy than hydride transfer and protonation pathways. **Error! Bookmark not defined.** In contrast, for isobutane, the hydride transfer transition pathway is a significantly lower energy route than C-H activation, which leads to *tert*-butyl cation and an Sb^{V} -H intermediates that provides a pathway to H_2 formation.



Publications Acknowledging this Grant in 2015-2018

- (I) a) Gustafson, S. J.; Konnick, M. M.; Periana, R. A.; Ess, D. H. “Mechanisms and Reactivity of Tl(III) Main-Group Metal-Alkyl Functionalization in Water” *Organometallics*, **2018**, *37*, 2723-2731.
- b) King, C. R.; Rollins, N.; Holdaway, A.; Konnick, M. M.; Periana, R. A.; Ess, D. H. “Electrophilic Impact of High-Oxidation State Main-Group Metal and Ligands on Methane C-H Activation and Functionalization Reactions” *Organometallics*, **2018**, *37*, 3045-3054.
- (II) a) Koppaka, A.; Park, S. H.; Hashiguchi, B. G.; Gunsalus, N. J.; King, C. R.; Konnick, M. M.; Ess, D. H.; Periana, R. A. “Selective C-H Functionalization of

Methane and Ethane by a Molecular Sb(V) Complex” *Angew. Chem. Int. Ed.* **2019**, *58*, 2241-2245.

b) Gunsalus, N. J.; Park, S. H.; Hashiguchi, B. G.; Koppaka, A.; Smith, S. J.; Ess, D. H.; Periana, R. A. “Selective N Functionalization of Methane and Ethane to Aminated Derivatives by Main-Group-Directed C-H Activation” *Organometallics* **2019**, DOI: 10.1021/acs.organomet.9b00246.

(III) *None*

Controlling Catalytic Activity by Redesigning Enzymatic Scaffolds

Bojana Ginovska, Greg Schenter, Joseph Laureanti and Wendy Shaw

Institute for Integrated Catalysis, Pacific Northwest National Laboratory, Richland, WA

Efficient interconversion of CO₂ to products can be utilized to store energy in chemical bonds. Molecular catalysts based on transition metals have been used as a platform to study approaches that can improve catalytic efficiency and modulate the reactions by utilizing a protein scaffold. Taking inspiration from nature, and to design more efficient catalysts, we are developing an understanding of the outer coordination sphere (OCS) effects on the reactivity of small molecule catalysts. The activity of metalloenzymes is extremely sensitive to the outer coordination sphere, i.e. the amino acid residues around the catalytic center, where positioning of functional groups can tune the electronic environment of the metal center and affect the delivery and positioning of substrate and solvent. We use a Rh-based molecular catalyst (Rh(bisdiphosphine) complex) to study the effects of the environment on the catalytic mechanism for converting CO₂ to formate. We hypothesize that *positioning diverse functionality around the active site creates an anisotropic environment to control the free energy landscape for H₂ addition and CO₂ substrate activation*. The molecular catalyst was embedded in a stable protein scaffold (LmrR) and studied by experimental and computational methods. Experimentally, we studied the rate of catalytic activity for CO₂ to formate using high pressure NMR. We used quantum mechanical calculations and molecular dynamics simulations to evaluate changes in the environment near the metal center, as a function of single amino acid variations. We studied the wild type scaffold and three variants (W99R, V18R and D103R), where residues near the active sites were replaced with arginine (Arg, R), a positively charged residue. These substitutions were selected in order to mimic the active site of formate dehydrogenase or CO dehydrogenase, where positively charged residues are believed to assist by stabilizing the negative charge in the transition state. By replacing an aspartic acid residue (Asp, D) with Arg, in each if the monomers of the LmrR homodimer, we increase the overall charge by +4, and by replacing the neutral tryptophan residues (Trp, W) to Arg or the two Val to Arg, we increase the charge by +2. Changes in the scaffold imposed by the single point variations affect both the electrostatic potential that the metal center experiences as well as the organization of water near the active site. Importantly we find that these changes correlate with the experimentally measured catalytic activity, where the D103R variant shows a more than 3-fold increase in catalytic activity. We are currently developing a mechanistic understanding by carrying out quantum mechanical calculations on the catalyst with and without the positioned centers and establishing changes in the electronic structure of the catalysts, as well as effects on the free energy surface in order to extract mechanistic details for this process. We are also investigating additional variants to evaluate the role of overall charge versus positioning of charge.

FWP 47319: Transdisciplinary Approaches to Realize Novel Catalytic Pathways to Energy Carriers

PI: Johannes Lercher

Spectroscopic Characterization of Polynuclear Copper Species in Chabazite Zeolites for Partial Methane Oxidation to Methanol

Laura N. Wilcox¹, Ishant Khurana¹, Hui Li², Christopher Paolucci², William F. Schneider²,
Rajamani Gounder^{1*}

¹Davidson School of Chemical Engineering, Purdue University, West Lafayette, IN

²Chemical and Biomolecular Engineering, University of Notre Dame, Notre Dame, IN

Presentation Abstract

Methane is an abundant and inexpensive alkane that can be sourced from natural and shale gas and upgraded to chemicals of higher value, including methanol. Cu-zeolites have received renewed attention as materials that may facilitate partial methane oxidation (PMO), with many proposed active site motifs, including mononuclear and polynuclear copper species. More precise identification of the copper structures that activate CH₄ can be facilitated by studying model heterogeneous supports that contain well-defined copper speciation, as a result of the synthetic and treatment procedures used to prepare them. Chabazite (CHA) zeolites are high-symmetry frameworks that contain a single, unique tetrahedral site (T-site) and serve as a model support to simplify the interpretation of experimental characterization data of Cu sites, which can be compared more faithfully to structural models using computational approaches. Mononuclear Cu sites in close proximity can condense to form binuclear oxo-bridged Cu species that can be quantified with the combination of H₂ and CO temperature programmed reduction (TPR). *In situ* diffuse reflectance UV-Visible and Raman spectroscopies were used to identify the presence of binuclear Cu site types. Spectral assignments in UV-Vis were corroborated by ab-initio molecular dynamics (AIMD) combined with time-dependent density functional theory (TD-DFT), which reveal the dynamic changes in structure and coordination even among nominally isolated Cu sites at finite temperature. Model Cu-CHA zeolites were used to measure methanol yields from stoichiometric PMO cycles, providing evidence that proximal mononuclear Cu sites that are able to form binuclear Cu complexes are precursors to the dominant PMO active sites.

DE-SC0019026: Dynamic Multinuclear Active Sites Formed from Mobilized Single Atoms on Heterogeneous Supports for Selective Oxidation Catalysis

PI: Rajamani Gounder

Student(s): Laura N. Wilcox, Andrew D. Mikes

RECENT PROGRESS

UV-Visible spectroscopy to distinguish Cu active sites in Cu-zeolites

The distribution of framework Al atoms ($\text{Al-O}(-\text{Si-O})_x\text{-Al}$) in CHA zeolites between isolated ($x \geq 3$) and paired ($x=1,2$) configurations influences the speciation of exchanged extraframework Cu cations. Cu^{2+} sites exchange at proximal Al sites (Z_2Cu) and $[\text{CuOH}]^+$ complexes exchange at isolated Al sites (ZCuOH). A suite of Cu-CHA samples was synthesized to contain solely Z_2Cu sites or solely ZCuOH sites at varying spatial density, or a mixture of both Z_2Cu and ZCuOH sites. *In situ* diffuse reflectance UV-Visible spectroscopy was used to monitor the structures of mononuclear and binuclear Cu sites present on these samples after high temperature oxidizing treatments in dioxygen (20 kPa O_2 , 673 K) and moderate temperature reducing treatments in carbon monoxide (5 kPa CO, 523 K).

UV-Visible spectra are shown for three model Cu-CHA zeolites that contain solely Z_2Cu sites or solely ZCuOH sites at two different spatial densities (Fig. 1). For the sample containing mononuclear Z_2Cu sites (Fig. 1a), d-d transition features characteristic of Cu^{2+} ($\sim 8,000\text{-}16,000\text{ cm}^{-1}$) and a ligand-to-metal charge transfer band ($\sim 30,000\text{-}50,000\text{ cm}^{-1}$) were observed after high temperature O_2 oxidation treatments. Importantly, these spectral features remained invariant after exposure to CO. For samples containing ZCuOH sites (Figs. 1b-c), several distinct d-d transition features ($\sim 11,059$, $\sim 13,593$, $\sim 16,379$, and $\sim 20,077\text{ cm}^{-1}$) and a shoulder representative of multinuclear copper species ($24,000\text{-}30,000\text{ cm}^{-1}$) are observed after O_2 oxidation treatments, and the intensities of these features depend on ZCuOH density.

These observations reproduce literature reports, yet specific assignments for these features have remained incompletely resolved to date. A key finding was observed after exposure to CO at 523 K, which has been reported to reduce

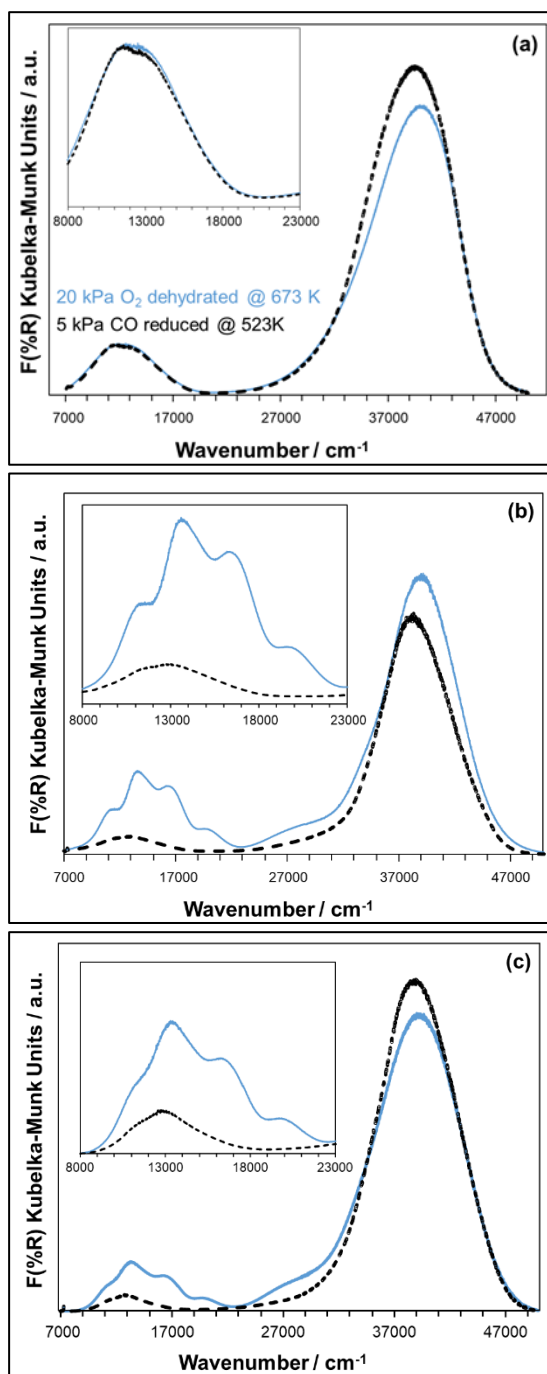


Figure 1. UV-Visible spectra of Cu-CHA zeolites containing (a) Z_2Cu sites ($\text{Si}/\text{Al}=5$, $\text{Cu}/\text{Al}=0.21$) or ZCuOH sites at (b) high ($\text{Si}/\text{Al}=15$, $\text{Cu}/\text{Al}=0.24$) and (c) low spatial density ($\text{Si}/\text{Al}=15$, $\text{Cu}/\text{Al}=0.15$) after high temperature oxidation (20 kPa O_2 , 673 K; blue) and CO reduction (5 kPa CO, 523 K; black).

multinuclear Cu-oxo complexes (e.g., $[\text{Cu-O-Cu}]^{2+}$) to Cu^+ , as it led to the disappearance of features at $\sim 16,379$, $20,077$, and $27,000 \text{ cm}^{-1}$. Thus, features that remain after CO reduction reflect d-d transitions of isolated ZCuOH sites that are sufficiently spatially isolated and do not condense to form multinuclear Cu-oxo complexes after high temperature O_2 oxidation. Features that disappear upon CO reduction are characteristic of multinuclear Cu-oxo sites formed upon condensation of proximal ZCuOH sites.

Consequences of finite-temperature dynamics investigated by theory

To further corroborate the spectral assignments inferred from experimental observations, UV-Visible spectra of candidate Cu structures were simulated using time-dependent density functional theory (TD-DFT), and to generate populations of Cu structures that are accessible for each Cu site type using *ab initio* molecular dynamics (AIMD) simulations. Computational models of Z_2Cu and ZCuOH sites in CHA were developed to predict the UV-Visible spectral features for each site type, and to compare with experimentally observed spectra. An important finding is that spectra for site models corresponding to static, minimum energy structures predict spectral features that do not reproduce experiment. Finite-temperature Cu ion dynamics lead to adoption of a distribution of Cu structures of different coordination and geometry, as evidenced from AIMD simulations even at ambient temperatures (300 K). Computed spectra for different initial configurations, when averaged over structures sampled during finite-temperature AIMD simulations (e.g., different ZCuOH rotational conformers in the 8-MR), are able to reproduce experimentally measured spectra (Fig. 2). The requirement to account for finite-temperature Cu site restructuring dynamics when predicting spectral features has wide-ranging implications in the scientific community for site assignments predicted by theory, as considerations only of static minimum-energy structures are insufficient to reproduce the complexity underlying experimentally-measured spectra.

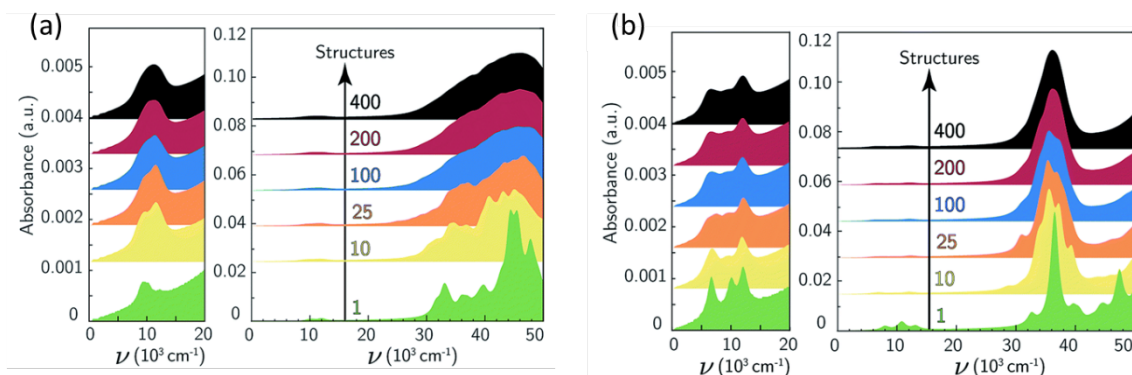


Figure 2. UV-Vis spectra simulated for (a) Z_2Cu and (b) ZCuOH sites in CHA, using structures from an *ab initio* molecular dynamics simulation (300 K), averaged over increasing numbers of equally spaced snapshots (1-400) during the AIMD simulation.

Publications Acknowledging this Grant in 2015-2018

Please classify your publications into three categories according to the source of support for the work published:

(XXXI) Exclusively funded by this grant

(XXXII) Jointly funded by this grant and other grants with leading intellectual contribution from this grant

5. Li, H.; Paolucci, C.; Khurana, I.; Wilcox, L. N.; Göttl, F.; Albarracin-Caballero, J. D.; Shih, A. J.; Ribeiro, F. H.; Gounder, R.*; Schneider, W. F.*. Consequences of Exchange-Site Heterogeneity and Dynamics on the UV-Visible Spectrum of Cu-Exchanged SSZ-13. *Chemical Science* **2019**, *10*, 2373-2384.

(XXXIII) Jointly funded by this grant and other grants with relatively minor intellectual contribution from this grant

Jeffrey P. Greeley

Electrocatalysis at Liquid-Solid Interfaces: Principles and Reactivity-Stability Trends

Siddharth Deshpande¹, Zhenhua Zeng¹, Ankita Morankar¹, Joseph Kubal¹, Jeffrey Greeley¹

Davidson School of Chemical Engineering, Purdue University, West Lafayette, IN 47907¹

Abstract

Fundamental principles of electrocatalysis and electrocatalytic reaction mechanisms at electrified solid/liquid interfaces are explored using periodic Density Functional Theory methodologies. This continuing effort seeks to identify and exploit efficient methods to elucidate complex electrocatalytic reaction mechanisms under realistic *in-situ* conditions, estimate the statistical thermodynamics and kinetics of charge transfer at interfaces, generate pH/potential-dependent phase diagrams of multifunctional interfaces in aqueous environments, and investigate new approaches for applying these fundamental insights to enhance the properties of electrocatalysts for energy-relevant chemistries. In the past project year, work has focused on development of enhanced structural models of layered double hydroxide catalysts under *in-situ* electrochemical conditions, development of freestanding, quasi-two dimensional metal nanosheets for catalysis of the oxygen reduction reaction, and analysis of solvent entropies in confined nanocatalytic environments.

DE-SC-0010379: Electrocatalysis at Liquid-Solid Interfaces: Principles and Reactivity-Stability Trends

Postdoc(s): Zhenhua Zeng

Student(s): Ankita Morankar, Joseph Kubal, Siddharth Deshpande

RECENT PROGRESS

In this update, we describe work in two primary topic areas related to thermodynamic and mechanistic analyses of electrochemical phenomena (we have also been investigating two other project, as well as several side projects that are maturing into longer-term research directions, but those are not described here).

Structural properties of layered double hydroxide oxygen evolution electrocatalysts

The first topic area focuses on prediction of electrocatalyst structure under *in-situ* reaction conditions, combined with first principles estimation of reactivity of these materials. We have considered, in particular, the Oxygen Evolution Reaction (OER), which is an electrochemical process wherein water is activated to produce hydrogen and oxygen. While catalysts in acidic environments are typically composed of costly ruthenium and iridium oxides, catalysts in alkaline environments, which are of increasing practical interest due to advances in alkaline

exchange membrane technology, may be composed of inexpensive metals such as perovskites and Ni-, Co-, or Fe-containing layered double hydroxides (LDH's). Numerous investigations of LDH-based OER catalysts have been carried out over the past several years, and exciting properties have been reported. Nevertheless, advances have been hindered by the lack of a clearly identifiable electronic descriptor for this chemistry and by the lack of understanding of the molecular-scale structure of the LDH's under high potential, *in-situ* reaction conditions.

We have made advances in determining the *in-situ* structure of layered NiFe- and CoFe-based layered double hydroxides, which are among the more promising such materials identified to date. The work, performed in collaboration with the group of Peter Strasser at the Technical University of Berlin, has combined periodic DFT analysis of the thermodynamic stability of the LDH structures with *in-situ* electrochemical characterization and WAXS measurements to determine that, at voltages relevant to the OER, the LDH structures transform from the *ex-situ* α -phase to a deprotonated γ -phase. The in-plane lattice constant and the interlayer distance are both reduced by 5-10% during this transformation. The computational analysis traces the origin of this transformation to a combination of cation oxidation and an exchange of anions and cations in the interlayer regions of the LDH; the latter mechanism has not, to our knowledge, been previously reported in the literature.

Building upon the accurate bulk structure that is determined, as described above, a descriptor-based reactivity model of the OER on layered double hydroxides is established (Figure 2). This analysis points to the central role of hydroxyl (OH) ligands that form bridges between Fe and Ni/Co sites in forming O₂. This insight, which modifies previous work that focused on hydroxyl adsorption on iron or Ni/Co only, is used to estimate reactivity trends for a series of heterocation/Fe pairs and reveals a possible tuning knob for future enhancements in OER catalyst performance.

Water structure around catalytic active sites in reduced dimensional environments

The second project bridges themes in electrocatalysis and heterogeneous catalysis by considering the structure of water in reduced dimensional environments. A central theme of electrocatalysis is the impact of water on surface chemical reactions and on the structure of the electrochemical double layer. The structure of the aqueous solvent often differs dramatically from that of bulk water due to the combined effects of confined geometries near surfaces and disruption of the water structure from solvated cations and adsorbed surface species. Over approximately the past 1.5 years, we have developed a strategy, based on the use of ab-initio molecular dynamics simulations, to estimate the entropy of water in such condensed phases by calculating the vibrational density of states of the water and decomposing this density into ideal gas, rotational, and vibrational contributions. The approach predicts the absolute entropy of bulk liquid water to within ~5%, and when combined with average potential energies from the AIMD runs, can be used to compute Helmholtz free energies of water in different condensed geometries and at different densities. We have recently completed application of this approach to the study of water in a well-known zeolite class, called Beta, that is used for a variety of industrially-relevant energy conversion processes. This analysis, whose results are summarized below, is a first step towards the application of similar techniques to the even richer environment of charged double layers near solid surfaces.

The study has considered a variety of point defects, which are often present in practical zeolitic materials, in the zeolite pore walls and has assessed the thermodynamically stable phases and structures of water near these defects. The structure of the various defects is sketched in Figure 3, and the computed Helmholtz free energies, referenced to the chemical potential of bulk water, are shown as a function of the average water density in Figure 4. The minima in the curves can be interpreted as stable phases at significantly different water densities. The hydrophobic defect-free zeolite is seen to have only a single phase, corresponding to quasi-linear strings of water molecules that avoid contact with the SiO₂ pore walls, while the other structures can exhibit either low density or high density phases that differ considerably in local detail. The figure gives a snapshot of these phases. The structures with lower average density are seen to consist of localized clusters of water molecules surrounding the defects, with sparser regions of water in other areas of the zeolite network.

The phases with higher average water densities correspond to more complete pore filling, and depending upon the local structure of the defect, the higher density water clusters may or may not persist at the higher average densities. We are beginning to explore the impact of these differing local water structures on catalytic events that occur near the defects, and we are additionally starting to adapt these techniques to calculation of the entropy of local water structures in electrocatalytic double layers near smooth and nanoparticle metal surfaces.

Future plans

In addition to continuing the work on the efforts described above, we are extending and applying the strategies developed in the past year to more efficiently quantify the effect of solvation on the thermodynamics and kinetics of complex elementary electrochemical reactions. We are extending the entropy estimation schemes described earlier to treat the thermodynamics of explicit electrochemical double layers, including the stabilization of reaction intermediates by hydrogen bonding with the solvent and entropy loss due to disruption of solvent-solvent hydrogen bonds. We are further evaluating strategies to extend these analyses to the kinetics of elementary surface reactions that involve both chemical bond activation and charge transfer. We are evaluating the efficacy of metadynamics and blue moon-based strategies to rigorously examine how solvent restructuring can impact free energies of activation for elementary reactions, and we are beginning at collaboration with Sapna Sarupria at Clemson to apply her hyperplane crossing methods to simple reactions at solvated interfaces. These and related methods are now being applied to the study of a complex, yet technologically exciting, electrocatalytic system, ethanol electrooxidation on Pt and Pt alloy single crystal surfaces with varying numbers of defects and other structurally undercoordinated features. We believe that the combination of these strategies, combined with

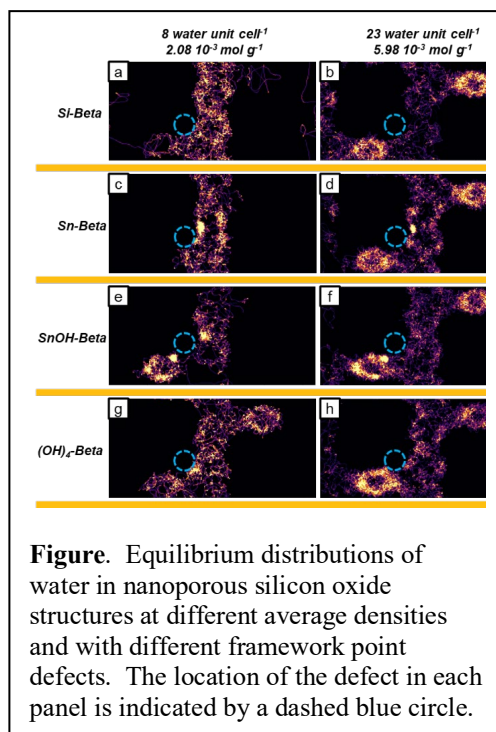


Figure. Equilibrium distributions of water in nanoporous silicon oxide structures at different average densities and with different framework point defects. The location of the defect in each panel is indicated by a dashed blue circle.

rigorous microkinetic modeling of the extended reaction mechanism, will enable a description of the ethanol electrooxidation process with unparalleled accuracy. It is anticipated that these techniques, as they mature, will find application to other elementary electrocatalytic processes, such as electrochemical oxygen evolution, that will be further explored later in the project year.

Up to Ten Publications Acknowledging these Grants in the last 3-4 years

1. “Tunable intrinsic strain in two-dimensional transition metal electrocatalysts,” L. Wang, Z. Zeng, W. Gao, T. Maxson, D. Raciti, M. Giroux, X. Pan, C. Wang, and J. Greeley, *Science* **363** (2019) 870-874.
2. “Ultralow-loading platinum-cobalt fuel cell catalysts derived from imidazolate frameworks,” L. Chong, J. Wen, J. Kubal, F. Sen, J. Zou, J. Greeley, M. Chan, H. Barkholtz, W. Ding, D. Liu, *Science* **362** (2018) 1276.
3. “In-situ surface stress measurement and computational analysis examining the oxygen reduction reaction on Pt and Pd,” Y. Ha, J. Oberst, Z. Zeng, T. Hoang, Y. Cohen, D. Wetzel, R. Nuzzo, J. Greeley, and A. Gewirth, *Electrochimica Acta* **260** (2018) 400.
4. “Stabilization of Ultrathin (Hydroxy)oxide Films on Transition Metal Substrates for Electrochemical Energy Conversion,” Z. Zeng, K. Chang, J. Kubal, N. Markovic, and J. Greeley, *Nature Energy* **2** (2017) 17070.
5. “Atomistic Insights into Nitrogen Cycle Electrochemistry: A Combined DFT and Kinetic Monte Carlo Analysis of NO Electrochemical Reduction on Pt(100),” H. Chun, V. Apaja, A. Clayborne, K. Honkala, and J. Greeley, *ACS Catalysis* **7** (2017) 3869.
6. “Platinum-nickel hydroxide nanocomposites for electrocatalytic reduction of water,” L. Wang, Y. Zhu, Z. Zeng, C. Lin, M. Giroux, L. Jiang, Y. Han, J. Greeley, C. Wang, and J. Jin, *Nano Energy* **31** (2017) 456-461.
7. “Characterization of oxygenated species at water/Pt(111) interfaces from DFT energetics and XPS simulations,” Z. Zeng and J. Greeley, *Nano Energy* **29** (2016) 369-377.
8. “Theoretical Heterogeneous Catalysis: Scaling Relationships and Computational Catalyst Design,” J. Greeley, *Annual Review of Chemical and Biomolecular Engineering* **7** (2016) 605-635.
9. “Towards First Principles-Based Prediction of Highly Accurate Electrochemical Pourbaix Diagrams.” Z. Zeng, M. Chan, Z. Zhou, J. Kubal, D. Fan, and J. Greeley, *J. Phys. Chem. C* **119** (2015) 18177-18187.
10. “Elucidation of Pathways for NO Reduction on Pt(111) From First Principles.” A. Clayborne, H. Chun, R. Rankin, and J. Greeley, *Ang. Chem. Int. Ed.* **54** (2015) 8255-8258.

Oliver Y. Gutierrez-Tinoco

From Single Atoms to Clusters: Controlling CO₂ Reduction through Molecular Affinity on Rh Catalysts

Oliver Y. Gutierrez, Janos Szanyi, Libor Kovarik, John Fulton, Johannes A. Lercher
Pacific Northwest National Laboratory

Presentation Abstract

Interest in single metal atoms stabilized by oxides is growing because these materials exhibit unique catalytic behavior with high metal atom efficiencies. Using hydrogenation of CO₂ as a research theme, we investigated the effects of environment and nuclearity of Rh on the rates of CO₂ conversion to CO and methane. A series of Rh catalysts were prepared in which the Rh loading was varied systematically from 0.05 to 0.5 wt. % on Fe₃O₄ and SiO₂. X-ray Adsorption Spectroscopy and Transmission Electron Microscopy showed that these catalysts contained sites ranging from single Rh atoms stabilized on Fe₃O₄ at low loadings via Rh-O-Fe linkages to Rh clusters on SiO₂ and Fe₃O₄ at high loadings.

We observed that the single Rh atom sites had one- to two-orders of magnitude higher catalytic activity for reduction of CO₂ than the corresponding Rh clusters. The ability of Rh sites to transfer H to adsorbed CO₂ or CO decreased as their metallic character declined. However, the ionic environment of the Rh-O-Fe sites caused them to have a strong affinity for CO₂ (determined from chemisorption isotherms), which enhanced the coverages of active species and overall reduction rates. Thus, we showed that the Rh-O-Fe sites are key to achieving such extraordinary increases in rate as well as high selectivity for transformation to CO.

Recent results obtained for analogous catalysts using Pt-group metals show that this strong affinity is a general feature of M-O-Fe sites. Based on this understanding, we are exploring new kinds of catalysts with precisely tuned concentrations of different types of active sites, which enables a high degree of control over reaction pathways.

FWP Number 47319: Transdisciplinary Approaches to Realize Novel Catalytic Pathways to Energy Carriers

PI: Johannes Lercher

Postdoc: Yifeng Zhu

N₂O Elimination from *cis*-Pt(PPh₃)₂(κ²-N₂O₂) and *trans*-Ph₃Sn-ONNO-SnPh₃

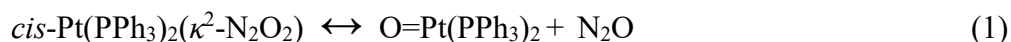
Jack V. Davis¹, Mohan M. Gamage¹, Musa Ahmadi¹, Leonardo Farias Serafim¹, Jake Sirlin¹,
Manuel Temprado², Burjor Captain¹, Carl D. Hoff¹.
University of Miami, Coral Gables, Florida¹, University of Alcala, Madrid, Spain².

Presentation Abstract

The long range goal of this project is to develop catalysts for oxidation of nitrous oxide to nitrate. A key first step in potential catalytic mechanisms may involve initial binding of N₂O at a metal oxo or a metal oxide complex to form bound hyponitrite complexes. The second step will involve further oxidation of these complexes to nitrite and then nitrate. This report focuses on detailed investigation of the reverse of N₂O binding, namely elimination of N₂O from *cis*-Pt(PPh₃)₂(κ²-N₂O₂) and *trans*-Ph₃Sn-ONNO-SnPh₃. From microscopic reversibility this yields insight into potential binding mechanisms. Reactivity of a mononuclear transition metal complex of Pt with *cis*-N₂O₂ binding will be compared to that of a bridging dinuclear main group Sn complex with a *trans*-N₂O₂ geometry.

DE-SC0019456: Catalytic Oxidation of Waste NxOy to Nitrate in Molten Salt and Fluorous Biphasic Solvents.**RECENT PROGRESS**

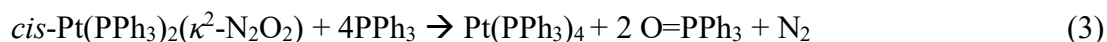
Investigation of Pt(PPh₃)₄ reaction with •NO. The reaction of Pt(PPh₃)₄ with •NO has been shown to lead to formation of the hyponitrite complex *cis*-Pt(PPh₃)₂(κ²-N₂O₂). In spite of the fact that this is one of the first transition metal hyponitrite complexes structurally characterized it is one of only a handful of hyponitrite complexes that can be prepared directly from •NO. There are conflicting reports in the literature regarding experimental yields of product and the mechanism of its formation is puzzling since •NO typically binds through N to a metal. Computational analysis of potential mechanisms of this reaction will be presented. Initially, irreproducible results were obtained until it was discovered that the •NO gas stream we were using contained N₂O in the tank itself. FTIR studies of the purified gas stream showed less than 1 ppm of •NO₂ and CO₂ but nearly 10 percent N₂O. This is presumably due to the known decomposition 3 •NO → N₂O + •NO₂. Under most situations N₂O would not be considered a contaminant and in fact it might be expected to stabilize *cis*-Pt(PPh₃)₂(κ²-N₂O₂) whose decomposition might occur via reaction (1):



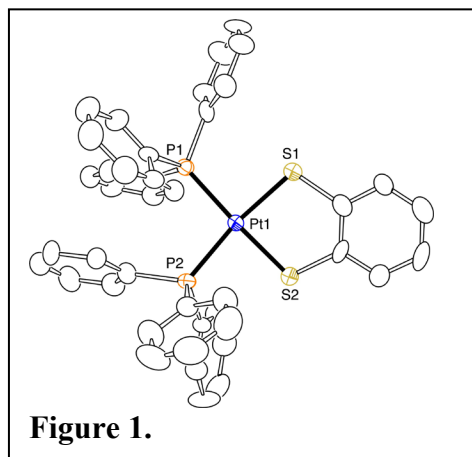
The presence of N₂O would be expected to suppress formation of the oxo complex. However, it was observed that the presence of N₂O in the gas stream did not lead to stabilization of the hyponitrite complex but to its decomposition and formation of a potent oxidant. Workup of the platinum containing products with CH₂Cl₂ leads to isolation of a nearly equimolar mixture of *cis*-Pt(PPh₃)₂(κ²-CO₃) and *cis*-Pt(PPh₃)₂Cl₂. This unusual reactivity is not observed when only •NO is present in the gas stream. The reaction of Pt(PPh₃)₄ with N₂O was investigated and found to be slow compared to the rapid reactions that occurs when Pt(PPh₃)₄ is exposed to an •NO/N₂O

mixture. Kinetic and mechanistic as well as computational results will be presented aimed at understanding how N₂O participates in this reaction sequence and whether or not that can be utilized to advantage.

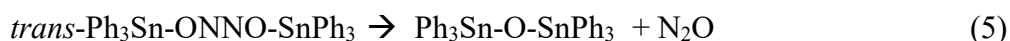
Investigation of reactions of *cis*-Pt(PPh₃)₂(κ²-N₂O₂). Reaction of *cis*-Pt(PPh₃)₂(κ²-N₂O₂) with carbon dioxide, triphenyl phosphine, and 1,2 C₆H₄(SH)₂ have been studied as shown in eqns. (2)-(4):



The reaction most suitable for calorimetric study is reaction (4) since it is rapid and finished in the time of mixing of the reagents. The reaction is clean and quantitative and should be suitable for comparative studies. The same quantitative reaction occurs with *cis*-Pt(PPh₃)₂(κ²-CO₃). This presents a better path to compare the thermochemical stability of carbonates to hyponitrites. The crystal structure of *cis*-Pt(PPh₃)₂(κ²-S₂-C₆H₄) is shown in Figure 1:



Investigation of *trans*-Ph₃Sn-ONNO-SnPh₃ and related complexes. The complex *trans*-Ph₃Sn-ONNO-SnPh₃ is one of only a few main group metal complexes of a hyponitrite that has been structurally characterized. It was decided to probe the reactivity of this species and compare it to reactions of *cis*-Pt(PPh₃)₂(κ²-N₂O₂). This could provide a basis for investigation of bimetallic Pt/Sn or other main group metal/transition metal systems in the future. Initial studies by both NMR and IR showed smooth extrusion of N₂O as shown in eqn. (5)



Reaction (5) occurs over a period of days at 20 °C in C₆D₆ solution and its rate has also been studied by both IR and NMR (in sealed tubes) in the range 20-80 °C. The reaction is first order in complex and unaffected by the presence of excess N₂O. Kinetic and spectroscopic data are shown in Figure 2 (left). Preliminary studies show that replacement of the phenyl group in *trans*-Ph₃Sn-ONNO-SnPh₃ with the bulkier 1,3,5 trimethyl benzene (mesityl) group results in a slower rate of N₂O loss from the hyponitrite. Synthesis of the bulkier complex *trans*-Cy₃Sn-ONNO-SnCy₃ (Cy = cyclohexyl) has been completed. Its crystal structure is shown in Figure 2 (right).

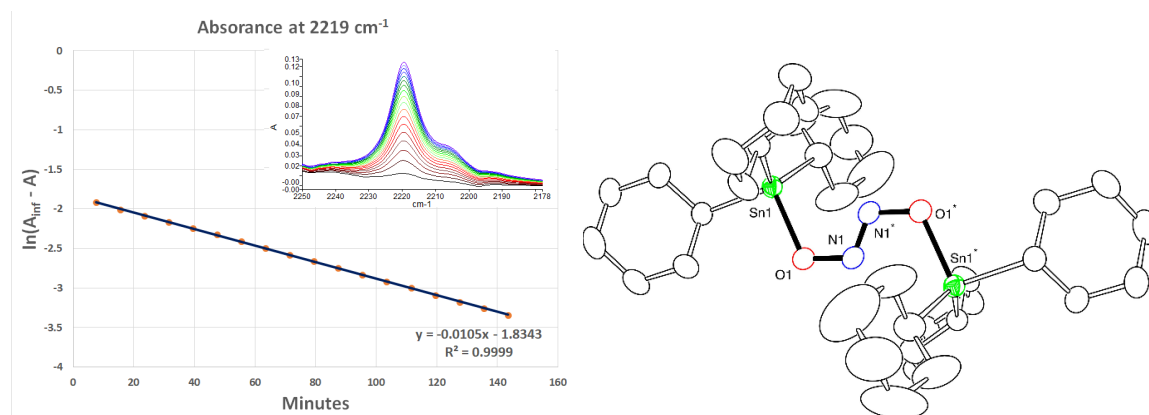


Figure 2. First order kinetic plot for extrusion of N_2O from *trans*- $\text{Ph}_3\text{Sn-ONNO-SnPh}_3$ at 60°C in C_6D_6 , inset shows growth in band at 2219 cm^{-1} due to N_2O (left); An ORTEP diagram for the molecular structure of *trans*- $\text{Cy}_3\text{Sn-ONNO-SnCy}_3$ (right).

It is important to point out that while this complex is not stable due to the relatively strong Sn-O-Sn bonded system, weaker complexes, such as Pt-O-Pt are expected to be favorable thermodynamically. Insight into the binding mechanism can be gained by study of the release mechanism by application of the principle of microscopic reversibility. The reaction is not influenced by the presence of added N_2O , CO_2 , or PPh_3 and in C_6D_6 it does not appear to be influenced by added water or oxygen. Studies by ^{119}Sn NMR do not reveal any intermediates or side products. The experimentally measured enthalpy of activation of 25 ± 2 kcal/mol is in keeping with the mechanism computed by DFT by Manuel Temprado for a truncated model and is shown in Figure 3.

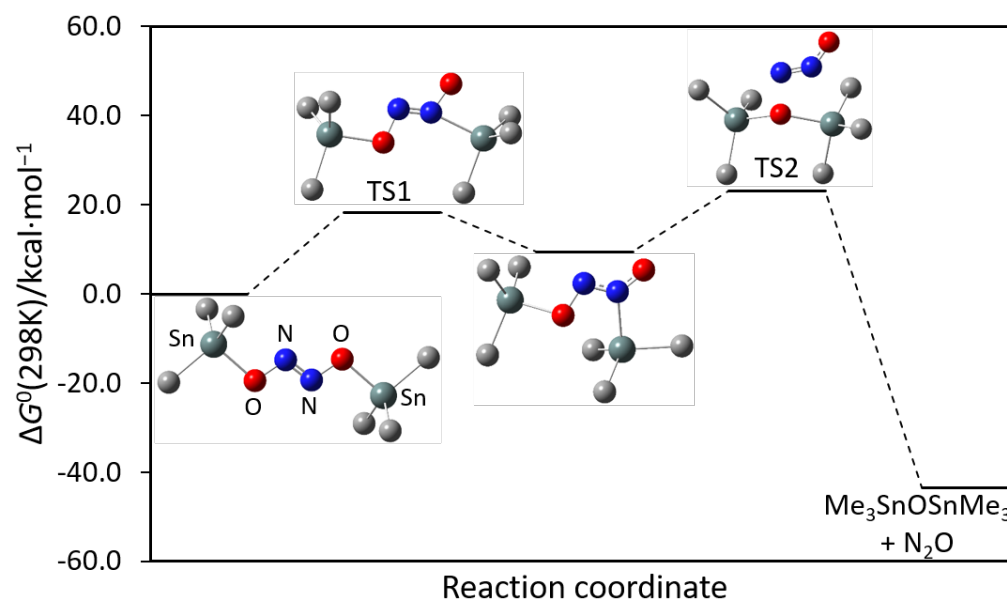


Figure 3. DFT-Computed energies (kcal/mol) for *trans*- $\text{Me}_3\text{SnONNOSnMe}_3 \rightarrow \text{Me}_3\text{SnOSnMe}_3 + \text{N}_2\text{O}$

The discovery of TS2 (see Figure 3) was a surprise to the investigators since it was anticipated that this reaction should proceed via initial isomerization of *trans*-Me₃Sn-ONNO-SnMe₃ to *cis*-Me₃Sn-ONNO-SnMe₃. The energy of that pathway was computed in Miami, but the value of collaboration was proven when the Alcala group discovered a lower energy pathway involving migration of the Me₃Sn group from terminal O to the adjacent N. This could have important consequences in attempts to design two site binding for addition rather than elimination of N₂O at the L_nM-O-ML_n bond. Thermochemical studies are in progress to compare reaction energetics for alkali metals, main group metals, early transition metals, late transition metals, and lanthanides. These early studies are preparing the ground for that work.

Investigation of the role of solvent, radicals, hydrides, and water on loss of N₂O from *trans*-Ph₃Sn-ONNO-SnPh₃. The direct loss of N₂O from *trans*-Ph₃Sn-ONNO-SnPh₃ only occurs rapidly at about 80 °C and even there has a half-life of about twenty minutes. This is inconvenient for direct calorimetric measurement. Differential scanning calorimetry will be done on this reaction but in the authors view solution calorimetric measurements are more reliable. Acceleration of this reaction was investigated and has led to a number of interesting results. It is important to study this model system since it may transfer knowledge and insight to the molten salt system. Radical attack and protonation are the two key accelerants. Reaction of the radical •Cr(CO)₃C₅Me₅ with *trans*-Ph₃Sn-ONNO-SnPh₃ was studied in excess and catalytic amounts. In small amounts it catalyzes N₂O loss. In stoichiometric amounts it yields a range of interesting products. The catalytic reaction is believed to proceed by generation of the stannoxyl radical •OSnPh₃ in a thermodynamically uphill initiation. This radical is trapped by excess metal radical but can react with *trans*-Ph₃Sn-ONNO-SnPh₃ to form Ph₃Sn-O-SnPh₃ and •ONNOSnPh₃ which losses N₂O to regenerate •OSnPh₃. Reaction of the hydride H-Cr(CO)₃C₅Me₅ with the tin hyponitrite has also been studied. It is complete by the time of taking the first scan (about 2 minutes) in dichloromethane that is not rigorously dry. In rigorously dry dichloromethane studies in the presence of activated molecular sieves to trap water it occurs smoothly over a half hour period. These results are interesting. They provide a basis for trying to understand and deal with factors which may be critical in catalyst design.

Publications Acknowledging this Grant in 2019-none to date.

Harold H. Kung

Catalysis by Au: Au-TiO₂ Interfacial Sites in Oxidation Catalysis and Selective Ethylbenzene Oxidation by Coupling with Au-catalyzed Cyclooctene Epoxidation

Harold H. Kung

Chemical and Biological Engineering, Northwestern University, Evanston, IL

Presentation Abstract

Efforts have focused on understanding Au-TiO₂ interfacial perimeter sites for selective oxidation and exploring and understanding the newly discovered phenomenon of Au-initiated coupled free radical reactions, which has the net effect of extending the catalytic effect of Au.

1. Characterization of Interfacial Perimeter Active Sites in TiO₂/AuNP Inverse Catalysts

Previously we have shown that the inverse catalyst system of TiO₂ cluster-decorated Au nanoparticles (NPs) are more active in selective oxidation of propane to acetone and decomposition of 2-propanol to acetone than Au or TiO₂, and the enhanced activity can be correlated to the Au-TiO_x interface. We also showed that such interfaces can be generated from several TiO₂ precursors. This period's efforts focused on structural characterization.

Surface Enhanced Raman Scattering (SERS) indicated that the TiO_x clusters that generate selective oxidation sites are distinct from crystalline rutile, anatase, or brookite. These TiO₂ clusters show a broad peak around 700 cm⁻¹ assigned to Ti-O-Ti vibrations, and whose peak position is sensitive to adsorbed species. Heating the sample in vacuum shifted the peak to 668 cm⁻¹. XANES showed an average Ti coordination in these TiO_x clusters of approximately five. UV-vis data also showed the TiO_x cluster absorption peak to be between that of TS-1 and anatase. Our current interpretation is that the TiO_x clusters are amorphous TiO₂ patches in which a mixture of 4-, 5-, and 6-coordinated Ti is present. 4-coordinated Ti is confirmed by acetone formation in the temperature programmed reaction of acetic acid. We believe that these 4-coordinated Ti at interfacial sites distinguish these samples from anatase-supported Au catalysts.

2. Enabling Selective Ethylbenzene Oxidation with Au-catalyzed Cyclooctene Epoxidation

When alone, ethylbenzene oxidation does not proceed in the presence of solubilized Au nanoclusters, but it occurs readily when Au nanoclusters and cyclooctene are present simultaneously. Control experiments showed: 1) Ethylbenzene oxidation can be initiated with free radical initiators, but it proceeds an order of magnitude slower than in the Au-cyclooctene system. 2) In the absence of Au nanoclusters, the reaction is suppressed by adding triphenylphosphine, but triphenylphosphine has minimal effect on the reaction if Au and cyclooctene are present. 3) Free radicals are detected using spin traps. From these and other results, a mechanistic description of the system was formulated in which Au initiates the reaction by catalyzing the formation of cyclooctenyl peroxy radicals. This radical is then responsible for initiating ethylbenzene oxidation. The net effect is that the catalytic effect of Au is extended to the ethylbenzene system. Such an "extended catalytic system" enables parallel reactions to proceed without constraints by stoichiometric relationships.

DE-FG02-03ER15457: Institute for Catalysis for Energy Processes (ICEP).

Tobin J. Marks

Surface Science Meets Homogeneous Catalysis. Surfaces as Unique Activators and Ligands

Tobin J. Marks

Department of Chemistry, Northwestern University, Evanston IL 60208 USA

Presentation Abstract

When chemisorbed upon certain surfaces, the reactivity of many types of earth-abundant organometallic molecules is dramatically enhanced in ways that historically have been poorly understood. Very high activities and selectivities for a variety of useful and instructive catalytic transformations are illustrative consequences of this altered reactivity. This presentation focuses on the intricate non-covalent and covalent multi-center interactions within and beyond the metal center active site that modulate these catalytic processes, focusing primarily on C-C bond formation, hydrogenation/dehydrogenation, and bond transposition processes. Specific interrelated topics include: 1) Understanding the marked differences in catalytic chemistry of mononuclear and multinuclear electrophilic d^0 catalysts electrostatically anchored on/activated to “weakly-coordinating” oxide surfaces versus those in homogeneous solution, 2) The definitive multi-dimensional solid state NMR, EXAFS, vibrational spectroscopic, and computational DFT structural characterization of these catalysts when adsorbed on “weakly-coordinating” oxide surfaces, and thereby elucidating the broad scope of their distinctive catalytic properties, including selective monomer polymerizations, oligomerizations, and arene hydrogenations, 3) The preparation, characterization by a battery of conventional and unique physical techniques, and the unusual transesterification, oxidative dehydrogenation, and reductive catalytic chemistry mediated by group 6 dioxo complexes adsorbed on activated carbon surfaces. It will be seen that the knowledge obtained from these studies opens the doors to design rules for next-generation surface as well as homogeneous catalysts, and for novel and useful polymerization and hydrogenation/dehydrogenation processes, including the catalytic detoxification of gasoline, stereoselective aromatics hydrogenation, biofeedstock trans-esterification, and bio-alcohol dehydrogenation.

DE-FG02-03ER15457: Institute for Catalysis for Energy Processes (ICEP)

Well-Defined Active-Site Environments on Silicate Supports

Alexander Katz,[#] Nicolás Grosso-Giordano,[#] Christian Schöttle,[#] Andrew Palermo,[#] Christian Schroeder,^{*} Alexander Okrut,[#] Andrew Solovyov,[#] Shengjie Zhang,[^] David Dixon,[^] Heinz Frei,[†] Bruce C. Gates,[%] Hubert Koller,^{*} Stacey I. Zones[‡]

[#]Department of Chemical and Biomolecular Engineering, University of California, Berkeley

^{*}Institut für Physikalische Chemie, Westfälische Wilhelms-Universität Münster, Germany

[^]Department of Chemistry, The University of Alabama, Tuscaloosa, Alabama

[†]Molecular Biophysics and Integrated Bioimaging Division, Lawrence Berkeley National Laboratory

[%]Department of Chemical Engineering, University of California at Davis

[‡]Chevron Energy Technology Company, Richmond, California

Presentation Abstract

We present a detailed evaluation of the environment present in MWW-type 2-dimensional zeolitic silicate supports. Simultaneously, we compare these zeotypes to traditional amorphous silica, demonstrating the advantages of the former as novel supports to design more efficient supported molecular catalysts. Silicates exhibit mildly acidic SiOH group on their surface, which dictate many of their functional properties. FTIR and ¹H NMR spectroscopies indicate four distinct environments are present for silanols on silicates, one of which is isolated, and three of which correspond to H-bound SiOH. By correlating FTIR vibrational frequencies, and ¹H NMR chemical shifts, and single quantum – double quantum ¹H dipolar correlation spectra, we demonstrate that one of these H-bound environments corresponds to silanols interacting with the siloxane backbone, while the other two correspond to mutually H-bound silanol pairs. These assignments resolve long-standing ambiguities about the speciation of silanols on silicates. We then demonstrate the role of silanols as condensation centers that control the environment onto which a macrocyclic calix[4]arene-Ti^{IV} complex (**cTi**) is grafted, on the external surface of a silicate zeotype. X-ray absorption and ¹³C{¹H} CP MAS NMR spectroscopies detect a different conformation of **cTi** when it is grafted at crystallographically equivalent locations adjacent to sub-nanometer surface cavities (7.1 Å in diameter). In a separate project, dealing with supported tetrairidium clusters (complexed with three calixarene-phosphine ligands on the basal plane – 2 in the equatorial position and the remaining one in the axial) on the surface silica, we use model compounds to understand the nature of dioxygen bonding as a ligand on the cluster frame. A combination of FTIR, XAS, and steady-state Raman spectroscopies demonstrates the permanent bonding of two dioxygen ligands on the supported tetrairidium cluster upon reaction with dioxygen under mild conditions. Electronic structure calculations predict (and experiments support) a change in mechanism of hydrogen transfer during ethylene hydrogenation as a result of the bound dioxygen ligands on the supported cluster.

DE-FG02-05ER15696: Control Of Supported Molecular Catalysts Using Metallocalixarene Active Sites

Postdoc(s): Alexander Okrut, Christian Schöttle

Student(s): Nicolás Grosso-Giordano, Andrew Palermo

Strategies for Enhancement of Catalytic Performance of Mo-based Catalysts in Methane Dehydroaromatization

Mustafizur Rahman¹, Apoorva Sridhar¹, Antonia Infantes-Molina², Alexey Boubnov³, Simon R. Bare³, Eli Stavitski⁴, Sheima J. Khatib¹

¹ Department of Chemical Engineering, Texas Tech University, Lubbock, TX

² Department of Inorganic Chemistry, Crystallography and Mineralogy. Faculty of Science. Campus de Teatinos, Malaga, Spain.

³ Stanford Synchrotron Radiation Lightsource, SLAC National Accelerator Laboratory, Menlo Park, CA

⁴ National Synchrotron Light Source II, Brookhaven National Laboratory, Upton, NY

Presentation Abstract

Finding new uses for methane as a fuel and chemical feedstock in the manufacturing industry is of increasing interest since CH₄ is the main constituent of natural gas, of which large reserves are being exploited. Non-oxidative methane aromatization reaction ($6 \text{CH}_4(\text{g}) \rightarrow \text{C}_6\text{H}_6(\text{g}) + 9\text{H}_2(\text{g})$) (MDA), falls within the group of direct processing reactions capable of converting CH₄ to value-added products in one step. Our group is carrying out systematic studies of this catalytic process with the goal to answer some fundamental questions to help mitigate the technological challenges of this process.

Zeolite-supported Mo catalysts have so far been the most widely studied catalysts in MDA, however, they do not fulfill the conversion and stability requirements for commercialization. It is agreed that Mo carbide species, originated by exposure of the Mo oxide species to the CH₄ reactant, are responsible for CH₄ activation, however, the nature and amount of carbide phases formed in this induction period of the reaction are not controlled. Our group has recently discovered the importance of the conditions at which the zeolite-supported Mo carbides are formed on the catalyst stability. We have tested different preparation conditions and contrasted the structure of the fresh and spent catalysts to explain the difference in catalytic behavior.

We have implemented the use of the optimum reduction and carburization conditions to synthesize supported Mo carbides ex situ, and found that modifying Mo/ZSM-5 catalysts with a second transition metal such as Co and Ni results in a synergistic effect rendering remarkably stable benzene yields over long periods of time in reaction.

Grant Number: Harnessing Metal-Carbon Interactions to Obtain Enhanced Yield in Aromatics and Improved Coking Resistance in Methane Aromatization

Student(s): Mustafizur Rahman, Apoorva Sridhar.

RECENT PROGRESS

Optimization of the *ex situ* formation of Mo carbide species in Mo/ZSM-5 catalysts

Traditionally, Mo/ZSM-5 catalysts employed in MDA are used in their oxide form as starting catalysts, and the active Mo carbide phases are formed in the reaction induction period. One of the specific objectives of our work has been to optimize the activation conditions that can render the most effective catalysts. In our previous work, we had demonstrated that reducing and carburizing the Mo oxide catalysts before reaction resulted in more stable catalysts and that this effect was especially evident at a high Mo loading of 10 wt%. This result was unexpected since usually catalysts containing such high Mo loadings have been reported to be highly unstable. Our findings point to the fact that the performance of the catalyst is not only governed by the Mo loading, but also by the conditions in which it is activated: reducing and carburizing the Mo oxide species at lower temperatures prevents their aggregation and consequent catalyst deactivation.

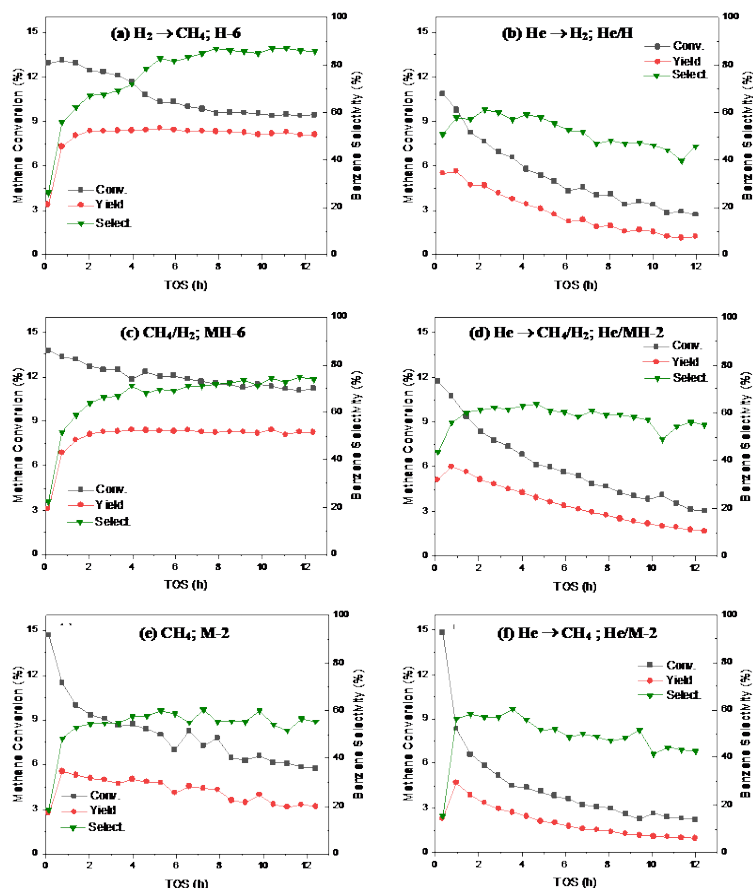


Figure 1. Evolution of the CH_4 conversion, benzene selectivity and benzene yield as a function of TOS (time on stream) for the $10MoO_x/HZSM-5$ catalysts after each type of reduction/carburization treatment.

the mechanism of formation of the carbide species by combining temperature programmed reduction and carburization (TPR&C) experiments with XRD characterization indicates that the

In the work presented here, we study the effect of different treatment conditions on a HZSM-5 supported MoO_x catalyst in order to optimize the formation of supported Mo carbide species *ex situ* for their application in MDA. The reduction/carburization conditions studied are: (1) heating the catalyst in a reducing gas, H_2 , up to reaction temperature and switching to CH_4 [$H_2 \rightarrow CH_4$]; (2) heating the catalyst in a reducing gas, H_2 , mixed with a small amount of CH_4 ; (3) heating the catalyst in CH_4 up to reaction temperature; and (4) heating the catalyst in an inert gas (commonly He) up to reaction temperature and then switching to CH_4 [$H_2 \rightarrow CH_4$]. **Figure 1** shows the benzene yield versus time on stream (TOS) for the different catalyst treatments: we find that heating the supported oxide slowly in either H_2 followed by CH_4 , or in a dilute mixture of CH_4/H_2 results in catalysts that are more stable in reaction compared to a MoO_x sample previously heated in He or CH_4 . Monitoring the

transformation of MoO_3 to more reduced species at lower temperature is linked to better catalytic performance. In the interest of space, the TPR&C and XRD results for only two types of treatment are shown in **Figures 2** and **3**. Heating the catalyst in He not only causes a drop in surface area before exposure to reaction conditions, but also results in a lower dispersion of Mo species compared to the H_2 or CH_4/H_2 treated samples, as observed by TEM imaging (**Figure 4**) and CO chemisorption. XPS analysis of fresh and spent catalysts indicates that the relative amount of Mo on the surface of the catalyst do not decrease with reaction in the case of the samples treated in $\text{H}_2 \rightarrow \text{CH}_4$, despite a large presence of carbon on the surface, suggesting an optimization in the carbon growth mechanics in supported Mo oxide samples treated in $\text{H}_2 \rightarrow \text{CH}_4$ before reaction. Modeling

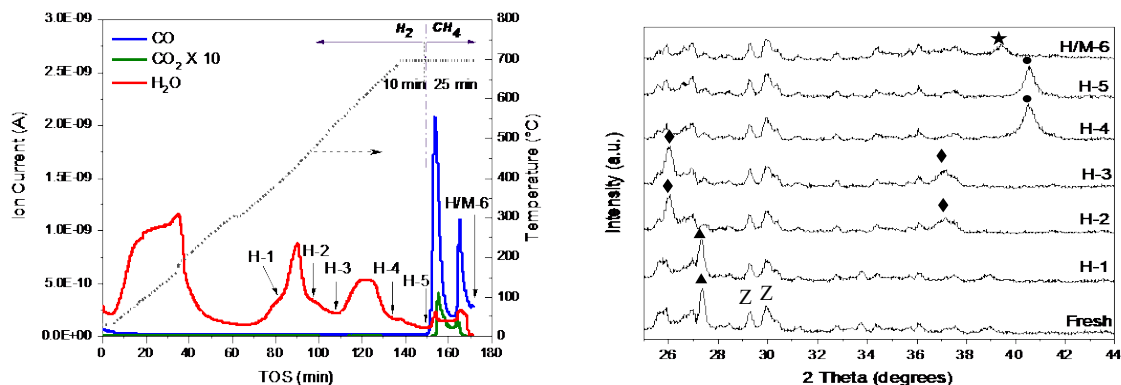


Figure 2 (left) TPR&C profile for treatment of $10\text{MoO}_x/\text{HZSM-5}$ in $\text{H}_2 \rightarrow \text{CH}_4$. Intermediate samples, recovered after each peak (arrows) are denoted H-1-H/M-6; (right) XRD patterns of $10\text{MoO}_x/\text{HZSM-5}$ before (denoted Fresh) and at the intermediate points of the TPR&C profile corresponding to $\text{H}_2 \rightarrow \text{CH}_4$ treatment. (▲) MoO_3 , (◆) MoO_2 , (●) Mo, (★) Mo_2C , (Z) ZSM-5. Observed evolution of bulk Mo species: $\text{MoO}_3 \rightarrow \text{MoO}_2 \rightarrow \text{Mo} \rightarrow \text{Mo}_2\text{C}$

with XAS data corroborates that while the nature of the Mo carbides present in the spent catalysts is the same for samples treated in He and in CH_4/H_2 , the Mo carbide particles in the latter are smaller. These results demonstrate that the major contributor to catalyst deactivation is the aggregation of MoO_3 species and that the catalyst stability can be enhanced dramatically by reducing the volatile and mobile MoO_3 species to their active form (Mo_2C) at lower temperature.

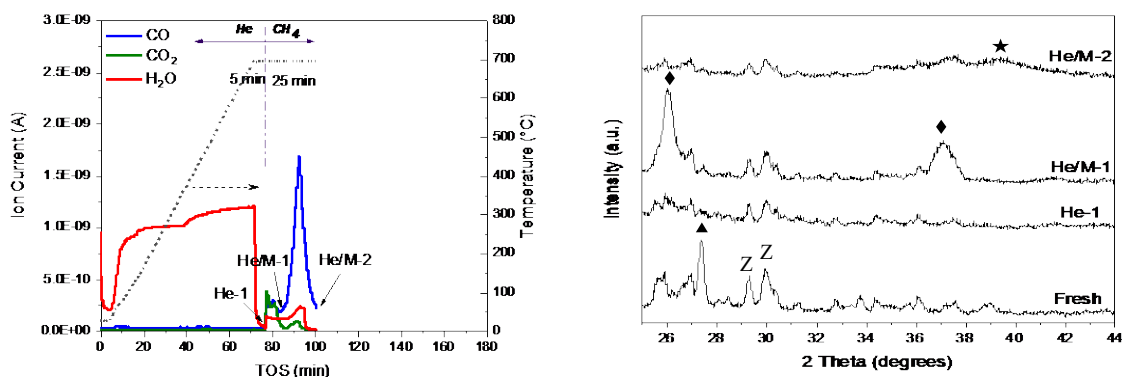


Figure 3 (left) TPR&C profile for treatment of 10MoO_x/HZSM-5 in He → CH₄. Intermediate points, taken right after each peak are denoted He-1 (before switching to CH₄), He/M-1 and He/M-2; (right) XRD patterns of 10MoO_x/HZSM-5 before (denoted Fresh) and at the intermediate points of the TPR&C profile corresponding to He → CH₄ treatment. (▲) MoO₃, (◆) MoO₂, (★) Mo₂C, (Z) ZSM-5. Observed evolution on Mo species: MoO₃ → MoO₂ → Mo₂C

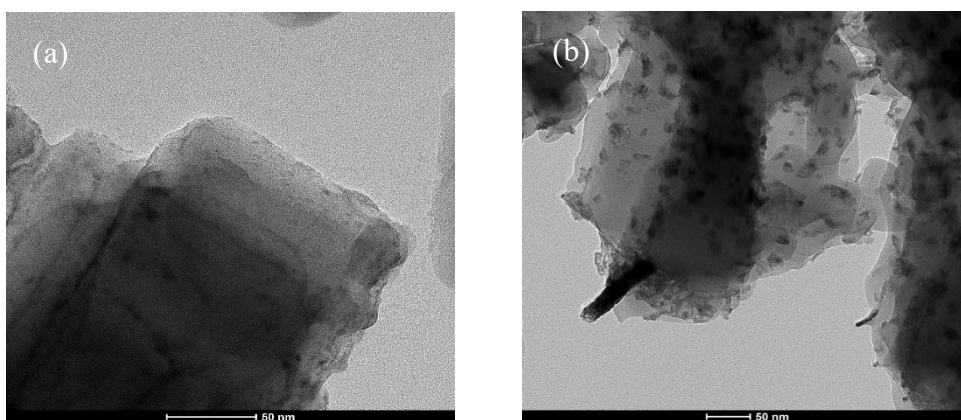


Figure 4. TEM images of (a) catalyst treated in H₂ → CH₄ (b) catalyst treated in He → CH₄

Ex situ formation of metal carbide species in bimetallic Mo-X/ZSM-5 (X=Co, Ni) catalysts

We have also studied bimetallic catalysts consisting of Mo-X (X = Co, Ni) with different metal loadings supported on ZSM-5. Various loadings of X were tested: 0.2, 0.6 and 1 wt% for a constant 6wt% loading of Mo. Single metal Mo and X catalysts were also prepared as references. Analysis of the activity of the catalysts shows that the effect of adding Co and Ni to Mo/ZSM-5 catalysts varies depending on the type of pretreatment received. When Mo carbides are formed *in situ*, during the reaction induction period (after He pretreatment) the presence of additives is detrimental to their catalytic activity and benzene yield (see blue points in **Figure 5**). However, when the catalysts are precarburized (pretreated in H₂+CH₄), a synergy between Mo and X is established for optimum loadings of both Co (0.6 wt%) and Ni (0.2 wt%) (red points in **Figure 5**), rendering catalysts that produce higher and more stable benzene yields. This behavior is due to the combination of various effects: 1) precarburization prevents migration of Mo species at high

temperature and pore blocking is reduced as indicated by surface area BET measurements and our previous work with single metal Mo catalysts; 2) thermogravimetric analysis of the fresh catalysts shows that the presence of additives further decreases the volatility and mobility of the Mo species, possibly enhancing the retention of the Mo species inside the zeolite channels and reducing catalyst deactivation; 3) structural characterization of the catalysts by XRD shows that when Mo and the additive species coexist, no crystalline mixed phases are observed, however TPR data pointed to a change in the electronic properties of Mo since its reducibility is modified in the presence of the both Co and Ni.

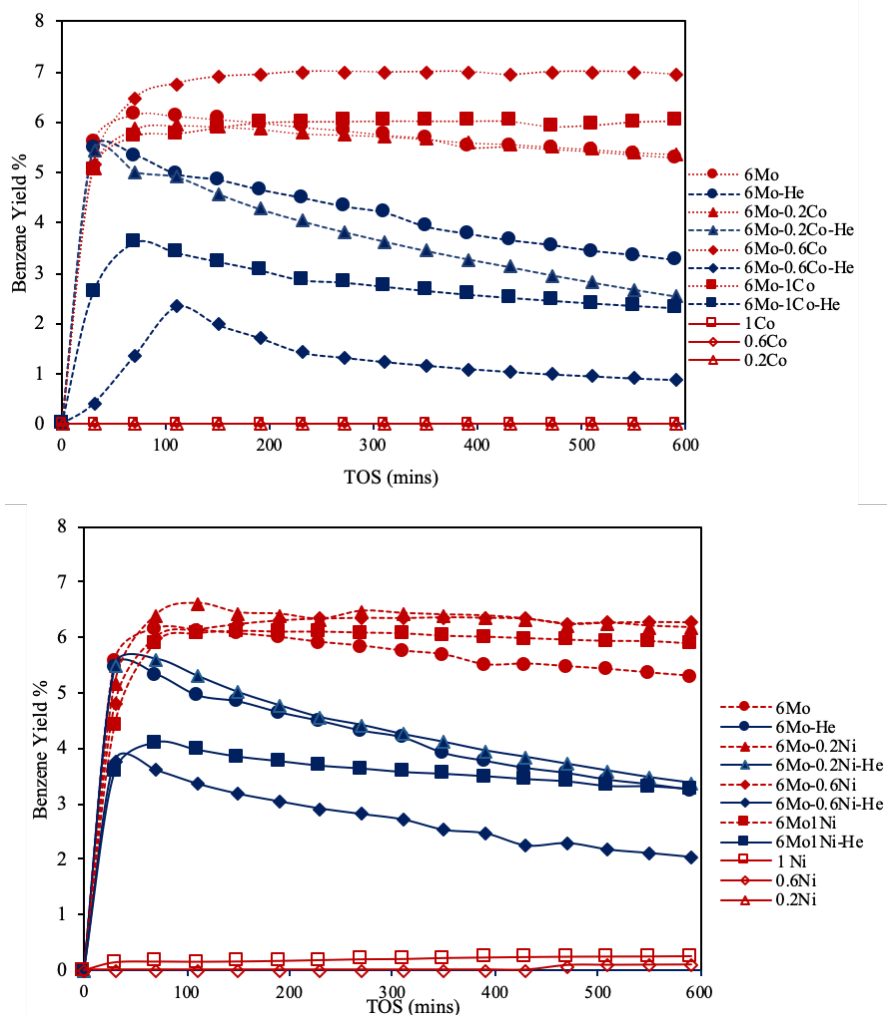


Figure 5. Benzene yield versus time on stream (TOS) for (a) Co-modified and (b) Ni-modified 6Mo/ZSM-5 catalysts. The shaded area corresponds to the induction period of the reaction. The blue symbols correspond to He-pretreated catalysts and red symbols correspond to precarburized catalysts. (The data points for unmodified 6Mo/ZSM-5, and single Co/ZSM-5 and Ni/ZSM-5 are included in both graphs to serve as reference for comparative purposes.)

Publications Acknowledging this Grant in 2015-2018

(XXXIV) *Exclusively funded by this grant;*

(XXXV) *Jointly funded by this grant and other grants with leading intellectual contribution from this grant;*

- 1) Rahman, M.; Infantes-Molina, A; Boubnov, A.; Bare, S. R.; Stavitski, E.; Sridhar, A.; Khatib, S. J. Increasing the Catalytic Stability by Optimizing the Formation of Zeolite-Supported Mo Carbide Species *ex situ* for Methane Dehydroaromatization. *J. Catal.* **2019**, 375, 314-328.
- 2) Sridhar, A.; Rahman, M.; Infantes-Molina, A; Khatib, S. J. Bimetallic Mo-Co/ZSM-5 and Mo-Ni/ZSM-5 Catalysts for Methane Dehydroaromatization: A Study of the Effect of Pretreatment and Metal Loadings on the Catalytic Behavior. *Applied Catal. A: Gen.* 2019 (*under review*).

(XXXVI) *Jointly funded by this grant and other grants with relatively minor intellectual contribution from this grant;*

Applications and advances in machine learned potentials

John Kitchin, Jenny Zhan, Mingjie Liu and Yilin Yang
Carnegie Mellon University, Department of Chemical Engineering

Presentation Abstract

Machine learned potentials (MLP) provide a powerful alternative to classical force fields for running simulations that are relevant to catalysis. The primary benefit over classical force fields is that one does not have to specify the physical form of the equations in advance; one simply needs to provide enough data to build the machine learned function that can predict new results between them. We have used this approach to model segregation in a ternary alloy (Cu-Pd-Au) surface by training a neural network potential to ~5000 DFT calculations of ternary alloy slabs. We could then run this potential hundreds of thousands of times to simulate segregation across ternary alloy space. The results were partially in agreement with experimental observations across the same space. The discrepancies have been attributed to DFT errors in the bonding between the alloy components. We have also developed a new approach to building machine learned potentials that addresses some limitations of the conventional approach. Finally, we have developed a simple approach to estimating uncertainty in machine learned potentials, which has implications in training them, as well as understanding when they are reliable.

Grant or FWP Number: DE-SC0018187

Student(s): Jenny Zhan, Mingjie Liu and Yilin Yang

RECENT PROGRESS

Modeling surface segregation of a ternary alloy

Modeling catalytic reactions on alloy surfaces is a challenge because segregation changes the surface composition compared to that of the bulk. If there are ordering tendencies the distribution of atoms in the surface will not be random. Modeling these effects accurately requires statistical sampling methods such as Monte Carlo simulations, and density functional theory is too expensive for this. Our approach is to use machine learned potentials for this purpose. We developed a neural network potential using the AMP code for Cu-Pd-Au using ~5000 DFT calculations as the source of the configurational energies. We then used the potential in a Monte Carlo simulation to estimate the surface composition across the ternary composition space. This approach was previously successful in quantitatively predicting the surface composition of a Au-Pd binary alloy.

The results of these simulations are shown in Figure 13. Overall, the tendency of Au to segregate to the surface was qualitatively correct, but slightly overestimated by the simulations. Interestingly, for Pd and Cu, the incorrect segregation tendency was predicted; we predict that Pd should segregate to the surface, but experimentally Cu segregation is observed. The root of this discrepancy appears to be in DFT; the formation energy of CuAu is too weak by DFT, PdAu is too strong, and the formation of CuPd is too negative. The result is that Pd prefers to be near Au,

which is enriched in the surface due to its size and lower surface energy. We are currently preparing these results for publication.

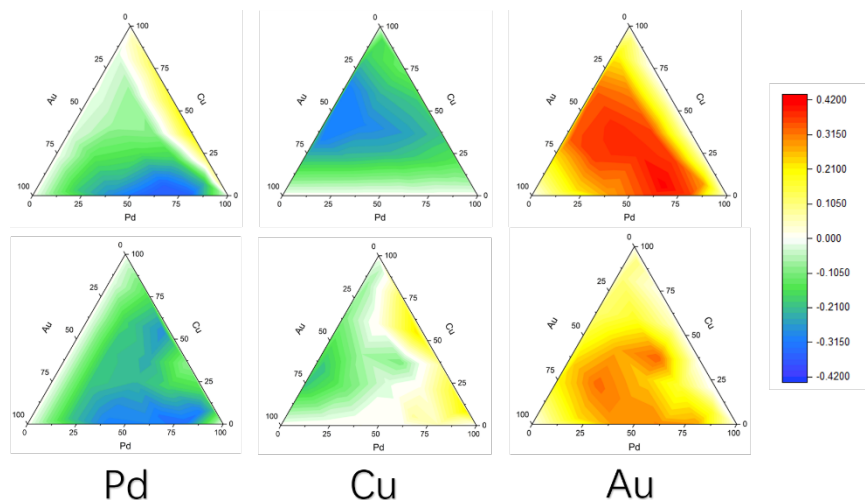


Figure 13. Comparison of simulated segregation surface compositions relative to the bulk composition (top) and experimental (bottom, courtesy of the Gellman group).

A multi-output neural network architecture for machine learned potentials

Machine learned potentials based on neural networks and the Behler-Parinello (BPNN) symmetry functions have been broadly used to simulate many materials. In this paradigm, the symmetry functions are used to create a feature vector that characterizes the local environment around each atom in terms of radial and angular distribution functions. A neural network is then used to provide a nonlinear mapping of the fingerprint vector to an atomic energy, where the sum of atomic energies provides the total energy of an atomic configuration. Derivatives of these neural networks provide forces, and stress for the configurations. The potentials are fitted using optimization methods that minimize the deviations between the predicted values and typically a database of corresponding density functional calculations. Although there are dozens of examples of success with this approach, there are some drawbacks that limit it as well.

The biggest drawbacks in the conventional BPNN implementation are that 1) the symmetry functions do not contain composition information directly, and 2) each element has its own neural network. The first limitation prevents transferability, essentially meaning each potential is only good for the conditions represented by the training data. The second limitation means the weights in each neural network are independent, and cannot leverage correlations between elements effectively. The first limitation is easily addressed by introducing weighting factors into the symmetry functions. The simplest weighting factor is to simply multiply each one by the atomic number of the species, but more sophisticated approaches that augment the fingerprint vector are also possible. This simple change makes the fingerprints more transferrable.

To address the second limitation, we have developed a new approach to implementing the BPNN, which uses a single neural network (SingleNN) with multiple outputs for the atomic energies, shown schematically in Figure 14. The hidden layers in this architecture compute an embedding vector that is finally linearly transformed in the output layer to provide an atomic energy for each species.

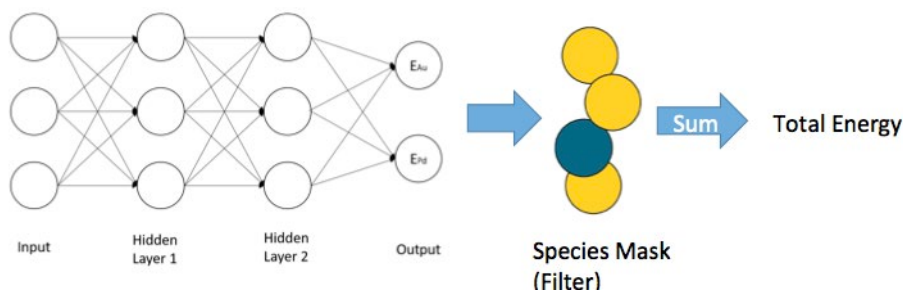


Figure 14. A schematic SingleNN for two elements - Au-Pd.

The combination of these two features enables an important new capability: transfer learning. We can train a BPNN on one system, freeze the hidden layer weights, and retrain only the output layer on a new data set. The hidden layers provide a nonlinear transformation of the fingerprint vector into a new vector that the atomic energies are linear in, making the subsequent training much easier. To illustrate this concept, we trained a SingleNN on a dataset of Zirconia containing bulk structures, defects, and molecular dynamic trajectories. Then, we froze the hidden layer weights, and retrained the potential on a data set of Au-Pd slabs. The results are shown in Figure 15 where good parity is observed for both energy and forces, *with only training of the output layer*.

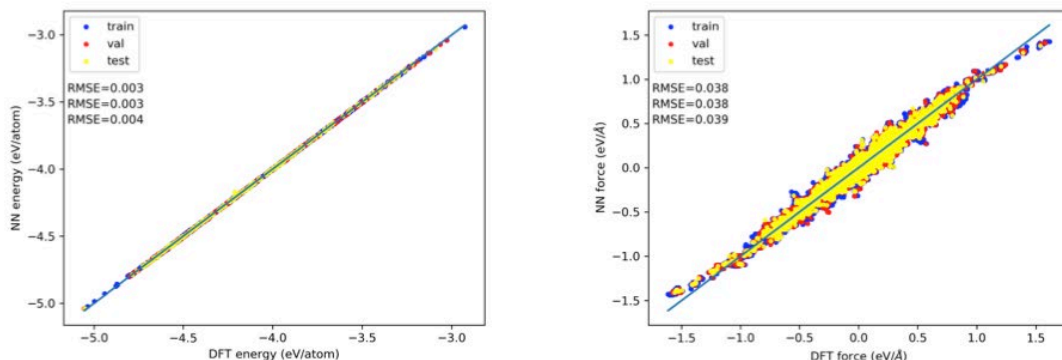


Figure 15. Demonstration of transfer learning from ZrO_2 to Au-Pd slabs. These are the parity plots of energy and forces for the Au-Pd data set.

Uncertainty quantification in machine learned potentials

One significant challenge with machine learned potentials (indeed any potential with many parameters) is estimating the uncertainty of predictions. It is not easy to tell when extrapolation is occurring in high-dimensional systems; in a machine learned potential it is common for the fingerprint vector to have 10-100 dimensions! Machine learned potentials seem mysterious, but they are just nonlinear models, and there are methods to estimate uncertainty for these. One method is called the delta-method. In essence, regression that minimizes the root mean squared error is equivalent to maximizing the log-likelihood of the regression parameters. In this scenario, the standard error of the parameters is related to the inverse square root of the Fisher information matrix, which in turn is closely related to the inverse square root of the Hessian of the objective function. The standard error is then simply related to the gradient of the model with respect to the parameters at the point of interest and the inverse Hessian at the minimum. The challenge has been a neural network may have hundreds of parameters, and these derivatives (and second derivatives) are inconvenient to derive and compute.

Machine learning has provided a breakthrough technology to mitigate this issue with the implementation of automatic differentiation in easy to use packages like autograd. This makes it

possible to automatically compute these derivatives in a few lines of code, and to easily estimate uncertainty from machine-learned potentials. An example application of this is shown in Figure 16 where a 95% confidence band is plotted around a neural network potential trained to mimic the Lennard Jones potential; near the data points the model is confident, and far from the points it is less confident. This suggests the MLP will not extrapolate reliably, which is expected since the neural network does not have any extrapolation constraints built into it. This work is also being prepared for publication.

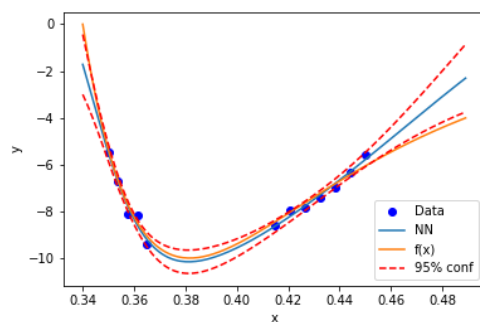


Figure 16. Illustration of uncertainty estimation in a machine learned potential. A neural network potential was trained to mimic the Lennard Jones potential.

Publications Acknowledging this Grant in 2015-2018

1. Kitchin, J. R., Machine learning in catalysis, *Nature Catalysis*, **2018**, *1*(4), 230–232.
<http://dx.doi.org/10.1038/s41929-018-0056-y>

Surface Chemistry and Reactions for Bimetallic Au Catalysis

Bruce E. Koel¹, Simon G. Podkolzin²

¹Department of Chemical and Biological Engineering, Princeton University, Princeton, NJ 08544

²Department of Chemical Engineering and Materials Science, Stevens Institute of Technology, Hoboken, NJ 07030

Presentation Abstract

Gold-based catalysts exhibit high catalytic activities and attractive selectivities for a wide range of reactions. They are especially promising in selective oxidation reactions. It is known that the catalytic properties of Au can be significantly enhanced by addition of other metals, but the development of improved Au-based catalysts is hindered by a lack of fundamental understanding of how the catalytic properties of Au can be controlled and tailored. The goal of our research program is to establish fundamental composition-structure-activity relationships for Au and bimetallic Au catalysts by synergistically combining experimental and computational studies.

In the past year we utilized this approach to investigate the structure and reactivity of atomic oxygen in gold catalysis. The interactions between oxygen and Au surfaces are fundamentally important in diverse areas of science and technology, but especially for understanding selective oxidation reactions in Au catalysis. Fundamental composition-structure-activity relationships for Au catalysts were established for H₂O₂ decomposition to H₂O and O₂. Adsorption and reactivity of reactants, products, and intermediates, along with catalytic reaction rates, were studied on monodisperse 5, 50, and 400-nm Au nanoparticles supported on SiO₂. In situ surface enhanced Raman spectroscopy measurements were performed to identify surface structures and species in the catalytic decomposition of H₂O₂. Density functional theory calculations with vibrational analyses were applied to interpret the Raman spectra and to identify the preferential oxygen structures. A new structure for an atomic oxygen intermediate at Au surfaces was found, and this discovery will advance the development of improved Au-based catalysts.

DE-SC0019052: Surface Chemistry and Reactions for Bimetallic Au Catalysis

PI: Bruce E. Koel,

Co-PI: Simon G. Podkolzin

Student(s): Yiteng Zheng

RECENT PROGRESS

H₂O₂ Decomposition Kinetics Measurements

Measurements of the kinetics of H₂O₂ decomposition to form gas-phase O₂ and liquid H₂O were performed under ambient conditions (room temperature, atmosphere pressure, and open to air) in a glass Raman cell that served as a batch reactor. Catalysts with 5, 50, and 400-nm monodisperse Au particles supported on SiO₂ were prepared using colloidal solutions and treated under flowing N₂ at 523 K for 2 h. Raman spectroscopy confirmed that the thermal treatment

produced spectroscopically clean Au surfaces without organic ligands. Catalytic decomposition of a 15 wt% aqueous H_2O_2 solution over clean Au catalysts was monitored utilizing in situ surface-enhanced Raman spectroscopy (SERS) measurements for evaluating the time-dependent H_2O_2 conversion.

The reaction rate of H_2O_2 decomposition decreased with increasing Au particle size (Figure 1). The 5 nm Au particles were more catalytically active than the 50 and 400 nm Au particles. After 45 min of reaction time, all H_2O_2 was decomposed over the 5 nm Au catalyst, whereas the H_2O_2 conversion was only 19 and 11 % for the 50 and 400 nm Au catalysts, respectively. A blank experiment conducted in the absence of Au showed that the rate of H_2O_2 decomposition was lower over the SiO_2 support alone, with a conversion of less than 1 % after 45 min of reaction time.

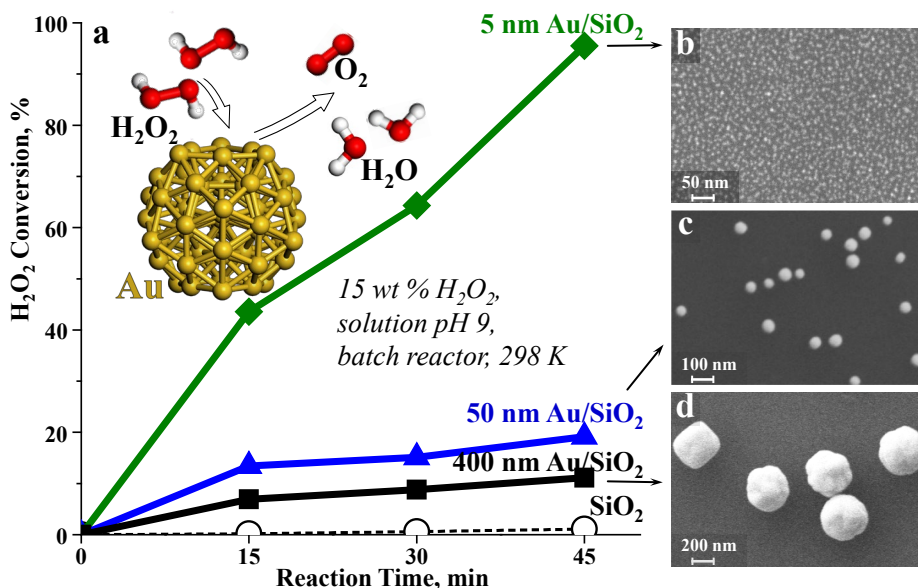


Figure 1. Dependence of H_2O_2 decomposition rates on the size of catalytic Au nanoparticles. (a) Kinetic measurements in a batch reactor with different sizes of Au nanoparticles. SEM images of the monodisperse Au/SiO₂ catalysts: (b) 5 nm, (c) 50 nm and (d) 400 nm.

Raman Spectroscopy Measurements

The time evolution of in situ Raman spectra for a 400 nm Au/SiO₂ catalyst at pH = 9 is compared (Figure 2) to a spectrum of the aqueous H_2O_2 solution collected in an experiment without Au under the same conditions. In addition to the Raman band at 940 cm^{-1} for SiO₂, liquid phase H_2O_2 exhibited a band at 975 cm^{-1} . After H_2O_2 started to decompose (15 and 30 min of reaction time), two new Raman bands at 590 and 822 cm^{-1} were observed. After 18 h, when most of the H_2O_2 had decomposed (92% conversion), the bands at 590 and 875 cm^{-1} became smaller and the band at 822 cm^{-1} was no longer observed. When all H_2O_2 decomposed after 26 h (100% conversion), bands at 590 and 875 cm^{-1} were no longer observed, leaving a single band at 940 cm^{-1} from the SiO₂ support. Since the bands at 590 and 822 cm^{-1} were only observed during H_2O_2 decomposition, they must be due to reaction intermediates.

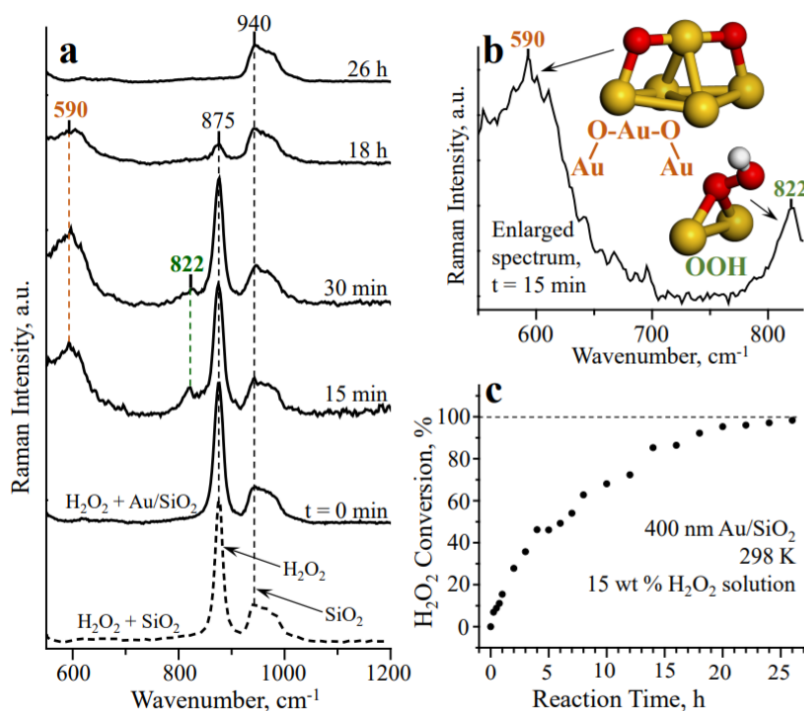


Figure 2. H₂O₂ decomposition over a 400-nm Au/SiO₂ catalyst. (a) In situ Raman spectra as a function on time. (b) An enlarged part of the spectrum at 15 min of reaction time along with assignments from DFT calculations. (c) Dependence of H₂O₂ conversion on the reaction time.

Density Functional Theory (DFT) Calculations

DFT calculations were utilized to identify structures formed by atomic oxygen adsorption on Au surfaces. Two structures described by other experimental and computational studies were identified. The first structure involved isolated O atoms binding on the Au surface at low surface oxygen coverage. The second structure was observed at higher coverage when two oxygen atoms push a neighboring Au atom from the surface into the adlayer to form a dimer denoted as Au₂-O-Au-O-Au₂, with the O atoms in pseudo threefold sites. In a recent result, we identify a new third structure found on the surface of Au nanoparticles. When O atoms do not need to displace an Au atom from a flat surface, an Au-O-Au-O-Au structure is formed with the O atoms in bridge sites (Figure 3D). The band at 590 cm⁻¹ is assigned to this newly identified Au-O-Au-O-Au structure. The calculated frequencies for this structure were 546-558 cm⁻¹ in good agreement with the experimental results.

DFT calculations were also used to assign the band at 822 cm⁻¹ to OOH surface species (Figure 2b). These calculations show that OOH adsorbs preferentially on an Au-Au bridge site with ν (O-O) modes in the range from 831 cm⁻¹ for small Au clusters to 806 cm⁻¹ for Au(111).

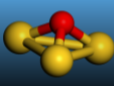

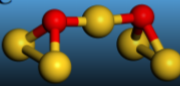
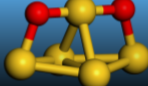
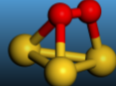
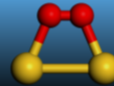
A	B	C	D	E	F
					
atomic oxygen on a threefold site	atomic oxygen on a bridge site	atomic oxygen as Au ₂ -O-Au-O-Au ₂	atomic oxygen as Au-O-Au-O-Au	molecular oxygen on a threefold site	molecular oxygen on a bridge site
$\nu(\text{O-Au})$	$\nu(\text{O-Au})$	$\nu_s(\text{O-Au-O})$	$\nu_s(\text{O-Au-O})$	$\nu(\text{O-O})$	$\nu(\text{O-O})$
373-431	451-467	450-508	546-558	1076	1049-1185

Figure 3. Oxygen structures on Au surfaces and their vibrational frequencies predicted by DFT calculations using multiple Au surfaces, ranging from small Au clusters to flat surfaces of Au single crystals: Au₅, Au₁₃ and Au₅₅ clusters, Au(111) and Au(211) surfaces, and an Au(111) surface with an additional Au atom.

Publications Acknowledging this Grant in 2015-2018. None to report.

Inter- and Intramolecular “Inverse” Frustrated Lewis Pairs – Catalysis and Small Molecule Activation

Clemens Krempner

Department of Chemistry & Biochemistry, Texas Tech University, Lubbock, Texas.

Presentation Abstract

The last decade has seen tremendous interest in the design and synthesis of inter- and intramolecular Frustrated Lewis Pairs (FLPs) as metal-free catalysts for organic transformations. In this context, our laboratory recently demonstrated that sterically congested organosuperbases can be combined with moderate to weak Lewis acids to generate so-called “inverse” FLPs. We showed that these *intermolecular* FLP systems are capable of cleaving H₂ heterolytically and, more importantly, catalyzing the hydrogenation of various imines and ketones. Herein, we report the synthesis of a new family of *intramolecular* “inverse” Frustrated Lewis Pairs that contain strongly basic guanidine units covalently linked to various moderately to weakly Lewis acidic organoboron moieties. Applications of these newly designed “inverse” *intramolecular* FLPs towards small molecule activation including H₂, CO, CO₂, alkynes and simple carbonyl compounds will be discussed.

DE-SC0019094: “Inverse” Frustrated Lewis Pairs as Transition Metal Free Catalysts for the Hydrogenation of Organic Carbonyl Compounds, CO₂ and CO.

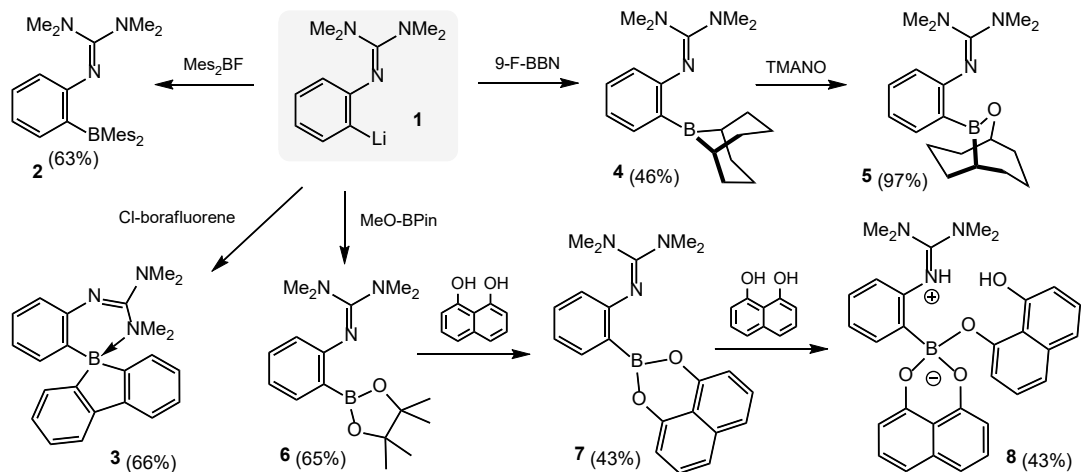
Postdoc: Suresh Mummadi

Students: Shipra Garg, Chamila Manankandayalage, Gordon Walker

RECENT PROGRESS

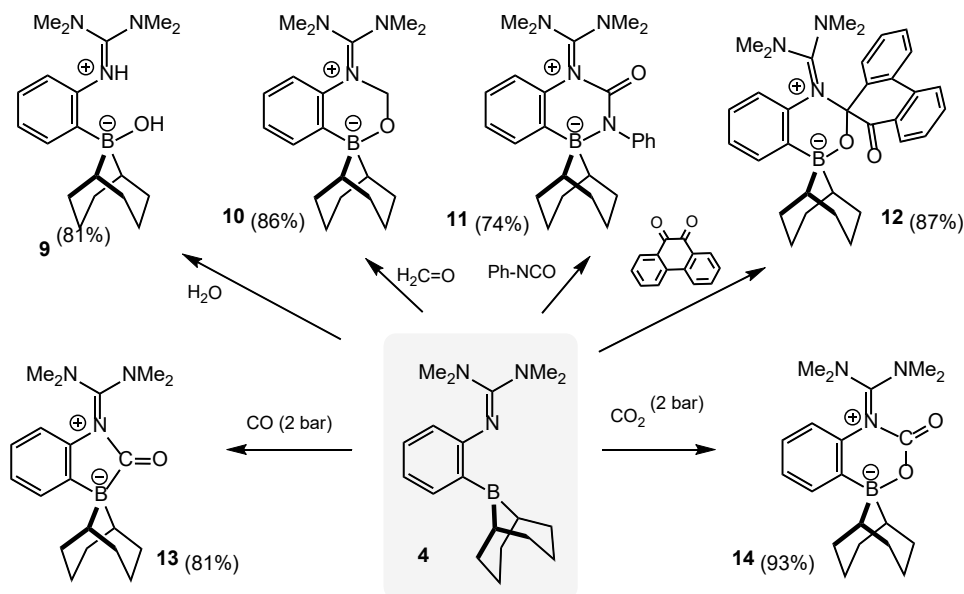
“Inverse” Intramolecular Frustrated Lewis Pairs

We recently discovered that the reaction of the 2-bromo-phenyl-tetramethylguanidine with BuⁿLi in toluene affords organolithium compound **1** in ca. 70% yields (Scheme 1). Treatment of **1** with FBMe₂ gave access to intramolecular FLP **2**, which was structurally fully characterized. To expand our arsenal of intramolecular FLPs for catalytic and stoichiometric activation of small molecules, the guanidino boranes **3**, **4** and **6** were synthesized from reactions of **1** with various halo- and alkoxy-boranes via salt metathesis. The X-ray data revealed that only **2** and **4** can be considered as intramolecular FLPs as no coordination of the guanidino group to the boron was noted. In contrast, **3** shows in the solid state and in solution donor-acceptor interaction between boron and one of the Me₂N groups. **4** can be selectively oxidized with TMANO to generate the liquid FLP **5**. Raw **6** was treated with 1,8-dihydroxynaphtalene but did not give the desired FLP **7**; instead a second equiv. of 1,8-dihydroxynaphtalene rapidly reacted with intermediate **7** to give the crystalline zwitterionic borate **8**.

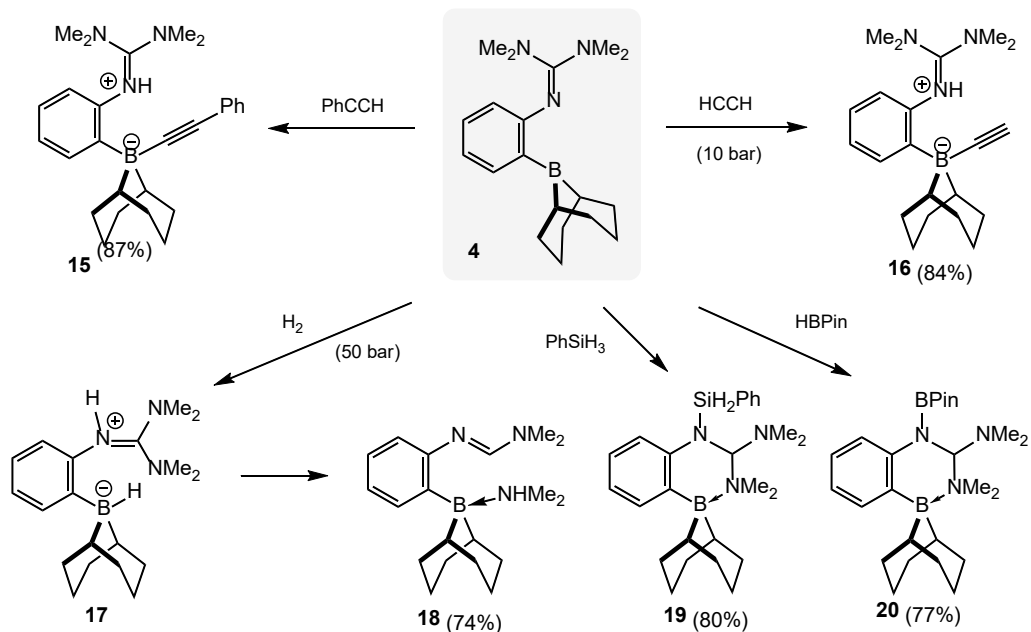


Scheme 1. Synthesis of guanidine-based “inverse” intramolecular FLPs.

The new FLPs **3-6** and zwitterionic **8** were isolated in good yields and structurally fully characterized by multi-nuclei NMR spectroscopy, combustion analysis and XRD. In addition the ability of **3-5** to form adducts with CO and CO₂ as well as to cleave C-H and H-H bonds was investigated. However, due to intramolecular donor-acceptor interactions in **3** adduct formation with CO and CO₂ as well as H₂-cleavage was not possible even at high temperatures and H₂ pressures. The oxidized FLP **5** was completely inactive in the presence of H₂ or Ph-C≡CH. No reaction occurred, even at high temperature over extended periods of time. We attribute the lack of reactivity to the reduced Lewis acidity of the boryl unit and the release of ring strain due to the insertion of oxygen into the B-C bond of the BBN unit. Gratifyingly, FLP **4** exhibited high reactivity towards a wide range of molecules (Schemes 2 and 3). For example, **4** readily reacts with H₂C=O and diketones to form the air- and moisture stable products of carbonyl addition **10** and **12**. PhCNO reacts with **4** in a similar manner to form addition product **11**. In this case addition of the C=N imino functionality and not the carbonyl group was noted according to the X-ray data. On the other hand, VT NMR studies indicate the formation of a second species in solution, which is believed to be the product of carbonyl addition. More importantly, also FLP **4** reacts smoothly with CO and CO₂ at relatively low pressures to furnish the corresponding adducts **13** and **14** in excellent isolated yields.



Scheme 2. Reactivity of intramolecular FLP **4** towards polar substrates.



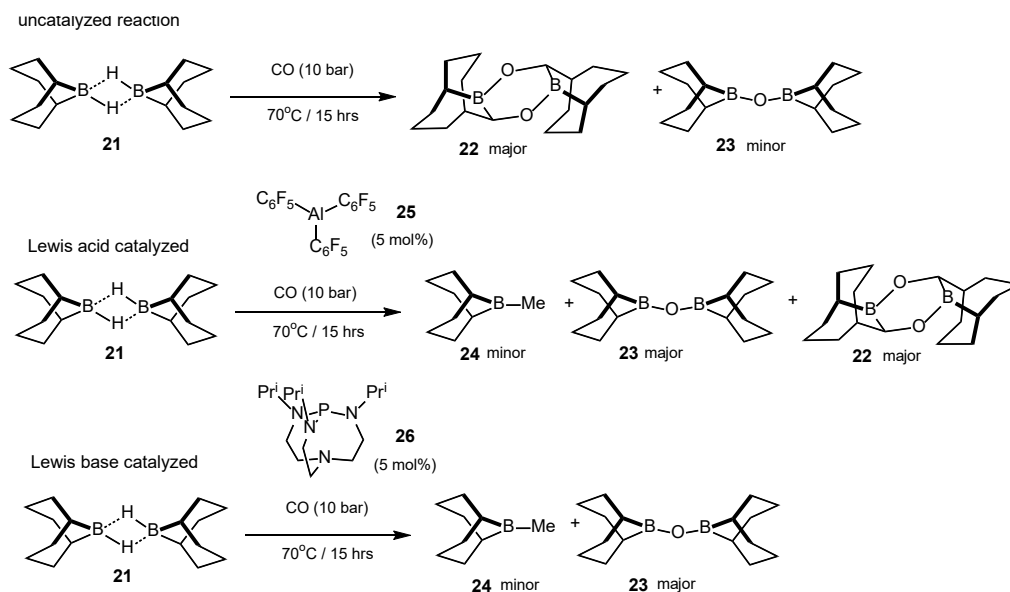
Scheme 3. C-H, B-H, Si-H and H-H bond cleavage with intramolecular FLP **4**.

Not surprising, FLP **4** rapidly reacted at 25°C with $\text{Ph-C}\equiv\text{CH}$ and also $\text{HC}\equiv\text{CH}$ via cleavage of the C-H bonds to form the corresponding alkyne substituted guanidinium borates **15** and **16** almost quantitatively (Scheme 3). Moreover, FLP **4** was capable of cleaving H_2 heterolytically at 25°C. However, under the conditions applied the guanidinium borohydride **17** appeared to be unstable and underwent an irreversible fragmentation reaction to give **18** as the major product, which was structurally characterized by XRD. Stoichiometric reactions of FLP **4** with PhSiH_3 and HBPIn ,

respectively, showed rapid Si-H and B-H bond cleavage, clearly demonstrating the high reactivity of **4**. But again subsequent transfer of the hydride from boron to carbon occurred with exclusive formation of products **19** and **20**.

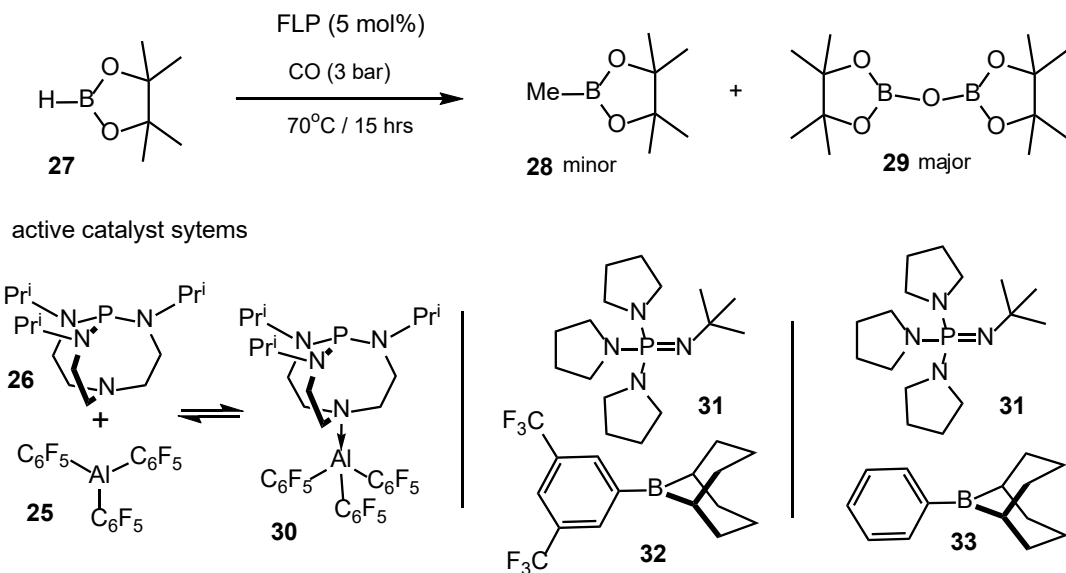
Catalytic Hydroboration of CO.

We reinvestigated the hydroboration of CO with 9-BBN (**21**). In agreement with the literature, the insertion product **22** was obtained as the major product of the reaction along with minor amounts of BBN-O-BBN (**23**) (Scheme 4). When the strong Lewis acid $\text{Al}(\text{C}_6\text{F}_5)_3$ (**25**) was used as a catalyst, **22** and **23** were detected as the major products along with 9-Me-BBN (**24**) as the minor product. Moreover, when Verkade's base $\text{P}[\text{N}(\text{Pr}^i)\text{CH}_2\text{CH}_2]_3\text{N}$ (**26**), known to form an FLP with 9-BBN that is capable of cleaving H_2 , was used as a catalyst only **23** (major) and **24** (minor) were obtained. The formation of **24** indicates that CO has been reduced according to the following equation: $3 \text{H-BBN} + \text{CO} \rightarrow \text{BBN-O-BBN} + \text{CH}_3\text{-BBN}$, and that FLP **26/21** catalyzes the reaction.



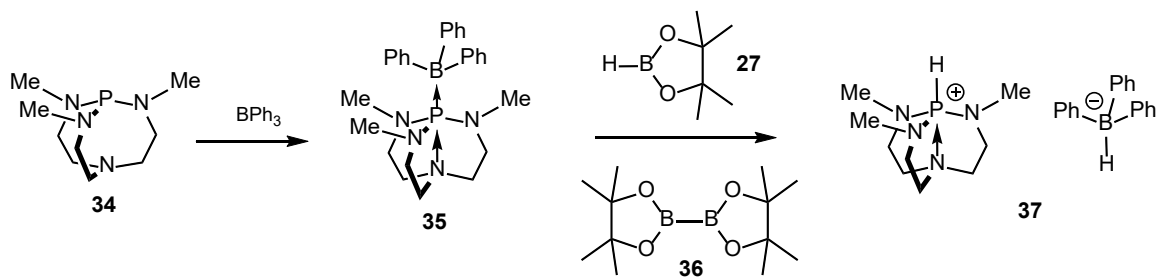
Scheme 4. Catalytic borylation of CO with 9-BBN.

Next, the hydroboration of CO with the less reactive borane HBPIn was investigated and no reaction with or without catalytic amounts of Verkade's base $\text{P}[\text{N}(\text{Pr}^i)\text{CH}_2\text{CH}_2]_3\text{N}$ (**26**) (Scheme 5) was noticed. On the other hand, various FLP catalysts including **31/32**, **31/33** and even the labile Lewis acid-base complex **30** proved to be active in the catalytic conversion of HBPIn and CO to Me-BPin (**28**) as the minor and PinB-O-BPin (**29**) as the major product. Again, these initial results indicate that CO has been reduced catalytically according to the following equation: $3 \text{H-Pin} + \text{CO} \rightarrow \text{PinB-O-BPin} + \text{CH}_3\text{-BPin}$.



Scheme 5. FLP catalyzed borylation of CO with HBPIn.

To gain insights into the mechanism, stoichiometric reactions of selected FLPs and Lewis acid base complexes have been performed (Scheme 6). Thus, the reaction of BPh_3 with the less sterically demanding Verkade's base $\text{P}[\text{N}(\text{Me})\text{CH}_2\text{CH}_2]_3\text{N}$ (**34**) generated Lewis acid base adduct **35**. Subsequent addition of HBin to **35** resulted in the formation of the phosphonium borohydride **37**, which formally is the product of H_2 cleavage. Since H_2 was not present, it is assumed that a dehydrogenation of HBPIn took place generating PinB-BPin (**36**) as a side product. The same behavior was noted when the FLP composed of Verkade's base $\text{P}[\text{N}(\text{Pr}^i)\text{CH}_2\text{CH}_2]_3\text{N}$ (**26**) and BPh_3 was treated with HBPIn; the borohydride salt $\{\text{HP}[\text{N}(\text{Pr}^i)\text{CH}_2\text{CH}_2]_3\text{N}\}[\text{HBPh}_3]$ and **37** were formed as the major products. These results support our hypothesis that in-situ generated borohydride anions, HBR_3^- , are active species in the catalytic borylation of CO.



Scheme 6. Synthesis and reaction of Lewis acid base adduct **35** with HBPIn.

Electrocatalytic H₂ Evolution by Metal Dithiolene Frameworks

Smaranda C. Marinescu,^a Keying Chen,^a Courtney A. Downes,^a Eugene Schneider,^b Jason D. Goodpaster^b

^aUniversity of Southern California, Los Angeles, CA

^bUniversity of Minnesota – Twin Cities, MN

Presentation Abstract

We have previously shown that metal dithiolene units can be successfully integrated into one- and two-dimensional frameworks, leading to materials that display unique electronic properties – they catalyze with remarkable activity the electrocatalytic conversion of water into hydrogen, and their electrical conductivity is switchable from semiconducting to metallic. To enhance the durability and charge transport properties of the MOF/electrode architecture in cobalt triphenylene-2,3,6,7,10,11-hexathiolate (**CoTHT**) system, we deposited **CoTHT** as an ink composite comprised of Nafion, a proton conductive polymeric binder, and carbon black, an inexpensive conductive additive. The utilization of the **CoTHT** composite leads to a huge improvement in the overpotential (η) to reach a current density of 10 mA/cm² ($\eta = 143$ mV) compared to prior reports, resulting in the most active MOF-based electrocatalyst for the HER. Density functional theory (DFT) calculations suggest that the catalytic cycle involves a Volmer discharge step to generate a cobalt hydride sandwiched between two layers, followed by a Heyrovsky step to form a cobalt-H₂ intermediate, and dissociate H₂. Taken together, theory and experiment suggest that carbon black significantly improves the activity of the dithiolene-based MOF by facilitating the electron transport process and influencing the rate-determining step in the mechanism. By suppressing the poor bulk properties of **CoTHT**, the composite outperforms all the reported dithiolene-based MOFs. Overall, these studies highlight the intrinsic activity of **CoTHT**, reveal the significance of the bulk properties in dictating the HER activity of the material, and provide insight into the HER mechanism of **CoTHT**.

Grant or FWP Number: Metal Dithiolene Coordination Polymers for Energy Applications

Publications Acknowledging this Grant

1. Chen, K.; Schneider, E.; Downes, C. A.; Goodpaster, J. D.; Marinescu, S. C. “Improving and Understanding the Hydrogen Evolving Activity of a Cobalt Dithiolene Metal-Organic Framework”, *submitted*.
2. Orchanian, N. M.; Hong, L. E.; Marinescu, S. C. “Electrocatalytic Syngas Generation with a Cobalt Phosphinothiolate Complex”, *submitted*.

Manos Mavrikakis

Atomic-scale Design of Metal and Alloy Catalysts: A Combined Theoretical and Experimental Approach

Manos Mavrikakis,[†] James A. Dumesic,[†] Younan Xia[‡]

[†] Department of Chemical & Biological Engineering, University of Wisconsin – Madison;

[‡] School of Chemistry & Biochemistry, Georgia Institute of Technology

Presentation Abstract

The main objective of this combined theoretical and experimental project is to: (i) *design* from first-principles, (ii) *synthesize* using advanced *nanosynthesis* techniques, and (iii) experimentally evaluate *new metal* and *alloy entities*, with unique *catalytic* properties for a number of important chemical reactions. Measurable impact can be found in a number of applications, including low temperature fuel cells, hydrogen production and purification, fuels/chemicals production, and pollution remediation. The importance of the atomic-scale architecture of these new theoretically-designed catalysts to their unique properties is driving the development of *new inorganic materials synthesis* approaches, which are capable of synthesizing the theoretically determined optimal, and in some cases, metastable, nanoscale catalytic architectures.

Grant or FWP Number: DOE Grant No. DE-FG02-05ER15731 (Atomic-scale Design of Metal and Alloy Catalysts: A Combined Theoretical and Experimental Approach)

PI: Manos Mavrikakis

Postdoc(s): Roberto Schimmenti (UW), Zhiheng Lyu (GIT)

Student(s): Saurabh Bhandari (UW)

Affiliations(s): University of Wisconsin-Madison, Georgia Institute of Technology

RECENT PROGRESS

Structure-Sensitivity of Formic Acid Electro-Oxidation on Transition Metal Surfaces¹

Formic acid (FA) is a non-toxic, renewable, and promising hydrogen storage material that can also be used as fuel in direct formic acid fuel cells (DFAFCs). Selective dehydrogenation of FA, however, remains a challenge: FA can either dehydrogenate to form CO₂ and protons or dehydrate to form CO and H₂O. Pt and Pd, the most active formic acid electrooxidation (FAO) catalysts, are not highly selective for dehydrogenation and are prone to poisoning by CO. Here, we use density functional theory (DFT) calculations together with the computational hydrogen electrode formalism to perform a systematic reactivity trends analysis and a structure-sensitivity study for FAO on model (111) and (100) transition metal surfaces.

We illustrate the different pathways available for FAO with the Pt surfaces at a potential of 0 V. FA can first deprotonate to form either formate (HCOO) or carboxyl (COOH). On Pt(111) (Figure

1A), the latter is thermodynamically favored by 0.29 eV. COOH can then undergo *direct oxidation* to form CO₂, or *dehydration* to form CO + H₂O(g). The latter is favored by 0.91 eV. This suggests that Pt(111) will be poisoned by CO even at low overpotentials. On the more open Pt(100) surface (**Error! Reference source not found.**B), reaction intermediates are stabilized relative to Pt(111). Although formation of CO is easier as all elementary steps are now thermodynamically downhill, Pt(100) is *less* prone to CO poisoning than Pt(111) as the *indirect oxidation* of CO is faster on it.

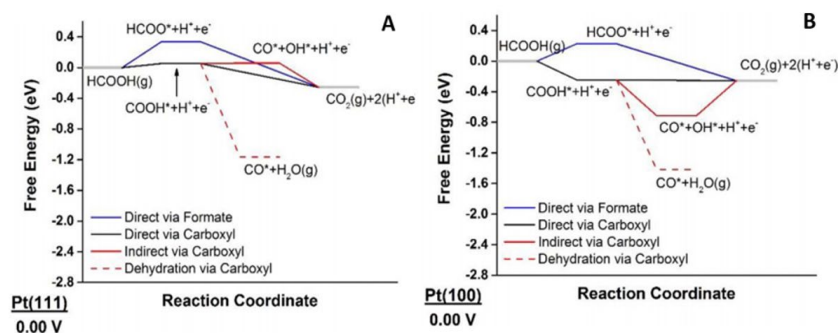


Figure 17 Free-energy diagrams of formic acid electrooxidation (FAO) on (A) Pt(111) and (B) Pt(100), both at 0.00 V. Figure adapted from reference 1.

To perform similar analyses on various other transition metals (Au, Ag, Cu, Pd, Ni, Ir, Rh, Co, Os, Ru, and Re), we used the calculated Gibbs free energy of adsorption of OH (G_{OH*}) and CO (G_{CO*}) as energy descriptors for creating generalized activity phase diagrams. These phase diagrams can guide the identification of surfaces

with improved FAO activity and selectivity. For example, we predict high activity for Ag and Cu, but they are unfortunately electrochemically unstable under reaction conditions. Pt and Pd are stable under reaction conditions, but rate-limited by water activation on both their (111) and (100) facets at both high and low potentials. Their poor ability to activate water explains why they are easily poisoned by CO. Alloying Pt and Pd with metals that bind O more strongly, could help them activate water and thus improve FAO activity and selectivity.

Subnanometric Au Clusters for Formic Acid Decomposition^{2,3}

Subnanometric metal clusters behave very differently depending on their size, down to differences in single atoms.⁴ Although subnanometric Au clusters have high activities and selectivities for the decomposition of formic acid (FA), the nature of the active site remains unresolved. To address this question, we performed first-principles DFT calculations on a series of Au clusters, and utilized the obtained DFT energetics in mean-field microkinetic models (MKM) to compare our findings with experimental measurements.² We then studied the most promising cluster in detail with rigorous, coverage-consistent kinetic Monte Carlo (KMC) simulations.³

Table 1 Adjustments to DFT-calculated parameters required for a microkinetic model to fit experimental kinetic data, for the Au₁₇, Au₁₈, and Au₁₉ clusters. Adapted from reference 2.

Adjustments (eV)	Au ₁₇	Au ₁₈	Au ₁₉
ΔBE(HCOO)	-0.09	-0.10	-0.10
ΔBE(H)	0.22	0.00	0.32
ΔE _{TS} (HCOOH→HCOO+H)	-0.36	-0.16	-0.33
ΔE _{TS} (HCOO→CO ₂ +H)	-0.41	-0.29	-0.21
ΔE _{TS} (H+H→H ₂)	-0.21	-0.05	-0.43

We first performed *ab initio* molecular dynamics simulations to determine the most stable structures of Au_n (n=2-25) clusters.² For each cluster, we evaluated the minimum energy pathway for FA decomposition to CO₂ and H₂. To connect this first-principles data with our experiments on Au/SiC catalysts⁵, we performed MKM studies on the most active clusters. We concluded that, out of the 24 Au clusters we studied, Au₁₈, whose structure is reported in Figure 2, was the most viable candidate for

rationalizing the experimental data; it required the least parameter adjustment to reproduce the high activities and selectivities observed in our reaction kinetics experiments.

Our MKM studies were, however, unable to explain a crucial experimental observation: selective formation of HD when monodeuterated FA was decomposed over Au.⁶ This is because Au clusters exhibit quasi-molecular properties such as *i*) discrete adsorbate coverages, *ii*) strong interactions between adsorbates due to quantum size-effects, and *iii*) non-homogeneity of surface sites, which lead to a breakdown of the mean-field approximation used in MKMs.

We therefore performed rigorous KMC simulations for FA decomposition on Au₁₈, which are able to capture the complexities of catalysis by clusters.³ To account for coverage effects, we specifically fitted a cluster expansion Hamiltonian that can be used on the fly to adapt to changes in the reaction energetics and activation energies of any reaction caused by interactions among adsorbates.

Our KMC simulations elucidated a detailed reaction mechanism for FA decomposition on Au₁₈ (Figure 2), in which the decomposition of FA occurs *one molecule at a time*. When a FA molecule dissociates on a clean Au₁₈ cluster, the resulting HCOO and H adsorbates end up occupying both active CN=5 sites (Figure 2; red triangles) on the cluster due to the strong stabilizing interactions between HCOO and H on these active sites. With no free active sites, the barriers for the dissociation of subsequent FA molecules are raised, preventing further dissociation of FA before the first FA molecule is completely decomposed to CO₂ and H₂. This kinetic isolation between turnovers explains the experimentally observed selectivity of decomposition of monodeuterated FA to HD.

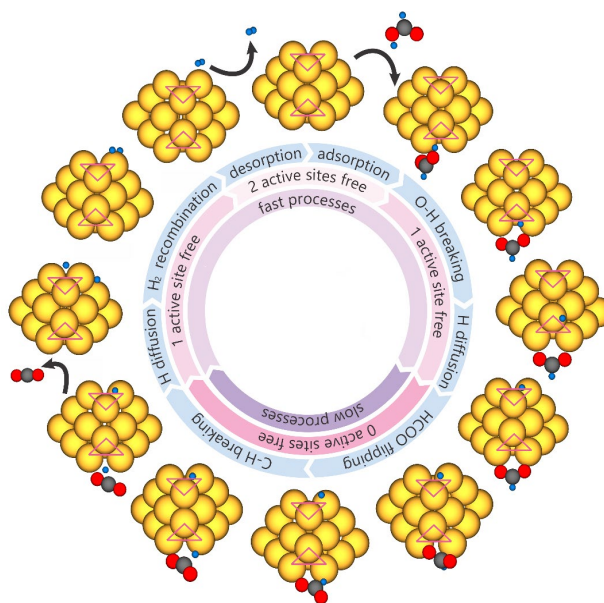


Figure 18 Proposed reaction mechanism of FA decomposition on Au₁₈. Descriptions of the elementary steps, the number of free active sites, and whether the steps are fast or slow processes, are marked in the blue, pink, and purple concentric circles respectively. Color code for structures: gold – Au, grey – C, red – O, blue – H. Red triangles mark the Au atoms with coordination number of 5. Adapted from reference 3.

Using experiments, first-principles calculations, and kinetic modeling, we pieced together a detailed picture of how FA decomposes on subnanometric Au clusters. We propose Au₁₈ as the active catalytic cluster, and elucidate, to our knowledge, the first example of heterogeneous catalysis by clusters one molecule at a time. These results enhance our understanding of how clusters may catalyze reactions with high activity and selectivity, and may guide the rational design of quasi-molecular subnanometric cluster catalysts for FA decomposition and other reactions.

Synthesis of Ru Icosahedral Nanocages with a Face-Centered-Cubic Structure and Evaluation of Their Catalytic Properties⁷

Shape-selected metal nanocrystals exhibit unique catalytic properties.⁸ Icosahedra in particular possess twin-boundary defects which exert inhomogeneous strain on the exposed (111) facets of the nanoparticles, modifying their reactivities.⁹ Here, we successfully synthesized Ru icosahedral nanocages,⁷ and evaluated their catalytic activity with experiments and DFT calculations.

We used Pd icosahedral nanocrystals, prepared using our previously developed procedure,¹⁰ as seeds and epitaxially deposited Ru atoms on them. Subsequently, we removed the Pd core by wet chemical etching. The resultant icosahedral Ru nanocages are approximately 1.1 nm (five atomic layers) thick and contain 12.5 wt. % Pd; complete removal of Pd during the etching process is not possible. Although bulk Ru has a hcp structure, the synthesized Ru nanocages have an fcc structure as the deposited layers adopt the packing of the underlying substrate. Experimentally, the Ru icosahedral nanocages were found to be twice as active as their cubic and octahedral counterparts for both the reduction of 4-nitrophenol and the decomposition of hydrazine.

We then used DFT calculations to probe the activity of the nanocages for a potential industrial application: ammonia synthesis. We focused on the N_2 dissociation elementary step, generally considered rate-determining for this reaction. The energy difference between the N_2^* dissociation transition state and gas-phase N_2 (Figure 3; $E_{N-N\ TS}$) determines the balance between the desirable dissociation of N_2^* and the undesired desorption of N_2^* ; lower $E_{N-N\ TS}$ values point to more competitive dissociation, leading to higher activities for ammonia synthesis. By this metric, our nanocages (**Error! Reference source not found.**; blue line) are more active than the (0001) facet of hcp Ru nanoparticles (Figure 3; red line) — they stabilize the N_2^* dissociation transition state by 0.48 eV. Subsurface Pd impurities remaining from the etching process are crucial for explaining this activity as the pure Ru icosahedral nanocage shows no activity enhancement.

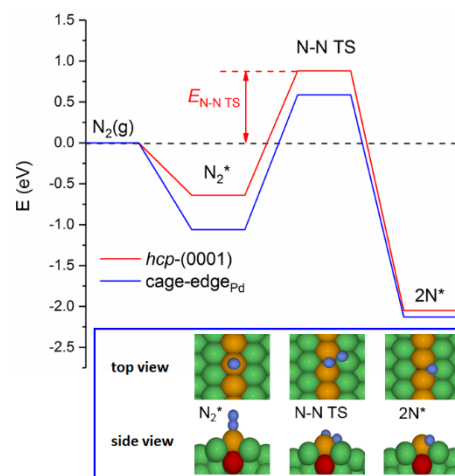


Figure 19 Calculated potential energy diagrams for N_2 dissociation on pure hcp-Ru(0001), and on the twin-boundary sites of the fcc-Ru icosahedral nanocage model with two subsurface Pd impurity atoms (cage-edge_{Pd}). N_2^* , $2N^*$, and $N-N\ TS$ denote adsorbed N_2 , two N^* adatoms at infinite separation and the N_2^* dissociation transition state, respectively. The inset depicts these states on cage-edge_{Pd}. Color code in the inset: blue – N, red – Pd, orange – step-edge Ru, green – other Ru. Figure adapted from reference 7.

References

- (1) Elnabawy, A. O.; Herron, J. A.; Scaranto, J.; Mavrikakis, M. Structure Sensitivity of Formic Acid Electrooxidation on Transition Metal Surfaces: A First-Principles Study. *J. Electrochem. Soc.* **2018**, *165*, J3109–J3121.
- (2) Li, S.; Singh, S.; Dumesic, J. A.; Mavrikakis, M. On the Nature of Active Sites for Formic Acid Decomposition on Gold Catalysts. *Catal. Sci. Technol.* **2019**, *9*, 2836–2848.
- (3) Chen, B. W. J.; Stamatakis, M.; Mavrikakis, M. Kinetic Isolation between Turnovers on Au_{18} Nanoclusters: Formic Acid Decomposition One Molecule at a Time. *Submitted* **2019**.
- (4) Vajda, S.; Pellin, M. J.; Greeley, J. P.; Marshall, C. L.; Curtiss, L. A.; Ballentine, G. A.; Elam, J. W.; Catillon-Mucherie, S.; Redfern, P. C.; Mehmood, F.; Zapol, P. Subnanometre

- Platinum Clusters as Highly Active and Selective Catalysts for the Oxidative Dehydrogenation of Propane. *Nat. Mater.* **2009**, *8*, 213–216.
- (5) Singh, S.; Li, S.; Carrasquillo-Flores, R.; Alba-Rubio, A. C.; Dumesic, J. A.; Mavrikakis, M. Formic Acid Decomposition on Au Catalysts: DFT, Microkinetic Modeling, and Reaction Kinetics Experiments. *AIChE J.* **2014**, *60*, 1303–1319.
 - (6) Ojeda, M.; Iglesia, E. Formic Acid Dehydrogenation on Au-Based Catalysts at near-Ambient Temperatures. *Angew. Chemie Int. Ed.* **2009**, *48*, 4800–4803.
 - (7) Zhao, M.; Xu, L.; Vara, M.; Elnabawy, A. O.; Gilroy, K. D.; Hood, Z. D.; Zhou, S.; Figueroa-Cosme, L.; Chi, M.; Mavrikakis, M.; Xia, Y. Synthesis of Ru Icosahedral Nanocages with a Face-Centered-Cubic Structure and Evaluation of Their Catalytic Properties. *ACS Catal.* **2018**, *8*, 6948–6960.
 - (8) Xia, Y.; Yang, X. Toward Cost-Effective and Sustainable Use of Precious Metals in Heterogeneous Catalysts. *Acc. Chem. Res.* **2017**, *50*, 450–454.
 - (9) Wang, H.; Zhou, S.; Gilroy, K. D.; Cai, Z.; Xia, Y. Icosahedral Nanocrystals of Noble Metals: Synthesis and Applications. *Nano Today* **2017**, *15*, 121–144.
 - (10) Lv, T.; Wang, Y.; Choi, S.-I.; Chi, M.; Tao, J.; Pan, L.; Huang, C. Z.; Zhu, Y.; Xia, Y. Controlled Synthesis of Nanosized Palladium Icosahedra and Their Catalytic Activity towards Formic-Acid Oxidation. *ChemSusChem* **2013**, *6*, 1923–1930.

Publications Acknowledging this Grant in 2016-2019

(I) Exclusively funded by this grant

1. Chen B. W. J.; Stamatakis M.; Mavrikakis M.; Kinetic Isolation between Turnovers on Au₁₈ Nanoclusters: Formic Acid Decomposition One Molecule at a Time, *Submitted* **2019**
2. Li S.; Singh S.; Dumesic J. A.; Mavrikakis M.; On the nature of active sites for formic acid decomposition on gold catalysts, *Catalysis Science and Technology* **2019**, *9*, 2836-2848
3. Chen B. W. J.; Kirvassilis D.; Bai Y.; Mavrikakis M.; Atomic and Molecular Adsorption on Ag(111), *Journal of Physical Chemistry C* **2019**, *123*, 7551-7566
4. Kropp T.; Lu Z.; Li Z.; Chin Y-H. C.; Mavrikakis M., Anionic Single-Atom Catalysts for CO Oxidation: Support-Independent Activity at Low Temperatures, *ACS Catalysis* **2019**, *9*, 1595-1604
5. Bai Y.; Kirvassilis D.; Xu L.; Mavrikakis M.; Atomic and Molecular Adsorption on Ni(111), *Surface Science* **2019**, *679*, 240-253
6. Tacey S. A.; Szilvási T.; Xu L.; Schauer J. J.; Mavrikakis M.; The role of iron-oxide aerosols and sunlight in the atmospheric reduction of Hg(II) species: A DFT+U study, *Applied Catalysis B: Environmental* **2018**, *234*, 347-356
7. Xu L.; Lin J.; Bai Y.; Mavrikakis M.; Atomic and Molecular Adsorption on Cu(111), *Topics in Catalysis* **2018**, *61*, 736-750
8. Bai Y.; Chen B. W. J.; Peng G.; Mavrikakis M.; Density functional theory study of thermodynamic and kinetic isotope effects of H₂/D₂ dissociative adsorption on transition metals, *Catalysis Science and Technology* **2018**, *8*, 3321-3335
9. Elnabawy A. O.; Herron J. A.; Scaranto J.; Mavrikakis M.; Structure Sensitivity of Formic Acid Electrooxidation on Transition Metal Surfaces: A First-Principles Study, *Journal of the Electrochemical Society* **2018**, *165*, 3109-3121
10. Xu L.; Kirvassilis D.; Bai Y.; Mavrikakis M.; Atomic and molecular adsorption on Fe(110), *Surface Science* **2018**, *667*, 54-65

11. Bai Y.; Mavrikakis M.; A Mechanistic Study of Nitric Oxide Reduction by Hydrogen on Pt(100) (I): A DFT Analysis of the Reaction Network, *Journal of Physical Chemistry B*, **2018**, *122*, 432-443
12. Rangarajan S.; Maravelias C. T.; Mavrikakis M.; **Sequential-Optimization-Based Framework for Robust Modeling and Design of Heterogeneous Catalytic Systems**, *Journal of Physical Chemistry C* **2017**, *121*, 25847-25863
13. Rangarajan S.; Mavrikakis M.; **On the Preferred Active Sites of Promoted MoS₂ for Hydrodesulfurization with Minimal Organonitrogen Inhibition**, *ACS Catalysis* **2017**, *7*, 501-509
14. Schimmenti R.; Cortese R.; Duca D.; Mavrikakis M.; **Boron Nitride-supported Sub-nanometer Pd₆ Clusters for Formic Acid Decomposition: A DFT Study**, *ChemCatChem* **2017**, *9*, 1610-1620
15. Vara M.; Roling L. T.; Wang X.; Elnabawy A. O.; Hood Z. D.; Chi. M.; Mavrikakis M.; Xia Y.; **Understanding the Thermal Stability of Palladium–Platinum Core–Shell Nanocrystals by *In Situ* Transmission Electron Microscopy and Density Functional Theory**, *ACS Nano* **2017**, *11*, 4571-4581
16. Gilroy K. D.; Elnabawy A. O.; Yang T.-H.; Roling L. T.; Howe J.; Mavrikakis M.; Xia Y.; **Thermal Stability of Metal Nanocrystals: An Investigation of the Surface and Bulk Reconstructions of Pd Concave Icosahedra**, *Nano Letters* **2017**, *17*, 3655-3661
17. Roling L. T.; Mavrikakis M.; **Toward Rational Nanoparticle Synthesis: Predicting Surface Intermixing in Bimetallic Alloy Nanocatalysts**, *Nanoscale* **2017**, *9*, 15005-15017
18. Vara M.; Lu P.; Yang X.; Lee C.-T.; Xia Y.; A photochemical, room-temperature, and aqueous route to the synthesis of Pd nanocubes enriched with atomic steps and terraces on the side faces, *Chemistry of Materials* **2017**, *29*, 4563-4571
19. Li S.; Scaranto J.; Mavrikakis M.; **On the Structure Sensitivity of Formic Acid Decomposition on Cu Catalysts**. *Topics in Catalysis* **2016**, *59*, 1580-1588.
20. Roling L. T.; Herron J. A.; Budiman W.; Ferrin P.; and Mavrikakis M.; **Dimethyl Ether Electro-Oxidation on Platinum Surfaces**. *Nano Energy* **2016**, *29*, 428-438
21. Herron J. A.; Morikawa Y.; and Mavrikakis M.; **Ab initio molecular dynamics of solvation effects on reactivity at electrified interfaces**. *Proceedings of the National Academy of Sciences of the United States of America* **2016**, *113*, E4937-E4945.
22. Xu L.; Yao X.; Khan A.; Mavrikakis M.; **Chloroform Hydrodechlorination over Palladium–Gold Catalysts: A First-Principles DFT Study**. *ChemCatChem* **2016**, *8*, 1739-1746.
23. Tacey S. A.; Xu L.; Mavrikakis M.; Schauer J. J.; **Heterogeneous Reduction Pathways for Hg(II) Species on Dry Aerosols: A First-Principles Computational Study**. *Journal of Physical Chemistry A* **2016**, *120*, 2106-2113.
24. Scaranto J.; Mavrikakis M.; **Density functional theory studies of HCOOH decomposition on Pd(111)**. *Surface Science* **2016**, *650*, 111-120.
25. Rangarajan S.; Mavrikakis M.; **DFT Insights into the Competitive Adsorption of Sulfur- and Nitrogen-Containing Compounds and Hydrocarbons on Co-Promoted Molybdenum Sulfide Catalysts**. *ACS Catalysis* **2016**, *6*, 2904-2917.
26. Scaranto J.; Mavrikakis M.; **HCOOH decomposition on Pt(111): A DFT study**, *Surface Science* **2016**, *648*, 201-211.

(II) Jointly funded by this grant and other grants with leading intellectual contribution from this grant

27. Zhao M.; Xu L.; Vara M.; Elnabawy A. O.; Gilroy K. D.; Hood Z. D.; Zhou S.; Figueroa-Cosme L.; Chi M.; Mavrikakis M.; Xia Y.; Synthesis of Ru Icosahedral Nanocages with a Face-Centered-Cubic Structure and Evaluation of Their Catalytic Properties, *ACS Catalysis* **2018**, *8*, 6948-6960
28. Liu Y.; Zhang L.; Göeßl F.; Ball M. R.; Hermans I.; Kuech T. F.; Mavrikakis M.; Dumesic J. A.; Synthesis Gas Conversion over Rh-Mn-W_xC/SiO_x Catalysts Prepared by Atomic Layer Deposition, *ACS Catalysis* **2018**, *8*, 10707-10720
29. Liu Y.; Göeßl F.; Ro I.; Ball. M. R.; Sener C.; Aragão I. B.; Zanchet D.; Huber G. W.; Mavrikakis M.; Dumesic J. A.; **Synthesis Gas Conversion over Rh-Based Catalysts Promoted by Fe and Mn**, *ACS Catalysis* **2017**, *7*, 4550-4563
30. Yang X.; Roling L. T.; Vara M.; Elnabawy A. O.; Zhao M.; Hood Z. D.; Bao S.; Mavrikakis M.; Xia Y.; Synthesis and Characterization of Pt–Ag Alloy Nanocages with Enhanced Activity and Durability towards Oxygen Reduction. *Nano Letters* **2016**, *16*, 6644-6649.
31. Merte L. R.; Bai Y.; Zeuthen H.; Peng G.; Lammich L.; Besenbacher F.; Mavrikakis M.; Wendt S.; **Identification of O-rich structures on platinum(111)-supported ultrathin iron oxide films**. *Surface Science* **2016**, *652*, 261-268.

(III) Jointly funded by this grant and other grants with relatively minor intellectual contribution from this grant

32. Zhu J.; Chen Z.; Xie M.; Lyu Z.; Chi M.; Mavrikakis M.; Jin W.; Xia Y.; Iridium-Based Cubic Nanocages with 1.1-nm-Thick Walls: A Highly Efficient and Durable Electrocatalyst for Water Oxidation in an Acidic Medium, *Angewandte Chemie International Edition* **2019**, *58*, 7244-7248
33. Jacobberger R.M.; Murray E. A.; Fortin-Deschênes M.; Göeßl F.; Behn W. A.; Krebs Z. J.; Levesque P. L.; Savage D. E.; Smoot C.; Lagally M. G.; Desjardins P.; Martel R.; Brar V.; Moutanabbir O.; Mavrikakis M.; Arnold M. S.; Alignment of semiconducting graphene nanoribbons on vicinal Ge(001), *Nanoscale* **2019**, *11*, 4864-4875
34. Özer E.; Sinev I.; Mingers A.; Araujo J.; Kropp T.; Mavrikakis M.; Mayrhofer K.; Cuenya B. R.; Strasser P.; Ir-Ni Bimetallic OER Catalysts Prepared by Controlled Ni Electrodeposition on Ir_{poly} and Ir(111), *Surfaces* **2018**, *1*, 165-186
35. Tao Z.; Chen C.; Szilvási T.; Keller M.; Mavrikakis M.; Kapteyn H.; Murnane M.; **Direct time-domain observation of attosecond final-state lifetimes in photoemission from solids**. *Science* **2016**, *353*, 62-67.

Gerard Parkin

**Selective Conversion of Carbon Dioxide to Formaldehyde via a Bis(silyl)acetal:
Carbon Dioxide as a C₁ Source for the Synthesis of Organic Molecules**

Michael Rauch and Gerard Parkin
Columbia University, Department of Chemistry

Presentation Abstract

The conversion of carbon dioxide to formaldehyde is a transformation that is of considerable significance in view of the fact formaldehyde is a very important industrial chemical. However, this transformation is challenging because CO₂ is both kinetically and thermodynamically resistant to chemical transformations. Therefore, we report here that formaldehyde can be readily obtained from CO₂ *via* the bis(silyl)acetal, H₂C(OSiPh₃)₂. Specifically, a system comprised of [Tism^{PriBenz}]MgX (X = H, Me) and B(C₆F₅)₃ is an effective catalysts for the selective hydrosilylation of CO₂ to the bis(silyl)acetal, H₂C(OSiPh₃)₂, from which formaldehyde is released upon treatment with CsF. H₂C(OSiPh₃)₂ thus serves as a formaldehyde surrogate and provides a means to incorporate reduced C₁ moieties into organic molecules by forming C–C, C–N, C–O and C–S bonds. For example, H₂C(OSiPh₃)₂ can also be used as a formaldehyde surrogate in the Pictet-Spengler reaction for the synthesis of heterocyclic compounds, as illustrated by the formation of 1,2,3,4-tetrahydro-β-carboline (tryptoline) *via* the reaction with tryptamine hydrochloride. H₂C(OSiPh₃)₂ is not only capable of delivering a methylene moiety, but it can also provide a CH moiety in the formation of benzazole derivatives. As an illustration, *N*-methylbenzimidazole is obtained upon reaction of H₂C(OSiPh₃)₂ with *N*-methyl-1,2-phenylenediamine in DMSO, while benzothiazole is obtained from the reaction of H₂C(OSiPh₃)₂ with 2-aminothiophenol. Isotopologues of H₂C(OSiPh₃)₂, *e.g.* D₂C(OSiPh₃)₂, H₂¹³C(OSiPh₃)₂, and D₂¹³C(OSiPh₃)₂, may be synthesized from the appropriate combinations of (¹²C/¹³C)O₂ and Ph₃Si(H/D), which thereby provide a direct and convenient means to use carbon dioxide as a source of isotopic labels in complex organic molecules.

DE-SC0019204: Metal Catalyzed Transformations involving C–X bonds for the Conversions of Carbon Dioxide and Organic Chemicals

Students: Michael Rauch, David Sambade, Matthew Hammond, Daniel Shlian

RECENT PROGRESS

1. Conversion of Carbon Dioxide to Formaldehyde

The conversion of carbon dioxide to formaldehyde is an important objective because the latter is a widely used industrial chemical (with an annual consumption of 30 million tons). However, formaldehyde is not obtained industrially by this process because the hydrogenation of CO₂ to afford formaldehyde is thermodynamically uphill, whereas the subsequent reduction to methanol is strongly exergonic. Formaldehyde is, therefore, instead produced industrially by the partial

oxidation of methanol. The synthesis of formaldehyde from CO₂ *via* methanol thus involves the circuitous reduction from C(IV) in CO₂ to C(-II) in CH₃OH, followed by oxidation to C(0) in CH₂O. Therefore, it is significant that we have developed a method to generate formaldehyde from carbon dioxide at room temperature *via* a readily isolable bis(silyl)acetal, namely H₂C(OSiPh₃)₂, by a process that does not involve unnecessary overreduction.

While the aforementioned addition of the H–H bond to CO₂ is thermodynamically uphill, the corresponding reaction of a Si–H bond is favorable and can occur in a stepwise manner to afford a series of reduced products with different carbon oxidation levels, namely silyl formates (HCO₂SiR₃), silyl acetals (H₂C(OSiR₃)₂), methoxysilanes (R₃SiOCH₃), and methane. In this regard, we recently demonstrated that a system comprised of [Tism^{PrⁱBenz}]MgX (X = H, Me) and B(C₆F₅)₃ was effective for the selective hydrosilylation of CO₂ to the bis(silyl)acetal, H₂C(OSiPh₃)₂, which corresponds to reduction to the formaldehyde level. We have investigated this transformation further and have demonstrated that the catalytic system can be modified from the milligram to multigram scale, thereby allowing H₂C(OSiPh₃)₂ to be isolated in a pure crystalline form and in excellent yield. The ability to isolate H₂C(OSiPh₃)₂ in a crystalline form is of note because it enabled the first structure determination of a bis(silyl)acetal by X-ray diffraction. In addition to affording H₂C(OSiPh₃)₂, the approach also allows for the facile synthesis of isotopologues. For example, D₂C(OSiPh₃)₂, H₂¹³C(OSiPh₃)₂, and D₂¹³C(OSiPh₃)₂ have been synthesized by reactions that use the appropriate combinations of Ph₃Si(H/D) and (¹²C/¹³C)O₂.

Of most significance, we have demonstrated that H₂C(OSiPh₃)₂ can be readily converted to anhydrous, monomeric, formaldehyde. Specifically, formaldehyde is produced rapidly at room temperature by treatment of a solution of H₂C(OSiPh₃)₂ with CsF, which serves as an initiator to induce the release of (Ph₃Si)₂O. Since the oxidation state of carbon in both CH₂O and H₂C(OSiPh₃)₂ is zero, it is evident that this approach for the synthesis of formaldehyde from CO₂ manages redox changes in a much more efficient manner than one which involves the unnecessary overreduction to methanol at the C(-II) level. Furthermore, both steps in the formation of formaldehyde from CO₂ *via* H₂C(OSiPh₃)₂ may be performed at room temperature, in contrast to the elevated temperatures that are employed in the process that proceeds *via* methanol. Another noteworthy feature of the synthesis *via* H₂C(OSiPh₃)₂ is that the method generates monomeric formaldehyde in an aprotic solvent by a procedure that does not require either (i) thermal cracking of paraformaldehyde, alpha-polyoxymethylene or trioxane, or (ii) the use of acidic reagents. Moreover, the synthetic method can also be used as a very convenient means to produce a variety of isotopically labeled formaldehyde derivatives, *e.g.* D₂CO, H₂¹³CO, and D₂¹³CO.

2. Carbon Dioxide as a C₁ Source for Organic Chemicals via a Bis(silyl)acetal

In view of the fact that H₂C(OSiPh₃)₂ can be used to generate formaldehyde, we have investigated its ability to serve as a methylene source in which the carbon is derived from CO₂. Excellent evidence that H₂C(OSiPh₃)₂ may serve this role is provided by its ability to participate in a Wittig reaction to form a terminal olefin. For example, in the presence of CsF, H₂C(OSiPh₃)₂ reacts immediately with the phosphonium ylid MeOC(O)C(H)PPh₃ to afford methyl acrylate in quantitative yield at room temperature; benzyl acrylate can likewise be obtained by an analogous procedure employing PhCH₂OC(O)C(H)PPh₃. The importance of CsF in promoting this reaction is underscored by the fact that, in its absence, H₂C(OSiPh₃)₂ does not react with MeOC(O)C(H)PPh₃ over a period of 1 day at elevated temperature. It is also important to note

that the formation of MeOC(O)C(H)CH₂ does not require isolation of H₂C(OSiPh₃)₂, such that the conversion of CO₂ to MeOC(O)C(H)CH₂ can be performed in a single reaction vessel.

H₂C(OSiPh₃)₂ can also be used to form C–C single bonds. For example, H₂C(OSiPh₃)₂ reacts with 5,5-dimethyl-1,3-cyclohexanedione (dimedone) to afford 2,2'-methylenebis(5,5-dimethylcyclohexane-1,3-dione) (formaldomedone), in which the two dimedone moieties are coupled *via* a CH₂ group. In addition to forming C–C bonds, H₂C(OSiPh₃)₂ can also be used to produce C–N, C–O and C–S bonds, thereby providing a means to obtain products that correspond to both functionalization and reduction of CO₂. For example, H₂C(OSiPh₃)₂ can be used as a formaldehyde surrogate in the Pictet-Spengler reaction for the synthesis of heterocyclic compounds, as illustrated by the formation of 1,2,3,4-tetrahydro-beta-carboline (tryptoline) *via* the reaction with tryptamine hydrochloride.

H₂C(OSiPh₃)₂ is not only capable of delivering a methylene moiety, but it can also provide a CH moiety in the formation of benzazole derivatives, which are often components of drugs. For example, the benzimidazole motif may be readily constructed by the reaction of an *o*-phenylenediamine with H₂C(OSiPh₃)₂, as illustrated by the formation of *N*-methylbenzimidazole upon reaction of H₂C(OSiPh₃)₂ with *N*-methyl-1,2-phenylenediamine in DMSO. Moreover, benzothiazole is obtained from the reaction of 2-aminothiophenol with H₂C(OSiPh₃)₂.

The ability of H₂C(OSiPh₃)₂ to afford the above compounds not only demonstrates its synthetic utility, but the transformations are also of interest because they are associated with the complete deoxygenation of CO₂, which is in contrast to many other transformations of CO₂ in which at least one C–O bond is typically preserved.

The utility of the above method to synthesize isotopologues of formaldehyde is of significance because it provides a means to incorporate isotopic labels into molecules with biological and medicinal applications. In this regard, although carbon dioxide is considered to be the universal precursor for incorporating isotopic labels (¹¹C, ¹³C and ¹⁴C), direct approaches are otherwise limited due to the aforementioned low reactivity of this molecule. The conversion of carbon dioxide into isotopically labeled formaldehyde is, thus, of considerable interest since its greater reactivity facilitates the incorporation of a carbon label.

Publications Acknowledging this Grant in 2015-2018

This grant did not exist in 2015 and so the publications listed below correspond to the preceding grant.

(I) Exclusively funded by this grant

1. Zuzek, A. A.; Parkin, G. Oxidative Addition of SiH₄ and GeH₄ to Ir(PPh₃)₂(CO)Cl: Structural and Spectroscopic Evidence for the Formation of Products Derived from *Cis* Oxidative Addition. *Dalton Trans.* **2015**, *44*, 2801-2808 (DE-FG02-93ER14339).
2. Sattler, W.; Ruccolo, S.; Chaijan, M. R.; Nasr Allah, T; Parkin, G. Hydrosilylation of Aldehydes and Ketones Catalyzed by a Terminal Zinc Hydride Complex, [κ³-Tptm]ZnH *Organometallics* **2015**, *34*, 4717-4731 (DE-FG02-93ER14339).
3. Rong, Y.; Sambade, D.; Parkin, G. Molecular Structures of Tris(1-tert-butyl-2-mercaptoimidazolyl)hydroborate complexes of Titanium, Zirconium and Hafnium *Acta Cryst.* **2016**, *C72*, 806-812 (DE-FG02-93ER14339).
4. Green, M. L. H.; Parkin, G. The Covalent Bond Classification Method and its Application to Compounds that Feature Three-Center Two-Electron Bonds *Struct. Bond.* **2017**, *171*, 79-140 (DE-FG02-93ER14339).

(II) Jointly funded by this grant and other grants with leading intellectual contribution from this grant

5. Neary, M. C.; Parkin, G. Dehydrogenation, Disproportionation and Transfer Hydrogenation Reactions of Formic Acid Catalyzed by Molybdenum Hydride Compounds. *Chem. Sci.* **2015**, *6*, 1859-1865 (DE-FG02-93ER14339).
6. Neary, M. C.; Parkin, G. Nickel-catalyzed Release of H₂ from Formic Acid and a New Method for the Synthesis of Zerovalent Ni(PMe₃)₄ *Dalton Trans.* **2016**, *45*, 14645-14650 (DE-FG02-93ER14339).
7. Neary, M. C.; Parkin, G. Structural Characterization of the Nickel(II) Formate Complex, Ni(py)₄(O₂CH)₂•2py, and Re-evaluation of the Nitrate Counterpart, Ni(py)₄(ONO₂)₂•2py: Evidence for Non-Linear Nitrate Coordination *Polyhedron* **2016**, *116*, 189-196 (DE-FG02-93ER14339).
8. Neary, M. C.; Parkin, G. Reactivity of Cyclopentadienyl Molybdenum Compounds Towards Formic Acid: Structural Characterization of CpMo(PMe₃)(CO)₂H, CpMo(PMe₃)₂(CO)H, [CpMo(μ-O)(μ-O₂CH)]₂ and [Cp*Mo(μ-O)(μ-O₂CH)]₂ *Inorg. Chem.* **2017**, *56*, 1511-1523 (DE-FG02-93ER14339).
9. Rauch, M.; Parkin, G. Zinc and Magnesium Catalysts for the Hydrosilylation of Carbon Dioxide *J. Am. Chem. Soc.* **2017**, *139*, 13264-13267 (DE-FG02-93ER14339).
10. Neary, M. C.; Quinlivan, P. J.; Parkin, G. Zerovalent Nickel Compounds Supported by 1,2-Bis(diphenylphosphino)benzene: Synthesis, Structures and Catalytic Properties *Inorg. Chem.* **2018**, *57*, 374-391 (DE-FG02-93ER14339).
11. Al-Harbi, A.; Hammond, M. J.; Parkin, G. Organometallic Zirconium Compounds in an Oxygen-Rich Coordination Environment: Synthesis and Structural Characterization of Tris(oxoimidazolyl)hydroborato Zirconium Compounds *Inorg. Chem.* **2018**, *57*, 1426-1437 (DE-FG02-93ER14339).

Understanding Kinetics of Reconstructed Catalyst Surfaces to Build Reactivity Descriptors

Felipe Polo-Garzon,¹ Victor Fung,² Yongqiang Cheng,³ Luke L. Daemen,³ Anibal J. Ramirez-Cuesta,³ Miaofang Chi,² Franklin Tao,⁴ De-en Jiang,⁵ Zili Wu^{1,2}

¹Chemical Sciences Division, ²Center for Nanophase Materials Sciences, ³Neutron Scattering Division, Oak Ridge National Laboratory, Oak Ridge, TN 37831; ⁴Department of Chemical Engineering and Chemistry, The University of Kansas, Lawrence, KS 66047; ⁵Department of Chemistry, University of California, Riverside, CA 92521

The overarching goal of our catalysis program is to control reaction pathways and enhance catalyst performances through detailed tuning of synergistic active sites. Reconstructed catalyst surfaces, far from ideal models, are often present under reaction conditions and we have aimed to characterize and manipulate the active sites on these reconstructed surfaces to tailor selectivity and boost rates. Three projects are covered in this presentation. First, we studied the underlying reasons that make a set of catalysts with the same elemental composition, but undergoing different synthesis and post-synthesis treatments, have different catalytic performances for select reactions. These different performances were found to be rooted on surface reconstructions. The surface reconstruction for a set of SrTiO₃ perovskites was studied, including the segregation of cations at the surface and the creation of highly active step-sites. The implications of this surface reconstruction for acid/base catalysis and CH₄ activation (combustion and oxidative coupling) will be presented.¹⁻² Second, we used a multi-modal approach involving computational and experimental techniques (including neutron scattering) to resolve the reaction mechanism for the high-temperature water-gas shift (WGS) reaction over the operating (reconstructed) surface of an industrial-type catalyst, CuCrFeO_x. Our work shows a ‘redox’ mechanism operating on the reconstructed catalyst surface and has settled a long-standing debate in the catalysis community.³ Third, we investigated the promotion of strong metal-support interactions (SMSIs) under the presence of a common organic compound. The tunability of these SMSIs is explored to untap better catalytic performances for CO oxidation. The understanding of surface reconstructions for a set of catalysts has naturally led to the establishment of reactivity descriptors. Future work will focus on establishing a feedback loop between experimentally- and computationally-derived reactivity descriptors of C-H activation in methane for a set of mixed-metal oxides with different elemental compositions. The reactivity of these catalysts will be measured in terms of intrinsic turnover frequencies with the aim of bridging the gap between computational predictions and experimental reaction rates.

FWP ERKCC96: Fundamentals of Catalysis and Chemical Transformations. For a full description of recent progress see Extended Abstract for ERKCC96.

References

1. Polo-Garzon, F.; Fung, V.; Liu, X.; Hood, Z. D.; Bickel, E. E.; Bai, L.; Tian, H.; Foo, G. S.; Chi, M.; Jiang, D.-e.; Wu, Z. *ACS Catal.* **2018**, *8* (11), 10306-10315.
2. Bai, L.; Polo-Garzon, F.; Bao, Z.; Luo, S.; Moskowitz, B. M.; Tian, H.; Wu, Z. *ChemCatChem* **2019**, *11* (8), 2107-2117.
3. Polo-Garzon, F.; Fung, V.; Nguyen, L.; Tang, Y.; Tao, F.; Cheng, Y.; Daemen, L. L.; Ramirez-Cuesta, A. J.; Foo, G. S.; Zhu, M.; Wachs, I. E.; Jiang, D.-e.; Wu, Z. *J. Amer. Chem. Soc.* **2019**, *141* (19), 7990-7999.

Characterization of, and Hydrocarbon Functionalization with, Lattice-Confined Reactive Intermediates

David C. Powers
Texas A&M University, Department of Chemistry

Presentation Abstract

Reactive metal–ligand (M–L) multiply bonded species, such as metal nitrides, oxos, and nitrenes, are critical reactive intermediates in both synthetic and biological C–H functionalization chemistry. The exquisite reactivity of intermediates capable of functionalizing C–H bonds renders these transient intermediates 1) challenging to observe or characterize and 2) difficult to harness for selective intermolecular C–H functionalization, such as during oxidative hydrocarbon upgrading. Metal-organic frameworks (MOFs), which are chemically manipulable porous materials, have garnered interest as potential platforms for hydrocarbon oxidation catalysis due to the potential to utilize substrate confinement within proximity of lattice-confined catalysts to enforce intermolecular group-transfer chemistry. This poster will detail efforts in our laboratory to develop new inorganic photochemical methods that enable direct structural characterization of reactive M–L multiply bonded species, as well as fundamental studies of the diffusional barriers that must be managed during intermolecular functionalization chemistry within porous catalyst materials. In particular, structural characterization of a Rh₂ nitrenoid relevant to C–H amination will be presented and progress towards the use of kinetic isotope effects as diffusion reporters in hierarchically porous catalyst materials will be detailed.

DE-SC0018977: Lattice-Templated Catalysts for Selective Hydrocarbon Upgrading

Student(s): Anuvab Das, Chen-Hao Wang, Gerard Van Trieste

RECENT PROGRESS

Synthesis of New Catalyst Platforms. *Templating Metastable Pd₂ Carboxylate Aggregates.* Evaluation of the potential for metal–metal (M–M) cooperation to enable catalysis requires access to specific polynuclear aggregates that display appropriate geometry and size. In many cases, exerting synthetic control over the aggregation of simple metal salts is a challenge. For example, Pd(II) acetate self-assembles as a trimer (*i.e.* Pd₃(OAc)₆) both in the solid state and in solution and does not feature close Pd–Pd interactions. Related carboxylate-supported Pd₂ aggregates (*i.e.* Pd₂(OAc)₄), which would feature close Pd–Pd interactions, are thermodynamically metastable in solution phase and thus largely unavailable. We demonstrate ion metathesis within pre-formed metal-organic frameworks (MOFs) to prepare metastable Pd₂ tetracarboxylates sites (Figure 1). The newly synthesized materials are characterized by elemental analysis, PXRD, SCXRD, EXAFS, XANES, and gas adsorption analysis. In addition, the critical role of network solvation on the kinetics of ion metathesis was revealed by coupled TGA-MS and ICP-MS experiments. The demonstration of templated ion metathesis to generate specific metastable coordination sites that

are inaccessible in solution phase chemistry represents a new opportunity to interrogate the chemistry of specific polynuclear metal aggregates.

Metallopolymerization to Translate Ligand-Modulated Chemoselectivity to Porous Catalysts

Porous catalysts have garnered substantial interest as potential platforms for group-transfer catalysis due to the ability to non-covalently co-localize substrates in proximity to site-isolated reactive intermediates. In contrast to soluble molecular catalysts, the limited synthetic toolbox available to prepare porous catalysts presents a formidable challenge to controlling the primary coordination sphere of lattice-confined catalysts and thus modulating the electronic structures of reactive catalyst intermediates. We have developed new

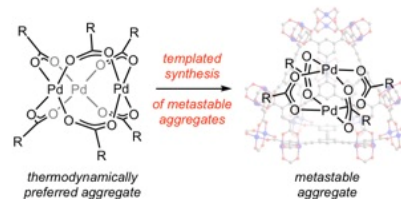


Figure 1. Ion methathesis within pre-formed template lattices provides access to Pd₂ sites that are metastable, and thus unavailable, in solution-phase chemistry.

synthetic methods to provide access to Ru₂-based porous materials in which the primary coordination sphere of the Ru₂ catalyst sites can be systematically varied (Figure 2). The method utilizes Sonogashira cross-coupling chemistry, a strategy common to the synthesis of porous organic polymers (POPs), to prepare a family of porous metallopolymers. The obtained materials are permanently porous (determined by N₂ uptake) and were characterized by IR, elemental analysis, gas sorption, powder X-ray diffraction, thermogravimetric analysis, X-ray absorption spectroscopy, and diffuse-reflectance UV-vis-NIR spectroscopy. X-ray absorption spectroscopy measurements confirm that both the valence and local coordination geometry are maintained during polymerization. The resulting porous materials are competent catalysts for nitrene-transfer chemistry and the chemoselectivity for allylic amination versus olefin aziridination can be tuned by modulating the primary coordination sphere of the catalyst sites.

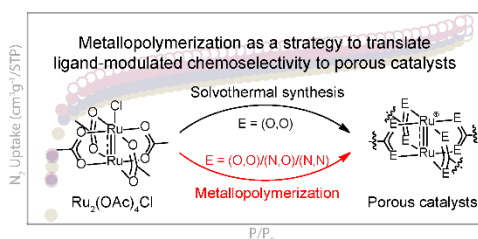


Figure 2. Five Ru₂L₄BF₄ complexes, featuring carboxylate (L = 4-I-OBz), amidate (L = 4-I-HNBz), 2-oxypyridinate (L = 4-I-hp or 5-I-hp), and 2-aminopyridinate (L = 4-I-ap) ligands, were prepared by a two-step procedure of ligand substitution and anion exchange. Ru₂-based porous polymers were synthesized from Sonogashira cross-coupling reaction between Ru₂ metallomonomers and alkyne-based linkers.

***In Operando* Characterization of Group Transfer Chemistry. Analysis of Diffusion in Hierarchically Porous Metal-Organic Framework Catalysts.** We have developed an experiment based on comparison of *intra*- and *intermolecular* kinetic isotope effects (KIEs) to evaluate the relative rates of diffusion and substrate functionalization in porous materials. Specifically, we demonstrated that diffusion of substrates in [Ru₆btc₄(N₃)₃] is the rate-determining step in toluene amination. We are now utilizing the developed experimental approach to understand the impact of material mesostructure on the mobility of substrate molecules during interstitial catalysis. To this end, we have prepared a family of mesoporous Ru₂-based materials by using a mixed-ligand feed comprised of benzene-1,3,5-tricarboxylic acid (H₃btc) and pyridine-3,5-dicarboxylic acid (H₂pydc). The resulting materials (def-Ru₆btc₄Cl₃) are isostructural (by PXRD) and feature different mesopore surface areas (by N₂ isotherms). Similar to the parent btc-derived material,

chloride-for-azide exchange in these materials is facile. Preliminary experiments indicate that toluene amination is viable with the family of mesoporous materials that have been prepared. Examination of the *intra*- and *intermolecular* kinetic isotope effects for nitrogen-atom transfer indicates that the intramolecular isotope effect decreases with increasing mesoporosity and the intermolecular isotope effect increases with increasing mesoporosity (Figure 3). These data indicate that toluene is effectively less confined as the mesoporous surface area increases. We anticipate these experiments will provide experimental probes to understand how to avoid diffusional issues in interstitial hydrocarbon oxidation catalysis.

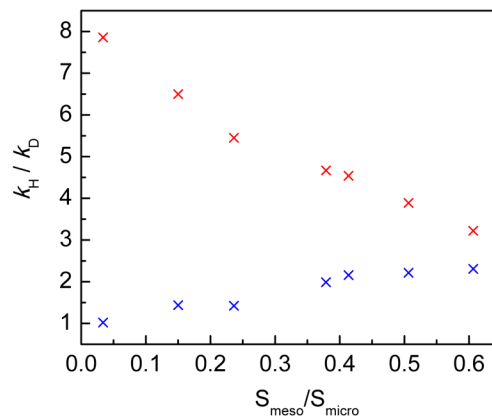


Figure 3. Intra- (x) and intermolecular (x) KIEs, determined for amination of d_1 -toluene and mixtures of d_8 - and H_8 -toluene, respectively, as a function of mesoporous surface area in mesoporous Ru_3btc_2 .

Publications Acknowledging this Grant in 2015-2018

No 2015-2018 publications to report.

Solvent Effects on Elementary Steps in Solid Acid Catalyzed Reactions: Acid-Base Interactions

Robert M. Rioux^{1,2}, Yanyu Mu¹, Susanna Ogozaly², William A Elliott¹, Christopher Titman¹
¹Department of Chemical Engineering, The Pennsylvania State University, University Park, PA
²Department of Chemistry, The Pennsylvania State University, University Park, PA

Presentation Abstract

Many biomass valorization reactions, such as bio-oil upgrading are conducted in liquid-phase and require acid-catalyzed conversion steps. Solvents influence the reaction rate of homogeneous and heterogeneous catalytic reactions by impacting the stability of reactants, products and transition states differently through solvation effects.¹ In this work, we investigated the influence of solvent effects on the activity of Brønsted acid sites in zeolite micropores. We measured the *apparent* heat of adsorption between pyridine and the Brønsted acid sites (BAS) in H-ZSM-5 in different solvents and solvent mixtures using isothermal titration calorimetry (ITC). ITC enables the complete thermodynamic profile (ΔG , ΔH , ΔS , n) to be determined from a single experiment. ITC experiments demonstrate the choice of the solvent strongly affects the apparent adsorption thermodynamics of pyridine on zeolite. The differences in apparent adsorption enthalpy measured in liquid-phase were evaluated through a Born-Haber cycle in the different solvents; gas-phase adsorption and solution thermodynamic properties measurements were conducted to construct the cycle. We found certain solvents yielded differing apparent heats of adsorption with varying Si/Al ratio in MFI, suggesting that solvent interactions may differ with the extent of hydrophilicity. Polar solvents (water and acetonitrile) were the most sensitive to Si/Al ratio, while the heat of adsorption measured for pyridine in water was invariant to the same ratio. Equilibrium adsorption isotherms confirm the formation of 1:1 pyridine-Brønsted acid adduct in all solvents, demonstrating changes in adsorption energies are not associated with acid site availability but the influence of solvent interactions with acid site.

DE-SC0016192: Catalytic Reactions at Solid-Liquid Interfaces: Solvent Effects on Activity, Selectivity and Reaction Mechanisms

PI: Robert M Rioux

Postdoc(s): N/A

Student(s): Yanyu Mu, Susanna Ogozaly, William Elliott, Christopher Titman

Affiliations(s): Pennsylvania State University

RECENT PROGRESS

Solvent effects on acid-base interactions distinguish differences in acid site strength in zeolite voids

To understand solvent effects on acid-base interactions in confined zeolite pores, we used isothermal titration calorimetry (ITC) to measure the apparent enthalpy of interactions between base (pyridine and isopropylamine) and Brønsted acid sites (BAS) in H-ZSM-5 in different solvents. We developed Born-Haber cycles to de-convolute the adsorption of pyridine on H-ZSM-

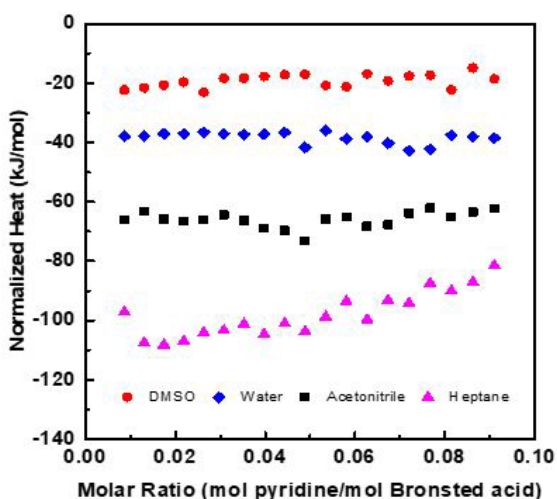


Figure 1. Measured enthalpies for binding pyridine to H-ZSM-5(Si/Al=11.5) at 25 °C in DMSO(circle), Water(diamond), Acetonitrile(square), and Heptane (triangle).

ITC experiments demonstrate the choice of the solvent strongly affects adsorption thermodynamics of pyridine on zeolite and the result is summarized in Figure 1. The adsorption enthalpy of pyridine on H-ZSM-5 at 298 K varied from -19 to -98 kJ/mol as the polarity of the solvent (DMSO, H₂O, CH₃CN, C₇H₁₆) decreased. We also investigated the influence of Si/Al on the measured heat of acid-base interactions in the presence of solvents. In H₂O, high Si/Al zeolites had larger heat of adsorption for pyridine compared to more Al-rich H-ZSM-5. We understand the origin of apparent heat measured in liquid phase by constructing a Born-Haber cycle. In the gas phase, the adsorption heat of pyridine on H-ZSM-5 is -224 kJ/mol at 200°C, while heptane adsorbs with -140 kJ/mol at 25°C, respectively. The heat of adsorption of heptane on H-ZSM-5, pre-adsorbed with pyridine is -47 kJ/mol at 25°C. The heat of mixing pyridine with heptane is measured to be +7.3 kJ/mol by solution calorimetry. The amount of pyridine adsorbed on H-ZSM-5 (Si/Al = 11.5) is measured to be 0.7 mmol/g in the gas phase at 200°C. The amount of heptane adsorbed on H-ZSM-5 is estimated to be 1.29 mmol/g according to the pore volume of H-ZSM-5 (0.19cm³/g) and the liquid density of heptane. The estimated enthalpy of pyridine adsorption on H-ZSM-5 in the gas phase is -264 kJ/mol, 40 kJ/mol higher than what we measured. Future effort will focus on Born-Haber cycles for the other solvents and understanding the non-linear influence

of solution composition (mixtures of CH₃CN and H₂O) on the apparent of heat of adsorption of pyridine by ITC.

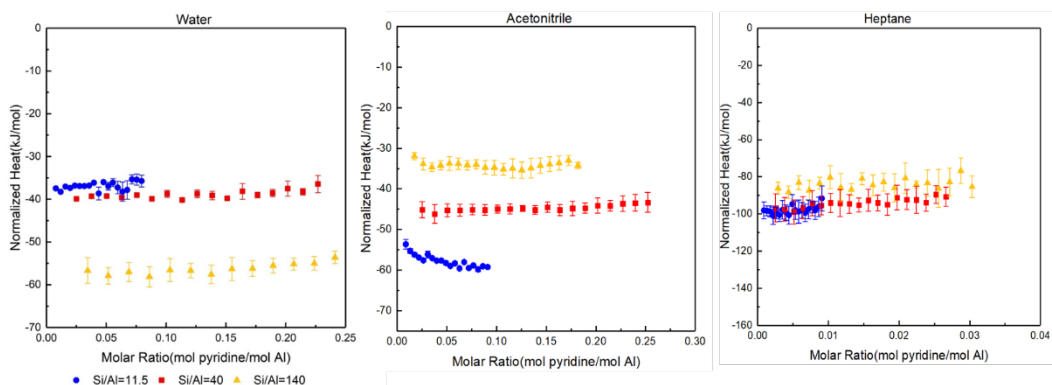


Figure 3. ITC thermograms for binding pyridine on H-ZSM-5 (Si/Al =11.5 (circle), 40 (square) and 140 (triangle)) at 25 °C in water, acetonitrile and heptane.

Thermograms for binding pyridine on three different H-ZSM-5 (Si/Al =11.5, 40 and 140) at 25 °C in water, acetonitrile and heptane are shown in Figure 3. The apparent enthalpies of binding pyridine on hydrophilic H-ZSM-5 (Si/Al =11.5 and 40) in water are about -38~-40 kJ/mol but the apparent enthalpy of binding pyridine on hydrophobic H-ZSM-5 (Si/Al =140) in water is about -60 kJ/mol. This is probably because hydrophilic zeolite (Si/Al = 11.5) has a much larger water uptake than hydrophobic zeolite (Si/Al =140). Water molecules stabilize the initial state via forming hydrogen bonds with protons in hydrophilic zeolite (Si/Al = 11.5) which decreases the apparent enthalpy of acid base interactions. In heptane, the apparent enthalpy of binding pyridine on hydrophobic H-ZSM-5 (Si/Al = 140) is about -84 kJ/mol but the apparent enthalpy of binding pyridine on hydrophilic zeolites are -98 for H-ZSM-5 (Si/Al = 11.5) and -94 kJ/mol for H-ZSM-5 (Si/Al = 40). This is probably because the main interaction between zeolite framework and heptane is van der Waals force. For the zeolite with different Si/Al ratio, the uptake of heptane can be estimated to be the same based on the pore volume of the zeolite and the liquid density of heptane. The interaction between heptane and hydrophobic zeolite is more favorable than hydrophilic zeolites which is reflected in the measured differential heats in gas phase which are -140 kJ/mol for Si/Al = 11.5, -134 kJ/mol for Si/Al = 40 and -154 kJ/mol for Si/Al=140. Heptane molecules stabilize the initial state via van der Waals interactions with the framework of the hydrophobic zeolite (Si/Al = 140) which decreases the apparent enthalpy of acid base interactions.

Publications Acknowledging this Grant in 2015-2018

(XXXVII) Exclusively funded by this grant

1. C. S. Sievers, Y. Noda, L. Qi, E. M. Albuquerque, R. M. Rioux, S. L. Scott. Phenomena in Catalytic Reactions at Solid-Liquid Interfaces. *ACS Catal.* **6** (2016) 8286-8307.
2. Y. Noda, K. Li, A. Engler, W. A. Elliott, R. M. Rioux. Development of Robust Sulfur Quantification and Speciation Method for SBA-15 Supported Sulfonic Acid Catalysts. *Catal. Sci. Technol.* **6** (2016) 5961-5971.
3. C. S. Spanjers, P. Guillo, M. J. Janik, T. D. Tilley, R. M. Rioux. Identification of Second Shell Coordination in Transition Metal Species Using Theoretical XANES: Example of Ti-O-(C,Si,Ge) Complexes. *J. Phys. Chem. A* **121** (2017) 162-167.

(XXXVIII) Jointly funded by this grant and other grants with leading intellectual contribution from this grant

1. M. E. Strayer, T. P. Senftle, J. P. Winterstein, N. M. Vargas-Barbosa, R. Sharma, R. M. Rioux, M. J. Janik, T. E. Mallouk. Charge Transfer Stabilization of Late Transition Metal Oxide Nanoparticles on a Layered Niobate Support. *J. Am. Chem. Soc.* **137** (2015) 16216-16224.
2. B. Panthi, A. Mukhopadhyay, L. Tibbits, J. Saavedra, C. J. Pursell, R. M. Rioux, B. D. Chandler. Using Thiol Adsorption on Supported Au Nanoparticle Catalysts to Evaluate Au Dispersion and the Number of Active Sites for Benzyl Alcohol Oxidation. *ACS Catal.* **5** (2015) 2232-2241.
3. L Qi, R. Alamillo, W. A. Elliott*, A. Andersen, D. W. Hoyt, E. D. Walter, K. S. Han, N. M. Washton, R. M. Rioux, J. A. Dumesic, S. L. Scott. Operando Solid-State NMR Observation of Solvent-Mediated Adsorption-Reaction of Carbohydrates in Zeolites, *ACS Catal.* **7** (2017) 3489-3500.
4. G. Kumar, L. Tibbits, J. Newell, B. Panthi, A. Mukhopadhyay*, R. M. Rioux, C. J. Pursell, M. Janik, B. D. Chandler. Evaluating differences in the active-site electronics of supported Au nanoparticle catalysts using Hammett and DFT studies. *Nature Chem.* **3** (2018) 268-274.
5. Y. Yang, J. W. Chang, R. M. Rioux, Structural elucidation of supported Rh complexes derived from RhCl (PPh₃)₃ immobilized on surface-functionalized SBA-15 and their catalytic performance for C-heteroatom (S, O) bond formation. *J. Catal.* **365** (2018) 43-54.

(XXXIX) Jointly funded by this grant and other grants with relatively minor intellectual contribution from this grant;

1. S. J. P. Varapragasam, C. Balasanthiran+, A. Gurung, Q. Q. Qiao, R. M. Rioux, J. D. Hoefelmeyer. Kirkendall Growth of Hollow Mn₃O₄ Nanoparticles upon Galvanic Reaction of MnO with Cu²⁺ and Evaluation as Anode for Lithium-Ion Batteries. *J. Phys. Chem. C* **121** (2017) 11089-11099.
2. C. Balasanthiran, S. Jensen, C. S. Spanjers, S. J. P. Vararagasam, R. M. Rioux, D. Kilin, J. D. Hoefelmeyer. Quantitative Attachment of Bimetal Combinations of Transition Metal Ions to the Surface of TiO₂ Nanorods. *Langmuir* **34** (2018) 5422-5434.

Activation of Atomically-dispersed Oxometal Catalysts for Olefin Transformations

Susannah L. Scott,¹ Albert E. Stiegman,² Baron Peters^{1,3}

¹ Department of Chemical Engineering, University of California, Santa Barbara

² Department of Chemistry, Florida State University

³ Department of Chemical Engineering, University of Illinois, Urbana-Champaign

Abstract

A major category of catalysts used in olefin transformations (metathesis, oligomerization, isomerization, polymerization) consists of transition metal ions (e.g., Cr(VI), Mo(VI), W(VI), Re(VIII)) that are atomically-dispersed on an oxide support (e.g., silica, alumina). The initially fully inorganic sites, which possess terminal metal-oxo bonds as well as M-O bonds to the support, activate spontaneously, by forming metal-carbon bonds in the presence of the olefin. The nature of the inorganic precursor sites and the mechanisms for their transformation to organometallic active sites were probed through a combination of spectroscopy, kinetic and product analysis, and computational modeling.

Grant or FWP Number: DE-FG02-03ER15467

Grant Title Hierarchical Design of Supported Organometallic Catalysis for Hydrocarbon Transformations

Postdoc(s): Fan Zhang (UCSB)

Student(s): Li Li (UCSB), Zachary Jones (UCSB), Michael Spears (UCSB), Craig Vandervelden (UCSB), Salman Khan (UCSB), Abigail Serrano (UCSB), David Jeffcoat (FSU), Nathan Peek (FSU)

RECENT PROGRESS

Spectroscopic and mechanistic studies of atomically dispersed catalysts. We have addressed, through detailed spectroscopic studies, a central question that exists for Cr(VI) sites supported on silica, which is whether two structurally different active sites coexist on the silica surface and participate in catalysis: a mono-oxo and a di-oxo site. Studies of the electronic structure of the Cr(VI) site, using UV-visible spectroscopy, supported with time-dependent density functional calculations, showed that the observed spectral features can be completely assigned by transitions associated with the di-oxo site. Moreover, calculations of the anticipated spectrum of the mono-oxo site indicate that it would have transitions at much lower energy than are observed, ruling it out as a contributor to the surface structure. Using complementary studies using Raman and Resonance Raman spectroscopy, coupled with a normal coordinate analysis, we were able to assign all of the observed Raman bands to normal modes of the di-oxo site. The study was comprehensive in that all Raman bands reported in different studies were analyzed using this model and all are in good agreement with the di-oxo model. Resonance Raman studies over a range of excitation wavelengths demonstrate unambiguously that bands previously assigned to a mono-oxo site are the result of a photo-degradation process.

We also advanced the understanding of activation in the MoO₃/SiO₂ olefin metathesis catalyst. In the conventionally prepared catalyst, a wide distribution of Mo(VI) sites are present, the majority of which are not active. A minority dioxomolybdenum site, Mo(=O)₂(-OSi≡)₂, is proposed to be the immediate precursor of the active site, which is suggested to be transformed by direct reaction with an olefin via a pseudo-Wittig mechanism. To investigate the connection between the pseudo-tetrahedral Mo(=O)₂(-OSi≡)₂ structure and the activation mechanism, we synthesized and characterized a well-defined version of silica-supported Mo(=O)₂(-OSi≡)₂ by anhydrous grafting of MoO₂(OR)₂ onto dry silica. Unexpectedly, this material failed to initiate propylene self-metathesis at temperatures ranging from 20 to 200 °C. However, exposure to olefins at much higher temperatures (> 500 °C) activates the precatalyst, allowing metathesis reactions to proceed at 20 °C. The fraction of resulting active sites, measured by the Chauvin-Commereuc method, can be as high as 36%. The activation of Mo(=O)₂(-OSi≡)₂ therefore has a significant energy barrier.

Perrhenate dispersed on γ -alumina is a very active olefin metathesis catalyst which spontaneously generates active sites (presumably carbenes) to catalyze olefin metathesis upon exposure to an olefin at near-ambient temperatures. We investigated the kinetics of activation of ReO_x/ γ -Al₂O₃ in propylene metathesis using a batch reactor, to facilitate measurement of precise rate constants. By observing the kinetics of activation by conducting propylene metathesis in a constant-temperature batch reactor, the activation barrier was measured to be (54.3 \pm 5.7) kJ/mol. This barrier is too low to be credibly associated with the widely-assumed pseudo-Wittig mechanism. The observation of a significant kinetic isotope effect provides evidence against this mechanism, which is further supported by IR demonstrating the absence of the pseudo-Wittig products formaldehyde or acetaldehyde. The formation of excess ethylene (ca. 1.5 times the number of active sites), as well as the absence of branched C₅ and C₆ products, are consistent with an allylic-H activation path.

Molecular complexes such as methyltrioxorhenium (MTO) are inactive as single-component metathesis catalysts, but activation by a Lewis acidic support leads even higher initial activities than catalysts based on perrhenate. The support plays a key role in determining both activity and stability in olefin metathesis. However, the organometallic system still suffers from low activation efficiency (in terms of the fraction of active sites), suggesting that the properties of the activator may be more important than the identity of the metal complex in this class of supported catalysts. We investigated how the local grafting environment affects the performance of MTO. The simple replacement of γ -Al₂O₃ by a mostly amorphous Al₂O₃ (*a*-Al₂O₃) results in a doubling of the number of active sites and much higher initial activity for grafted MTO. IR and 2D NMR spectra provide evidence of interactions between adsorbed MTO and the surface hydroxyls of alumina. The abundant basic (terminal) hydroxyls of γ -Al₂O₃ suppress tautomerization simply by coordinating to Re. Amorphous alumina, with more and stronger Lewis acid sites and a lower population of surface hydroxyl groups, promotes tautomerization in the presence of olefin, activating a much higher fraction of grafted Re sites. Thus isolated strong Lewis sites (i.e., Lewis acid sites remote from hydroxyl groups) which are relatively more abundant on *a*-Al₂O₃ are responsible for activating and stabilizing grafted MTO.

Nuclearity effect in supported Ga clusters for propane dehydrogenation. The reactions of Ga(*i*-Bu)₃ with the dehydrated and partially dehydroxylated surfaces of alumina and silica were studied by IR, high field solid-state NMR and EXAFS spectroscopies, as well as elemental analysis. Grafting onto Al₂O₃ occurs selectively by protonolysis at individual surface hydroxyl groups, resulting in the formation of mononuclear [(≡AlO)Ga(*i*-Bu)₂L] (L = surface oxygen) sites

as the major surface organometallic entities. Conversely, grafting on silica affords dinuclear species $[(\equiv\text{SiO})_2\text{Ga}_2(i\text{-Bu})_3]$ by a combination of protonolysis and isobutyl group transfer to Si. Further evidence for the difference in nuclearity was obtained by analysis of the WT-EXAFS. The mononuclear alumina-supported Ga sites show much higher activity in propane dehydrogenation than their dinuclear silica-supported counterparts. The propane dehydrogenation reaction may require the presence of Al–O–Ga bonds to promote heterolytic C–H bond activation. Comparisons with benchmark catalysts show that the effect of the catalyst diluent is significant under the reaction conditions and must be carefully assessed in order to attribute reactivity correctly.

Computational modeling of amorphous catalytic materials. Predicting the overall kinetics of catalysts on amorphous supports requires that we overcome two challenges: (1) we must understand how catalyst preparation history shapes the distribution of active sites, and (2) we must average over potentially large variations in site activity because the overall activity may be due to a small minority of sites. In pursuit of goal (1), we learned how variations in hydroxyl arrangement, specifically, the dihedral angle between vicinal silanols, influence the grafting of TiCl_4 onto amorphous silica and correctly predict experimental observations of this reaction. We developed machine learning tools that use *ab initio* calculations to parameterize a population balance model of the catalyst grafting process. In pursuit of goal (2), we developed rare events tools to efficiently compute site averaged kinetics given the grafted site distribution.

Publications Acknowledging this Grant in 2015-2018

(XL) Exclusively funded by this grant

- B. Peters, S.L. Scott, Single Atom Catalysts on Amorphous Supports: A Quenched Disorder Perspective. *J. Chem. Phys.* **2015**, *142*, 104708.
- A. Fong, Y. Yuan, S.L. Ivry, S.L. Scott, B. Peters, Computational Kinetic Discrimination of Ethylene Polymerization Mechanisms for the Phillips (Cr/SiO_2) Catalyst. *ACS Catal.* **2015**, *5*, 3360-3374.
- B. Goldsmith, T. Hwang, S. Seritan, B. Peters, S.L. Scott, Rate-Enhancing Roles of Water Molecules in Methyltrioxorhenium-Catalyzed Olefin Epoxidation by Hydrogen Peroxide. *J. Am. Chem. Soc.* **2015**, *137*, 9604-9616.
- C. Brown, J. Krzystek, R. Achey, R. Fu, R. Meulenberg, M. Polinski, N. Peek, Y. Wang, L. van de Burgt, S. Profeta, A.E. Stiegman, S.L. Scott, Mechanism of Initiation in the Phillips' Ethylene Polymerization Catalyst: Redox Processes Leading to the Active Site. *ACS Catal.* **2015**, *5*, 5574-5583.
- D.C. Collier, B.C. Vicente, S.L. Scott, Rapid Extraction of Quantitative Kinetic Information from Variable-Temperature Reaction Profiles. *Chem. Eng. J.* **2016**, *303*, 183-192.
- A. Fong, B. Peters, S.L. Scott, One-Electron Redox Activation of the Reduced Phillips Polymerization Catalyst via Alkylchromium(IV) Homolysis: A Computational Assessment. *ACS Catal.* **2016**, *6*, 6073-6085.
- C. Brown, A. Lita, M. Crosswhite, Y. Tao, M. Mileham, J. Krzystek, R. Achey, R. Fu, M. Polinski, N. Peek, Y. Wang, L. van de Burgt, S. Profeta, A.E. Stiegman, S.L. Scott, Mechanism of Initiation in the Phillips Ethylene Polymerization Catalyst: Ethylene Activation by Cr(II) and the Structure of the Resulting Active Site. *ACS Catal.* **2017**, *7*, 7442.
- A. Fong, C. Vandervelden, S.L. Scott, B. Peters, Computational Support for Phillips Catalyst Initiation via Cr-C Bond Homolysis in a Chromacyclopentane Site. *ACS Catal.* **2018**, *8*, 1728-1733.

- N. Peek, D.B. Jeffcoat, C. Moisii, L. van de Burgt, S. Profeta, S.L. Scott, A.E. Stiegman, A Reassessment of the Electronic Structure of Cr(VI) Sites Supported on Amorphous Silica and Implications for Cr Coordination Number. *J. Phys. Chem. C* **2018**, *122*, 4349-4358.
- C. Moisii, D. Jeffcoat, N. Peek, L. van de Burgt, S.L. Scott, A. E. Stiegman, Do Mono-Oxo Sites Exist in Silica-Supported Cr(VI) Materials? Reassessment of the Resonance Raman Spectra. *J. Phys. Chem. C* **2018**, *122*, 17149-17160.
- (XLI) *Jointly funded by this grant and other grants with leading intellectual contribution from this grant*
- K.C. Szeto, A. Gallo, S. Hernández-Morejudo, U. Olsbye, F. Lefebvre, L. Delevoye, R.M. Gauvin, S.L. Scott, M. Taoufik, Selective Grafting of Ga(*i*-Bu)₃ on Mesoporous H-ZSM-5 by Surface Organometallic Chemistry for Catalytic Propane Aromatization. *J. Phys. Chem. C* **2015**, *119*, 26611-26619.
- T.D. Nguyen, Z.R. Jones, B.R. Goldsmith, W.R. Buratto, G. Wu, B. Peters, S.L. Scott, T.W. Hayton, A Cu₂₅ Nanocluster with Metallic Copper Character. *J. Am. Chem. Soc.* **2015**, *137*, 13319-13324.
- T.-A. D. Nguyen, B. R. Goldsmith, H. T. Zaman, G. Wu, B. Peters, and T. W. Hayton, Synthesis and Characterization of a Cu₁₄ Hydride Cluster Supported by Neutral Donor Ligands, *Chem. Eur. J.* **2015**, *21*, 2351.
- T. Bligaard, R.M. Bullock, C.T. Campbell, J.G. Chen, B.C. Gates, R.J. Gorte, C.W. Jones, W.D. Jones, J.R. Kitchin, S.L. Scott, Toward Benchmarking in Catalysis Science: Best Practices, Challenges, and Opportunities. *ACS Catal.* **2016**, *6*, 2590-2602.
- A. Gallo, A. Fong, K.C. Szeto, J. Rieb, L. Delevoye, R.M. Gauvin, M. Taoufik, B. Peters, S.L. Scott, Ligand Exchange-Mediated Activation and Stabilization of a Re-based Olefin Metathesis Catalyst by Chlorinated Alumina. *J. Am. Chem. Soc.* **2016**, *138*, 12935-12947.
- T.D. Nguyen, Z.R. Jones, D.F. Leto, G. Wu, S.L. Scott, T.W. Hayton, Ligand-Exchange-Induced Growth of an Atomically Precise Cu₂₉ Nanocluster from a Smaller Cluster. *Chem. Mater.* **2016**, *28*, 8385-8390.
- B.R. Goldsmith, B. Peters, J.K. Johnson, B.C. Gates, S.L. Scott, Beyond Ordered Materials: Understanding Catalytic Sites on Amorphous Solids. *ACS Catal.* **2017**, *7*, 7543-7557.
- D. B. K. Chu, J. S. Owen, and B. Peters, Nucleation and Growth Kinetics from LaMer Burst Data. *J. Phys. Chem. A* **2017**, *121*, 7511.
- A.W. Cook, Z. Jones, G. Wu, S.L. Scott, T.W. Hayton, An Organometallic Cu₂₀ Nanocluster: Synthesis, Characterization, Immobilization on Silica, and “Click” Chemistry. *J. Am. Chem. Soc.* **2018**, *140*, 394-400.
- K.C. Szeto, N. Merle, C. Rios, A. Gallo, Z.R. Jones, L. Delevoye, R.M. Gauvin, S.L. Scott, M. Taoufik, A Strong Support Effect in Selective Propane Dehydrogenation Catalyzed by Ga(*i*-Bu)₃ Grafted onto Silica and □-Alumina. *ACS Catal.* **2018**, *8*, 7566-7577.
- F. Zhang, K. C. Szeto, M. Taoufik, L. Delevoye, R.M. Gauvin, S.L. Scott, Enhanced Metathesis Activity and Stability of Methyltrioxorhenium on a Mostly Amorphous Alumina: Role of the Local Grafting Environment. *J. Am. Chem. Soc.* **2018**, *140*, 13854-13868.
- (XLII) *Jointly funded by this grant and other grants with relatively minor intellectual contribution from this grant*
- F. Che, J.T. Gray, S. Ha, N. Kruse, S.L. Scott, J.-S. McEwen, The Role of the Electric Field in Catalysis: A Perspective. *ACS Catal.* **2018**, *8*, 5153-5174.

Sanjaya D. Senanayake

**Pathways for Methanol Synthesis from the Conversion of C-H bonds over
Well-defined Metal-Oxide Surfaces**

Sanjaya D. Senanayake, Feng Zhang, Zongyuan Liu, Ivan Orozco, Luis E. Betancourt
Ping Liu, Jose A. Rodriguez

Chemistry Department, Brookhaven National Laboratory, Upton, NY

Methane remains a valuable yet underutilized resource. Our recent studies indicate that, in spite of the high stability of methane, systems such as Ni-CeO₂(111) and CeO₂-Cu(111) can break C-H bonds even at room temperature, through careful manipulation of interfaces and metal-support interactions, using C1 oxidants (CO₂, O₂/H₂O). Our approach is to rely on *in-situ* studies, using real time in situ measurements with XRD, XAFS, AP-XPS, infrared spectroscopy and TEM/STM coupled with DFT to study powder and model systems to elucidate C-H activation and conversion steps that produce CH₃OH and CO+H₂.

We have employed Dry Reforming of Methane (DRM: CH₄+CO₂→2CO+2H₂) conditions to establish benchmark steps for low temperature oxidative conversion of C-H bonds (using CO₂) on several metal supported CeOx, including Pd, Ru, Ni, Co, Fe, where the active species and reaction mechanism are complex while a strong interaction between small M nanoparticles (M⁰/M^{δ+}) and reduced CeOx surfaces (Ce⁴⁺/Ce³⁺) prevail. We have also started to develop a method for the direct conversion of methane to methanol building on these studies. We have found that a CeO₂/Cu₂O/Cu(111) inverse system is able to activate methane at room temperature and then, with the help of water, performs a highly selective catalytic cycle, for the production of methanol. The interfacial interaction between CeOx-CuOx is crucial while the pressure of water has a strong effect on the selectivity towards the production of methanol. We have mapped surface chemical pathways using C1s and O1s AP-XPS to sequence the steps that can produce methanol directly from methane. Our model system insights will be employed in powder systems.

1. Liu et al. *Angewandte Chemie* (2016) 128 (26), 7581-7585.
2. Lustemberg et al. *ACS Catalysis* (2016) 6 (12), 8184-8191.
3. Zuo et al. *JACS* (2016) 138 (42), 13810-13813.
4. Liu et al. *Angewandte Chemie* (2017) 56 (42) 13041-13046.
5. Zhang et al. *ACS Catalysis* (2018) 8 (4), 3550–3560.
6. Lustemberg et al. *JACS* (2018) 140 (24), 7681–7687.
7. Liu et al. *ACS Catalysis* (2019) 9 3349-3359.
8. Zhang et al. *J. Phys. Chem.* (2019) 122 (50), 28739-28747.

Design of Highly Durable Multimetallic Electrocatalysts

Jocelyn T. L. Gamler,¹ Hannah M. Ashberry,¹ Alberto Leonardi,² Xiahan Sang,³ Raymond R. Unocic,³ Michael Engel,² and Sara E. Skrabalak^{1,*}

¹Department of Chemistry, Indiana University, 800 East Kirkwood Avenue, Bloomington, Indiana

²Institute for Multiscale Simulation, Friedrich-Alexander Universität Erlangen-Nürnberg, Cauerstraße 3, Erlangen, Germany

³Center for Nanophase Materials Sciences, Oak Ridge National Laboratory, One Bethel Valley Road, Oak Ridge, Tennessee

Presentation Abstract

Pt catalysts are widely studied for the oxygen reduction reaction, but their cost and susceptibility to poisoning limit their use. A strategy to address both problems is to incorporate a second transition metal to form a bimetallic alloy; however, the durability of such catalysts can be hampered by leaching of non-noble metal components. Here, we show that random alloyed surfaces can be stabilized to achieve high durability by depositing the alloyed phase on top of intermetallic seeds using a model system with PdCu cores and PtCu shells. Specifically, random alloyed PtCu shells were deposited on PdCu seeds that were either the atomically random face-centered cubic phase (FCC A1, Fm3m) or the atomically ordered CsCl-like phase (B2, Pm3m). Precise control over crystallite size, particle shape, and composition allowed for comparison of these two core@shell PdCu@PtCu catalysts and the effects of the core phase on electrocatalytic durability. Indeed, the nanocatalyst with the intermetallic core saw only an 18% decrease in activity after stability testing (and minimal Cu leaching), whereas the nanocatalyst with the random alloy core saw a 58% decrease (and greater Cu leaching). The origin of this enhanced durability was probed by classical molecular dynamics simulations of model catalysts, with good agreement between model and experiment. This work is coupled with advances in synthesis which show that a variety of PtX (where X = Co, Fe, Ni, and Cu) shells can be deposited on intermetallic seeds by seed-mediated co-reduction to provide a general platform for nanocatalysts with enhanced durability. Moreover, the synthesis of intermetallic seeds is being advanced by revealing that the disorder-to-order transition can be mediated by size refocusing, with in situ TEM studies being undertaken to better understand the apparent size-dependence of the ordering temperature.

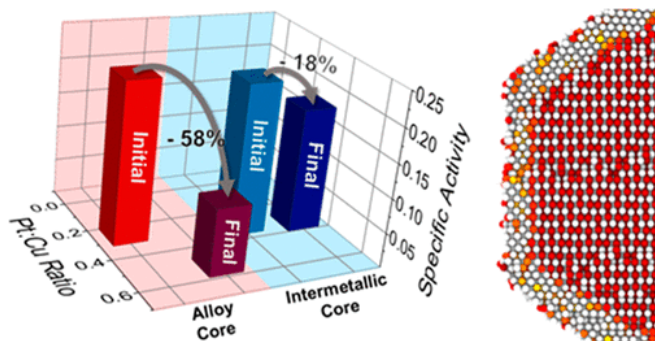
DE-SC0018961: Dynamics and Strain-Engineering of Multimetallic Nanocatalyst

Student(s): Jocelyn T. L. Gamler and Hannah M. Ashberry

RECENT PROGRESS

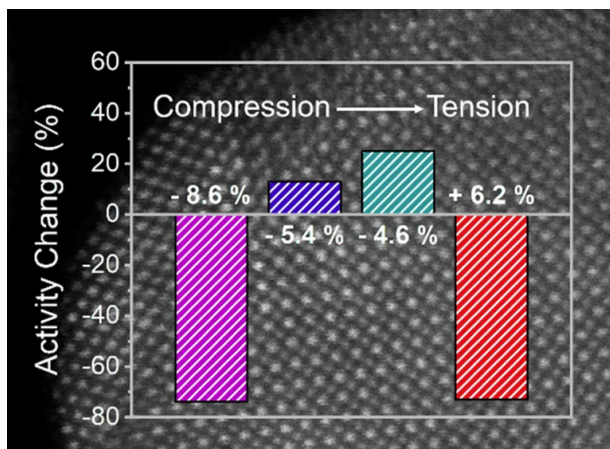
Achieving Highly Durable Random Alloy Nanocatalysts through Intermetallic Cores

We show that random alloyed surfaces can be stabilized to achieve high durability by depositing the alloyed phase on top of intermetallic seeds using a model system with PdCu cores and PtCu shells. Specifically, random alloyed PtCu shells were deposited on PdCu seeds that were either the atomically random face-centered cubic phase (FCC A1, $Fm\bar{3}m$) or the atomically ordered CsCl-like phase (B2, $Pm\bar{3}m$). Precise control over crystallite size, particle shape, and composition allowed for comparison of these two core@shell PdCu@PtCu catalysts and the effects of the core phase on electrocatalytic durability. Indeed, the nanocatalyst with the intermetallic core saw only an 18% decrease in activity after stability testing (and minimal Cu leaching), whereas the nanocatalyst with the random alloy core saw a 58% decrease (and greater Cu leaching). The origin of this enhanced durability was probed by classical molecular dynamics simulations of model catalysts, with good agreement between model and experiment. Although many random alloy and intermetallic nanocatalysts have been evaluated, this study directly compares random alloy and intermetallic cores for electrocatalysis with the enhanced durability achieved with the intermetallic cores likely general to other core@shell nanocatalysts.



Building Random Alloy Surfaces from Intermetallic Seeds: A General Route to Strain-Engineered Electrocatalysts with High Durability

Here, the concepts of a core@shell architecture, alloyed surfaces, and high-durability intermetallics are integrated into one nanostructure platform using seed-mediated co-reduction (SMCR). Specifically, random alloy PtM (where M = Ni, Co, Cu, or Fe) shells are deposited on intermetallic PdCu B2 seeds. Control of shell thickness and Pt:M ratios is also demonstrated, providing a general route to strain-engineered alloyed surfaces. The performance of these nanocatalysts was evaluated for the oxygen reduction reaction as a function of shell thickness and shell composition, where PtCu and PtNi shells showed a 230% and 270% activity increase, respectively, compared to the Pt reference. This evaluation is coupled with Tafel plot analysis which shows significant changes in the Tafel slopes, which indicate a shift in the rate-limiting step when a core@shell architecture is incorporated. Significantly, this work demonstrates the versatility of

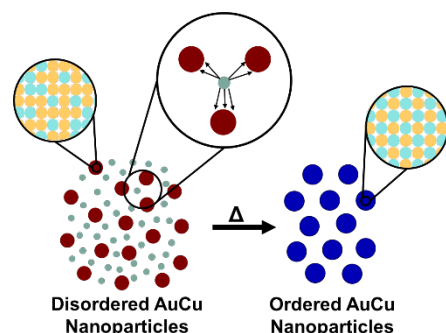


SMCR as a facile way to integrate a core@shell architecture, alloyed surfaces, and high-durability intermetallics within one platform.

Disorder-to-Order Transition Mediated by Size Focusing: a Route towards Monodisperse Intermetallic Nanoparticles

Intermetallic nanoparticles are remarkable due to their often enhanced catalytic, magnetic, and optical properties, which arise from their ordered crystal structures and high structural stability. Typical syntheses of intermetallic nanoparticles include thermal annealing of the disordered counterpart in atmosphere (or vacuum) and colloidal syntheses where the phase transformation is achieved in solution. While both methods can produce intermetallic nanoparticles, there is difficulty in achieving *monodisperse* nanoparticles, which is critical to exploiting their properties for various applications.

Here, we show that overgrowth on random alloy AuCu nanoparticles mediated by size refocusing yields monodisperse intermetallic AuCu nanoparticles. Size refocusing has been used in syntheses of semiconductor and upconverting nanocrystals to achieve monodisperse samples, but now we demonstrate size refocusing as a mechanism to achieve the disorder-to-order phase transformation in multimetallic nanoparticles. The phase transformation was monitored by time evolution experiments, where analysis of reaction aliquots with transmission electron microscopy and powder X-ray diffraction revealed the generation and dissolution of small nanoparticles coupled with an increase in the average size of the nanoparticles and conversion to the ordered phase. This demonstration advances the understanding of intermetallic nanoparticle formation in colloidal syntheses, which can expedite the development of electrocatalysts and magnetic storage materials.



Publications Acknowledging this Grant

Jointly funded by this grant and other grants with leading intellectual contribution from this grant;

Gamler, J. T. L.; Leonardi, A.; Ashberry, H. M.; Daanen, N. N.; Losovyj, Y.; Unocic, R. R.; Engel, M.; Skrabalak, S. E. Achieving Highly Durable Random Alloy Nanocatalysts through Intermetallic Cores. *ACS Nano* **2019**, *13*, 4008-4017.

Gamler, J. T. L.; Ashberry, H. M.; Sang, X.; Unocic, R. R.; Skrabalak, S. E. Building Random Alloy Surfaces from Intermetallic Seeds: A General Route to Strain-Engineered Electrocatalysts with High Durability. *ACS Appl. Nano. Mater.* **2019**, DOI: 10.1021/acsnm.9b00901.

Two-State Reactivity in Iron(I)-Catalyzed Alkene Isomerization

Yafei Gao, Sean A. Lutz, Anne K. Hickey and Jeremy M. Smith
Indiana University

Presentation Abstract

The high spin ($S = 3/2$) Fe(I) complex, $[\text{Ph}_2\text{B}(\text{}^t\text{BuIm})_2\text{Fe}(\text{CH}_2\text{}^t\text{Bu})\text{N}_2]^-$ is a catalyst for the isomerization of alkenes. Interestingly, the catalyst shows high resistance to the presence of σ -bases. A combined experimental and theoretical investigation has been undertaken to understand the mechanism of alkene isomerization. Experimental results are consistent with isomerization occurring by the allyl mechanism, with alkene C-H oxidative addition rate-determining, providing a kinetic isotope effect, $k_{\text{H}}/k_{\text{D}} = 2.8 \pm 0.1$ (303-333 K). Experimentally calibrated computations reveal the complex interplay of spin, relative alkene orientation and spin-orbit coupling on the mechanism of catalysis. Thermodynamically, two spin surfaces are accessible ($S = 1/2$ and $S = 3/2$), both of which provide access to an η^1 -allyl intermediate, but the η^3 -allyl isomer stable on the $S = 1/2$ surface only. The relative spin-orbit coupling between the two spin surfaces depends on the orientation of alkene binding to iron. This in turn influences the likely isomerization pathway.

DE-SC0019466: Harnessing Spin as a Design Element in Low Valent Iron Catalysis

Postdoc: Yafei Gao

Student(s): Juan A. Valdez-Moreira

RECENT PROGRESS

Isolation of Fe(V) and Fe(VI) Complexes: As part of a preliminary survey of the reactivity of the iron(I) complex, $\text{H}_2\text{B}(\text{MesIm})_2\text{Fe}(\eta^2\text{-dvtms})$ (dvtms = divinyltetramethyldisiloxane), we have found that reaction with the organoazide provides the structurally bis(imido) complex, $\text{H}_2\text{B}(\text{MesIm})_2\text{Fe}(=\text{NMes})_2$ in high yield. The complex has been assigned as having a low spin ($S = 1/2$) Fe(V) formulation, based on Mössbauer ($\delta = -0.25$ mm/s, $\Delta E_{\text{Q}} = 0.82$ mm/s) and X-band EPR ($g_{\text{ave}} = 1.972$) spectroscopy. Additionally, no hyperfine coupling to the imido nitrogen atoms is observed, which is supported by preliminary ENDOR measurements. The electronic structure, as computed by DFT, reveal the SOMO is mainly localized on the Fe atom, as is most of the unpaired spin density. Consistent with the reversible oxidative process observed in the CV ($E_{1/2} = -0.61$ V vs Fc^+/Fc), chemical oxidation affords an air-stable, diamagnetic complex, formulated as the iron(VI) complex $[\text{H}_2\text{B}(\text{MesIm})_2\text{Fe}(=\text{NMes})_2]\text{BPh}_4$. Here, the Mössbauer spectrum reveals a more negative isomer shift ($\delta = -0.48$ mm/s) and larger quadrupole splitting ($\Delta E_{\text{Q}} = 1.29$ mm/s), consistent with metal-based oxidation. This is supported by the electronic structure, which shows two d-electrons housed in a metal-based HOMO.

Copper-Catalyzed Oxidation of O–H and N–H Bonds

Shannon S. Stahl

Department of Chemistry, University of Wisconsin-Madison

This poster will outline our advances in understanding two classes fundamental reactions relevant to copper-catalyzed aerobic oxidation of organic molecules: (1) Cu-catalyzed oxidation of O–H bonds to generate oxyl radicals, and (2) Cu-catalyzed oxidation of N–H bonds that provide the basis for aerobic oxidative coupling of N–N bonds. The first of these efforts builds upon our previous work on Cu/nitroxyl-catalyzed aerobic alcohol reactions in which the nitroxyl cocatalyst is generated via oxidation of a hydroxylamine O–H bond under the aerobic reaction conditions. Our studies provide key insights in the basis for redox cooperativity between Cu^{II} and an oxyl radical that enable efficient alcohol oxidation. The studies of N–H oxidation and oxidative N–N bond formation is motivated by the prevalence of N–N bonds in industrial chemicals (e.g., azo dyes, hydrazine), together with the growing interest in the use of ammonia as liquid hydrogen carrier for energy-conversion applications. Our studies of aerobic and electrochemical oxidative N–N coupling reactions provide unprecedented insights into the kinetic and thermodynamic principles underlying these reactions and set the stage for new route to leverage ammonia as a hydrogen carrier.

DE-FG02-05ER15690: Copper-Catalyzed Aerobic Oxidation of O–H and N–H Bonds

Postdoc(s): Damian P. Hruszkewycz, Alistair J. J. Lennox, Amit Das, Michael C. Ryan, Fei Wang, James B. Gerken

Student(s): Scott D. McCann, Aristidis Vasilopoulos, Kelsey C. Miles, Lauren D. Whitmire, Jordan E. Nutting

Collaborator: Kyle M. Lancaster (Cornell)

RECENT PROGRESS

Cu^{II}-Mediated O–H Oxidation of Hydroxylamines, Cu^{II}/Aminoxyl Electronic Structural Studies, and O–H Oxidation of Fe–OH₂ Complexes.

Proton-Coupled Oxidation of TEMPO-H by Cu^{II}X₂ Species (X = OAc, TFA, OTf). Over the past decade our lab has developed two complementary catalyst systems, abbreviated Cu/TEMPO and Cu/ABNO, that have proven to be highly effective for aerobic alcohol oxidation (Fig. 1). Cu/TEMPO is very chemoselective, oxidizing primary alcohols even in the presence of unprotected secondary alcohols, while Cu/ABNO oxidizes virtually all alcohols (1°/2°, activated/unactivated) with excellent efficiency. These methods have been implemented in industrial applications, initially in smaller-scale efforts (e.g., pharmaceutical, fine chemical), but more recently in larger scale chemical processes. Our mechanistic studies show that the Cu^{II} and aminoxyl engage in a cooperative mechanism in which the two one-electron oxidants promote

efficient two-electron oxidation of the substrate, and experimental data and DFT calculations support the formation of an η^1 -nitroxyl adduct that mediates hydride transfer via a six-membered transition state (Fig. 1).

In our original mechanistic study of Cu/TEMPO-catalyzed alcohol oxidation, we proposed that oxidation of TEMPOH to TEMPO• proceeds via H-atom transfer (HAT) from TEMPOH to a reactive Cu/O₂ species, such as a binuclear copper μ - η^2 : η^2 -peroxide or bis- η -oxo species (Fig. 2A). A subsequent study of electrochemical Cu/TEMPO-catalyzed alcohol oxidation under anaerobic conditions, however, provided support for an alternative mechanism in which a Cu^{II}X₂ species mediates proton-coupled oxidation of TEMPOH (Fig. 2B), using an exogenous tertiary amine (not shown) or an anionic ligand as the Brønsted base. Mechanistic data obtained during our study of electrochemical alcohol oxidation revealed a discrepancy between our data and an earlier report by Sheldon et al. (*Org. Biomol. Chem.* 2003, 3232), concerning the relative redox potentials of Cu(II) and TEMPO•. Specifically, Sheldon suggested that TEMPO• oxidizes Cu^I to Cu^{II}, while our data showed that Cu^{II} salts promote rapid oxidation of TEMPOH (Fig. 3). In order to probe the origin of this discrepancy, Cu^{II}-mediated proton-coupled oxidation of TEMPOH to TEMPO radical was investigated by using UV-visible and EPR spectroscopy, cyclic voltammetry, and kinetic methods under anaerobic conditions (ref 11). Our studies revealed that, when Cu(OAc)₂ is the oxidant, the rapid oxidation of TEMPOH by Cu^{II} is followed by a much slower reoxidation of Cu^I to Cu^{II}(OAc)₂. The latter process occurs via disproportionation of TEMPOH into tetramethylpiperidine and TEMPO⁺, and the latter species oxidizes Cu^I. In other words, Cu^I oxidation is driven by cleavage of the N–O bond to form the strong oxidant TEMPO⁺. These observations show that TEMPO is not capable of direct oxidation of Cu^I, as proposed by Sheldon, while Cu^{II}-mediated oxidation of TEMPOH is facile and kinetically competent under aerobic alcohol oxidation conditions.

Electronic-Structural Basis for Cu/TEMPO Redox Cooperativity. Aminoxyl radicals are mild oxidants. In spite of their electron deficient character, they can serve as ligands for transition metals. The frontier orbitals of the aminoxyl ligands are energetically similar to those of the transition metals, thereby complicating the electronic structural description of the resulting aminoxyl/metal complexes. Three possible resonance structures may be considered for the Cu/aminoxyl species proposed as intermediates in alcohol oxidation (Fig. 4). In one limit, formal electron transfer occurs from R₂NO• to Cu^{II}, producing Cu^I-oxoammonium configuration: Cu^I–(O=⁺NR₂). The opposite extreme features reduction of the aminoxyl by

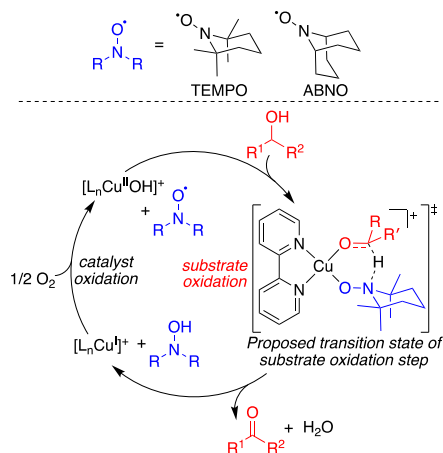


Fig. 1. Cu/TEMPO and Cu/ABNO aerobic alcohol oxidation catalyst systems with Cu^{II}(η^1 -nitroxyl)(alkoxide) six-membered transition state ($L_n = 2,2'$ -bipyridine +/- *N*-methylimidazole).

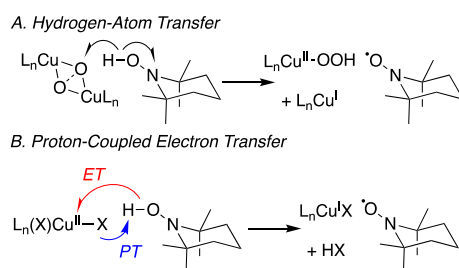


Fig. 2. Possible mechanisms for Cu-mediated oxidation of TEMPOH.

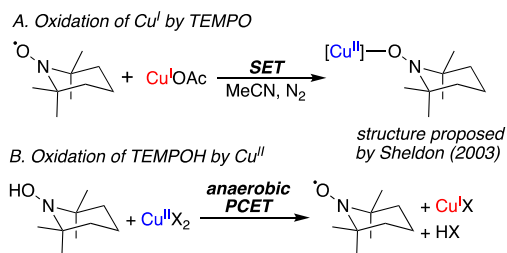


Fig. 3. Conflicting proposed reaction pathways involving redox reactions between Cu^{I/II} and TEMPOH/TEMPO.

Cu^{II} to afford a Cu^{III}–(–O–NR₂) species, and the intermediate case corresponds to a covalent Cu^{II}–(•ONR₂) adduct.

To elucidate the nature of the interaction between Cu^{II} and an aminoxyl species, we undertook a joint experimental/computational study of four [Cu–ONR₂]²⁺ complexes in collaboration with Prof. Kyle Lancaster

(Cornell) (ref 8). In addition to investigating two previously reported Cu/TEMPO adducts, we prepared and obtained X-ray crystal structures of two Cu/ABNO adducts (Fig. 5A). Cu K-edge, Cl K-edge, and Cu L_{2,3}-edge X-ray absorption spectroscopy was used to probe the molecular orbital energy levels and oxidation state of each of the copper complexes. Within error, all four aminoxyl complexes investigated have essentially the same Cu 3d character in their LUMOs: 28 ± 3%. This may be construed as the absence of 56% of a 3d electron from the Cu manifold (i.e. intermediate between the Cu^I–(O=⁺NR₂) and Cu^{II}–(•ONR₂) electronic configurations).

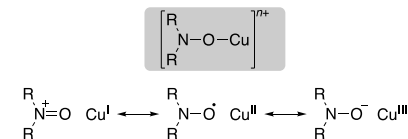


Fig. 4. Accessible valence tautomers of [Cu–ONR₂]ⁿ⁺ complexes.

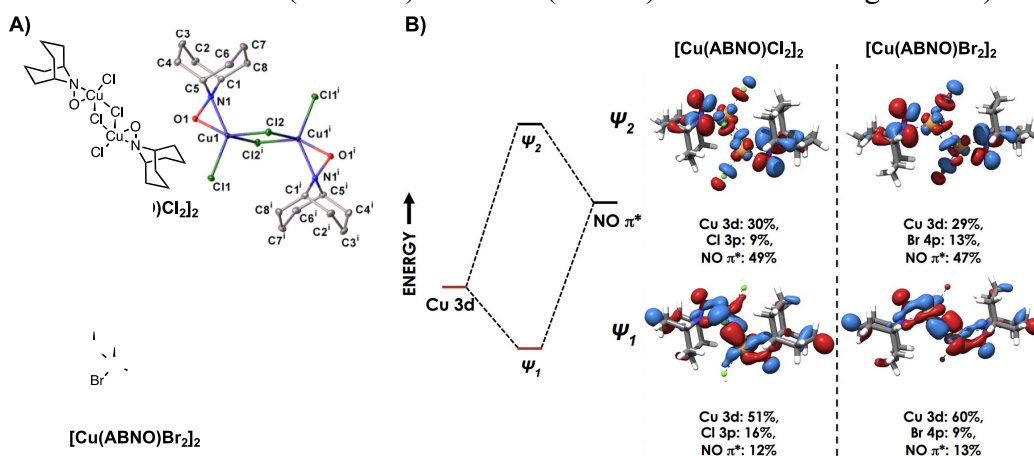


Fig. 5. A) Structure and X-ray crystal structure of the complexes [Cu(ABNO)Cl₂]₂ and [Cu(ABNO)Br₂]₂, and B) partial MO diagrams for the same complexes derived from DFT calculations. Depicted MOs correspond to the interaction between the Cu^{II}X₂ 3d SOMO and the R₂NO π* SOMO.

DFT calculations were used to corroborate the experimental oxidation state assignments. Simplified MO diagrams depicting the principal orbital interactions between the Cu^{II}X₂ fragment SOMO and R₂NO π* SOMO are shown in Fig. 5B. The electronic structure picture reveals appreciable electron density transferred from R₂NO π* to Cu^{II}, conferring oxoammonium character to the R₂NO ligand. The computational methodology was extended to one of the intermediates invoked in Cu/aminoxyl-catalyzed alcohol oxidation, [(bpy)Cu(TEMPO)(OⁿPr)] (cf. Fig. 1), and these studies again supported a Cu^I–(O=⁺NR₂)-like electronic structure.

(TAML)Fe-OH₂ oxidation to TAML-Fe-oxo species and C-H oxidation. Building on our previous report of Co/N-hydroxyphthalimide-catalyzed aerobic oxygenation of benzylic C-H bonds (ref. 6), we initiated a study focused on electrochemical generation of high-valent iron-oxo species from the corresponding iron-aqua complexes (ref 12). Whereas this reactivity has been evaluated in the context of catalytic water oxidation (Fig. 6), our recent report represents the first example of preparative electrochemical oxidation of organic molecules involving generation of a molecular metal-oxo species using water as the source of oxygen. After evaluating several previously reported Fe complexes, we focused on an iron complex bearing TAML (TAML = tetraamido macrocyclic ligand), an ancillary ligand pioneered by Collins and co-workers for iron-catalyzed oxidation of organic molecules with hydrogen peroxide. Cyclic voltammetry (CV) studies revealed the presence of Fe^{III/IV} and Fe^{IV/V} redox processes at 800 mV and 1250 mV, respectively (vs Ag/AgCl). Spectroelectrochemical studies showed that the catalyst resting state in bulk solution corresponds to the same dimeric oxo-bridged Fe^{IV} complex, irrespective of the electrolysis potential (i.e., 800 mV and 1250 mV vs Ag/AgCl); however, the rates of C-H oxygenation and alcohol dehydrogenation of a number of different substrates proceeds more rapidly during electrolysis at high potential due to the formation of the transient, but highly reactive, Fe^V-oxo species. These results establish an important benchmark for electrochemical C-H oxidation of organic molecules.

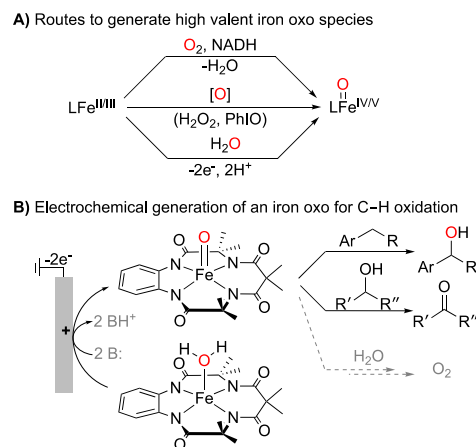


Fig. 6. Use of high-valent Fe complexes for oxidation of benzylic C-H and/or alcohol substrates to ketones.

Copper-Catalyzed Aerobic N-H Bond Oxidation and Oxidative Coupling of N-N Bonds.

We recently initiated a complementary research effort focused on Cu-catalyzed N-H oxidation and oxidative N-N coupling. Organometallic chemists and other catalysis researchers are well versed in carbon-hydrogen and carbon-heteroatom bond formation. But, aside from the extensive study of water oxidation to molecular oxygen, comparatively little attention has been given to catalytic methods for heteroatom-heteroatom bond formation. The mechanistic principles underlying Cu-catalyzed N-N bond-forming reactions are similarly poorly developed and understood. This topic has particular relevance to the use of ammonia as a hydrogen-carrier, including the development of fuel cells capable of using hydrazine or ammonia as the fuel.

We initiated our studies of N-N coupling by investigating the aerobic oxidative intermolecular coupling of *N*-substituted anilines and carbazoles (Fig. 7 and ref 10). Previously reported methods for the preparation of these compounds feature stoichiometric oxidants, such as KMnO₄, Ag₂O, or dichromate, in addition to a recent direct electrolysis method. Our reaction conditions achieve oxidative dimerization of carbazoles and diarylamines to N-N coupled bicarbazoles and tetraarylhydrazines under mild conditions (1 atm O₂, 60-80 °C) with a catalyst composed of CuBr·dimethylsulfide and N,N-dimethylaminopyridine. The reactions between

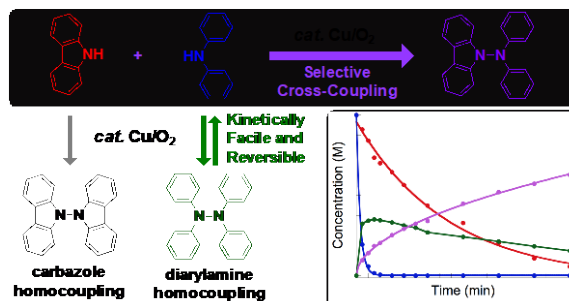


Fig. 7. Time course of the cross coupling of a carbazole (red) and a diarylamine (blue).

carbazole and diarylamine partners exhibit selective cross-coupling, even with a 1:1 ratio of the two substrates, with yields >80-90% of the cross-coupled product. NMR spectroscopic studies showed that the tetraarylhydrazine is a kinetically-favored product (Fig 7, green trace), but it is consumed as the reaction proceeds, with concomitant formation of the more thermodynamically stable cross-coupled product (Fig. 7, purple trace). The N–N bond of tetraarylhydrazine is weak (BDE = 23.5 kcal/mol for Ph₂N–NPh₂), and control experiments show that N–N cleavage of the tetraarylhydrazines occurs in the absence of copper, with EPR spectroscopic experiments providing evidence for N-centered radical formation under catalytic reaction conditions.

More recent (unpublished) studies are targeting mechanistic characterization of more challenging N–N coupling reactions. We anticipate that such reactions could proceed by a two-stage oxidase-type mechanism, such as that shown in Fig. 8. We have nearly completed a study focusing on mechanistic investigation of two reactions reported previously by others (Fig. 9): intramolecular N–N coupling to afford a triazole (Nagasawa), intermolecular N–N coupling to afford an azine (Hayashi). Neither reaction has been the subject of mechanistic investigation, and our results aligned with the two-state cycle in Fig. 8). Specifically, gas-uptake studies show clear evidence for a 2:1 N–N product:O₂ stoichiometry during catalytic turnover. In addition, stoichiometric oxidative N–N coupling under anaerobic conditions mediated by Cu^{II} and a Brønsted base affords product consistent with each Cu^{II} center serving as a one-electron oxidant. Kinetic studies have been carried out for both of the catalytic N–N coupling reactions shown in Fig. 9, and the results show that both feature aerobic oxidation of Cu^I as the turnover-limiting half-reaction (i.e., rate = $k_{\text{obs}}[\text{Cu}]^n[\text{O}_2]$, with $n \sim 2$).

Ongoing studies are focused on more thorough characterization of Cu-catalyzed azine synthesis, as this reaction has been developed to a level that it has been considered for industrial production of hydrazine. Upon hydrolysis, azines liberate hydrazine and benzophenone, and the latter may be reconverted to imine via ammonolysis. Insights gained during the course of this work are anticipated to lead to new strategies for the use of ammonia as a chemical building block and as an energy carrier.

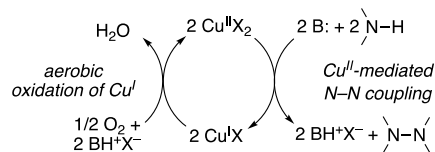


Fig. 8. Simplified oxidase-type mechanism for Cu-catalyzed aerobic oxidative N–N coupling.

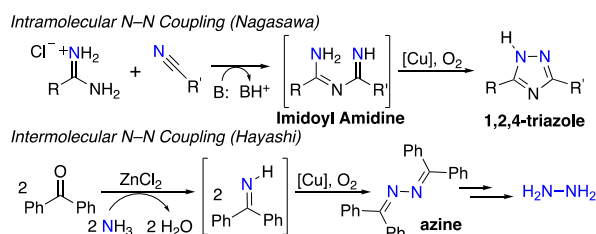


Fig. 9. N–N bond formation of azines and 1,2,4-triazoles mediated by a Cu/O₂ catalyst system.

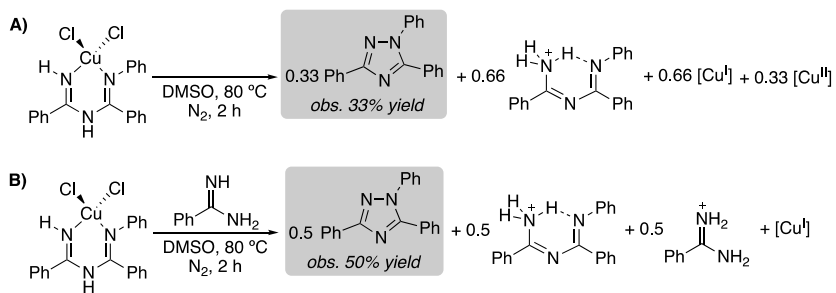


Fig. 10. Balanced equations for stoichiometric N–N coupling mediated by Cu^{II}, with product yields matching that expected if Cu^{II} serves as a one-electron oxidant and two equivalents of Brønsted base are required.

Publications Acknowledging this Grant in 2015-2019

Jointly funded by this grant and other grants with leading intellectual contribution from this grant:

1. Xie, X.; Stahl, S. S. Efficient and Selective Cu/Nitroxyl-Catalyzed Methods for Aerobic Oxidative Lactonization of Diols. *J. Am. Chem. Soc.* **2015**, *137*, 3767-3770.
2. McCann, S. D.; Stahl, S. S. Copper-Catalyzed Aerobic Oxidations of Organic Molecules: Pathways for Two-Electron Oxidation with a Four-Electron Oxidant and a One-Electron Redox-Active Catalyst. *Acc. Chem. Res.* **2015**, *48*, 1756-1766.
3. Steves, J. E.; Stahl, S. S. Stable TEMPO and ABNO Catalyst Solutions for User-Friendly (bpy)Cu/Nitroxyl-Catalyzed Aerobic Alcohol Oxidation. *J. Org. Chem.* **2015**, *80*, 11184-11188.
4. McCann, S. D.; Stahl, S. S. Mechanism of Copper/Azodicarboxylate-Catalyzed Aerobic Alcohol Oxidation: Evidence for Uncooperative Catalysis. *J. Am. Chem. Soc.* **2016**, *138*, 199-206.
5. Zhang, W.; Wang, F.; McCann, S. D.; Wang, D.; Chen, P.; Stahl, S. S.; Liu, G. Enantioselective Cyanation of Benzylic C–H Bonds via Copper-Catalyzed Radical Relay. *Science*, **2016**, *353*, 1014-1018.
6. Hruszkewycz, D. P.; Miles, K. C.; Thiel, O. R.; Stahl, S. S. Co/NHPI-mediated aerobic oxygenation of benzylic C–H bonds in pharmaceutically relevant molecules. *Chem. Sci.* **2017**, *8*, 1282-1287.
7. Vasilopoulos, A.; Zultanski, S. L.; Stahl, S. S. Feedstocks to Pharmacophores: Cu-Catalyzed Oxidative Arylation of Inexpensive Alkylarenes Enabling Direct Access to Diarylalkanes. *J. Am. Chem. Soc.* **2017**, *139*, 7705-7708.
8. Walroth, R. C.; Miles, K. C.; Lukens, J. T.; MacMillan, S. M.; Stahl, S. S.; Lancaster, K. M. Electronic Structural Analysis of Copper(II)–TEMPO/ABNO Complexes Provides Evidence for Copper(I)–Oxoammonium Character. *J. Am. Chem. Soc.* **2017**, *139*, 13507-13517.
9. Lennox, A. J. J.; Nutting, J. E.; Stahl, S. S. Selective Electrochemical Generation of Benzylic Radicals Enabled by Ferrocene-Based Electron-Transfer Mediators. *Chem. Sci.* **2018**, *9*, 356-361.
10. Ryan, M. C.; Martinelli, J. R.; Stahl, S. S. Cu-Catalyzed Aerobic Oxidative N–N Coupling of Carbazoles and Diarylamines Including Selective Cross-Coupling. *J. Am. Chem. Soc.* **2018**, *140*, 9074-9077.
11. Ryan, M. C.; Whitmire, L. D.; McCann, S. D.; Stahl, S. S. Copper/TEMPO Redox Redux: Analysis of PCET Oxidation of TEMPOH by Copper(II) and the Reaction of TEMPO with Copper(I). *Inorg. Chem.* **2019**, *Accepted for publication*.
12. Das, A.; Nutting, J. E.; Stahl, S. S. Electrochemical C–H Oxygenation and Alcohol Dehydrogenation Involving Fe-oxo Species using Water as the Oxygen Source. *Chem. Sci.* **2019**, *10*, *Accepted for publication* (DOI: 10.1039/C9SC02609F).

Jointly funded by this grant and other grants with relatively minor intellectual contribution from this grant:

1. Osterberg, P. M.; Niemeier, J. K.; Welch, C. J.; Hawkins, J. M.; Martinelli, J. R.; Johnson, T. E.; Root, T. W.; Stahl, S. S. Experimental Limiting Oxygen Concentrations for Nine Organic Solvents at Temperatures and Pressures Relevant to Aerobic Oxidations in the Pharmaceutical Industry. *Org. Process Res. Dev.* **2015**, *19*, 1537-1543.

2. Miles, K. C.; Stahl S. S. Practical Aerobic Alcohol Oxidation with Cu/Nitroxyl and Nitroxyl/NO_x Catalyst Systems. *Aldrichimica Acta* **2015**, *48*, 8-10.
3. Kim, J.; Stahl, S. S. Cu-Catalyzed Aerobic Oxidative Three-Component Coupling Route to *N*-Sulfonyl Amidines via an Ynamine Intermediate. *J. Org. Chem.* **2015**, *80*, 2448-2454.

Influence of Temperature and Ti substitution on Oxygen Electroadsorption and Electrocatalysis: A Progress on Theory-Experiment Convergence

Jin Suntivich

Cornell University, Department of Materials Science and Engineering

Presentation Abstract

We present our study on the convergence between theoretical and experimental electrocatalysis by using direct oxygen-electroadsorption measurements on transition-metal-oxide catalysts. The use of renewable electricity to synthesize fuels and materials offers a tantalizing opportunity to address concerns over energy and sustainability. Oxygen electrocatalysis, which includes the oxygen reduction reaction (ORR) and oxygen evolution reaction (OER), is currently the major contributor of inefficiency in fuel cells and electrolyzers. A superior electrocatalyst can reduce this inefficiency by stabilizing intermediates via electroadsorption. Currently, the most common approach is to find a superior catalyst by applying density functional theory (DFT) to screen for materials that can efficiently stabilize ORR/OER intermediates such as OH_{ad} , O_{ad} , and OOH_{ad} . Our work provides an experimental test of these calculated electroadsorption values. In our last report, we presented the O_{ad} and OH_{ad} electroadsorption measurement on $\text{IrO}_2(110)$ and $\text{RuO}_2(110)$. This year, we investigate the influence of temperature and Ti addition. Using the temperature experiment, we have isolated the enthalpy and entropy of the electroadsorption to check the accuracy of DFT assumptions. The Ti alloying study further reveals how a doping of an isovalent metal can influence the electroadsorption energies. Our major findings are that (1) the Ti addition protects the scaling relation, an idea that the first surface bond can approximate the trend of the intermediates adsorption, and (2) the attractive adsorbate-adsorbate interaction is a result of entropy. The second finding is counterintuitive as it suggests that the degree of freedom of (likely) the water layer governs the adsorbate interaction instead of direct chemical bonding.

DE-SC0018029: Rational Selection of Transition-Metal Oxide Electrocatalysts from Structure-Electronic Structure-Activity Relations: The Role of Defects, Strain, and Sub-Surface Layering

Students: Chuhyon (John) Eom, Ding-Yuan Kuo

RECENT PROGRESS

i. Measurement of the Oxygen Electroadsorption on Well-defined Rutile Surfaces

In the last report period, we described our measurement of the oxygen electroadsorption (O_{ad} and OH_{ad}) on well-defined rutile $\text{IrO}_2(110)$ and $\text{RuO}_2(110)$ grown on TiO_2 single-crystal substrates along the (110) orientation using molecular-beam epitaxy (MBE). Our observation shows a peculiar behavior of the adsorbate-adsorbate interaction, which was repulsive for OH_{ad} but attractive for O_{ad} . To better understand this observation, we in this report period carried out a temperature-dependent electroadsorption experiment to get at the underlying physics behind the adsorbate-adsorbate interactions (**Fig. 1**). We fit the background-corrected electroadsorption

measurements to surface adsorption models of a Frumkin isotherm, which factors into account a mean-field interaction parameter (g). The fitted results are vastly improved (see **Fig. 1.**) We use this model for our analysis.

From the fitted Frumkin isotherms, we can assess the O_{ad} and OH_{ad} electroadsorption free energies as a function of temperature by converting electrochemical potential to free energy (using RHE reference, 1st peak: $H_2O \rightarrow OH_{ad} + \frac{1}{2} H_2$ and 2nd peak: $OH_{ad} \rightarrow O_{ad} + \frac{1}{2} H_2$, **Fig. 2**). Then, from the temperature-dependent result, we can separate the enthalpy and the entropy terms (assuming that entropy is temperature-independent, **Fig. 2**).

The O_{ad} and OH_{ad} electroadsorption enthalpy and entropy results reveal insights into the electrochemical process at the liquid-oxide interfaces. We find that O_{ad} adsorbates *repel* each other enthalpically despite O_{ad} having an attractive O_{ad} - O_{ad} interaction. This result reflects a counterintuitive point: the origin of the O_{ad} - O_{ad} attraction is actually *entropy*. Our measurement shows that an O_{ad} - O_{ad} cluster formation have higher degree of freedom than OH_{ad} - OH_{ad} (and O_{ad} - OH_{ad}). This entropy gain in turn enables an overall attractive O_{ad} - O_{ad} interaction, which manifested as the attractive Frumkin isotherm.

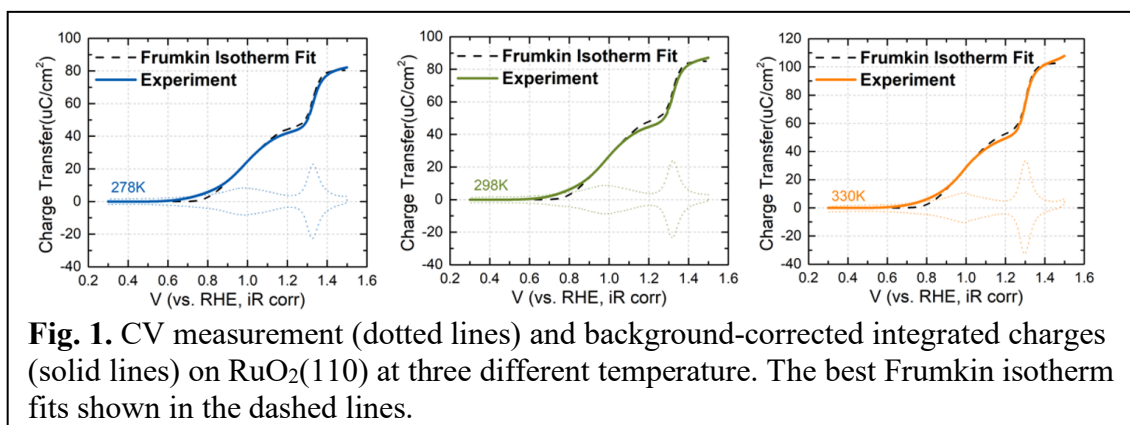
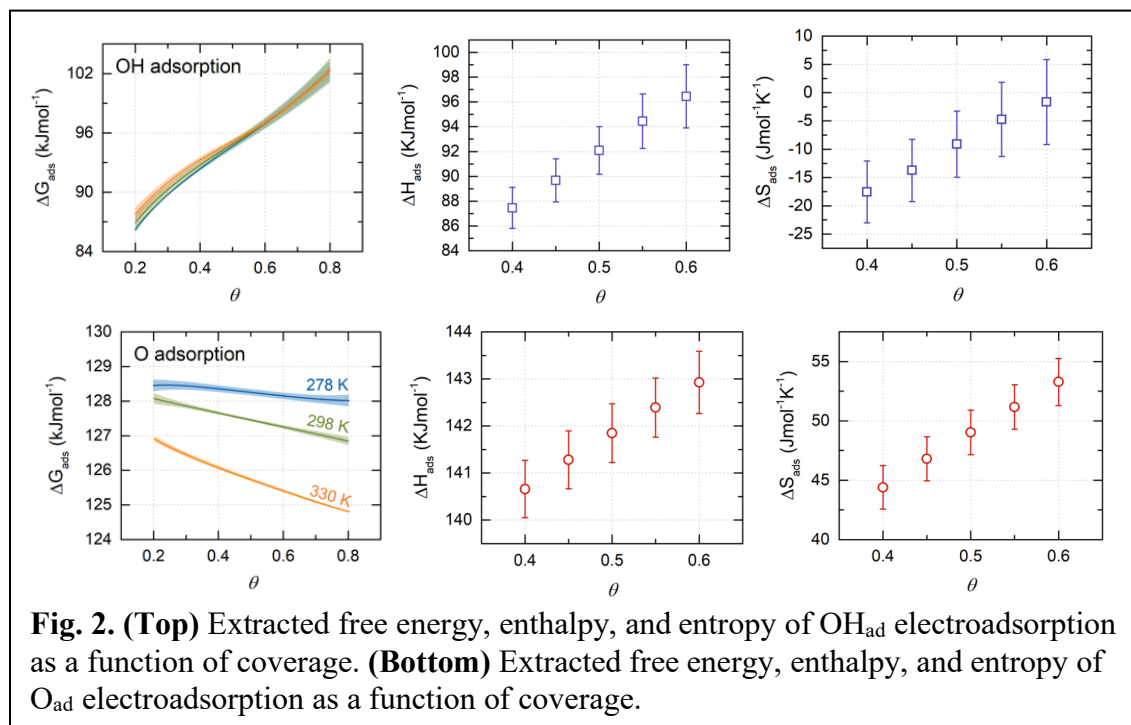


Fig. 1. CV measurement (dotted lines) and background-corrected integrated charges (solid lines) on $RuO_2(110)$ at three different temperature. The best Frumkin isotherm fits shown in the dashed lines.

ii. Measurement of the Role of Ti addition on the Oxygen ElectroadSORPTION

We have grown Ti-doped IrO_2 films using MBE. These films were characterized with X-ray diffraction (XRD) and reflective high-energy electron diffraction (RHEED). Both XRD and RHEED patterns are consistent with the Ti-doped IrO_2 films behaving as a solid solution epitaxially growing along the (110) termination.

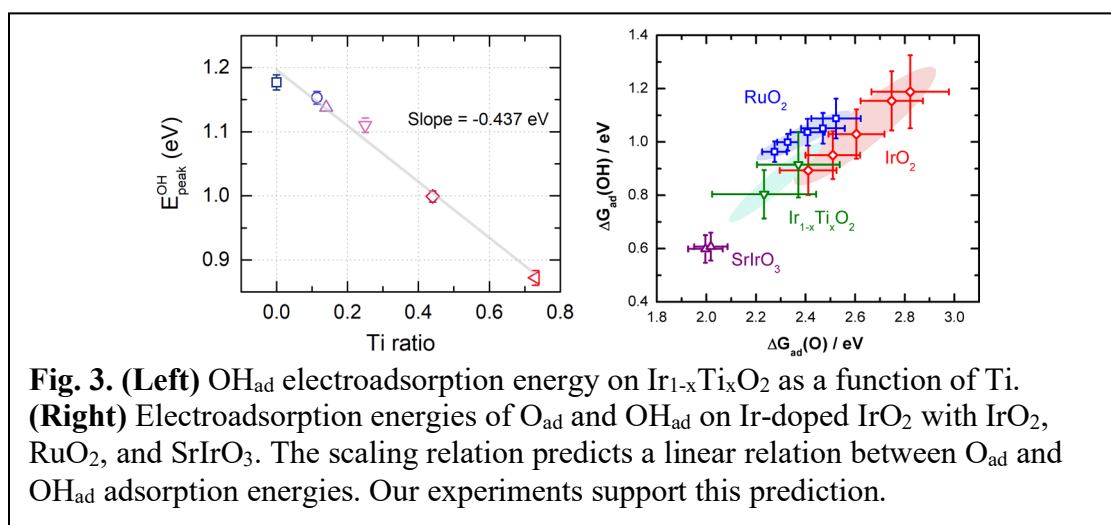
We use cyclic voltammetry (CV) to measure the O_{ad} and OH_{ad} electroadsorption on the Ti-doped IrO_2 films. We can measure from the CV spectra the OH_{ad} electroadsorption ($H_2O_{ad} \rightarrow OH_{ad} + H^+ + e^-$) and O_{ad} ($OH_{ad} \rightarrow O_{ad} + H^+ + e^-$). We use the peak positions as estimates for the O_{ad} and OH_{ad} electroadsorption energies. We find that the inclusion of Ti strengthens the OH_{ad} electroadsorption energy on IrO_2 (**Fig. 3 left**). We use these measurements to test the scaling relation, a hypothesis that the first surface bond can approximate the trend of the adsorption of similar species (*i.e.*, $\Delta G_O \propto \Delta G_{OH}$). **Fig. 3 right** shows that the electroadsorption results on the Ti-doped $IrO_2(110)$ films support this hypothesis, even when combined with IrO_2 , RuO_2 , and $SrIrO_3$ data from the previous report period. One implication from the scaling relation is the prediction of



a volcano plot or the Sabatier principle. We are currently verifying this prediction. In our previous report, we made this comparison by using ΔG_{OH} on RuO_2 and IrO_2 at different pH, which may not provide a fair comparison since the electrocatalysis at low and high pH may obey different mechanisms. We are comparing all data at the same pH in this new analysis, which is anticipated to be completed within the next few months.

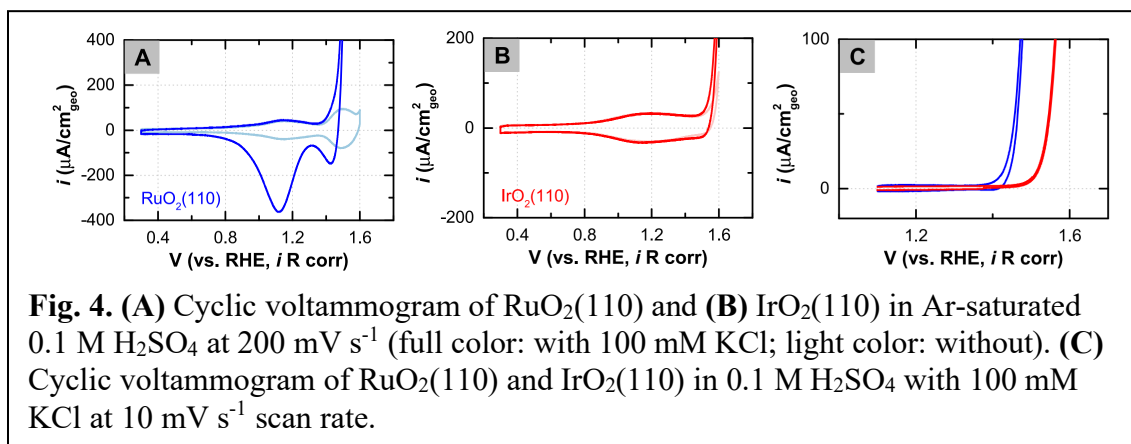
iii. Measurement of the Chlorine Evolution Reaction on $\text{IrO}_2(110)$ and $\text{RuO}_2(110)$

We used the chlorine evolution reaction (CER, $2\text{Cl}^- \rightarrow \text{Cl}_2 + 2\text{e}^-$) to probe the surface chemistry of $\text{IrO}_2(110)$ and $\text{RuO}_2(110)$ at oxidizing potential. DFT calculation predicted that the CER proceeds via the Volmer-Heyrovsky mechanism on O_{ad} -covered RuO_2 surface ($\text{O}_{\text{ad}} + \text{Cl}^- \rightarrow \text{OCl}_{\text{ad}} + \text{e}^-$ followed by $\text{OCl}_{\text{ad}} + \text{Cl}^- \rightarrow \text{O}_{\text{ad}} + \text{Cl}_2 + \text{e}^-$). From this mechanism, the CER is expected



to occur at potential higher than the O_{ad} formation, which if true would verify that our assignment of the O_{ad} formation on the CV.

Indeed, the CER occurs near the onset of the O_{ad} formation on both $RuO_2(110)$ and $IrO_2(110)$ surfaces (~ 1.4 and ~ 1.5 V vs. RHE, respectively, **Fig. 4**). On both materials, the OH_{ad} formation was virtually unaffected by Cl^- , which is consistent with the DFT prediction. We carried out this experiment to provide additional evidence to verify our assignment of the O_{ad} formation to the features at $\sim 1.4 - 1.5$ V vs. RHE. Our finding confirms this assignment, which highlights one of the main conclusions so far in our Project: oxide materials are likely terminated with OH_{ad} and O_{ad} at oxidizing potential relevant for oxygen electrocatalysis.



Publications Acknowledging this Grant in 2015-2018

(XLIII) Exclusively funded by this grant;

1. Kuo, D.Y., Paik, H., Nelson, J.N., Shen, K.M., Schlom, D.G., Suntivich, J., “Chlorine Evolution Reaction Electrocatalysis on $RuO_2(110)$ and $IrO_2(110)$ grown using Molecular-Beam Epitaxy”, *J. Chem. Phys.* **2019**, *150*, 4, 041726.
2. Kuo, D.Y., Paik, H., Kloppenburg, J., Faeth, B., Shen, K.M., Schlom, D.G., Hautier, G., Suntivich, J., “Measurements of Oxygen Electroadsorption Energies and Oxygen Evolution Reaction on $RuO_2(110)$: A Discussion of the Sabatier Principle and its Role in Electrocatalysis”, *J. Am. Chem. Soc.* **2018**, *140* 50, 17597-17605.

(XLIV) Jointly funded by this grant and other grants with leading intellectual contribution from this grant;

3. Eom, C.J., Kuo, D.Y., Adamo, C., Moon, E.J., May, S.J., Crumlin, E.J., Schlom, D.G., Suntivich, J., “Tailoring Manganese Oxide with Atomic Precision to Increase Surface Site Availability for Oxygen Reduction Catalysis”, *Nat. Commun.* **2018**, 4034.
4. Kuo, D.Y., Eom, C.J., Kawasaki, J.K., Petretto, G., Nelson, J.N., Hautier, G., Crumlin, E.J., Shen, K.M., Schlom, D.G., Suntivich, J., “Influence of Strain on the Surface–Oxygen Interaction and the Oxygen Evolution Reaction of $SrIrO_3$ ”, *J. Phys. Chem. C* **2018**, *122* 8, 4359-4364.

Bridging Molecular and Heterogeneous Catalysis Through Graphite-Conjugated

Yogesh Surendranath
Massachusetts Institute of Technology, Department of Chemistry

Presentation Abstract

The interconversion of electrical and chemical energy requires catalysts that can efficiently transfer multiple electrons to or from small molecules. Heterogeneous catalysts have extended band structures with high densities of states at the Fermi level, allowing these surfaces to engage in concerted electron transfer and substrate activation; however, it is difficult, if not impossible, to obtain significant molecular-level understanding for most heterogeneous catalysts because surface active sites are inherently dynamic, difficult to modify at the molecular level, and hard to identify, much less characterize. Recently, we have developed a new class of catalysts that incorporate molecularly well-defined, highly-tunable active sites into heterogeneous graphite surfaces. These graphite-conjugated catalysts (GCCs) feature a unique conjugated linkage between a discrete molecular active site and the delocalized states of graphitic carbons. Electrochemical and spectroscopic investigations establish that GCCs exhibit strong electronic coupling to the electrode, leading to electron transfer (ET) behavior that diverges fundamentally from that of solution phase or surface-tethered analogues. We find that: (1) ET is not observed between the electrode and a redox-active GCC moiety regardless of applied potential. (2) ET is observed at GCCs *only* if the interfacial reaction is ion-coupled. (3) Even when ET is observed, the oxidation state of a transition metal GCC site remains unchanged. From these observations, we construct a mechanistic model for GCC sites in which ET proceeds exclusively through inner-sphere mechanisms. This behavior is identical to that of catalytically active metal surfaces rather than to that of molecules in solution, making GCCs the first platform in which molecular active sites behave as metal surface sites. Our results demonstrate that GCCs provide a versatile platform for investigating and controlling interfacial inner-sphere reactivity in both elementary ET steps and electrocatalysis at the molecular level. To expand our efforts further, we have now investigated the influence of strong electronic coupling on proton-coupled electron transfer reactions at substituted phenazines and also on oxygen reduction at graphite-conjugated cobalt porphyrin active sites.

DE-SC0014176: Tunable Oxygen Reduction Electrocatalysis by Phenazine-Modified Carbons

PI: Yogesh Surendranath

Postdoc(s): Tomohiro Fukushima, Michael Pegis

Student(s): Megan Jackson, Seokjoon Oh, Corey Kaminsky, Travis Marshall-Roth

Affiliations(s): Massachusetts Institute of Technology

RECENT PROGRESS

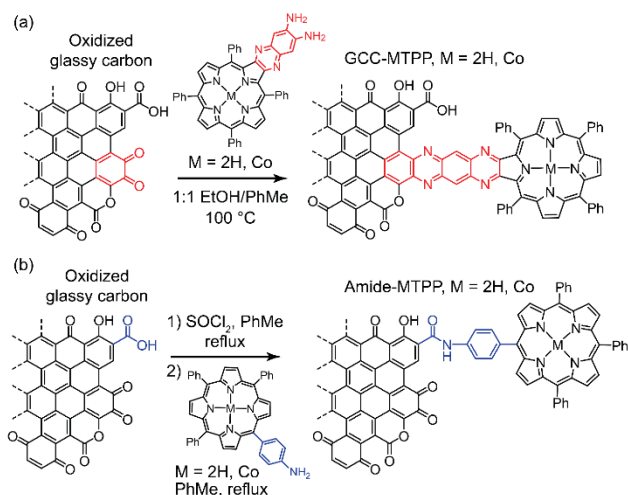


Figure 20. a) Synthesis of the strongly electronically coupled GCC-CoTPP. b) Synthesis of the weakly electronically coupled Amide-CoTPP. The development of this GCC-porphyrin platform opens up a vast space for electrochemical and thermal catalytic studies as well as enabling numerous spectroscopic studies that previously remained elusive.

Before examining the emergent reactivity of the conjugated porphyrins, we sought to understand how conjugation impacts the catalytic behavior relative to similar porphyrins that were heterogenized with linkages that do not confer strong electronic coupling. Heterogenized porphyrins have been used for electrocatalytic purposes for over sixty years and display a remarkable diversity in reactivity depending on the surface ligation methodology. While this variation in activity has been observed for numerous metalloporphyrins, the origin remains largely unknown. We hypothesized that the electronic interaction of the porphyrin with the surface may be a contributing factor to the observed variation in reactivity. In order to test this hypothesis, we ligated cobalt tetraphenylporphyrin (CoTPP) to glassy carbon surfaces following two methods that provide strong and weak electronic coupling. The strongly-coupled system consists of the conjugated porphyrin, GCC-CoTPP, whereas the weakly-coupled system consists of CoTPP ligated via an amide linkage to the surface, called Amide-CoTPP (**Figure 1b**). Both systems were rigorously characterized by spectroscopic and electrochemical techniques.

We evaluated the oxygen reduction activity of the two systems as probe for the impact of electronic coupling on defining catalytic activity. Both systems display activity for oxygen reduction in aqueous acidic media (**Figure 2**), however, the strongly coupled

In the past year we expanded the scope of GCCs to a new ligand platform that can support earth-abundant yet labile first-row transition metals. To that end, we synthesized a diaminoporphyrin that readily condenses onto graphitic carbon surfaces (**Figure 1a**). Porphyrins are an ideal platform as they strongly chelate metals in the central cavity resulting in remarkable stability of the resulting complex. Furthermore, metalloporphyrins demonstrate an enormous breadth of reactivity in both synthetic and biological systems where they are known catalysts for CO₂ reduction, O₂ reduction, oxidative C-H activation and nitrene transfer, among many other reactions. As a result, the

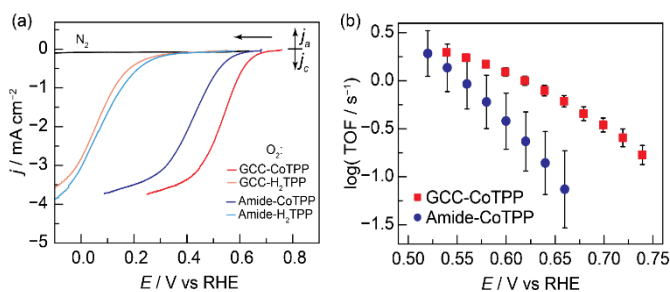


Figure 21. a) Linear sweep voltammograms (LSVs) of GCC-CoTPP (red), amide-linked CoTPP (dark blue), GCC-H₂TPP (pink), amide-linked H₂TPP (sky blue) and GCox (grey) recorded under an O₂ atmosphere. LSV of GCC-CoTPP under an N₂ atmosphere (black). All data were recorded in 0.1 M HClO₄ at a 5 mV/s scan rate with the electrode rotated at 2000 rpm. b) Turnover frequencies for the ORR as a function of potential for GCC-CoTPP (red) and Amide-CoTPP (blue). Error bars represent one standard deviation. All data were recorded in 0.1 M HClO₄ with the electrode rotated at 2000 rpm.

GCC-CoTPP shows an earlier onset potential by 60 mV as compared to the weakly-coupled Amide-CoTPP. Both systems reach similar peak current densities, suggesting similar product fractionation. Indeed, quantification of the peroxide byproduct reveals that the two catalysts show nearly identical selectivity for the four-electron reduction to water. In order to determine the relative rates of the oxygen reduction reaction on a per-site basis, we quantified the surface coverage of cobalt for each catalyst and determined the turnover frequencies for each catalyst. In the activation-controlled region, we found that GCC-CoTPP displays an order of magnitude rate enhancement relative to the weakly coupled Amide-CoTPP. This result reveals that the electronic coupling engendered by the linkage chemistry directly impacts the catalytic rate and should be considered when designing new methods for the heterogenization of molecular catalysts.

Our continued interest in investigating the fundamentals of inner-sphere chemistry at GCC sites also motivated our pursuit for understanding how the installation of other PCET-active groups onto the GCC scaffold would influence the resulting electrochemistry. As such, we prepared a variety of graphite-conjugated phenazine complexes with substitution on the backbone of the diamine precursors and studied the resulting surface electrochemistry (**Figure 3**).

To our surprise, surface PCET is not limited to phenazine functional groups. For example, installation of phenolic-functional groups (GCC-phen-*m/o*-OH) resulted in the formation of a new surface confined redox waves near -0.2 V vs NHE in addition to the standard phenazine PCET process near -0.8 V vs NHE. Unlike the molecular analogue of the phenolic GCC, the redox process for GCC-phen-*m*-OH displays reversible waves for both phenazine *and* phenol-based PCET. These results are not limited to functional groups that undergo PCET in homogeneous solutions- both aniline and carboxy- functionalized GCCs also display new PCET waves once conjugated on the electrode surface.

The overall PCET process can be visualized within a partial square scheme (**Figure 4**), which partitions the overall free energy for PCET (diagonal, black) as contributions from the proton transfer (horizontal, red) and electron transfer (vertical, blue) thermochemistry. A remarkable feature of interfacial PCET square schemes is that the ET and PT driving force can be independently tuned via the identity of the metallic solid and the identity of the protic functional group, respectively. This independence is distinct from square schemes for PCET on small molecules, where the proximity between the proton and electron donor/acceptor states renders independent tuning to be difficult if not impossible. These insights provide an important design criterion for tuning the thermochemistry of PCET at interfaces. For example, our model suggests that the rational tuning of the thermochemistry of important PCET intermediates in electrocatalysis can be envisaged through changing the work function of the material (E_{PZFC}) or via changes in the surface acidity.

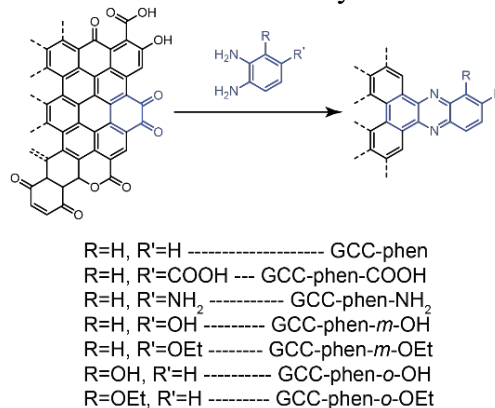


Figure 3. Synthesis of substituted phenazine GCCs.

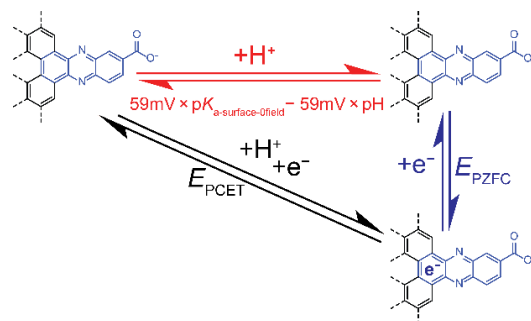


Figure 4. Partial square scheme for interfacial proton-coupled electron transfer (PCET) at GCC-phen-COOH as an example reaction.

Publications Acknowledging this Grant in 2015-2018

(XLV) Exclusively funded by this grant;

None

(XLVI) Jointly funded by this grant and other grants with leading intellectual contribution from this grant;

1. Oh, S.; Gallagher, J. R.; Miller, J. T.; Surendranath, Y. Graphite-Conjugated Rhenium Catalysts for Carbon Dioxide Reduction. *J. Am. Chem. Soc.* **2016**, *138*, 1820–1823.
2. Fukushima, T.; Drisdell, W.; Yano, J.; Surendranath, Y. Graphite-Conjugated Pyrazines as Molecularly Tunable Heterogeneous Electrocatalysts. *J. Am. Chem. Soc.* **2015**, *137*, 10926–10929.
3. Chu, S. B.; Fukushima, T.; Surendranath, Y. Minor Impact of Ligand Shell Steric Profile on Colloidal Nanocarbon Catalysis. *Chem. Mater.* **2017**, *29*, 495-498.
4. Murray, A. T.; Surendranath, Y. Reversing the Native Aerobic Oxidation Reactivity of Graphitic Carbon: Heterogeneous Metal-Free Alkene Hydrogenation. *ACS Catal.* **2017**, *7*, 3307-3312.
5. Ricke, N. D.; Murray, A. T.; Shepherd, J. J.; Welborn, M. G.; Fukushima, T.; Van Voorhis, T.; Surendranath, Y. Molecular-Level Insights into Oxygen Reduction Catalysis by Graphite-Conjugated Active Sites. *ACS Catal.* **2017**, *7*, 7680-7687.
6. Jackson, M. N.; Oh, S.; Kaminsky, C. J.; Chu, S. B.; Zhang, G.; Miller, J. T.; Surendranath, Y. Strong Electronic Coupling of Molecular Sites to Graphitic Electrodes via Pyrazine Conjugation. *J. Am. Chem. Soc.* **2018**, *140*, 1004-1010.
7. Kaminsky, C. J.; Wright, J.; Surendranath, Y. Graphite-Conjugation Enhances Porphyrin Electrocatalysis *ACS Catal.* **2019**, *9*, 3667–3671.
8. Jackson, M. N.; Pegis, M. L.; Surendranath, Y. Graphite-Conjugated Acids Reveal a Molecular Framework for Proton-Coupled Electron Transfer at Electrode Surfaces. *ACS Cent. Sci.* **2019**, *5*, 831-841

Activation of Shale Gas on Singly Dispersed Catalytic Sites Anchored on Oxide

Yu Tang,^a Luan Nguyen,^a De-en Jiang,^b Philippe Sautet,^c Franklin (Feng) Tao^a

Department of Chemical and Petroleum Engineering, University of Kansas^a

Department of Chemistry, University of California, Riverside^b

Department of Chemical and Biomolecular Engineering, University of California, Los Angeles^c

Supported metal nanoparticles are the main catalysts for activation of methane in chemical industries. Coupling of C_nH_m species ($n \geq 0, m \geq 0$) on continuously packed metal sites such as adjacent Ni atoms on surface of Ni nanoparticles leads to formation of coke layers on a metal catalyst. Rational design of catalysts with high tolerance for coke formation and exhibiting high activity and selectivity for transforming shale gas component to high value chemicals is significant for efficient utilization of shale gas. In this project, activations of CH_4 at low temperature ($\leq 150^\circ C$) and at high temperature ($\geq 500^\circ C$) on singly dispersed cationic sites are two approaches for efficient transforming CH_4 to high value chemicals. In low-temperature activation of CH_4 , we have designed singly dispersed cationic sites anchored in microporous oxide or on open oxide support. Pd_1O_4 and Rh_1O_5 sites exhibit high activities for productions of alcohol and carboxylic acid, respectively. DFT calculations suggest that Rh-O bonds can activate C-H of CH_4 , forming CH_3 and OH species bonded to Rh_1 atom; coupling of the adsorbed HO and CO forms -COOH intermediate which subsequently couples with CH_3 to form a product molecule. In terms of high temperature activation, CeO_2 with singly dispersed Ni_1+Ru_1 sites, CeO_2 with singly dispersed Rh-Rh dimer and TiO_2 with singly dispersed Rh_1 were prepared. These singly dispersed Ni_1 and Ru_1 atoms play a synergetic role in activations of CH_4 and CO_2 , respectively, making this catalyst exhibiting higher activity than CeO_2 anchored with only Ni_1 or on Ru_1 sites. TiO_2 anchored with Rh_1 atoms exhibits high activity and thermal stability for partial oxidation of methane to form syngas at $600^\circ C$; the high thermal stability results from the nearly saturated coordination of a Rh atom with nearest five oxygen atoms upon substituting for Ti atoms on (110) face of TiO_2 nanoparticles. Different from the rigid surface of TiO_2 , singly dispersed Rh_1 atoms form Rh-Rh dimers during reforming CH_4 with H_2O or CO_2 due to the high mobility of surface lattice oxygen atoms of CeO_2 . These studies suggested that cationic sites can efficiently activate CH_4 and the local chemical and coordination environments of the central atom of a catalytic site are crucial for performing a catalytic event at a molecular level.

Grant Number: Understanding of catalytic transformation of shale gas and development of catalysts with high activity and selectivity through experimental exploration and theoretical simulation

PI: Franklin (Feng) Tao

Postdoc(s): Luan Nguyen

Student(s): Yu Tang

RECENT PROGRESS

Synergy effect of Ga and Pt in/on ZSM-5 leading to high activity and selectivity for producing benzene through aromatization of ethane

ZSM-5 with anchored Ga, Pt or both Ga and Pt were synthesized for aromatization of ethane. As shown in Figure 1c, 20 mg of 0.20wt%Ga+0.20wt%Pt/ZSM-5 can convert more than 70% of ethane to benzene at 600°C and generate benzene with a yield of 55%. Compared to 20 mg of 0.20wt%Ga/ZSM-5 (Figure 1a) and 20 mg of 0.20wt%Pt/ZSM-5 (Figure 1b), 0.20wt%Ga/0.20wt%Pt/ZSM-5 demonstrated an obviously higher activity and selectivity for producing benzene (Figure 1c). In addition, the yield of benzene from ethane catalyzed by 0.20wt%Ga+0.20wt%Pt/ZSM-5 (almost 55%) was obviously larger than the sum of yields from 0.2wt%Ga/ZSM-5 and 0.2wt%Pt/ZSM-5 (nearly 35%), suggesting that the synergetic effect of gallium and platinum sites of this catalyst played a significant role in aromatization of ethane.

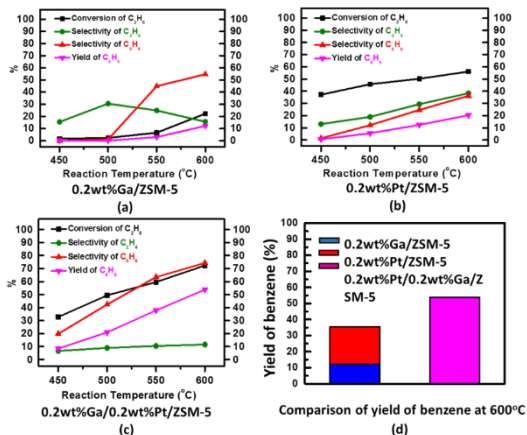
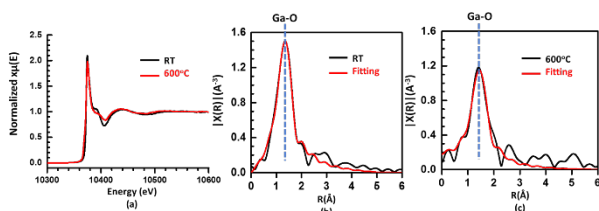


Figure 1. Catalytic performance of 0.20wt%Ga/ZSM-5 (a), 0.20wt%Pt/ZSM-5 (b), and 0.20wt%Ga+0.20wt%Pt/ZSM-5 (c), and yield of the three catalysts at 600°C (d).

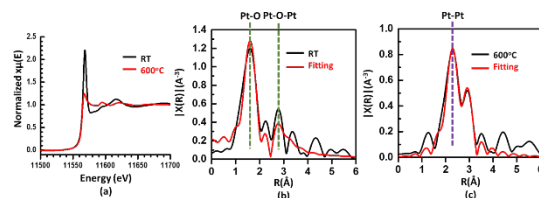
In order to reveal the role of gallium and platinum sites on the aromatization of ethane, extensive characterizations were performed to study these catalysts. For instance, operando XANES and EXAFS experiments of 0.20wt%Ga+0.20wt%Pt/ZSM-5 were carried out. The energy space and r space of Ga K-edge and Pt L₃-edge were plotted in Figures 2 and 3, respectively. As seen from Figure 2b, the first peak at approximately 1.3 Å (before phase correction) was assigned to Ga-O bonds. The lack of peak of the second shell of Ga-(O)-Ga of Ga₂O₃ suggests that Ga atoms in the as-synthesized RT catalyst are singly dispersed; the single dispersion of Ga atoms was maintained during the aromatization at 600°C.

In terms of Pt-L₃ edge, the peak of the as-prepared 0.2wt%Ga+0.2wt%Pt/ZSM-5 is ~1.5 Å (before the phase correction) (Figure 3b). It was assigned to the first shell Pt-O bond of platinum



sample	Bond	CN	R(Å)
0.2wt%Pt+0.2wt%Ga/ZSM-5 RT	Ga-O	4.92±0.84	1.817±0.016
0.2wt%Pt+0.2wt%Ga/ZSM-5 600C	Ga-O	3.37±0.34	1.924±0.026

Figure 2. XAS studies of 0.20wt%Ga/HZSM-5. (a) XANES of 0.20wt%Ga/HZSM-5 at RT and after catalysis at 600°C. (b) r -space spectra of 0.20wt%Ga/HZSM-5 before catalysis. (c) r -space spectra of 0.20wt%Ga after catalysis at 600°C. The lower panel is the table of the parameters used for fitting r -space spectra of 0.20wt%Ga/HZSM-5 at RT (b) or after catalysis at 600°C (c).



sample	Bond	CN	R(Å)
0.2wt%Pt/0.2wt%Ga/ZSM-5 RT	Pt-O	4.07 ± 1.74	2.006±0.038
0.2wt%Pt/0.2wt%Ga/ZSM-5 600C	Pt-O-Pt	1.76 ± 1.5	2.846±0.080
	Pt-Pt	8.84 ± 1.77	2.750±0.012

Figure 3. XAS studies of 0.20wt%Pt/HZSM-5. (a) XANES of 0.20wt%Pt/HZSM-5 at RT and after catalysis at 600°C. (b) r -space spectra of 0.20wt%Pt/HZSM-5 before catalysis. (c) r -space spectra of 0.20wt%Pt after catalysis at 600°C. The lower panel is the table of the parameters used for fitting r -space spectra of 0.20wt%Pt/HZSM-5 at RT (b) or after catalysis at 600°C (c).

oxide. It confirmed that Pt atoms bond with O atoms; there is lack of Pt-Pt metal bonds in as-synthesized catalyst (Figure 3b). Notably, during aromatization at 600°C, platinum nanoparticles were formed, evidenced by the peak observed around 2-3 Å (Figure 3c) which is assigned to Pt-Pt bonds of Pt nanoparticles. The formations of Pt nanoparticles on 0.20wt%Pt /HZSM-5 and 0.20wtGa%+0.20wt%Ga/HZSM-5 were confirmed by the observation of Pt nanoparticles in TEM images. These characterizations suggest that Ga atoms are singly dispersed and Pt is at metallic state during aromatization of ethane at 600°C.

In summary, through the integration of in-situ/operando characterization of the catalysts and their catalytic performance in aromatization of ethane, we have found that the active sites of Pt and Ga are metallic Pt atoms of Pt nanoparticles supported on ZSM-5 and singly dispersed cationic Ga atoms encapsulated in micropores of ZSM-5. Extensive catalysis studies suggest that the singly dispersed Ga atoms and metallic Pt nanoparticles play a synergic role in aromatization of ethane at 600°C (Figure 1).

Efficient transformation of CH₄ to syngas through reforming CH₄ with CO₂ on Ce_{0.95}Ni_{0.025}Ru_{0.025}O₂ and synergistic effect of singly dispersed Ni₁ and Ru₁ sites

We have designed a new catalyst Ce_{0.95}Ni_{0.025}Ru_{0.025}O₂ which exhibits higher activity and selectivity in producing syngas at 500°C than Ce_{0.95}Ni_{0.05}O₂ and Ce_{0.95}Ru_{0.05}O₂ (Figures 4 and 5). The high activity of Ce_{0.95}Ni_{0.025}Ru_{0.025}O₂ in transformation of CH₄ to syngas results from a synergistic effect between the singly dispersed Ni and Ru cations. The synergistic effect was confirmed by kinetics studies of CH₄ reforming in the temperature range of 480-550°C. Computational studies suggest that (1) CH₄ is activated by Ni₁ site; (2) CO₂ is activated by a site consisting of oxygen vacancy (O_v) and its nearest Ru₁ atom; and (3) coupling of H atoms (derived from activation of CH₄) to form a H₂ molecule is performed on Ru₁ site. For instance, these differences in barriers for activating CH₄ on Ni₁ and Ru₁ site achieved from computational studies are listed in Table 1.

Transformation of CH₄ to syngas through partial oxidation of CH₄ on TiO₂ anchored with singly dispersed Rh₁ atoms

Durability of catalytic performance on a catalyst in reforming CH₄ at high temperature has been a great challenge in utilization of CH₄. For reactions

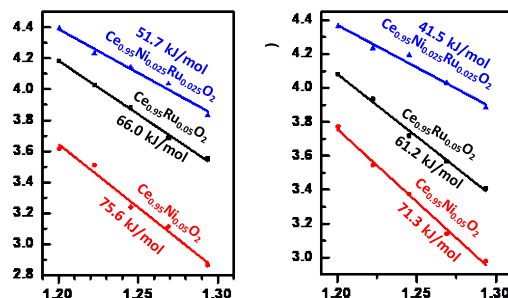


Figure 4. Arrhenius plot in term of the rate of product of (a) H₂ and (b) CO catalyzed by the Ce_{1-x}Ni_xRu_yO₂ catalysts. Blue: 5 mg Ce_{0.95}Ni_{0.025}Ru_{0.025}O₂ diluted with 300 mg purified quartz; black: 15 mg Ce_{0.95}Ru_{0.05}O₂ diluted with 300 mg purified quartz; red: 20 mg Ce_{0.95}Ni_{0.05}O₂ diluted with 300 mg purified quartz.

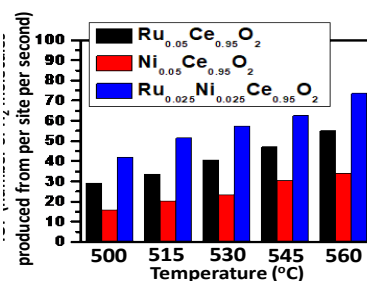


Figure 5. Turnover frequency (TOF) of reforming CH₄ with CO₂ in term of hydrogen production from per Ni₁ site of Ce_{0.95}Ni_{0.05}O₂, from per Ru₁ site of Ce_{0.95}Ru_{0.05}O₂, from per Ni₁ or Ru₁ site for Ce_{0.95}Ni_{0.025}Ru_{0.025}O₂ at 500°C-560°C.

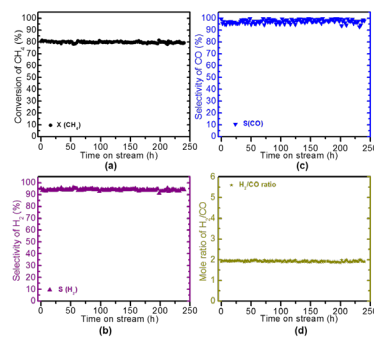


Figure 6. Catalytic stability of Rh₁/TiO₂ catalyst (a) conversion of CH₄; (b) selectivity of H₂; (c) selectivity of CO and (d) H₂/CO mole ratio. 50 mg Rh₁/TiO₂, flow rate of 10% CH₄ is 25 mL/min and 5% O₂ is 25 mL/min, temperature: 650 °C.

such as reforming of methane and aromatization of methane, deactivation of catalysts resulting from the formation of coke layers through coupling CH_n ($n \geq 0$) species on continuously packed metal atoms on surface of metal catalysts is a long-standing issue. Here we have designed a catalyst consisting of discontinuously packed metal sites in terms of single dispersion. The singly dispersed Rh_1 sites are active for reforming methane to produce syngas. The single dispersion of Rh_1 atoms prevents potential coupling of CH_n species, thus exhibiting high stability of catalytic performance for ten days without any decay (Figure 6). The high thermal stability of this single-atom catalyst results from the nearly saturated coordination of Rh_1 atom with its nearest five oxygen atoms based on structural characterization (Figures 7e and 7f). This active and thermally stable site Rh_1O_5 anchored on TiO_2 was formed through substituting for Ti cations of (110) face of TiO_2 .

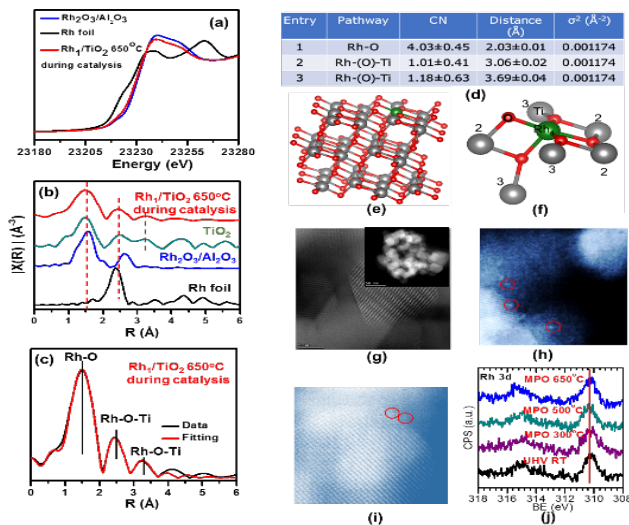


Figure 7. (a-b) In-situ XANES and EXAFS studies of Rh_1/TiO_2 catalyst: Rh K-edge XANES data of (a1) Rh foil; (a2) $\text{Rh}_2\text{O}_3/\text{Al}_2\text{O}_3$; (a3) Rh_1/TiO_2 during catalysis at 650°C ; k^2 -weighted Rh K-edge EXAFS data in r space of (b1) Rh foil; (b2) $\text{Rh}_2\text{O}_3/\text{Al}_2\text{O}_3$; (b3) Rh_1/TiO_2 during catalysis at 650°C ; (c) results of quantitative analyses for Rh-O and Rh-(O)-Ti of Rh_1/TiO_2 during catalysis at 650°C ; And (d) High resolution aberration-corrected HAADF-STEM images visualizing singly dispersed Rh atoms anchored on TiO_2 marked in red arrows.

Table 1. Gibbs free energy barriers (G_a) and Gibbs free energy changes (ΔG) for the elementary steps in CH_4 dehydrogenation and oxidation of CH_n ($n=0-3$) on Ni_1 and Ru_1 .

step	Reaction	Ni_1		Ru_1		
		G_a	ΔG	Reaction	G_a	ΔG
1	$\text{CH}_4(\text{g})+2^* \leftrightarrow \text{CH}_3^*+\text{H}^*$	1.88	0.94	$\text{CH}_4(\text{g})+2^* \leftrightarrow \text{CH}_3^*+\text{H}^*$	2.01	0.82
2	$\text{CH}_3^*+\text{O}^* \leftrightarrow \text{CH}_3\text{O}^*+^*$	1.33	0.03	$\text{CH}_3^*+^* \leftrightarrow \text{CH}_2^*+\text{H}^*$	1.73	0.69
3	$\text{CH}_3\text{O}^*+^* \leftrightarrow \text{CH}_2\text{O}^*+\text{H}^*$	1.52	1.04	$\text{CH}_2^*+\text{O}^* \leftrightarrow \text{CH}_2\text{O}^*+^*$	1.30	0.34
4	$\text{CH}_2\text{O}^*+^* \leftrightarrow \text{CHO}^*+\text{H}^*$	0.01	0.03	$\text{CH}_2\text{O}^*+^* \leftrightarrow \text{CHO}^*+\text{H}^*$	0.48	0.28
5	$\text{CHO}^*+^* \leftrightarrow \text{CO}^*+\text{H}^*$	0.17	0.20	$\text{CHO}^*+^* \leftrightarrow \text{CO}^*+\text{H}^*$	0.00	0.44
6	$\text{CO}^* \leftrightarrow \text{CO}(\text{g})+^*$		0.64	$\text{CO}^* \leftrightarrow \text{CO}(\text{g})+^*$		1.70

Formation of Rh dimer on CeO_2 under catalytic condition and its catalytic performance during catalysis

Different from Rh_1 single atoms anchored on TiO_2 (Figure 7), singly dispersed Rh_1 atoms anchored on CeO_2 formed Rh-Rh dimers during catalysis of reforming of methane through H_2O and CO_2 (Figure 8). Computational studies show that the dimerization is a thermodynamics-driven

process. It results from the high mobility of surface lattice oxygen atoms of CeO₂. Compared to the high thermal stability of Rh₁ anchored on TiO₂(110), the dimerization of Rh₁ on CeO₂ suggests that the support is a crucial component in building a catalyst with high thermal stability. Notably, the formed Rh-Rh dimers are highly active for reforming CH₄ to produce syngas (Figure 9).

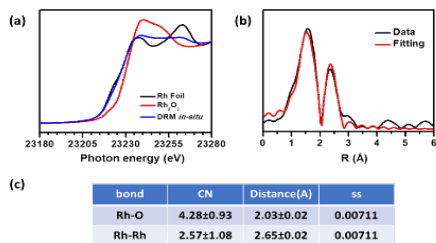


Figure 8. In-situ XAS studies of the Rh₁/CeO₂ catalyst. (a) XANES of the Rh K edge of Rh₁/CeO₂ catalyst compared with foil and oxide reference; (b) fitting of r-space spectrum of EXAFS from the Rh K edge of Rh₁/CeO₂ catalyst, (c) the fitting parameters summarized.

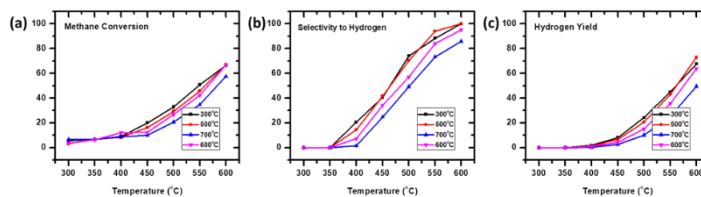


Figure 9. Catalysis performance of the Rh dimer/CeO₂ catalyst in term of (a) the conversion of methane, (b) selectivity to hydrogen and (c) yield of hydrogen. Pretreatment was performed before catalysis test, which was reduced by 5% H₂ for 30 min at given temperature.

Publications Acknowledging this Grant in 2015-2018

(I) Exclusively funded by this grant;

1. Tang, Y.; Li, Y. T.; Fung, V.; Jiang, D. E.; Huang, W. X.; Zhang, S. R.; Iwasawa, Y.; Sakata, T.; Nguyen, L.; Zhang, X. Y.; Frenkel, A. I.; Tao, F., Single rhodium atoms anchored in micropores for efficient transformation of methane under mild conditions. *Nat. Commun.* **2018**, *9*, 11.
2. Huang, W. X.; Zhang, S. R.; Tang, Y.; Li, Y. T.; Nguyen, L.; Li, Y. Y.; Shan, J. J.; Xiao, D. Q.; Gagne, R.; Frenkel, A. I.; Tao, F., Low-Temperature Transformation of Methane to Methanol on Pd1O4 Single Sites Anchored on the Internal Surface of Microporous Silicate. *Angew. Chem.-Int. Edit.* **2016**, *55* (43), 13441-13445.
3. Tao, F.; Crozier, P. A., Atomic-Scale Observations of Catalyst Structures under Reaction Conditions and during Catalysis. *Chemical Reviews* **2016**, *116* (6), 3487-3539.
4. Tao, F.; Shan, J.; Nguyen, L.; Wang, Z.; Zhang, S.; Zhang, L.; Wu, Z.; Huang, W.; Zeng, S.; Hu, P. Understanding complete oxidation of methane on spinel oxides at a molecular level, *Nat. Comm.* **2015**, *6*, 7798.
5. Liu, J. J.; Fung, V.; Wang, Y.; Du, K. M.; Zhang, S. R.; Nguyen, L.; Tang, Y.; Fan, J.; Jiang, D. E.; Tao, F. F., Promotion of catalytic selectivity on transition metal oxide through restructuring surface lattice. *Applied Catalysis B-Environmental* **2018**, *237*, 957-969.
6. Shan, J. J.; Zhang, S. R.; Choksi, T.; Nguyen, L.; Bonifacio, C. S.; Li, Y. Y.; Zhu, W.; Tang, Y.; Zhang, Y. W.; Yang, J. C.; Greeley, J.; Frenkel, A. I.; Tao, F., Tuning Catalytic Performance through a Single or Sequential Post Synthesis Reaction(s) in a Gas Phase. *ACS Catal.* **2017**, *7* (1), 191-204.
7. Fung, V.; Tao, F.; Jiang, D. E., Low-temperature activation of methane on doped single atoms: descriptor and prediction. *Phys. Chem. Chem. Phys.* **2018**, *20* (35), 22909-22914.
8. Nguyen, L.; Tao, P. P. C.; Liu, H. M.; Al-Hada, M.; Amati, M.; Sezen, H.; Gregoratti, L.; Tang, Y.; House, S. D.; Tao, F. F., X-ray Photoelectron Spectroscopy Studies of Nanoparticles Dispersed in Static Liquid. *Langmuir* **2018**, *34* (33), 9606-9616.

- 9 Nguyen, L.; Tang, Y.; Li, Y. T.; Zhang, X. Y.; Wang, D.; Tao, F., Dual reactor for in situ/operando fluorescent mode XAS studies of sample containing low-concentration 3d or 5d metal elements. *Rev. Sci. Instrum.* **2018**, *89* (5), 054103.
- 10 Zhang, X. Y.; House, S. D.; Tang, Y.; Nguyen, L.; Li, Y. T.; Opalade, A. A.; Yang, J. C.; Sun, Z. C.; Tao, F. F., Complete Oxidation of Methane on NiO Nanoclusters Supported on CeO₂ Nanorods through Synergistic Effect. *Acs Sustainable Chemistry & Engineering* **2018**, *6* (5), 6467-6477.
11. Nguyen, L.; Tao, F., Reactor for tracking catalyst nanoparticles in liquid at high temperature under a high-pressure gas phase with X-ray absorption spectroscopy. *Rev. Sci. Instrum.* **2018**, *89* (2), 024102
12. Tao, F.; Nguyen, L., Interactions of gaseous molecules with X-ray photons and photoelectrons in AP-XPS study of solid surface in gas phase. *Phys. Chem. Chem. Phys.* **2018**, *20* (15), 9812-9823.
13. Tang, Y.; Ma, L. J.; Dou, J.; Andolina, C. M.; Li, Y. T.; Ma, H. B.; House, S. D.; Zhang, X. Y.; Yang, J.; Tao, F., Transition of surface phase of cobalt oxide during CO oxidation. *Phys. Chem. Chem. Phys.* **2018**, *20* (9), 6440-6449.
14. Fung, V.; Tao, F.; Jiang, D. E., Trends of Alkane Activation on Doped Cobalt (II,III) Oxide from First Principles. *Chemcatchem* **2018**, *10* (1), 244-249.
15. Fung, V.; Tao, F.; Jiang, D. E., Understanding oxidative dehydrogenation of ethane on Co₃O₄ nanorods from density functional theory. *Catal. Sci. Technol.* **2016**, *6* (18), 6861-6869.
16. Fung, V.; Tao, F. F.; Jiang, D. E., General Structure-Reactivity Relationship for Oxygen on Transition-Metal Oxides. *J. Phys. Chem. Lett.* **2017**, *8* (10), 2206-2211.
17. Liu, J. J.; Zhang, S. R.; Zhou, Y.; Fung, V.; Nguyen, L.; Jiang, D. E.; Shen, W. J.; Fan, J.; Tao, F. F., Tuning Catalytic Selectivity of Oxidative Catalysis through Deposition of Nonmetallic Atoms in Surface Lattice of Metal Oxide. *ACS Catal.* **2016**, *6* (7), 4218-4228.
18. Zhang, S. R.; Shan, J. J.; Nie, L. H.; Nguyen, L.; Wu, Z. L.; Tao, F., In situ studies of surface of NiFe₂O₄ catalyst during complete oxidation of methane. *Surface Science* **2016**, *648*, 156-162.
19. Tang, Y.; Nguyen, L.; Li, Y. T.; Wang, N.; Tao, F., Surface of a catalyst in a gas phase. *Curr. Opin. Chem. Eng.* **2016**, *12*, 52-61.
20. Nguyen, L.; Tao, F., Development of a reaction cell for in-situ/operando studies of surface of a catalyst under a reaction condition and during catalysis. *Rev. Sci. Instrum.* **2016**, *87* (6), 12.

(II) *Jointly funded by this grant and other grants with leading intellectual contribution from this grant;*

1. Chen, Y.; deGlee, B.; Tang, Y.; Wang, Z. Y.; Zhao, B. T.; Wei, Y. C.; Zhang, L.; Yoo, S.; Pei, K.; Kim, J. H.; Ding, Y.; Hu, P.; Tao, F. F.; Liu, M. L., A robust fuel cell operated on nearly dry methane at 500 degrees C enabled by synergistic thermal catalysis and electrocatalysis. *Nat. Energy* **2018**, *3* (12), 1042-1050.
2. Dou, J.; Tang, Y.; Nie, L. H.; Andolina, C. M.; Zhang, X. Y.; House, S.; Li, Y. T.; Yang, J.; Tao, F. F., Complete Oxidation of Methane on Co₃O₄/CeO₂ Nanocomposite: A Synergic Effect. *Catal. Today* **2018**, *311*, 48-55.
3. Zhang, X. Y.; Sun, Z. C.; Wang, B.; Tang, Y.; Nguyen, L.; Li, Y. T.; Tao, F. F., C-C Coupling on Single-Atom-Based Heterogeneous Catalyst. *J. Am. Chem. Soc.* **2018**, *140* (3), 954-962.

4. Bergman, S. L.; Granstrand, J.; Tang, Y.; Paris, R. S.; Nilsson, M.; Tao, F. F.; Tang, C. H.; Pennycook, S. J.; Pettersson, L. J.; Bernasek, S. L., In-situ characterization by Near-Ambient Pressure XPS of the catalytically active phase of Pt/Al₂O₃ during NO and CO oxidation. *Applied Catalysis B-Environmental* **2018**, *220*, 506-511.
5. Zhang, S. R.; Tang, Y.; Nguyen, L.; Zhao, Y. F.; Wu, Z. L.; Goh, T. W.; Liu, J. J. Y.; Li, Y. Y.; Zhu, T.; Huang, W. Y.; Frenkel, A. I.; Li, J.; Tao, F. F., Catalysis on Singly Dispersed Rh Atoms Anchored on an Inert Support. *ACS Catal.* **2018**, *8* (1), 110-121.
6. Takanebe, K.; Khan, A. M.; Tang, Y.; Nguyen, L.; Ziani, A.; Jacobs, B. W.; Elbaz, A. M.; Sarathy, S. M.; Tao, F., Integrated In Situ Characterization of a Molten Salt Catalyst Surface: Evidence of Sodium Peroxide and Hydroxyl Radical Formation. *Angew. Chem.-Int. Edit.* **2017**, *56* (35), 10403-10407.
7. Mueannern, Y.; Yang, X.; Tang, Y.; Tao, F.; Baker, L. R., Catalysis at Multiple Length Scales: Crotonaldehyde Hydrogenation at Nanoscale and Mesoscale Interfaces in Platinum-Cerium Oxide Catalysts. *J. Phys. Chem. C* **2017**, *121* (25), 13765-13776.
8. Dou, J.; Sun, Z. C.; Opalade, A. A.; Wang, N.; Fu, W. S.; Tao, F., Operando chemistry of catalyst surfaces during catalysis. *Chem. Soc. Rev.* **2017**, *46* (7), 2001-2027.
9. Nguyen, L.; Liu, L. C.; Assefa, S.; Wolverton, C.; Schneider, W. F.; Tao, F. F., Atomic-Scale Structural Evolution of Rh(110) during Catalysis. *ACS Catal.* **2017**, *7* (1), 664-674.
10. Sohn, H.; Soykal, I.; Zhang, S. R.; Shan, J. J.; Tao, F.; Miller, J. T.; Ozkan, U. S., Effect of Cobalt on Reduction Characteristics of Ceria under Ethanol Steam Reforming Conditions: AP-XPS and XANES Studies. *J. Phys. Chem. C* **2016**, *120* (27), 14631-14642.
11. Cao, S. W.; Tao, F.; Tang, Y.; Li, Y. T.; Yu, J. G., Size- and shape-dependent catalytic performances of oxidation and reduction reactions on nanocatalysts. *Chem. Soc. Rev.* **2016**, *45* (17), 4747-4765.
12. Nguyen, L.; Zhang, S. R.; Wang, L.; Li, Y. Y.; Yoshida, H.; Patlolla, A.; Takeda, S.; Frenkel, A. I.; Tao, F., Reduction of Nitric Oxide with Hydrogen on Catalysts of Singly Dispersed Bimetallic Sites Pt1Co1 and Pd1Co1. *ACS Catal.* **2016**, *6* (2), 840-850.
13. Zhang, S. R.; Nguyen, L.; Liang, J. X.; Shan, J. J.; Liu, J. Y.; Frenkel, A. I.; Patlolla, A.; Huang, W. X.; Li, J.; Tao, F., Catalysis on singly dispersed bimetallic sites. *Nat. Commun.* **2015**, *6*, 10.
14. Nguyen, L.; Zhang, S. R.; Yoon, S. J.; Tao, F., Preferential Oxidation of CO in H₂ on Pure Co₃O_{4-x} and Pt/Co₃O_{4-x}. *Chemcatchem* **2015**, *7* (15), 2346-2353.

(III) *Jointly funded by this grant and other grants with relatively minor intellectual contribution from this grant;*

1. Khivantsev, K.; Jaegers, N. R.; Kovarik, L.; Hanson, J. C.; Tao, F.; Tang, Y.; Zhang, X. Y.; Koleva, I. Z.; Aleksandrov, H. A.; Vayssilov, G. N.; Wang, Y.; Gao, F.; Szanyi, J., Achieving Atomic Dispersion of Highly Loaded Transition Metals in Small-Pore Zeolite SSZ-13: High-Capacity and High-Efficiency Low-Temperature CO and Passive NO_x Adsorbers. *Angew. Chem.-Int. Edit.* **2018**, *57* (51), 16672-16677.
2. Cai, W. T.; Mu, R. T.; Zha, S. J.; Sun, G. D.; Chen, S.; Zhao, Z. J.; Li, H.; Tian, H.; Tang, Y.; Tao, F.; Zeng, L.; Gong, J. L., Subsurface catalysis-mediated selectivity of dehydrogenation reaction. *Sci. Adv.* **2018**, *4* (8), eaar5418.
3. Celik, G.; Ailawar, S. A.; Sohn, H.; Tang, Y.; Tao, F. F.; Miller, J. T.; Edmiston, P. L.; Ozkan, U. S., Swellable Organically Modified Silica (SOMS) as a Catalyst Scaffold for Catalytic Treatment of Water Contaminated with Trichloroethylene. *ACS Catal.* **2018**, *8* (8), 6796-6809.

4. Rawal, T. B.; Acharya, S. R.; Hong, S.; Le, D.; Tang, Y.; Tao, F. F.; Rahman, T. S., High Catalytic Activity of Pd-1/ZnO(10(1)over-bar0) toward Methanol Partial Oxidation: A DFT plus KMC Study. *ACS Catal.* **2018**, *8* (6), 5553-5569.
5. Pei, Y. C.; Qi, Z. Y.; Goh, T. W.; Wang, L. L.; Maligal-Ganesh, R. V.; MacMurdo, H. L.; Zhang, S. R.; Xiao, C. X.; Li, X. L.; Tao, F.; Johnson, D. D.; Huang, W. Y., Intermetallic structures with atomic precision for selective hydrogenation of nitroarenes. *J. Catal.* **2017**, *356*, 307-314.
6. Sohn, H.; Celik, G.; Gunduz, S.; Dogu, D.; Zhang, S. R.; Shan, J. J.; Tao, F. F.; Ozkan, U. S., Oxygen Mobility in Pre-Reduced Nano- and Macro-Ceria with Co Loading: An AP-XPS, In-Situ DRIFTS and TPR Study. *Catalysis Letters* **2017**, *147* (11), 2863-2876.
7. Lu, Y.; Zhang, R. G.; Cao, B. B.; Ge, B. H.; Tao, F. F.; Shan, J. J.; Nguyen, L.; Bao, Z. H.; Wu, T. P.; Pote, J. W.; Wang, B. J.; Yu, F., Elucidating the Copper-Hagg Iron Carbide Synergistic Interactions for Selective CO Hydrogenation to Higher Alcohols. *ACS Catal.* **2017**, *7* (8), 5500-5512.
8. Nie, L. H.; Yu, J. G.; Jaroniec, M.; Tao, F. F., Room-temperature catalytic oxidation of formaldehyde on catalysts. *Catal. Sci. Technol.* **2016**, *6* (11), 3649-3669.

Catalytic Transformations and Bond Activation Processes Promoted by Zr/Co Heterobimetallic Complexes

Christine M. Thomas, Hongtu Zhang, Kathryn M. Gramigna, and Nathanael H. Hunter
The Ohio State University, Department of Chemistry and Biochemistry

Presentation Abstract

Early/late heterobimetallic complexes have been designed and synthesized using dinucleating tris- and bis(phosphinoamide) ligand frameworks, with the ultimate goal of either developing more sustainable catalytic processes using base metals or uncovering entirely new reaction spaces through metal-metal cooperativity. In this context, we have found Zr/Co complexes to exhibit the ideal balance of stability and reactivity, allowing our group to uncover a series of unique reactions promoted by heterobimetallic Zr/Co complexes, each with unusual mechanisms facilitated by metal-metal cooperativity. For example, a tris(phosphinoamide) Zr^{IV}/Co^I complex has been shown to rapidly react with O₂ to generate a terminal Zr^{IV}/Co^I peroxo complex. This reaction exemplifies a unique cooperative reaction pathway in which two-electron O₂ reduction occurs at a formally d⁰ Zr^{IV} center and is facilitated by the appended d¹⁰ Co^I fragment, which serves as an electron-reservoir. More coordinative unsaturated bis(phosphinoamide) Zr/Co complexes are much more reactive than their tris(phosphinoamide) congeners, and have proven to be active catalysts for the hydrogenation of alkene and alkyne substrates under mild conditions. Interestingly, internal alkynes are selectively semi-hydrogenated to alkene products by the Zr/Co bis(phosphinoamide) catalyst, but nearly 1:1 mixtures of *Z* and *E* olefin products are formed. Careful analysis of the product distribution over time suggests that the *E* olefin is formed directly rather than via *Z*-to-*E* isomerization, a phenomenon we believe to be closely linked to the bimetallic nature of the H₂ activation process. The bis(phosphinoamide) Zr/Co complexes also readily activate the C-H bonds of pyridine derivatives and terminal alkynes. Ongoing progress in understanding the mechanism and further catalytic applications of these reactions will be discussed.

DE-SC0019179: Metal-Metal Cooperativity in Early/Late Heterobimetallic Complexes as a Strategy for Promoting Catalysis with Earth-Abundant Metals

PI: Christine M. Thomas

Postdocs: Jeffrey W. Beattie, Elizabeth M. Lane

Students: Hongtu Zhang, Nathanael H. Hunter, Brett A. Barden, Canning Wang, David Ullery

Affiliations: The Ohio State University, Department of Chemistry and Biochemistry

DE-SC0014151: Metal-Metal Interactions in Heterobimetallic Complexes as a Strategy to Promote Multielectron Redox and Small Molecule Activation Processes

PI: Christine M. Thomas

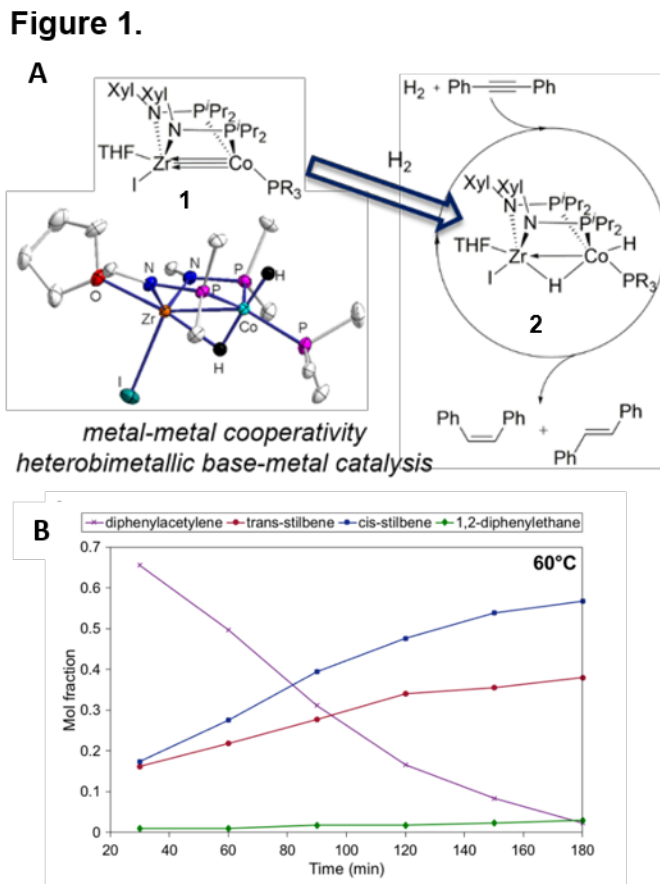
Student: Kathryn M. Gramigna

Affiliation: Brandeis University, Department of Chemistry

RECENT PROGRESS

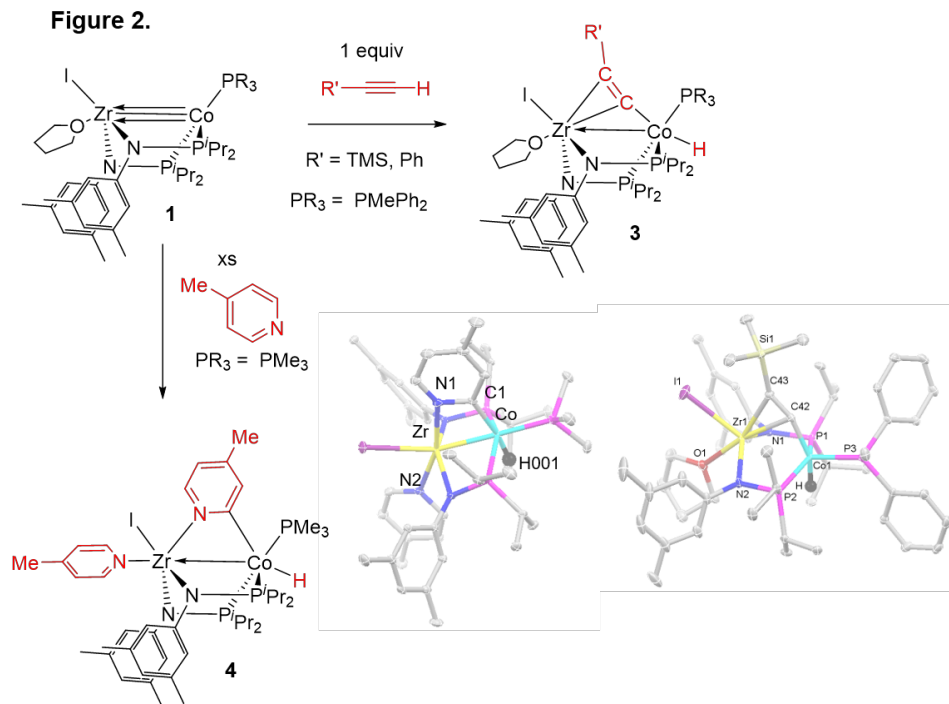
Catalytic Applications of Zr/Co Bis(phosphinoamides) Complexes

The hydrogenation of unsaturated hydrocarbons is typically performed using precious metal catalysts, but a heterobimetallic approach enables this catalytic transformation with a combination of two base metals. A reduced Zr^{IV}/Co^{-I} bis(phosphinoamide) complex **1** is shown to readily add H_2 across the Zr/Co multiple bond to afford an isolable dihydride complex **2**. This reactivity can be effectively incorporated into a catalytic cycle for the hydrogenation of alkenes and semi-hydrogenation of alkynes (Figure 1A). Monitoring product distribution over time suggests two operative mechanisms for alkyne semi-hydrogenation, including a mechanism for the direct formation of *trans* alkene products that is uniquely enabled by metal-metal cooperativity (Figure 1B). The Ti/Co analogue of **1** exhibits significantly diminished catalytic activity, and shows no evidence for direct formation of *trans* alkene products in semi-hydrogenation reactions. The effect of varying the early metal in early/late heterobimetallic catalysts showcases the ways that both catalyst activity and selectivity can be tuned by changing the metal-metal combination.

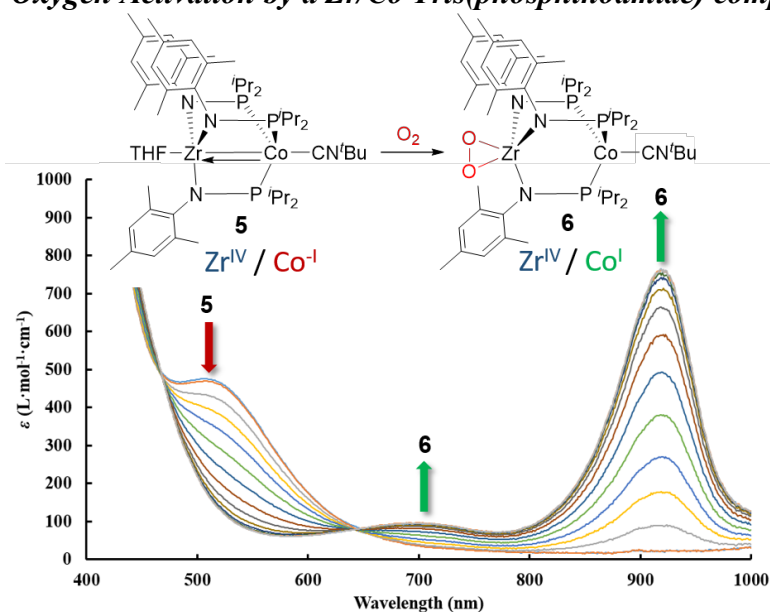


In addition to dihydrogen, complex **1** has been found to activate C-H bonds at room temperature (Figure 2). For example, the C-H bond of terminal alkynes readily adds across the Zr/Co bond of **1** to generate the Co-hydride/ μ -acetylide complex **3** via C-H oxidative addition. Furthermore, addition of excess 4-methylpyridine to **1** affords complex **4**, in which pyridine has been C-H activated in the *ortho*-position. We are hopeful that these C-H activation reactions can be incorporated into a catalytic cycle for C-H functionalization reactions.

A better understanding of reaction mechanisms that incorporate bimetallic cooperativity will allow the design of more sustainable base metal catalysts and the development of new catalytic transformations.



Oxygen Activation by a Zr/Co Tris(phosphinoamide) complex



Our group have previously shown that early and late metals linked together through a tris(phosphinoamide) dinuclear ligand framework are uniquely capable of activating strong σ and π bonds via cooperative bond activation pathways that involve simultaneous interaction of both metals with incoming substrates. We have recently uncovered a new mode of bimetallic cooperativity in which one metal binds a substrate molecule while the second metal plays the role of a redox active metalloligand. For example, when access to the low valent Co center is

effectively blocked using a tightly binding ligand such as $^t\text{BuNC}$ in complex **5**, we have found that incoming substrates are forced to interact exclusively with the $d^0 \text{Zr}^{\text{IV}}$ center. In a recent example of this, we have shown that Zr/Co tris(phosphinoamide) complex **5** reacts rapidly with excess dry O_2 to afford the peroxo complex **6** (Figure 3). Monitoring the reaction at -80°C reveals a clean transformation with no build-up of intermediates, with a reaction rate of $2 \times 10^{-3} \text{ mM/s}$. The pendent Co^{I} center in **5** does not interact directly with O_2 but rather serves as a redox-active metalloligand, mediating two-electron reduction of O_2 to O_2^{2-} at a formally $d^0 \text{Zr}^{\text{IV}}$ center.

Publications Acknowledging these Grants in 2018-2019

(XLVII) Exclusively funded by these grants;

1. Zhang, H.; Hatzis, G. P.; Moore, C. E.; Dickie, D. A.; Bezpalko, M. W.; Foxman, B. M.; Thomas, C. M. O₂ Activation by a Heterobimetallic Zr/Co Complex. *J. Am. Chem. Soc.* **2019**, *accepted*. DOI: 10.1021/jacs.9b04215
2. Barden, B. A.; Culcu, G.; Krogman, J. P.; Bezpalko, M. W.; Hatzis, G. P.; Dickie, D. A.; Foxman, B. M.; Thomas, C. M. Assessing the Metal-Metal Interactions in a Series of Heterobimetallic Nb/M (M = Fe, Co, Ni, Cu) and Their Effect on Multielectron Redox Properties. *Inorg. Chem.* **2019**, *58*, 821-833.
3. Gramigna, K. M.; Dickie, D. A.; Foxman, B. M.; Thomas, C. M. Cooperative H₂ Activation Across a Metal-Metal Multiple Bond and Hydrogenation Reactions Catalyzed by a Zr/Co Heterobimetallic Complex. *ACS Catalysis* **2019**, *9*, 3153-3164.

(XLVIII) Jointly funded by this grant and other grants with leading intellectual contribution from this grant;
none

(XLIX) Jointly funded by these grants and other grants with relatively minor intellectual contribution from these grants;

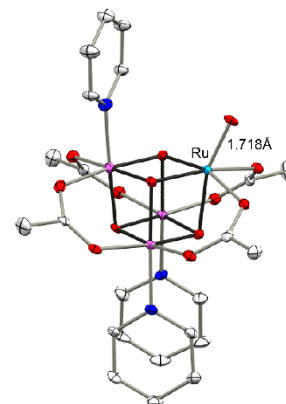
1. Coombs, J.; Perry, D.; Kwon, D.-H.; Thomas, C. M.; Ess, D. H. Why Two Metals are Better Than One for Heterodinuclear Cobalt-Zirconium-Catalyzed Kumada Coupling. *Organometallics* **2018**, *37*, 4195-4203.
2. Greer, S. M.; McKay, J.; Gramigna, K. M.; Thomas, C. M.; Stoian, S. A.; Hill, S. Probing Fe-V Bonding in a C₃-Symmetric Heterobimetallic Complex. *Inorg. Chem.* **2018**, *57*, 5870-5878.

Synthesis and Properties of Ruthenium–Cobalt Oxo Cubane Clusters Bearing a High-Valent, Terminal Ru^V–Oxo with Significant Oxo Radical Character

Jaruwan Amtawong and T. Don Tilley
Chemical Sciences Division, Lawrence Berkeley National Laboratory

Presentation Abstract

High-valent Ru^V–oxo intermediates have long been proposed in catalytic oxidation chemistry, but investigations into their electronic and chemical properties have been rather limited due to their reactive nature and rarity. The incorporation of Ru into the [Co₃O₄] subcluster via the single-step assembly reaction of Co^{II}(OAc)₂(H₂O)₄ (OAc = acetate), perruthenate (RuO₄[−]), and pyridine (py) yielded an unprecedented Ru(O)Co₃(μ₃-O)₄(OAc)₄(py)₃ cubane featuring an isolable, yet reactive Ru^V–oxo moiety. EPR, ENDOR, and DFT studies reveal a valence-localized [Ru^V(S=½)Co^{III}₃(S=0)O₄] configuration and a small degree of covalency in the cubane core. Significant oxyl radical character in the Ru^V–oxo unit is experimentally demonstrated by radical coupling reactions between the oxo cubane and both 2,4,6-tri-*tert*-butylphenoxy and trityl radicals. The oxo cubane oxidizes organic substrates and, notably, reacts with water to form an isolable μ-oxo *bis*-cubane complex [(py)₃(OAc)₄Co₃(μ₃-O)₄Ru]–O–[RuCo₃(μ₃-O)₄(OAc)₄(py)₃]. Redox activity of the Ru^V–oxo fragment is easily tuned by the electron-donating ability of the distal ligand set at the Co sites demonstrating strong electronic communication throughout the entire oxo cubane cluster. Natural bond orbital (NBO) calculations reveal cooperative orbital interactions of the [Co₃O₄] unit in supporting the Ru^V–oxo moiety *via* a strong π-electron donation. This contribution provides an understanding of important factors that favor formation of metal–oxo species especially those in heterobimetallic oxo systems.



Contract No. DE-AC02-05CH11231

Student: Jaruwan Amtawong

Timothy H. Warren

Chemical and Electrocatalytic Oxidation of Ammonia

Mahdi Raghibi Borougeni, Christine Greene, and Timothy H. Warren
Georgetown University, Department of Chemistry

Presentation Abstract

Produced on a massive scale, easily liquefied, and transported through thousands of miles of pipelines, ammonia (NH₃) has nearly the same energy content as does H₂ per H atom. Efficient ammonia oxidation electrocatalysts would enable the efficient use of ammonia in fuel cells. The development of homogeneous molecular electrocatalysts for ammonia oxidation offers the opportunity to uncover effective mechanistic pathways to convert NH₃ to protons, electrons and N₂.

We describe two new ammonia oxidation systems based on first row transition metals. Copper β -diketiminato complexes serve as homogeneous ammonia oxidation electrocatalysts. Cyclic voltammetry, structural, kinetic, and computational studies support a mechanism in which ammonia is first oxidized to hydrazine via copper(II) amides [Cu^{II}]-NH₂ unstable towards N-N coupling. The simple iron complex ferrocenium (Fc⁺) efficiently converts NH₃ to N₂ along with protons and electrons captured as NH₄⁺ and Fc, respectively. Kinetic and computational studies suggest a related mechanism that involves coupling of Fc-NH₂ intermediates. Ferrocene serves as an electrocatalyst for NH₃ in MeCN while liquid ammonia soluble ferrocene derivatives enable electrooxidation in 80% ammonia / MeCN solutions at -40 °C.

Grant or FWP Number: DE-SC001779

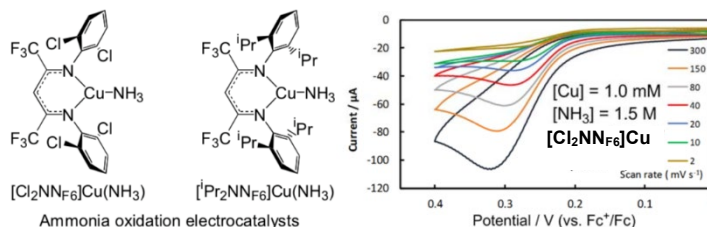
Catalytic Interconversion of Ammonia and Dinitrogen at Base Metals

Student(s): Mahdi Raghibi Borougeni, Evan J. Gardner, Christine Greene, David Lucas Kane

RECENT PROGRESS

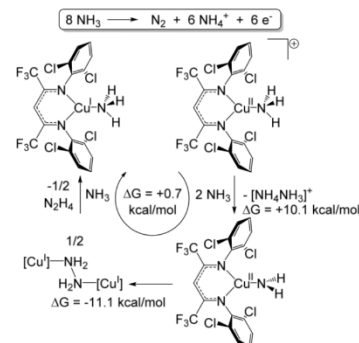
Ammonia Oxidation at Copper β -diketiminato Complexes

Although copper(II) ammine complexes have been known since the time of Werner, we find that sterically restricting the coordination environment at copper enables the chemical and electrocatalytic oxidation of ammonia. The copper(I) β -diketiminato complexes [Cl₂NNF₆]Cu and [iPr₂NNF₆]Cu each exhibit smooth electrocatalytic behavior as measured by cyclic voltammetry in 1.5 M NH₃ solution in MeCN at a glassy carbon working electrode and 0.1 M [Bu₄N]PF₆ as supporting electrolyte. While the more electron-poor [Cl₂NNF₆]Cu has an onset potential of approximately +200 mV vs. Fc⁺/Fc, the somewhat more



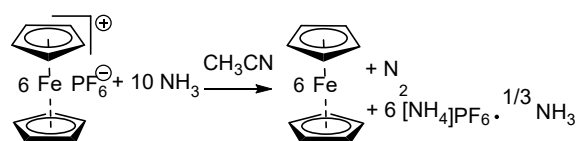
electron-rich $[\text{Pr}_2\text{NNF}_6]\text{Cu}$ has a significantly lower onset potential of -240 mV vs. Fc^+/Fc , representing approximate overpotentials of 1140 and 700 mV in MeCN.

DFT studies suggest that isolable monovalent $[\text{Cu}^{\text{I}}](\text{NH}_3)$ species undergo oxidation to the corresponding copper(II) monoammine complexes $\{[\text{Cu}^{\text{II}}](\text{NH}_3)\}^+$ which undergo deprotonation by NH_3 to give $[\text{Cu}^{\text{II}}]-\text{NH}_2$ species unstable towards N-N coupling to form hydrazine and $[\text{Cu}^{\text{I}}]$. In support of this mechanism, chemically isolable $\{[\text{Cl}_2\text{NNF}_6]\text{Cu}(\text{NCMe})_2\}^+$ reacts quickly with excess NH_3 to give $[\text{Cu}^{\text{I}}](\text{NH}_3)$ and N_2H_4 as well as the dicopper hydrazine adduct $\{[\text{Cl}_2\text{NNF}_6]\text{Cu}\}_2(\mu-\text{N}_2\text{H}_4)_2$ that also forms under electrocatalytic conditions.



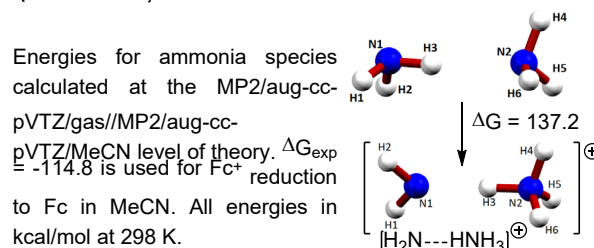
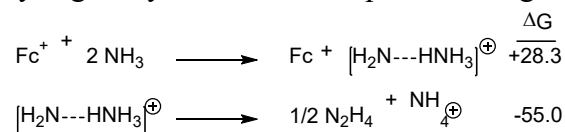
Chemical and Electrocatalytic Ammonia Oxidation by Ferrocenium

The simple iron complex ferrocenium (Fc^+) efficiently converts NH_3 to N_2 along with protons and electrons captured as NH_4^+ and Fc , respectively. Addition of excess ammonia gas to a solution of ferrocenium hexafluorophosphate (FcPF_6) in acetonitrile at room temperature results in rapid conversion of Fc^+ to Fc with concomitant formation of N_2 and NH_4^+ in a 6 electron reaction.

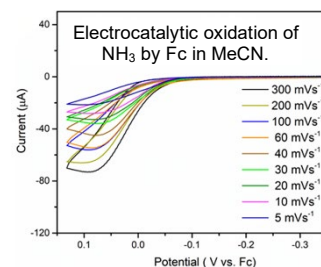


Analysis of the headspace by GC-TCD reveals 95% yield of N_2 and ^1H NMR analysis indicates the formation of Fc in 90-100% yield. Protons derived from the oxidation of ammonia are captured by excess ammonia and appear in quantitative yield as NH_4^+ , isolated as $\text{NH}_4\text{PF}_6 \cdot 1/3 \text{NH}_3$ under our workup conditions. Addition of $^{15}\text{NH}_3$ to Fc^+ forms $^{15}\text{N}_2$ and hydrazine is even more quickly oxidized than ammonia.

Kinetic analysis by UV-vis spectroscopy reveals clean first-order decay of Fc^+ in the presence of excess NH_3 . Analysis of the NH_3 dependence reveals second and third order terms in $[\text{NH}_3]$ to give the rate law: $\text{rate} = (k_2[\text{NH}_3]^2 + k_3[\text{NH}_3]^3)[\text{Fc}^+]$. Eyring analysis over the temperature range -20 to 10 °C with $[\text{NH}_3] = 1.0 \text{ M}$ allows us to estimate $\Delta H^\ddagger = 8.4(7) \text{ kcal/mol}$ and $\Delta S^\ddagger = -37.3(25) \text{ cal/mol}$ with $\Delta G^\ddagger = 19.5 (15) \text{ kcal/mol}$. High level DFT calculations reveal that ammonia oxidation by Fc^+ likely takes place via an inner sphere mechanism. Considered in MeCN solvent, simple oxidation of 2 equiv. NH_3 via the ammonia dimer to give the amidyl-ammonium radical cation is 28.3 kcal/mol higher in energy than the experimentally determined reduction of Fc^+ of Fc .

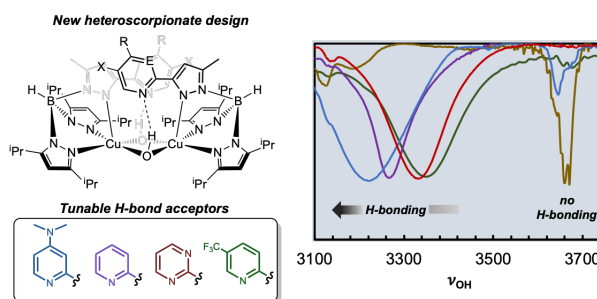


Cyclic voltammetry of 1.0 mM Fc in a 3.6 M NH₃ solution in MeCN using a glassy carbon electrode with 0.1 M [Bu₄N]PF₆ shows a large, irreversible oxidative wave corresponding to electrocatalytic ammonia oxidation. Controlled potential electrolysis (CPE) allows for the catalytic oxidation of ammonia. CPE of a 4.6 M NH₃ solution at 50 mV vs. Fc with 1 mM Fc is long-lived. Monitoring the headspace for N₂ formed after 13 h indicates Faradaic efficiency of 44%. The Faradaic efficiency may be limited due to the reactivity of the intermediates with the glassy carbon electrode: multi-scan CV of the Fc / NH₃ system results in a 40% loss in current that becomes stable. Importantly, use of a sulfonated ferrocene enables electrocatalysis in very concentrated NH₃ solutions or even liquid ammonia at -40 °C.

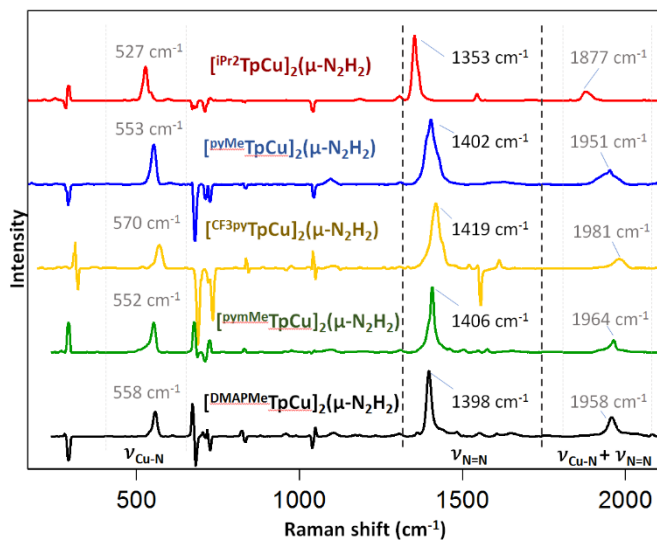


Diazene Activation via Tris(pyrazolyl)borate Complexes with Pendant Pyridine Arms

We have developed efficient synthetic pathways to a family of tris(pyrazolyl)borate ligands ^{py}TpK that possess pyridyl groups with different substituents that are appended to one pyrazolyl ring of the ^{py}Tp ligand. We have been able to incorporate electron-withdrawing CF₃ groups as well as electron-donating Me and NMe₂ substituents. This has enabled the synthesis of a family of {^{py}TpCu}₂(μ-OH)₂ complexes that possess py···H-OCu H-bonding between the pyridyl arm and the hydroxyl O-H. The electron-poor CF₃ gives a broad ν(OH) band centered at 3335 cm⁻¹ whereas the electron-rich NMe₂ substituent gives a broad ν(OH) band at 3217 cm⁻¹. These decreased stretching frequencies relative to {^{iPr}2TpCu}₂(μ-OH)₂ at 3670 cm⁻¹ that possesses no H-bonding clearly indicate the ability to modulate H-bonding.



These {^{py}TpCu}₂(μ-OH)₂ complexes are useful precursors to the corresponding diazene species {^{py}TpCu}₂(μ-N₂H₂) by simple reaction with hydrazine. The X-ray structure of the parent {^{py}TpCu}₂(μ-N₂H₂) complex clearly shows H-bonding between the py-arm of the Tp ligand and the bridging diazene ligand. In collaboration with Prof. Hannah Shafaat at Ohio State University we have obtained the resonance Raman spectra of several {^{py}TpCu}₂(μ-N₂H₂) complexes. The trend is clear: the more electron-poor the N-heterocycle substituent, the less activated the stronger the N=N bond.



Resonance Raman spectra of {^{py}TpCu}₂(μ-N₂H₄) complexes

These ^{py}TpM scaffolds have been extended to Fe, Co, and Ni with the goal to examine the effect of the N-heterocycle pendant on the interconversion of N₂H₂ and N₂ ligands.

Publications Acknowledging this Grant in 2018-2019

(1) *Exclusively funded by this grant*

“Tris(pyrazolyl)borate Copper Hydroxide Complexes Featuring Tunable Intramolecular H-bonding” Gardner, E. J.; Cobb, C. R.; Bertke, J. A.; Warren, T. H.* *ChemRxiv* preprint: <https://doi.org/10.26434/chemrxiv.7878065.v1>

Alkane Activation and Oxidation on IrO₂(110)

Jason F. Weaver,¹ Aravind Asthagiri,² Minkyu Kim,² Rachel Martin,¹ Austin Franklin,¹
Yingxue Bian,¹ Tao Li¹

¹ Department of Chemical Engineering, University of Florida, Gainesville, FL

² Department of Chemical and Biomolecular Engineering, The Ohio State University, Columbus,
OH

Presentation Abstract

The IrO₂(110) surface efficiently promotes the C-H bond activation of light alkanes (C1-C3) at temperatures as low as 100 K, producing adsorbed alkyl fragments that remain stable to nearly 400 K. These characteristics may provide opportunities for developing IrO₂-based catalysts that can selectively and efficiently convert light alkanes to value-added products. In this presentation, I discuss our recent investigations of alkane activation and oxidation on IrO₂(110), and focus on clarifying the mechanisms for C-H bond activation and subsequent oxidation. We find that light alkanes (C1-C3) adsorb strongly on the IrO₂(110) surface by forming σ -complexes along rows of coordinatively-unsaturated Ir atoms, and that this adsorbed state acts as the precursor for initial C-H bond cleavage. I will discuss recent results showing that ethane dehydrogenation to ethylene occurs on IrO₂(110) just above room temperature during temperature programmed reaction spectroscopy (TPRS), and that partially hydrogenating surface O-atoms prior to ethane adsorption enhances the selectivity toward ethylene formation. In contrast, similar experiments with propane fail to yield propylene, with extensive oxidation to CO_x ensuing instead. I will discuss the elementary rate processes that govern selectivity in these oxidative dehydrogenation reactions as determined from experiment and DFT, and show that deactivation of surface O-atoms provides a means for promoting selectivity toward alkane dehydrogenation to alkenes on IrO₂(110).

DE-FG02-03ER15478: Alkane Oxidation on Late Transition-Metal Oxide Surfaces

Postdoc(s): M. Kim

Student(s): R. Martin, A. Franklin, T. Li, V. Mehar, Y. Bian, F. Feng

RECENT PROGRESS

AP-XPS investigations of CH₄ oxidation on IrO₂(110)

During the last year, we have characterized IrO₂(110) film growth and reaction with CH₄ using *in situ* AP-XPS at the NSLS-2 light source in Brookhaven and MAX IV in Sweden.

We have successfully generated and characterized IrO₂(110) films with high-resolution XPS at the synchrotron facilities by oxidizing Ir(100) at ~775 K and O₂ pressures greater than 1 Torr, and find that the films are highly reactive toward pure CH₄ over a range of *in situ* conditions. Figure 1a shows a representative series of Ir 4f spectra collected at NSLS- 2 during exposure of an IrO₂(110) film to 10⁻⁵ Torr of CH₄ at a surface temperature of 600 K. The spectra show that CH₄ reduces the ~15 layer IrO₂(110) film nearly completely within about 50 minutes, demonstrating that an efficient Mars van Krevelan mechanism is operative wherein O-atoms from the subsurface rapidly migrate to the surface to sustain CH₄ oxidation and thereby cause the oxide film to be

almost completely reduced to metal. We also find that ~ 0.1 to 1 Torr of pure CH₄ reduces the IrO₂ film to metal within seconds at 600 K, further demonstrating the extraordinary reactivity of IrO₂(110) toward methane. Figure 1b shows rough estimates of the IrO₂(110) film thickness as a function of time during exposure to 10⁻⁵ Torr of CH₄ at various temperatures. The data shows that temperature enhances the IrO₂ reduction rate, with an estimated activation energy of 43 kJ/mol. Our experiments also provide evidence of steady state CH₄ oxidation during exposure of IrO₂(110) films to CH₄/O₂ mixtures of varying compositions and total pressures between 0.1 and 3.0 Torr. We are continuing to analyze the spectra using peak deconvolution as well as DFT calculations of the core-level shifts, aiming to develop molecular-scale models of the surface reactivity.

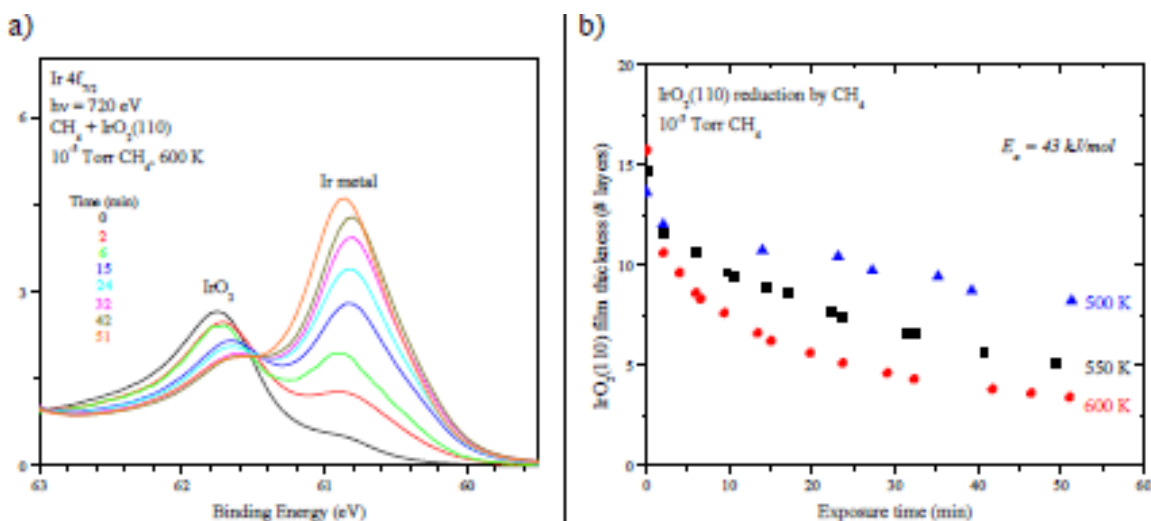


Figure 1: a) Ir 4f_{7/2} spectra collected as a function of time during exposure of an IrO₂(110) film to 10⁻⁵ Torr of CH₄ at 600 K, and b) estimated IrO₂(110) film thickness as a function of time during exposure to 10⁻⁵ Torr of CH₄ at surface temperatures of 500, 550 and 600 K.

Local effects of surface OH groups on the CH₄ oxidation kinetics on IrO₂(110)

We have recently investigated the influence of surface OH groups on the adsorption and activation of CH₄ on IrO₂(110), and developed a microkinetic model, based on DFT calculations, to simulate TPRS spectra for comparison with experimental results. Our DFT results predict that surface OH groups strongly destabilize CH₄ σ -complexes on IrO₂(110) in addition to deactivating surface O-atoms that are needed to achieve CH₄ activation at

low temperature. We demonstrate that a microkinetic model that incorporates the influence of surface OH groups on the CH₄ binding and reactivity reproduces experimental TPRS results which show that adsorbed CH₄ π -complexes preferentially dissociate at low CH₄ coverage, but that an increasing fraction of the adsorbed CH₄ desorbs at low temperature (~120 K) with increasing initial CH₄ or H pre-coverage. The simulations reveal that low-temperature CH₄ desorption during TPRS arises primarily from CH₄ π -complexes that are kinetically-trapped between adjacent surface OH groups, and are thus destabilized and unable to access reactive O-atoms. Our results demonstrate that the local effect of adjacent OH groups must be incorporated into any microkinetic models to properly capture the selectivity between extensive and partial oxidation in alkane conversion on IrO₂(110) under reaction conditions.

Publications Acknowledging this Grant in 2015-2018

(I) Exclusively funded by this grant;

1. Mehar, V.; Kim, M.; Shipilin, M.; Van den Bossche, M.; Gustafson, J.; Merte, L. R.; Hejral, U.; Gronbeck, H.; Lundgren, E.; Asthagiri, A.; Weaver, J. F., "Understanding the intrinsic surface reactivity of single-layer and multilayer PdO(101) on Pd(100)". *ACS Catal* **2018**, *8*, 8553-8567.
2. Martin, R.; Kim, M.; Franklin, A.; Bian, Y.; Asthagiri, A.; Weaver, J. F., "Adsorption and oxidation of propane and cyclopropane on IrO₂(110)". *Phys. Chem. Chem. Phys.* **2018**, *20*, 29264 - 29273.
3. Li, T.; Kim, M.; Liang, Z.; Asthagiri, A.; Weaver, J. F., "Dissociative chemisorption and oxidation of H₂ on the stoichiometric IrO₂(110) surface". *Top. Catal.* **2018**, *61*, 397-411.
4. Li, T.; Kim, M.; Liang, Z.; Asthagiri, A.; Weaver, J., "Hydrogen oxidation on oxygen-rich IrO₂(110)". *Catalysis, Structure and Reactivity* **2018**, *4*, 1-13.
5. Kim, M.; Pan, L.; Weaver, J. F.; Asthagiri, A., "Initial reduction of the PdO(101) surface: Role of oxygen vacancy formation kinetics". *J. Phys. Chem. C* **2018**, *122*, 26007-26017.
6. Bian, Y. X.; Kim, M.; Li, T.; Asthagiri, A.; Weaver, J. F., "Facile dehydrogenation of ethane on the IrO₂(110) surface". *J. Am. Chem. Soc.* **2018**, *140*, 2665-2672.
7. Weaver, J. F.; Choi, J.; Mehar, V.; Wu, C. J., "Kinetic coupling among metal and oxide phases during CO oxidation on partially reduced PdO(101): Influence of gas-phase composition". *ACS Catal* **2017**, *7*, 7319-7331.

8. Pan, L.; Weaver, J. F.; Asthagiri, A., "First principles study of molecular O₂ adsorption on the PdO(101) surface". *Top. Catal.* **2017**, *60*, 401-412.

9. Choi, J.; Pan, L.; Mehar, V.; Zhang, F.; Asthagiri, A.; Weaver, J. F., "Promotion of CO oxidation on PdO(101) by adsorbed H₂O". *Surf. Sci.* **2016**, *650*, 203-209.

10. "Catalytic chemistry of oxide nanostructures", A. Asthagiri, D. Dixon, Z. Dohnálek, B. Kay, R. Rousseau, J. Rodriguez, D. Stacchiola, and J. F. Weaver in *Oxide materials at the two-dimensional limit*, Springer Series in Materials Science, Vol. 234 (**2016**). Editors: F. Netzer and A. Fortunelli.

11. Zhang, F.; Pan, L.; Choi, J.; Mehar, V.; Diulus, J. T.; Asthagiri, A.; Weaver, J. F., "Propane sigma-complexes on PdO(101): Spectroscopic evidence of the selective coordination and activation of primary C-H bonds". *Angew. Chem., Int. Ed.* **2015**, *54*, 13907-13911.

12. Weaver, J. F.; Zhang, F.; Pan, L.; Li, T.; Asthagiri, A., "Vacancy-mediated processes in the oxidation of CO on PdO(101)". *Acc. Chem. Res.* **2015**, *48*, 1515-1523.

13. Choi, J.; Pan, L.; Zhang, F.; Diulus, J. T.; Asthagiri, A.; Weaver, J. F., "Molecular adsorption of NO on PdO(101)". *Surf. Sci.* **2015**, *640*, 150-158.

(II) Jointly funded by this grant and other grants with leading intellectual contribution from this grant;

1. Busch, M.; Mehar, V.; Merte, L. R.; Shipilin, M.; Lundgren, E.; Weaver, J. F.; Gronbeck, H., "Adsorption of NO on Fe₃O₄(111)". *Chem. Phys. Lett.* **2018**, *693*, 84-87.

2. Shipilin, M.; Lundgren, E.; Gustafson, J.; Zhang, C.; Bertram, F.; Nicklin, C.; Heard, C. J.; Gronbeck, H.; Zhang, F.; Choi, J.; Mehar, V.; Weaver, J. F.; Merte, L. R., "Fe oxides on Ag surfaces: Structure and reactivity". *Top. Catal.* **2017**, *60*, 492-502.

3. Merte, L. R.; Heard, C. J.; Zhang, F.; Choi, J.; Shipilin, M.; Gustafson, J.; Weaver, J. F.; Gronbeck, H.; Lundgren, E., "Tuning the reactivity of ultrathin oxides: NO adsorption on monolayer FeO(111)". *Angew. Chem., Int. Ed.* **2016**, *55*, 9267-9271.

4. Mehar, V.; Merte, L. R.; Choi, J.; Shipilin, M.; Lundgren, E.; Weaver, J. F., "Adsorption of NO on FeO_x films grown on Ag(111)". *J. Phys. Chem. C* **2016**, *120*, 9282-9291.

Size-Selected Metal Oxide Clusters as Model Inverse Catalysts

Michael G. White,^{1,2} Kenneth R. Goodman,¹ Yilin Ma,¹ and Jason Wang¹

¹Department of Chemistry, Stony Brook University, Stony Brook, NY

²Chemistry Division, Brookhaven National Laboratory, Upton, NY

Presentation Abstract

Size-selected cluster deposition is being used to prepare model inverse catalysts of metal oxides on Cu, Cu₂O and Au surfaces that have proved to be highly active for the water-gas-shift reaction and CO₂ hydrogenation. Size-selected cluster deposition is unique in its ability to control cluster stoichiometry which provides a means of introducing oxygen “vacancies” and varying the average cation oxidation state. The recent introduction of a vacuum suitcase makes it possible to access characterization instrumentation, e.g., STM and AP-XPS, without exposing the samples to air, thereby reducing carbon contamination and preserving the as-deposited cluster stoichiometry. STM imaging of stoichiometric and “reduced” oxide clusters of Ti and Nb deposited on Au(111) exhibit surprisingly different binding sites and morphologies, with the stoichiometric clusters, e.g., Ti₃O₆ forming small assemblies of 3-5 clusters on terraces while individual clusters decorate the step edges with nearly uniform spacing. By comparison, the “reduced” clusters (Ti₃O₅, Nb₃O₆) form larger fractal-like assemblies consisting of 10-100’s of clusters in close contact that can extend across steps edges. The assemblies are composed of individual clusters in close contact, but not chemically fused to form MO_x islands, and thus retain their unique structural and chemical properties. Combined STM and AP-XPS studies have also been performed on Zr modified Cu₂O/Cu(111) surfaces as model catalysts for CO₂ hydrogenation to methanol. The as-deposited surfaces are composed of small ZrO_x clusters (a few atoms) on a disordered Cu₂O/Cu surface, which becomes more reduced as the surface temperature is increased. Under ambient pressures of CO₂ and H₂, the CuO_x regions of the surface are fully reduced and the C1s and O1s XPS spectra show evidence of multiple reaction products, H_xCOO, CO₂^{δ-}, H_xC-O, and OH, which are expected intermediates for the formate and reverse-WGS pathways for methanol formation. These results demonstrate the importance of the Cu-ZrO_x interface for promoting CO₂ activation and hydrogenation.

FWP-BNL-CO040: Catalysis for Advanced Fuel Synthesis and Energy

Force/Activity Relationships in Transition Metal-Catalysis

Ross A. Widenhoefer, Stephen L. Craig, Liqi Wang, Yichen Yu
Department of Chemistry, Duke University

Presentation Abstract

Strategies to increase the efficiency of catalytic reactions remain a fundamental need in basic energy sciences. A promising and emerging approach is to reversibly switch ligand geometry within a catalytic cycle, so that the catalyst is optimized for each of multiple elementary reaction steps. Our program is focused on using mechanical force to reversibly perturb the ligand geometry of transition metal complexes, ultimately to bias catalysis. A key effort is directed at identifying quantitative relationships between a force of tension applied to a ligand and the energetics of elementary steps at the associated metal center. Specifically, we use computationally calibrated macrocycles to apply force to the alkoxy position in MeO-BIPHEP derivative ligands that are coordinated to Pd and Pt. The resulting organometallic complexes have subsequently been applied to oxidative insertion and reduction elimination reactions and the effect of force has been quantified. Key findings include the first demonstration of qualitatively differential response to force for these two elementary reactions, which supports the hypothesis that a switching force applied to a ligand can open up reactivity space in catalysis. The contributions from distortion of the complex vs. force-coupled ligand motion during the catalytic cycle are assessed. These studies are impacting our understanding of ligand geometry effects broadly and inspiring new designs for catalytic approaches that have the potential to reach broadly across the basic energy catalysis spectrum.

DE-SC0018188: Multi-State Catalysts Modulated by Mechanical Force

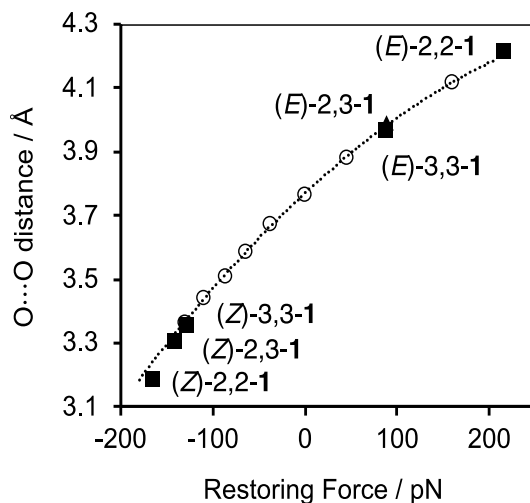
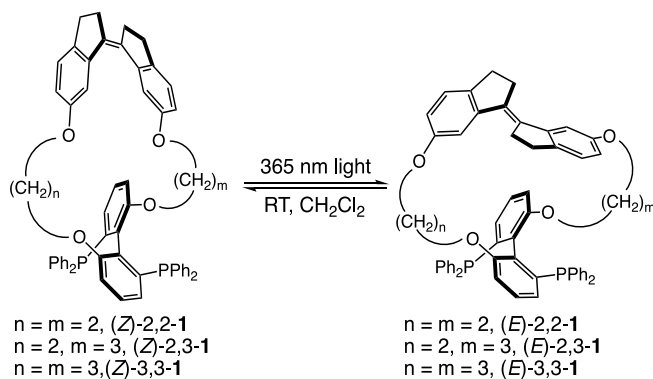
PIs: Ross A. Widenhoefer, Stephen L. Craig

Students: Liqi Wang, Yichen Yu

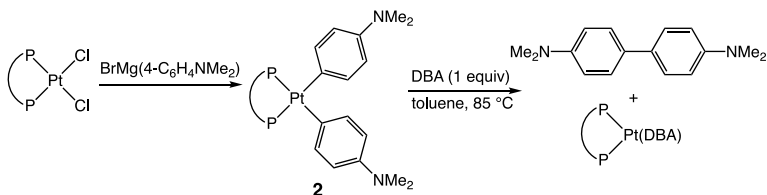
RECENT PROGRESS

The long-term objective of this project is to funnel mechanical forces to the molecular level and use those forces to improve catalyst activity and/or selectivity. Key questions include: how does an applied force of tension to a ligand affect reactivity in the various elementary steps of a catalytic cycle? What types of ligands, metals, and reactions are most susceptible to mechanical perturbation? How precise must the quantity of delivered force be to achieve a specific outcome? And ultimately, what materials are the most promising supports for bulk multi-state mechanocatalysis? Our current activities are directed toward understanding the fundamental underpinnings required to develop mechanically-responsive catalysts, including the elucidation of force-reactivity relationships, force-modulated catalytic reaction mechanisms, and force-modulated potential energy landscapes.

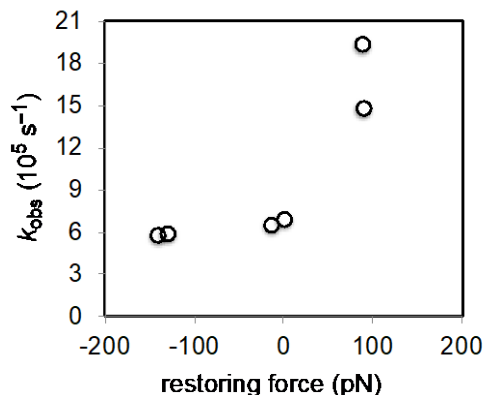
Quantitative force-activity relationships for elementary steps within catalytic coupling reactions. Recent efforts have been directed toward understanding and quantifying the effects of applied mechanical force on the energetics of reductive elimination and oxidative addition from palladium and/or platinum bis(phosphine) complexes under stoichiometric conditions. These transformations were targeted for initial investigation because (1) they represent two of the most important steps required for the synthetically-important cross-coupling reactions and (2) both transformations potentially involve significant perturbation of the P–M–P bond angle in the ground state relative to the transition state and, for this reason, are likely to be strongly affected by external mechanical force. Our approach to this objective employs force probe ligands **1** comprised of a photochemically active stiff stilbene (1,1'-biindane) chromophore tethered to a MeO-BIPHEP-derived bis(phosphine) ligand. Light-induced Z to E isomerization of the stiff stilbene moiety leads to force-induced modulation (compression and extension, respectively) of the BIPHEP dihedral angle, and hence the P–M–P bite angle. The applied mechanical force has been quantified by DFT calculations at the B3LYP/6-311+G(d) level and ultimately correlated with the energetics of reductive elimination and oxidative addition. We now have access to a family of six force-probe ligands **1** comprised of three E/Z pairs which differ in the length of the tethering chains. These ligands allow access to applied forces ranging from –166 pN (compression) to 215 pN (extension) relative to untethered MeOBiphep.



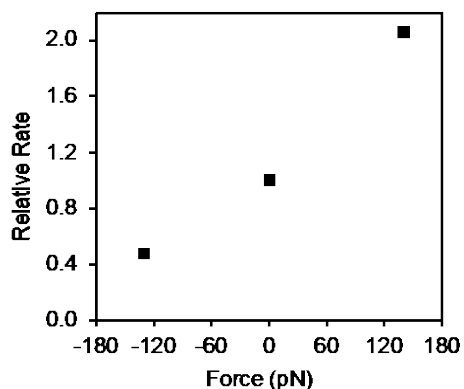
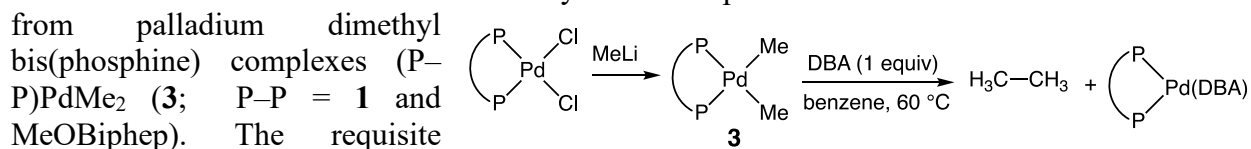
Force Modulated sp^2 - sp^2 reductive elimination from platinum diaryl bis(phosphine) complexes. We have established the force-activity relationship for the reductive elimination of 4,4'-bis(dimethylamino)-1,1'-biphenyl from platinum diaryl bis(phosphine) complexes containing force probe ligands **1** and MeOBiphep. The requisite platinum complexes were synthesized in two steps via reaction of bis(phosphine) ligand with (COD)PtCl₂ to form complexes (P–P)PtCl₂ followed by reaction with BrMg(4-C₆H₄NMe₂) to form diaryl complexes (P–P)Pt(4-C₆H₄NMe₂)₂ (**2**). Importantly, ³¹P NMR analysis of complexes **2** revealed that the one-bond platinum-phosphorous coupling constants (¹J_{Pt–P}), which are a sensitive probe of P–Pt–P bond angle, for the series of complexes **2** did not differ significantly (< 5 Hz), which strongly suggest that the applied force does not significantly affect the ground state geometry of complexes **2**. Heating solutions of complexes **2**



in toluene- d_8 containing DBA as a trapping ligand at 85 °C led to first-order decay through ≥ 3 half-lives to form 4,4'-bis(dimethylamino)-1,1'-biphenyl in >85% yield as the exclusive organic product along with (P-P)Pt(DBA) as the exclusive organometallic component. Relative to the force-free benchmark complex (MeOBiphep)Pt(4-C₆H₄NMe₂)₂ ($k = 6.9 \times 10^{-5} \text{ s}^{-1}$), compressive forces of up to -166 pN led to the small but significant decrease of the rate of reductive elimination ($k = 5.8 \times 10^{-5} \text{ s}^{-1}$). Conversely, extension forces of 140 pN led to a three-fold increase in the rate of reductive elimination ($k = 1.94 \times 10^{-5} \text{ s}^{-1}$).

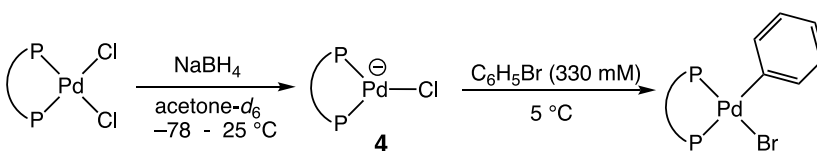


Force Modulated sp^3 - sp^3 reductive elimination from palladium dimethyl complexes. We have likewise established the force-activity relationship for the reductive elimination of ethane from palladium dimethyl



Force modulated oxidative addition to Pd(0) bis(phosphine) complexes. We have established the force-activity relationship for the oxidative addition of bromobenzene to palladium(0) bis(phosphine) complexes [(P-P)PdCl]⁻ (**4**; P-P = **1** and MeOBiphep). To avoid potential complications arising from the presence of excess chloride ion, the requisite palladium(0) chloride complexes **4** were generated in situ via reduction of (P-P)PdMeCl with NaBH₄ in acetone- d_6 at -78 °C. Treatment of complexes **4** (20 mM) with bromobenzene (200 mM) at 5 °C led to first-order decay to form the palladium aryl bromide complexes (P-P)PdBrPh as the exclusive products. As was anticipated, the effect of applied mechanical force was the opposite of that observed for reductive elimination with compressive forces increasing the rate of oxidative addition and extension forces decreasing the rate. For example, as compared to the force-free benchmark complex

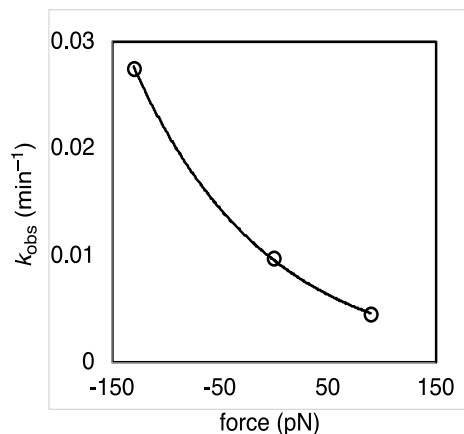
(MeOBiphep)PdCl]⁻ ($k_{\text{obs}} = 1.6 \times 10^{-4} \text{ s}^{-1}$), a compressive force of -130 pN produced a 2.8-fold increase in the rate of oxidative



addition ($k_{\text{obs}} = 4.5 \times 10^{-4} \text{ s}^{-1}$), whereas extension forces of 140 pN led to a two-fold decrease in the rate of oxidative addition ($k_{\text{obs}} = 7.5 \times 10^{-5} \text{ s}^{-1}$).

Taken together, these results represent the first demonstration of enhanced reactivity in a transition metal catalyzed reaction via a mechanically perturbed ligand, and more importantly it provides a first quantitation of a force-rate relationship of this type. Furthermore, we have demonstrated the differential effects of force on the rates of elementary metal-mediated reaction steps (oxidative addition and reductive elimination). Gratifyingly, the methodology should be applicable to a range of forces and ultimately other substrates, catalysts, and reactions (including reductive elimination, above), but even these early results are raising interesting questions. For example,

^{31}P NMR chemical shifts suggest that the electronic structure of the catalyst is trivially perturbed. That is, the change in reactivity is not due to changes in the ground state of the catalyst, but due to the effect of force on restricting catalyst conformation during the reaction. Further experiments will be needed to fully assess this hypothesis, but the nature of quantitative force-activity relationships have the potential to provide new insights into the factors that underlie ligand effects more broadly.



LIST OF PARTICIPANTS

Last Name	First Name	E-mail Address
Abild-Pedersen	Frank	abild@slac.stanford.edu
Abu-Omar	Mahdi	abuomar@chem.ucsb.edu
Bare	Simon	simon.bare@slac.stanford.edu
Bell	Alexis T.	alexbell@berkeley.edu
Bernskoetter	Wesley	bernskoetterwh@missouri.edu
Betley	Theodore	betley@chemistry.harvard.edu
Bhan	Aditya	abhan@umn.edu
Biddinger	Elizabeth	ebiddinger@ccny.cuny.edu
Bligaard	Thomas	bligaard@stanford.edu
Bradley	Chris	chris.bradley@sciecne.doe.gov
Bullock	R. Morris	morris.bullock@pnnl.gov
Byers	Jeffery	jeffery.byers@bc.edu
Campbell	Charles T.	charliec@uw.edu
Chen	Donna	dachen@sc.edu
Chen	Jingguang	jc3972@columbia.edu
Chi	Miaofang	chim@ornl.gov
Coates	Geoff	gc39@cornell.edu
Craig	Stephen	stephen.craig@duke.edu
Cundari	Thomas	tomc@unt.edu
Dai	Sheng	dais@ornl.gov
Datye	Abhaya	datye@unm.edu
Davis	Robert	rjd4f@virginia.edu
Delferro	Massimiliano	delferro@anl.gov
Ess	Daniel	dhe@chem.byu.edu
Flytzani- Stephanopoulos	Maria	mflytzan@tufts.edu
Gaffney	Kelly	kgaffney@slac.stanford.edu
Garrett	Bruce	Bruce.Garrett@science.doe.gov
Ginovska	Bojana	bojana.ginovska@pnnl.gov
Goldberg	Karen	kig@sas.upenn.edu
Gounder	Rajamani	rgounder@purdue.edu
Greeley	Jeffrey	jgreeley@purdue.edu
Gutiérrez	Oliver	oliver.gutierrez@pnnl.gov
Harris	Alexander	alexh@bnl.gov
Hartwig	John	jhartwig@berkeley.edu
Heinz	Tony	tony.heinz@stanford.edu
Hermans	Ive	hermans@chem.wisc.edu
Hoff	Carl	c.hoff@miami.edu
Jaramillo	Thomas	jaramillo@stanford.edu
Jenks	Cynthia	cjenks@anl.gov
Kaphan	David	kaphand@anl.gov
Katz	Alexander	askatz@berkeley.edu
Khatib	Sheima	sheima.khatib@ttu.edu

Kitchin	John	jkitchin@andrew.cmu.edu
Koel	Bruce	bkoel@princeton.edu
Krempner	Clemens	clemens.krempner@ttu.edu
Kung	Harold	hkung@northwestern.edu
Lercher	Johannes	johanneslercher@hotmail.com
Liu	Ping	pingliu3@bnl.gov
Liu	Cong	congliu@anl.gov
Marinescu	Smaranda	smarines@usc.edu
Marks	Tobin	t-marks@northwestern.edu
Mavrikakis	Manos	manos@engr.wisc.edu
McEwen	Jean-Sabin	js.mcewen@wsu.edu
Mindiola	Daniel	mindiola@sas.upenn.edu
Mueller	Karl	karl.mueller@pnnl.gov
Notestein	Justin	j-notestein@northwestern.edu
Ozkan	Umit	ozkan.1@osu.edu
Parkin	Gerard	parkin@columbia.edu
Peters	Jonas	jpeters@caltech.edu
Polo-Garzon	Felipe	pologarzonf@ornl.gov
Powers	David	david.powers@chem.tamu.edu
Pruski	Marek	mpruski@iastate.edu
Rappe	Andrew	rappe@sas.upenn.edu
Rioux	Robert	rioux@engr.psu.edu
Rodriguez	Jose	rodriguez@bnl.gov
Sadow	Aaron	sadow@iastate.edu
Schwartz	Viviane	Viviane.Schwartz@science.doe.gov
Scott	Susannah	sscott@ucsb.edu
Senanayake	Sanjaya D.	ssenanay@bnl.gov
Skrabalak	Sara	sskrabal@indiana.edu
Slowing	Igor	islowing@iastate.edu
Smith	Jeremy	smith962@indiana.edu
Stahl	Shannon	stahl@chem.wisc.edu
Suntivich	Jin	jsuntivich@cornell.edu
Surendranath	Yogesh	yogi@mit.edu
Tao	Franklin	franklin.feng.tao@ku.edu
Thomas	Christine	thomasc@chemistry.ohio-state.edu
Tilley	T. Don	tdtilley@berkeley.edu
Tran	Ba	ba.tran@pnnl.gov
Vura-Weis	Josh	vuraweis@illinois.edu
Warren	Timothy	thw@georgetown.edu
Waymouth	Robert	waymouth@stanford.edu
Weaver	Jason	weaver@che.ufl.edu
White	Michael	mgwhite@bnl.gov
Widenhoefer	Ross	rwidenho@chem.duke.edu
Wu	Zili	wuz1@ornl.gov

Cover images courtesy of: Morris Bullock (PNNL), Daniel Ess (Brigham Young University), Carl Hoff (University of Miami), Aditya Bhan (University of Minnesota), Thomas Jaramillo (SLAC and Stanford University), David Powers (Texas A&M University) and Thomas Cundari (University of North Texas).



U.S. DEPARTMENT OF
ENERGY

Office of
Science